Late Stage ^{18}F-Fluorination and ^{123}I-Iodination for PET and SPECT Imaging

A thesis submitted to the Board of the Faculty of Physical Sciences, in partial fulfilment of the requirements for the degree of Doctor of Philosophy at the University of Oxford

Thomas C. Wilson

Somerville College

University of Oxford

The work presented in this thesis was conducted under the supervision of Prof. Véronique Gouverneur and carried out at the Chemistry Research Laboratory, University of Oxford, unless otherwise specified. All the work is my own, except where otherwise stated, and has not been submitted for any other degree at this or any other university.

Thomas C. Wilson

5th September 2018

Thomas Wilson Somerville College DPhil Chemistry Trinity Term 2018

Abstract: Late Stage ^{18}F-Fluorination and ^{123}I-Iodination for PET and SPECT Imaging

This thesis consists of the development and application of novel radiochemical transformations for both Positron Emission Tomography (PET) and Single Photon Emission Computered Tomography (SPECT). A general introduction is presented in **Chapter I** and covers PET, the production of fluorine-18 and the current state-of-the-art for ^{18}F-radiolabelling. **Chapter IV** provides a brief overview of SPECT, production of radionuclides in SPECT and the current state-of-the-art.

The results chapters consist of three different approaches for the development and application of novel radiochemical transformations within PET or SPECT imaging. **Chapter II** discusses the application of the copper mediated nucleophilic ^{18}F-fluorination of aryl pinacol boronic esters to the radiofluorination of [^{18}F]olaparib. Subsequently, the imaging of DNA damage in pancreatic adenocarcinoma cell lines is examined. **Chapter III** discusses the synthesis of the novel ^{18}F-trifluoromethylation reagent, [^{18}F]-5-(trifluoromethyl)dibenzothiophenium trifluoromethanesulfonate and its application to the ^{18}F-trifluoromethylation of unmodified peptides. **Chapter IV** is comprised of the development of the copper mediated ^{123}I-Iodination of aryl boron reagents and its application to four clinically relevant SPECT tracers.

Finally, **Chapter V** provides experimental data for compounds discussed within this thesis.

Acknowledgements

First and foremost, I would like to thank Véronique for giving me the opportunity to work in her fantastic group. It has been a great experience in which I have loved (almost) every minute of it. Throughout all four years she has been supportive and has taught me so much. Her passion for chemistry is truly inspiring and something I will take with me the rest of my life.

I would also like to thank Cancer Research UK for my generous funding and giving me the opportunity to work with the whole CRUK and OCIC network. I would like to thank Graham, Bart, Veerle, Eugene and Maria for all their patience and support throughout all our collaborations.

Over my four years the group has changed a lot. I want to thank Thomas Cailly for teaching me so much (and for being very patient!) when I first arrived in the group as well as the whole of F12 including: Faye, Plum, Enrico, Gruber, Gabriele, Anna, Francesco, Osman and Natan.

I want to thank Matt, Sean, Kee, Patrick and, Stefan for teaching me everything there to know in SOMIL. I will never forget those early mornings during the winter! Gregor, thank you for all the tea breaks over the years. No matter how chemistry was going, you would always be there to chat. Your drive throughout all four years was an inspiration. Jeroen, I want to thank you for all our conversations over the last two years, our trips to Brothers, and even the occasional pint!

Over my four years in Somerville I have met many amazing individuals. Thomas, Ruben, Rita, James, Fergus, Joanna, Emily, JM, it has been great to get to know you all. Jeff, whilst you are a source of occasional frustration, you are always there come rain or shine. To the Abingdon crew, Ben, Davis, Minty, Ed, Andy, Joe,

Ramon, Swain and Anthony, I want to thank you all for all the fun memories, from our Risk nights to Pub Golf.

Of course, I should not pass mention on the three musketeers, Michael, Nick and Raul. Michael 'Rear-Admiral' Schedler, you are as much a source of knowledge as you are of beer and it was a pleasure to work with you during my first two years. Nicholas 'Burly Field Marshall' Taylor, you are a great colleague and an even better friend. It was a privilege to work with you. Finally, Raul 'The Snake' Pereira, I was great working in the hood with you and I hope one day we can blast 'Loona' out of the lab again.

I want to thank my brother and sister, Alex and Evie for all their support thought my PhD. To my parents, Liz and Rod, you were always there when I needed you and I am grateful for all the support you have given me throughout my studies. Lulu, thank you for being a source of amusement throughout my time. To Lydia and Joel, thank you for the wonderful memories in California.

Finally, I want to thank my wife, Rebecca. You have always been there for me, in the good times and in the bad. I am so lucky to have met such a wonderful person, let alone marry one!

Abbreviations

[^{11}C]	Enriched in carbon-11
[^{18}F]	Enriched in fluorine-18
[^{18}F]FDA	6-[^{18}F]Fluorodopamine
[^{18}F]FDG	2-[^{18}F]Fluoro-2-deoxy-D-glucose
[^{18}F]FDOPA	6-[^{18}F]Fluoro-3,4-dihydroxy-L-phenylalanine
[^{18}F]FMT	6-[^{18}F]Fluoro-3-hydroxy-L-phenylalanine
[^{18}F]FMTEB	3-[^{18}F]Fluoro-5-[(2-methyl-1,3-thiazol-4-yl)ethynyl]benzonitrile
[^{18}F]FPEB	3-[^{18}F]Fluoro-5-[(pyridinyl-3-yl)ethynyl]benzonitrile
[^{18}F]MFBG	(3-[^{18}F]Fluorobenzyl)guanidine
[^{18}F]NFSI	*N*-[^{18}F]Fluorobenzenesulfonimide
[^{18}F]Selectfluor	1-Chloromethyl-4-[^{18}F]fluoro-1,4-diazoniabicyclo[2.2.2]octane
bis-triflate	bis(triflate)
[^{18}F]SFB	Succinimidyl 4-[^{18}F]fluorobenzoate
[^{123}I]	Enriched in iodine-123
[^{124}I]	Enriched in iodine-124
[^{125}I]	Enriched in iodine-125
[^{131}I]	Enriched in iodine-131
[^{123}I]IMPY	(6-[^{123}I]iodo-2-(4'-dimethylamino-)phenyl-imidazo[1,2-a]pyridine)
[^{123}I]IPEB	3-[^{123}I]Iodo-5-[(pyridinyl-3-yl)ethynyl]benzonitrile
[^{123}I]MIBG	(3-[^{123}I]Iodobenzyl)guanidine
[^{123}I]SIB	Succinimidyl 4-[^{123}I]iodobenzoate
Å	Angstrom
APE	Apurinic/apyrimidinic endonuclease
Boc	*Tert*-Butoxycarbonyl
Bq	Becquerel
BrettPhos	2-(Dicyclohexylphosphino)3,6-dimethoxy-2',4',6'-triisopropyl-1,1'-biphenyl
BRCA	Breast cancer 1
Bu	Butyl
Ci	Curie
COD	1,5-cyclooctadiene
CuAAC	Copper catalysed azide alkyne cycloaddition
dba	dibenzylideneacetone
d.c.	decay corrected
DCE	1,2-dichloroethane
DCM	Dichloromethane
DMA	Dimethylacetamide
DMF	Dimethylformamide
DMI	1,3-Dimethyl-2-imidazolidinone
DMSO	Dimethyl sulfoxide
DNA	Deoxyribonucleic acid
DNA-PK	DNA-dependent protein kinase
dppf	1,1'-Bis(diphenylphosphino)ferrocene
dtbpy	4,4'-Di-*tert*-butyl-2,2'-dipyridyl
EF5	2-(2-Nitro-1H-imidazol-1-yl)-N-(2,2,3,3,3-pentafluoropropyl) acetamide
ESI	Electrospray ionisation
Et_2O	Diethyl ether
equiv.	Equivalents

G	Giga
g	Grams
HBA	Hydrogen bond acceptor
HBD	Hydrogen bond donor
HBTU	(2-(1*H*-benzotriazol-1-yl)-1,1,3,3-tetramethyluronium hexafluorophosphate
HCl	Hydrochloric acid
HI	Hydroiodic acid
HLB	Hydrophobic-Lipophilic Balanced
HR	Homologous recombination
HRMS	High resolution mass spectrometry
Hz	Hertz
^{i}AmONO	Isopentyl nitrite
IEDDA	Inverse electron demand Diels Alder
impy	Imidazo[1,2-*b*]pyridazine
^{i}Pr	*Iso*-propyl
^{i}PrNEt$_2$	*N,N'*-Diisopropylethylamine
k	Kilo
K_{222}/Kryptofix$_{222}$	Kryptofix®
LIG1	Ligase 1
LIG3	Ligase 3
L-SeMeT	L-Selenomethionine
M	Mega
m	Milli
m	Multiplet
MA	Molar activity
MAX	Mixed mode anion exchange
MCX	Mixed mode cation exchange
MeOH	Methanol
mol	Moles
MTBE	Methyl-*tert*-butyl ether
MW	Molecular weight
NaDT	Sdoium decatungstate
NBS	*N*-Bromosuccinimide
^{n}BuLi	*n*-ButylLithium
NCS	*N*-Chlorosuccinimide
nep	Neopentyl glycol
NEt$_3$	Triethylamine
NFSI	*N*-Fluorobenzenesulfonamide
NHEJ	Non-homologous end joining
NIS	*N*-Iodosuccinimide
NMP	*N*-methyl-2-pyrrolidone
NTF	Triflamide
o	*Ortho*
OAc	Acetate
OTf	Triflate
OTs	Tosylate
p	*Para*
PARP	Poly (ADP-ribose) polymerase
PARPi	Poly (ADP-ribose) polymerase inhibitor
PDAC	Pancreatic adenocarcinoma cell

PDFA	Difluoromethylene phosphobetaine
PET	Positron emission tomography
pin	Pinacol
Ph	Phenyl
pK_a	Acid dissociation constant
PSMA	Prostate specific membrane antigen
Pol β	DNA polymerase beta
Prep	Preparative
py	Pyridine
RCC	Radiochemical conversion
RCP	Radiochemical purity
RCY	Radiochemical yield
SA	Specific activity
salen	*N,N'*-Ethylenebis(salicylimine)
SEM	2-(trimethylsilyl)ethoxy methyl
SOMIL	Siemens Oxford Molecular Imaging Laboratory
SPAAC	Strain promoted azide alkyne cycloaddition
SPECT	Single photon emission computed tomography
t	Triplet
t	*Tert*
TBAF	*Tetra*-n-butyl ammonium fluoride
TCEP	Tris(2-carboxyethyl)phosphine
TFA	Trifluoroacetic acid
THF	Tetrahydrofuran
TLC	Thin-Layer Chromatography
TMEDA	*N,N,N',N'*-tetramethylethylenediamine
TREAT.HF	Triethylamine trihydrofluoride
Tris	Tris(hydroxymethyl)aminomethane
TSPO	Translocator protein
μ	Micro
UV	Ultraviolet
WAX	Weak anion exchange
WCX	Weak cation exchange
XLF	Non-homologous end joining factor 1

Table of Contents

Chapter I: Application of Fluorine-18 in Positron Emission Tomography

1.1 Positron Emission Tomography:

Positron emission tomography (PET) is a powerful, non-invasive imaging technique typically used for clinical diagnosis and treatment analysis,[1] as well as for drug discovery and development.[2] Furthermore, PET imaging may provide information on human physiology, metabolic status and molecular level events that cannot be generated by structural imaging techniques, such as X-ray or ultrasound. Finally, the use of PET imaging in conjugation with structural imaging techniques such as X-ray computed tomography (X-ray CT) or magnetic resonance imaging (MRI),[3,4] is seen as particularly valuable due to the information provided on both physiological and anatomical events which cannot be generated using either method alone.

Radionuclide	Production	Half-Life ($t_{1/2}$, min)	Decay Process	Decay Product	Maximum β^+ Energy (keV)	Range (mm (in H_2O))[5]
Carbon-11	$^{14}N(p,\alpha)^{11}C$	20.4	99.8% β^+	^{11}B	960	4.1
Nitrogen-13	$^{16}O(p,\alpha)^{13}N$	9.97	100% β^+	^{13}C	1190	5.4
Oxygen-15	$^{15}N(d,n)^{15}O$	2.04	99.9% β^+	^{15}N	1720	8.2
Fluorine-18	$^{18}O(p,n)^{18}F$[a]	109.8	97% β^+	^{18}O	635	2.4

Table 1.1. List of common PET radionuclides [a]Production of [^{18}F]fluoride: See section 1.4.3 for other production methods and sources

PET utilises positron-emitting radioisotopes as direct labels on tracer compounds. The radioisotopes that are most commonly used for PET tracers are short-lived and decay almost exclusively by positron emission (β^+). Carbon-11, nitrogen-13, oxygen-15 and fluorine-18 (Table 1.1) represent some of the most common PET radionuclides, which may be used to replace their stable counterparts (carbon-12, nitrogen-14, oxygen-16 and fluorine-19).[5] This differentiates from other

techniques in which a radiolabelled prosthetic group containing a positron emitting radionuclide is used which may otherwise impact upon the biological properties of the radiotracer in question.

The radioisotopes used for PET are produced in cyclotrons; compact particle accelerators capable of producing proton and deuteron beams *via* bombardment of a specific target. Due to the short half-lives ($t_{1/2}$) of these isotopes, the preparation of tracers typically involves the radioisotope being attached in the final steps of the synthesis. Ideally, this will be undertaken at the same location as both the isotope production and final use of the tracer. Fluorine-18, with its relatively long half-life, enables greater flexibility compared to other radionuclides (Table 1.1). As a rough guide, three isotope 'half-lives' is used for the maximum time between end-of-bombardment (EoB) to injection.[5] Taken, together, this presents scientists with a complex challenge when developing late stage ^{18}F-fluorination techniques for the radiolabelling sensitive (bio)molecules.

During the imaging process, the positron emitted throughout the decay process is not detected directly but undergoes annihilation with an electron within the surrounding material, producing two gamma (γ) rays emitted at 180 °C (Figure 1.1). A ring of highly sensitive detectors picks up these coincidental γ-rays, initially converting them into light and then electrical impulses using a photo-multiplier thus allowing for 2D or 3D images to be generated. The distance travelled by the positron before annihilation, is controlled by the energy of emission, and thus dictates the resolution of the image. The shorter the range, the closer the annihilation is to the actual decay site and therefore the higher the resolution of the final image. Of those isotopes used in PET, fluorine-18 has the lowest emission energy (511 keV) and

therefore has the lowest range (2.4 mm in water), resulting in the highest resolution images.[5]

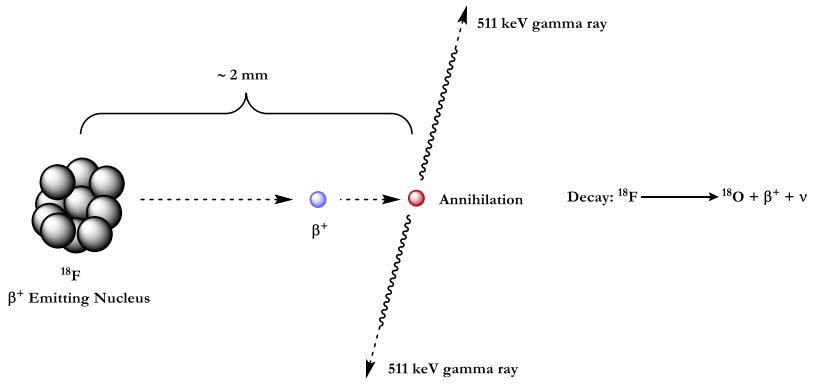

Figure 1.1. Decay of positron emitting radionuclide

Because of its high sensitivity, typically only sub-nanomolar quantities of the tracer in question is required to generate enough annihilation events to produce a suitable image. This means that the *in vivo* system remains unperturbed upon the introduction of the tracer, allowing for accurate information to be gathered.[6] Additionally, highly potent or toxic compounds can be investigated at sub-pharmacological or sub-toxicological doses.[2] These advantages are reflected in the wide range of medical disciplines that PET is utilised in, including oncology for the detection and monitoring of tumours, in cardiology for the imaging of myocardial perfusion, and in neurology for the early detection and monitoring of debilitating disorders such as Alzheimer's and Parkinson's disease. PET may also be used to monitor long term physiological and biochemical changes which may otherwise alter the distribution and concentration of the tracer over time, thus yielding important clinical information.

1.2 Application of Fluorine-19 Bioactive Molecules

Whilst fluorine-19 is the most common halogen found in the Earth's crust,[7] it's rarity within natural products is notable.[8] Nonetheless, the incorporation of fluorine has found a pivotal role in both pharmaceutical and agrochemical industries with 20% – 25% of approved drugs containing at least one fluorine atom (Figure 1.2).[9] This can be pin-pointed to the unique properties of fluorine and the subsequent influences it can exert on a target molecule.

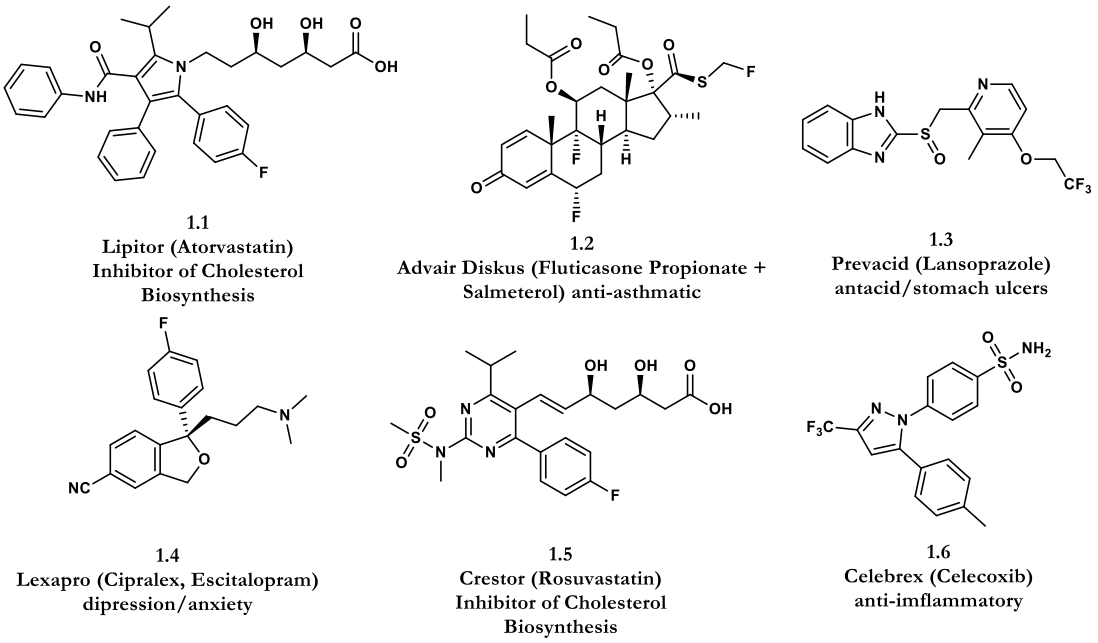

Figure 1.2. Examples of top selling fluorine containing pharmaceuticals[10,11,12]

The first of these properties is that of fluorine's size (Table 1.2). Due to its minimal size, fluorine can be used in place of a hydrogen atom or hydroxyl group without any considerable impact on the molecular structure in solution.[13] The second is the high electronegativity of fluorine; indeed, it is the most electronegative element (3.98).[14] This electronegativity leads to highly polarised C-F bonds, which can significantly influence the acidity or basicity of the proximal functional groups.[11]

Typically, with increased fluoride incorporation, acids are made more acidic whilst the basicity of bases is decreased (pK_a).[15] This influence can aid in tuning binding affinity to specific sites as well as influencing the pharmacokinetic properties of pharmaceutical molecules.[16]

In the presence of fluorine, the lipophilicity of drug molecules can also be modulated. In the case of aromatic fluorination, the incorporation of fluorine will increase the lipophilicity of the molecule through the adjacent π-bonds. However, the inclusion of fluorine to saturated alkyl chains, can decrease the lipophilicity due to fluorine's strong electron withdrawing capabilities. Fluorine is also utilised as a way of increasing the metabolic stability of molecules, owing to the high dissociation energy of the C-F bond compared to the C-H bond (Table 1.2),[17] the increased binding affinity by means of structural conformation as well as direct site contact or indirect contact mediated by water molecules.[18]

X	Van der Waal's Radius (Å)	Bond Length C-X (Å)	Bond Dissociation Energy C-X ($kJmol^{-1}$)
H	1.20	1.09	431
O	1.40 – 1.52	1.43	377*, 431**
F	1.35 – 1.47	1.35 – 1.41	452*, 485**

Table 1.2. Comparison of Influences between H, O and F Substitution *$C(sp^3)$-X bond dissociation energy **$C(sp^2)$-X bond dissociation energy

1.3 Application of Fluorine-18 in Bioactive Molecules

Three avenues are available when utilising PET imaging in drug discovery. The first being the radiolabelling of drug candidates and analysis *in vivo* for simple biodistribution. The second being the use of occupancy studies to determine the displacement of known radioligands upon administration of new candidates. Finally, PET allows for the monitoring of the pharmacological response to novel drug

candidates, by tracking with known tracers such as 2-[^{18}F]fluoro-2-deoxy-D-glucose **[^{18}F]1.7** ([^{18}F]FDG) (Figure 1.3).[2,19]

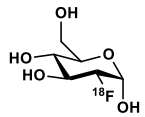

[^{18}F]1.7
[^{18}F]FDG

Figure 1.3. 2-[^{18}F]Fluoro-2-D-glucose ([^{18}F]FDG)

As PET imaging only requires the administration of small quantities of the drug, these levels fall below toxicity levels. This allows for studies in rodent, non-human, primate and human subjects prior to phase 1 clinical trials.[20,21] This permits for information of the pharmacodynamics and pharmacokinetic properties of a compound to be established to a higher degree than that gained by *in vitro* analysis alone. Consequently, the use of PET to screen potential drug candidates can aid in eliminating poor candidates prior to expensive and/or long clinical trials, therefore saving both time and money.[22,23]

1.4 ^{18}F-Fluorination

The stoichiometry of fluorine-18 in reactions, for both research and radiosynthesis of PET tracers, typically falls in the pico- to nanomolar range, well below that of traditional fluorine-19 chemistry.[5] Due to the vast stoichiometric excesses of precursors and other reagents, resulting in pseudo-first order kinetics with respect to the radioisotope concentration, reactions that previously took hours or days to reach completion, can now be completed in minutes.

Nonetheless, the low amounts of fluorine-18 present in these reactions leads to significant challenges and drawbacks. The main problem being that it is highly challenging to translate 'cold' chemistry into the 'hot' radio-lab. This problem is

amplified when metal catalysts are used, where minor impurities in reagents or solvents previously ineffectual, are now substantial.

1.4.1 Fluorine-18: Concepts and Considerations

There are two primary sources of fluorine-18 for radiofluorination; nucleophilic [^{18}F]fluoride and [^{18}F]F_2.[24] As highlighted earlier, the most desirable option is for the ^{18}F-fluorination step to occur as late as possible, although post-fluorination reactions are feasible due to the relatively long half-life of fluorine-18.

Of the two sources, nucleophilic [^{18}F]fluoride is favoured due to its greater selectivity, ease of which it can be handled and the capability this reagent has in affording tracers with high molar activity (MA). In comparison, [^{18}F]F_2, being highly reactive often suffers from poor selectivity whilst the relatively few facilities that are equipped to handle [^{18}F]F_2 limits its geographical impact.[24]

Of those factors highlighted, MA of the final product is an important consideration for radiosynthesis. Defined as the measure of activity per unit mass of the labelled compound, it is commonly quoted as giga-becquerel per micromole (GBq μmol^{-1}) and is a measure of the activity over the total amount of the compound present, including that bearing fluorine-19. Presence of the ^{19}F-analogue is unavoidable due to its presence in the reaction, be it deliberate or unintentional. Sources of fluorine-19 stem from absorption, isotopic exchange or trace quantities in reagents and solvents used. Whilst this means that the theoretical maximum MA can never be achieved, it can be maximised by the application of non-carrier added procedures. Whilst the use of a carrier can be useful to direct the reaction pathway, or is simply unavoidable as in the case of [^{18}F]F_2, these reactions lead to much lower MA due to the increased quantities of the ^{19}F-analogue formed.

Radiochemical reaction efficiency can be measured by radiochemical conversion (RCC), radiochemical yield (RCY) or as an activity yield (AY). RCC, typically measured by the combination of radio-TLC and radio-HPLC, is a measure of radio-fluorinated product against remaining ^{18}F-reagent and is inherently, decay corrected (d.c). RCY is the collected product expressed as the percentage of related starting activity utilised in the process (e.g. synthesis, separation, etc.). RCY can be decay corrected to time at start of synthesis, which negates total synthesis time, or non-decay corrected (n.d.c.), which accounts for synthesis time. The "activity yield" is the amount of radioactive product expressed in Bq, MBq, GBq etc, which is obtained from a starting amount of activity (e.g. produced at a cyclotron) and is not corrected for decay. This term is useful, or necessary to indicate the efficiency of a labelling procedure. The activity yield is, of course, dependent on the effectiveness and duration of all technical manipulations used, in addition to the yield of the labelling reaction.[25] For this thesis, all RCYs and AYs are listed as non-decay corrected unless stated otherwise.

1.4.2 Fluorine-18: Production and Derivatisation

The type of fluorine-18 desired dictates the cyclotron target and method of bombardment, as shown in Table 1.3. [^{18}F]Fluoride is produced by proton bombardment of ^{18}O-enriched water, under the ^{18}O(p,n)^{18}F nuclear reaction, and is delivered from the cyclotron as [^{18}F]fluoride in ^{18}O-enriched water. This method of production affords the highest MA source of fluorine-18, which permits the radiosynthesis of high MA radiotracers. This in turn allows for reduced amounts of tracer compound to be injected for the same amount of activity. For tracers targeting

rare receptor sites, this is vital, as the receptor may become saturated with unlabelled compound, should a lower MA tracer be used.

^{18}F Source	Target	Nuclear Reaction	MA (GBq μmol^{-1})
[^{18}F]F$^-$	[^{18}O]H_2O	^{18}O(p,n)^{18}F	5000
[^{18}F]F_2	Ne + F_2	^{20}Ne(d,α)^{18}F	0.37 – 0.74
[^{18}F]F_2	$^{18}O_2$ + F_2	^{18}O(p,n)^{18}F	1
[^{18}F]F_2[a]	[^{18}O]H_2O	^{18}O(p,n)^{18}F	55

Table 1.3. Production methods for ^{18}F-containing sources [a] 'Post-Target' Method[26]

As the [^{18}F]fluoride is delivered as an aqueous solution, this results in a species that is highly solvated and weakly nucleophilic; a poor reagent for radiofluorination. Consequently, it requires separation from the ^{18}O-enriched water and activation prior to its use. This is typically achieved with an anion exchange cartridge (QMA) to trap the [^{18}F]fluoride, which can then be eluted with a basic solution containing an appropriate cation. This is most frequently accomplished by use of potassium carbonate in a mixture of acetonitrile and water prior to further additions of anhydrous acetonitrile for azeotropic drying. A cryptand, usually Kryptofix 2.2.2 (K_{222}), is included in the elution solution to aid in the re-solvation of the [^{18}F]KF in the reaction solvent as [^{18}F]KF/K_{222}. Other commonly used cations include tetraalkylammonium ions (tetraethylammonium and tetrabutylammonium) from their bicarbonate salt, which do not require the use of cryptands.

Electrophilic fluorine-18, as [^{18}F]F_2, can be produced directly by two nuclear reactions; irradiation of a Ne/F_2 gas mixture with deuterium (^{20}Ne(d,α)^{18}F) or irradiation of [^{18}O]O_2 gas with protons (^{18}O(p,n)^{18}F) in an analogous manner to the production of [^{18}F]fluoride. The former of these two procedures is rarely used as it is

low yielding and affords [^{18}F]F_2 in very low MA due to the high amount of F_2 used as a carrier.[27] This is exemplified by the 1/2-hour bombardment with 8 – 9 MeV deuterons results in < 37 MBq when [^{18}F]F_2 with a MA of 0.37 – 0.74 GBq/μmol.[28] The latter procedure is used more frequently. After the initial bombardment allowing the formation of the excited ^{18}F* atoms, the F_2 carrier gas (~ 0.1% in Ne or Kr is introduced followed by a second irradiation of the target that incites the isotopic exchange process to form the [^{18}F]F_2 gas. In this method, a lower amount of carrier is required resulting in higher MA, albeit limited to ~1 GBq μmol^{-1}.[29]

An alternative, indirect, route has been reported by Bergman and Solin. Using [^{18}F]fluoride, produced by the ^{18}O(p,n)^{18}F nuclear reaction, which is azeotropically dried and reacted with methyl iodide to form [^{18}F]CH_3F. Upon purification by gas chromatography, transfer to an electrical discharge chamber with a small amount of carrier F_2 gas is carried out. The electrical discharge results in atomisation and ^{18}F/^{19}F isotopic exchange to form [^{18}F]F_2 with a MA up to 55 GBq μmol^{-1}.[26]

Whilst [^{18}F]F_2 allowed for the labelling of electron rich substrates, the high reactivity of the reagent often led to poor selectivity and undesired side reactions.[30] To overcome this, scientists have been able to manipulate the reactivity of [^{18}F]F_2 gas by the synthesis of more tempered ^{18}F-containing reagents. Gouverneur and Solin reported the synthesis of the *N*-fluoro containing reagents: [^{18}F]Selectfluor **[^{18}F]1.13** bis(triflate) and [^{18}F]NFSI **[^{18}F]1.12** from [^{18}F]F_2.[31,32] Other [^{18}F]N-F reagents include [^{18}F]*N*-fluoropyridinium triflate **[^{18}F]1.9**, 1-[^{18}F]fluoro-2-pyridone **[^{18}F]1.10** along with various *N*-fluoro-*N*-alkylsulfonamides **[^{18}F]1.11**.[33] Other electrophilic fluorination reagent derived from [^{18}F]F_2 include [^{18}F]AcOF **[^{18}F]1.14**, [^{18}F]CF_3OF

[^{18}F]1.15 and [^{18}F]$FClO_3$ although the handling of these highly reactive [^{18}F]O-F reagents has limited uptake and application.[34] Finally, the electrophilic fluorination reagent [^{18}F]XeF_2 **[^{18}F]1.8** can be accessed directly by the reaction of Xe with [^{18}F]F_2 gas in a nickel reactor.[35] Alternatively, [^{18}F]XeF_2 can be accessed *via* isotopic exchange with [^{18}F]fluoride,[36] as reported by Pike and co-workers in 2001 and later in 2010 under microfluidics (Figure 1.4).[37]

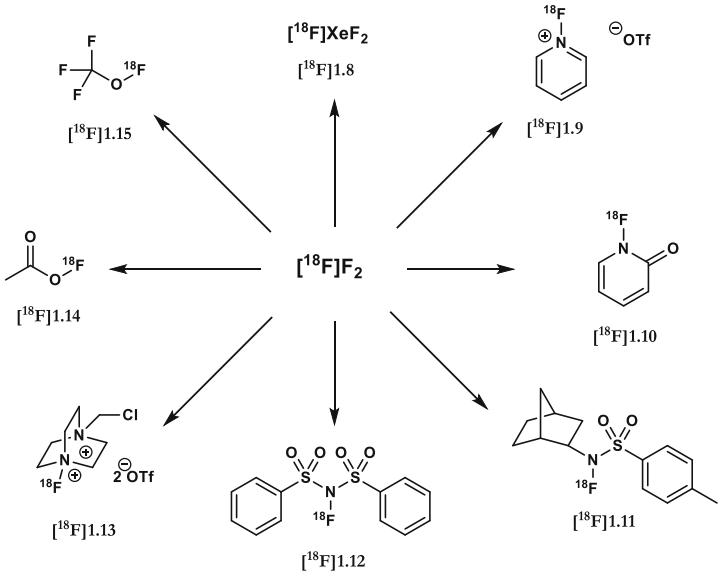

Figure 1.4. Examples of electrophilic ^{18}F-fluorination reagents derived from [^{18}F]F_2

1.5 Application of Fluorine-18

The following sections discuss the application of nucleophilic and electrophilic ^{18}F-fluorination reagents. This will be discussed in the context of the ^{18}F-fluorination of small molecules. For further information on the developments in the field of radiolabelled biomolecules, see **Chapter III**.

1.6 Electrophilic ^{18}F-Fluorination

Electrophilic ^{18}F-fluorination with $[^{18}F]F_2$ has been shown to facilitate ^{18}F-incorporation into systems that are difficult to access by nucleophilic routes. Whilst the highly reactive nature of $[^{18}F]F_2$ is prohibitive to selective ^{18}F-fluorination of aliphatic compounds, $[^{18}F]F_2$ has been used for the preparation of several imaging agents. An example of this being the direct addition of $[^{18}F]F_2$ across a per-fluorinated olefin to access [^{18}F]EF5 **[^{18}F]1.17**, an imaging agent for hypoxia (Scheme 1.1).[38]

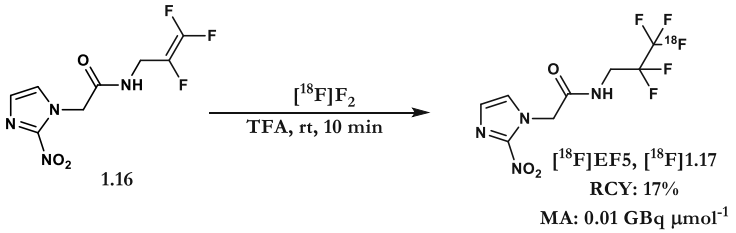

Scheme 1.1. Electrophilic ^{18}F-fluorination toward [^{18}F]EF5

The direct electrophilic fluorination of (hetero)arenes with $[^{18}F]F_2$ often yields complex mixtures due to the potent oxidizing strength of fluorine. Nevertheless, $[^{18}F]F_2$ has been used for the radiosynthesis of radiotracers such as [^{18}F]FDOPA **[^{18}F]1.21**, by tempering $[^{18}F]F_2$ and its reactivity with low temperatures and by dilution in neon gas. Chirakal and co-workers reported that 0.5% $[^{18}F]F_2$ in neon gas reacts directly with L-DOPA in a solution of HF at –65 °C to produce a mixture of 2- (**[^{18}F]1.19**), 5- (**[^{18}F]1.20**), and [^{18}F]FDOPA **[^{18}F]1.21**.[39] In that instance, the solvent and Lewis acid additives were found to have a profound effect of RCYs and product distributions.[40] The direct electrophilic radiofluorination of L-DOPA can also be accomplished with milder electrophilic fluorinating reagents such as $[^{18}F]XeF_2$ and [^{18}F]AcOF (Scheme 1.2).[41,42] More recently, the groups of Gouverneur and Solin

reported the use of [^{18}F]Selectfluor bis(triflate) for the silver mediated ^{18}F-fluorination of aryl boronic ester **1.22** (Scheme 1.3).[31]

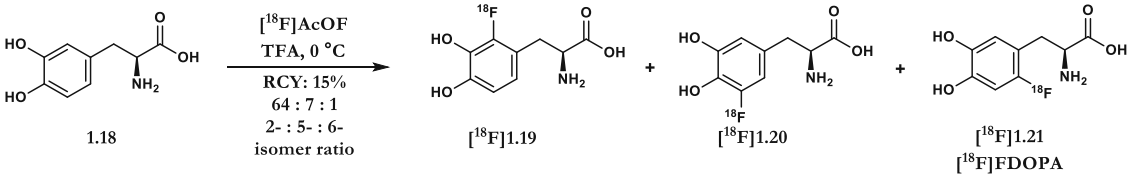

Scheme 1.2. Electrophilic ^{18}F-fluorination towards [^{18}F]FDOPA with [^{18}F]AcOF

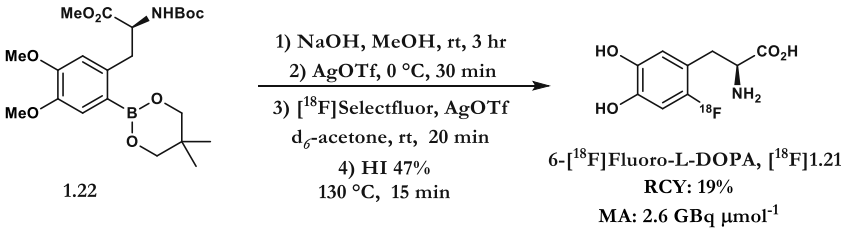

Scheme 1.3. Electrophilic ^{18}F-fluorination methods toward [^{18}F]FDOPA with [^{18}F]Selectfluor *bis*(triflate)

Reagents derived from [^{18}F]F_2 have found supplementary use in recent years. Gouverneur and co-workers established the importance of [^{18}F]NFSI **[^{18}F]1.12** with the first examples of an organo-mediated asymmetric ^{18}F-fluorination to give enantioenriched α-[^{18}F]fluoro-aldehydes (*ee* > 90%).[43] This transformation was exemplified with the radiosynthesis of (2*S*,4*S*)-4-[^{18}F]fluoroglutamic acid **[^{18}F]1.27** (Scheme 1.4) which has shown potential for imaging lung and breast tumours or as an alternative to [^{18}F]FDG **[^{18}F]1.7** in [^{18}F]FDG negative tumours.

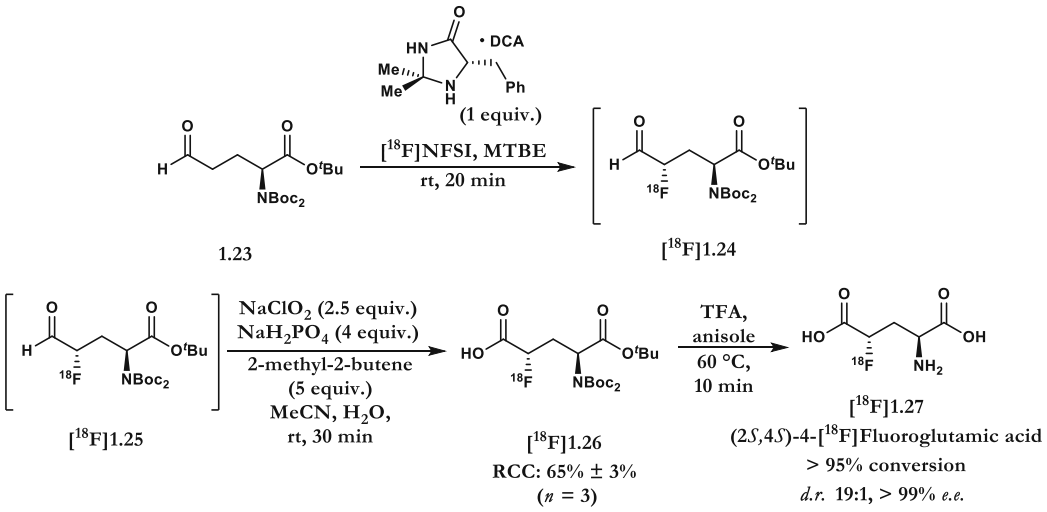

Scheme 1.4. Organo-mediated ^{18}F-fluorination with [^{18}F]NFSI

Despite these innovative works, the use of [^{18}F]F_2 is becoming less common, especially so with the advent of new nucleophilic radiofluorination methods. This reasoning is concentrated around four areas. The first being the limited number of facilities equipped to handle [^{18}F]F_2. The second being the low selectivity, due to the high reactivity of [^{18}F]F_2, which results in multiple ^{18}F-products requiring longer purification methods. Third, the radiochemical yield is inherently limited to 50% and finally, the low MA of the final product due to the use of F_2 as a carrier.[24]

1.7 Metal Free Nucleophilic ^{18}F-Fluorination

1.7.1 Aliphatic ^{18}F-Fluorination

Thermally induced S_N2 mechanisms are most commonly applied to the radiofluorination of aliphatic and aromatic motifs respectively. In both instances, precursors are designed with the appropriate leaving groups. In the case of aliphatic ^{18}F-fluorination, this includes sulfonates (tosyl, trifyl, mestyl, nosyl) and halides (I, Br).[24]

[^{18}F]FDG **[^{18}F]1.7**, is the most widely used tracer for clinical PET imaging. This radio-fluorinated analogue of glucose is typically labelled by the substitution of a mannose triflate or tosylate precursor, and allows for the tracking of increased metabolism in cells and, as such, is used in oncology for the diagnosis and disease mapping due to the up-regulation of aerobic glycolysis in cancerous cells (Scheme 1.5).[44]

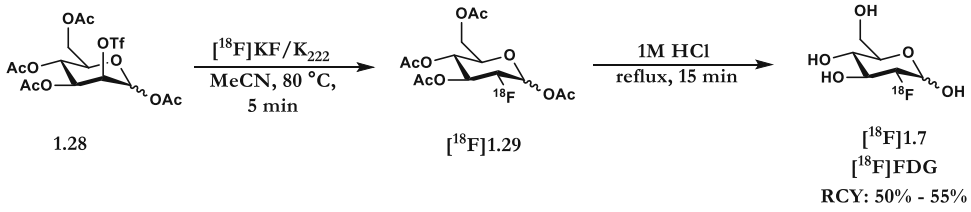

Scheme 1.5. Synthesis of [^{18}F]FDG **[^{18}F]1.7**

1.7.2 Aromatic ^{18}F-Fluorination

Nucleophilic aromatic substitution (S_NAr) serves as the most common method for the radiofluorination of (hetero)aromatics. This is primarily due to the ease at which the precursors can be prepared and the ability for this protocol to facilitate good [^{18}F]fluoride incorporation (Scheme 1.6). Along with some of those leaving groups described for aliphatic ^{18}F-fluorination, trimethylammonium salts and nitro-based precursors are also used, with the reaction typically undertaken at high temperature and in polar aprotic solvents such as DMF or DMSO.[24] Nevertheless, this approach is limited to suitably activated precursors, bearing electron withdrawing groups situated *ortho* or *para* to the leaving group in question.

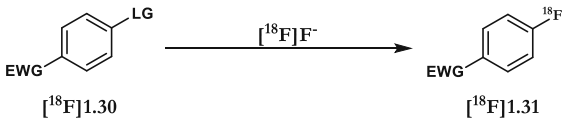

[18F]1.30 [18F]1.31

EWG = Electron withdrawing group (NO_2, CN, CHO etc.)
LG = Leaving group (NO_2, halo, triflate, mesylate, tetraalkylammonium)

Scheme 1.6. General overview of S_NAr ^{18}F-fluorination reactions

Whilst these factors limit the precursor to bearing thermally stable functional groups as well as favourable substitution patterns, scientists continue to invest significantly in this transformation when developing novel ^{18}F-containing tracers. As demonstrated by the radiofluorination of 6-[^{18}F]fluoro-L-dihydroxy-phenylalanine ([^{18}F]FDOPA **[^{18}F]1.21**) by Luxen and Lemaire,[45] in cases where the target compound does not bear the necessary electron deficient ring, rapid and efficient post-fluorination strategies have been devised (Scheme 1.7). Whilst this approach proved highly effective for the radiosynthesis of [^{18}F]FDOPA **[^{18}F]1.21**, the rigorous testing and optimisation of each step is time consuming and has encouraged the development of alternative strategies for late stage nucleophilic ^{18}F-fluorination of aromatics and in particularly, electron rich aromatics.

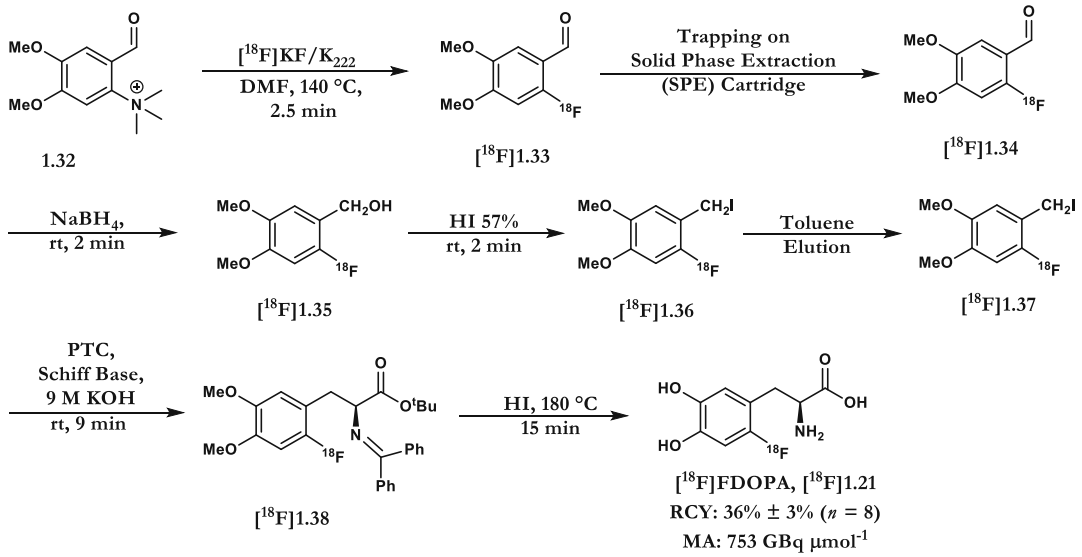

Scheme 1.7. [^{18}F]FDOPA synthesis using a nucleophilic source of fluorine-18

Early works for the ^{18}F-fluorination of electron neutral and electron rich (hetero)aromatics centred on thermally induced fluorodediazonation reactions using aryl diazonium [^{18}F]tetrafluoroborates.[46] Nonetheless, due to competing incorporation of fluorine-19, the maximum theoretical incorporation of 25% in combination with the very low MA meant further optimisation was needed. To this end, Zwernemann and co-workers, reported an improved process with high molar activity for the fluorodediazonation of the diazonium 2,4,6-triisopropylbenzenesulfonate precursor **1.39 + 1.40** (Scheme 1.8).[47] Nonetheless, the limited stability of these precursors has led to negligible uptake within the community.

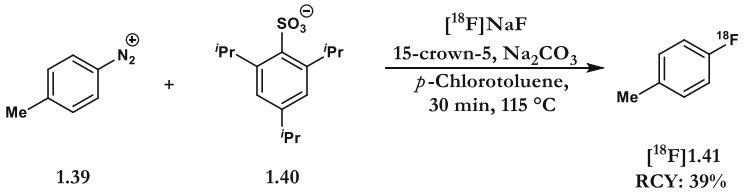

Scheme 1.8. ^{18}F-Fluorodediazonation Reactions

The ^{18}F-fluorination of tri-arylsulfonium salts **1.42**, **1.44** and di-aryl sulfoxides **1.47** has shown to be useful for the labelling of electron neutral and electron deficient arenes (Scheme 1.9A, Scheme 1.9B, Scheme 1.9C).[48,49] However, it is the radiofluorination of diaryliodonium salts that has been one of the most popular novel transformation to ^{18}F-containing arenes. First reported by Pike and Aigbirhio in 1995, the use of diaryliodonium salts has proved effective for the late-stage ^{18}F-fluorination of electron rich, neutral and poor ^{18}F-conatining aromatics (Scheme 1.10).[50,51,52]

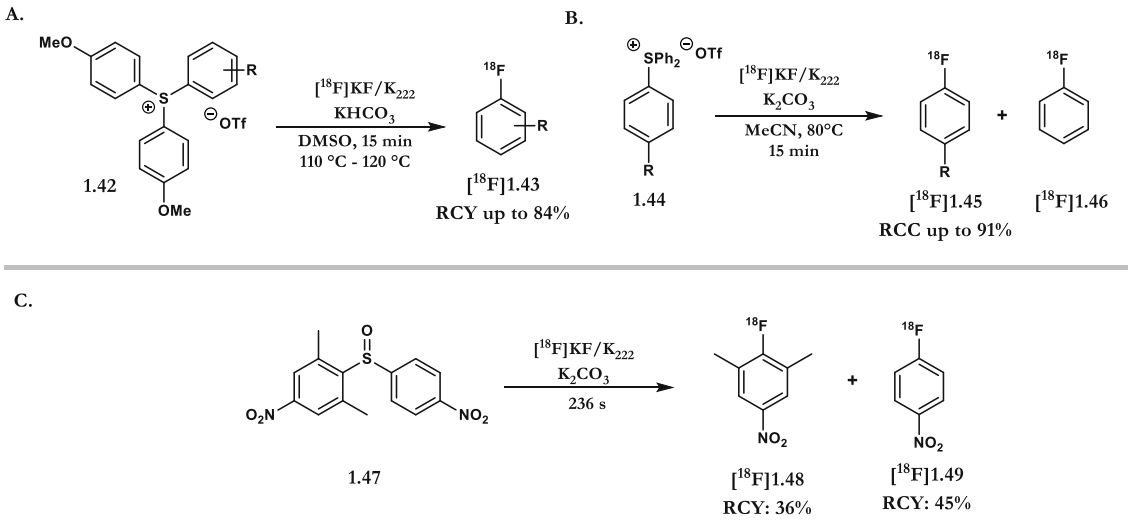

Scheme 1.9. ^{18}F-Fluorination of tri-arylsulfonium salts and diaryl sulfoxides

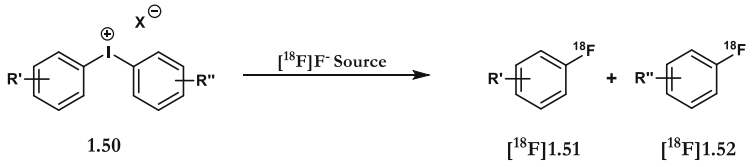

Scheme **1.10.** ^{18}F-Fluorination of diaryliodonium salts

When reacted with [^{18}F]fluoride, [^{18}F]fluoroarene and the corresponding iodoarene are produced. The regioselectivity is dictated primarily by the relative electron density of the two arenes with the radiofluorination favouring the more electron deficient of the two arenes. Nonetheless, there is invariably, a degree of the secondary ^{18}F-arene forming. To minimise this by-product formation, *para*-methoxy substitution is often used to direct the radiofluorination to the other aromatic. More recently, the 2-thienyl has shown to be a promising candidate for regio-specific ^{18}F-lablling, although this is shown to be more likely due to the challenges of identification of the by-product under radiofluorination conditions.[53]

A recent study by Coenen proposed that the counter-ion may also play a significant role in the reactivity of the substrate.[53] Exemplified with a series of (2-methoxyphenyl)(2-thienyl)iodonium salts, it was found that the counter effect on the

RCC of the reaction followed the order of tosylate < iodide < triflate < bromide whilst for the reaction rates it is tosylate < bromides < iodides < triflates. Further to this, he found the substitution at the *ortho* position on one aromatic ring to have a profound effect in shifting the selectivity towards that arene.

This *ortho* effect, is attributed to mechanistic considerations. Starting from a trigonal bipyramidal complex **1.53**, the transition state in which the *ortho* substituent lies in an equatorial position is favoured (Scheme 1.11). Pike and co-workers determined that the capacity of the *ortho* substituent to direct the radiofluorination towards its respective aromatic ring follows 2-methoxy < hydrogen < 2-iso-propyl ≈ 2-ethyl < 2-methyl < 2-bromo < 2,4,6-trimethyl < 2,6-dimethyl.[52] However, the appearance of the 2-methoxy substituent at the lower end of this series suggest that the *ortho* effect is not solely a steric effect.

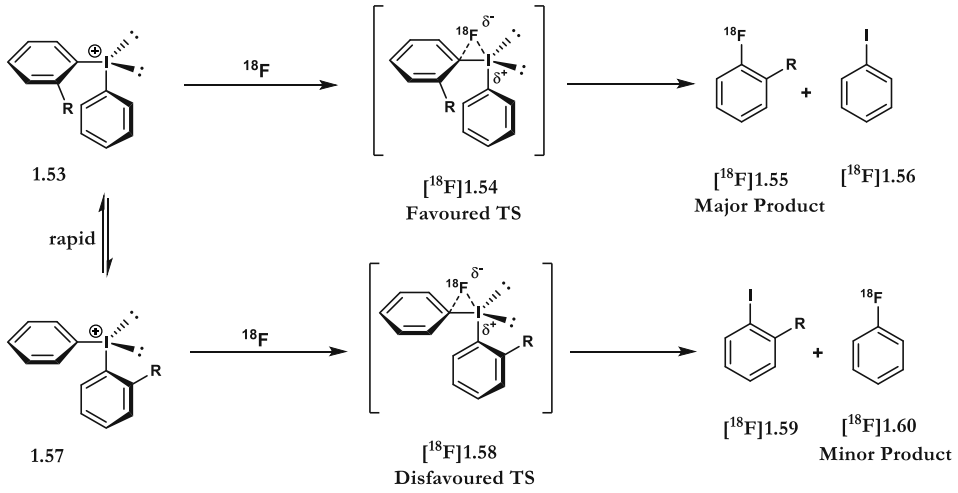

Scheme 1.11. ^{18}F-Fluorination of Diaryliodonium Salts: The *Ortho* Effect

More recently, Vasdev and co-workers expanded the field of hypervalent iodine(III) precursors in radiochemistry by the introduction of iodonium ylides.[54] Using a spirocyclic auxiliary **1.61**, Vasdev reported increased precursor stability and ^{18}F-incorporation during radiofluorination. Applicability of this precursor was

described for a series of substrates bearing electron donating and withdrawing functionalities, including four compounds of interest to the radiopharmaceutical industry (Scheme 1.12A). This transformation was validated as a method for human use via the preparation of [^{18}F]FPEB **[^{18}F]1.64** in a RCY of 20% and a MA of 670 GBq μmol^{-1} (Scheme 1.12B).[55] Finally, in 2016, Vasdev and Liang disclosed mechanistic studies via DFT calculation, in addition to the use of iodonium ylides derived from adamantone **1.65**; a substituent which increased stability and improved RCC's for electron-rich substrates (Scheme 1.12C).[56]

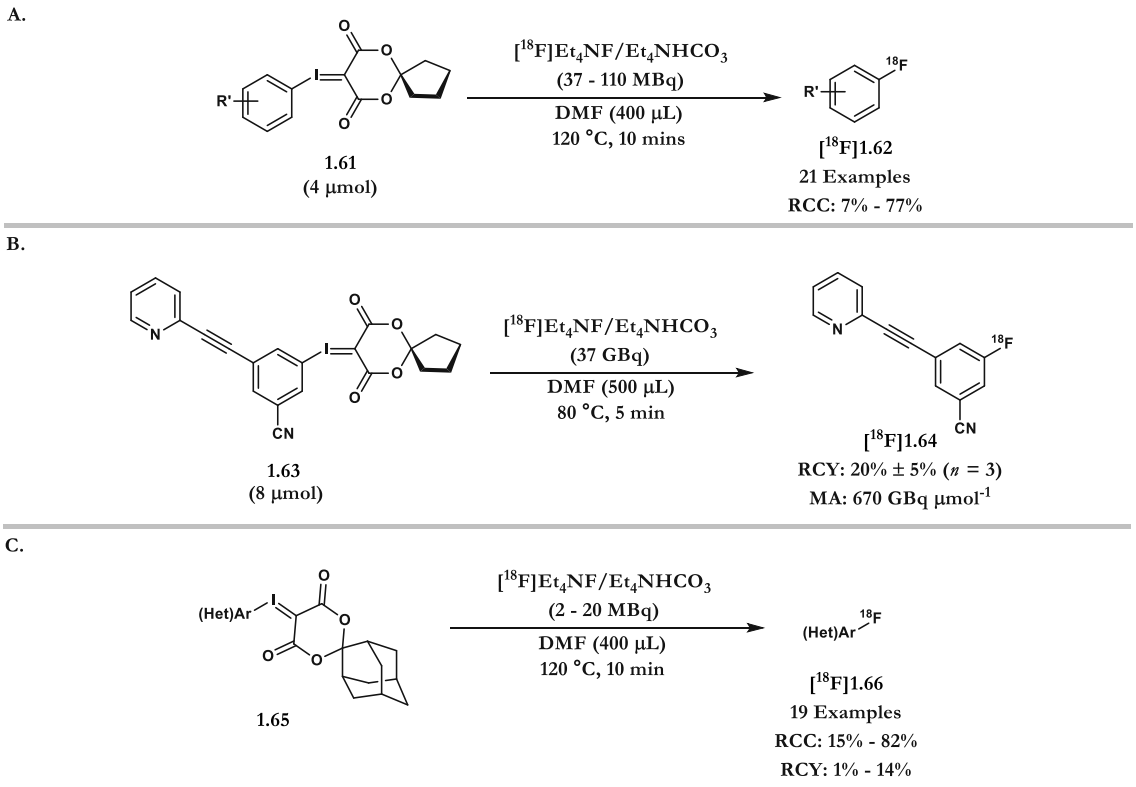

Scheme 1.12. ^{18}F-Fluorination of iodonium ylides

1.7.3 ^{18}F-Fluorination of Other Motifs

The first example of a ^{18}F-trifluoromethylated aryl was achieved *via* isotopic exchange of an α,α,α-trifluorotoluene with [^{18}F]KF/K$_{222}$.[57] Halogen exchange reactions with chloro- **1.67** or bromodifluoromethyl-arene **1.69** precursors in combination with various [^{18}F]fluoride sources have also been described, though harsh conditions are required (Scheme 1.13A). Typically, temperature greater than 150 °C are reported. This in turn has been shown to lead to precursor decomposition and the subsequent release of fluoride leading to very low MA being reported (Scheme 1.13B).[58,59]

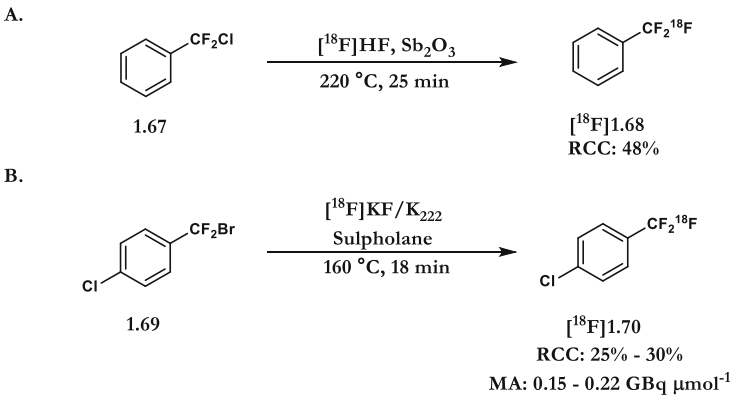

Scheme 1.13. Metal free ^{18}F-fluorination for the preparation of aryl-CF$_2$^{18}F motifs

In 2015, Liang and co-workers, reported the ^{18}F-trifluoromethylthiolation of electrophilic alkyl with *in situ* generated difluorocarbene in the presence of elemental sulfur and [^{18}F]KF/K$_{222}$ (Scheme 1.14).[60] This reaction proceeded under mild reaction conditions and in fast reaction times. Although a relatively broad substrate scope was demonstrated, the low MA of 0.8 GBq μmol^{-1} is a drawback.

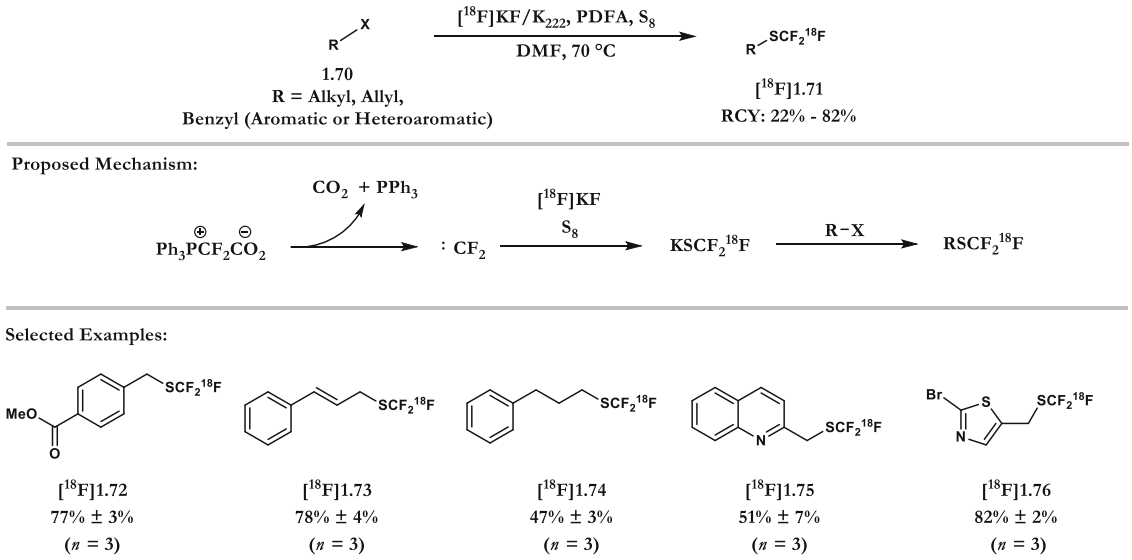

Scheme 1.14. Metal free ^{18}F-fluorination for the preparation of alkyl-$SCF_2{}^{18}F$ motifs

In 2017, Labar and Jubault reported the ^{18}F-trifluoromethylation of symmetrical aryl disulfides or diselenides for the synthesis of the corresponding ^{18}F-trifluoromethylthiolated or ^{18}F-trifluoromethylselenylated arenes **1.77** (Scheme 1.15).[61] Reacting [^{18}F]KF/K_{222} with a bench stable (difluoromethyl)(mesityl)(phenyl) sulfonium salt **1.80**, [^{18}F]fluoroform ([^{18}F]HCF_3) **[^{18}F]1.81** could be isolated under a flow of N_2. [^{18}F]Fluoroform could then be passed directly to a solution of disulphide or diselenide, KO^{t}Bu in DMF to afford the corresponding ^{18}F-trifluoromethylthiolated products.

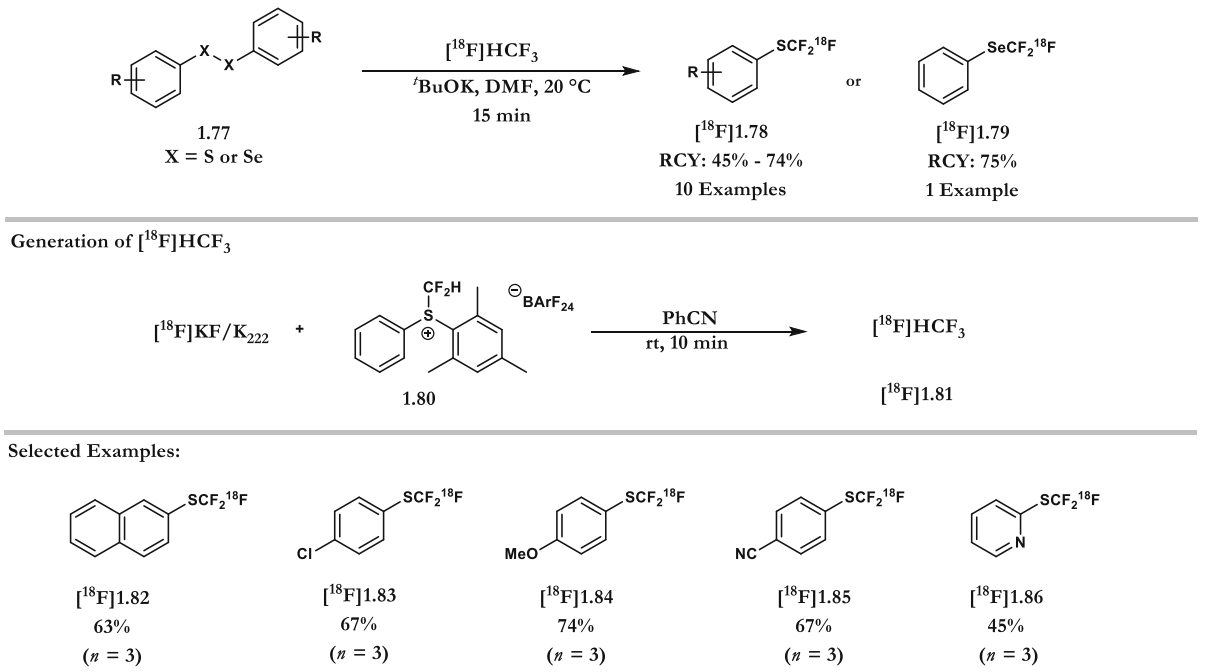

Scheme 1.15. Metal free ^{18}F-fluorination for the preparation of aryl-$SCF_2{}^{18}F$ and aryl-$SeCF_2{}^{18}F$ motifs

1.8 Metal Mediated Nucleophilic ^{18}F-Fluorination:

The use of transition metals and their complexes to mediate radiofluorination processes is becoming increasingly popular throughout the scientific community with a wide range of metals and associated transformations being described. Typically requiring lower temperature compared to their metal free counterparts, this can aid in selectivity and can be a particularly important consideration for sensitive precursors or for the radiosynthesis of enantioenriched tracers.[62]

1.8.1 Aliphatic ^{18}F-Fluorination:

Recently, the Gouverneur group reported two routes for the radiosynthesis of allyl ^{18}F-fluorides using $Pd(dba)_2$ or $[Ir(COD)Cl]_2$. The use of the Pd(0) complex facilitated the radiofluorination of [^{18}F]cinnamyl fluoride in good RCC (9% – 42% (*n* = 12)) at room temperature in only 5 minutes (Scheme 1.16A).[63] Using the Ir(II) complex, excellent ^{18}F-incorporation could be obtained, along with the retention of

stereochemistry (Scheme 1.16B). For both transformations, the use of tetraalkylammonium salts as the source of [^{18}F]fluoride was found to be beneficial over the use of [^{18}F]KF/K_{222}.[64]

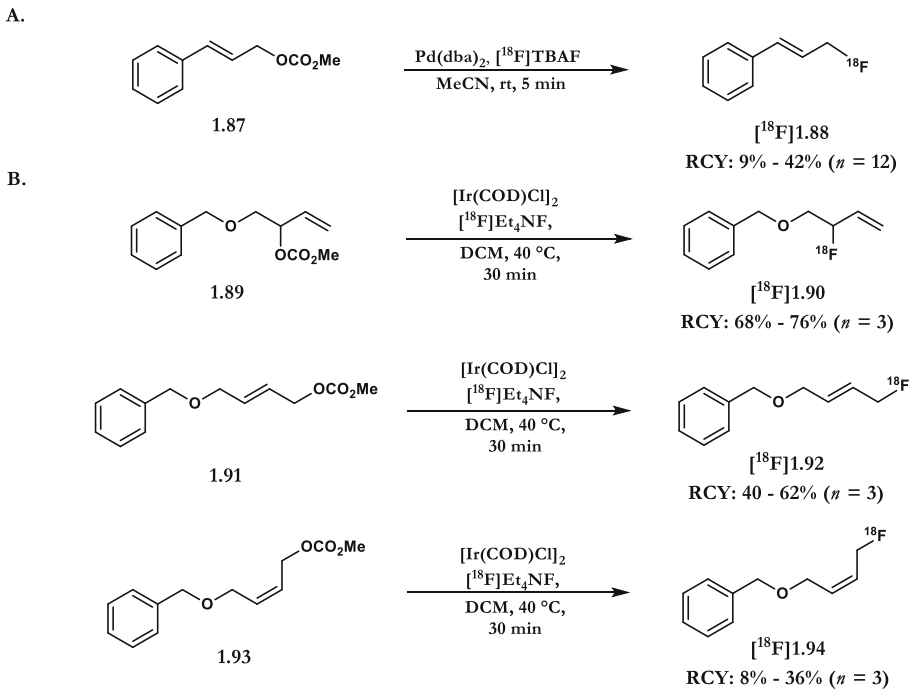

Scheme 1.16. Ir and Pd mediated allylic ^{18}F-fluorination

In 2014, Doyle and co-workers developed an enantioselective ^{18}F-fluorination *via* the Co(II) catalysed ring opening of epoxides (Scheme 1.17).[65] Doyle and Kung, by use of a solution of (*R,R*)-(salen)Co(III)OTs **1.97** to elute the trapped [^{18}F]fluoride, were able to form a (*R,R*)-(salen)Co(III)-^{18}F species. Doyle and Kung were subsequently able to carry out the same epoxide opening reaction with excellent ^{18}F-incorporation and enantioselectivity reported.

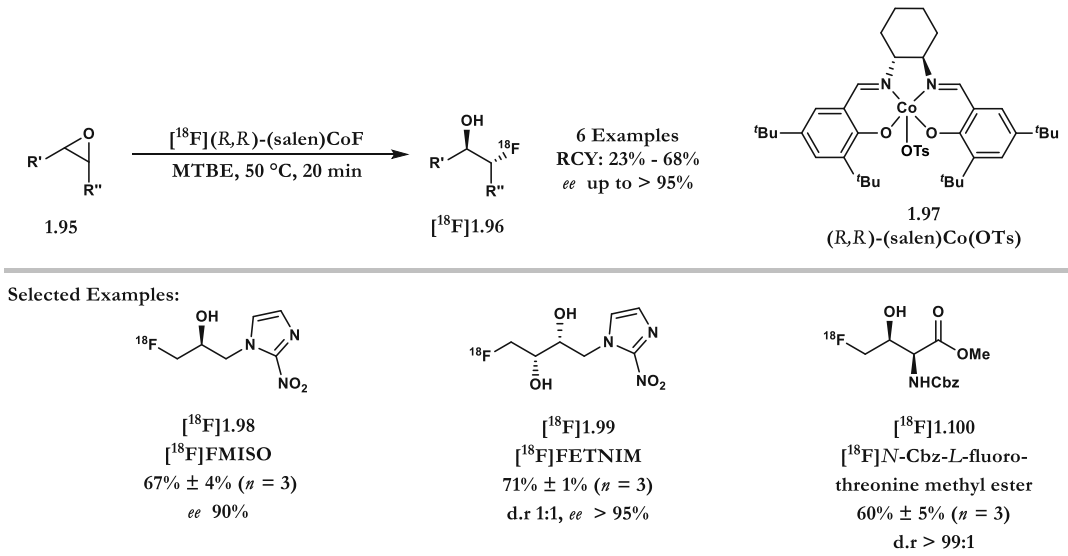

Scheme 1.17. Co(III) mediated ^{18}F-fluorination of epoxides

The need for pre-functionalisation was dispensed with by Groves and Hooker who reported the benzylic C-H ^{18}F-fluorination mediated by a Mn(III) complex, Mn(salen)OTs **1.103** (Scheme 1.18).[66]

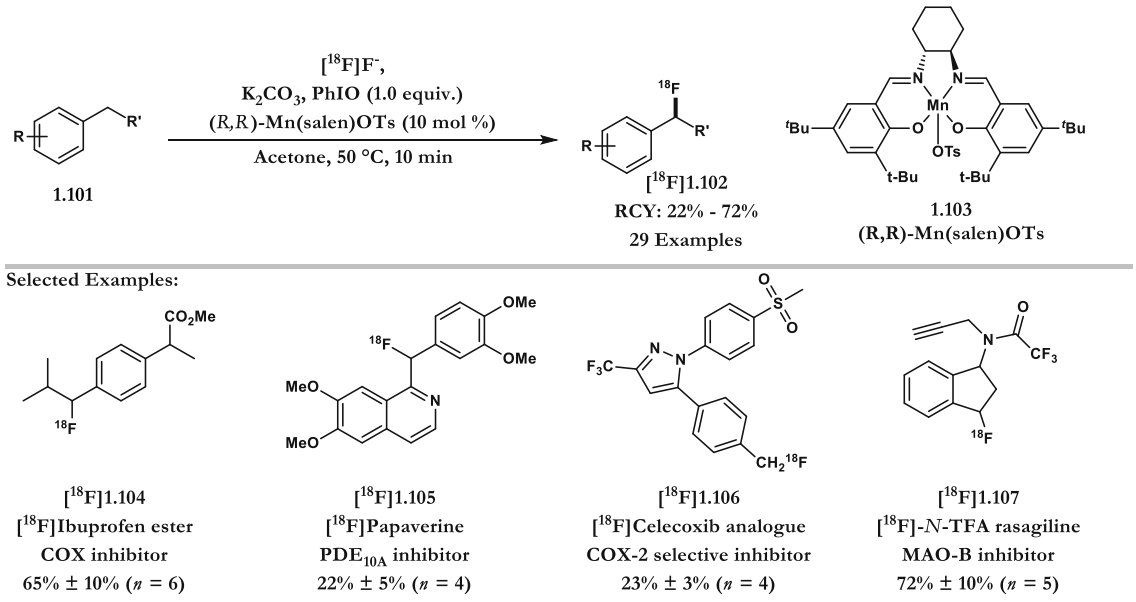

Scheme 1.18. Mn(III) mediated benzylic ^{18}F-fluorination

This procedure demonstrated a wide applicability with the radiolabelling of 20 small molecules and a further nine bioactive molecules. Furthermore, they demonstrated a dry-down free procedure by use of a solution of the Mn(III) complex in acetone to

elute the [^{18}F]fluoride. This technology was also reported by Carroll and co-workers for the synthesis of ^{18}F-trifluoromethyl functionalities.[67]

1.8.2 Aromatic ^{18}F-Fluorination:

In 2013, Sanford and co-workers reported the copper-catalysed ^{19}F-fluorination of (mesityl)(aryl)iodonium salts with KF.[68] The authors proposed that the high selectivity of this reaction was controlled primarily by sterics. With fluorination on the mesitylene ring strongly disfavoured, the alternative aryl fluoride product was formed in at least 19:1 selectivity in most cases. Later that year, Sanford and Scott translated this method to the ^{18}F-labelling of fluoroarenes (Scheme 1.19A) with RCCs ranging from 14% to 79%.[69] Following this work, Neumaier and co-workers demonstrated the capacity to substitute potassium carbonate and 18-crown-6 in favour of the mesityl)(aryl)iodonium salt in methanol for the elution of the [^{18}F]fluoride (Scheme 1.19B).[70]

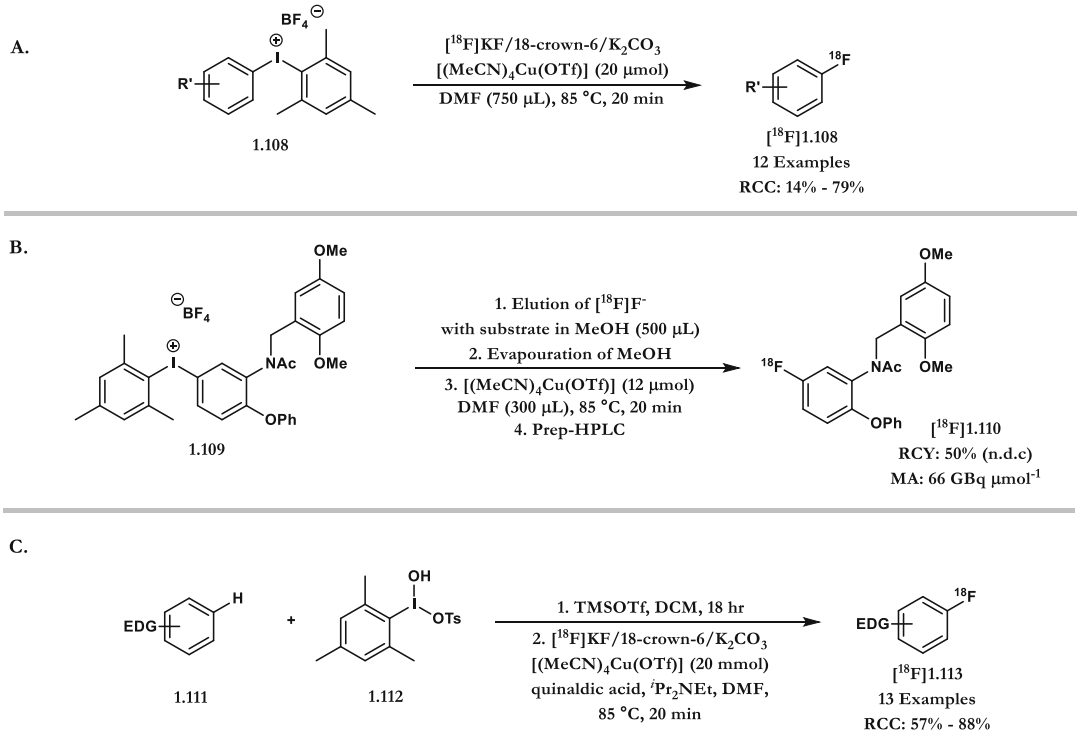

Scheme 1.19. Cu-mediated ^{18}F-fluorination of (mesityl)(aryl)iodonium salts

In 2017, Sanford and Scott reported a protocol for the *in-situ* synthesis of (mesityl)(aryl)iodonium salts from electron-rich (hetero)arenes and their subsequent ^{18}F-fluorination (Scheme 1.19C).[71] Whilst RCCs from electron-rich aromatics was generally excellent, the ^{18}F-fluorination of pyrrole and thiophene gave multiple ^{18}F-containing products. Furthermore, when starting from 55 GBq of [^{18}F]fluoride, an isolated yield of 2.8% was reported suggesting further work is required before this method is suitable for the preparation of radiotracers when using clinically relevant doses of [^{18}F]fluoride.

In 2011, Ritter and co-workers approached the radiofluorination of electron rich (hetero)arenes with an umpolung approach (Scheme 1.20).[72] Reaction of [^{18}F]KF/18-crown-6 with a highly fluorophilic Pd(IV) complex **1.114** gave 90% ^{18}F-incorporation as a Pd(IV)-^{18}F complex **[^{18}F]115**. This complex is considered as an electrophilic ^{18}F-species, derived from [^{18}F]fluoride. In so doing, this circumvents the low MA and handling issues associated with [^{18}F]F_2. At this stage, a second, preformed Pd(II)-aryl complex **1.116**, is introduced. Following an initial single electron transfer (SET), the [^{18}F]fluoride is transferred from the Pd(III)-^{18}F complex to the Pd(III)-aryl complex. A second SET precedes the reductive elimination to form the desired ^{18}F-aryl bond. Following this work, Ritter and co-workers reported that Ni(II)-aryl complex **1.118** can undergo an analogous process.[73] However, rather than two preformed Pd complexes being required, a single complex can be used to achieve the capture and subsequent reductive elimination steps with [^{18}F]fluoride (Scheme 1.21). One criticism of both works however, was the use of air sensitive Pd and Ni complexes. Furthermore, neither work had shown to be amenable to ^{18}F-fluorination

with clinically relevant doses of [^{18}F]fluoride with low isolated yields reported (Scheme 1.20 and Scheme 1.21).[74,75]

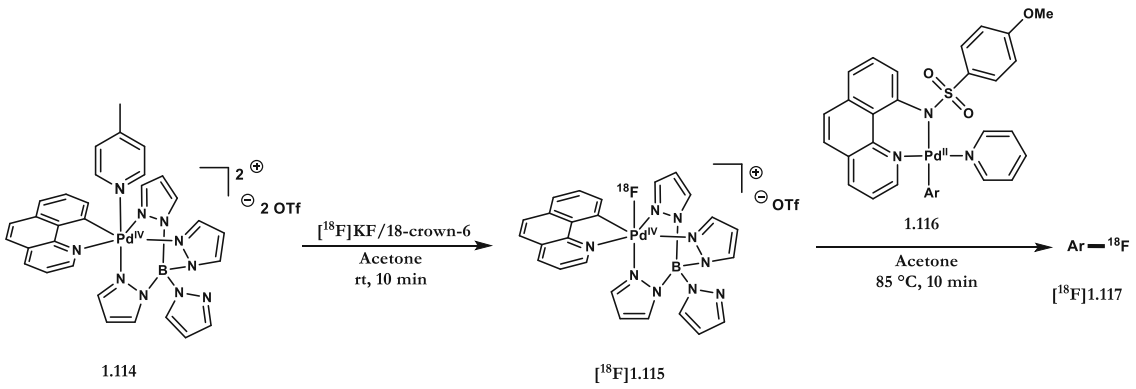

Scheme 1.20. Nucleophilic ^{18}F-fluorination via a Pd(IV) complex

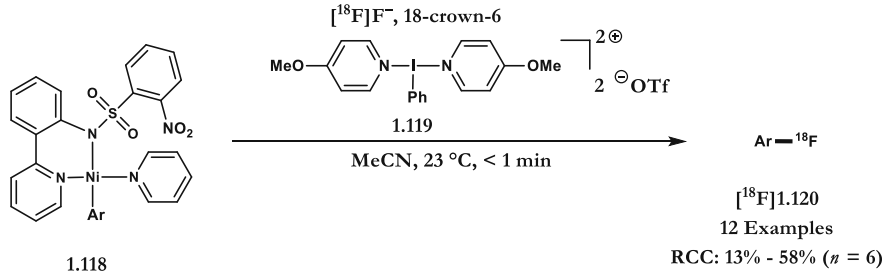

Scheme 1.21. Nucleophilic ^{18}F-fluorination via a Ni(III) complex

In 2011, the Ritter group described the use of an imidazoline-type reagent for the deoxyfluorination of phenol.[76] A follow-up study in 2016 by Ritter and Hooker presented computational and kinetic mechanistic studies, as well as the translation of this method to the preparation of [^{18}F]fluoro(hetero)arenes (Scheme 1.22A).[77] The initial step of the process involved the reaction of chloroimidazolium chloride with phenols to form aryloxyimidazolium chloride **1.122**, which was isolated by filtration. A solution of aryloxyimidazolium chloride **1.122** and either potassium bicarbonate or tri-*n*-butylamine in a 10:1 mixture of butanone and ethanol was used to elute [^{18}F]fluoride from an anion exchange cartridge. Following azeotropic drying, stirring at 130 °C for 20 minutes afforded [^{18}F]fluoro(hetero)arenes in 13% - 99% RCC. A

range of free O-H and N-H groups were tolerated, although this method was restricted to electron-deficient phenols; a consequent of the concerted nucleophilic aromatic substitution mechanism.

In 2017, Ritter and Hooker, with the use of a ruthenium π-complex, broadened the substrates scope of the transformation via reduction of the electron density of the arene (Scheme 1.22B).[78] The requirement of 30 – 40 mg of reagent along with the low elution efficiency (60% – 70%) was a disadvantage however. It should also be noted that although the ruthenium complex employed is air and moisture stable, a criticism of the previous works with Pd and Ni, the Ru complex is not commercially available and requires a glovebox for preparation and the use of a highly toxic organothallium reagent.

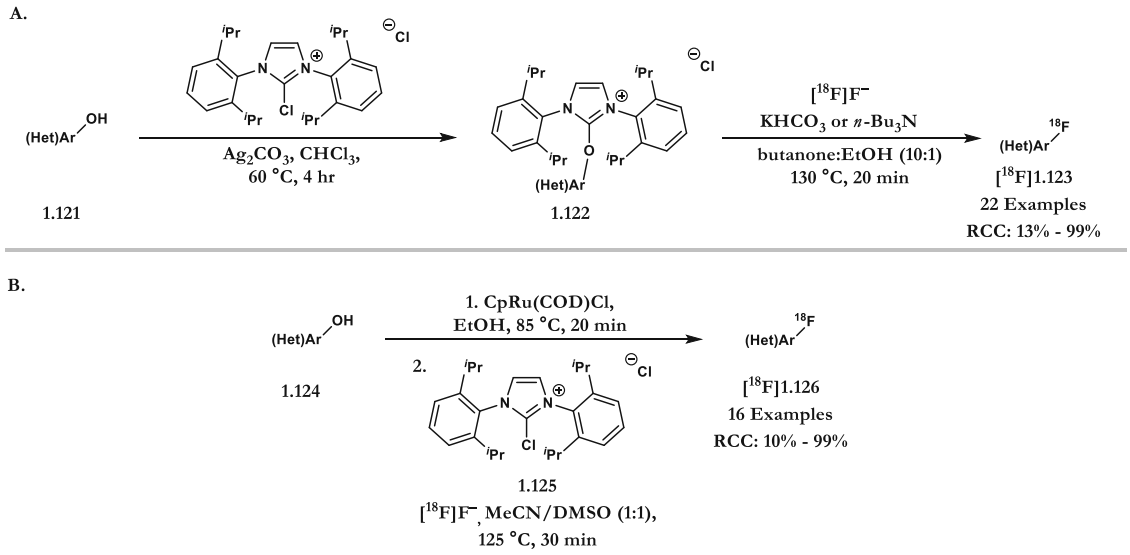

Scheme 1.22. Nucleophilic ^{18}F-deoxyfluorination of phenols

As highlighted in Section 1.6, the use of boron reagents in combination with the electrophilic fluorination reagent, [^{18}F]Selectfluor *bis*(triflate) **1.13**,[31] has been reported for the synthesis of the tracer, [^{18}F]FDOPA **[^{18}F]1.21**. A nucleophilic variant of this process emerged in 2014 building on advances made in the field of copper-

mediated ^{19}F-fluorination. Ribas followed by Wang demonstrated that Cu(III) intermediates in geometrically-constrained systems are amenable to nucleophilic fluorination (Scheme 1.23A).[79,80] Following these studies, Hartwig reported the fluorination of aryl iodides with [Cu(OTf)(*t*-BuCN)$_2$] and AgF evoking a mechanism involving a Cu(III) intermediate and C-F reductive elimination pathway (Scheme 1.23B).[81] Sanford and co-workers subsequently reported the reaction of (hetero)aryl trifluoroborate salts with KF and Cu(OTf)$_2$ (Scheme 1.23C).[82] Bridging the gap between ^{19}F and ^{18}F-fluorination, Gouverneur and co-workers demonstrated that the pre-formed Cu(III) complex **1.134** is responsive to nucleophilic ^{18}F-fluorination in the presence of carrier-added [^{18}F]fluoride (Scheme 1.23D).[83] This experiment paved the way for a general procedure to access ^{18}F-(hetero)arenes from boron species using nucleophilic [^{18}F]fluoride.

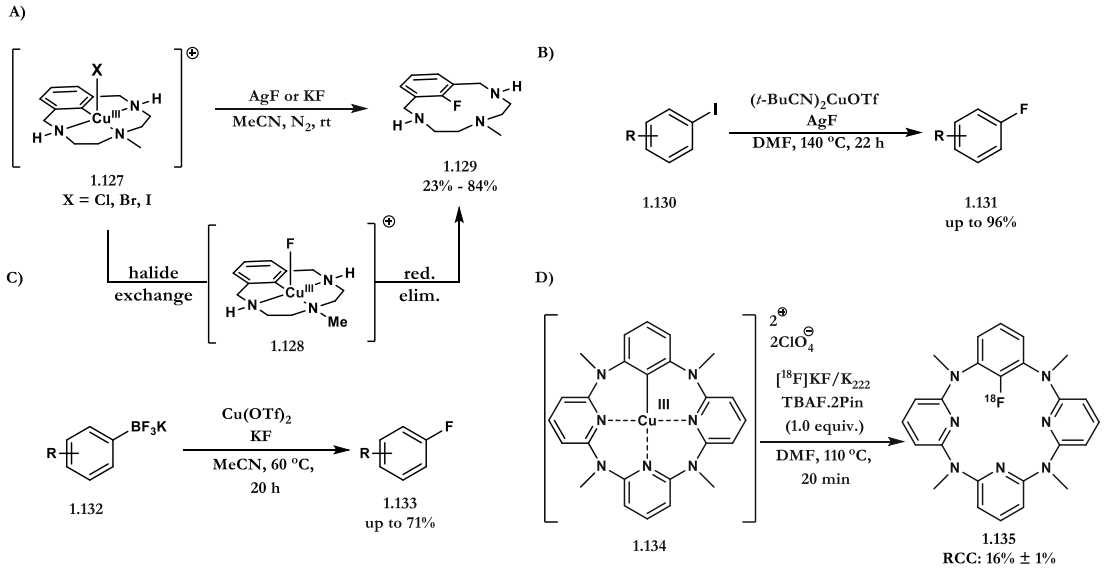

Scheme 1.23. Nucleophilic ^{19}F-fluorination of boron reagents under copper catalysis

In 2014, the Gouverneur group demonstrated that the direct labelling of aryl boronic esters *via* a nucleophilic source of fluorine-18, [^{18}F]KF/K$_{222}$, is feasible. Starting from aqueous [^{18}F]fluoride and after a conventional drying step, [^{18}F]KF was

reacted with boronic pinacol esters in the presence of tetrakis pyridine copper(II) triflate to give a variety of ^{18}F-labelled (hetero)arenes (Scheme 1.24).[84] This method facilitates the labelling of electron poor and electron rich arenes, and more functionalised molecules such as DAA-1106 and protected racemic 6-[^{18}F]fluoro-*m*-tyrosine. Of particular note, the method provides direct access to 6-[^{18}F]fluoro-*L*-DOPA from [^{18}F]fluoride with a protocol requiring a single deprotection step post-labelling.

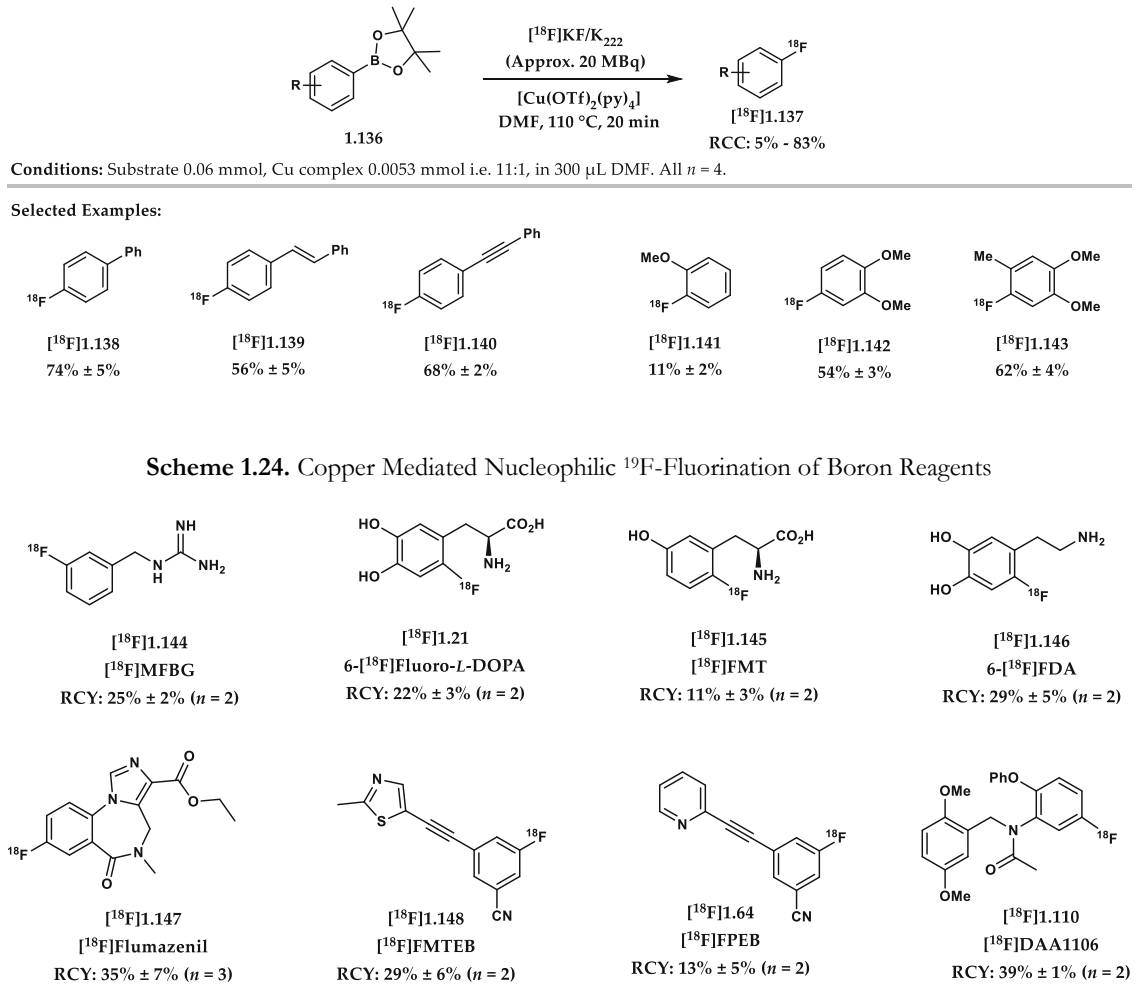

Scheme 1.24. Copper Mediated Nucleophilic ^{19}F-Fluorination of Boron Reagents

Scheme 1.25. Copper mediated nucleophilic ^{19}F-fluorination of eight clinically relevant tracers. Conditions: electron rich substrates: substrate (0.02 mmol), Cu complex (0.02 mmol), DMA (400 μL); electron poor substrates: substrate (0.03 mmol), Cu complex (0.04 mmol), DMA (400 μL); elution conditions for electron rich substrates: QMA Carbonate $K_2C_2O_4$ (1 mg), K_2CO_3 (0.1 mg), $K_{2.2.2}$ (6.3 mg), CH_3CN/H_2O (900 μL); Elution conditions for electron poor substrates: QMA Oxalate, $K_2C_2O_4$ (1 mg), K_2CO_3 (0.1 mg), $K_{2.2.2}$ (6.3 mg), CH_3CN/H_2O (900 μL)

Further optimisation tailored for either electron-rich or electron-poor boron reagents enabled access to eight clinically relevant PET tracers using up to 26 GBq [^{18}F]fluoride (Scheme 1.25).[85] Key optimisation parameters include change of solvent (DMA instead of DMF), the ratio between the boron reagent and the copper complex, and/or cartridge pre-conditioning ($K_2C_2O_4$ instead of K_2CO_3).

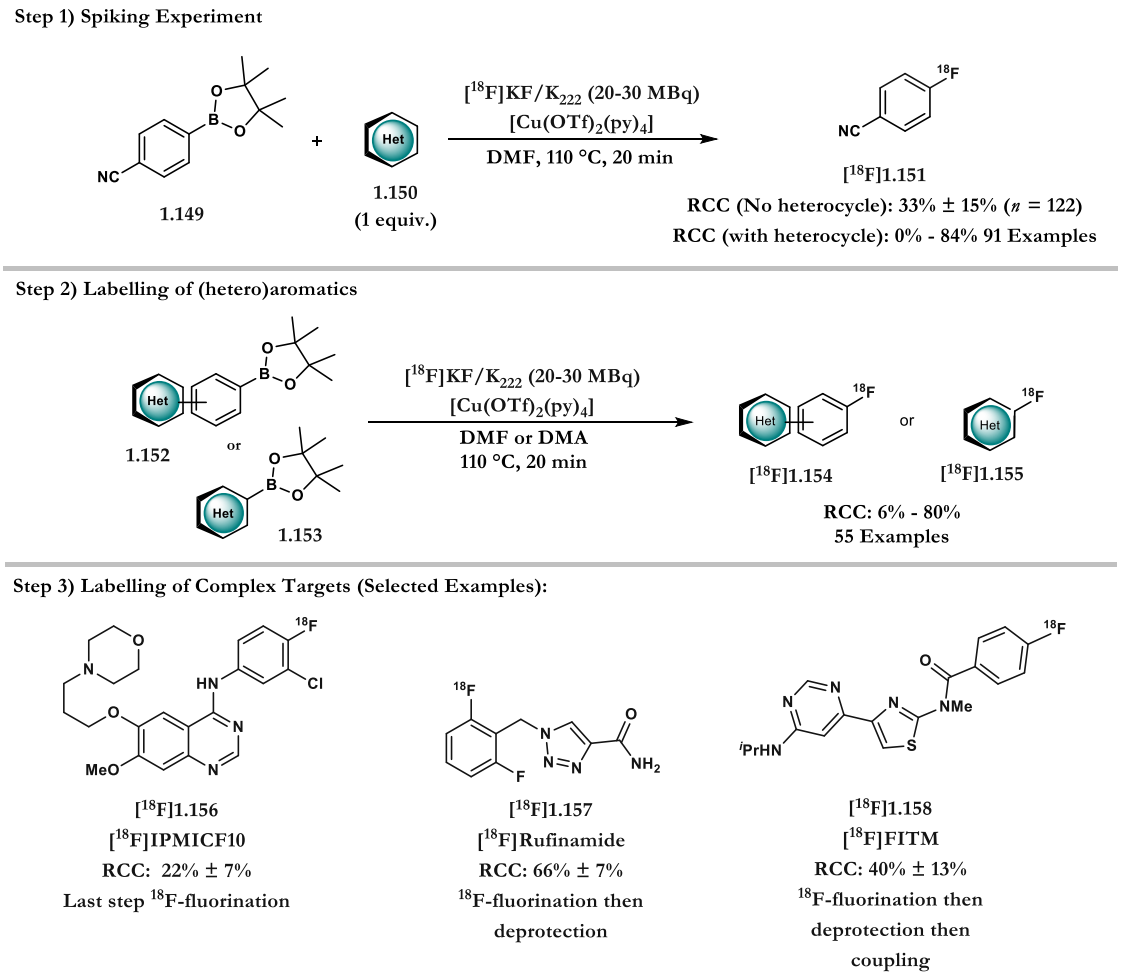

Scheme 1.26. De-Risking the copper mediated nucleophilic ^{19}F-fluorination

In 2017, an in-depth evaluation of the scope and limitation of the copper-mediated ^{18}F-fluorination of (hetero)aryl boronic species was accomplished.[83] The approach inspired by the robustness screening technique of Collins and Glorius,[86] consisted of assessing the compatibility of the methodology with close to 100 heterocycles and carrying out the ^{18}F-labelling of over 50 small molecules all

containing at least one heterocyclic ring. The large data set arising from this study proved extremely useful for designing low-risk retro-radiosynthetic routes for complex targets. Rewardingly, this rational approach culminated in the successful radiosynthesis of seven complex targets labelled applying one of three strategies: 1) last step ^{18}F-fluorination, 2) ^{18}F-fluorination followed by a single conventional deprotection step, and 3) more than one step post ^{18}F-labelling (Scheme 1.26).

The value of this ^{18}F-radiochemistry was further broadened with boron reagents other than boronic pinacol esters. Sanford and Scott reported that aryl boronic acids are equally suitable for Cu-mediated ^{18}F-fluorination and investigated in depth how cartridge pre-conditioning influences the extent of side-reactions such as protodeboronation (Scheme 1.27A).[87,88] This study also indicated that the pre-formed tetrakis pyridine copper (II) triflate can be conveniently replaced by $Cu(OTf)_2$ in the presence of pyridine. A follow-up study from Neumaier demonstrated that the use of primary and secondary alcohols as co-solvent further increases the radiochemical yield for the ^{18}F-fluorination of a range of (hetero)aryl boronic pinacol esters, boronic acids, and stannanes (Scheme 1.27B).[89]

During this time, the value of Cu-mediated ^{18}F-fluorination of aryl boron reagents as a route to access ^{18}F-(hetero)arenes has been illustrated in various laboratories worldwide (Scheme 1.28). Selected examples include the ^{18}F-fluorination of [^{18}F]dihydrofluvastatin analogue **[^{18}F]1.163**,[90] [^{18}F]fluorobenzyl triphenylphosphonium triflate **[^{18}F]1.164**,[91] [^{18}F]volinanserin ([^{18}F]MDL100907) **[^{18}F]1.166**,[92,] [^{18}F]IPMICF17 **[^{18}F]1.165** and BMS-986205 **[^{18}F]1.167**.[93,94]

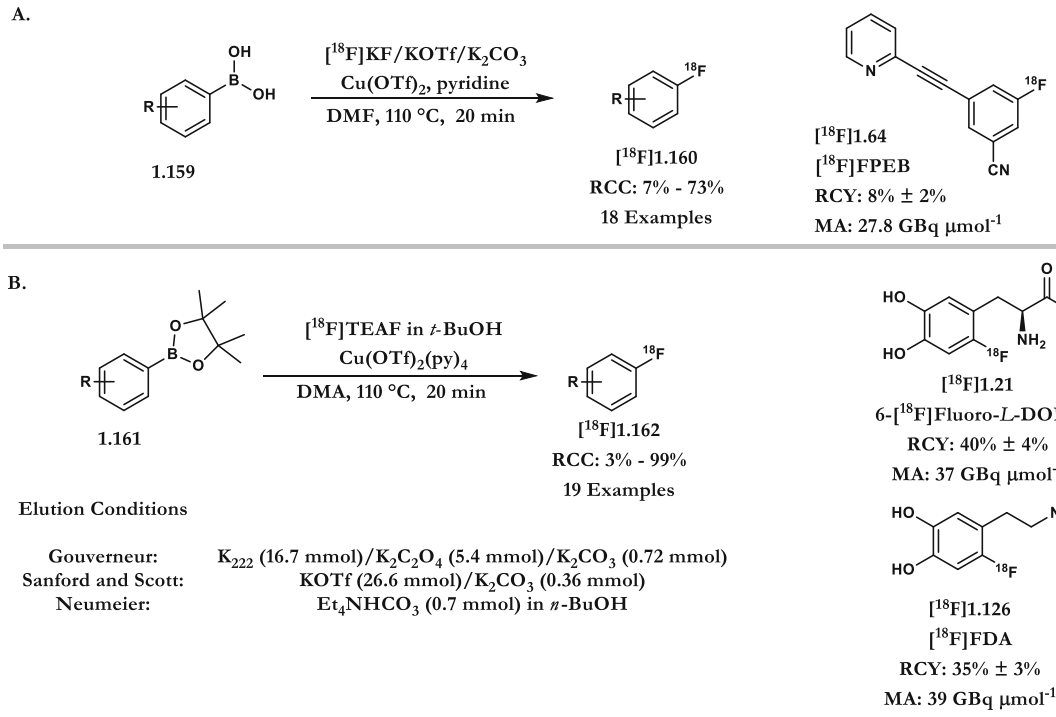

Scheme 1.27. Copper mediated nucleophilic ^{19}F-fluorination of boron reagents

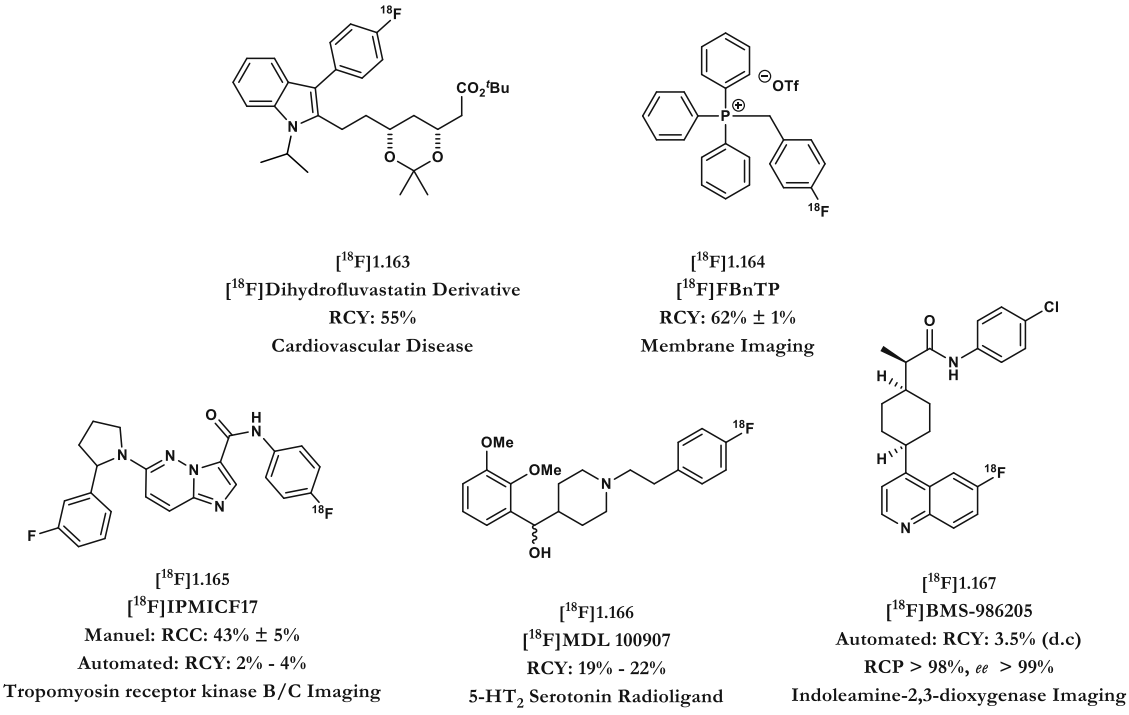

Scheme 1.28. Application of the copper mediated nucleophilic ^{19}F-fluorination

1.8.3 ^{18}F-Fluorination of Other Motifs

Typical routes for the introduction of the ^{19}F-trifluoromethyl group is by copper(I) catalysed cross-coupling with CF_3-sources.[95] Huiban and co-workers, were able to generate Cu(I)-$^{18}CF_3$ from difluorocarbenes, generated from methyl chlorodifluoroacetate and [^{18}F]KF/K_{222}.[96] Using this Cu(I)-$^{18}CF_3$ source, a broadly applicable ^{18}F-trifluoromethylation of aryl halides was reported (Scheme 1.29). Compared to halogen exchange reactions, the substrate scope was broadened, however, the modest MA of 0.1 GBq μmol^{-1} is a drawback.

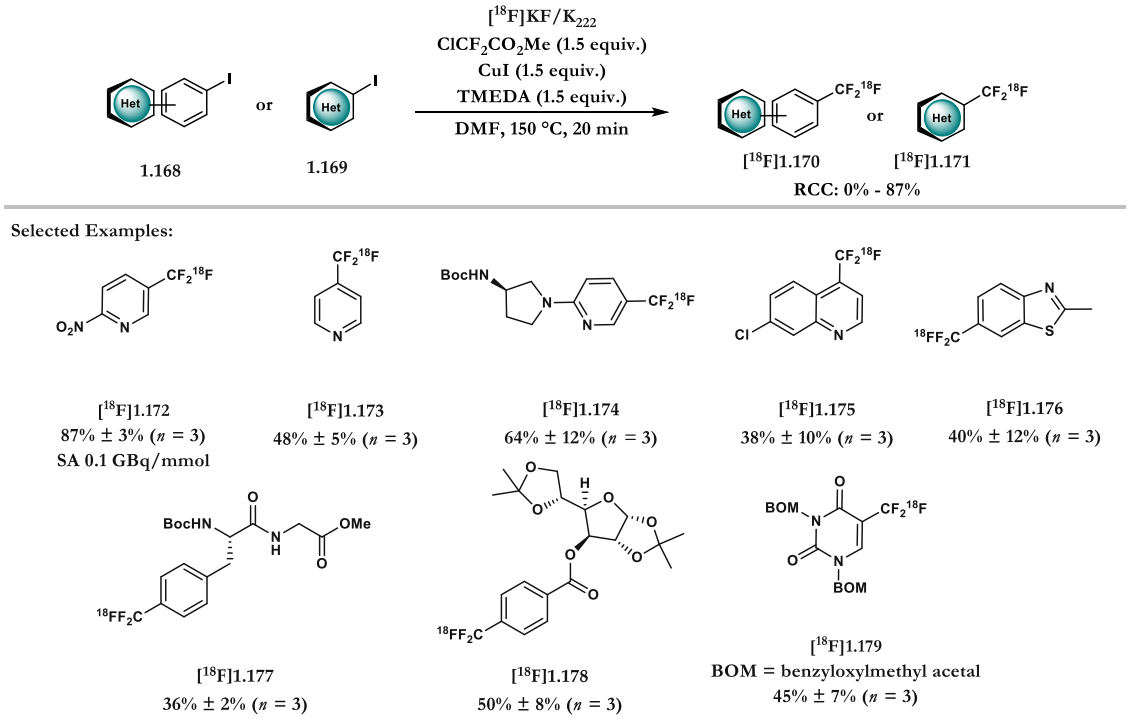

Scheme 1.29. A broadly applicable ^{18}F-trifluoromethylation of aryl halides

Riss and co-workers presented an alternative method for the generation of Cu(I)-$^{18}CF_3$, utilising Vugts radiosynthesis of [^{18}F]trifluoromethane from difluoroiodo-methane followed by potassium *tert*-butoxide in the presence of CuBr.[97] Whilst this procedure was shown to be amenable to electron rich, neutral and deficient arenes, the MA of 0.139 GBq μmol^{-1} remains a drawback. To overcome this,

Vugts and co-workers, using triethylammonium trihydrofluoride (TREAT.3HF) to stabilise the [^{18}F]Cu(I)-CF_3 **[^{18}F]1.181** species, were able to increase the MA up to 32 GBq μmol^{-1} for the ^{18}F-trifluoromethylation of aryl iodides and aryl boronic acids (Scheme 1.30).[98]

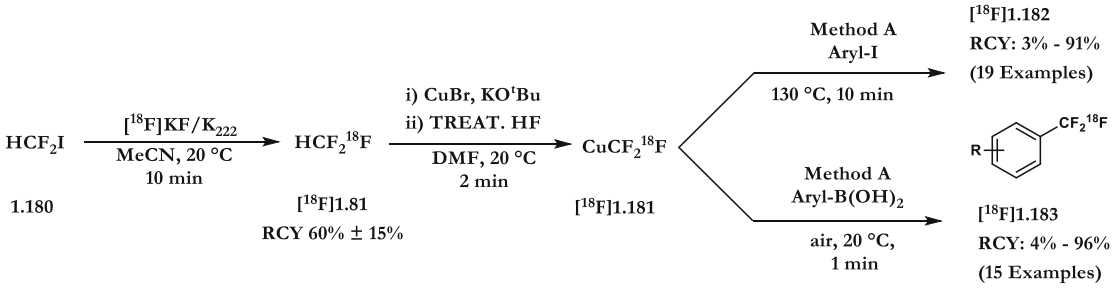

Scheme 1.30. ^{18}F-Trifluoromethylation of aryl halides and aryl boronic acids

Whilst the use of thermal activation for the synthesis of (hetero)aryl-$CF_2{}^{18}F$ motifs, it has proven incompatible for the synthesis of more complex functional groups including, trifluoromethoxy, difluoromethoxy and trifluoromethyl thiol groups. In 2015, Gouverneur and co-workers reported the first radiosynthesis of such groups with the silver mediated ^{18}F-fluorination from the corresponding chloro- and bromo-precursors (Scheme 1.31).[99] A modest scope was reported with MA in the range of 0.1 – 0.2 GBq μmol^{-1}.

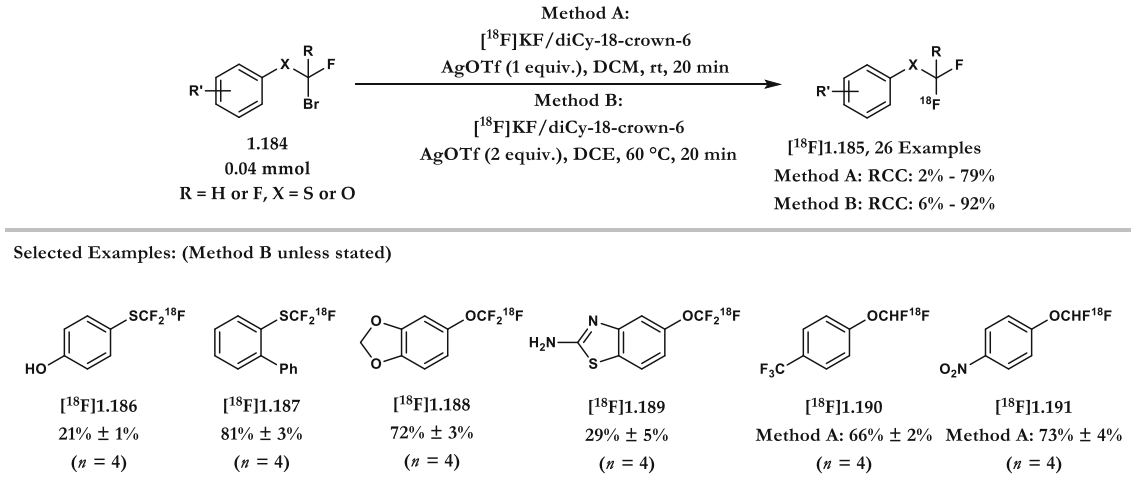

Scheme 1.31. Silver mediated nucleophilic ^{18}F-fluorination

1.9 Thesis Outline

This thesis discusses of the development and application of novel radiochemical transformations for both Positron Emission Tomography (PET) and Single Photo Emission Computered Tomography (SPECT) using [^{18}F]fluoride and [^{123}I]NaI respectively. A general introduction is presented in **chapter I** and **chapter IV**. **Chapter I**, covers PET, the production of fluorine-18 and the current state-of-the-art for ^{18}F-radiolabelling. **Chapter IV** provides a brief overview of SPECT, production of radionuclides in SPECT and the current state-of-the-art.

The results chapters consist of three different approaches for the development and application of novel radiochemical transformations within PET or SPECT imaging. **Chapter II** entails the application of the copper mediated nucleophilic ^{18}F-fluorination of aryl pinacol boronic esters to the radiofluorination of [^{18}F]olaparib. Subsequently, the imaging of DNA damage in pancreatic adenocarcinoma cell lines is examined. **Chapter III** discusses the synthesis of the novel ^{18}F-trifluoromethylation reagent, [^{18}F]-5-(trifluoromethyl)dibenzothiophenium trifluoromethanesulfonate and its application to the ^{18}F-trifluoromethylation of unmodified peptides. **Chapter IV** consists of the development of the copper mediated ^{123}I-Iodination of aryl boron reagents and its application to four clinically relevant SPECT tracers.

Finally, **Chapter V** provides experimental data for compounds discussed within this thesis.

1.10 References

1 M. E. Phelps. *Proc. Natl. Acad. Sci., USA* 2000, **97**, 9226; b) S. M. Ametamey, M. Honer, P. A. Schubiger, *Chem. Rev.*, 2008, **108**, 1501; c) S. L. Pimlott, A. Sutherland, *Chem. Soc. Rev.*, 2011, **40**, 149; d) L. Zhu, K. Ploessl, H. F. Kung, *Chem. Soc. Rev.*, 2014, **43**, 6683; e) R. Chakravarty, H. Hong, W. Cai, *Mol. Pharmaceutics,* 2014, **11**, 3777; f) M. S. Placzek, W. Zhao, H.-Y. Wey, T. M. Morin, J. M. Hooker, *Semin. Nucl. Med.*, 2016, **46**, 20.

2 P. M. Matthews, E. A. Rabiner, J. Passchier, R. N. Gunn, *Br. J. Clin. Pharmacol.,* 2012, **73***,* 175.

3 F. Champion, F. Lerebours, P. Cherel, V. Edeline, A. L. Giraudet, M. Wartski, D. Bellet, J. L. Alberini, *Eur. J. Nucl. Med. Mol. Imaging,* 2013, **40**, 1206.

4 L. Ceriani, G. Treglia, G. Paone, M. Bongiovanni, S. Franscella, L. Giovanella, *J. Clin. Endocrinol. Metab.,* 2013, **98**, 2208.

5 P. W. Miller, N. J. Long, R. Vilar, A. D. Gee, *Angew. Chem. Int. Ed.,* 2008, **47**, 8998.

6 C. Levin, *Eur. J. Nucl. Med. Mol. Imaging*, 2005, **32**, S325.

7 C. Murphy, C. Schaffrath, D. O'Hagan, *Chemosphere*, 2003, **52**, 455.

8 K. Chan, D. O'Hagan, D. Hopwood, *Natural Product Biosynthesis By Microorganisms and Plants, Pt B*, 2012, **516**, 219.

9 D. O'Hagan, *Chem. Soc. Rev.,* 2008, **37**, 308.

10 D. O'Hagan, *J. Fluorine Chem.,* 2010, **131**, 1071.

11 A. Vulpetti, C. Dalvit, *Drug Disc. Today,* 2012, **17**, 890.

12 W. K. Hagmann, *J. Med. Chem.,* 2008, **51**, 4359.

13 K. Muller, C. Faeh, F. Diederich, *Science*, 2007, **317**, 1881.

14 L. Pauling, *The Nature of the Chemical Bond and the Structure of Molecules and Crystals. An introduction to modern structural chemistry*, Cornell University Press, Ithaca, 1939.

15 P. Jeschke, *ChemBioChem.,* 2004, **5**, 570.

16 S. Purser, P. R. Moore, S. Swallow, V. Gouverneur, *Chem. Soc. Rev.,* 2008, **37**, 320.

17 L. Hunter, *Beilstein J. Org. Chem.,* 2010, **6.**

18 B. Chamberlain, V. Batra, W. Beard, A. Kadina, D. Shock, B. Kashemirov, C. McKenna, M. Goodman, S. Wilson, *Chembiochem,* 2012, **13**, 528.

19 G. Kelloff, J. Hoffman, B. Johnson, H. Scher, B. Siegel, E. Cheng, B. Cheson, J. O'Shaughnessy, K. Guyton, D. Mankoff, L. Shankar, S. Larson, C. Sigman, R. Schilsky, D. Sullivan. *Clin. Cancer Res.,* 2005, **11**, 2785.

20 E. Aboagye, *Mol. Imaging Bio.,* 2005, **7**, 53.

21 M. Bergstom, A. Grahnen, b. Langstrom, *Eur. J. Clin. Pharmacol.,* 2003, **59**, 357.

22 K. Kaitin, J. Dimasi, *Clin. Pharamocol. Ther.,* 2011, **89**, 183.

23 J. Dimasi, H. Grabowski, R. Hansen, *N. Eng. J. Med.,* 2015, **372**, 1972.

24 S. Preshlock, M. Tredwell, V. Gouverneur, *Chem. Rev.,* 2016, **116**, 719.

25 H. H. Coenen, A. D. Gee, M. Adam, G. Antoni, C. S. Cutler, Y. Fujibayashi, J. M. Jeong, R. H. Mach, T. L. Mindt, V. W. Pike, A. D. Windhorst, *Nucl. Med. Biol.,* 2017, **55**, 5.
26 J. Bergman, O. Solin, *Nucl. Med. Biol.,* 1997, **24**, 677.
27 G. Blessing, H. Coenen, K. Franken, S. Qaim, *App. Radiat. Isot.,* 1986, **37**, 1135.
28 G. Bida, R. Ehrenkaufer, A. Wolf, J. Fowler, R. Macgregor, T. Ruth, *J. Nucl. Med.,* 1980, **21**, 758.
29 R. Nickles, R. Hichwa, M. Daube, G. Hutchins, D. Congdon, *Int. J. Appl. Radioat. Isot.,* 1983, **34**, 625.
30 a) N. Fukuhara, L. A. Bigelow, *J. Am. Chem. Soc.,* 1941, **63**, 2792; b) F. Cacace, A. P. Wolf, *J. Am. Chem. Soc.,* 1978, **100**, 3639.
31 I. S. R. Stenhagen, A. K. Kirjavainen, S. J. Forsback, C. G. Jørgensen, E. G. Robins, S. K. Luthra, O. Solin, V. Gouverneur, *Chem. Commun.,* 2013, **49**, 1386.
32 H. Teare, E. G. Robins, E. Årstad, S. K. Luthra, V. Gouverneur, *Chem. Commun.,* 2007, **23**, 2330.
33 N. Satyamurthy, G. T. Bida, M. E. Phelps, J. R. Barrio, *Appl. Radiat. Isot.,* 1990, **41**, 733.
34 A. Hiller, C. Ficher, A. Jordanova, J. T. Patt, J. Steinbach, *Appl. Radiat. Isot.,* 2008, **66**, 152.
35 R. Chirakal, G. Firnau, G. Schrobilgen, J. McKAy, E. Garnett, *Int. J. Appl. Radiat. Isot.,* 1984, **35**, 401.
36 M. Constantinou, F. Airbirhio, R. Smith, C. Ramsden, V. Pike, *J. Am. Chem. Soc.,* 2001, **123**, 1780.
37 S. Lu, V. Pike, *J. Fluorine Chem.,* 2010, **131**, 1032.
38 W. Dolbier, A. Li, C. Kock, C. Shiue, A. Kachur, *Appl. Radiat. Isot.,* 2001, **54**, 73.
39 R. Chirakal, G. Firnau, E. S. Garnett, *J. Nucl. Med.,* 1986, **27**, 417.
40 R. Chirakal, N. Vasdev, G. J. Schrobilgen, C. Nahnias, *J. Fluorine Chem.,* 1999, **99**, 87.
41 G. Finrau, R. Chirakal, S. Sood, S. Garnett, *Can. J. Chem.,* 1980, **58**, 1449.
42 a) R. Chirakal, G. Firnau, J. Couse, E. S. Garnett, *Int. J. Appl. Radiat. Isot.,* 1984, **35**, 651; b) M. J. Adam, T. J. Ruth, J. R. Grierson, B. Abeysekera, B. D. Pate, *J. Nucl. Med.,* 1986, **27**, 1462; c) M. J. Adam, J. R. Grierson, T. J. Ruth, S. Jiyn, *Appl. Radioat. Isot.,* 1986, **37**, 877; d) H. H. Coenen, K. Franken, P. Kling, G. Stocklin, *Appl. Radioat. Isot.,* 1988, **39**, 1243.
43 F. Buckingham, A. K. Kirjavainen, S. Forsback, A. Krzycamonik, T. Keller, I. M. Newington, M. Glaser, S. K. Luthra, O. Solin, V. Gouverneur, *Angew. Chem. Int. Ed.,* 2015, **54**, 13366.
44 M. L. Richards, P. J. H. Schott, *Radiochemical Syntheses,* Joh Willey & Sons, Inc., 2012, 1.
45 L. Libert, X. Franci, A. Plenevaux, T. Ooi, K. Maruoka, A. Luxen, C. Lemaire, *J. Nucl. Med.,* 2013, **54**, 1154.

46 T. Nozaki, Y. Tanaka, *Int. J. Appl. Radiat. Isot.,* 1967, **18**,111.
47 A. Knochel, O. Zwernemann, *J. Label. Compd. Radiopharm.,* 1996, **38**, 325.
48 T. Tewson, M. Welch, *J. Chem. Soc. Chem. Commun.,* 1979, 1149.
49 J. Chun, C. Morse, F. Chinz, V. W. Pike, *Chem. Commun.,* 2013, **49**, 2151.
50 V. W. Pike, F. I. Aighirhio, *J. Chem. Soc., Chem. Commun.,* 1995, 2215.
51 S. M.-Santamaria, M. A. Carroll, V. W. Pike, H. S. Rzepa, D. A. Widdowson, *J. Chem. Soc., Perkin Trans.,* 2000, **2**, 2158.
52 J.-H. Chun, S. Lu, Y.-S. Lee, V. W. Pike, *J. Org. Chem.,* 2010, **75**, 3332.
53 T. Ross, J. Ermert, C. Hocke, H. H. Coenen, *J. Am. Chem. Soc.,* 2007, **129**, 8018.
54 B. H. Rotstein, N. A. Stephenson, N. Vasedev, S. H. Liang, *Nat. Commun.,* 2014, **5** 5365.
55 N. A. Stephenson, J. P. Holland, A. Kassenbrock, D. L. Yokell, E. Livni, S. H. Liang, N. Vasdev., *J. Nucl. Med.,* 2015, **56**, 489.
56 B. H. Rotstein, L. Wang, R. Y. Liu, J. Patteson, E. E. Kwan, N. Vasdev, S. H. Liang, *Chem. Sci.,* 2016, **7**, 4407.
57 T. Ido, T. Irie, Y. Kasida, *J. Label. Compd. Radiopharm.,* 1979, **16**, 153.
58 G. Angelini, M. Speranza, C. Shiue, A. Wolf, *J. Chem. Soc., Chem. Commun.,* 1986, 924.
59 A. Hammadi, C. Crouzel, *J. Label. Compd. Radiopharm.,* 1993, **33**, 703.
60 J. Zheng, L. Wang, J.-H. Lin, J.-C. Xiao, S. H. Liang, *Angew. Chem. Int. Ed.,* 2015, **54**, 13240.
61 E. Carbonnel, T. Besset, T. Poisson, D. Labar, X. Pannecoucke, P. Jubault, *Chem. Commun.,* 2017, **53**, 5706.
62 F. Buckingham, V. Gouverneur, *Chem. Sci.,* 2016, **7**, 1645.
63 C. Hollingworth, A. Hazari, M. Hopkinson, M. Tredwell, E. Benedetto, M. Huiban, A. Gee, J. Brown, V. Gouverneur, *Angew. Chem. Int. Ed.,* 2011, **50**, 2613.
64 E. Benedetto, M. Tredwell, C. Hollingworth, T. Khotavivattana, J. M. Brown, V. Gouverneur, *Chem. Sci.,* 2013, **4**, 89.
65 T. Graham, R. Lambert, K. Ploessl, H. Kung, A. Doyle, *J. Am. Chem. Soc.,* 2014, **136**, 5291.
66 X. Huang, W. Liu, H. Ren, R. Neelamegam, J. M. Hooker, J. T. Groves, *J. Am. Chem. Soc.,* 2014, **136**, 6842.
67 L. Carroll, H. L. Evans, A. C. Spivey, E. O. Aboagye, *Chem. Commun.,* 2015, **51**, 8439.
68 N. Ichiishi, A. J. Canty, B. F. Yates, M. S. Sanford, *Org. Lett.,* 2013, **15**, 5134.
69 N. Ichiishi, A. F. Brooks, J. J. Topczewski, M. E. Rodnick, M. S. Sanford, P. J. H. Scott, *Org. Lett.,* 2014, **16**, 3224.
70 B. D. Zlatopolskiy, J. Zischler, P. Krapf, F. Zarrad, E. A. Urusova, E. Kordys, H. Endepols, B. Neumaier, *Chem. Eur. J.,* 2015, **21**, 5972.
71 M. S. McCammant, S. Thompson, A. F. Brooks, S. W. Krska, P. J. H. Scott, M. S. Sanford, *Org. Lett.,* 2017, **19**, 3939.

72 E. Lee, A. S. Kamlet, D. C. Powers, C. N. Neumann, G. B. Boursalian, T. Furuya, D. C. Choi, J. M. Hooker, T. Ritter, *Science,* 2011, **334**, 639.
73 E. Lee, J. M. Hooker, T. Ritter, *J. Am. Chem. Soc.,* 2012, **134**, 17458.
74 A. S. Kamlet, C. N. Neumann, E. Lee, S. M. Carlin, C. K. Moseley, N. Stephenson, J. M. Hooker, T. Ritter, *PLoS One,* 2013, **8**, e59187
75 A. J. Hoover, M. Lazari, H. Ren, M. K. Narayanam, J. M. Murphey, R. M. Dam, J. M. Hooker, T. Ritter, *Organometallics,* 2016, **35**, 1008.
76 P. Tng, W. Wang, T. Ritter, *J. Am. Chem. Soc.,* 2011, **133**, 11482.
77 C. N. Neumann, J. M. Hooker, T. Ritter, *Nature,* **534**, 369.
78 M. H. Bevzavi, D. Mandal, M. G. Strebl, C. N. Neumann, E. M. D'Amato, J. Chen. J. M. Hooker, T. Ritter, *ACS Cent. Sci.,* 2017, **3**, 944.
79 A. Casitas, M. Canta, M. Solà, M. Costas and X. Ribas, *J. Am. Chem. Soc*., 2011, **133**, 19386.
80 B. Yao, Z.-L. Wang, H. Zhang, D.-X. Wang, L. Zhao and M.-X. Wang*, J. Org. Chem*., 2012, **77**, 3336.
81 P. S. Fier, J. Luo and J. F. Hartwig, *J. Am. Chem. Soc*., 2013, **135**, 2552.
82 Y. Ye, S. D. Schimler, P. S. Hanley and M. S. Sanford, *J. Am. Chem. Soc.,* 2013, **135**, 16292.
83 N. J. Taylor, E. Emer, S. Preshlock, M. Schedler, M. Tredwell, S. Verhoog, J. Mercier, C. Génicot and V. Gouverneur, *J. Am. Chem. Soc.,* 2017, **139**, 8267.
84 M. Tredwell, S. M. Preshlock, N. J. Taylor, S. Gruber, M. Huiban, J. Passchier, J. Mercier, C. Genicot and V. Gouverneur *Angew. Chem. Int. Ed*., 2014, **53**, 7751.
85 S. Preshlock, S. Calderwood, S. Verhoog, M. Tredwell, M. Huiban, A. Hienzsch, S. Gruber, T. C. Wilson, N. J. Taylor, T Cailly, M. Schedler, T. L. Collier, J. Passchier, R. Smits, J. Mollitor, A. Hoepping, M. Mueller, C. Génicot, J. Mercier and V. Gouverneur, *Chem. Commun.,* 2016, **52**, 8361.
86 K. D. Collins and F. Glorius, *Nat. Chem.,* 2013, **5**, 597.
87 A. V. Mossine, A. F. Brooks, K. J. Makaravage, J. M. Miller, N. Ichiishi, M. S. Sanford and P. J. H. Scott, *Org. Lett.,* 2015, **17**, 5780.
88 A. V. Mossine, A. F. Brooks, N. Ichiishi, K. J. Makaravage, M. S. Sanford and P. J. H. Scott, *Scientific Reports,* 2017, **7**, 1.
89 J. Ziachler, M. Kolks, D. Modemann, D. Neumaier and B. D. Zlatopolskiy *Chem. Eur. J.,* 2017, **23**, 3251.
90 T. Niwa, H. Ochiai, Y. Watanabe and T. Hosoya, *J. Am. Chem. Soc.,* 2015, **137**, 14313.
91 Zhang, C. Zhang, J. Lau, N. Colpo, F. Bénard and K.-S. Lin, *J. Label. Compd. Radiopharm.*, 2016, **59**, 467.
92 X. Zhang, R. Dunlow, B. N. Blackman and R. E. Swenson, *J. Label. Compd. Radiopharm.*, 2018, **61**, 427.

93 A. V. Mossine, A. F. Brooks, V. B.-Gauthier, J. J. Bailey, N. Ichiishi, R. Schirrmacher, M. S. Sanford and P. J. H. Scott, *J. Label. Compd. Radiopharm.,* 2018, **61**, 228.

94 E. Cole, D. Donnelly, M. Wallace, T. Tran, R. Burrell, W. Turley, A. Allentoff, A. Huang, A. Balog and S. Bonacorsi, *J. Nucl. Med.,* 2018, **59**, 605.

95 A. Lishchvnski, M. A. Novikov, E. Martin, E. C. E.-Adán, P. Novák, V. V. Grushin, *J. Org. Chem.,* 2013, **78**, 11126.

96 M. Huiban, M. Tredwell, S. Mizuta, Z. Wan, X. Zhang, T. L. Collier, V. Gouverneur, J. Passchier, *Nat. Chem.,* 2013, **5**, 941.

97 T. Rühl, W. Rafique, V. T. Lien, P. J. Riss, *Chem. Commun.,* 2014, **50**, 6056.

98 D. van der Born, C. Sewing, J. D. M. Hersceid, A. D. Windhorst, R. V. A. Orru, D. J. Vugts, *Angew. Chem. Int. Ed.,* 2014, **53**, 11046.

99 T. Khotavivattana, S. Verhoog, M. Tredwell, L. Pfeifer, S. Calderwood, K. Wheelhouse, T. L. Collier, V. Gouverneur, *Angew. Chem. Int. Ed.,* 2015, **54**, 9991.

Chapter II:

Imaging of DNA Damage with [^{18}F]Olaparib

2.1 Application of Novel ^{18}F-Methodology Towards [^{18}F]Olaparib

As summarised in **chapter I**, several innovative methodologies for the ^{18}F-fluorination of (hetero)aromatics have been reported. This chapter discusses the application of the copper mediated nucleophilic ^{18}F-fluorination of (hetero)aryl boronic pinacol esters for the radiosynthesis of [^{18}F]olaparib, an isotopologue of the PARP inhibitor, olaparib (AZD-2281, Lynparza) (Figure 2.1).

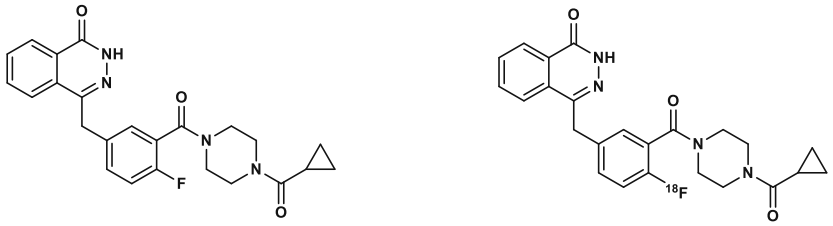

2.1
Olaparib:
(AZD-2281, Lynparza)

[^{18}F]2.1
[^{18}F]Olaparib

Figure 2.1. Structure of olaparib and [^{18}F]olaparib

2.2 DNA Damage

Within every cell of the human body, the DNA double helix is constantly exposed to damaging agents, leading to tens of thousands of DNA lesions occurring each day.[1] If a lesion is not repaired correctly, it may lead to the cell becoming senescent, apoptotic, or even malignant. Over recent years, a multitude of causes of DNA damage have been identified.[2,3] These can be split into endogenous and exogenous processes. Endogenous processes are responsible for the majority of DNA damage, and can be divided into three main categories: oxidative (i.e. produced by reactive oxygen species), hydrolytic (e.g. deamination of cytosine to uracil), and alkylation reactions (e.g. methylation of the N7-position of guanine residues).[4] Examples of exogenous sources for DNA damage include ultraviolet light, ionising radiation, certain chemotherapy drugs, industrial chemicals and carcinogens

associated with tobacco products.[5] The recognition and repair of this damage to DNA is accomplished by a set of complex, yet finely tuned DNA damage response (DDR) signalling pathways that inhibit cell cycle progression and subsequently repair DNA lesions (Figure. 2.2).

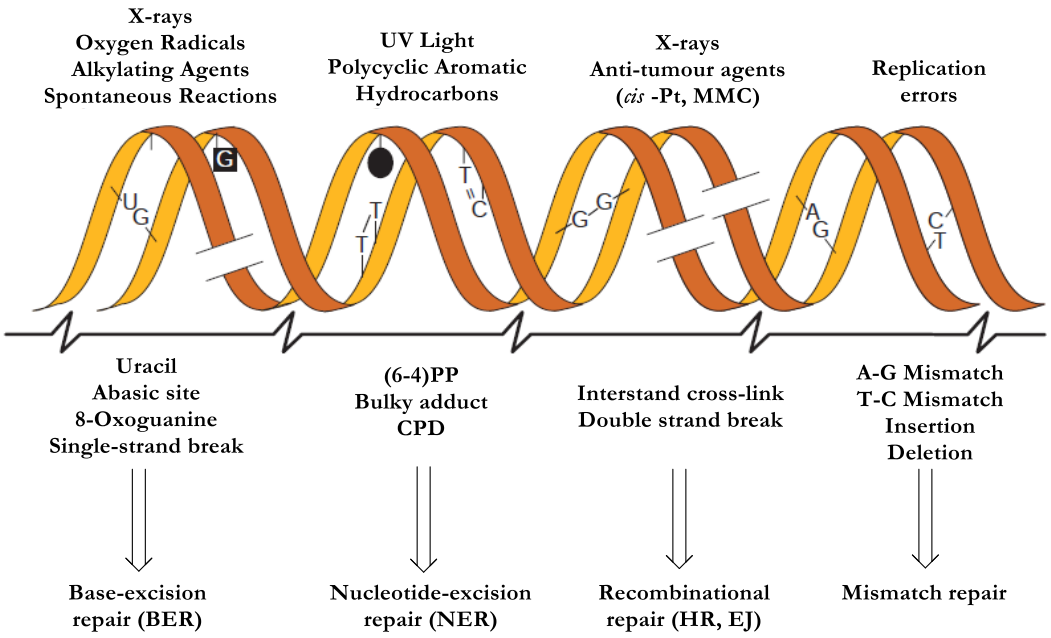

Figure 2.2. Schematic of DNA damage causes and SSB/DSB repair pathways

2.2.1 Single-Strand Break Repair Mechanisms

The repair of SSBs in DNA is facilitated mainly, by base excision repair (BER).[6] Deficiencies and mutations of proteins in this pathway are linked to genomic instability, ageing, and cancer.[7] BER has two sub-pathways referred to as short-patch repair (Figure. 2.3) and long-patch repair; the former being responsible for up to 90% of all BER.[8] Short-patch BER is made up of five major steps: (i) recognition of the damaged base by a DNA glycosylase and the consequent removal of the base, creating an apurinic or apyrimidinic (AP) site intermediate, (ii) incision of the basic site by an AP endonuclease (APE) or AP lyase, (iii) removal of the remaining sugar fragment by a lyase or phosphodiesterase, (iv) filling of the remaining gap by a DNA polymerase

(commonly, DNA polymerase β, POLB) with the correct nucleotide, and finally (v) sealing of the remaining nick by a DNA ligase (LIG1 or LIG3/XRCC1 complex, Figure. 2.3).[9]

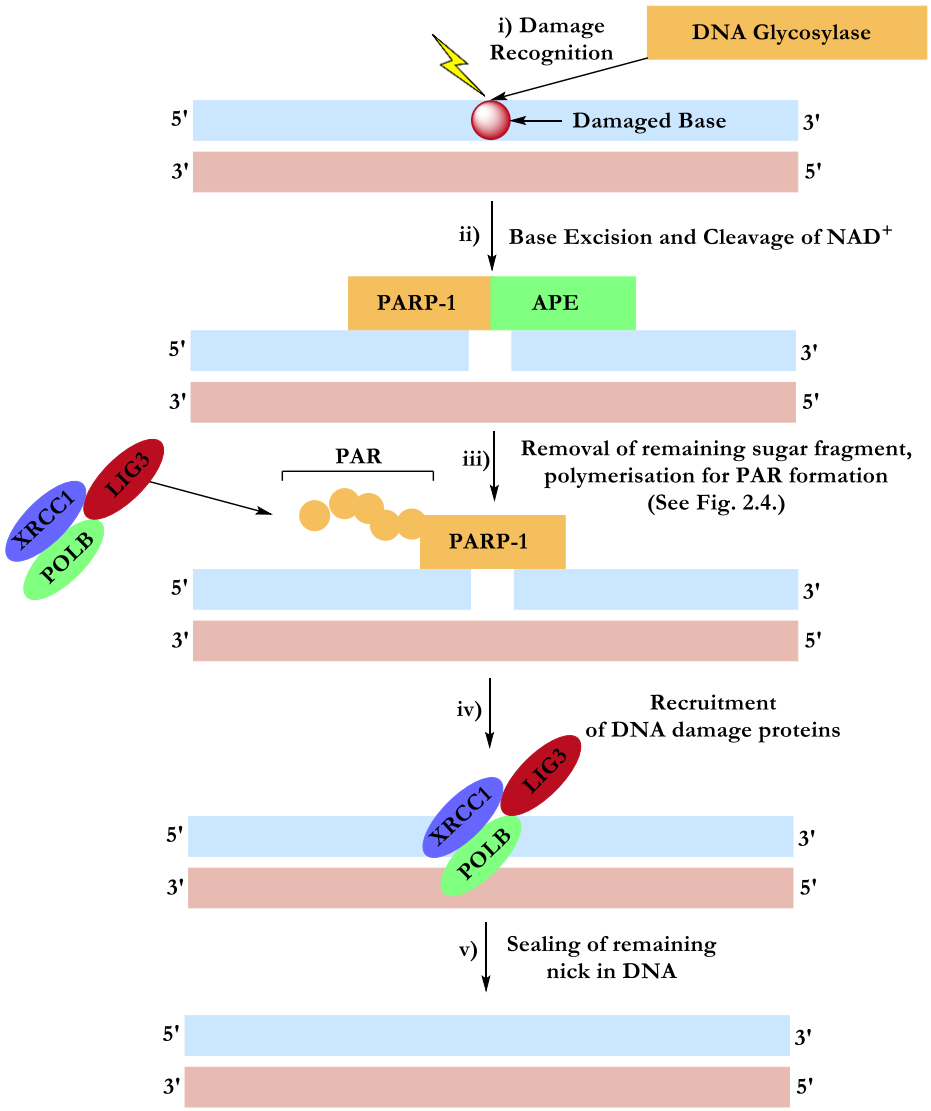

Figure 2.3. Base excision repair (BER); short patch single strand break (SSB) repair pathway

Of the sensors utilised in the BER of SSBs, poly(ADP-ribose) polymerase 1 (PARP-1) is particularly influential.[10,11] Upon binding to nicked DNA, PARP-1 cleaves nicotinamide adenine dinucleotide (NAD^+), at which point it catalyses the polymerisation of ADP-ribose units into long, branched chains of poly(ADP ribose) (PAR) (Figure 2.4).[12] While the chief target for poly(ADPribosylation) is PARP-1

itself, other DNA damage repair proteins and histones are also PARylated. PARP-1 is subsequently responsible for the recruitment of additional DDR proteins which cooperate for the completion of SSB repair.[13]

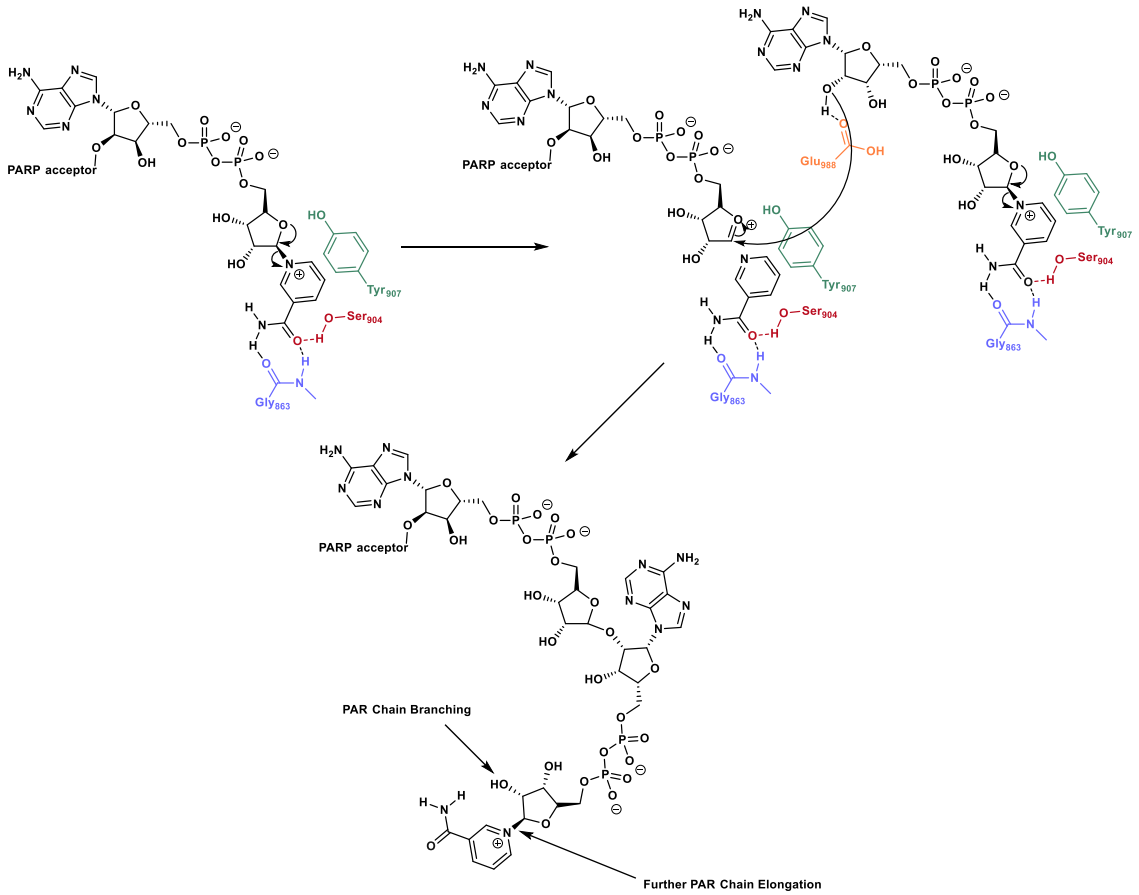

Figure 2.4. Mechanism of PARP catalysed poly(ADP-ribosyl)ation

2.2.2 Double-Strand Break Repair Mechanisms

Double-strand breaks are the most harmful form of DNA damage, since a single occurrence can lead to chromosomal translocation or cell death.[14] The repair of DSBs is executed by two main pathways: homologous recombination (HR) and non-homologous end joining (NHEJ, Figure. 2.5).[15] HR is initiated when ataxia telangiectasia mutated (ATM) kinase protein binds to a DSB, whereupon the DNA damage response process is triggered.[16] In the HR pathway, the MRN complex (Mre11, Rad50, Nbs1), replication protein A (RPA), Rad51, and BRCA1/2 make up

the most integral components. The MRN complex is responsible for the resection of 5'-3' ends upon DSB recognition which are then coated with RPA.[17] Recombination is performed by Rad51, which replaces RPA in a BRCA1/2-dependent manner to assemble presynaptic Rad51 filaments.[18] A displacement loop (D-Loop) containing the novel heteroduplex DNA is then formed via DNA strand exchange between the target DNA and the Rad51 filament. Lastly, the broken 3' end primes DNA synthesis using the duplex DNA as a template.[19]

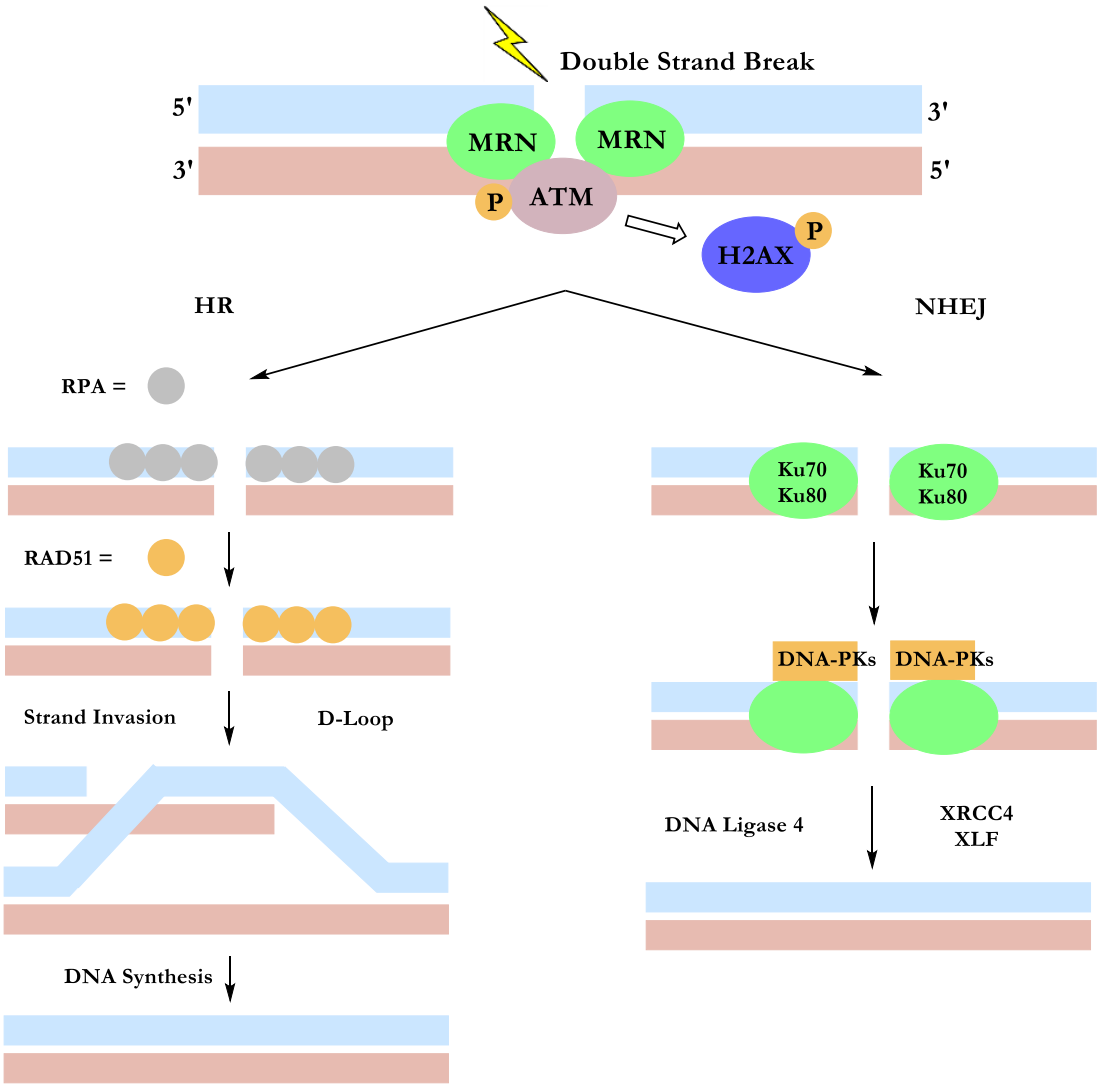

Figure 2.5. Schematic of HR and NHEJ pathways

NHEJ involves binding of the Ku70-Ku80 protein heterodimer to the DNA lesion, followed by the attachment of DNA dependent protein kinase catalytic subunit

(DNA-PKcs). The ensuing DNA-PK holoenzyme binds and phosphorylates the protein Artemis, which cleaves the single-stand overhangs of DNA. Lastly, a complex of proteins, including DNA ligase 4 (LIG4), XRCC4 and XLF, completes the process by joining the DNA ends.[20] As with HR, NHEJ is important for genomic integrity since alterations of the Ku complex or LIG4 can cause genome rearrangements.[21]

The level of control over both these processes (SSB repair and DSB repair) ultimately minimises genomic instability and impedes the formation of tumours.[22] Defects in this defensive mechanism have been found to occur with significantly higher prevalence in many human cancers compared to normal tissues.[23,24,25] As such, extensive DNA damage and DDR signalling is present and critically important in virtually all stages of tumour development.[26,27] Taken together, the ability to monitor and respond to DDR *in vivo* is crucial for those populations whom otherwise may possess deficiencies and/or mutations. One such example is populations bearing BRCA1 and BRCA2 mutations/deficiencies in which the likelihood of contracting breast and/or ovarian cancers is drastically enhanced. In response, several lines of research are currently being undertaken, one of which, is the development of PARP inhibitors for the treatment of those patients bearing a BRCA1/2 mutation.[28]

2.3 PARP Inhibitors and Synthetic Lethality

Small molecule inhibitors of PARP-1 can disrupt the BER repair pathway, leading to collapsed replication forks and ultimately DSBs upon replication.[29,30] By disrupting PARP catalytic activity, the formation of PAR polymers is prevented. Cancer cells with defects in HR have exhibited vastly increased sensitivity to PARP-1 inhibitors due to their high dependency on PARP.[31] In such cases, damaged DNA either persists unrepaired or is subjected to a more error prone DNA repair

mechanism.[32] This process ultimately leads to cell apoptosis (Scheme 2.6). Healthy cells can compensate for this inhibition of PARP by relying on other repair mechanism such as HR.[33]

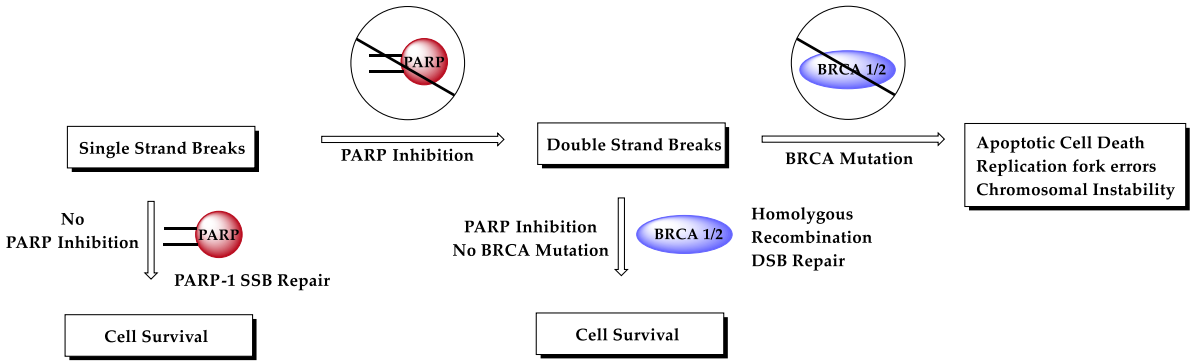

Figure 2.6. Synthetic lethality in the treatment of cancer cells

This type of targeting is known is synthetic lethality and provides scientists with a broader selection of therapeutic possibilities, to the point whereby chemotherapy and radiation can potentially be avoided (Figure 2.6)

2.4 PARP Inhibitors: Structural Development and Binding Modes

In the 1980s, nicotinamide and 3-aminobenzamide were shown to be inhibitors of PARP (IC_{50} 210 μM and 30 μM respectively) which provided the starting point for further optimisation.[34,35] By screening over 100 compounds from several structural classes, Ueda and Banasik discovered multiple bicyclic and tricyclic lactams with sub-micromolar levels of potency. This work refined those initial PARP-1 pharmacophores by demonstrating that fusing the arylamide to another ring could restrict the degrees of freedom for the amide moiety, thus locking it into a geometry beneficial for PARP-1 inhibitory potency.

Another family of scaffolds was developed in the early 1990s in the laboratories of Griffin and Golding. This consisted of, imidazole and benzoxazole

carboxamides in which the azole acts as an intramolecular hydrogen bond acceptor for the amide NH. This intramolecular hydrogen bond facilitated a "pseudoring", locking the primary amide in the geometry most beneficial for PARP-1 binding.[36]

The inherent potency of such a small core spawned multiple subseries of compounds from which several clinical candidates were derived.[37] The common feature of each of the inhibitors was a hydrogen bonding network between the amide functionality of the inhibitor core and Ser904 and Gly863 of PARP-1. This mimics the H-bonding network with which NAD^+ bind to PARP. Lactam based inhibitors such as isoquinolinone NU1025 (Figure. 2.7A) form three hydrogen bonds in the nicotinamide-subsite of the NAD^+ pocket, two from Gly863 and one from Ser904.

The necessity of this H-bonding network for the binding of inhibitors to PARP-1 rationalised both the improved potency observed with fused arylamides and the detrimental effect of substituents close to the amide pharmacophore on enzymatic potency. Other features of the nicotinamide pocket include the two aryl residues Tyr896 and Tyr907 forming a π-electron sandwich for the flat arylamide groups. This further enhanced the reasoning for the improvement in potency of arylamides versus saturated amides. The back wall of the nicotinamide subsite bordered by Ala898 and Lys903 formed a tight pocket just large enough for small substituents (e.g. CH_3, F, Cl) on the benzamide-containing ring (Figure. 2.8 A-ring). In some instances, Glu988 also formed a hydrogen bond with the inhibitor. This glutamate residue explains why heteroatoms in certain positions on the A-ring increase the potency of inhibitors. The last feature of the nicotinamide binding pocket is the large hydrophobic pocket adjacent to the nicotinamide binding site. This pocket is often referred to as the adenine ribose binding site (AD site),[38] and most series of PARP-1 inhibitors take

advantage of this spacious pocket to improve potency, solubility, and other pharmaceutical properties of the series. Figure 2.7B and Figure 2.7C illustrate the binding modes for two other PARP-1 inhibitors.[39,40]

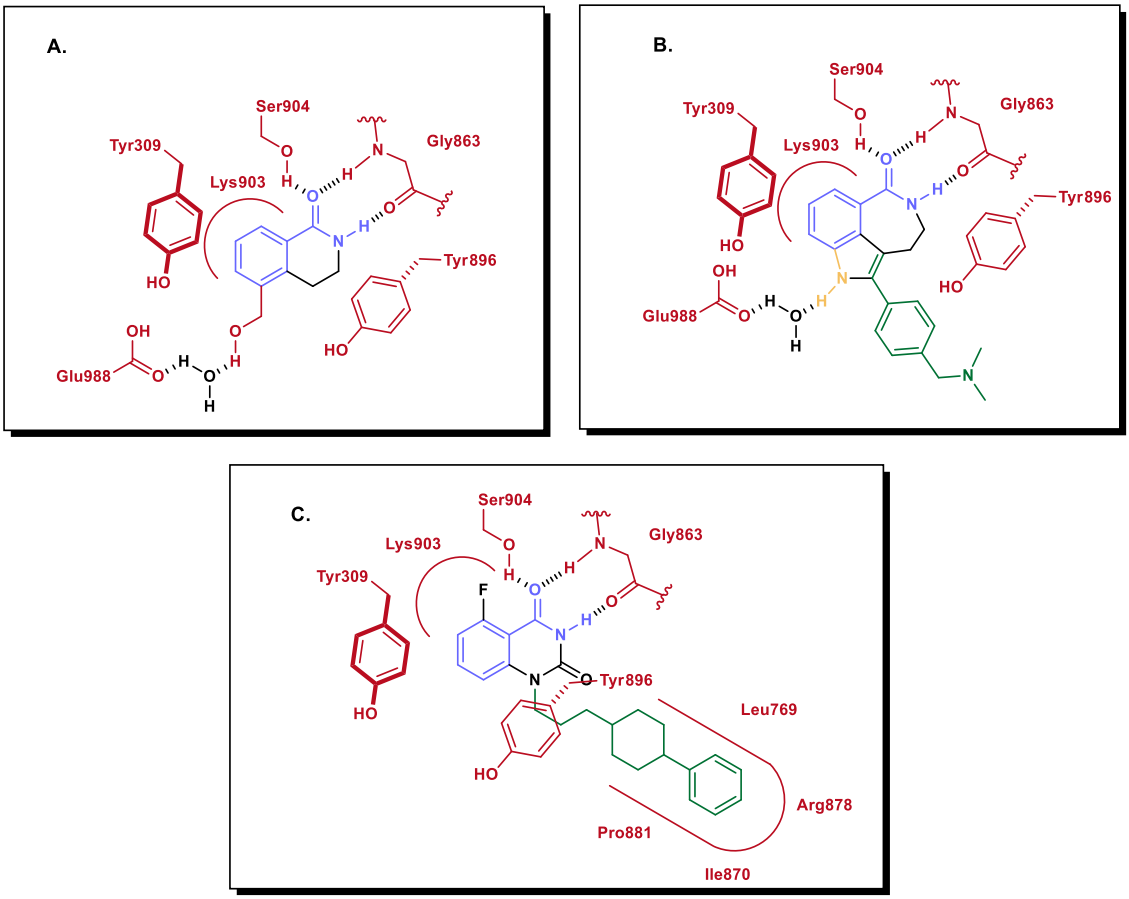

Figure 2.7. Binding modes of several PARP-1 inhibitors in the nicotinamide binding pocket: A) dihydroisoquinolinone; B) indolobenzazepine binding model; C) quinazolidione binding model.

Taking into account the aforementioned interactions and multiple X-ray co-crystal structures, the optimal PARP-1 pharmacophore is summarised in Figure 2.8. This should contain an amide moiety fused within a bicyclic ring system or "pseudo bicyclic ring" system as outlined in by rings A and B (Figure. 2.8). Furthermore, this pharmacophore should contain at least one of the following; (1) hydrogen bond donors and acceptors on the opposite side of the A-ring from the amide (purple, Figure 2.8); (2) small hydrophobic substituents on the A-ring, adjacent to the amide

(red, Figure 2.8); (3) large hydrophobic groups in the southeast portion of the pharmacophore (orange, Figure 2.8).[29]

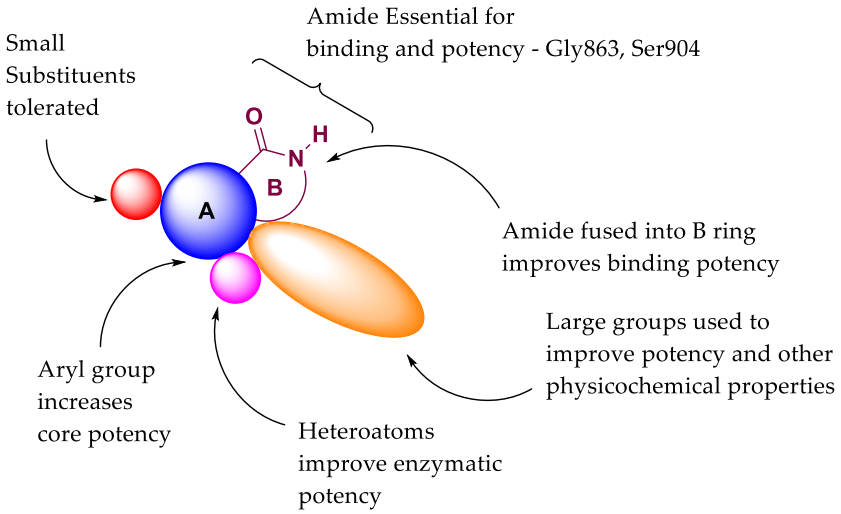

Figure 2.8. General structural overview and design of PARP inhibitors

It is all these structural investigations that have led to a wide variety of PARP inhibitors being developed for clinical investigation (Figure. 2.9).

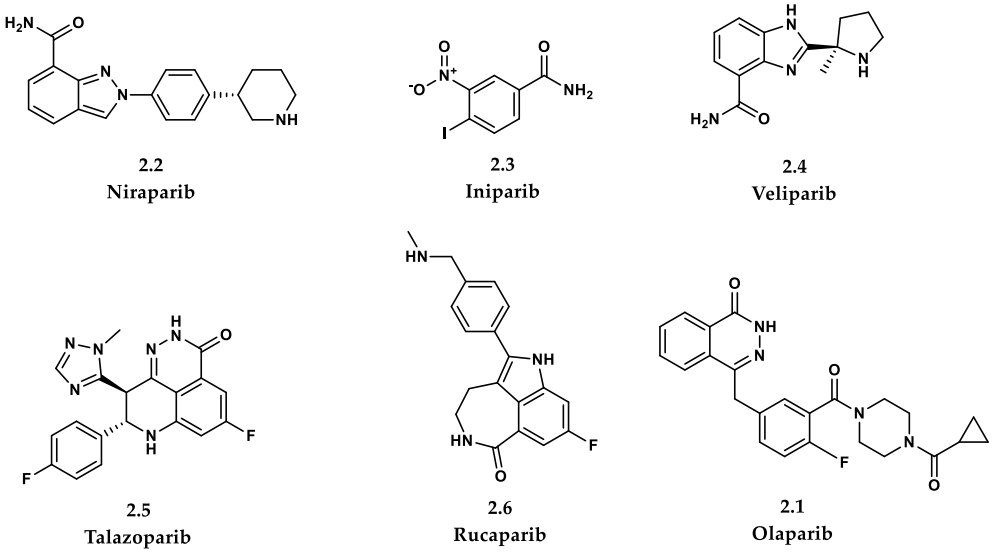

Figure 2.9. PARP inhibitors currently under clinical investigation

2.5 Olaparib

Of the PARP inhibitors currently under clinical investigation, the first clinically approved was olaparib (ku-0059436, AZ2281, Lynparza®). Initially investigated in the early 2000s by KuDOS/Maybridge, the two companies found promising results via high throughput screening. Following this, a range of bicyclic ring systems was narrowed down to a selection of phthalazinones from which initial optimisations resulted in good PARP-1 inhibitory potency but poor cellular activity (Figure 2.10).

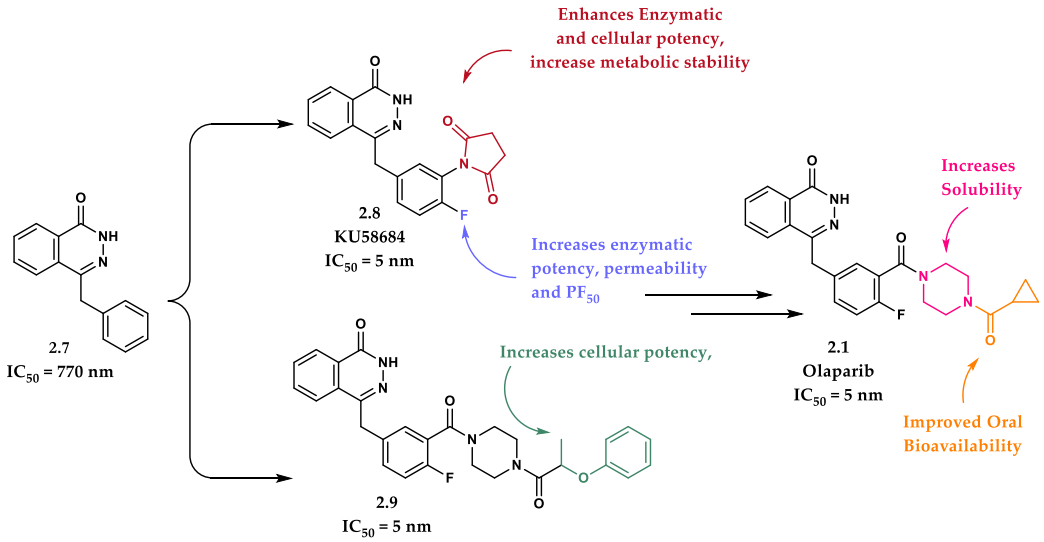

Figure 2.10. Evolution of olaparib: a) Initial high throughput screening hits b) Key preliminary optimisations c) Key structural features and properties of olaparib

Through optimisation of the benzyl substituted phthalazinones, KuDOS were able to find the desired balance between pharmacokinetics, cytotoxicity potentiation, metabolic stability and the ability to potentiate the toxicity of various anticancer chemotherapies *in vivo*. Ultimately, focusing efforts towards compounds that fit within 'druglike' parameters (MW < 500, PSA < 140 Å, rotatable bonds < 7, HBD and HBA <10, solubility of 0.1< mg/kg), KuDOS arrived at the structure now known as olaparib (Figure 2.10).

Well tolerated *in vivo*, olaparib advanced into clinical trials in 2005 with AstraZeneca acquiring KuDOS in 2006. The phase III results indicated that when dosed orally, olaparib was rapidly absorbed and eliminated but still inhibited PARP. Furthermore, it was found that for 1/3 of the patient population within this study whom were carriers of the BRCA mutation, much of this subgroup (≈ 60%) responded to treatment with olaparib. In December 2014, olaparib was approved for use as a single agent by the EMA and the FDA for germline BRCA mutated (gBRCAm) advanced ovarian cancer patients that had received three or more prior lines of chemotherapy. Later, in January 2018, olaparib became the first PARP inhibitor to be approved by the FDA for gBRCAm metastatic breast cancer. These approvals inspired the investigation of radiolabelled PARP inhibitors based on olaparib.

2.6 Resistance to PARP Inhibitors

Whilst significant strides have been made in the field of PARP inhibition for the treatment of cancer, resistance to PARP inhibitors, is common. It has been reported that 30% -70% of patients with mutations in areas of DDR do not respond to therapies including PARP inhibitors.[41] Resistance is often due to either low PARP enzyme expression, or the inability of the drug to penetrate tumour tissue, or part of the tumour tissue, due to increased interstitial pressure and desmoplasia. These factors are particularly relevant in pancreatic adenocarcinomas or an intact blood-brain-barrier, such as in the case of brain tumours or brain metastases. Increased expression of ATP binding cassette (ABC) drug efflux pumps may also prevent drug uptake in the tumour, most relevant for gastro-intestinal and pancreatic tumours.

Recently, several reports have suggested that accurately measuring and monitoring PARP expression *in vivo* may provide critical information regarding the state of disease,[42] as it has been found to independently correlate with worse outcomes in breast, ovarian, and other tumours.[43,44] Assessment of DDR signalling activation may also contribute to genotoxic treatment evaluation, following chemo- or radiotherapy. To date, PARP expression and BRCA status in tumours can be determined by immunohistochemistry or genetic sequencing on biopsy samples. However, many tumours however are known to be extremely heterogeneous due to their increased genomic instability. This heterogeneity is unnoticed when sampling tissue from a single biopsy site. Furthermore, acquisition of reliable and high-quality biopsies is significantly invasive and in many disease sites, such as lung, brain, or pancreas, these biopsies may be non-trivial.

2.7 PET and SPECT Imaging of PARP

A more advantageous prospect compared to invasive biopsies, is the use of PET or SPECT imaging agents. These imaging techniques have excellent sensitivity in comparison to other clinical imaging modalities and are routinely used for *in vivo* tracking of biomolecular processes.[45] The principal advantages of *in vivo* imaging of DDR over conventional tissue biopsies are: (1) the ability to analyse larger tissue volumes compared with a small, potentially unrepresentative sample, (2) an improved insight into tumour heterogeneity, (3) the lack of need for an invasive operation to access the area of interest, which removes the risk of serious complications related to infection, haemorrhaging etc., and (4) the option to perform repeated imaging of the same area which would allow longitudinal assessment.

Due to the well-established role of PARP-1 as a mediator in the repair of DNA SSBs, it represents an attractive biomarker for PET and SPECT imaging. Over the last decade, there have been several attempts to develop radiolabelled imaging agents that permit visualisation of this DDR protein. Amongst those markers available for imaging, radiolabelled PARP inhibitors occupy a prominent place.

2.7.1 Radiolabelled Derivatives of Olaparib

2.7.1.1 [^{18}F]Olaparib Derivatives

In 2011, Weissleder and co-workers, *via* an inverse electron demand Diels-Alder reaction, reported access to [^{18}F]bioorthogonally-labelled olaparib ([^{18}F]BO, **[^{18}F]2.12**), a molecule which deviates significantly from that of the parent molecule olaparib (Scheme 2.1).[46] This structural deviation means **[^{18}F]2.12** exhibits a poorer IC_{50} compared to olaparib (Table 2.1).

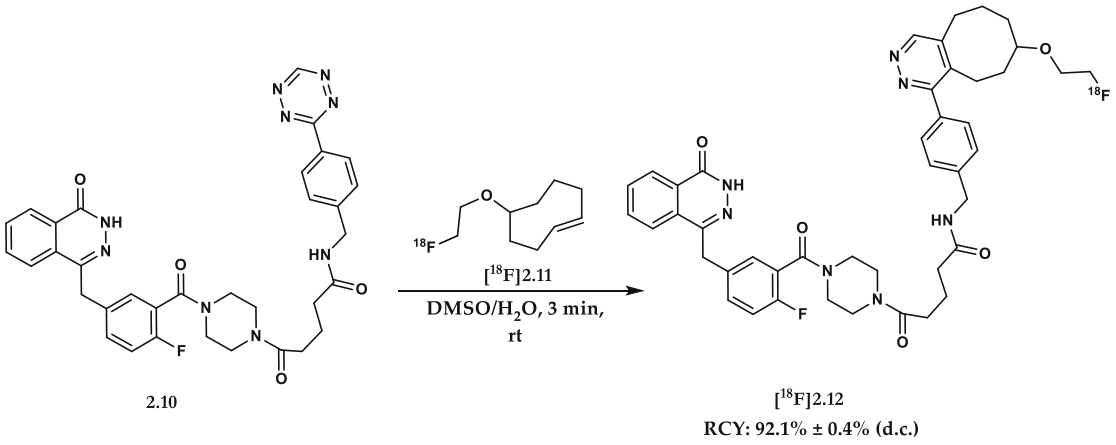

Scheme 2.1. Preparation of [^{18}F]BO **[^{18}F]2.12** via an inverse electron demand Diels Alder

More recently, [^{18}F]PARPi-FL **[^{18}F]2.13**, and [^{18}F]PARPi **[^{18}F]2.18** (Scheme 2.2, 2.3), the latter exhibiting greater structural similarity to olaparib, have been used to successfully measure uptake and distribution of PARP *in vivo*.[47,48] Finally, in 2018, the

groups of Sutherland and Pimlott reported the radiosynthesis of **[^{18}F]2.20** via displacement of the chloro-precursor **2.19** (Scheme 2.4).[49]

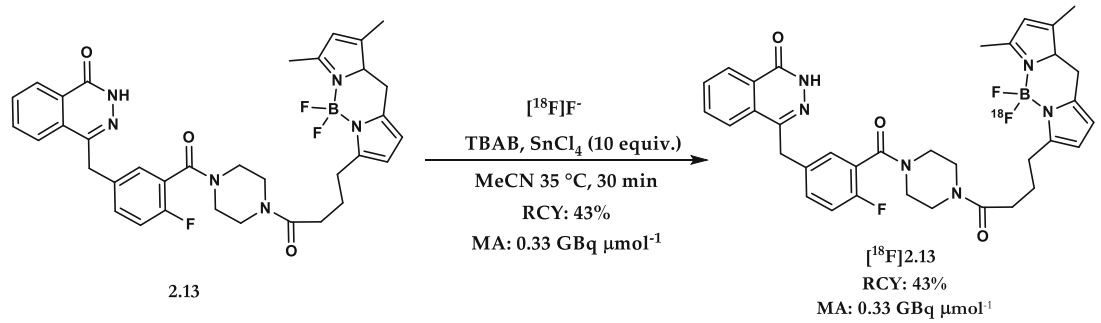

Scheme 2.2. Labelling of [^{18}F]PARPi-FL **[^{18}F]2.13** via isotopic exchange

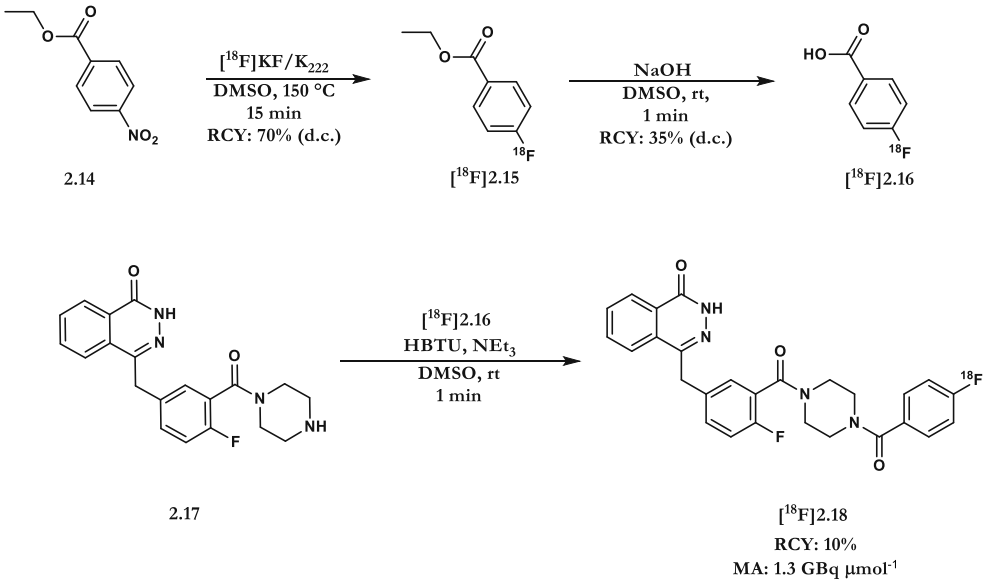

Scheme 2.3. Preparation of [^{18}F]PARPi **[^{18}F]2.18** via S_NAr

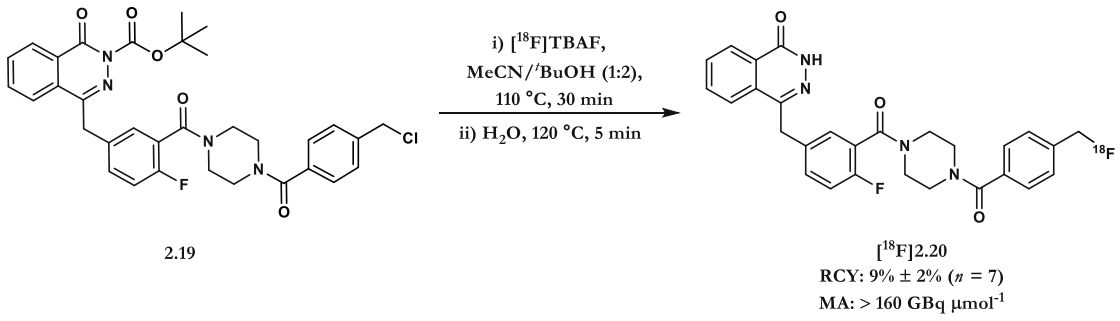

Scheme 2.4. Preparation of **[^{18}F]2.20** via S_N2

Compound	IC_{50}*	LogP
Olaparib **2.1**	5 nM	0.8
[^{18}F]BO **[^{18}F]2.12**	18 nM	-
[^{18}F]PARPi-FL **[^{18}F]2.13**	12 nM	2.9
[^{18}F]PARPi **[^{18}F]2.18**	2.8 nM	1.8
[^{18}F]2.20	2.0 nM	2.51

Table 2.1. IC_{50} and LogP of: Olaparib **2.1**, [^{18}F]BO **[^{18}F]2.12**, [^{18}F]PARPi-FL **[^{18}F]2.13**, [^{18}F]PARPi **[^{18}F]2.18** and **[^{18}F]2.20** *Cell free assay values

2.7.1.2 ^{11}C-Labeled Olaparib

In 2015, Skrydstrup and co-workers, via a three component ^{11}C-carbonylation of aryl palladium species, reported a method to access a carbon-11 labelled isotopologue of olaparib, [^{11}C]olaparib **[^{11}C]2.1**.[50] In this instance, Skrydstrup was successfully able to isolate the oxidative addition species **2.21/2.22** and therefore avoid what was thought to otherwise be the most challenging step within the catalytic cycle (Scheme 2.5).

Preliminary efforts by Skrydstrup and co-workers used the ligand, Xantphos, to generate the stable species **2.21**. When subject to the standard ^{11}C-carbonylation conditions, no product formation was observed. Therefore, in order to access [^{11}C]olaparib **[^{11}C]2.1** however, a compromise with regards to the stability of the precursor had in be made. Whilst the use of *t*Bu ligands to generate species **2.22** proved effective for the subsequent ^{11}C-carbonylation, **2.22** was noted as being unstable under ambient atmosphere and therefore prohibitive for translation towards pre-clinical/clinical studies (Scheme 2.6).

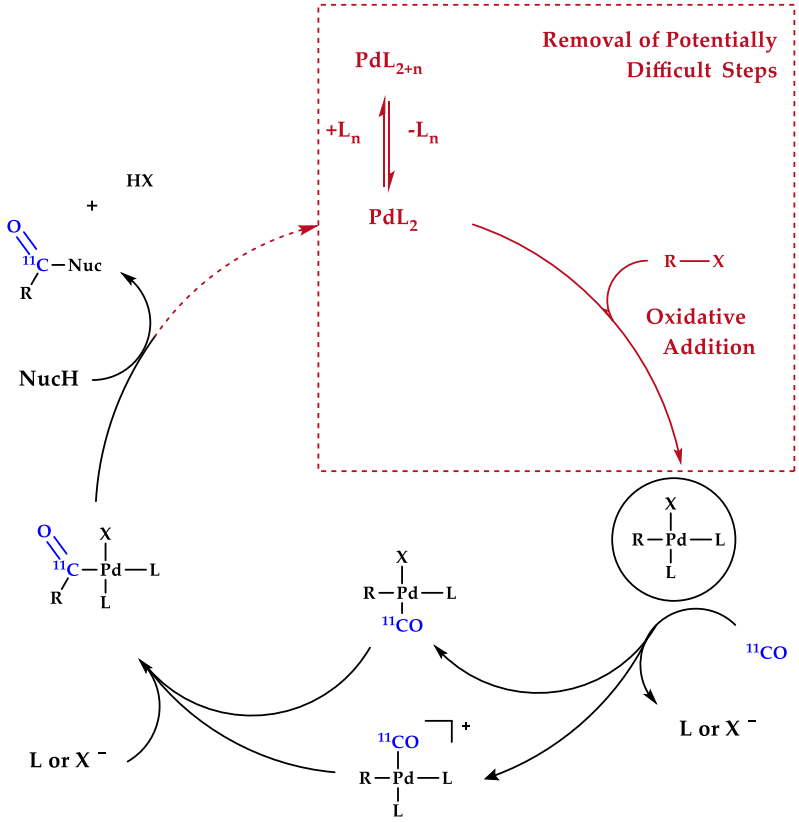

Scheme 2.5. ^{11}C-Carbonylation of preformed aryl palladium complexes

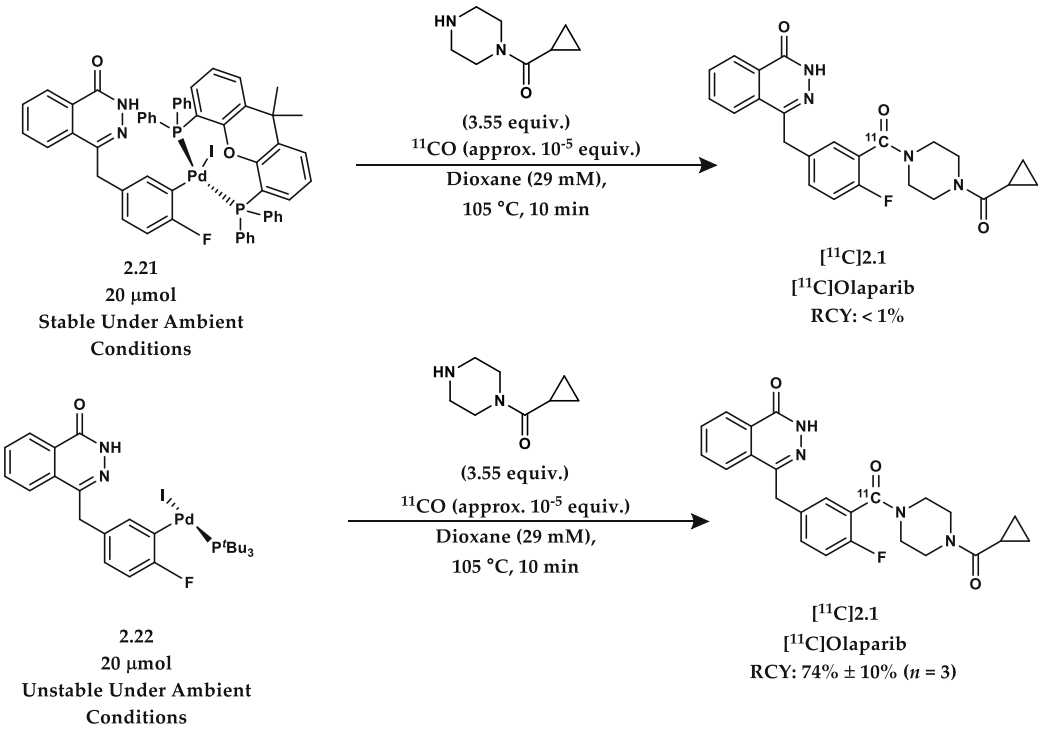

Scheme 2.6. Preparation of [^{11}C]olaparib **[^{11}C]2.1**

2.8 ^{18}F-Labelled Isotopologue of Olaparib

As shown so far, a wide variety of radiolabeled PARP inhibitors based on olaparib have been developed. Of those works described in the literature, only the work of Skrydstrup and co-workers offers a direct path to an isotopologue of the parent compound, olaparib **2.1**, albeit with the short-lived radioisotope carbon-11. Given the improved flexibility that fluorine-18 offers over carbon-11, development of a strategy that would allow for access to [^{18}F]olaparib **[^{18}F]2.1** was of significant interest. As an isotopologue of the unlabelled drug, [^{18}F]olaparib would benefit from the wealth of clinical data already available which would further aid in its translation to the clinic. In addition, [^{18}F]olaparib would allow direct imaging of the delivery of olaparib to tumour tissues, and could therefore act as a direct companion imaging biomarker for patient stratification.

2.8.1 Project Aim: Application of Novel ^{18}F-Fluorination Methodology

Considering the precedent in the literature, it was clear that the synthesis of an ^{18}F-labelled isotopologue of olaparib would be non-trivial. To justify such an investigation, several requirements would have to be met. Firstly, the precursor must be bench stable and readily accessible using 'facile' transformations. This precursor should allow direct access to the ^{18}F-labelled isotopologue, with a maximum of one post-labelling transformation. The procedure must make use of non-carrier added ^{18}F-fluoride and be amenable to automation. In addition, the radiolabelled product should be accessed in high yields and in high molar activities. Finally, [^{18}F]olaparib must be shown to be a suitable tracer for the imaging of DNA damage (Figure 2.11).

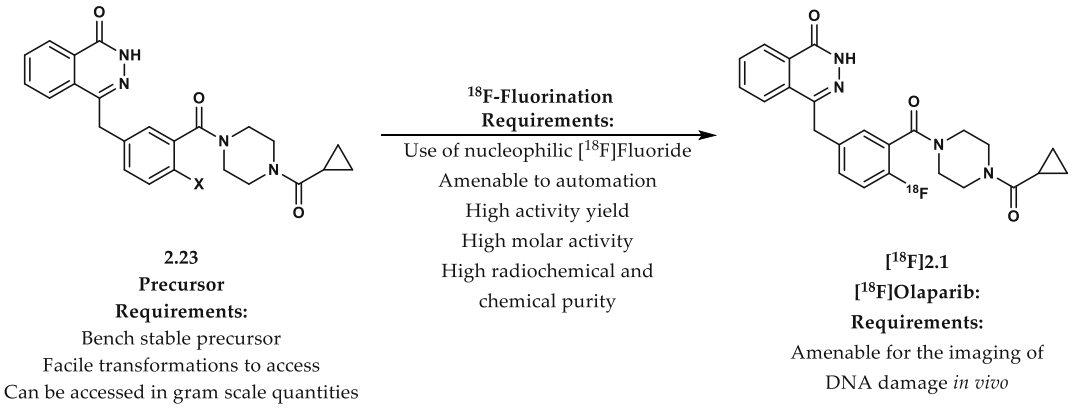

Figure 2.11. Project requirements for the ^{18}F-fluorination towards [^{18}F]olaparib

2.8.2 Selection of Methodology

In light of these requirements (Figure 2.11), the choice of methodology used to access [^{18}F]olaparib was seen as crucial to the success of the project. Gouverneur and co-workers had recently reported the de-risking of the copper mediated nucleophilic ^{18}F-fluorination of aryl pinacol boronic esters (See Chapter I, Section 1.7.2).[51] In this work, Gouverneur described how one could determine whether a given target would likely be compatible with the methodology before significant time had been invested into precursor synthesis. As such, it was proposed that this investigation be applied to olaparib in order to probe the feasibility of the copper mediated ^{18}F-fluorination of aryl pinacol boronic esters in a radiosynthesis of [^{18}F]olaparib **[^{18}F]2.1** (Figure 2.12).

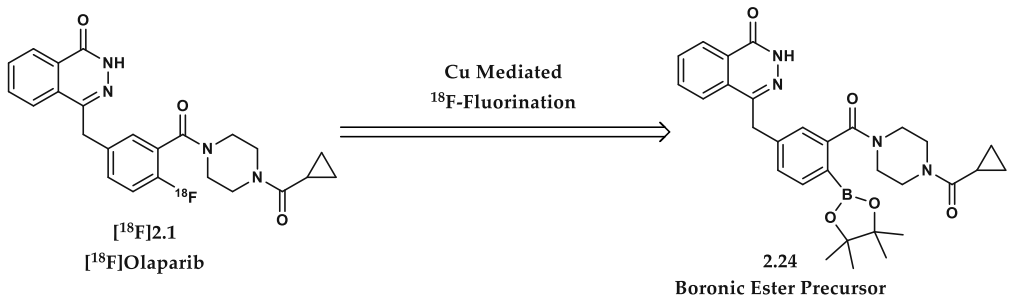

Figure 2.12. Retro-radiosynthesis for [^{18}F]olaparib **[^{18}F]2.1**

2.8.3 Screening Experiments: Olaparib

The first steps described by Gouverneur and co-workers involved an additive screening experiment. Based on the work of Collins and Glorius,[52] Gouverneur and co-workers proposed that, should one possess the ^{19}F-target in question, an additive screening experiment using a model reaction of known RCC/RCY should be enough to validate a targets level of compatibility.

In this instance, the ^{18}F-fluorination of boronic ester **2.25** with $[^{18}F]KF/K_{222}$ (20 – 30 MBq) and $Cu(OTf)_2(py)_4$ (0.0053 mmol) in DMF (300 μL) served as the benchmark reaction, with a reported RCC of 35% ± 14% without any additive.[51] Repeating the reaction in the presence of one equivalent of olaparib resulted in a radiochemical conversion of 0% was observed, possibly to due to competing Chan-Lam pathways (Scheme 2.7).

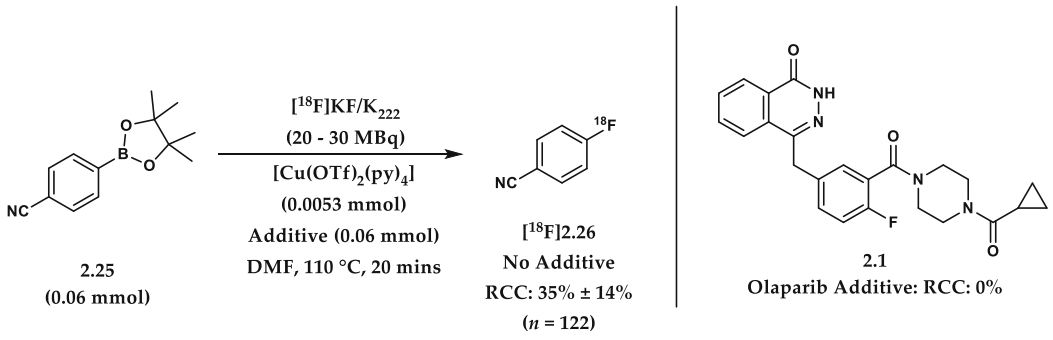

Scheme 2.7. Spiking experiment with olaparib **2.1**

2.8.4 Spiking Experiments: Protecting Group Studies

Since the NH phthalazinone of olaparib was thought to be problematic, a range of *N*-protected phthalazinone was synthesised. Again, the RCC of **[^{18}F]2.25** was determined in the presence of one equivalent of each. In the preliminary screening process, unprotected **2.27**, methylated **2.28** and Boc protected **2.29**

phthalazinones were examined (Scheme 2.8). Both unprotected **2.27** and Boc protected **2.29** proved incompatible with the labelling reaction. In the latter case, this was likely due to the *in-situ* cleavage of the Boc group liberating the incompatible amide group.

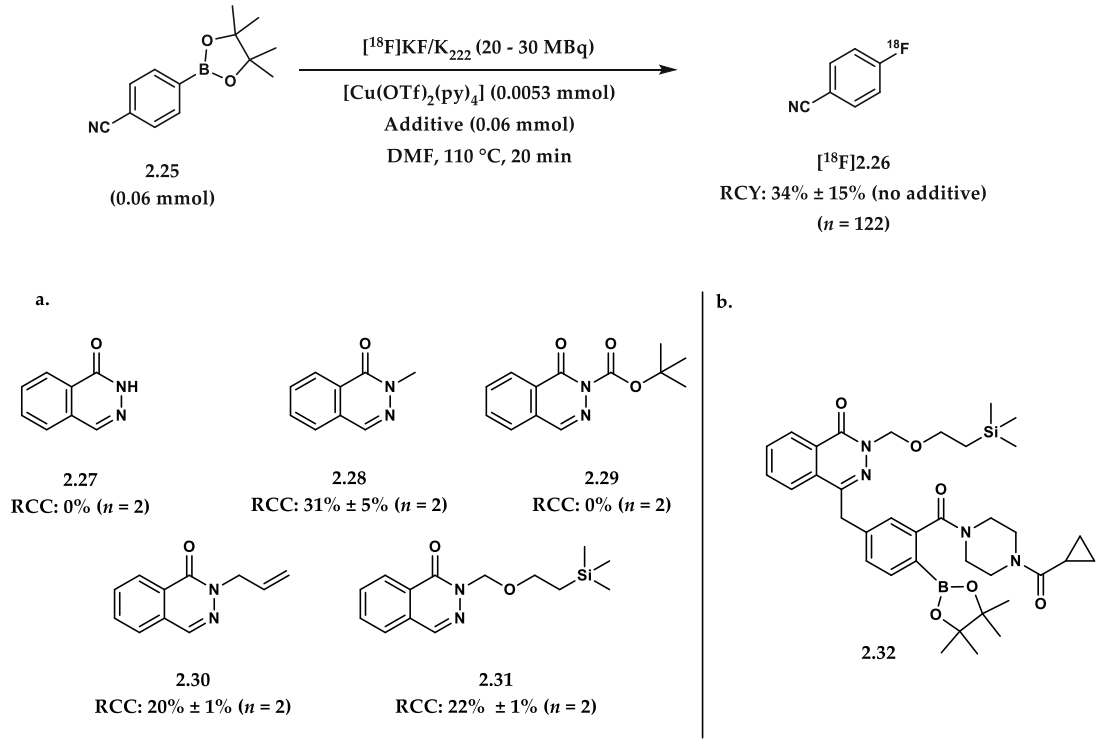

Scheme 2.8. A) Additive experiments for the ^{18}F-fluorination of **2.25** B) Optimal protected boronic ester precursor **2.32** based on additive experiments

The high compatibility of the methylated phthalazinone **2.28**, confirmed that the NH was the source of incompatibility and led to a further examination of more easily cleavable methylene based protecting groups. Both allyl-protected phthalazinone **2.30** and 2-(trimethylsilyl)ethoxymethyl acetal (SEM) **2.31** proved compatible with only minor reductions in radiochemical conversion (Scheme 2.8). Given the range of conditions known for cleavage of the SEM group, it was decided that this would serve as a suitable protecting group for the radiosynthesis of

[^{18}F]olaparib. This decision served as a guide for the synthesis of precursor **2.32** and corresponding ^{19}F-containing references.

An important point to note at this stage is that when spiking the ^{18}F-fluorodeboronation reaction of **2.25** in the presence of **2.31**, no significant loss of activity was observed. This indicated that the formation of the volatile trimethylsilyl [^{18}F]fluoride, a product of deprotection, was not occurring.

2.8.5 ^{19}F-Olaparib Reference

Having identified a precursor likely to be compatible for the copper mediated ^{18}F-fluorodeboronation reaction, the next step was to synthesise the corresponding protected references. Within radiochemistry, radiolabelled products are typically identified by the matching of HPLC retention of the ^{18}F-containing compound and the corresponding ^{19}F-containing reference. To this end, the synthesis of **2.33** was required prior to labelling studies (Figure 2.13).

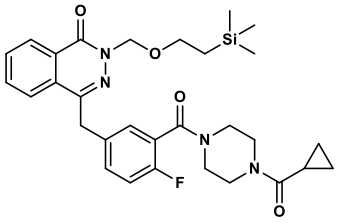

2.33

Figure 2.13. ^{19}F *N*-SEM protected reference **2.33**

Upon isolation of phosphonate **2.35** *via* the reaction of 2-carboxylbenzaldehyde and dimethylphosphite, subsequent coupling to 2-fluoro-5-formyl-benzonitrile *via* a Horner-Wadsworth-Emmons reaction afforded **2.36** in 92% yield with an isomeric ratio of 1.5:1. Without further purification, the mixture of isomers were subjected to hydrolysis with (9M) NaOH. After stirring at 90 °C for 4

hours, hydrazine monohydrate to form phthalazone **2.37**. Activation of the carboxylic acid group of **2.37** using HBTU enabled the subsequent coupling to 1-(cyclopropylcarbonyl)-piperazine afforded **2.1** in 72% yield. Finally, deprotonation using sodium hydride, followed by addition of 2-(trimethylsilyl)ethoxy methyl chloride furnished the corresponding, protected ^{19}F reference **2.33** as an inseparable mixture with regioisomer **2.38** (57:43) (Scheme 2.9). This observation was confirmed with ^{13}C-NMR spectroscopy by the characteristic shift at 94.2 ppm for the *O*-isomer **2.38** compared to a shift at 67.3 ppm for the *N*-isomer **2.33** (Figure. 2.14).

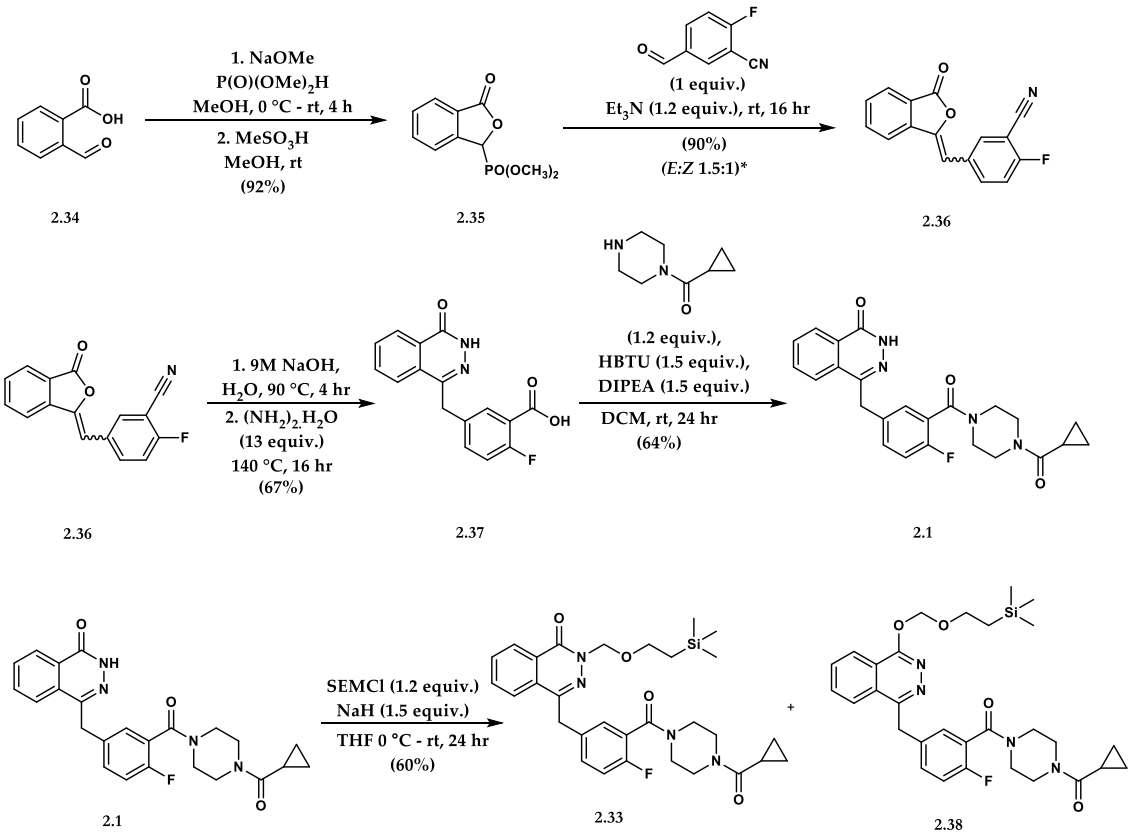

Scheme 2.9. Synthesis of ^{19}F references **2.1** and **2.33** **E:Z* ratio assigned arbitrarily using ^{1}H NMR Spectroscopy

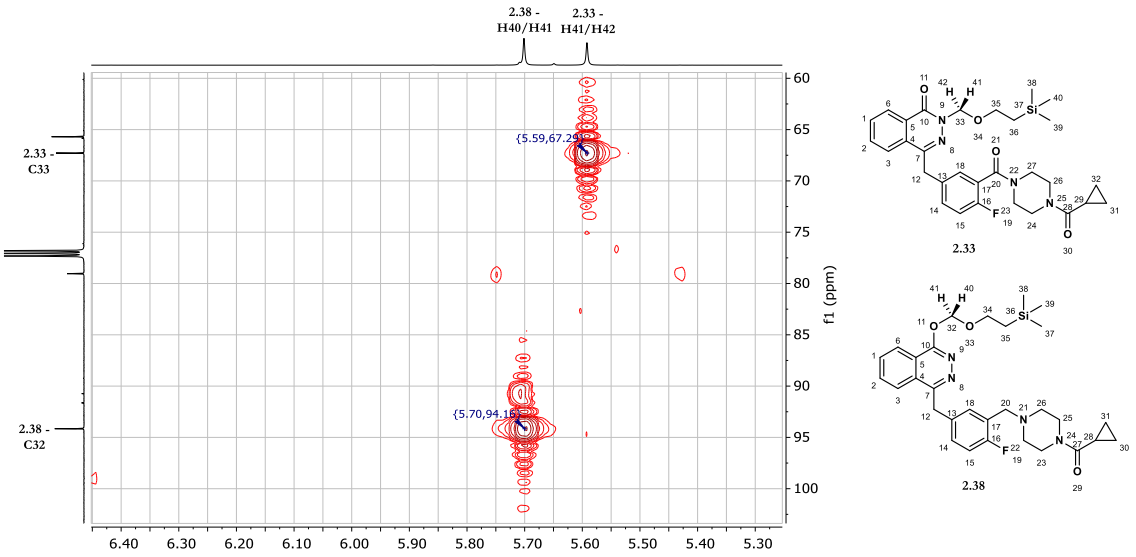

Figure 2.14. HSQC of **2.33** and **2.38**

2.8.6 [^{18}F]Olaparib Precursor Synthesis: Model Screening

Given previous works undertaken within the group for the synthesis of boronic ester precursors,[53] it was anticipated that a late stage borylation may prove the most optimal strategy to access boronic pinacol ester **2.32**. To this end, both brominated **2.39** and iodinated **2.40** model compounds were synthesised *via* the coupling of the corresponding benzoic acids and 1-(cyclopropylcarbonyl)piperazine. Subsequently, **2.39** and **2.40** were subject to a range of known conditions to access boronic pinacol ester **2.41**. Under conditions described by Miyaura for the palladium catalysed borylation of aryl halides,[54] rapid reduction to the protonated compound **2.42** was observed (Table 2.2, Entries 1 – 4). When subjected to lithium halogen exchange followed by quenching with ^{i}PrOBpin, a complex mixture was detected with degradation of the starting material observed. Whilst the brominated model **2.42** offered superior conversion to that of iodinated model **2.41**, significant levels of protodeboronation still took place.

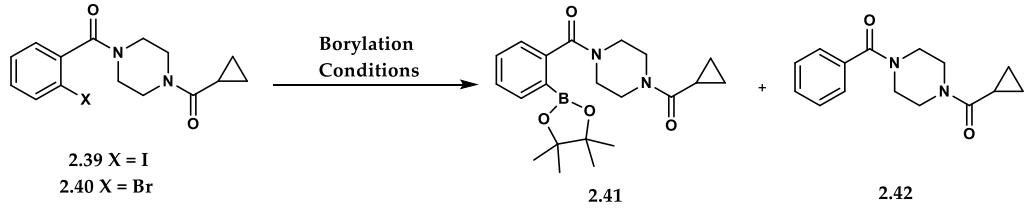

2.39 X = I
2.40 X = Br

2.41

2.42

Entry	X	Conditions	Conversion/Ratio (2.43:2.44)[a]
1	I	$Pd(dppf)Cl_2$ (3 mol%), B_2pin_2 (2.2 equiv.), KOAc (3 equiv.), DMF, 80 °C, 16 hr	100%/0:100
2	I	$Pd(dppf)Cl_2$ (3 mol%), B_2pin_2 (2.2 equiv.), KOAc (3 equiv.), PhMe, 120 °C, 16 hr	100%/0:100
3	I	$Pd(dppf)Cl_2$ (3 mol%), B_2pin_2 (2.2 equiv.), KOAc (3 equiv.), 1,4-Dioxane, 80 °C, 16 hr	100%/0:100
4	I	$Pd(dppf)Cl_2$ (3 mol%), B_2pin_2 (2.2 equiv.), KOAc (3 equiv.), DMF, 80 °C, 10 mins	100%/0:100
5	I	1. *n*-BuLi (1.1 equiv.), THF, -78 °C, 30 mins, 2. ^{i}PrOBpin (1.4 equiv.)	100%/Decomposition
6	I	1. *n*-BuLi (1.1 equiv.), THF, -78 °C, 30 mins, ^{i}PrOBpin (1.4 equiv.) *(in situ)*	0%/NA
7	Br	$Pd(dppf)Cl_2$ (3 mol%), B_2pin_2 (2.2 equiv.), KOAc (3 equiv.), DMF, 80 °C, 16 hr	100%/50:50
8	Br	$Pd(dppf)Cl_2$ (3 mol%), B_2pin_2 (2.2 equiv.), KOAc (3 equiv.), PhMe, 120 °C, 16 hr	100%/0:100
9	Br	1. *n*-BuLi (1.1 equiv.), THF, -78 °C, 30 mins, 2. ^{i}PrOBpin (1.4 equiv.)	0%/NA
10	Br	1. *n*-BuLi (1.1 equiv.), THF, -78 °C, 30 mins, ^{i}PrOBpin (1.4 equiv.) *(in situ)*	0%/NA

Table 2.2. Screening reactions for the borylation of **2.39** or **2.40** [a]Determined by ^{1}H NMR Spectroscopy

To probe the influence of the side chain upon the reaction, both **2.43** and **2.46** were synthesised and subjected to the most optimal conditions described previously (Table 2.2). Whilst full conversion was observed in both cases, significant quantities of the protonated products **2.44** and **2.48** were observed (Table 2.10, 2.12). With this information in hand, it was proposed that the less hindered *ortho*-methyl ester **2.49**

would offer greater compatibility. Taking the most optimal conditions for the borylation of **2.40**, full conversion to the desired product **2.50** was observed (Scheme 2.12).

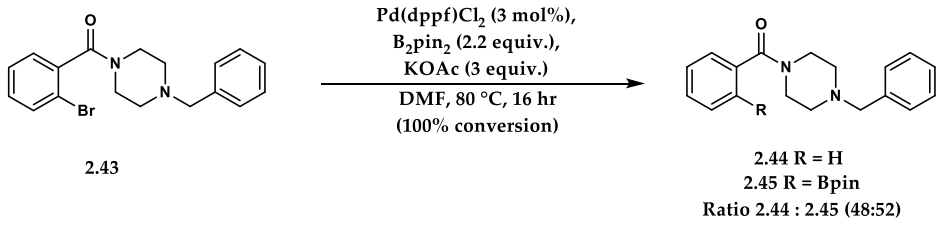

Scheme 2.10. Borylation of **2.43** [a] Determined by ^{1}H NMR Spectroscopy [a]

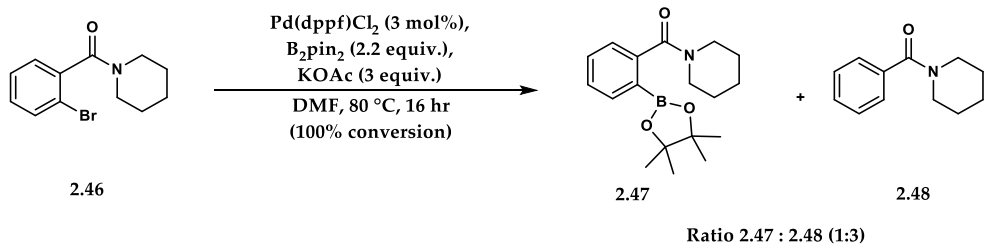

Scheme 2.11. Miyaura-Borylation of **2.46** [a]Determined by ^{1}H NMR Spectroscopy [b]

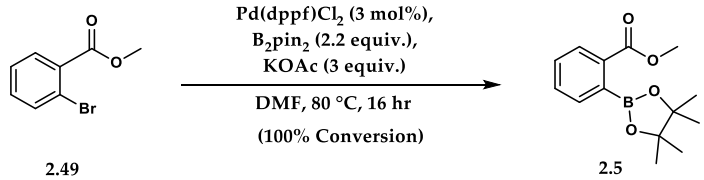

Scheme 2.12. Miyaura-Borylation of **2.49**[c]

2.8.7 Bpin-Olaparib Retrosynthetic Analysis

Having established an optimal precursor for the installation of the aryl pinacol boronic ester, a retrosynthetic analysis was carried out. This would follow a strategy

[a] ^{1}H NMR Spectroscopy of **2.44** confirmed with literature: M. Zhu, K.-I. Fujita, R. Yamaguchi, *J. Org. Chem.,* 2012, **77**, 9102.
[b] ^{1}H Spectroscopy NMR of **2.48** confirmed with literature: Y. Liu, S. Shi, M. Achtenhagen, R. Liu, M. Szostak, *Org. Lett.,* 2017, **19**, 1614.
[c] Confirmed by ^{1}H NMR Spectroscopy of commercially available pinacol boronic ester (CAS: 653589-95-8)

analogous to that taken for the synthesis of the fluorinated reference **2.33**. However, two points of note stood out: 1) the need to prepare 2-bromo-5-formyl-benzonitrile **2.57** in multi-gram quantities and 2) the need to carry out protections on both acid and phthalazinone moieties prior to the 'early-stage' borylation (Scheme 2.13).

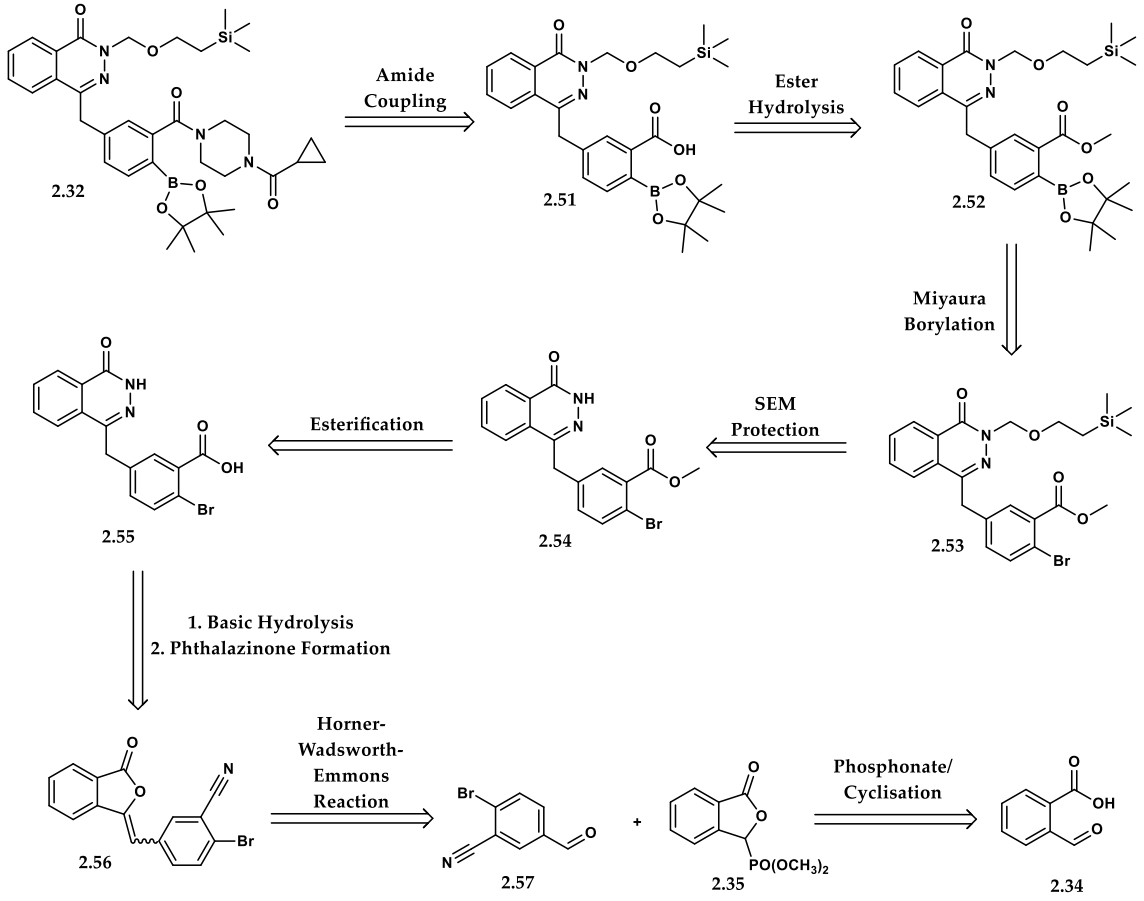

Scheme 2.13. Retrosynthetic analysis for the synthesis of aryl boronic pinacol ester **2.32**

2.8.8 Bpin-Olaparib Synthesis

Following the strategy described for the synthesis of reference **2.33**, early efforts focused on the synthesis of aldehyde **2.57**. Given the electron withdrawing cyano- and aldehyde groups found at *ortho/para* substitutions respectively, nucleophilic aromatic substitution (S_NAr) of the commercially available aryl fluoride

2.58 was pursued. Even under the harshest conditions however, no conversion was observed with only starting material recovered (Table 2.5).

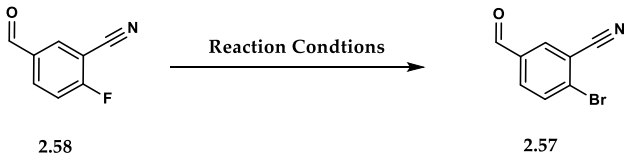

2.58 2.57

Reaction N°	Conditions	Conversion (%)
1	LiBr (5 equiv.), DMF, 110 °C, 48 hrs	0%
2	LiBr (5 equiv.), DMSO, 130 °C, 48 hrs	0%
3	LiBr (5 equiv.), NMP, 180 °C, 48 hrs	0%

Table 2.5. Screening reactions for the S_NAr of **2.58**

Taking an alternative approach, in 2013, Sun and co-workers described the cyano- directed *ortho* halogenation of arenes using $Pd(OAc)_2$ and *p*-toluenesulfonic acid (PTSA) in DCE with either NCS, NBS or NIS as the electrophilic source of halogen (Scheme 2.14).[55] Whilst trace amounts of conversion of starting material **2.63** was observed (Table 2.6), numerous regioisomers were detected within the ^1H NMR spectrum. This observation rendered this approach impractical to scale-up and was abandoned.

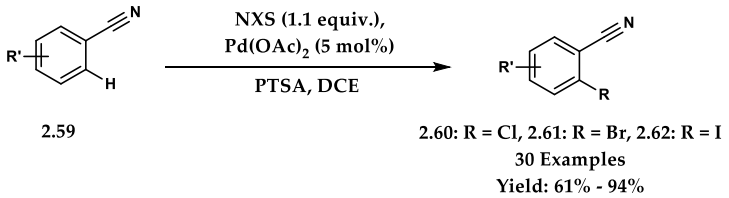

2.59

2.60: R = Cl, 2.61: R = Br, 2.62: R = I
30 Examples
Yield: 61% - 94%

Scheme 2.14. Palladium-Catalyzed *ortho*-Halogenation (I, Br, Cl) of Aryl-nitriles via sp^2 C–H Bond Activation Using Cyano as Directing Group

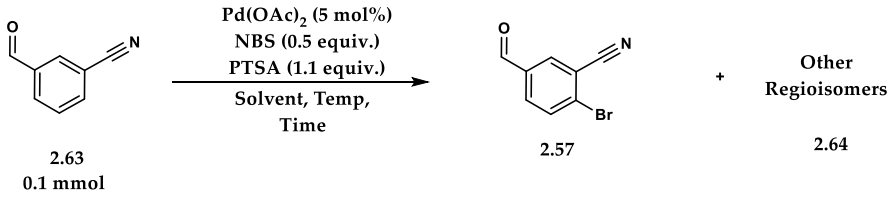

Entry	Conditions	Conversion (%) (Ratio 2.63+2.57+2.64)[a]
1	DCE, rt, 16 hr	0%
2	DCE, 40 °C, 8 hr	0%
3	DCE, 40 °C, 16 hr	5% (1:1.4)
4	DCE, 70 °C, 2 hr	0%
5	DCE, 70 °C, 16 hr	7% (1:1.4)

Table 2.6. Screening reactions for the C-H bromination of **2.63** [a] Determined by ^{1}H NMR Spectroscopy

With no viable route to aldehyde **2.57** in a single step, a multi-step approach was devised. By subjecting **2.65** to lithium halogen exchange with *n*-BuLi (1.1 equiv.) followed by quenching with DMF, aldehyde **2.66** could be obtained in 57% conversion (Table 2.7, Entry 1). Increasing the amount of *n*-BuLi led to 63% conversion (Entry 2). Increasing the reaction time led to the formation of the protonated by-product **2.67** (Entry 3). Further screening of temperature, solvent and base led to no improvement. When scaled up to 5 mmol, **2.66** was isolated in 71% yield (Table 2.7). Subsequently, by exposing **2.66** to conventional Sandmeyer conditions, aldehyde **2.57** could be isolated in 64% (Scheme 2.13). Importantly, this reaction was scalable, with over 16 grams (80 mmol) of **2.71** being isolated in a single run.

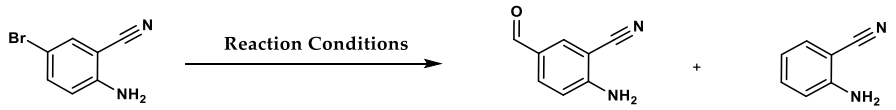

2.65
0.01 mmol

2.66

2.67

Entry	Conditions	Ratio **2.65 : 2.66 : 2.67**[a]
1	*n*-BuLi (1.1 eq.), THF, - 78 °C, 1 hr, DMF (1.4 eq.)	1: 1.3: 0
2	***n*-BuLi (2.2 eq.), THF, - 78 °C, 1 hr, DMF (2.5 eq.)**	**1: 1.7: 0**
3	*n*-BuLi (1.1 eq.), THF, - 78 °C, 4 hr, DMF (1.4 eq.)	1: 0.2: 0.9
4	*n*-BuLi (1.1 eq.), Et_2O, - 78 °C, 1 hr, DMF (1.4 eq.)	1: 0: 0
5	*n*-BuLi (1.1 eq.), THF, - 40 °C, 1 hr, DMF (1.4 eq.)	1: 2.3: 1.6
6	*n*-BuLi (1.1 eq.), THF, - 78 °C, 10 min, DMF (1.4 eq.)	1: 1: 0
7	*t*-BuLi (1.1 eq.), THF, - 78 °C, 1hr, DMF (1.4 eq.)	1: 1.2: 0.8
Scale Up (5 mmol): 1. *n*-BuLi (2.2 eq.), THF, -78 °C, 1 hr, DMF (2.5 eq.)		**Yield: 71%**

Table 2.7. Optimisation for the Formylation of **2.65** [a]Determined by ^{1}H NMR Spectroscopy

With aldehyde **2.57** in hand, analogous conditions to that of the synthesis of fluorinated reference **2.33** were used (Scheme 2.15). An initial Horner-Wadsworth-Emmons reaction of phosphonate **2.35** and **2.57** afforded **2.56** in 92% yield in an isomeric ratio of 10:1. Hydrolysis under basic conditions to the corresponding carboxylic acid followed by the *in-situ* addition of hydrazine monohydrate at reflux afforded phthalazinone **2.55** in 88% yield. Subsequent methylation of carboxylic acid **2.55** and selective *N*-SEM protection respectively afforded bromide **2.53** in 64% yield over two steps. Applying those conditions described previously (Scheme 2.10), full conversion to the corresponding aryl pinacol boronic ester **2.52** could be achieved (Scheme 2.16).

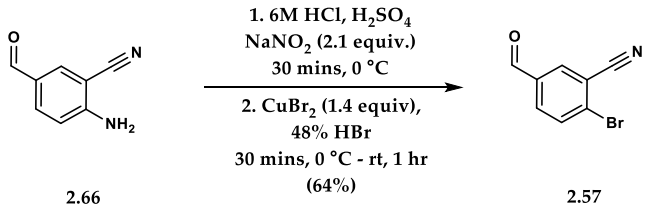

Scheme 2.15 Bromination of **2.66**

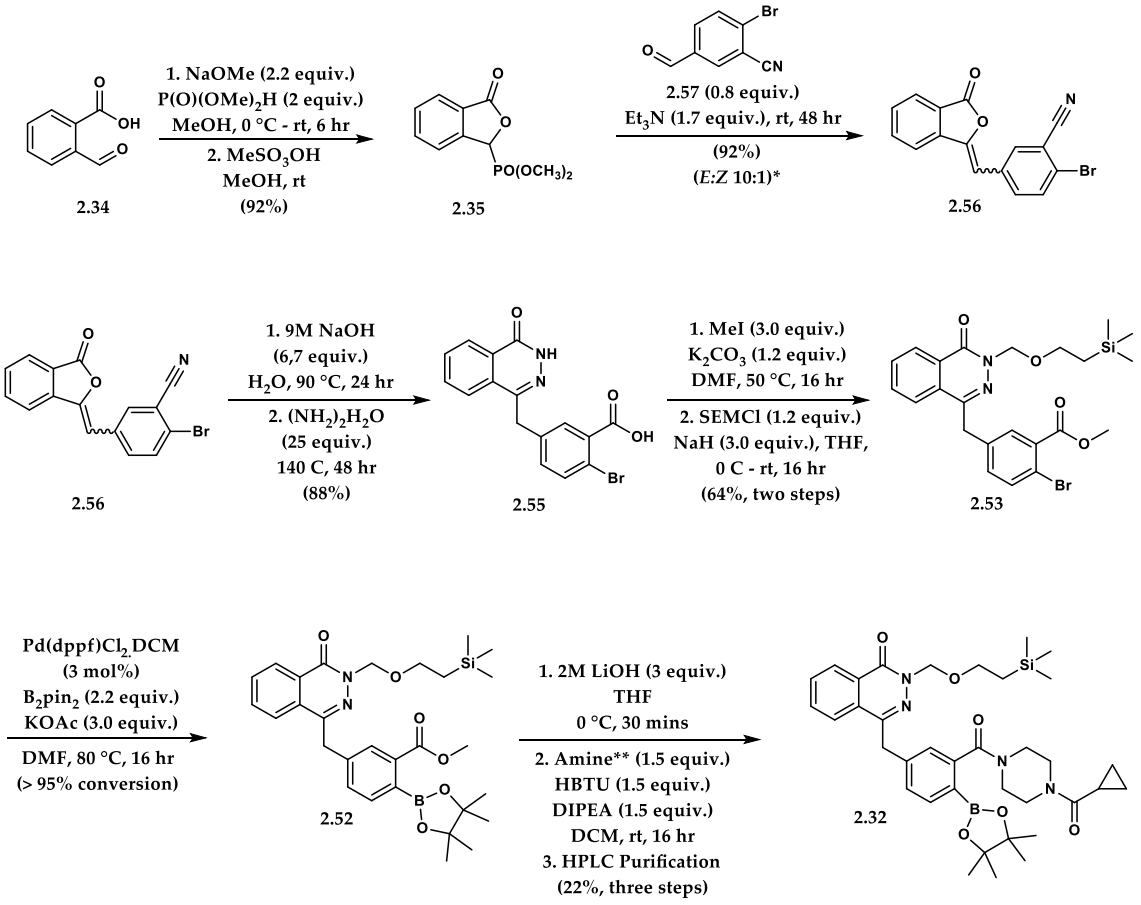

Scheme 2.16. Synthesis of 4-(3-(4-(cyclopropanecarbonyl)piperazine-1-carbonyl)-4-(4,4,5,5-tetra methyl-1,3,2-dioxaborolan-2-yl)benzyl)-2-((2-trimethlsilyl)ethoxy)methyl)phthalzin-1(*2H*)-one **2.32**, **E:Z* ratio assigned arbitrarily using ^{1}H NMR Spectroscopy **1-(cyclopropyl carbonyl)piperazine.

Exposing ester **2.52** to standard hydrolysis conditions, a complex mixture of products was observed. When carried out at lower temperatures and under higher dilution (0.03M) however, greater selectivity for the corresponding carboxylic acid could be achieved. Upon isolation of acid **2.51**, the crude material was exposed

directly to those coupling conditions described for the synthesis of **2.33** (Scheme 2.9). Ultimately, reverse phase prep-HPLC afforded **2.32** in 22% yield over three steps.

2.8.9 Optimisation of the Radiolabelling towards [^{18}F]Olaparib

Subjecting **2.32** to the conditions described by Gouverneur in 2017 for the labelling of electron deficient aromatics ([^{18}F]KF/K_{222} (20-30 MBq), substrate (0.02 mmol), $Cu(OTf)_2(py)_4$ (0.03 mmol), DMA (300 µL), 110 °C, 20 mins),[51] a 9% radiochemical conversion to **[^{18}F]2.33** was observed (Scheme 2.17).

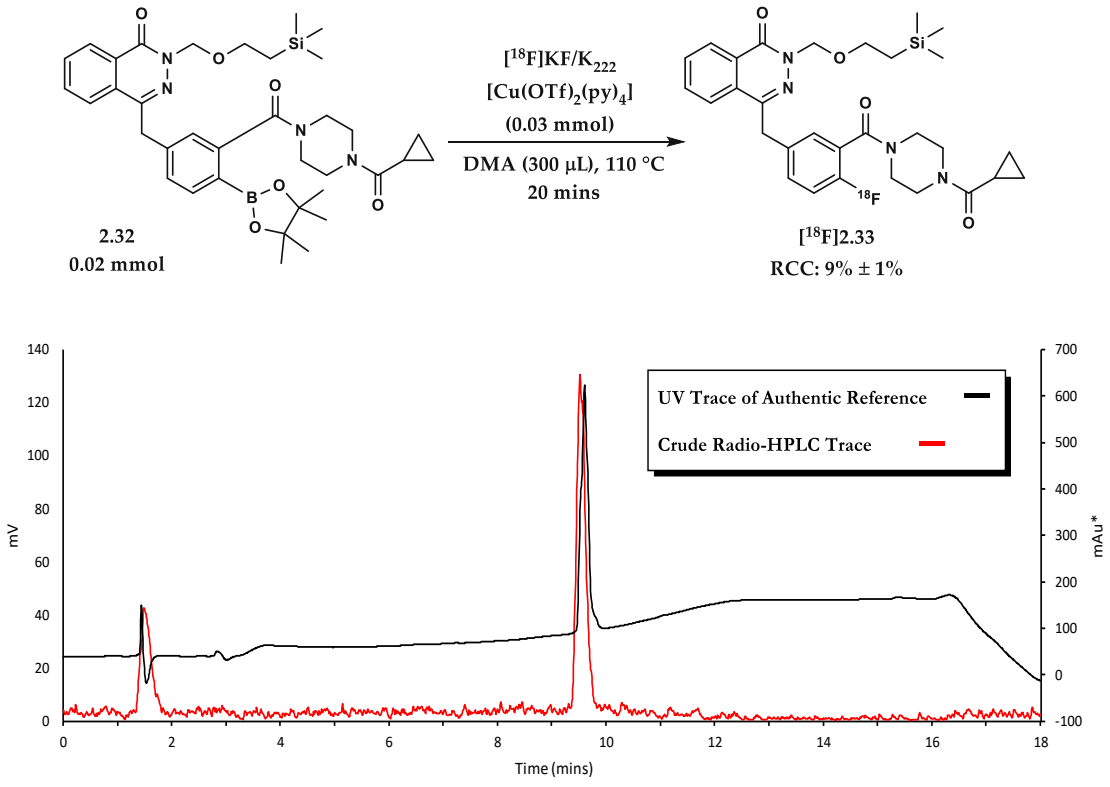

Scheme 2.17. ^{18}F-Radiofluorination and Radio-HPLC Trace of **[^{18}F]2.33**

It had already been recognised that when translating from small scale (20 – 30 MBq) to batch scale (typically > 1 GBq), a significant reduction in radiochemical yield is often observed due to the increased amount of base present within the reaction.[53]

Therefore, efforts were devoted to improving the small scale ^{18}F-fluorodeboronation of **2.32** before proceeding to batch scale isolations.

2.8.10 Optimisation of the ^{18}F-Fluorodeboronation

For the additive data reported by Gouverneur and co-workers in 2017,[51] it was noted that when imidazo[1,2-*b*]pyridazine (impy) **2.68** was spiked into the standard reaction (Scheme 2.18), a significantly improved RCC was observed. Given the propensity for impy derivatives to coordinate to copper, it was proposed that this may offer a superior catalyst to that of the $Cu(OTf)_2(py)_4$ reported by Gouverneur. $Cu(impy)_4(OTf)_2$ could be isolated and recrystallised with the structure confirmed by X-ray crystallography.

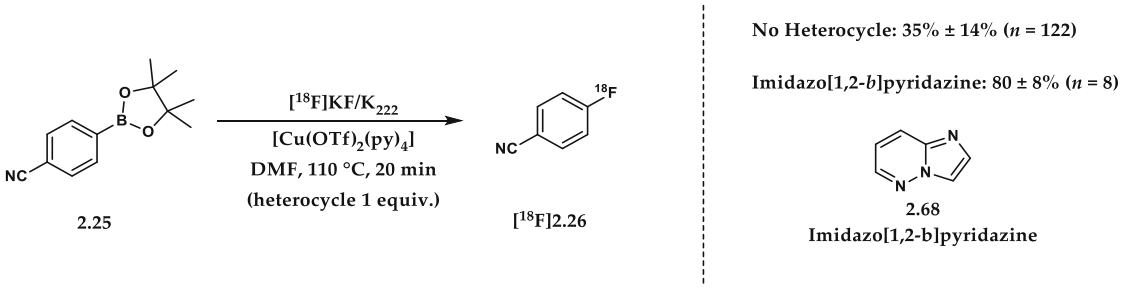

Scheme 2.18. Spiking Data for the ^{18}F Labelling of **2.25**

When $Cu(OTf)_2(impy)_4$ **2.68** was implemented for the labelling of **2.41**, an increase from 17% to 48% was observed (Table 2.9). Following this, a range of solvents were examined.[56] Subjected **2.69** to a range of polar aprotic solvents, it was found that 1,3-dimethyl-2-imidazolidinone (DMI) was similarly beneficial to DMA for the ^{18}F-fluorodeboronation of **2.69** (Scheme 2.19). When combing DMI with $Cu(OTf)_2(impy)_4$ **2.68** for the ^{18}F-labelling of **2.41**, a pronounced increase in radiochemical conversion from 48% to 82% was observed (Table 2.9).

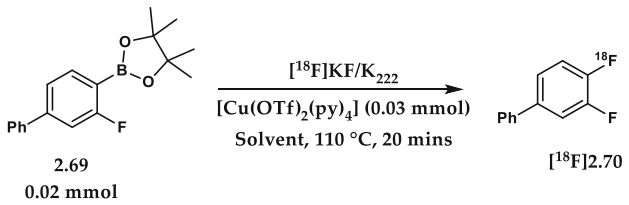

Solvents:

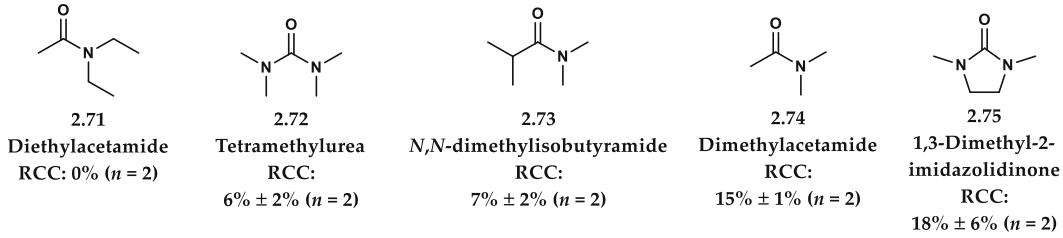

Scheme 2.19. Solvent Screening for the ^{18}F-Labelling of **2.69**[d]

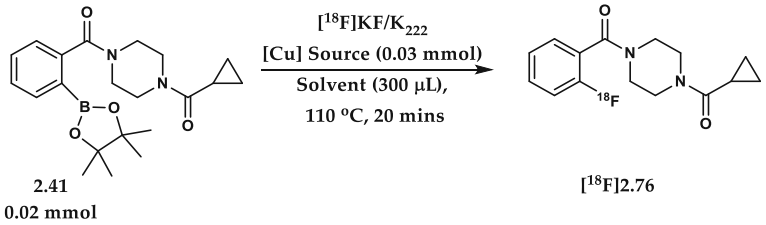

Entry	Cu Source	Solvent	RCC (*n* = 2)
1	$Cu(OTf)_2(py)_4$,	DMA	17% ± 3%
2	$Cu(OTf)_2(impy)_4$	DMA	48% ± 1%
3	$Cu(OTf)_2(impy)_4$	DMI	82% ± 1%

Table 2.9. Optimisation for the ^{18}F-Fluorodeboronation of **2.41**

When applied to the precursor for the synthesis of [^{18}F]olaparib, an increase in radiochemical conversion from 9% to 56% was observed (Scheme 2.20), sufficient for future efforts to be directed towards to the isolation of **[^{18}F]2.1** using levels of non-carrier added [^{18}F]fluoride suitable for clinical doses.

[d] Work carried out by N. Taylor and S. Preshlock

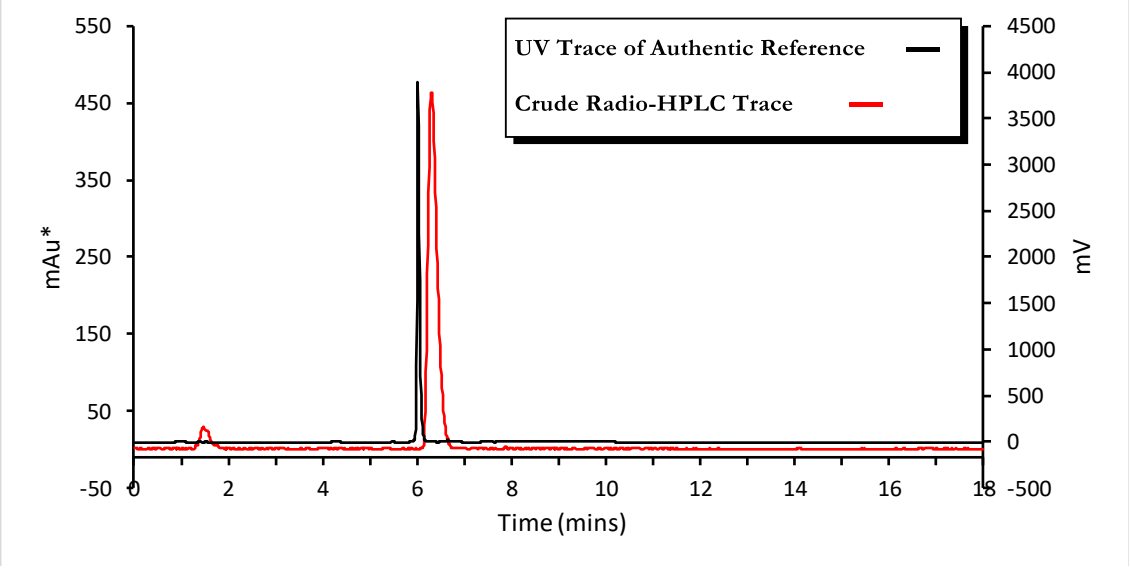

Figure 2.16. HPLC UV Trace and Radio-HPLC trace of **2.76** and **[^{18}F]2.76**

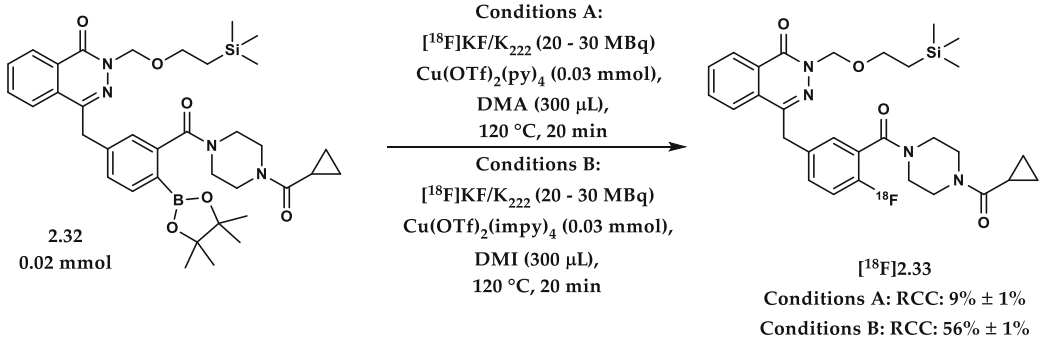

Scheme 2.20. Optimised procedure for the ^{18}F-radiolabelling of **2.32**

2.8.11 [^{18}F]Olaparib: Deprotection Screening of 2.33

Having established an effective protocol for the ^{18}F-labelling of **2.32**, investigations were carried out for the *in situ* deprotection of **[^{18}F]2.33**. Taking a range of conditions described within the literature, the use of TFA in a 1:1 mixture with DMI at 120 °C for 20 minutes proved the most effective (Scheme 2.21) affording **2.1** in > 95% conversion (confirmed by ^{1}H NMR spectroscopy).

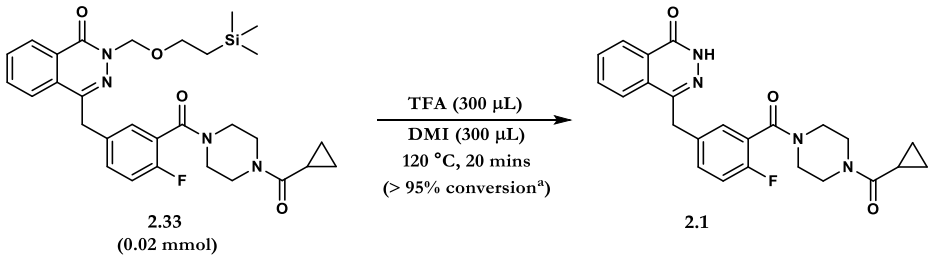

Scheme 2.21. Deprotection of **2.33** [a]Determined by ^{1}H NMR Spectroscopy

2.8.12 Batch Scale Isolation of [^{18}F]Olaparib

Work towards the isolation of [^{18}F]olaparib **[^{18}F]2.1** using up to 10 GBq of non-carrier added ^{18}F-fluoride began with the investigation into the base present on the QMA cartridge. Given the electron withdrawing nature of the aromatic ring in question,[57,58] and encouraged by the work of Gouverneur and co-workers in 2016,[53] it was proposed that less basic oxalate ($C_2O_4^{2-}$) may offer improved compatibility to that of carbonate (CO_3^{-}) (Scheme 2.22).

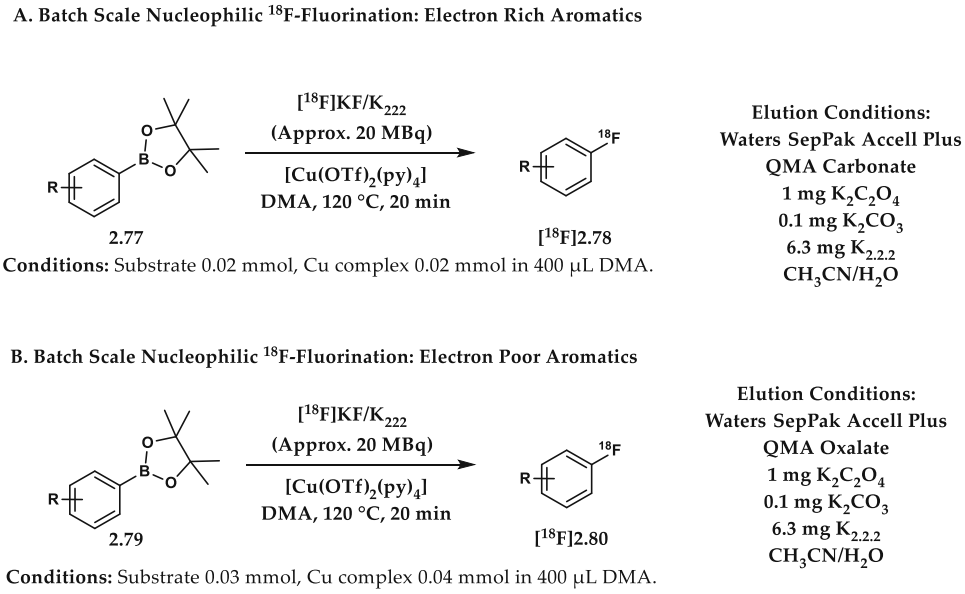

Scheme 2.22. Elution Conditions for the Batch Scale Nucleophilic ^{18}F-Fluorination of Electron Rich and Electron Poor Aromatics[85]

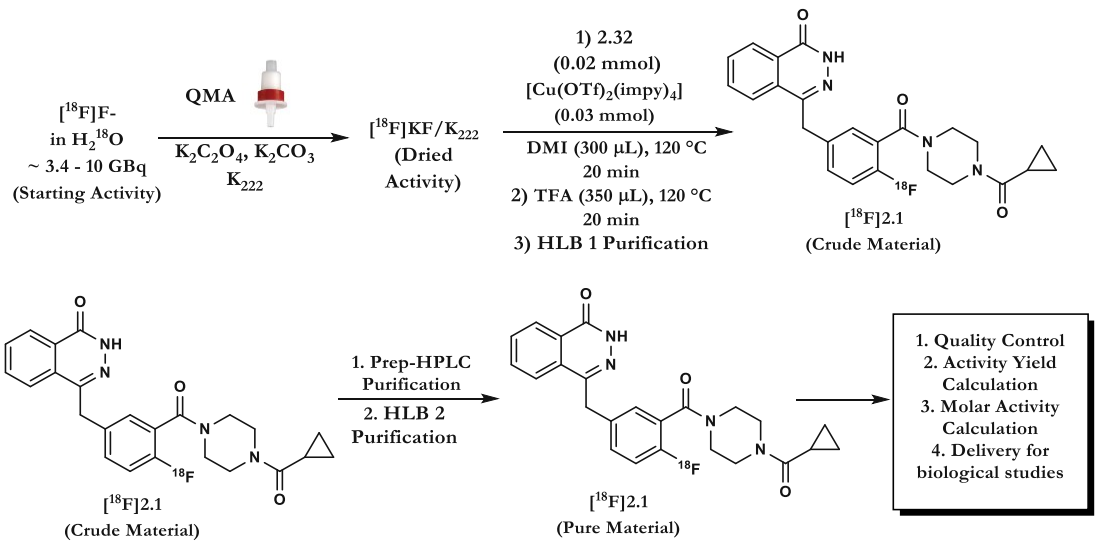

Run	QMA Ion	Activity (MBq)				AY (%)	Synthesis Time (min)	Molar Activity (GBq µmol^{-1})
		Starting	Dried	HLB 1	HLB 2			
1	Oxalate[a]	5500	3070	1050	290	5	149	7.2
2	Oxalate[a]	3620	2650	1076	550	15	136	10.1
3	Oxalate[a]	3400	1502	711	220	6	154	2.8
4	Oxalate[a]	7750	3120	1215	309	4	135	9.8
5	Oxalate[a]	8080	3140	1152	470	6	135	21.3
Activity Yield: 7% ± 4% (*n* = 5)								

Table 2.10. Activity Yield of **[18F]2.1** [a]Pre-conditioned with 3 mL of a 10 mg/mL $K_2C_2O_4$(aq) solution followed by 5 mL H_2O at a flow rate of 3 mL/min.

Poor retention of [18F]fluoride upon drying however, hindered the overall activity yield (AY) of **[18F]2.1**. By changing to carbonate as the base present on the QMA cartridge, the AY improved from 7% ± 4% to 18% ± 3% (Table 2.10 and 2.11.) with molar activities up to 26 GBq µmol^{-1} (Graph 2.1, Table 2.12). As had been noted for the small-scale reactions, no deprotection of the SEM group was observed with radiochemical yields after HLB cartridge purification upwards of 40% (Table 2.10, Table 2.11, HLB 1).

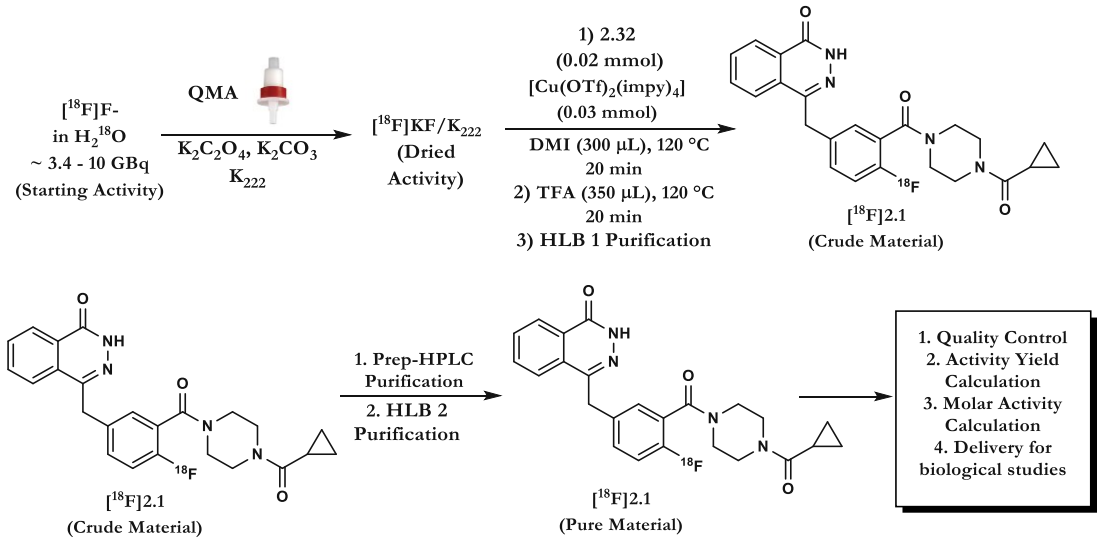

Run	QMA Ion	Activity (MBq)				AY (%)	Synthesis Time (min)	Molar Activity (GBq µmol^{-1})
		Starting	Dried	HLB 1	HLB 2			
1	Carbonate	8510	7420	3890	1168	14	140	10.9
2	Carbonate	10000	8420	4330	2300	23	130	21.3
3	Carbonate	10000	8950	3510	1836	18	129	25.7
4	Carbonate	1510	1281	640	278	18	144	2.7
5	Carbonate	7780	6730	3100	1343	17	132	15.4
Activity Yield: 18% ± 3% (*n* = 5)								

Table 2.11. Activity Yield of **[18F]2.1**

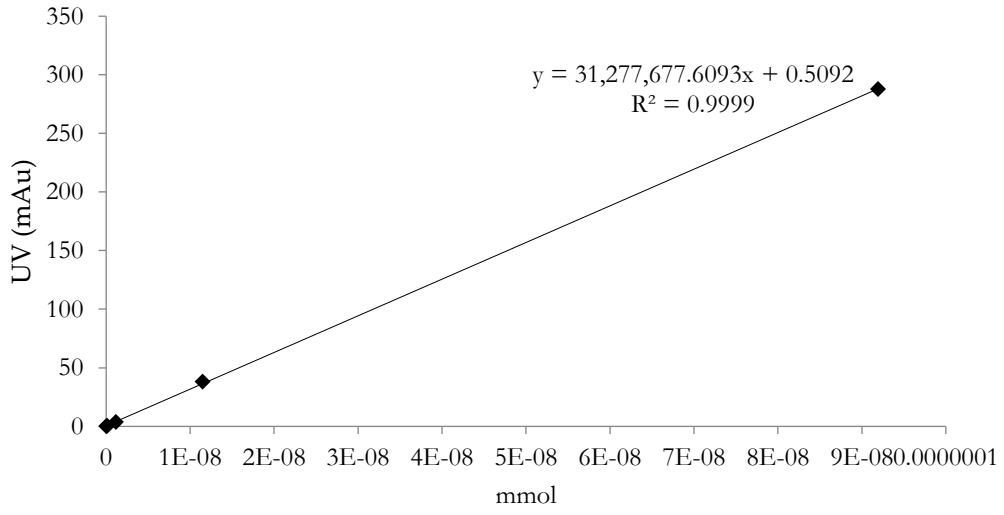

Graph 2.1. Calibration curve for olaparib

Injection Number	Activity (MBq)	Area (mAu)	mmol injected ($*10^{-7}$)	Molar Activity (GBq μmol^{-1})
1	2.0	9.16	2.7	7.2
2	1.4	4.82	1.3	10.4
3	1.6	18.29	5.6	2.8
4	0.7	2.73	0.71	9.8
5	3.1	5.06	1.4	21.3
6	1.1	3.67	1.0	10.9
7	1.6	2.86	0.75	21.3
8	1.7	2.58	0.66	25.7
9	2.2	25.79	8.1	2.7
10	2.6	5.79	1.7	15.4

Table 2.12. Molar activity data for [^{18}F]olaparib **[^{18}F]2.1**

2.8.13 Labelling of [^{18}F]Olaparib: Chemical Purity

Upon isolation and reformulation in 10% DMSO/PBS, analysis by reverse phase HPLC was carried out revealing the high radiochemical purity of product **[^{18}F]2.1** (Figure 2.17). Whilst the UV trace of the isolated product **[^{18}F]2.1** suggested a high chemical purity, further confirmation was required before biological studies were undertaken. One common byproduct of the Cu mediated ^{18}F-fluorination process, that of protodeboronation, has been investigated by several groups for the ^{18}F-labelling of a variety of radiotracers.[59,51] As such, the corresponding compound **2.84** was synthesised in 25% yield over 4 steps (Scheme 2.23). From this, HPLC analysis confirmed successful separation was achieved and therefore, any competitive binding *in vivo*/*in vitro*, avoided (Figure. 2.18, 2.19).

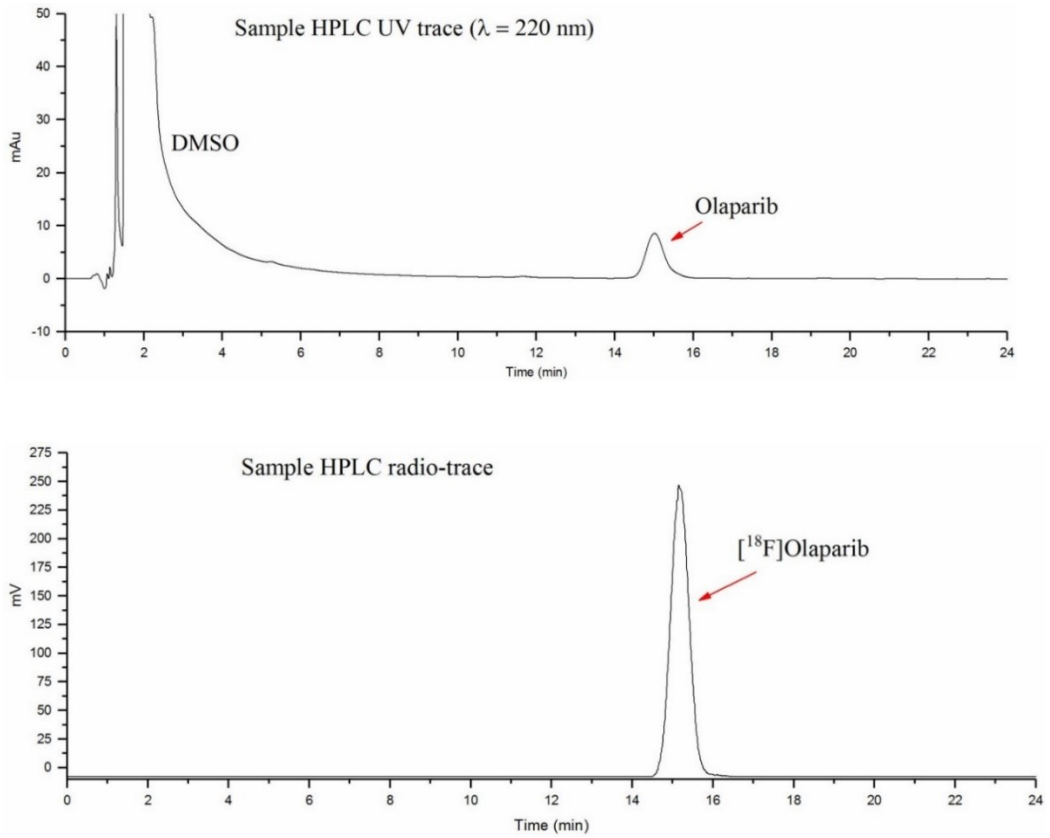

Figure 2.17. Semi-prep radioHPLC purification of [^{18}F]olaparib; HPLC Eluent: Synergi 4 µm Hydro-RP 80Å, 150 x 4.6 mm with 25% MeCN/75% H_2O (isocratic 1 mL/min) monitoring with UV (220 nm).

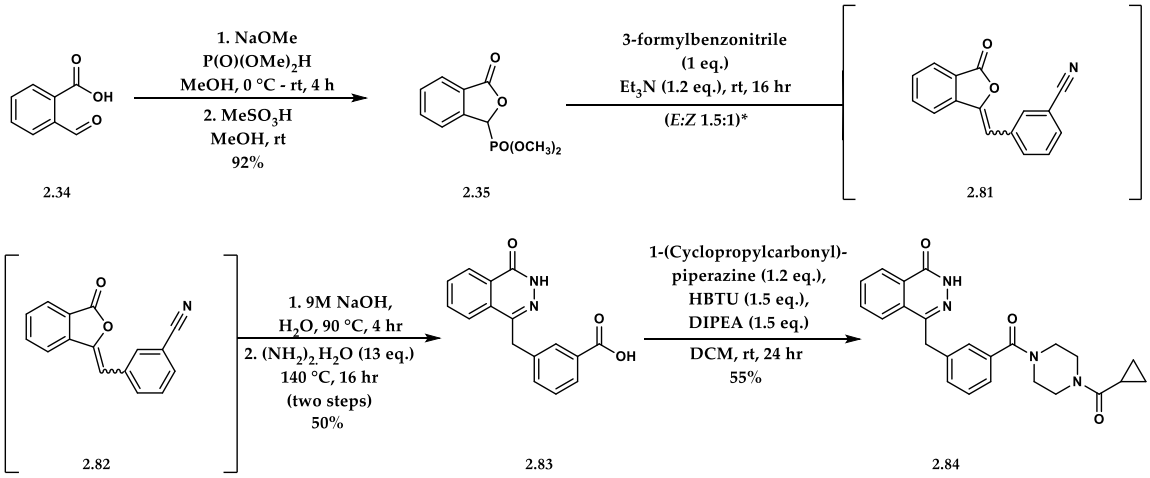

Scheme 2.23. Synthesis of **2.84** **E:Z* ratio assigned arbitrarily using ^{1}H NMR Spectroscopy

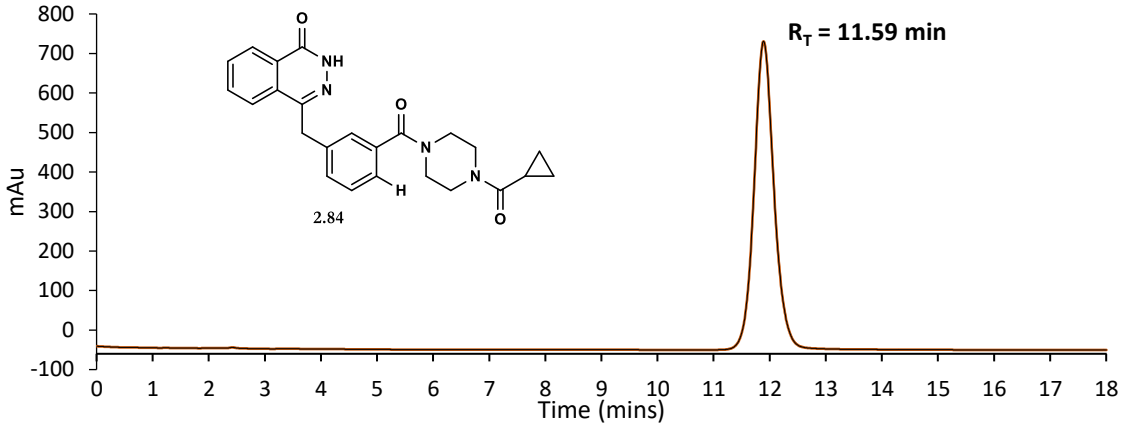

Figure 2.18. Synthesis and Analysis of **2.84**; HPLC Eluent: Synergi 4 μm Hydro-RP 80A, 150 x 4.6 mm with 25% MeCN/75% H_2O (isocratic 1 mL/min) monitoring with UV (220 nm).

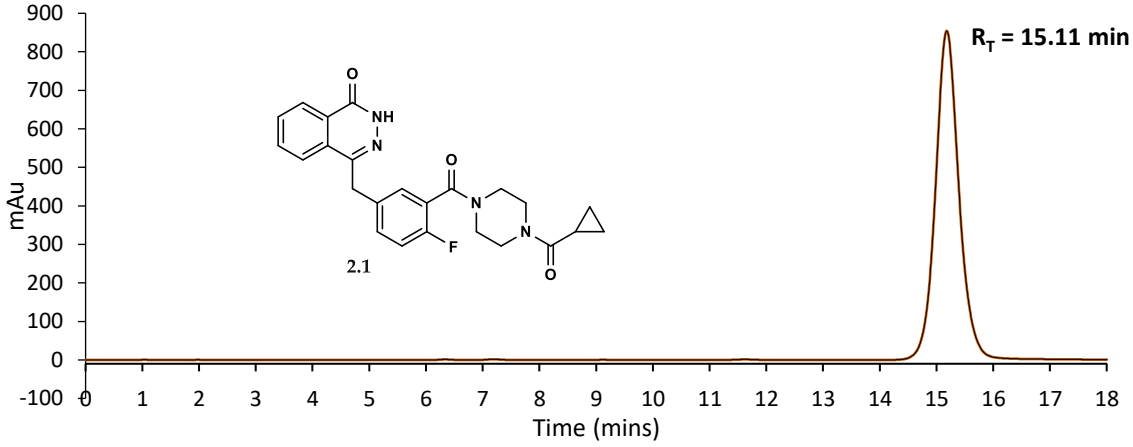

Figure 2.19. HPLC UV Trace of Olaparib **2.1**. HPLC Eluent: Synergi 4 μm Hydro-RP 80A, 150 x 4.6 mm with Figure% MeCN/75% H_2O (isocratic 1 mL/min) monitoring with UV (220 nm).

2.9 In Vitro and In Vivo Evaluation of [^{18}F]Olaparib[e]

As previously described (Section 2.3.4), increased interstitial pressure and desmoplasia can result in resistance to PARP inhibitors. As such, a range of pancreatic ductal adenocarcinoma (PDAC) cell lines expressing PARP were selected; namely PSN-1, MiaPaCa-2 and CaPan-1 cell lines. This class of cells typically express increased interstitial pressure and desmoplasia *in vivo* and therefore were seen as ideal for the imaging with [^{18}F]olaparib. This study was carried out over the course of 8 deliveries of [^{18}F]olaparib. [^{18}F]Olaparib was delivered as a solution in 10% DMSO/PBS at pH 7.4 at a dilution of ~ 475 MB qmL^{-1}. All biological data was obtained at least in triplicate with results reported as mean ± standard deviation unless stated otherwise (Statistical methods reported in section 5.5.18).

2.9.1 [^{18}F]Olaparib in Naïve Mice

Initial studies sought to establish the basic biodistribution of [^{18}F]olaparib. *In vivo* dynamic PET imaging of wild type naïve CBA mice revealed fast pharmacokinetics and a hepatobiliary clearance pattern (Figure 2.20). Based on volume-of interest analysis of ^{18}F signal originating from a region drawn around the heart, the blood clearance of [^{18}F]olaparib followed a biphasic pattern (Figure 2.21), with fast and slow half-lives of 2.8 min (44%; 95%CI: 2.1-4.0 min) and 32.3 min (56%; 95% CI 27.6-39.1 min), respectively, resulting in a weighted half-life of 19.3 min (Figure 2.20). Given the very small injected dose of compound (0.0065 mg/kg), the blood half-life of [^{18}F]olaparib was markedly shorter than the previously reported half-life of 58 min (in female mice) after intravenous administration of a bolus of 20

[e] The following work was carried out by J. Knight and M.-A. Xavier

mg/kg of olaparib, but slower than the 5.5 min for an ^{18}F-labelled olaparib-based PARP inhibitor reported by Reiner and co-workers.[48] Removal of selected tissues after imaging and measurement of their ^{18}F-content confirmed the results obtained though image-based quantification (Figure 2.20B, Figure 2.21, Figure 2.25), showing low blood retention and high intestinal uptake of [^{18}F]olaparib at 1 h post injection.

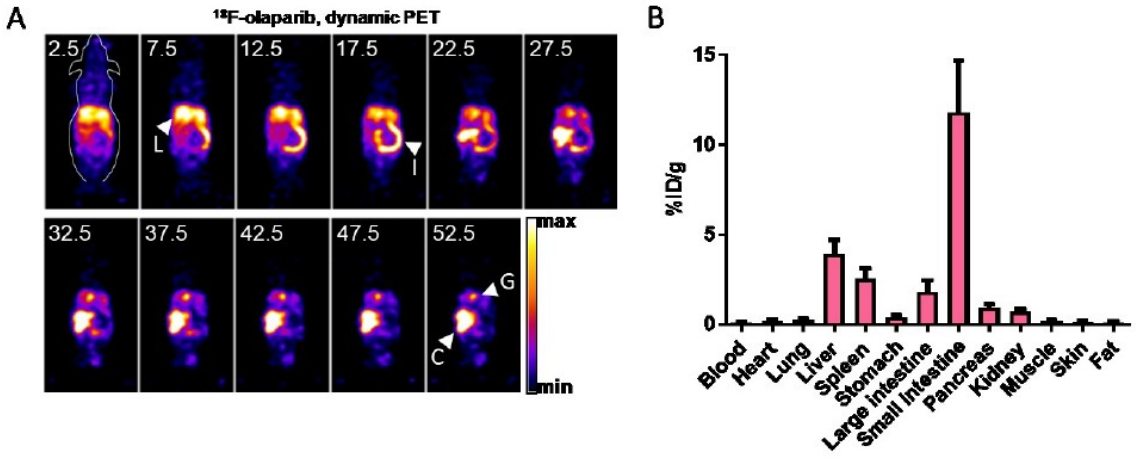

Figure 2.20. (A) Representative dynamic PET images after an intravenous bolus injection of [^{18}F]olaparib (3 MBq). The middle of the timeframes are indicated in min. Images are presented as MIPs (B) Biodistribution in wild type CBA mice, at 1 h post injection of [^{18}F]olaparib. L: liver, G: gall bladder, I: small intestine, C: caecum.

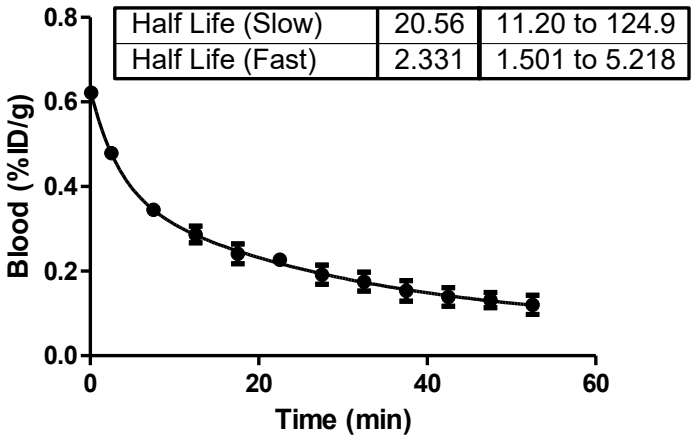

Figure 2.21. Concentration of [^{18}F]olaparib in blood of naïve CBA mice. Half Life reported in minutes

2.9.2 [^{18}F]Olaparib in PARP-1 expressing PDAC cell lines *In Vitro*

In vitro, [^{18}F]olaparib was taken up within 30 min in a small panel of PDAC cells lines with PSN-1 showing the highest uptake (Figure 2.22A). Results at 60 min after initial exposure of the cells to [^{18}F]olaparib were similar. Cell-associated uptake of [^{18}F]olaparib in all three cell lines could be blocked almost completely (>99%) by addition of a large excess of cold, unlabelled olaparib ($P < 0.0001$), suggesting a highly specific interaction of [^{18}F]olaparib and binding sites (on PARP-1, 2, and 3) (Figure 2.22A). In PSN-1 cells, efficient blocking was also achieved using an excess of three NAD^+-pocket binding PARP inhibitors, olaparib (IC_{50} = 20(16-25) nM, mean (95% CU)), talazoparib (IC50 = 5.2(3.2-8.5) nM) and rucaparib (IC_{50} = 12(8.2-18) nM; all $P < 0.001$) (Figure 2.22B).

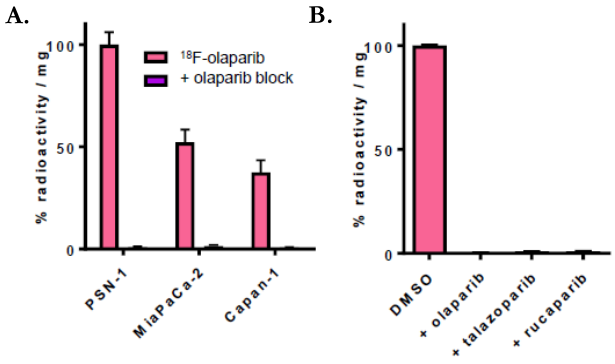

Figure 2.22. (A) Uptake of ^{18}F in PSN-1, MiaPaCa-2 and Capan-1 cells, 30 min after addition of [^{18}F]olaparib. Uptake can be blocked using an excess of cold, unlabelled olaparib. (B) Uptake of [^{18}F]olaparib in PSN-1 could be blocked by an excess of olaparib, talazoparib, or rucaparib..

Having established a highly specific binding interaction between [^{18}F]olaparib and all three cell lines, the next step was to investigate the correlation between DNA damage and the uptake of [^{18}F]olaparib. The hypothesis being that, upon exposure to external beam radiation, the increased DNA damage to those cell lines would lead to an increase in PARP expression and therefore an increased uptake of [^{18}F]olaparib.

To this end, all three cell lines were exposed to incremental increases of external beam radiation. *In vitro*, 2 hours after gamma-irradiation (10 Gy) of cells, Western blot analysis revealed an increase in PARP-1 expression in MiaPaCa-2 and PSN-1 cells (Figure. 2.23A). PARP-1 expression in Capan-1 cells proved low, and beyond the detection limit of Western blotting (Figure 2.23A). For *in vitro* however, [^{18}F]olaparib uptake was increased in all cells after gamma-irradiation, in a radiation dose-dependent manner (Figure 2.23B).

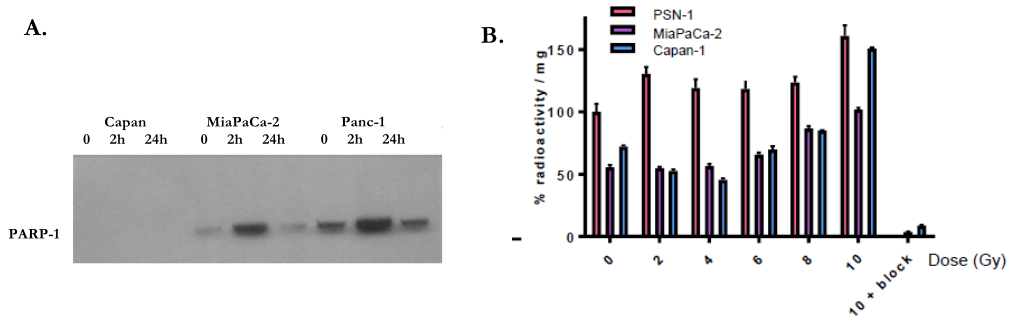

Figure 2.23. (A) Western blot probing for PARP-1 in a panel of PDAC cell lines, before, and after 2 or 24 h of external beam irradiation (10 Gy); (B) Uptake of [^{18}F]olaparib in a panel of cell lines, 48 h after external beam irradiation with increasing doses. As a control, uptake of [^{18}F]olaparib irradiated at 10 Gy could additionally be blocked by an excess of cold, unlabelled olaparib.

2.9.3 [^{18}F]Olaparib in PARP-1 expressing PDAC cell lines *In Vivo*

To confirm if this correlation is also observed *in vivo*, xenograft mouse models of all three cell lines were subject to either external beam radiation (10 Gy) or sham radiation. Two hours post-irradiation, [^{18}F]olaparib was administered intravenously. After 1 hour, each animal was sacrificed, the tissues removed and an *ex vivo* biodistribution undertaken. Overall, correlation between PARP-1 expression, as measured by Western Blot, correlated well with the uptake of [^{18}F]olaparib in xenograft tissues ($R = 0.84$, $P < 0.0001$, Figure. 2.24).

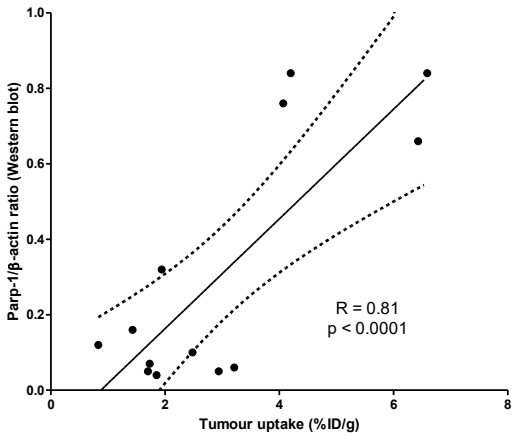

Figure 2.24. [^{18}F]olaparib uptake for PSN-1, MiaPaCA-2 and Capan-1 xenografts (both irradiated and not irradiated). Correlation determined by *ex vivo* biodistribution (*x*-axis) and PARP-1 expression measured via Western Blot (*y*-axis)

2.9.4 [^{18}F]Olaparib in PSN-1 cells and xenografts after external beam irradiation

Finally, in an effort to explore whether [^{18}F]olaparib could be used to measure the effects of DNA damaging therapies such as external beam radiotherapy, irradiation of a given of cell line, and the subsequent measuring of PARP-1 expression was undertaken. Given the high specific binding and PARP expression, the PSN-1 cell line was selected for *in vivo* analysis (Figure 2.23). For this study, irradiation of the PSN-1 xenograft would be carried out two hours prior to intravenous injection of [^{18}F]olaparib.

The biodistribution and clearance pattern in xenograft-bearing animals was found to be similar to that in naïve wild type mice (Figure 2.25, Figure 2.26). Uptake in tissues expressing PARP-1, 2, and 3 such as the spleen, bone, and the pancreas was observed, and this uptake could be blocked by co-injection of an excess of cold, unlabelled olaparib, again demonstrating the specificity of PARP-targeting. Uptake of [^{18}F]olaparib in PARP-1 expressing PSN-1 xenografts amounted to 3.16 ± 0.36%ID/g, measured by biodistribution experiments at 1 h after intravenous bolus injection. *In vivo*, 2 h after irradiation of PSN-1 xenografts (10 Gy), uptake of ^{18}F-

olaparib in the tumour tissue was increased by 70%, to 5.35 ± 1.16 %ID/g (P = 0.025). The specificity of this uptake was demonstrated by a significant decrease in tumour uptake following co-injection of an excess of cold, unlabelled olaparib, where uptake dropped to 1.20 ± 0.17 %ID/g (P = 0.0016).

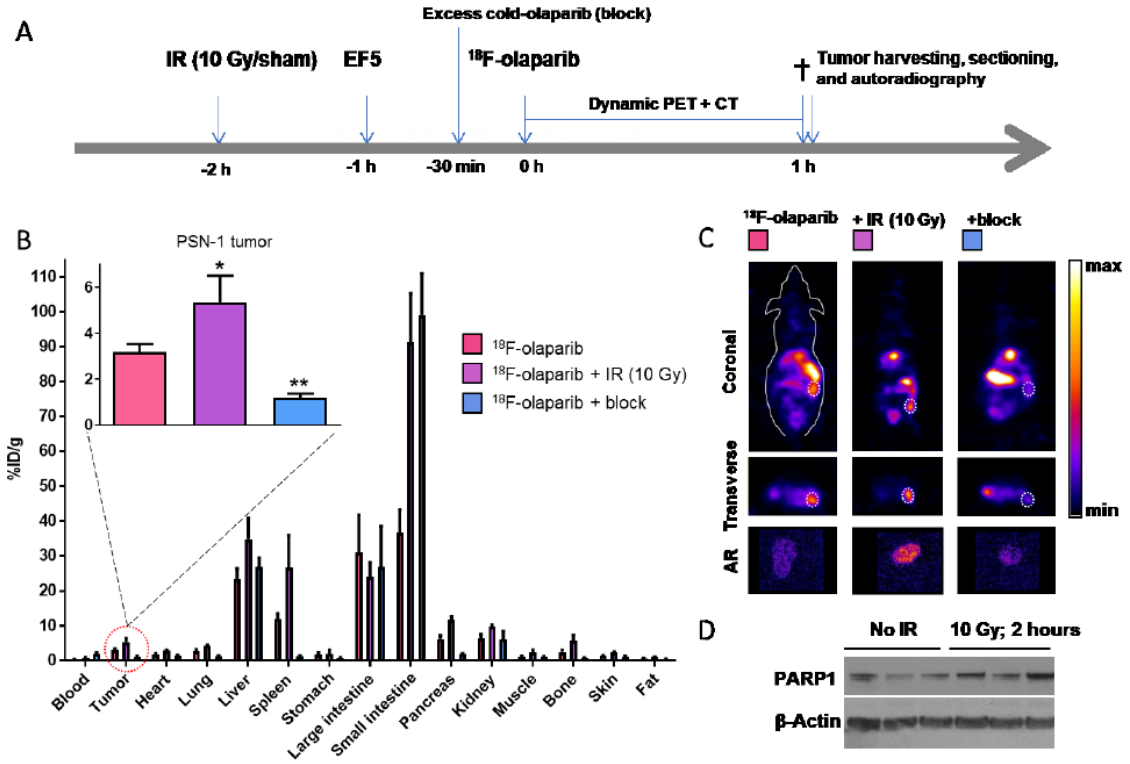

Figure 2.25. (A) Schematic of the experimental design of imaging experiments. (B) Biodistribution in mice bearing PSN-1 xenografts, at 1 h post injection of [^{18}F]olaparib (3 MBq). *5.35 ± 1.16 %ID/g (P = 0.025) **1.20 ± 0.17 %ID/g (P = 0.0016) (C) Representative MIP images of PSN-1 xenograft-bearing mice, 1 h post injection of [^{18}F]olaparib. Arrowheads indicate the position of the xenograft tumour. Insets represent autoradiograms of tumour sections, corroborating PET imaging results. (D) Western Blot showed increased PARP-1 levels in three irradiated compared to three non-irradiated PANC1-xenografts.

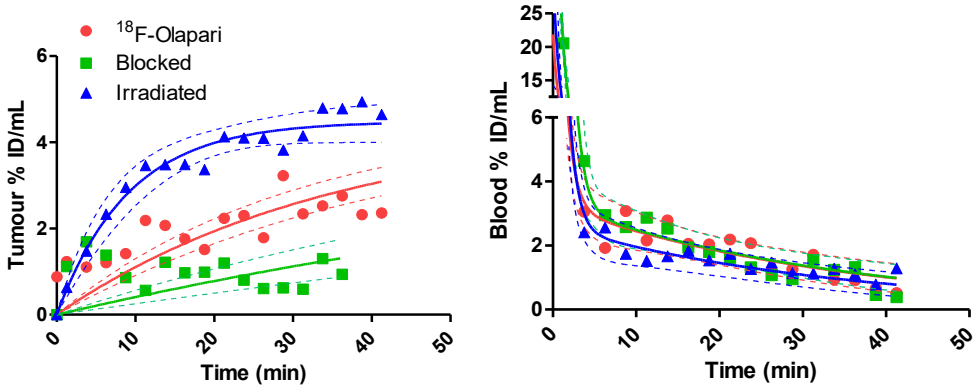

Figure 2.26. Image quantification of **[^{18}F]2.1** in mice bearing PSN-1 xenografts

2.10 Conclusion and Future Work

Using the copper-mediated ^{18}F-fluorination of aryl boronic esters, the first radiosynthesis of [^{18}F]olaparib was achieved. [^{18}F]Olaparib was taken up selectively in cells overexpressing PARP-1. Irradiation increased PARP-1 expression and [^{18}F]olaparib uptake in a radiation-dose-dependent fashion. PET imaging in mice showed specific uptake of [^{18}F]olaparib in tumour xenografts expressing PARP-1 (3.2±0.36%ID/g in PANC1 xenografts), correlating linearly with PARP-1 expression. Two hours after irradiation of the tumour (10 Gy), uptake of [^{18}F]olaparib increased by 70% (P = 0.025).

Future aims of this project are to: 1) investigate the use of [^{18}F]olaparib to measure PARP expression for other cancers *in vivo*; 2) expand the radiolabelling to other platforms for the automated synthesis of [^{18}F]olaparib under GMP conditions; 3) through clinical trials, aim to establish [^{18}F]olaparib as a commercial radiotracer for patient stratification.

2.11 Reference

1 S. P. Jackson, J. Bartek, *Nature* 2009, **461**, 1071.
2 J. H. J. Hoeijmakers, *N. Engl. J. Med.,* 2009, **361**, 1475.
3 B. M. Sirbu, D. Cortez, *Cold Spring Harb. Perspect. Biol.,* 2013, **5**, 1.
4 B. M. Brenerman, J. L. Illuzzi, D. M. Watson, *Carcinogenesis* 2014, **35**, 2643.
5 C. J. Lord, A. Ashworth, *Nature* 2012, **481**, 287.
6 E. Seeberg, L. Eide, M. Bjørås, *Trends Biochem. Sci.,* 1995, **10**, 391.
7 G. L. Dianov, U. Hübscher, *Nucleic Acids Res.,* 2013, **41**, 3483.
8 S. T. Dexheimer, *Springer* 2013, 19.
9 Y.-J. Kim, D. M. Wilson, *Curr. Mol. Pharmacol.,* 2012, **5**, 3.
10 D. D'Amours, S. Desnoyers, I. D'Silva, G. G. Poirier, *Biochem. J.,* 1999, **342**, 249.
11 V. Schreiber, F. Dantzer, J. C. Amé, G. De Murcia, *Nat. Rev. Mol. Cell Biol.,* 2006, **7**, 517.
12 T. Lindahl, M. S. Satoh, G. G. Poirier, A. Klungland, *Trends Biochem. Sci.,* 1995, **20**, 405.
13 G. De Murcia, V. Schreiber, M. Molinete, B. Saulier, O. Poch, M. Masson, C. Niedergang, J. M. De Murcia, *Mol. Cell Biochem.,* 1994, **138**, 15.
14 K. K. Khanna, S. P. Jackson, *Nat. Genet.,* 2001, **27**, 247.
15 P. J. McKinnon, K. W. Caldecott, *Annu. Rev. Genomics Hum. Genet.,* 2007, **8**, 37.
16 A. Cerbinskaite, A. Mukhopadhyay, E. R. Plummer, N. J. Curtin, R. J. Edmondson, *Cancer Treat Rev.,* 2012, **38**, 89.
17 M. Krajewska, R. S. N. Fehrmann, E. G. E. De Vries, M. A. T. M. Vugt, *Front. Genet.,* 2015, **6**, 1.
18 Helleday. T, *Carcinogenesis* 2010, **31**, 955.
19 J. Renkawitz, C. A. Lademann, S. Jentsch, *Nat. Rev. Mol. Cell Biol.,* 2014, **15**, 369.
20 S. F. Bunting, A. Nussenzweig, *Nat. Rev. Cancer* 2013, **13**, 443.
21 C. T. Yan, C. Boboila, E. K. Souza, S. Frnaco, T. R. Kickernell, M. Murphy, S. Gurnaste, M. Geyer, A. A. Zarrin, J. P. Manis, K. Raiewsky, F. W. Alt, *Nature* 2007, **449**, 478.
22 X. Li, H. Xu, C. Xu, M. Lin, X. Song, F. Yi, *Int. J. Mold. Sci.,* 2013, **14**, 2431.
23 T. D. Halazonetis, V. G. Gorgoulis, J. Bartek, *Science* 2008, **319**, 5868.
24 J. B. M. Koorstra, S. M. Honf, C. Shi, A. K. Meeker, J. K. Ryu, G. J. Offerhaus, M. G. Goggins, R. H. Hruban, A. Maitra, *Mod. Pathol.,* 2009, **22**, 1439.
25 M. Kshirsagar, W. Jiang, I. M. Shih, *J. Oncol.,* 2011, **2012**, 1.
26 V. G. Gorgoulis, L. V. F. Vassiliou, P. Karakaidos, P. Zacharatos, A. Kotsinas, T. Liloglou, M. Venere, R. A. DiTullio Jr, N. G. Kastrinakis, B. Levy, D. Kletsas, A. Yoneta, M. Herlyn, C. Kittas, T. D. Halazonetis, *Nature* 2005, **434**, 907.
27 O. A. Sedelnikova, W. M. Bonner, *Cell Cycle* 2006, **5**, 2909.
28 SEER Cancer Statistics Review 1975 - 2013

29 D. V. Ferraris, *J. Med. Chem.,* 2010, **53**, 4561.
30 J. C. Knight, S. Koustoulidou, B. Cornelissen, *Eur. J. Nucl. Med. Mold. Imaging* 2017, **44**, 1065.
31 H. E. Bryant, N. Schults, H. D. Thomas, K. M. Parker, D. Flower, E. Lopez, S. Kyle, M. Meuth, N. J. Curtin, T. Heeleday, *Nature* 2005, **434**, 913.
32 A. G. Patel, J. N. Sarkaria, S. H. Kaufmann, *Proc. Natl. Acad. Sci.,* 2011, **108**, 3406.
33 S. Shall, G. De Murcia, *Mutat. Res. DNA Repair* 2000, **460**, 1.
34 M. Banasik, K. Ueda, *Mol. Cell Biochem.,* 1994, **137**, 185.
35 B. W. Durkacz, O. Omidiji, D. A. Gray, S. Shall, *Nature* 1980, **283**, 593.
36 A. W. White, R. Almassy, A. H. Calvert, N. J. Curtin, R. J. Griffin, Z. Hostomsky, K. Maegley, D. R. Newell, S. Srinicasan, B. T. Golding, *J. Med. Chem.,* 2000, **43**, 4084.
37 F. Dantzer, G. de La Rubia, M.-D. Murcia, Z. Hostomsky, G. De Murcia, V. Schreiber, *Biochemistry* 200, **39**, 7559.
38 T. Kinoshita, I. Nakanishi, M. Warizaya, A. Iwashita, Y. Kido, K. Hattori, T. Fujii, *FEBS Lett.,* 2004, **556**, 43.
39 D. J. Skalizky, J. T. Marakovits, K. A. Margley, A. Ekker, X. H. Yu, Z. Hostomsky, S. E. Webber, B. W. Eastman, R. Almassy, J. Li, N. J. Curtin, D. R. Newell, A. H. Calvery, R. J. Griffin, B. T. Golding, *J. Med. Chem.,* 2003, **46**, 210.
40 K. Hattori, Y. Kido, H. Yamamoto, J. Ishida, K. Kamijo, K. Murano, M. Ohkubo, T. Kinoshita, A. Iwashita, K. Mihara, S. Yamazaki, N. Matsuoka, Y. Teramura, H. Miyake, *J. Med. Chem.,* 2004, **47**, 4151.
41 L. Livraghi, G. E. Garber, *BMC Med.,* 2015, **13**, 188.
42 L. O'Driscoll, N. Walsh, A. Larken, J. Ballot, W. S. Ooi, G. Gullo, R. O'Conner, M. Clynes, J. Crown, S. Kennedy, *Anticancer Res.,* 2007, **27**, 2115.
43 S.-H. Park, S. J. Noh, K. M. Kim, J. S. Bae, K. S. Kwon, S. H. Jung, J. R. Kim, H. Lee, M. J. Chung, W. S. Moon, M. J. Kang, K. Y. Jang, *Transl. Oncol.,* 2015, **8**, 239.
44 P. Pournazari, R. F. Padmore, F. Kosari, P. Scalia, M. T Shahbani-Rad, S. Shariff, D. J. Demetrick, M. Bosch, A. Mansoor, *Hum. Pathol.,* 2014, **45**, 1582.
45 P. M. Matthews, E. A. Rabiner, J. Passchier, R. N. Gunn, *Br. J. Clin. Pharmacol.,* 2012, **73***,* 175.
46 T. Reiner, E. J. Keliher, S. Earley, B. Marinelli, R. Weissleder, *Angew. Chem. Int. Ed. Engl.,* 2011, **50**,1922.
47 G. Carlucci, B. Carney, C. Brand, S. Kossatz, C. P. Irwin, S. D. Carlin, E. J. Keliher, W. Weber, T. Reiner, *Mol. Imaging Biol.,* 2015, **17**, 848.
48 B. Carney, G. Carlucci, B. Salinas, V. Di Gialleonardo, S. Kossatz, A. Vansteene, V. A. Longo, A. Bolaender, G. Chiosis, K. R. Keshari, W. A. Weber, T. Reiner, *Mol. Imaging Biol.,* 2016, **18**, 386.
49 F. Zmuda, A. Blair, M. C. Liuzzi, G. Malviya, A. J. Chalmers, D. Lewis, A. Sutherland, S. L. Pimlott, *J. Med. Chem.,* 2018, **61**, 4103.
50 T. L. Andersen, S. D. Friis, H. Audrain, P. Nordeman, G. Antoni, T. Skrydstrup, *J. Am. Chem. Soc.,* 2015, **137**, 1548.

51 N. J. Taylor, E. Emer, S. Preshlock, M. Schedler, M. Tredwell, S. Verhoog, J. Mercier, C. Genicot, V. Gouverneur, *J. Am. Chem. Soc.,* 2017, **139**, 8367.
52 K. D. Collins, F. Glorius, *Nat. Chem.*, 2013, **5**, 597.
53 S. Preshlock, S. Calderwood, S. Verhoog, M. Tredwell, M. Huiban, A. Hienzsch, S. Gruber, T. C. Wilson, N. J. Taylor, T. Cailly, M. Schedler, T. L. Collier, J. Passchier, R. Smits, J. Mollitor, A. Hoepping, M. Mueller, C. Genicot, J. Mercier, V. Gouverneur *Chem. Commun.*, 2016, **52**, 8361.
54 T. Ishiyama, M. Murata, N. Miyaura, *J. Org. Chem.,* 1995, **60**, 7508.
55 B. Du, X. Jiang, P. Sun, *J. Org. Chem.,* 2013, **78**, 2786.
56 N. Ichiishi, A. F. Brooks, J. J. Topczewski, M. E. Rodnick, M. S. Sanford, P. J. H. Scott, *Org. Lett.,* 2014, **16**, 3224.
57 A. Katsifis, K. Hamacher, J. Schnitter, G. Stöcklin, *Appl. Radiat. Isot.,* 1993, **44**, 1015.
58 K. Hamacher, W. Hamkens, *Appl. Radiat. Isot.*, 1995, **4**, 911.
59 A. V. Mossine, A. F. Brooks, V. B.-Gauthier, J. J. Bailey, N. Ichiishi, R. Schirrmacher, M. S. Sanford, P. J. H. Scott, *J. Label. Compd. Radiopharm.,* 2018, **1**, 11.

Chapter III:

^{18}F-Trifluoromethylation of Unmodified Peptides

3.1 Radiolabelling of Biomolecules

As discussed in Chapter I, PET imaging, using radiolabeled molecules, provides valuable *in vivo* functional information.[1] Due to their favourable pharmacokinetics and high specificity targeting characteristics, biomolecules such as nucleotides, peptides, aptamers and antibodies have attracted significant attention as candidates for radiolabelling. Furthermore, the spatial and temporal information of biomolecules *in vivo* present scientists with viable probes for research into areas such as clinical diagnostic studies, monitoring biochemical processes, and evaluation of the pharmacological properties of pharmaceutical candidates in support of drug discovery programs.[2-3]

3.2 Site Selective Modification of Biomolecules

Compared to the late stage radiofluorination of small molecules, the installation of fluorine-18 into biomolecules comes with unique challenges due to the high functionality present within many substrates as well as their heightened sensitivity to changes in pH and temperature.[4] Nonetheless, all these obstacles must be overcome whilst maintaining a high level of selectivity for a given residue. To achieve this selectivity, many of the works discussed within this chapter take inspiration from strategies that use stable isotopes (fluorine-19, carbon-12 etc.). In recent years, the field of site selective protein modification has expanded rapidly with a plethora of transformations having been reported.[5] Some of the most important considerations when developing novel strategies include; the abundance of a given amino acid, the reactivity of a given residue and how this reactivity may be affected by its location within a given biomolecule.

For the first of these factors, this is illustrated by the targeting of cysteine and lysine residues. For the cysteine residue, the relatively low abundance (< 3.5%) has allowed for high levels of precision to be attained.[6] However, this rarity can also be problematic should these residues be buried within a given biomolecule and therefore, inaccessible. Concerning the lysine residue, its high abundance (> 7.5%) makes it an logical target for modification. Yet with high abundance, full reaction of all lysine residues is unlikely and therefore, reactions may generate mixtures of many products.

For the second of these considerations, that of reactivity, both lysine and cysteine residues provide a good illustration of the challenges involved. Both functional groups are nucleophilic in nature and therefore the ability to control the selectivity towards a given residue is crucial.[5] One strategy for the conjugation with amines over nucleophilic thiol residues has been the use of 'harder' electrophiles including activated esters, sulfonyl chlorides and isothiocyanates.[7] In comparison, α-halocarbonyls and maleimides have been well documented for their selectivity towards thiol residues (Table 3.1).[8]

Aligned closely to both aforementioned challenges is the positional control exerted upon a given amino acid.[5] It has already been stated that should a residue be buried within a peptide/protein, it is less open to modification; although this can be overcome through partial denaturation of the protein allowing the site of interest to undergo modification.[9] Other factors include the surrounding microenvironment as well as the proximity to other reactive residues which can aid or inhibit chemical ligation.[10] A fine illustration of positional control upon the reactivity of a given residue is the comparison of α-amino groups and ε-amino groups. Whilst a protein only bears a single α-amino group, it will typically have multiple ε-amino groups. Nonetheless,

the higher pK_a of the lysine side chains (pK_a: 10.67) compared to the α-amino group (pK_a = 9.16) makes the latter an attractive target for site selective functionalisation.[11,12]

Amino Acid	Abundance (%)	pK_a (C-terminus, N-terminus, side chain)*	Nucleophilicity (*N*)	Isoelectric Point
alanine	7.4	2.33, 9.71, NA	13.01	6.01
arginine	4.2	2.03, 9.00, 12.10	12.96	10.76
asparagine	4.4	2.16, 8.76, NA	13.03	5.41
aspartic acid	5.9	1.95, 9.66, 3.71	13.81	2.77
Cysteine	3.3	1.91, 10.28, 8.14	23.43	5.07
glutamic acid	5.8	2.16, 9.58, 4.15	13.96	3.22
glutamine	3.7	2.18, 9.00, NA	13.45	5.65
glycine	7.4	2.34, 9.58, NA	13.51	5.97
histidine	2.9	1.70, 9.09, 6.04	13.83	7.59
isoleucine	3.8	2.26, 9.60, NA	-	6.02
leucine	7.6	2.32, 9.58, NA	14.01	5.98
lysine	7.2	2.15, 9.16, 10.67	-	9.74
methionine	1.8	2.16, 9.08, NA	13.13	5.74
phenylalanine	4.0	2.18, 9.09, NA	14.12	5.48
proline	5.0	1.95, NA, 10.47	18.08	6.48
serine	8.1	2.13, 9.05, 13*	13.16	5.68
threonine	6.2	2.20, 8.96, 13*	12.69	5.87
tryptophan	1.3	2.38, 9.34, NA	-	5.88
tyrosine	3.3	2.24, 9.04, 10.10	-	5.66
valine	6.8	2.27, 9.52, NA	13.65	3.97

Table 3.1 Key parameters of the 20 naturally occurring amino acids including: abundance, pK_a, Nucleophilic (*N*) according to Mayr's reactivity scale towards benzhydrylium ions,[13] and Isoelectric point, *approximate

3.3 ^{18}F-Fluorination of Biomolecules

Taking all these factors into account and combined with the known challenges in radiochemistry, such as the low stoichiometry of reagent, poor reactivity of fluoride in water and short half-life of fluorine-18,[14] the installation of fluorine-18 into biomolecules is certainly not a trivial matter. To date, fluorine-18 incorporation into biomolecules falls broadly, into two categories: 1) direct methods whereby fluorine-18 is incorporated straight into the biomolecule of interest through the formation of C-^{18}F, B-^{18}F and Si-^{18}F bonds or *via* chelation with Al-^{18}F complexes (Scheme 3.1A); 2) indirect methods whereby the radiosynthesis of a prosthetic group labelled with fluorine-18 is undertaken prior to conjugation with a given biomolecule (Scheme 3.1B).[15]

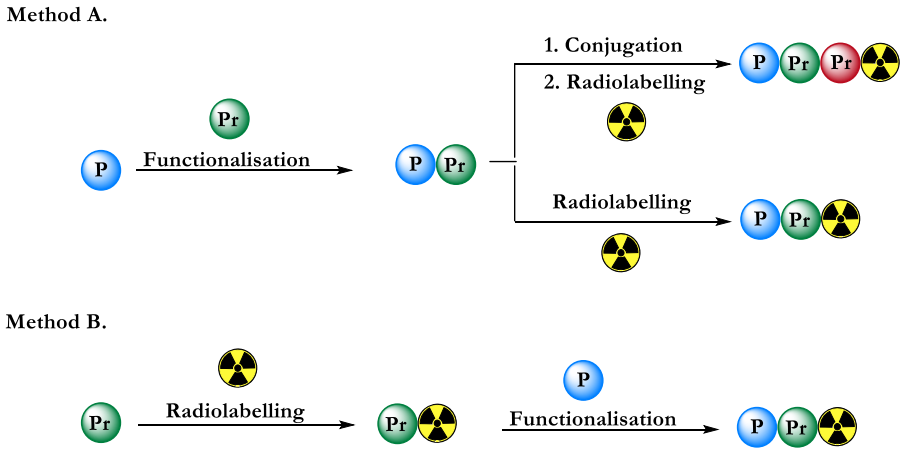

Scheme 3.1 General scheme for the incorporation of fluorine-18 into biomolecules A) Direct incorporation of fluorine-18 into biomolecules; B) Indirect incorporation of fluorine-18 into biomolecules via formation of prosthetic groups; P: peptide; Pr: Prosthetic group

3.4 Direct Radiolabelling of Biomolecules

The use of S_NAr reactions to incorporate fluorine-18 into small molecules is well documented.[16] For biomolecules however, this strategy from ^{18}F-fluorination was not reported till 2009. Berndorff and co-workers reported the trimethylammonium leaving group for the radiofluorination of **3.1** (Scheme 3.2A).[17]

For efficient ^{18}F-incorporation, the C-terminus required modification prior to ^{18}F-fluorination. Following this work, Chen and co-workers utilised the nitro leaving group for the radiolabelling of modified monomeric and dimeric cyclic RGD peptides **3.3** and **3.5** respectively (Scheme 3.2B).[18]

3.4.1 C-^{18}F Bond Formation

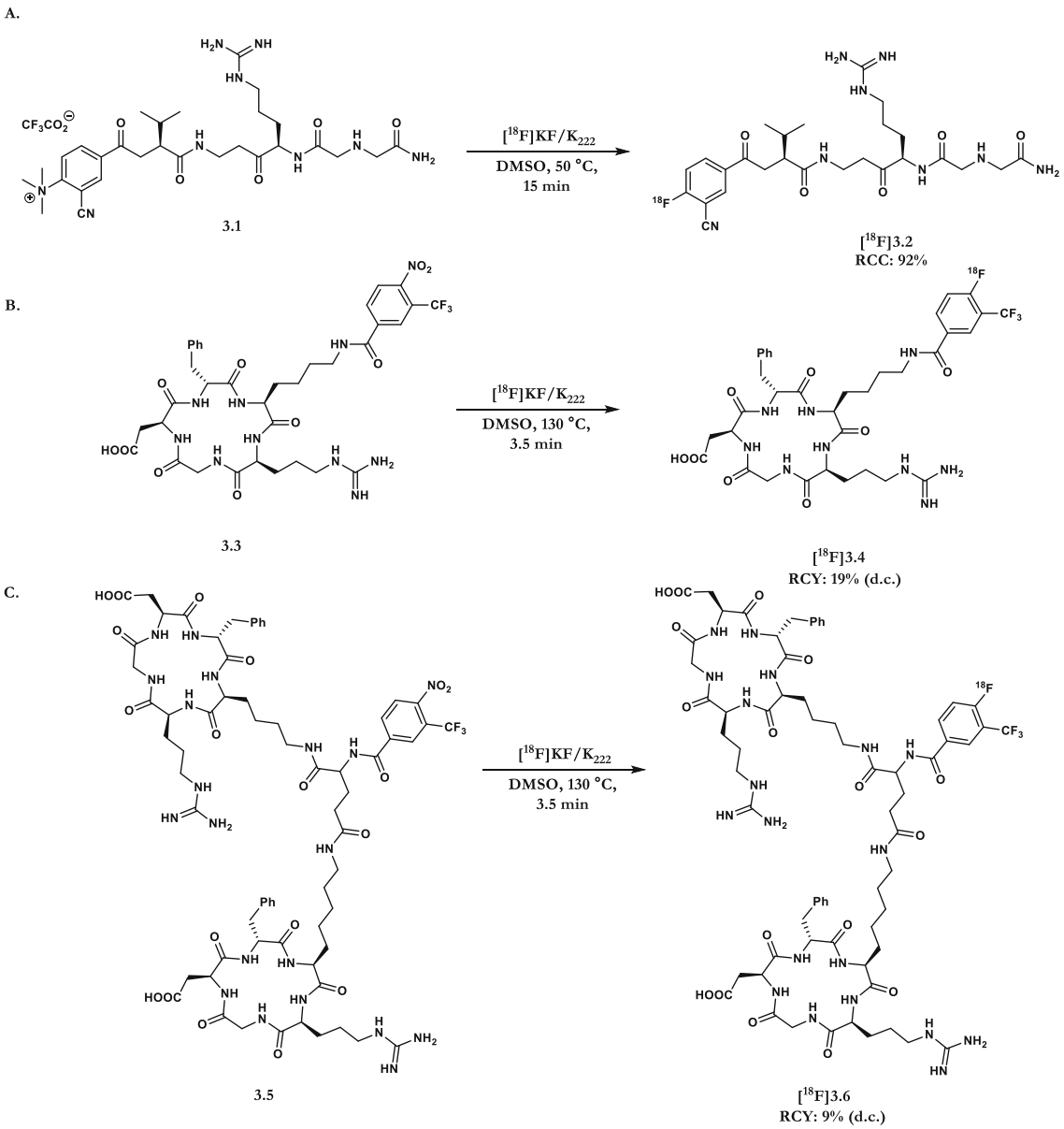

SCHEME 3.2. Nucleophilic aromatic substitution of biomolecules

For the direct aliphatic C-^{18}F bond formation in biomolecules, few examples have been disclosed. In 2009, Ametamey and co-workers reported the labelling of peptides via the ring opening of aziridines. This methodology was used to access tetrapeptide **[^{18}F]3.9**, thymidine derivative **[^{18}F]3.10** and octapeptide **[^{18}F]3.11** (Scheme 3.3).[19]

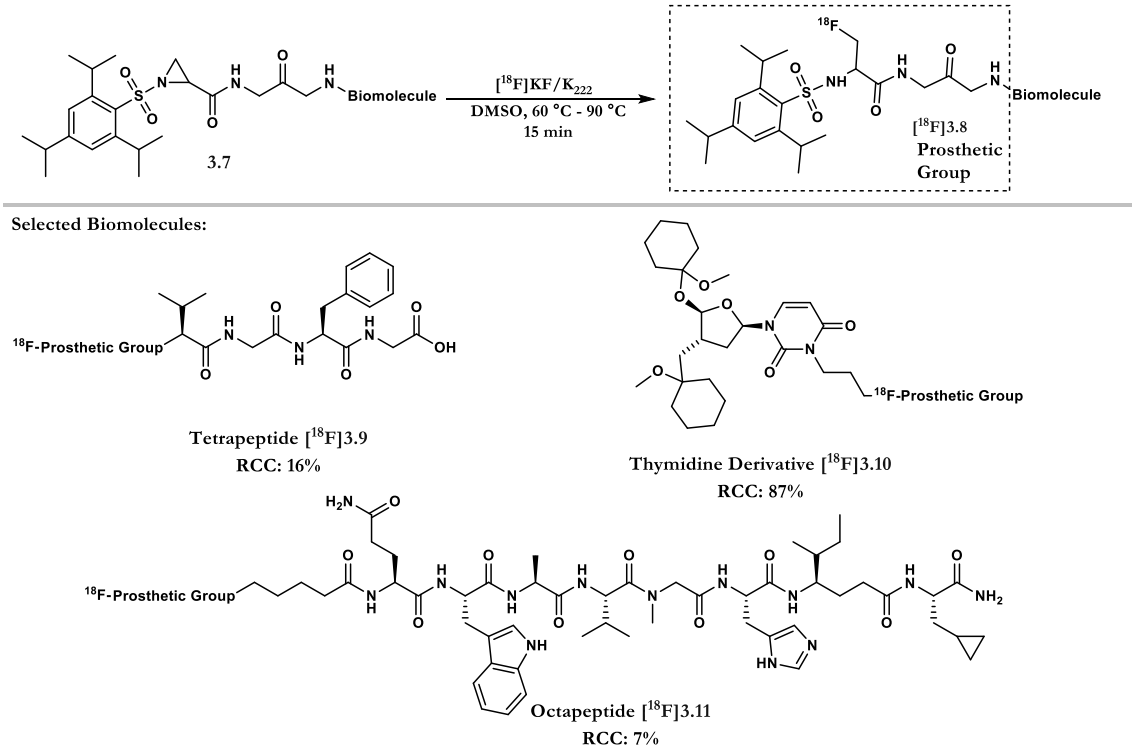

Scheme 3.3. ^{18}F-Fluorination of biomolecule *via* ring opening of aziridines

Whilst demonstrating some utility, both S_NAr and S_N2 reactions typically require biomolecules be able to survive in polar organic medium and moderate to high temperatures; factors that limit the scope of both strategies. O'Hagan and co-workers, in an effort to develop more favourable condition, sought inspiration from the biocatalytic transformation of the naturally occurring fluorinase enzyme (Scheme 3.4A).[20] This allowed for the first time, the use of nucleophilic [^{18}F]fluoride in water under ambient conditions for a S_N2 type transhalogenation reaction. In this seminal work, the late stage ^{18}F-fluorination of RGD-TEG-CIDEA **3.14** in the presence of

L-SeMeT (Scheme 3.4B) was described. Whilst highly innovative, expansion of this strategy to other (bio)molecules has stalled due to the limited scope of the reaction. Furthermore, several modifications to the lysine residue were required prior to ^{18}F-fluorination. This led to a precursor that structurally deviates significantly from the native cRGD peptide.

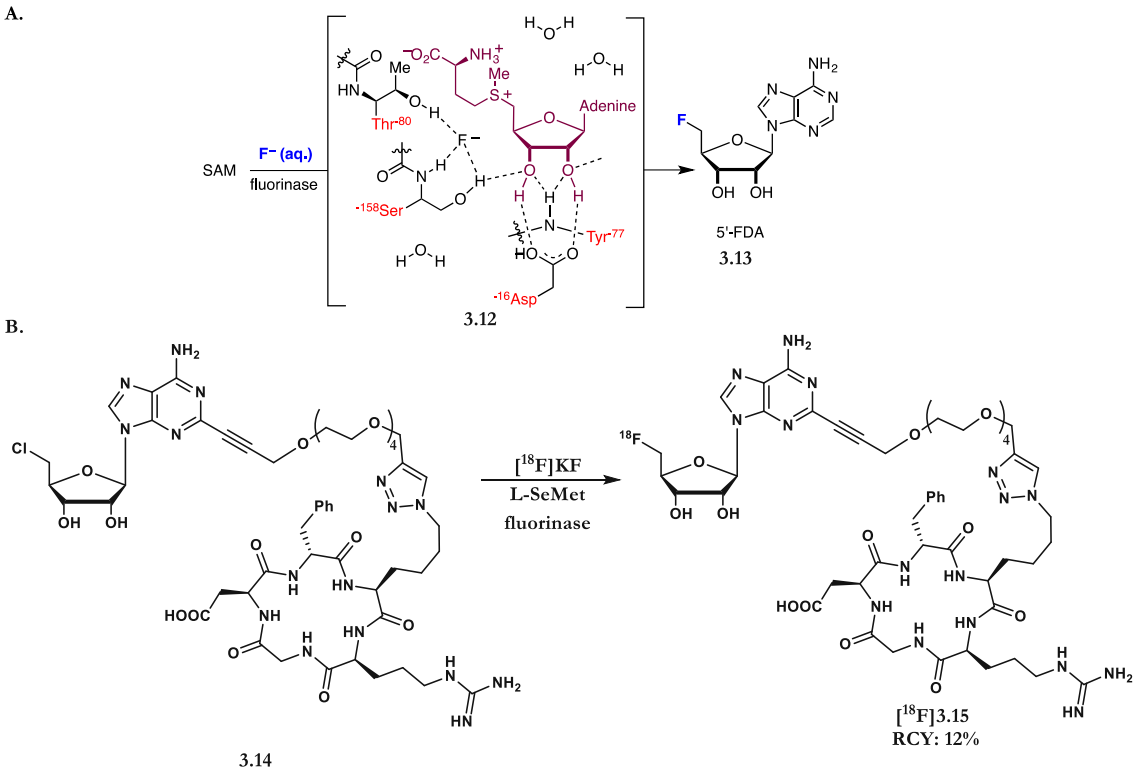

Scheme 3.4. Biocatalytic ^{18}F-fluorination in aqueous medium with fluorinase

3.4.2 B-^{18}F Bond Formation

B-^{18}F bond formation in small molecules has been widely used since the 1960's,[21,22] it was not till 2005 that it was applied to biomolecules (Scheme 3.5A).[23] In this instance, [^{18}F]KHF_2 was reacted in aqueous media with pinacol phenyl boronate diester **3.16** conjugated to biotin. This pioneering work was extended to biotinylated arylboronic ester **3.18** under carrier added conditions (Scheme 3.5B).[24] Further examples of this transformation have been reported by Keller and co-workers for the

^{18}F-labelling of Marimastat **3.20**, and later by Li and Perrin for the ^{18}F-labelling of dimeric cyclo-RGD **3.22** (Scheme 3.5C, D).[25,26]

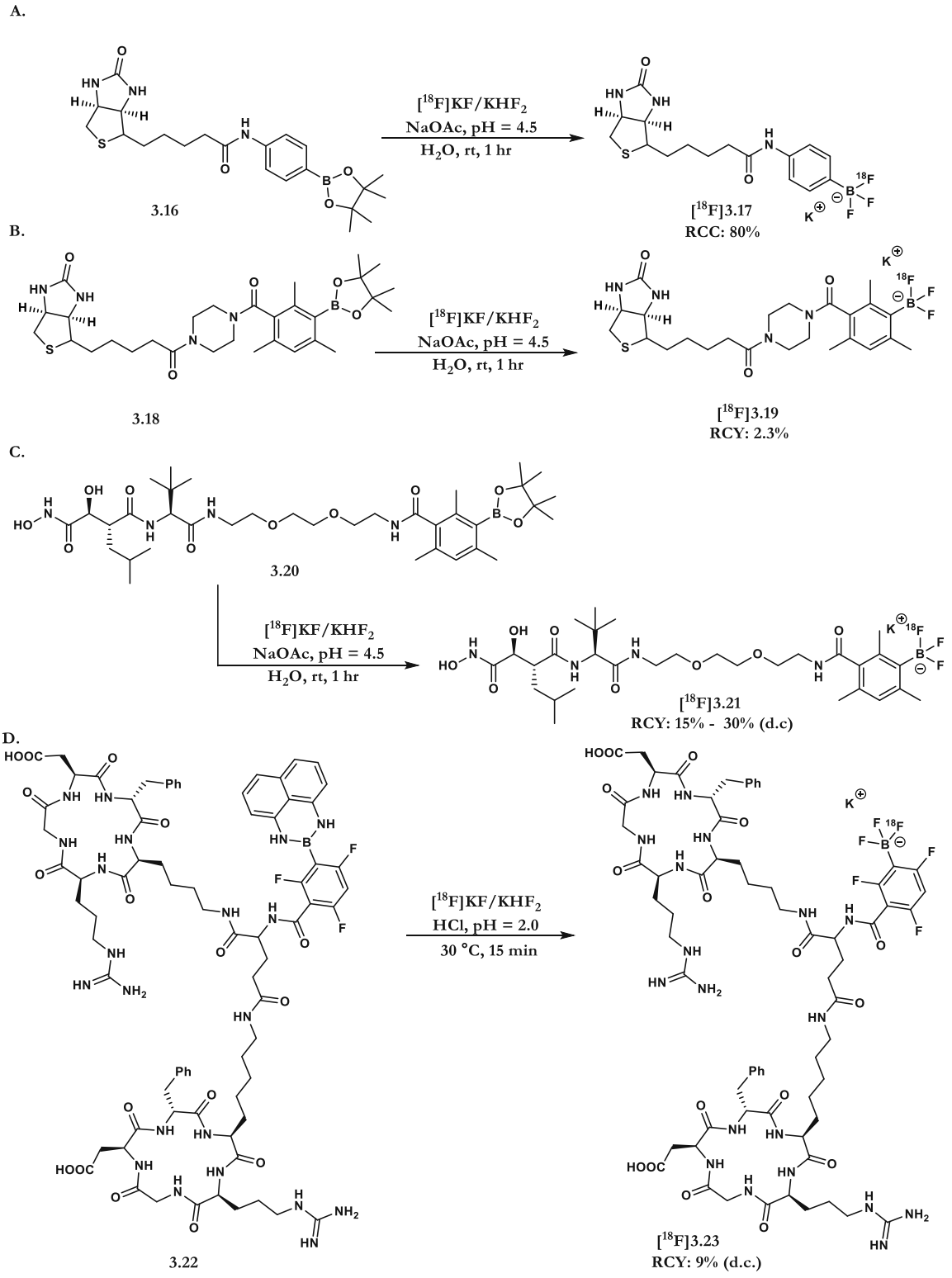

Scheme 3.5. Examples of B-^{18}F bond formation within biomolecules

Direct access for the preparation of the ^{18}F-trifluoroborate motif has also been reported *via* isotopic exchange of the corresponding ^{19}F-containing precursor. This facile transformation has since been used to access a range of drug molecules and biologically relevant targets (Scheme 3.6A, B).[27,28,29]

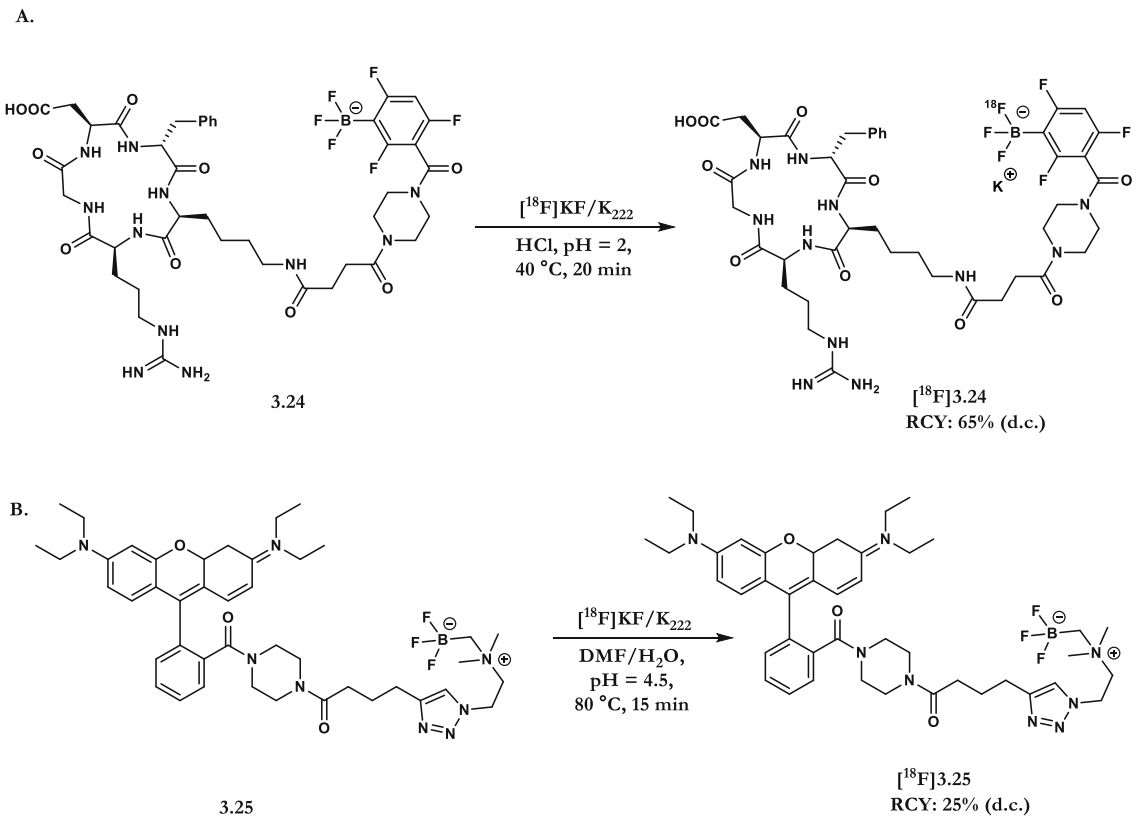

Scheme 3.6. Examples of B-^{18}F bond formation within biomolecules *via* isotopic exchange

Compared to C-^{18}F bond formation, B-^{18}F bond forming processes offer improved biocompatibility in terms of reaction medium and/or reaction temperature. Both strategies still have drawbacks however. First, the need for acidic medium is prohibitive to those biomolecules with greater pH sensitivity. Furthermore, both transformations can result in low molar activities. This stems from the use of KHF_2 as a carrier or, from the release of fluorine-19 during isotopic exchange. This can have implications when exploring occupancy studies *in vivo*.

3.4.3 Si-^{18}F Bond Formation

The development of Si-^{18}F bond formation for the radiolabelling of biomolecules was first reported by Perrin and co-workers using the alkyltriethoxysilane conjugated biotin **3.26** as a precursor to **[^{18}F]3.27**.[23] Whilst high incorporation of fluorine-18 was reported, the moderate stability of the ^{18}F-containing group in aqueous solution hindered application for *in vitro*/*in vivo* studies (Scheme 3.7).

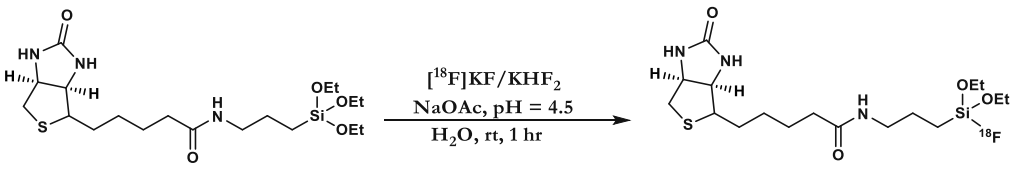

3.26 **[^{18}F]3.27**
ca. 100% ^{18}F-incorporation

Scheme 3.7. Si-^{18}F bond formation in biomolecules

Niemeyer, by substituting the ethoxy side chains for ^{t}Bu, reported improved stability of the Si-^{18}F bond *in vitro* over 60 minutes.[30] This strategy was illustrated by the ^{18}F-labelling of an oxime-derivatised Tyr$_3$-octreotate **3.28** bearing triorganofluorosilane functionality (Scheme 3.8A). Later, Voigtmann and co-workers reported an alternative strategy for the ^{18}F-labelling of biomolecules *via* the nucleophilic displacement of alkoxy, hydroxy or hydride leaving groups (Scheme 3.8B).[31]

As was highlighted for B-^{18}F bond formation, many of these reactions still require acidic conditions. Furthermore, the lipophilic nature of silicon functionalities may potentially influence the biological properties of the substrate in question; such as the increased non-specific binding of the molecule.[32] To overcome this, the use of PEG groups or zwitterion containing functional groups have been used to reduce this effect upon lipophilicity (Scheme 3.8C).[33]

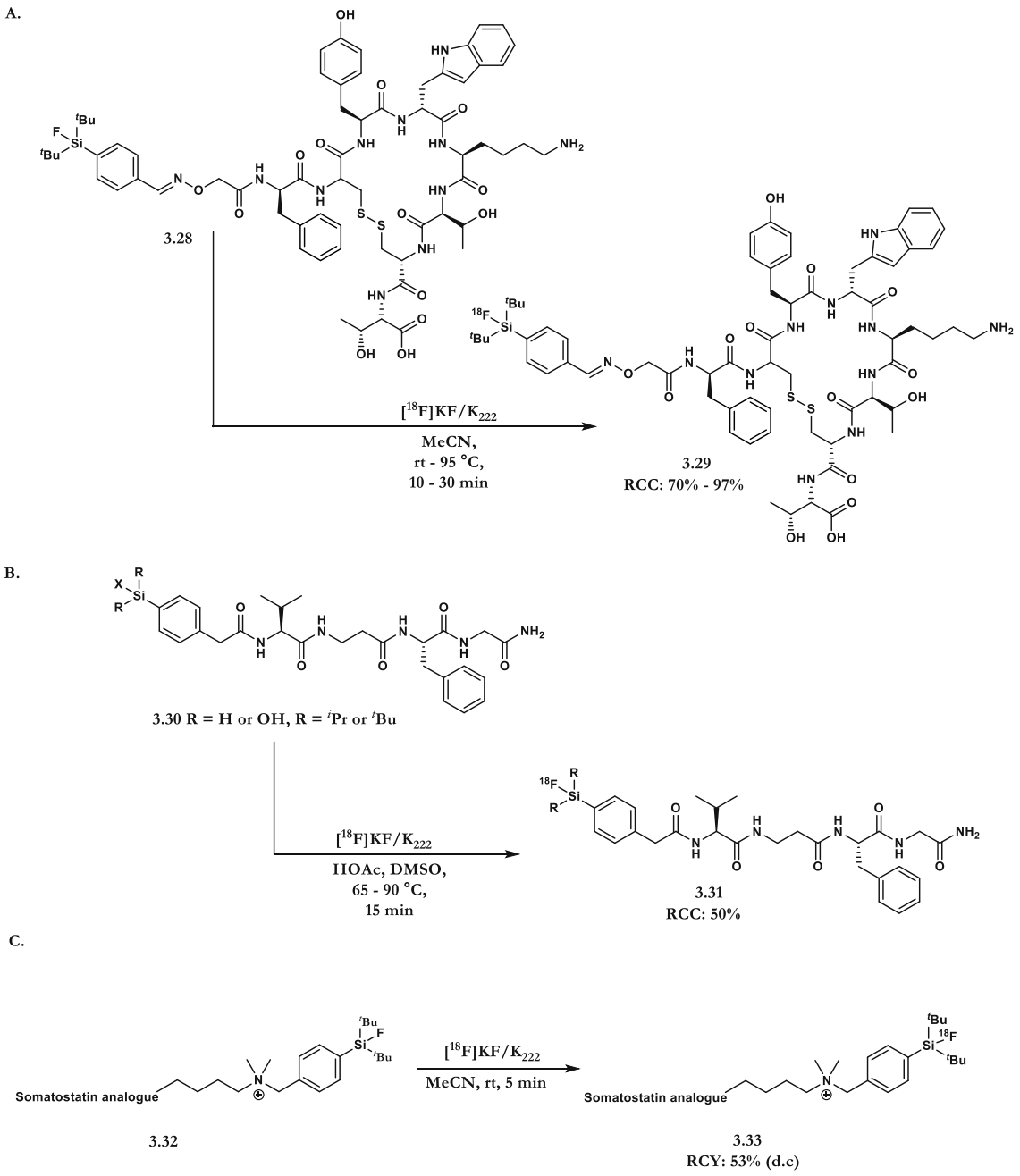

Scheme 3.8. Examples of Si-^{18}F Bond formation within biomolecules

3.4.4 Al-^{18}F Bond Chelation

^{18}F-labelling *via* chelation has greatly enhanced the field of labelled biomolecules for PET imaging.[34] Taking advantage of fast kinetics of chelation chemistry whilst potentially eliminating the need for HPLC purification, this approach has clear benefits when compared to C-^{18}F, B-^{18}F and Si-^{18}F bond forming processes.

Goldenberg and co-workers, in a one pot process, reported the synthesis of the stable Al-^{18}F complex **3.35**.[35] The authors noted that Al-^{18}F complexes could bind tightly to 1,4,7-triazacyclononane-1,4,7-triacetic acid **3.34** (NOTA) chelating ligands (Scheme 3.9).

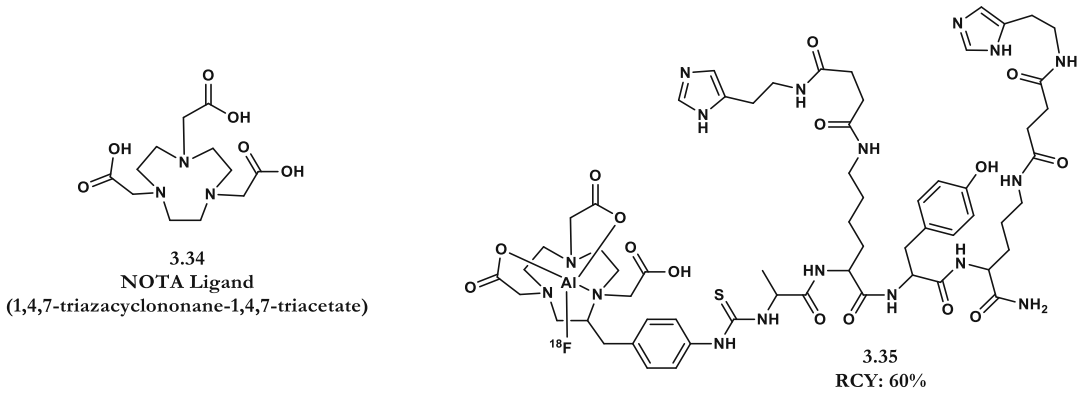

Scheme 3.9. Al-^{18}F bond formation with NOTA ligand **3.34**

Whilst this chelation strategy has been used extensively for the radiofluorination of biomolecules, many of the Al-^{18}F chelation methods using NOTA of NODA (1,4,7-triazacyclononane-1,4-diacetate) chelators require elevated reaction temperatures.[36-38] To this end, scientists have sought to develop both chelators and reaction conditions that have a greater compatibility to sensitive biomolecules. In 2016, Bormans and co-workers developed a polydentate ligand **3.36** for the complexation of Al-^{18}F at a relatively mild temperature of 40 °C. This ligand was subsequently used for the radiolabeling of peptide Glu-NHCO-NH-Lys(Ahx)L3 **[^{18}F]3.37** in 25% RCY (Scheme 3.10).[39]

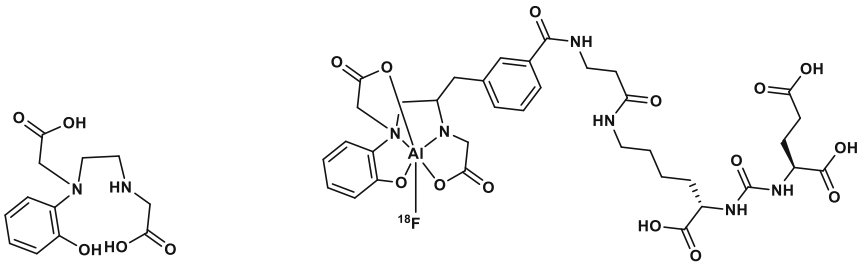

3.36

[^{18}F]3.37
RCY: 25%
MA: 27 GBq μmol^{-1}

Scheme 3.10. Al-^{18}F bond formation with ligand **3.36**

3.5 Indirect ^{18}F-fluorination of Biomolecules

As emphasised throughout the previous section (3.4), direct nucleophilic ^{18}F-fluorination is usually undertaken under relatively harsh conditions for biomolecules; such as at low pH and high temperature. These non-physiological conditions are not tolerated by many biomolecules, many of which are susceptible to hydrolysis and/or degradation. Therefore, the applicability of this type of approach for the radiofluorination of biomolecules can be limited.[4]

To circumvent this problem, scientists have developed indirect methods which involve the radiosynthesis and conjugation of radiolabeled prosthetic groups (Scheme 3.11). These prosthetic groups typically contain orthogonally reactive functionalities that allow for the rapid and efficient conjugation to biomolecules. This multiple step process has been illustrated within a wide range of transformations including alkylation, amidation, acylation, imidation, oxime, hydrazine bond formation as well as glycosylation.[4,15,40,41]

3.5.1 Prosthetic Groups for Functionalisation of Amino Residues

The most common fluorine-18 containing prosthetic group for conjugation to amino groups is *N*-succinimidyl-4-[^{18}F]fluorobenzoate ([^{18}F]SFB) **[^{18}F]3.41**, an

acylating agent amenable to conjugation with amino groups found at *N*-termini or within lysine residues. The first reported synthesis by Vaidyanathan and Zalutsky in the early 1990's required a multistep approach (Scheme 3.11).[42] Initial displacement of the trifluoromethylammonium group with [^{18}F]KF/K_{222} was followed by oxidation of aldehyde **[^{18}F]3.39** with $KMnO_4$. Lastly, activation of ester **[^{18}F]3.40** with NHS and DIC in THF afforded **[^{18}F]3.41** in an activity yield of 25% and molar activity of 10 GBq μmol^{-1}. During this study, Vaidyanathan and Zalutsky were able to conjugate [^{18}F]SFB to a monoclonal antibody fragment (F(ab')$_2$) in up to 60% RCY.[42] In 2012, Löser and co-workers demonstrated the value of **[^{18}F]3.41** *via* conjugation to four resin bound peptides (Scheme 3.12).[43]

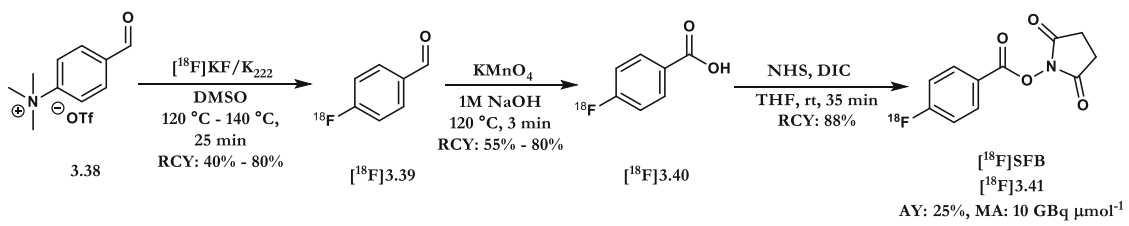

Scheme 3.11 Radiosynthesis of [^{18}F]SFB **[^{18}F]3.41**

With a synthesis time close to two hours and a decay corrected yield of 25% however, there was scope for further optimisation and derivatisation. To this end, scientists have sought to either, optimise the radiosynthesis of [^{18}F]SFB or,[44] investigate other ^{18}F-labelled prosthetic groups amenable to conjugation with amino groups. This includes, *N*-succinimidyl-*o*-(di-*tert*-butyl[^{18}F]fluorosilyl)-benzoate ([^{18}F]SiFB) **[^{18}F]3.44**,[45] 6-[^{18}F]fluoronicotinic acid tetrafluorophenyl ester ([^{18}F]F-Py-TFP) **[^{18}F]3.46** and 3-[^{18}F]fluoropropanesulfonyl chloride **[^{18}F]3.49** (Scheme 3.13, Scheme 3.14, Scheme 3.15).[46,47]

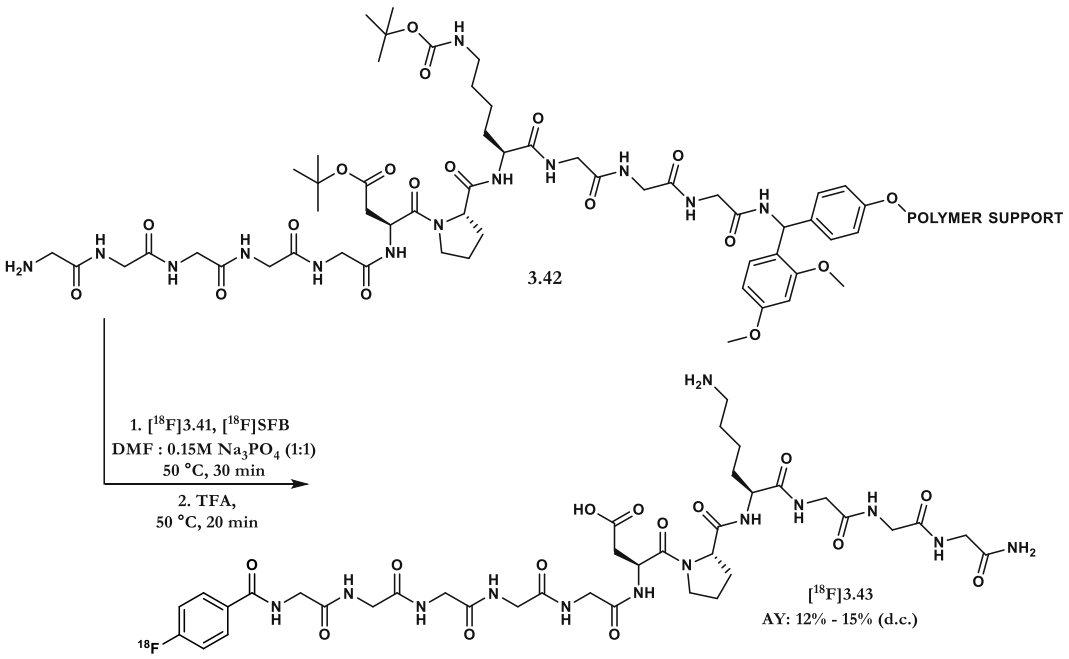

Scheme 3.12 Conjugation of **[^{18}F]3.41** to resin bound peptides

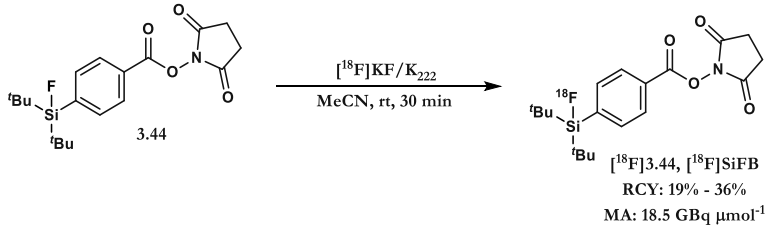

Scheme 3.13 Radiosynthesis of [^{18}F]SiFB **[^{18}F]3.44**

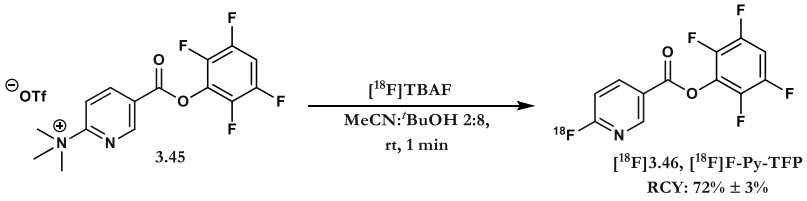

Scheme 3.14 Radiosynthesis of [^{18}F]F-Py-TFP **[^{18}F]3.46**

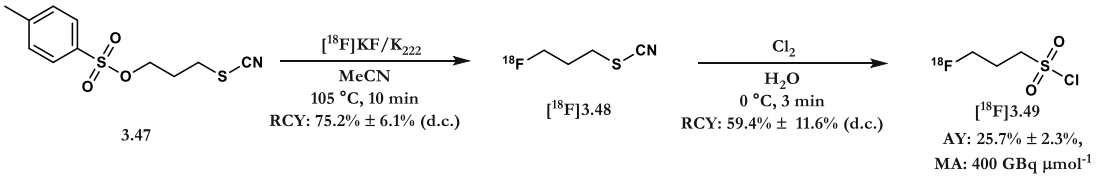

Scheme 3.15 Radiosynthesis of 3-[^{18}F]fluoropropanesulfonyl chloride **[^{18}F]3.49**

Bioconjugation reactions for oxime formation have also received attention for the radiosynthesis of amino-oxy-functionalised peptides bearing fluorine-18.[4] Such prosthetic groups typically contain aldehydes/hemi-acetal functional groups amenable to conjugation with amino groups (Scheme 3.16A). Cuthbertson and co-workers reported the radiosynthesis of **[^{18}F]3.53** in 62% RCY (d.c.) by conjugation of **[^{18}F]3.51** with hydroxyl amine derived-RGD-PEG (Scheme 3.16A).[48] In addition to this work, Schirrmacher and co-workers reported the use of [^{18}F]SiFa derived aldehyde, **[^{18}F]3.44** for the labelling of amino-oxy derived cRGD peptide **3.54** at room temperature in 50% RCY (d.c.) (Scheme 3.16B).[49]

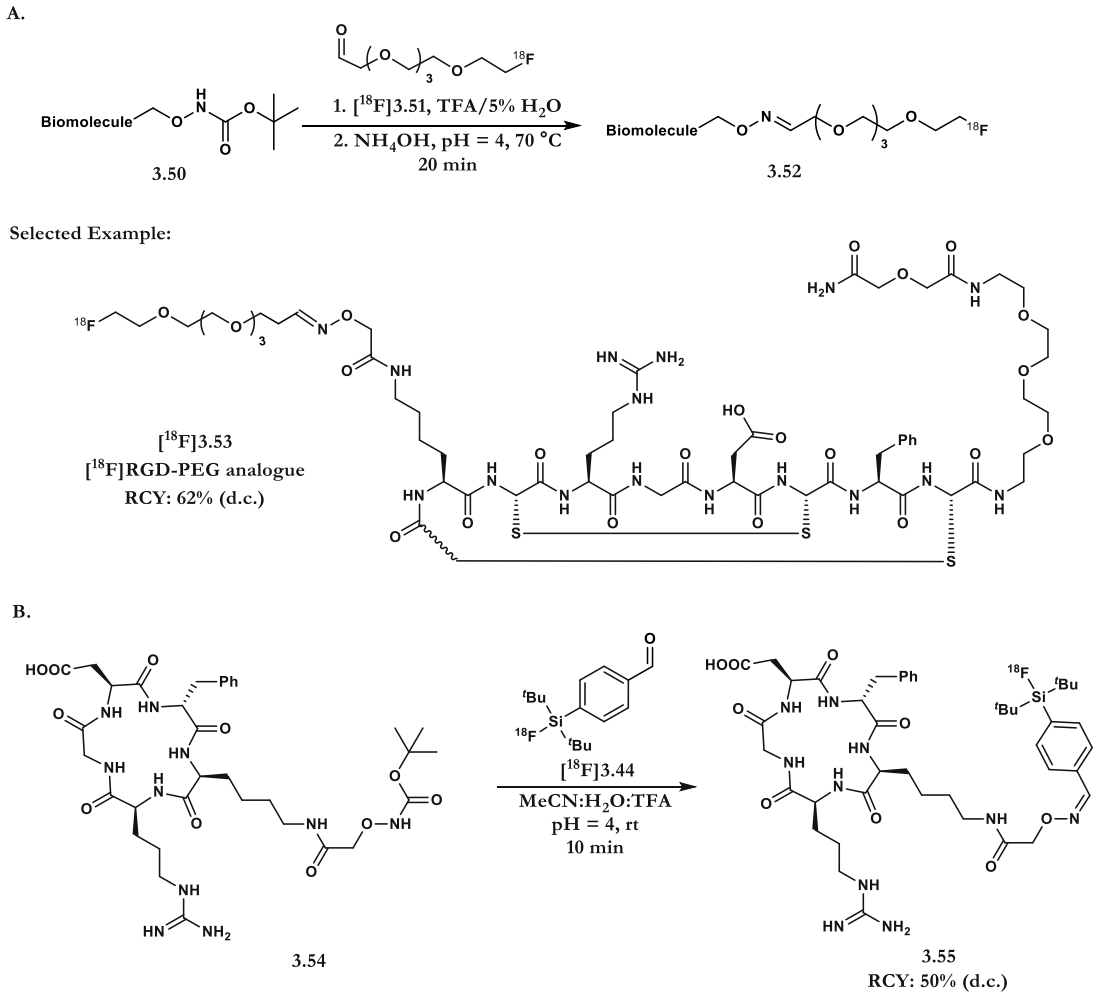

Scheme 3.16 Conjugation of aldehyde based prosthetic groups for the ^{18}F-labelling of biomolecules

Storr and co-workers developed multiple sulfonyl-based prosthetic groups including 3-/4-formyl, 4-maleimido and other functionalised [^{18}F]arylsulfonyl fluorides which can be accessed by reacting the corresponding sulfonyl chlorides with [^{18}F]CsF/Cs_2CO_3 (Scheme 3.17).[50] Subsequently, Storr applied **[^{18}F]3.58** for the conjugation to BBN-ONH_2, a 9 amino acid bombesin analogue, in 35% RCY (d.c.) (Scheme 3.18).

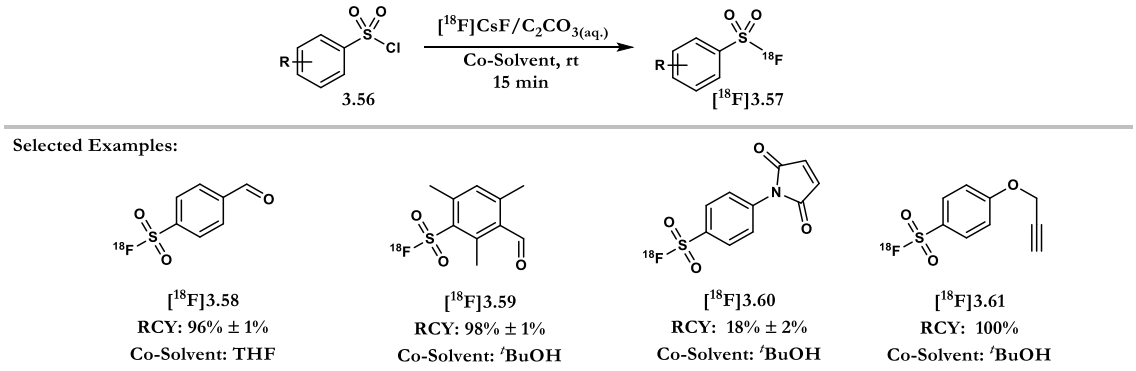

Scheme 3.17 ^{18}F-labeled aryl-sulfonyl-fluoride derivatives

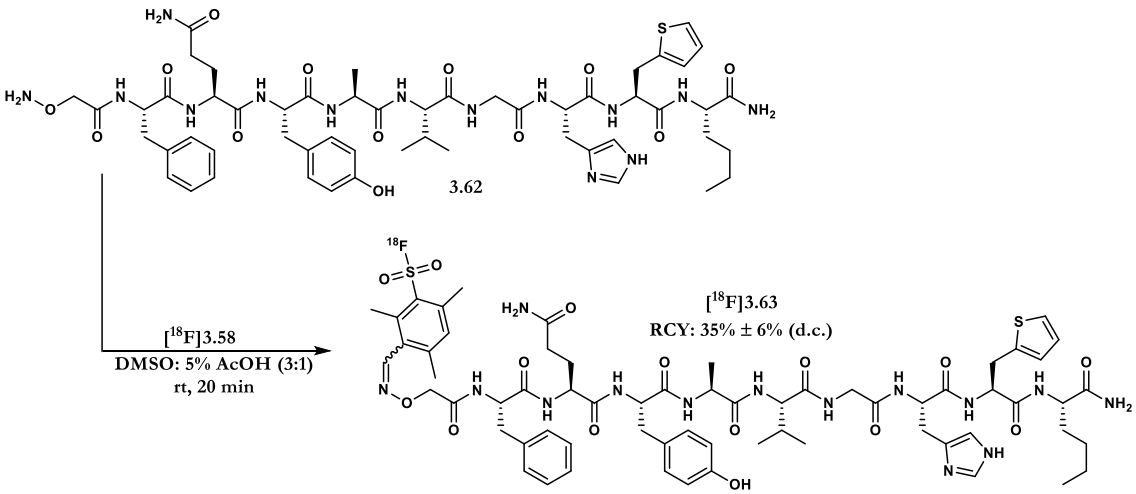

Scheme 3.18 Application of **[^{18}F]3.58** for conjugation to bombesin analogue **3.62**

3.5.2 Prosthetic Groups for Conjugation to Thiol Groups

Whilst [^{18}F]SFB **[^{18}F]3.41** has shown moderate compatibility for the conjugation to cysteine residues,[51] further examples of prosthetic groups exhibiting improved selectivity for thiol over amino-targeting prosthetic groups have been developed. Prosthetic groups amenable to thiol-alkylation include *N*-(4-fluorobenzyl)-2-bromoacetamide **[^{18}F]3.63** ([^{18}F]FBBA) and 2-bromo-*N*-[3-(2-[^{18}F]fluoropyridine-3-yloxy)propyl]acetamide **[^{18}F]3.64** ([^{18}F]FpyBrA) (Scheme 3.19).[52,53] A selection of maleimides derivatives have also been reported for chemoselective Michael addition with cysteine or methionine residues (Scheme 3.19, Scheme 3.20).[54,55,56]

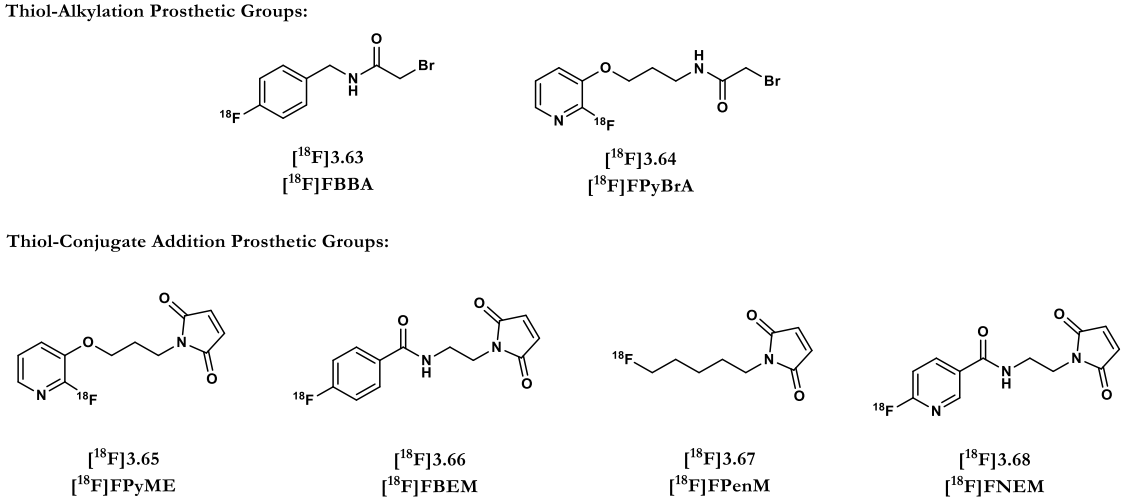

Scheme 3.19 Examples of thiol selective prosthetic groups

Recently, Chen and co-workers reported an alternative strategy with introduction of [^{18}F]hexafluorobenzene **[^{18}F]3.73** into dimeric RGD peptides (Scheme 3.21). Through isotopic exchange, **[^{18}F]3.73** could be accessed readily in 25% RCY and 1.4 GBq μmol^{-1} MA prior to thiol-substitution reaction with c(RGDfK) peptide **3.72**.[57]

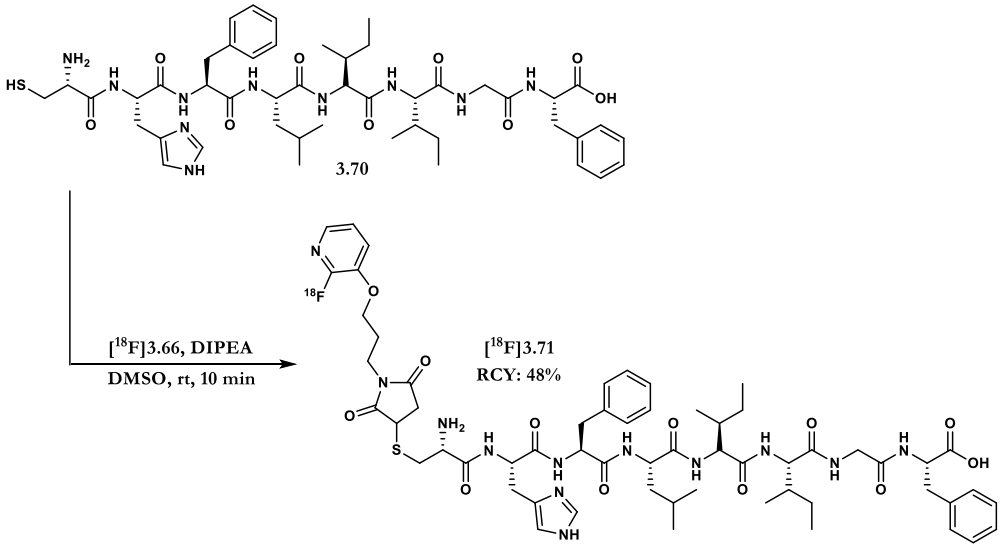

Scheme 3.20 Radiosynthesis of **[^{18}F]3.71** via Michael addition

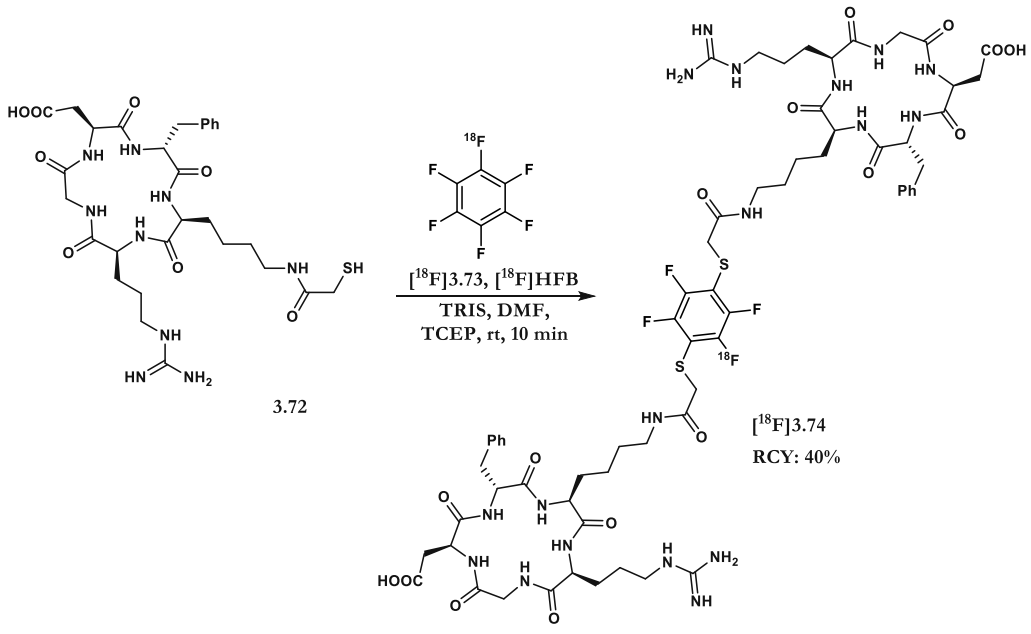

Scheme 3.21 Radiosynthesis of **[^{18}F]3.74** with [^{18}F]HFB **[^{18}F]3.73**

3.5.3 Copper Catalysed Alkyne Azide Cycloaddition (CuAAC)

One of the most widely used transformations for the labelling of biomolecules is that of the copper catalysed alkyne-azide cycloaddition (CuAAC). This variant of the Huisgen 1,3-dipolar cycloaddition was first reported in 2002.[58] The reaction can be performed at ambient temperatures in aqueous medium making it favourable for

functionalising biomolecules. The first use of CuAAC within radiofluorination was in 2006 by the groups of Marik and Sutcliff. In this instance the authors modified the lysine residue prior to conjugation for ^{18}F-labelled prosthetic **[^{18}F]3.75**. This strategy has inspired the development of a wide range of prosthetic groups amenable to CuAAC (Scheme 3.22A, Scheme 3.22B).[59,34,60-61]

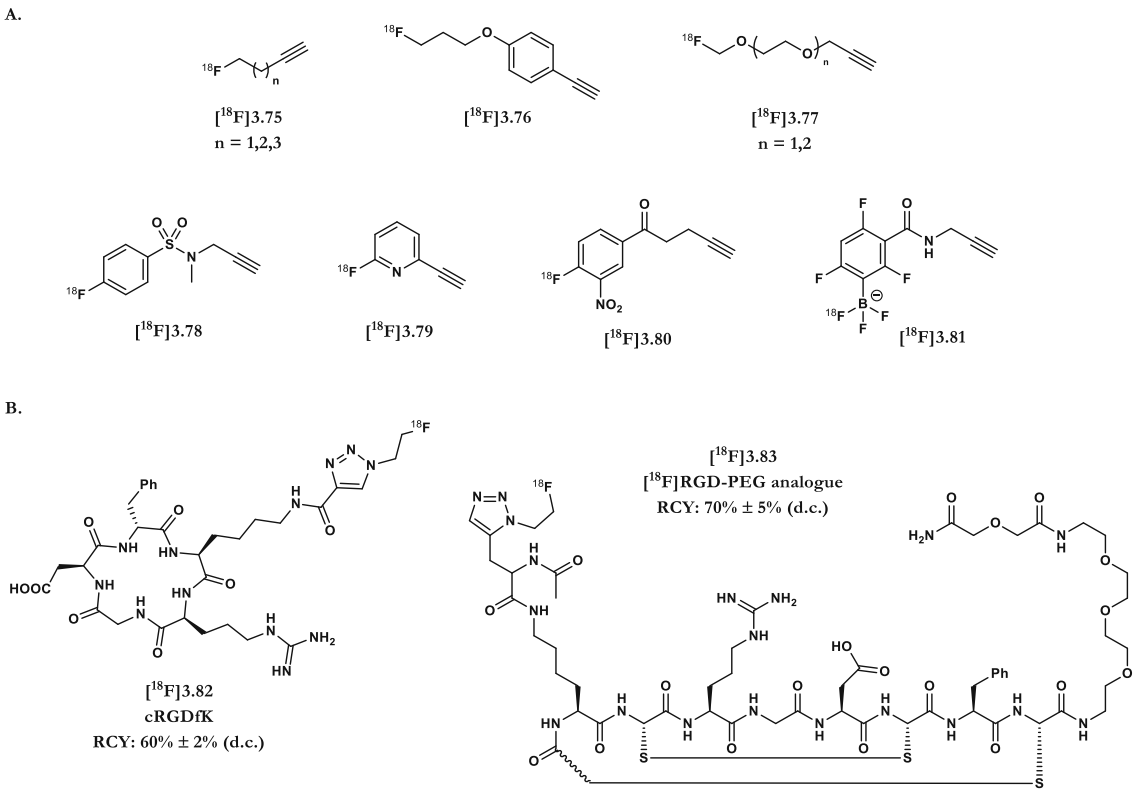

Scheme 3.22. A) Examples of ^{18}F-containing prosthetic groups for CuAAC B) Examples of the CuAAC reaction for the ^{18}F-labelling of biomolecules

3.5.4 Strain Promoted Alkyne-Azide Cycloaddition (SPAAC) Reaction

A lesser known derivative of the CuAAC, namely the strain promoted alkyne-azide cycloaddition (SPAAC) reaction, takes advantage of the ring-strain of a cyclooctyne ring to promote 1,2,3-triazole formation with the corresponding azide

(Scheme 3.23).[34,62] Without the need for copper, this reaction has a distinct advantage over the CuAAC coupling reaction (Scheme 3.23 A, B).[63-64]

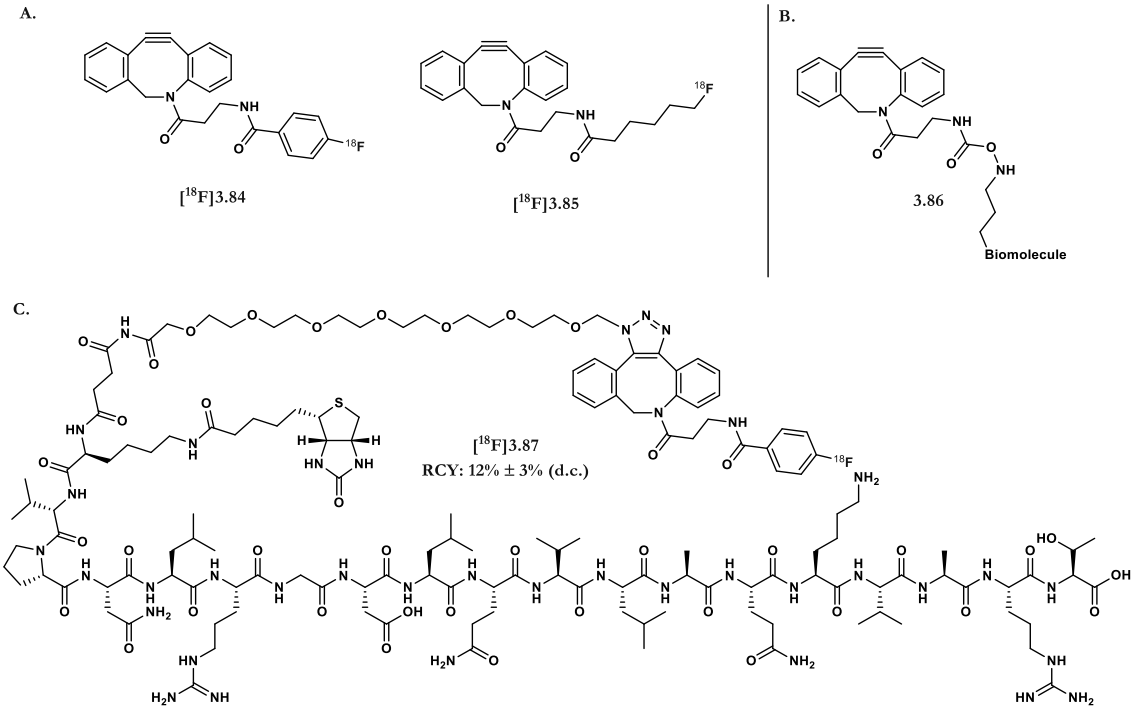

Scheme 3.23. A) List of commonly used ^{18}F-containing prosthetic groups for SPAAC B) Examples of the SPAAC reaction for the ^{18}F-labelling of biomolecules

3.5.5 Inverse Electron Demand Diels-Alder (IEDDA) Reaction

Another innovative reaction is that of the inverse electron demand Diels Alder (IEDDA) reaction. In this instance, an electron rich ^{18}F-labelled tetrazine moiety is utilised, typically in conjugation with the radiolabelled alkene, *trans*-cyclooctene [^{18}F]TCO **[^{18}F]3.89** (Scheme 3.24).[65-66] The extremely fast reaction kinetics (k_2 = 2000 M^{-1} s^{-1} in 9:1 MeOH:H_2O) have been taken advantage of for pre-targeting strategies for the radiolabelling of antibodies *in-vivo*, a class of biomolecules previously inaccessible to radiofluorination due to their prohibitively slow pharmacokinetics (Scheme 3.24).[34,67]

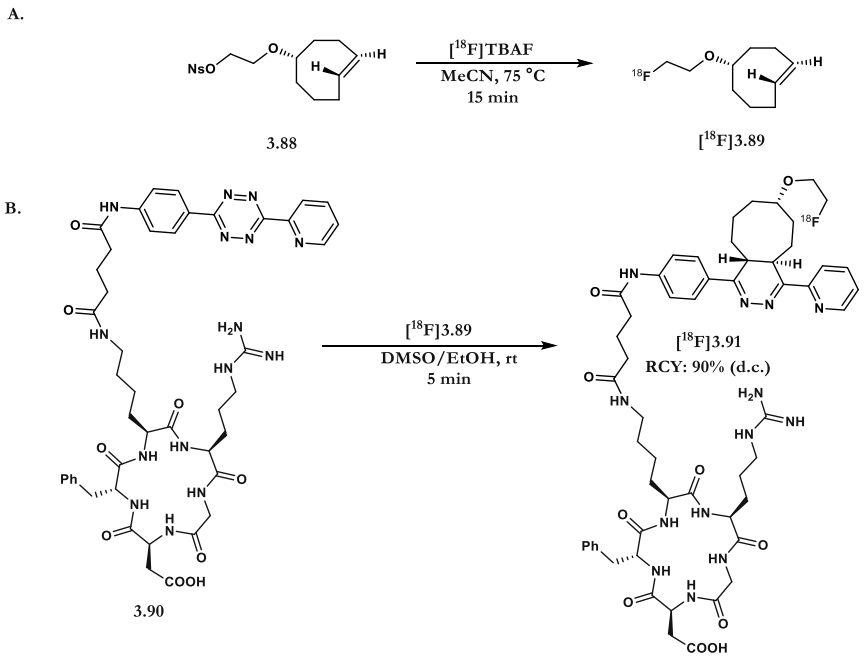

Scheme 3.24. A) Radiosynthesis of [^{18}F]TCO **[^{18}F]3.89** B) Application of **[^{18}F]3.89** within the IEDDA reaction for the labelling of biomolecules

3.6 Radiolabelling of Biomolecules with 'Zero-Sized' Motifs

For many of the works discussed so far, the biomolecule of choice must undergo a modification. For both direct and indirect radiolabelling, this has typically been illustrated *via* conjugation to thiol-, amino- or carboxy- residues. This process is carried out either, prior to radiolabelling or, post-labelling with a given radiolabelled prosthetic group. For both strategies, should major structural modifications be required, alteration of the biomolecules' biological function can occur.[4] This has encouraged the development of innovative labelling methodologies with minimally sized radiolabelled prosthetic groups. Recent studies have focused on radiolabelling with carbon-11. For example, Skrydstrup and co-workers reported that methyl bisphosphine–ligated complexes enable *N*-^{11}C-acetylation of lysine residues within native peptides (3.25A).[68] Following this study, the direct ^{11}C-cyanation of unprotected peptides at a cysteine residue was illustrated by the groups of Buchwald and Hooker. By applying a palladium-mediated cross-coupling for arylation of

cysteine residues, subsequent ^{11}C-cyanation was achieved in good RCYs (3.25B).[69] Whilst both are highly efficient processes, the short half-life of carbon-11 can be restrictive when targeting biomolecules with relatively slow pharmacokinetics.

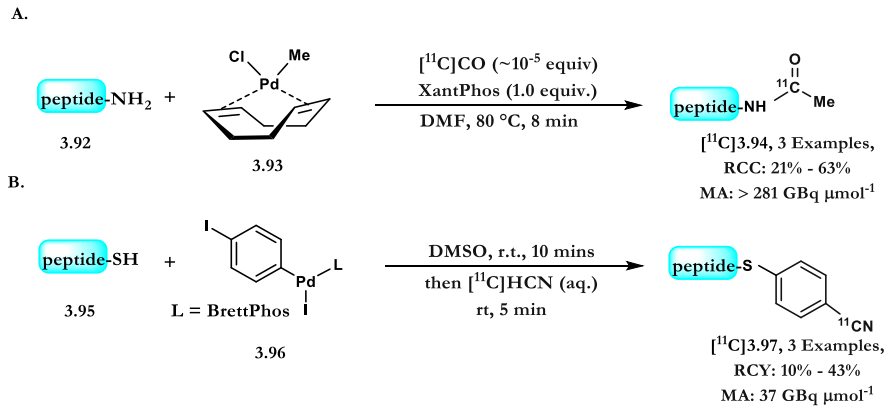

Scheme 3.25 A) ^{11}C-Acetylation of lysine residues B) ^{11}C-Cyanation of cysteine residues

3.7 Fluorination of Biomolecules

Fluorine and its isotopes fluorine-18 and fluorine-19 present scientists with widespread opportunities when developing novel strategies for the installation of zero-sized motifs into biomolecules. Compared to carbon-11, fluorine-18 offers improved flexibility for the radiosynthesis and subsequent PET imaging due to its longer half-life and enhanced resolution.[70] Alternatively, by using fluorine-19, 'zero-background' ^{19}F-NMR studies can be undertaken.[71,72] The high sensitivity of this technique has already been used to elucidate structural, functional and dynamic interactions between receptors and enzyme catalyst.[72]

3.7.1 ^{18}F-Fluorination of Unmodified Peptides

For the direct ^{18}F-fluorination of biomolecules, Britton and co-workers reported the site selective ^{18}F-fluorination of unprotected peptides using *N*-[^{18}F]fluorobenzenesulfonamide ([^{18}F]NFSI) **[^{18}F]3.99**, a reagent derived from [^{18}F]F_2. In this work, Britton and co-workers targeted the leucine residue using

sodium decatungstate (NaDT) for hydrogen atom abstraction prior to ^{18}F-fluorination. This procedure was shown to be tolerant to free carboxylic acid, amide and amine residues. However, the use of [^{18}F]F_2 and the resulting low molar activity of this transformation (1.3 – 5.3 MBq μmol^{-1}) is a drawback (Scheme 3.26).

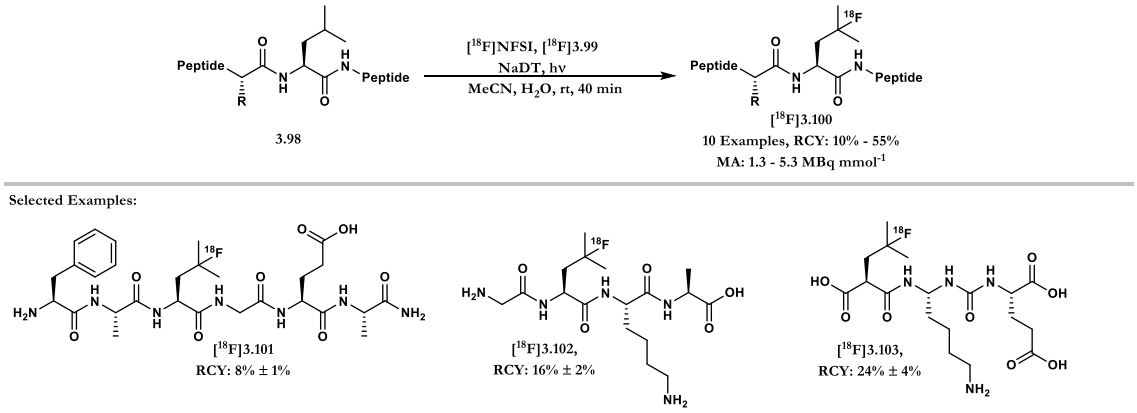

Scheme 3.26. Late stage ^{18}F-fluorination of unprotected peptides with [^{18}F]NFSI **[^{18}F]3.99**

3.8 Trifluoromethylation of Unmodified Peptides

Whilst the radiolabelling of biomolecules with fluorine-18/fluorine-19 itself is a valuable transformation, one notable challenge is overcoming the degree of chemical shift anisotropy (CSA); a process leading to chemical shielding differences of the electrons surrounding the nucleus relative to the external magnetic field. The impact is the broadening of protein NMR resonance and the loss of key information.[73] To this end, our group, in a complementary approach to the work of Davis and co-workers,[71] sought to develop a strategy for the installation of the smallest symmetrical per-fluorinated group, the trifluoromethyl 'CF_3' group. Not only would this serve as a highly useful transformation for the installation of fluorine-18 into biomolecules,[2,4] but the reduced CSA effect on the fluorine nuclei themselves would be advantageous when investigating structural information using ^{19}F-NMR spectroscopy.

Nevertheless, for the installation of the ^{18}F-trifluoromethyl group, the design and radiosynthesis of a novel ^{18}F-trifluoromethylation reagent would be required.

3.8.1 Trifluoromethylation Reagents

Several prominent commercially available trifluoromethylation reagents exist including: Togni **3.104**, Togni II **3.105**, Ruppert-Prakash **3.106**, Langlois **3.107**, Baran **3.108** and Umemoto's reagent **3.109** (Figure 3.1).[74] At the outset of this investigation into the ^{18}F-trifluoromethylation of biomolecules, reagent selection was seen as crucial for the success of the project. In this instance, both the viability of the radiosynthesis to access the reagent as well as its feasibility for the ^{18}F-trifluoromethylation of biomolecules would need to be considered.

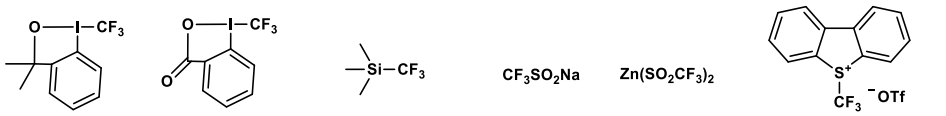

Figure 3.1. Commercially available trifluoromethylation reagents

3.8.2 ^{19}F-Fluorination of Unmodified Peptides

In 2008, Togni and co-workers reported the trifluoromethylation of the cysteine residue using the hypervalent trifluoromethylation reagent **3.105** (Scheme 3.27). In this work, Togni and co-workers reported a high selectivity for the cysteine residue in the presence of amino, hydroxy, carboxy, amide, thioacetal and alkenyl groups. Whilst the tryptophan residue was shown to compete with the thiol group for the trifluoromethyl group, at higher pH, this chemoselectivity could be influenced to favour trifluoromethylation of the thiol residue.[75]

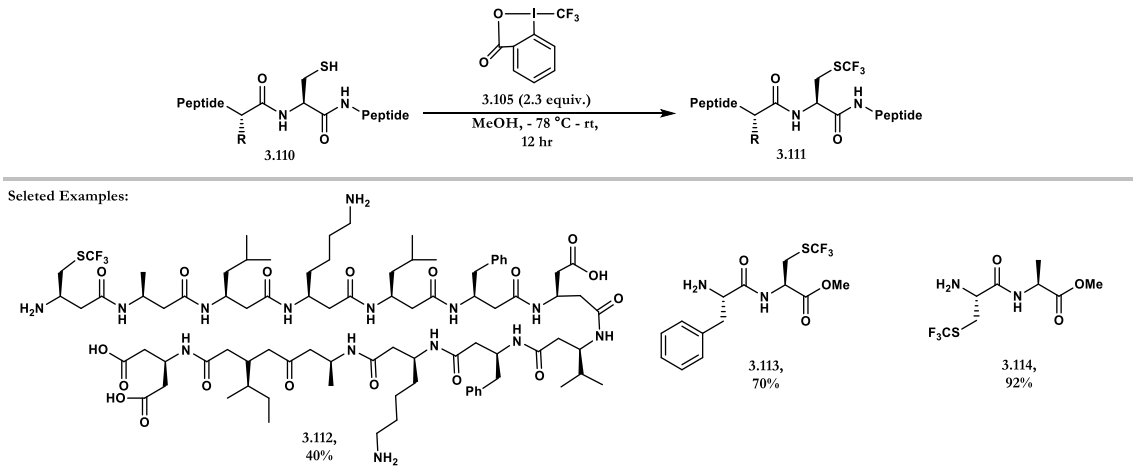

Scheme 3.27 Trifluoromethylation of cysteine residues with **3.105**

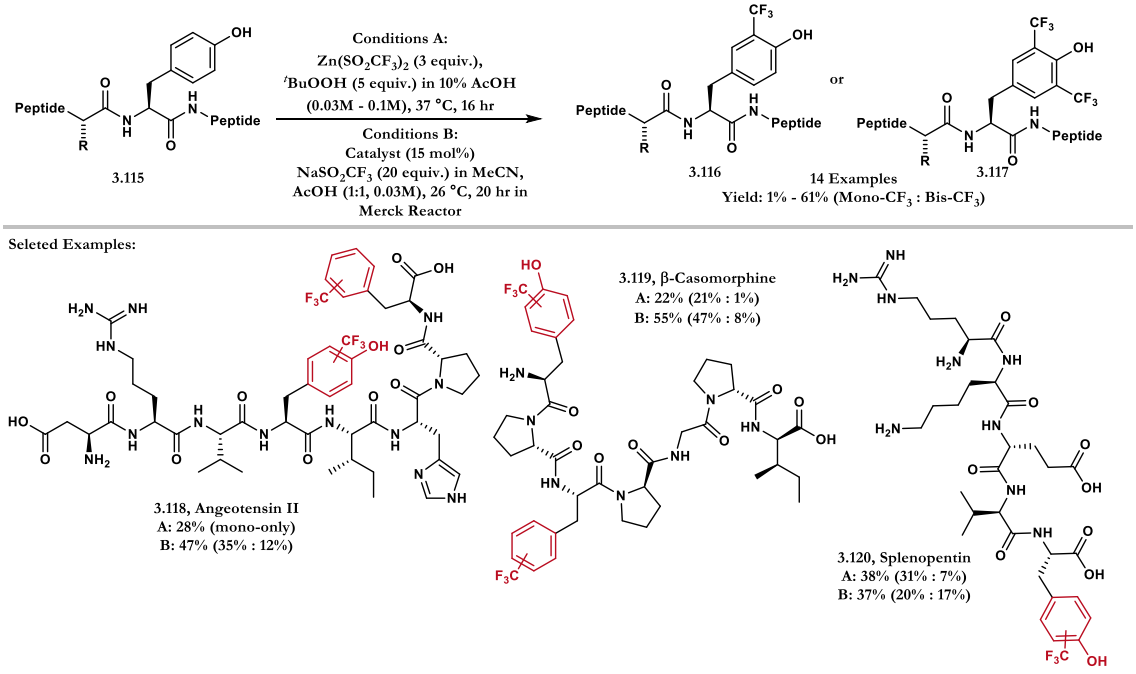

Scheme 3.28. Trifluoromethylation of tyrosine residues (yield quoted accounts for total CF_3 incorporation into biomolecule) Catalyst: Ir[dFCF3ppy]

More recently, Krska and co-workers reported the radical C-H trifluoromethylation of unmodified peptides at the tyrosine residue. Using either $Zn(SO_2CF_3)_2$ in combination with ^{t}BuOOH or $NaSO_2CF_3$ under photoredox catalysis, the authors were able to incorporate the trifluoromethyl group into tyrosine residues of peptides as complex as human insulin (Scheme 3.28).[76]

While both transformations are appealing for translation to ^{18}F-trifluoromethylation, none of the reagents used were seen as being trivial to prepare. Focusing on **3.105**; although it can be prepared in a single step (Scheme 3.29), this would require a route to **[^{18}F]3.106**.[77] Given the high affinity of fluoride for silicon, the radiosynthesis of **[^{18}F]3.106** would most likely require a multiple step approach. Given the short half-life of fluorine-18, such as strategy was unlikely to afford **[^{18}F]3.105** in appreciable RCYs. Turning to **3.128**; although numerous routes towards CF_3SO_2M are known (Scheme 3.30), for ^{18}F-radiochemistry, these approaches would require a route towards the necessary [^{18}F]CF_3-precursor, and one or more reactions post-labelling.[78]

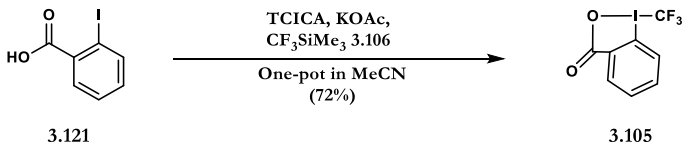

Scheme 3.29. One-Pot preparation of **3.105**

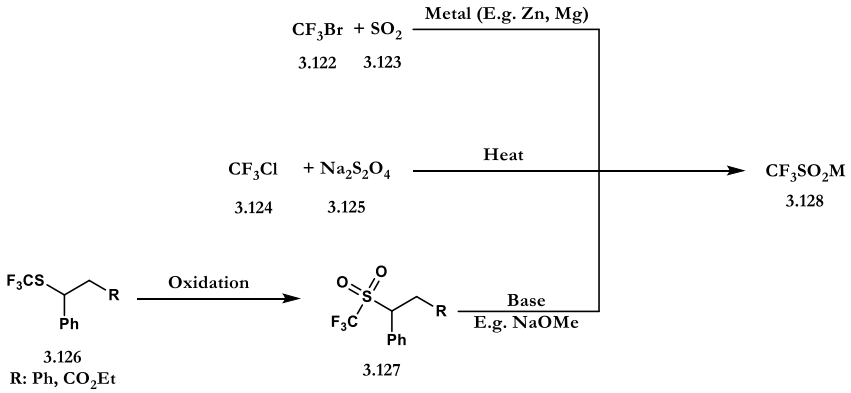

Scheme 3.30. General overview for the preparation of MSO_2CF_3 reagents

Ultimately, we focused on the reagent known as Umemoto **3.109**. Due to its solubility in water and the ability to tune its reactivity through interchange of sulfur with selenium or tellurium, and/or substitution on the aryl groups, it was proposed

that the Umemoto reagent would serve as a suitable candidate (Figure 3.2).[79-80] Furthermore, given the soft electrophilic nature of the reagent, it was hoped that selectivity would be similar to that observed by Togni and co-workers when using reagent **3.105**.[81]

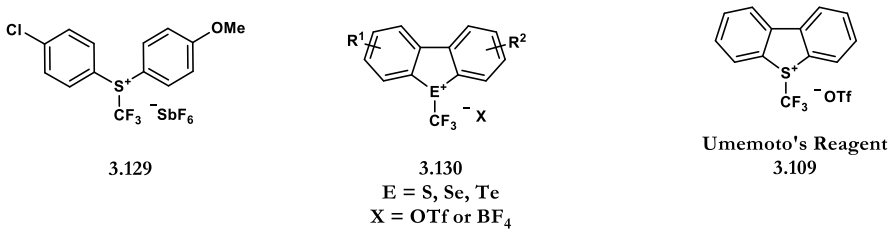

Figure 3.2. Derivatives of S-CF_3 electrophilic trifluoromethylation reagents

3.8.3 Umemoto's Reagent: Design and Radiosynthesis

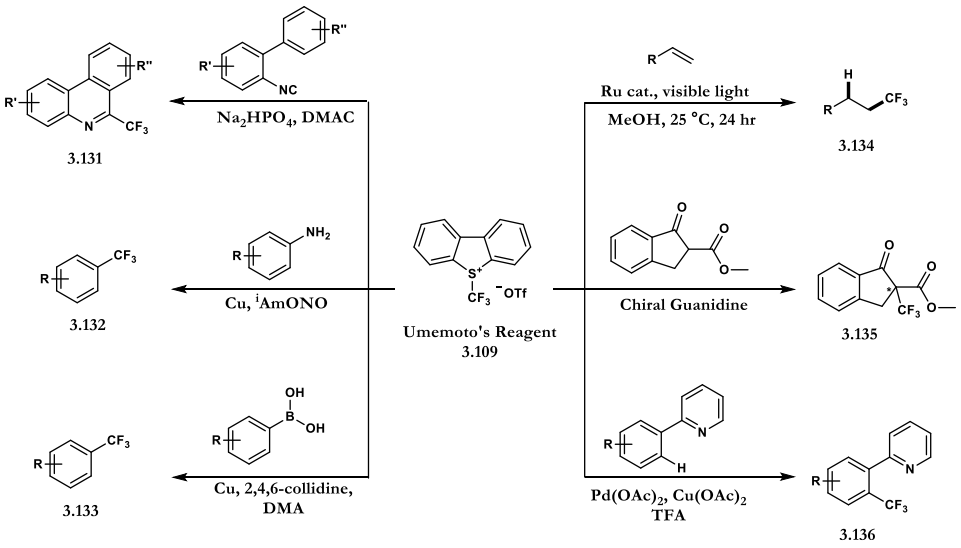

Scheme 3.31. Application of Umemoto's reagent **3.109**

Since its first documented use in 1990,[82] the reagent known as Umemoto's (5-trifluoromethyl)dibenzothiophenium trifluoromethane sulfonate) **3.109** has been used extensively for the electrophilic trifluoromethylation of numerous functional groups (Scheme 3.31).[83-89] The most streamlined protocol to prepare **3.109** consists of treating 1,1'-biphenyl **3.137** with CF_3SO_2K and two equivalents of Tf_2O.[90] For

radiolabeling, this method would require a route to ^{18}F-labeled CF_3SO_2K, by no means a trivial process at that time (Scheme 3.32A).

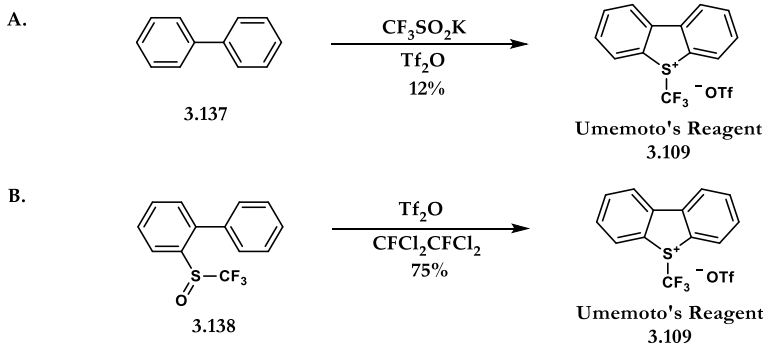

Scheme 3.32. Synthesis of Umemoto's reagent **3.109**

An alternative approach reported by Umemoto and co-workers consisted of subjecting 2-((trifluoromethyl)sulfinyl)-1,1'-biphenyl **3.138** to cyclisation with triflic acid/anhydride (Scheme 3.32B).[91] This approach was more attractive as, in 2015, Gouverneur and co-workers reported the silver mediated ^{18}F-fluorination using [^{18}F]KF/K_{222} to access ^{18}F-aryl-SCF_3 motifs (Scheme 3.33) including that of **[^{18}F]3.141** in radiochemical conversions up to 80%.[92] This served as a starting point for the synthesis of [^{18}F]Umemoto's reagent (Scheme 3.34).

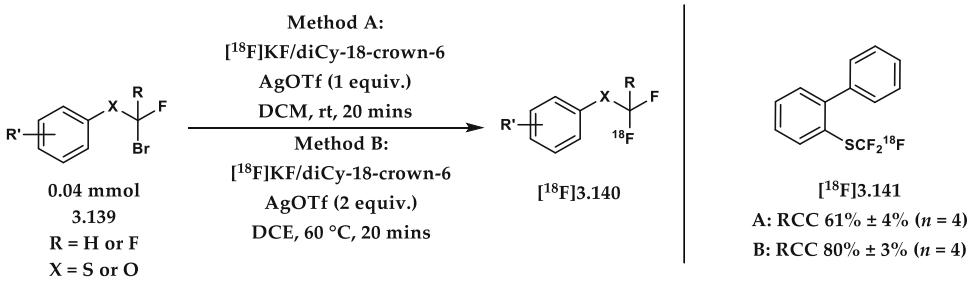

Scheme 3.33. Silver mediated ^{18}F-Fluorination of bromodifluoromethylthiolated arenes

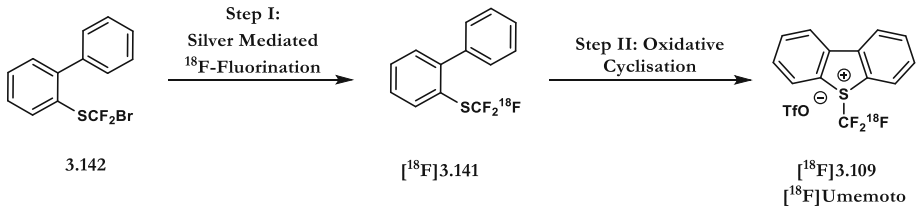

Scheme 3.34. Proposed strategy for the preparation of [^{18}F]Umemoto **[^{18}F]3.109**

3.8.4 Umemoto's Reagent: Optimisation for the Batch Scale Isolation of [^{18}F]3.109[a]

For the silver mediated ^{18}F-fluorination reported by Gouverneur in 2015, only nominal effort had been invested in the optimisation of the reaction using larger quantities of non-carrier added ^{18}F-fluoride. To this end, initial efforts were devoted towards the optimisation of the silver mediated ^{18}F-fluorination to access **[^{18}F]3.141**.

3.8.5 Influence of Silver Salts

Using the conditions reported previously by Gouverneur and co-workers for the radiofluorination of **3.142**, a 12% RCY for **[^{18}F]3.141** was obtained (Table 3.2, Entry 1). The use of a larger amount of AgOTf (2 equiv.) in DCE (300 μL) at elevated temperatures (60 °C) saw an increase in RCY to 20% (Table 3.2, Entry 2). This served as a benchmark for the screening of other non-coordinating silver salts. Under these conditions the use of AgOTf was found to be superior to $AgNTf_2$ (Table 3.2, Entry 3).

In each of the instances described so far, the AgOTf had to transferred to the 5 mL vial containing dried [^{18}F]KF/K_{222} in a mixture of 3:2 MeOH:MeCN (500 μL). Upon addition, the solvent had to be removed under a flow of nitrogen at 100 °C prior to carrying out the ^{18}F halex in DCE. During this drying process a significant amount of activity loss, typically 500 – 1000 MBq was observed (5% – 10% loss). As such, complexes **3.143** and **3.144**, both soluble in DCE, were evaluated. However, both resulted in low RCYs (Table 3.2, Entries 4 and 5). The *bis*-1,5-cyclooctadiene complex **3.145** showed a similar yield to uncomplexed AgOTf (Table 3.2, Entry 6)

[a] The work described in the following section was carried out in collaboration with Dr. S. Verhoog and Dr. M. Tredwell

but solid residues remained after SepPak purification. The use of PPh_3AuNTf_2 afforded **[^{18}F]3.141** in 4% (Table 3.2, Entry 7).[93]

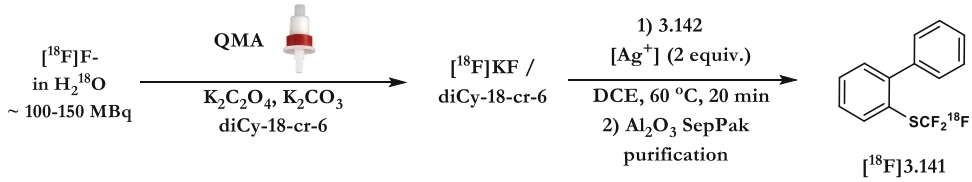

Entry[a]	Elution conditions[b]	[Ag$^+$]	RCY[c]
1	A	AgOTf[d]	12% ± 1% (*n* = 3)
2	A	AgOTf	20% ± 2% (*n* = 2)
3	A	$AgNTf_2$	14% (*n* = 1)
4	A	$[Ag(pyr)_2]OTf$	6% (*n* = 1)
5	A	[Ag(2,4,6-collidine)$_2$]OTf	2% (n = 1)
6	A	$[Ag(COD)_2]OTf$	17% ± 2% (*n* = 2)[e]
7	A	PPh_3AuNTf_2[f]	4% (*n* = 1)

[a]**3.142** (40 μmol), [Ag$^+$] (80 μmol), DCE (300 μL); [b] $K_2C_2O_4.H_2O$ (22 μmol), K_2CO_3 (1.5 μmol), diCy-18-cr-6 (38 μmol) in CH_3CN/H_2O 4/1 (1 mL); [c]non decay corrected; Radiochemical purity of **[^{18}F]3.141** >95% as determined by radioHPLC. [d] AgOTf (0.04 mmol), rt, 20 min. [e] Incomplete removal of solids after SepPak purification. [f] PPh_3AuNTf_2 (0.04 mmol), DCM, rt, 20 min.

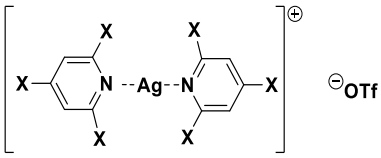

3.143, X = H, $[Ag(pyr)_2]OTf$

3.144, X = Me, [Ag(2,4,6-collidine)$_2$]OTf

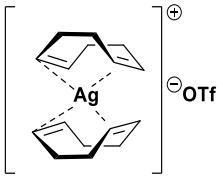

3.145

$[Ag(COD)_2]OTf$

Table 3.2. Investigation of different Ag(I)-sources in the preparation of **[^{18}F]3.141**

3.8.6 Influence of ^{18}F-Elution Conditions[b]

Having established the optimal silver(I) salt, solvent and temperature, the influence of the elution mixture upon RCY of **[^{18}F]3.141** was investigated. From

[b] The work described in the following section was carried out in collaboration with Dr. S. Verhoog and Dr. M. Tredwell

previous works it had been established that larger amounts of both $K_{2.2.2}$ and K_2CO_3 were detrimental to ^{18}F-incorporation.[92] The weaker base, $K_2C_2O_4$ (pK_a of the conjugated acid of oxalate = 4.19 vs 10.3 for CO_3^{2-}) had minimal influence on the ^{18}F-incorporation (Table 3.3, Entry 1). Investigation into other weak inorganic bases such as KH_2PO_4 (pKa = 7.21) resulted in 13% RCY (Table 3.3, Entry 2). The use of cesium as a counterion in the elution mixture was examined. In this case, an improved RCY of 33% was observed (Table 3.3, Entry 3). Finally, tetra-alkyl ammonium salts Et_4NHCO_3 and Et_4OTf were examined with RCYs of 26% and 34% observed respectively (Table 3.3, Entries 4-5). In both instances however, significant amounts of precipitate were observed, an issue which would be highly prohibitive for automation.

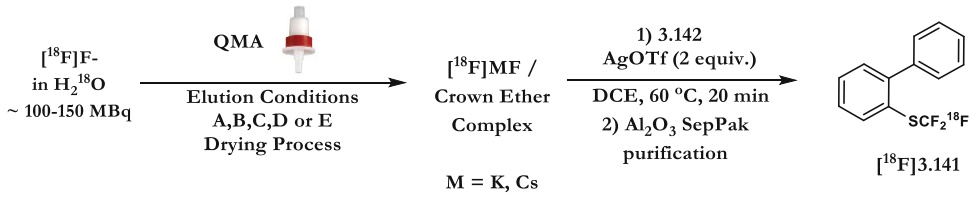

Entry[a]	Elution Conditions[b]	RCY (n = 2)[c]
1	$K_2C_2O_4$, diCy-18-cr-6 (A)	20% ± 2%
2	KH_2PO_4, diCy-18-cr-6 (B)	13% ± 2%
3	$Cs_2C_2O_4$, diPh-24-cr-8 (C)	33% ± 1%
4	Et_4NHCO_3 (D)	26% ± 1%
5	Et_4NOTf (E)	34% ± 7%

[a] **3.142** (40 μmol), AgOTf (80 μmol), DCE (300 μL). [b] **A** = $K_2C_2O_4.H_2O$ (22 μmol), K_2CO_3 (1.5 μmol), diCy-18-cr-6 (38 μmol) in CH_3CN/H_2O 4/1 (1 mL); **B** = $KH_2PO_4.2H_2O$ (26 μmol), diCy-18-cr-6 (38 μmol) in CH_3CN/H_2O 4/1 (1 mL); **C** = $Cs_2C_2O_4$ (22 μmol), Cs_2CO_3 (1.5 μmol), diPh-24-cr-8 (38 μmol) CH_3CN/H_2O 4/1 (1 mL); **D** = Et_4NHCO_3 (26 μmol), CH_3CN/H_2O 4/1 (1 mL); **E** = Et_4NOTf (26 μmol) in MeOH (1 mL). [c] non-decay corrected; Radiochemical purity of **[18F]3.141** >95% as determined by radio-HPLC.

Table 3.3. Investigation of Different Elution Conditions in the Synthesis of **[18F]3.141**

3.8.7 Oxidative Cyclisation of [^{18}F]3.141[c]

Having established both elution conditions and reaction conditions for the halogen exchange, the next step was to examine the oxidative cyclisation of **[^{18}F]3.141**. Taking aliquots of **[^{18}F]3.141** and exposing the crude material to *m*-CPBA afforded the desired product **[^{18}F]3.109** in high conversion (Table 3.4, Entries 1-3). However, taking larger aliquots led to a drop-in conversion (Table 3.4, Entry 4). The reason for this likely being the presence of unreacted **3.142**, which is not separated from **[^{18}F]3.141** after Al_2O_3 SepPak purification.

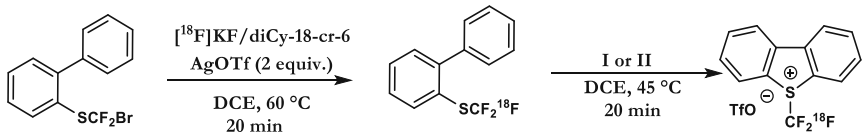

3.142 [^{18}F]3.141 [^{18}F]3.109

Entry	[^{18}F]3.141	additive[a]	purification	RCC
1	~ 30 MBq[b]	I (2 equiv.)	Al_2O_3 (N) SepPak	95% ± 0%[c]
2	~ 30 MBq[b]	I (3 equiv.)	Al_2O_3 (N) SepPak	98% ± 1%[c]
3	~ 30 MBq[b]	I (4 equiv.)	Al_2O_3 (N) SepPak	97% ± 3%[c]
4	106 MBq[d]	I (3 equiv.)	Al_2O_3 (N) SepPak	13%[e]
5	120 MBq	I (3 equiv.)	HPLC	30%[f]
6	224 MBq	II (3 equiv.)	HPLC	42%[f]
7	0.2-1.6 GBq	II (3 equiv.)	HPLC	49% ± 9%[f,g]

[a] I = *m*-CPBA/Tf_2O; II = Oxone®/Tf_2O. [b] ~ 50 μL aliquot of a solution of **[^{18}F]3.141** in 1 mL DCE; [c]determined by radio-TLC (n = 2); [d] ~ 300 μL aliquot of a solution of **[^{18}F]3.141** in 1 mL DCE; [e] RCC determined by radio-TLC; [f] Isolated RCY; [g] n = 44

Table 3.4. Investigation into the Oxidative Cyclisation of **[^{18}F]3.141**

This problem was overcome by purification of **[^{18}F]3.141** using reverse phase prep-HPLC, which resulted in complete removal of **3.142**. Following prep-HPLC,

[c] The work described in the following sub-section was carried out in collaboration with Dr. S. Verhoog and Dr. M. Tredwell

[^{18}F]3.141 was trapped on a C18 cartridge before eluting with DCE (1.4 mL). During this process it was also found that a SepPak silica dry cartridge was necessary to remove trace quantities of water that otherwise had a detrimental effect upon the oxidative cyclisation of **[^{18}F]3.141**. Whilst this procedure led to an overall reduction in RCY of **[^{18}F]3.141**, it was found to be necessary for efficient cyclisation (Scheme 3.34).

With a protocol to prepare **[^{18}F]3.141** as both a chemically and radio-chemically pure product in hand, both organic and inorganic oxidants were re-evaluated for the oxidative cyclisation. To do this however, a procedure for the analysis of **[^{18}F]3.109** were required. It was found that, by eluting the crude reaction mixture from the oxidative cyclisation reaction over a Waters SiO_2 light SepPak, all apolar impurities could be removed. After elution of impurities with DCE, **[^{18}F]3.109** could then be eluted from the SepPak with CH_3CN in high radiochemical purity (Scheme 3.35). This served as the standard protocol when discriminating between oxidants.

Whilst *m*-CPBA proved to be highly efficient for the cyclisation process (Table 3.4, Entry 5), HPLC analysis of purified **[^{18}F]3.109** identified benzoic acid impurities. In order to remove these chemical impurities, the inorganic oxidant Oxone® was chosen, as it could easily be removed upon transfer to the Waters SiO_2 light SepPak (Table 3.4, Entry 7). In so doing, **[^{18}F]3.109** was isolated as both a chemically and radio-chemically pure product.

When combined, the overall non-decay corrected activity yield of **[^{18}F]3.109** calculated from [^{18}F]fluoride was 5% ± 2% (n = 41) (Scheme 3.35). Using this protocol up to 840 MBq of **[^{18}F]3.109** was isolated from ~6–10 GBq of [^{18}F]fluoride.

The identity of **[^{18}F]3.109** was established by HPLC and electrospray ionization (ESI) mass spectrometry (**[^{19}F]3.109**, $C_{14}H_8F_4O_3S_2$ *m/z* 253.1, calcd 253.0). The molar activity of **[^{18}F]3.109** was calculated to be 0.08 GBq μmol^{-1} (Figure 3.3, Figure 3.4). This was primarily due to the halogen exchange during the first step, a process which afforded intermediate **[^{18}F]3.141** in a molar activity of 0.24 GBq μmol^{-1}.

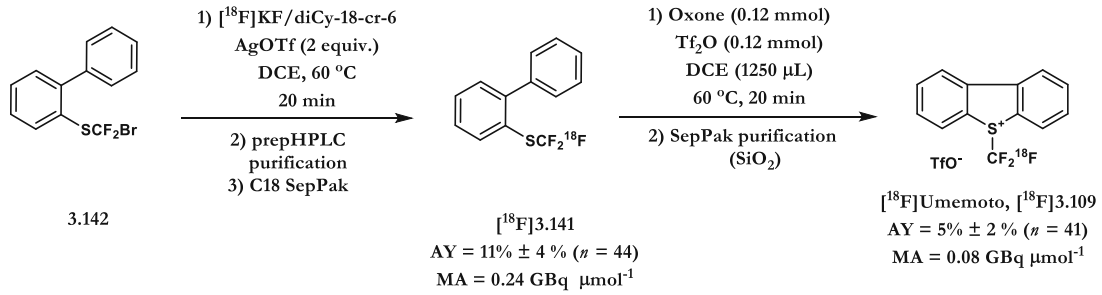

Scheme 3.35. Semi-Automated Isolation Procedure for **[^{18}F]3.109**

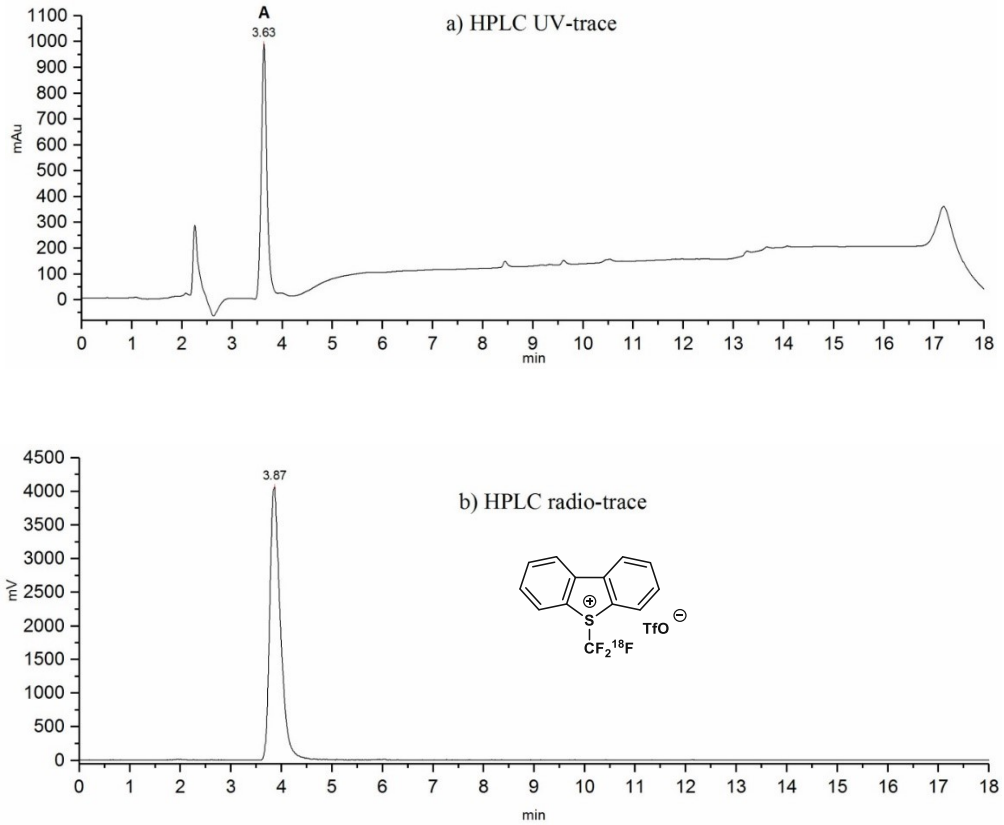

Figure 3.3. a) HPLC UV-trace (254 nm) and b) HPLC radio-trace of a sample of **[^{18}F]3.109** after isolation. Phenomenex Synergi Hydro RP 4 μm 80A 150x4.6mm column (Eluent A, flow rate = 0.7 mL/min**)**.

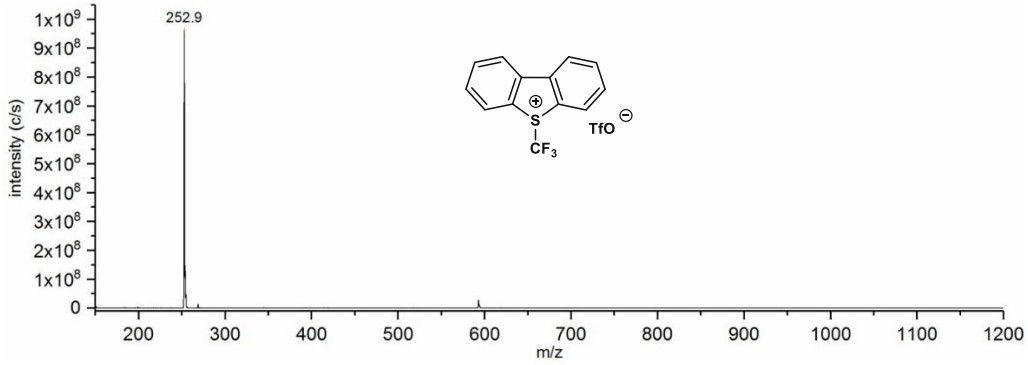

Figure 3.4. Peak A. *m/z* Calcd for $C_3H_8F_3S_1$ $[M]^+$ 253.0, found 252.9.

3.8.8 [^{18}F]Umemoto: Optimisation for the ^{18}F-Trifluoromethylation of Cysteine Residues[d]

With a procedure for the radiolabeling of **[^{18}F]3.109** established, attention was turned towards its reactivity for the ^{18}F-trifluoromethylation of cysteine residues. Although the strategy for the trifluoromethylation of cysteine residues with **3.106** gave encouragement that this would be possible, the drastic change in relative stoichiometry between **[^{18}F]3.109** and peptide, meant this may not be a totally trivial process.

Initially, the reactivity of the novel ^{18}F-trifluoromethylation reagent **[^{18}F]3.109** was examined with ethyl benzoyl-*L*-cysteinate **3.143** and (*tert*-butoxycarbonyl)-*DL*-homocysteinate **3.144** (Table 3.5). ^{18}F-Trifluoromethylation of **3.143** took place upon treatment of **[^{18}F]3.109** with DMAP in MeCN (0.2M), with the RCC of **[^{18}F]3.146** increasing to 60% at higher concentration (0.4M) (Table 3.5, Entries 1 – 3). DMF and DMSO were both found to be suitable solvents for this transformation (Table 3.5, Entry 4). As a control experiment, it was found that base was essential for ^{18}F-trifluoromethylation to take place (Table 3.5, Entry 6).

[d] The work described in the following section was carried out in collaboration with Dr. S. Verhoog and Dr. C. W. Kee

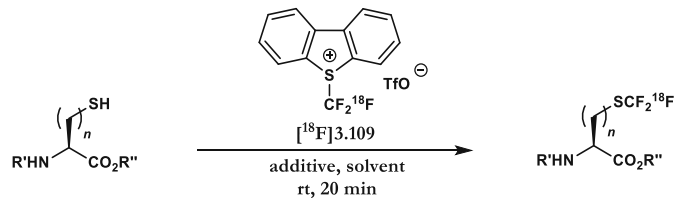

3.143, *n* = 1, R' = COPh, R'' = Me
(±)-3.144, *n* = 2, R' = Boc, R'' = Me
3.145, *n* = 2, R', R'' = H

[^{18}F]3.146, *n* = 1, R' = COPh, R'' = Me
(±)-[^{18}F]3.147, *n* = 2, R' = Boc, R'' = Me
[^{18}F]3.148, *n* = 2, R', R'' = H

Entry[a]	3.143-3.145[b]	Additive[c]	Solvent[d]	RCC [^{18}F]3.146 - [^{18}F]3.148 [%][e]
1	**3.143** (40)	DMAP	CH_3CN[f]	0%
2	**3.143** (40)	DMAP	CH_3CN[g]	6% ± 1%
3	**3.143** (40)	DMAP	CH_3CN	60% ± 7%
4	**3.143** (40)	DMAP	DMF	65% ± 2%
5	**3.143** (40)	DMAP	DMSO	59% ± 2%
6	**3.143** (40)	-	DMSO	2% ± 1%
7	**3.143** (20)	DMAP	DMSO	72% ± 4%[h]
8[i]	**3.143** (20)	DMAP	DMSO	69% ± 1%
9[i]	**3.143** (20)	DMAP	DMSO/H_2O, 4/1	66% ± 4%
10	**3.143** (20)	$KHCO_3$	DMSO/H_2O, 1/1	71% ± 6%[h]
11	**3.144** (20)	DMAP	DMSO/H_2O, 4/1	75% ± 8%
12[j]	**3.145** (20)	$KHCO_3$[k]	DMSO/H_2O, 1/9	26% ± 6%[l]

Table 3.5. Optimisation for the ^{18}F-trifluoromethylation of **3.143** and **3.144** [a] ~20-25 MBq of **[^{18}F]3.109** per reaction; [b] μmol; [c] 1 equiv; [d] 100 μL; [e] determined by radio-TLC and radio-HPLC (*n* = 2); [f] 400 μL; [g] 200 μL; [h] *n* = 4; [i] reaction time = 10 mins; [j] reaction time = 20 min, reaction temp. = 40 °C; [k] 2 equiv; [l] RCY after Oasis MCX cartridge purification.

Initial results found 10% water to be compatible as a co-solvent (Table 3.5, Entry 9). Due to the relatively poor solubility of DMAP in DMSO:H_2O (1:1) however, a switch to $KHCO_3$ was required (Table 3.5, Entry 10). When reacted in a 4:1 mixture of DMSO:H_2O (*tert*-butoxycarbonyl)-*DL*-homocysteinate **3.144** underwent successful ^{18}F-trifluoromethylation in 75% ± 8% (Table 3.5, Entry 11). Increasing the H_2O ratio to 90%, a solvent system with higher compatibility for the

^{18}F-trifluoromethylation of unprotected amino acids, afforded **[^{18}F]3.148** in 26% ± 6% after SepPak purification (Table 3.5, Entry 12).

3.8.9 [^{18}F]Umemoto: ^{18}F-Trifluoromethylation of Dipeptides Bearing Cysteine Residues[e]

Prior to the ^{18}F-trifluoromethylation of biologically relevant targets, an orthogonality screening of dipeptides bearing cysteine residues was undertaken. In all cases, both *C*- and *N*-termini were protected to minimise interference of these functionalities at this stage (Scheme 3.36).

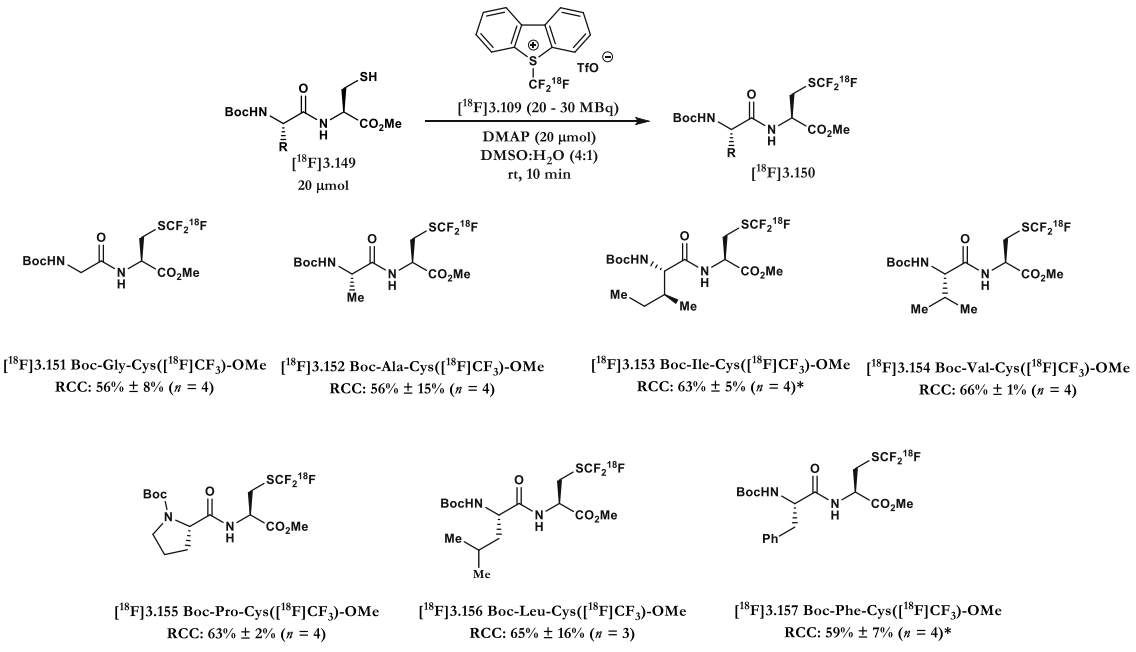

Scheme 3.36 ^{18}F-Trifluoromethylation of dipeptides *DMSO (100 μL) used as solvent

At first, dipeptides bearing unreactive side chains were investigated, namely, Gly, Ala, Val, Ile, Phe, Leu and protected Boc-proline residues (Scheme 3.36). By treating the corresponding thiols with **[^{18}F]3.109**, DMAP (20 μmol) in either

[e] The work described in the following section was carried out in collaboration with Dr. S. Verhoog and Dr. C. W. Kee

DMSO/H_2O (4:1) or DMSO at room temperature for 10 minutes, the ^{18}F-trifluoromethylated products were formed in good RCCs and radiochemical purities (RCP).

Peptides bearing potentially problematic residues such as Met, Asn, Gln, Thr, Lys, Ser, Tyr and Glu were examined. Using those conditions described previously (Scheme 3.37), ^{18}F-trifluoromethylation of dipeptides containing amide, phenol and sulfide functionality was successful with high RCC and RCP observed. No oxidation of the methionine residue was observed in this instance. For residues containing hydroxy side chains, namely Ser and Tyr, treatment with $KHCO_3$ (1 equiv.) instead of DMAP led to improved RCCs.

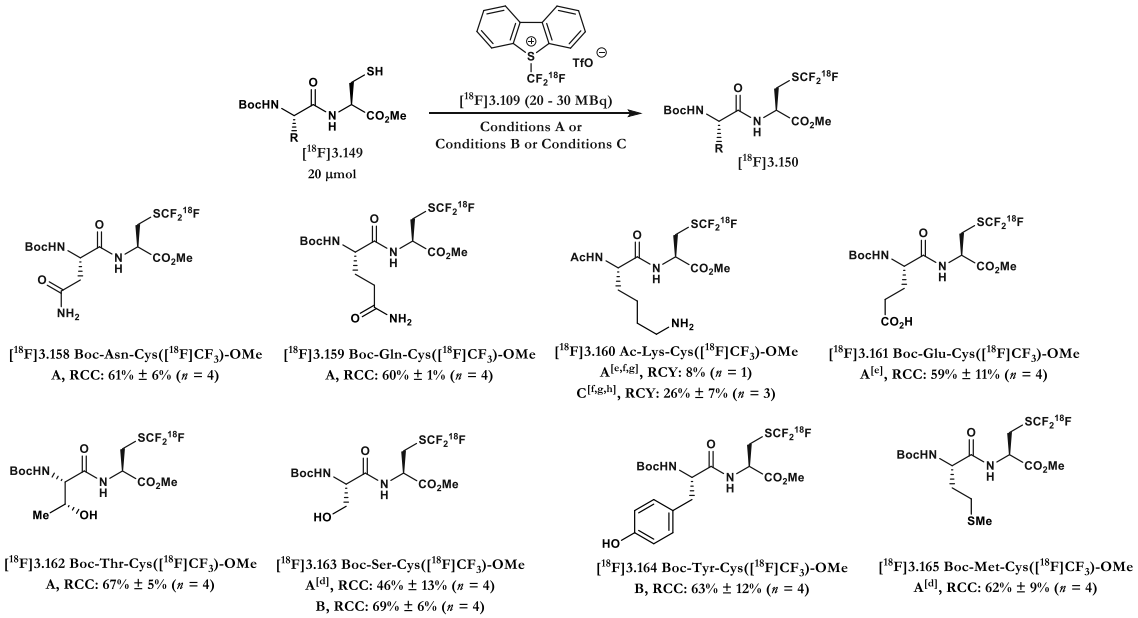

Scheme 3.37 ^{18}F-Trifluoromethylation of Dipeptides Conditions: A) 20 µmol peptide, 20 µmol DMAP, DMSO/H_2O 4:1 (100 µL), rt, 10 min, *DMSO (100 µL) used as solvent; Conditions B) 20 µmol peptide, 20 µmol $KHCO_3$, DMSO/H_2O 1:1 (100 µL), rt, 10 min. Conditions C: 20 µmol peptide, 20 µmol Et_4NHCO_3, DMSO/H_2O 4:1 (100 µL), 40 °C, 20 min. [d] DMSO (100 µL) was used. [e] 40 µmol DMAP was used. [f] Substrate is Ac-Lys-Cys-Ome.TFA. [g] Isolated yield after cartridge purification (Oasis HLB). [h] 40 µmol Et_4NHCO_3 was used

For the ^{18}F-trifluoromethylation of the dipeptide bearing lysine as a residue, two equivalents of Et_4NHCO_3 was required for successful incorporation. Finally, for

the ^{18}F-trifluoromethylation of the dipeptide bearing a glutamic acid residue, two equivalents of DMAP as a base was required, affording **[^{18}F]3.161** in 59% ± 11% RCC. This was seen as a crucial result given the prevalence of carboxylic acid residues found within unmodified peptides.

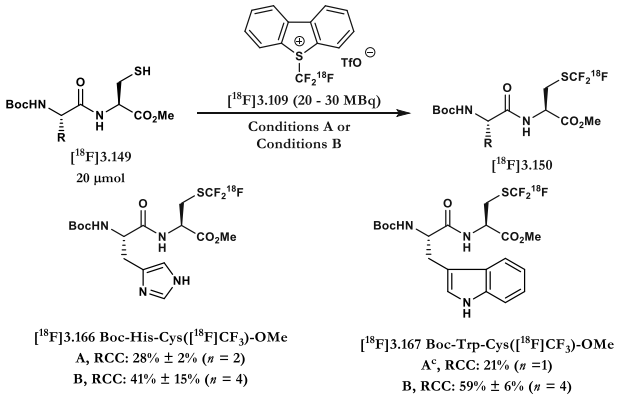

Scheme 3.38. ^{18}F-Trifluoromethylation of histidine and tyrtophan containing dipeptides [a]Conditions A: 20 μmol peptide, 20 μmol DMAP, DMSO/H_2O 4:1 (100 μL), rt, 10 min. [b]Conditions B: 20 μmol peptide, 20 μmol $KHCO_3$, DMSO/H_2O 1:1 (100 μL), rt, 10 min. [c]DMSO (100 μL) was used.

Dipeptides featuring tryptophan and histidine gave rise to the formation of more than one ^{18}F-radiolabeled product (Scheme 3.38). The ^{18}F-trifluoromethylation of methyl (*tert*-butoxycarbonyl)-*L*-histidyl-*L*-cysteinate led to the ^{18}F-labeled peptide **[^{18}F]3.166** in 41% ± 15% RCC (n = 4) as the major product (68% RCP). In addition to predominant ^{18}F-trifluoromethylation at the cysteine residue (64% RCP), similar competitive pathways were observed for the tryptophan-containing dipeptide precursor of **[^{18}F]3.167**. To determine the side products observed within each reaction, HPLC and ESI analysis was undertaken.

For the reaction of the tryptophan-containing dipeptide, a single major byproduct with a retention time of 15.3 min was observed (Figure 3.5). This was confirmed as the ^{18}F-trifluoromethylated product due to labelling on the indole.

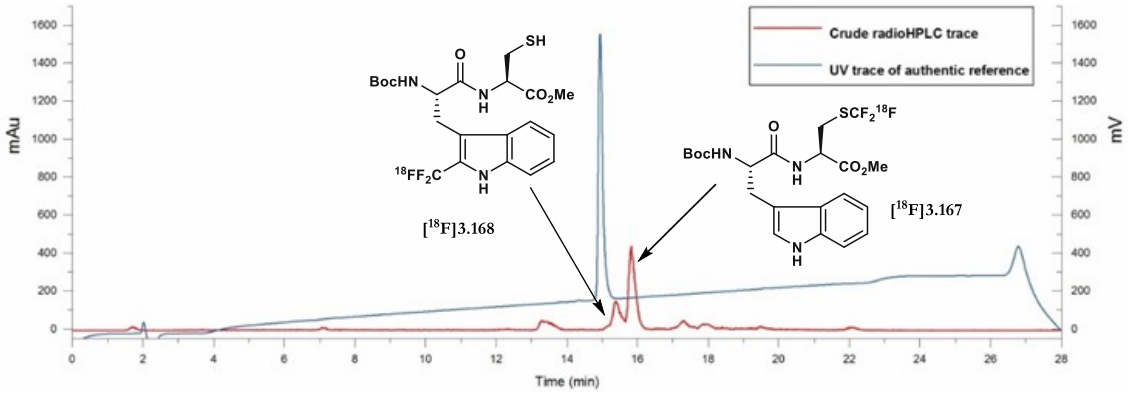

Figure 3.5. HPLC radio-trace of **[^{18}F]3.168/[^{18}F]3.167** (red) overlaid with HPLC UV-trace (220 nm) of **[^{19}F]3.168** (blue).

For the reaction of the histidine-containing dipeptide, multiple byproducts were observed (Figure 3.6). For this complex mixture, ESI mass spectrometry was used. Within the crude mixture, five radiolabelled products were identified (Figure 3.6).

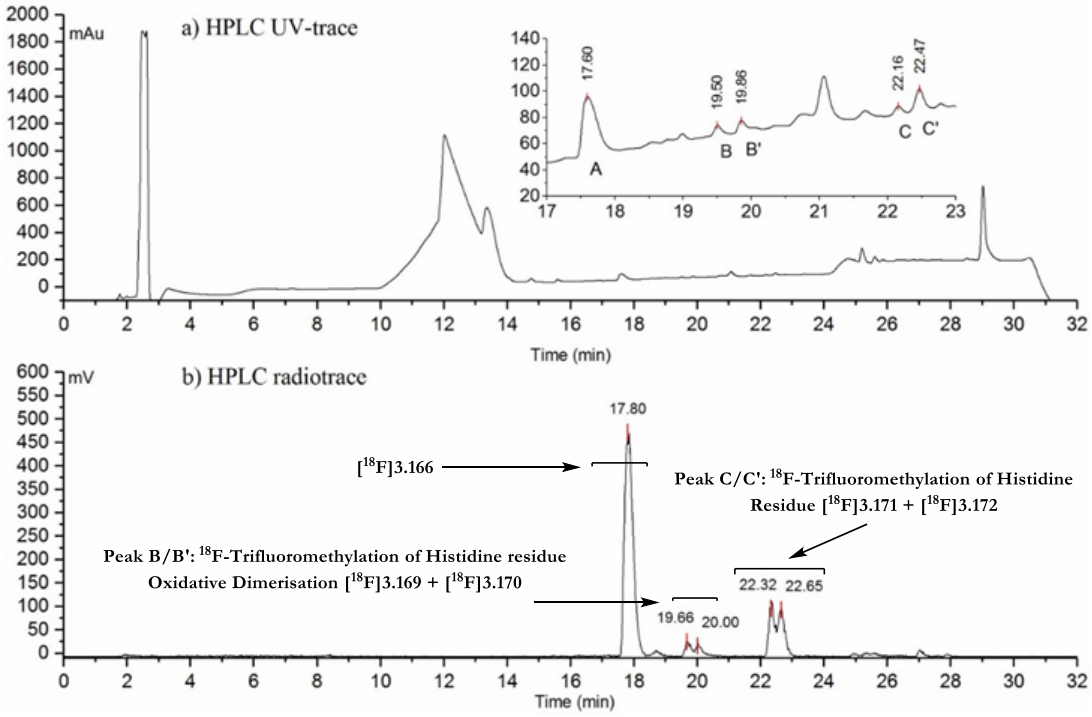

Figure 3.6. Crude HPLC UV-trace (220 nm) and radio-HPLC trace of the ^{18}F-trifluoromethylation of methyl (tert-butoxycarbonyl)-*L*-histidyl-*L*-cysteinate in DMSO/H_2O 1/1 using $KHCO_3$ as base.

The ^{18}F-trifluoromethylated product **[^{18}F]3.166** (t_R: 17.80 min), could be unambiguously identified using the corresponding ^{18}F-containing reference. Peaks B

and B' (t_R = 19.50, t_R = 19.86), *m/z* values of 810.8 were recorded (Figure 3.7, Figure 3.8). Given the propensity for **3.109** to trifluoromethylate histidine, it was proposed that the observed peak corresponding to the product of ^{18}F-trifluoromethylation on the histidine ring followed by oxidative dimerisation (**[^{18}F]3.169** + **[^{18}F]3.170**). Peaks C and C' (t_R = 22.16, t_R = 22.47), *m/z* values of 440.9 were recorded (Figure 3.9, Figure 3.10). In this instance it was believed that the observed peaks corresponding to the product of ^{18}F-trifluoromethylation on the histidine ring (**[^{18}F]3.171** + **[^{18}F]3.172**).

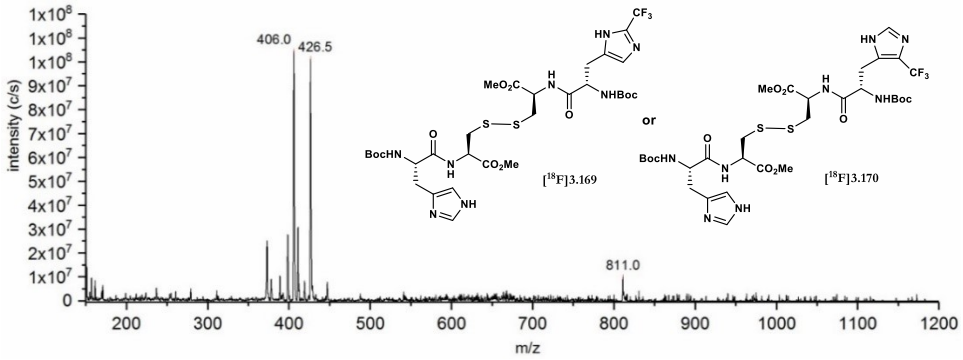

Figure 3.7. Peak B. *m/z* Calcd for $C_{31}H_{46}F_3N_8O_{10}S_2$ $[M+H]^+$ 811.3, found 811.0.

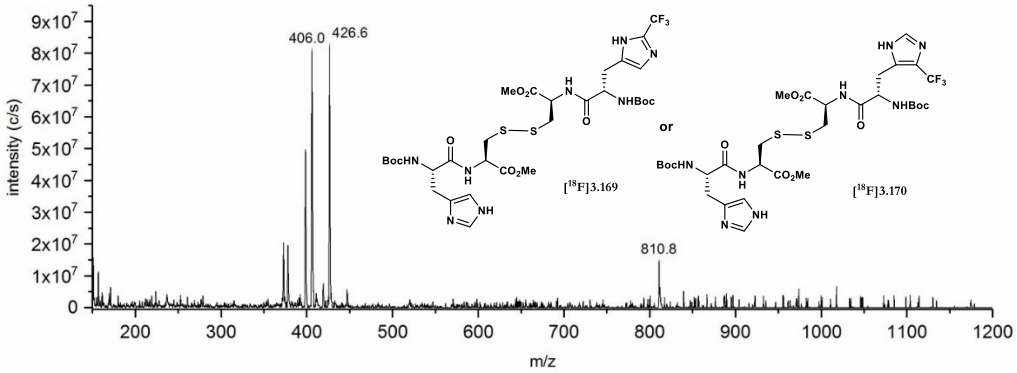

Figure 3.8. Peak B'. *m/z* Calcd for $C_{31}H_{46}F_3N_8O_{10}S_2$ $[M+H]^+$ 811.3, found 810.8.

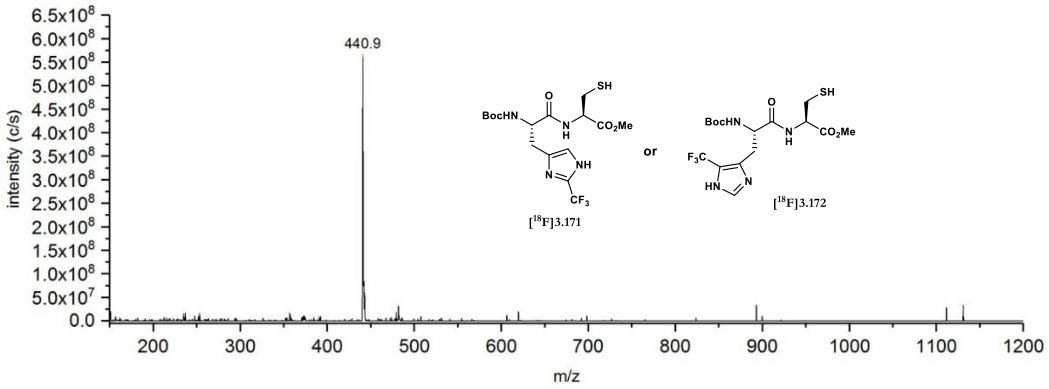

Figure 3.9. Peak C. *m/z* Calcd for $C_{16}H_{24}F_3N_4O_5S$ $[M+H]^+$ 441.1, found 440.9.

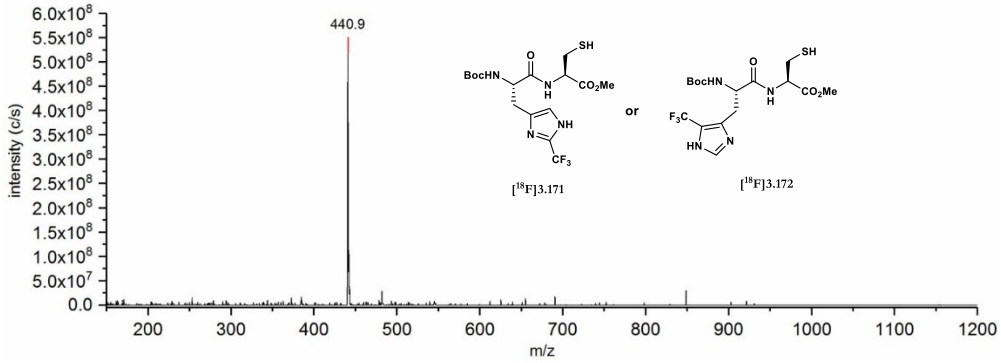

Figure 3.10. Peak C'. *m/z* Calcd for $C_{16}H_{24}F_3N_4O_5S$ $[M+H]^+$ 441.1, found 440.9.

This selectivity profile for both tryptophan and histidine dipeptides is consistent with the observation that both indoles and imidazoles are amenable to direct C-H ^{18}F-trifluoromethylation with **[^{18}F]3.109**. To maximise thiol ^{18}F-trifluoromethylation, the ratio of ^{18}F-radiolabeled products was investigated. However, side reactions could not be totally suppressed (41% vs 21% for **[^{18}F]3.166**, 59% vs 28% for **[^{18}F]3.167**). Nonetheless, a high level of compatibility had been demonstrated for all other naturally occurring amino acid residues.

3.8.10 ^{18}F-Trifluoromethylation of Unmodified Peptides

Having established a high level of orthogonality for the ^{18}F-trifluoromethylation of cysteine residues with **[^{18}F]3.109**, attention turned to the ^{18}F-trifluoromethylation of biologically relevant unmodified peptides. Initially, this focus was directed to smaller biomolecules (< 5 amino acid residues) bearing multiple carboxylic acid residues. As such, glutathione **3.173** and ((1-carboxy-2-mercaptoethyl)-carbamoyl)-glutamic acid, a core structure found in PET radioligands targeting prostate specific membrane antigen **3.174** (PSMA),[94] were selected (Figure 3.11).

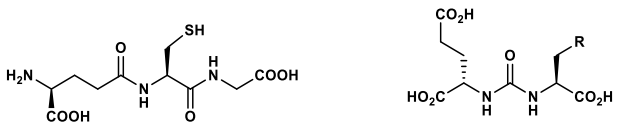

Glutathione, 3.173

PSMA, 3.174
R = Cys or Lys

Figure 3.11. Glutathion **3.173** and PSMA **3.174**

Previous work for the ^{18}F-labelling of both **3.173** and **3.174** had focused on using prosthetic groups for indirect radiofluorination. In 2014, Yu and co-workers reported the conjugation of an ^{18}F-labeled fluoro-butyl ethacrynic acid derivative **[^{18}F]3.176** to glutathione for the imaging of brain tumours expressing Lipocalin-type prostaglandin D synthase (L-PGDS), an enzyme shown to correlate with neurological disorders such as Alzheimer's and Parkinson's disease (Scheme 3.39).[95] Similar strategies have been used for the ^{18}F-labelling of PSMA **3.174** at the cysteine residue (Scheme 3.40). Furthermore, **[^{18}F]3.180** has already shown to be highly useful to the

imaging of metastatic prostate cancer due to its improved specific binding compared to [^{18}F]FDG.[96,97]

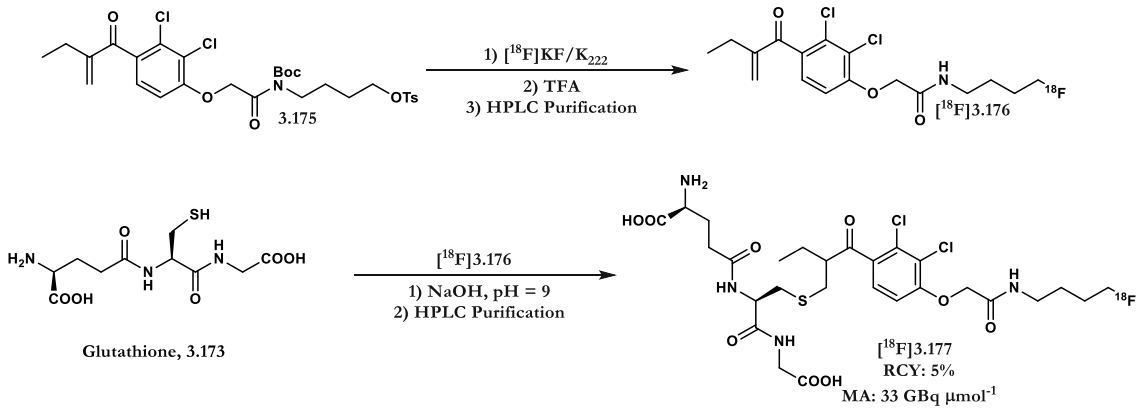

Scheme 3.39. Conjugation of Glutathione **3.173** with an ^{18}F-labeled fluoro-butyl ethacrynic acid derivative

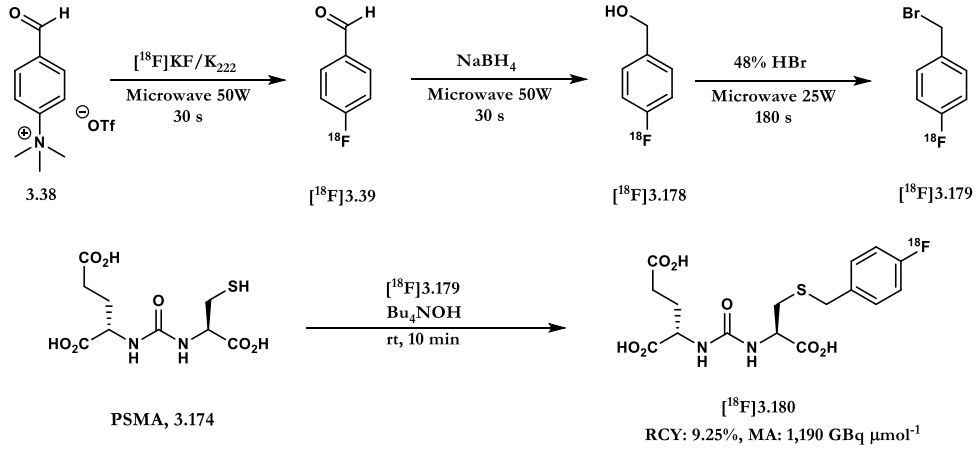

Scheme 3.40. Conjugation of PSMA **3.174** with an ^{18}F-labeled **[^{18}F]3.179**

Using **[^{18}F]3.109**, glutathione **3.173** underwent successful thiol ^{18}F-trifluoromethylation in 26% ± 4% RCY (n = 2) when the reaction was carried out with an excess of $KHCO_3$ (3 equiv.) in DMSO/H_2O (1/1). Similar conditions afforded **[^{18}F]3.182** in a RCY of 10% ± 2% (Scheme 3.41).

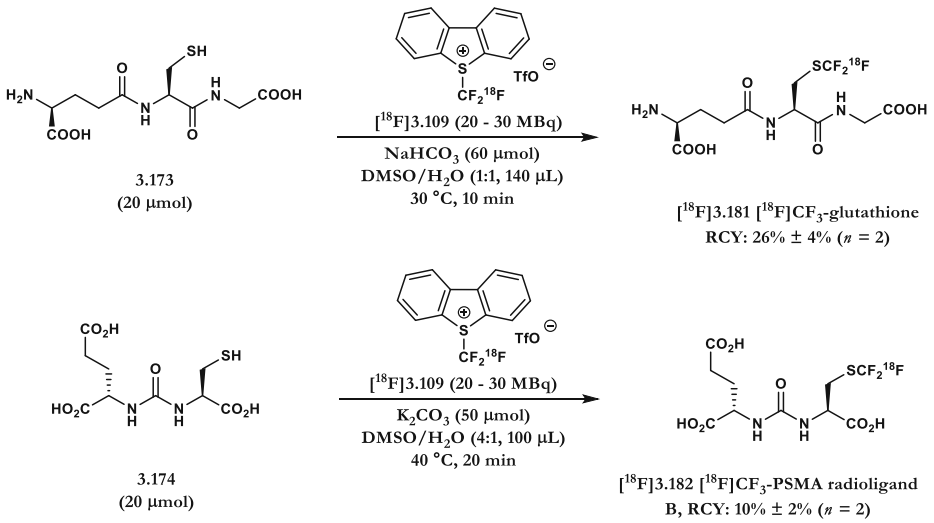

Figure 3.41 ^{18}F-Trifluoromethylation of Unmodified Peptides **[^{18}F]3.181** and **[^{18}F]3.182**

Having demonstrated the capacity of **[^{18}F]3.109** to ^{18}F-trifluoromethylate cysteine residues in the presence of multiple carboxylic acid, the next stage was to examine a larger peptide (> 10 amino acids). The challenge at this point was to examine whether, larger peptides bearing increased functionality, can undergo ^{18}F-trifluoromethylation when under higher levels of dilution (Scheme 3.42).

To this end, the beta-amyloid peptide fragment **3.183** (1 μmol, MW = 1034) was selected. **3.183** underwent successful ^{18}F-trifluoromethylation in 40 μL of solvent (DMSO/H_2O 1/1). The reaction proceeded exclusively at the cysteine residue affording the single product **[^{18}F]3.184** isolated in 30% ± 11% RCY (Scheme 3.43). This structural assignment was confirmed by mass spectrometry (ESI) and comparison of the authentic reference by UV- and radio-HPLC. This was an important advance given the desire to expand this methodology to larger peptides and eventually, that of proteins.

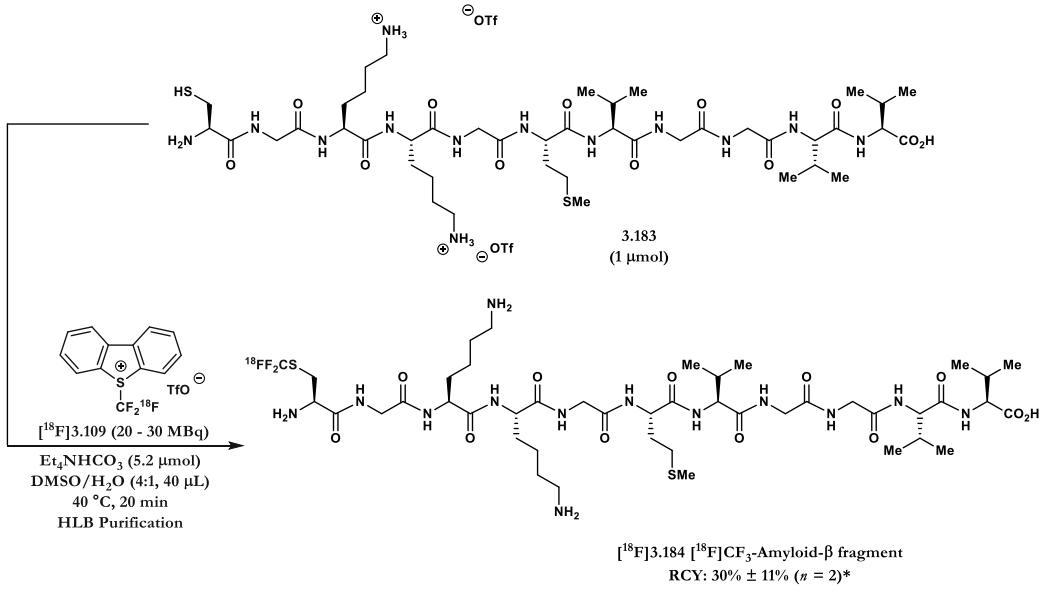

Scheme 3.42 ^{18}F-Trifluoromethylation of **3.183**

3.8.11 In Vivo Imaging and Stability Studies[f]

To investigate the *in-vivo* stability of peptides functionalised with an [^{18}F]SCF_3 moiety, a biodistribution profile was obtained by injecting naïve CBA mice (n = 3) with cRGDfC([^{18}F]CF_3) **[^{18}F]3.186**, followed by dynamic whole-body PET imaging.

Radiolabeled Arg-Gly-Asp (RGD) peptides have been a major focus for non-invasive assessment of angiogenesis because of their high affinity and selectivity for integrin $\alpha_v\beta_3$.[98] It was therefore of interest to study the ^{18}F-labeling of cyclic peptide containing the RGD sequence. The ^{18}F-trifluoromethylation was performed with 3 μmol of peptide and 10 μmol of Et_4NHCO_3 at 40 °C in 40 μL of solvent (DMSO/H_2O 1/1). After 20 minutes of reaction, cRGDfC([^{18}F]CF_3) **[^{18}F]3.186** was obtained in 33% ± 9% after cartridge purification. Following reverse phase HPLC

[f] The work described in the following section was carried out in collaboration with Dr. S. Verhoog, Dr. C. W. Kee, Dr. V. Kersemans and Dr. S. Smart.

was carried out affording **[^{18}F]3.186** as both a radio-chemically and chemically pure product in 19% ± 5% RCY (Scheme 3.43, Figure 3.11).

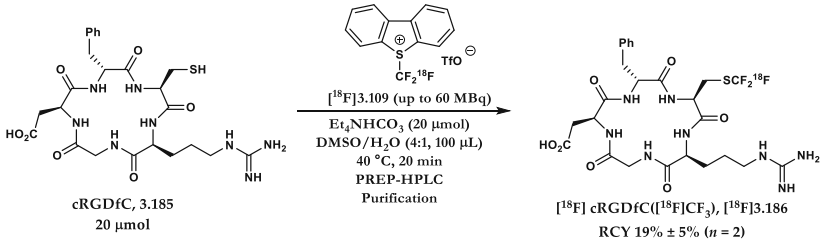

Scheme 3.43 ^{18}F-Trifluoromethylation of cRGDfC **[^{18}F]3.186**

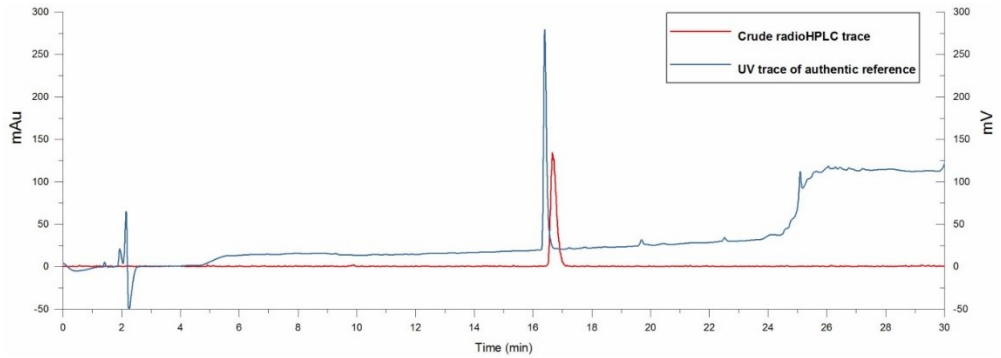

Figure 3.12. HPLC radio-trace of **[^{18}F]3.186** (red) overlaid with HPLC UV-trace (220 nm) of **[^{19}F]3.186** (blue).

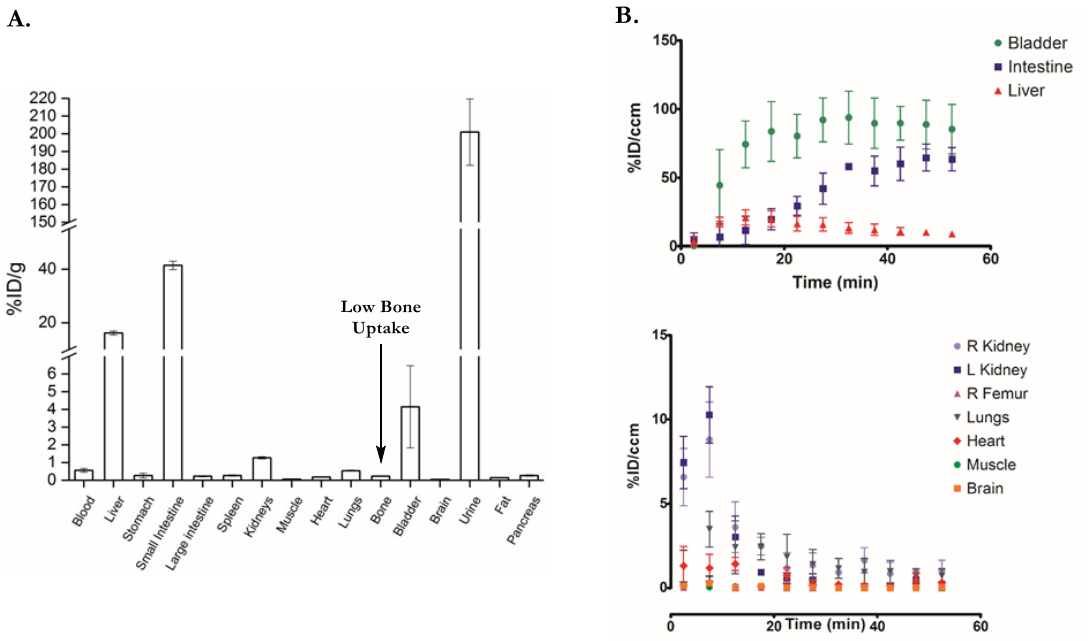

Figure 3.12. A) **[^{18}F]3.186** over 60 min after intravenously injection into a naïve CBA mouse. B) Time averaged image; Biodistribution in selected organs of cRGDfC([^{18}F]CF_3) **[^{18}F]3.186** 1 hr post injection in naïve CBA mice (n = 3); C) Time-activity curves of accumulation of cRGDfC([^{18}F]CF_3) **[^{18}F]3.186** in selected organs in naïve CBA mice (n = 3)

Biodistribution studies by imaging and dissection show that **[^{18}F]3.186** is predominantly excreted by the hepatobiliary route and to a lesser extent by the kidneys. Although these excretion organs still contain a considerable amount of radioactivity at 1 hr post injection, most radioactivity in non-targeted tissues and blood was cleared. This biodistribution profile is consistent with RGD peptides labeled applying alternative methods.[98] Notable was the absence of bone uptake. Brigaud and co-workers had reported that under basic conditions, cysteine residues are susceptible to β-elimination, a process which ultimately leads to the release of fluoride and difluorothiophosgene.[99] In this instance, the distinct lack of bond uptake indicated that **[^{18}F]3.186** is metabolically stable towards [^{18}F]SCF_3 elimination and that no [^{18}F]fluoride was released (Figure 3.12).[100]

3.9 Conclusion and Future Work

In summary, this chapter reports the first protocol enabling direct ^{18}F-trifluoromethylation of unmodified peptides at the cysteine residue with the novel [^{18}F]Umemoto's reagent **[^{18}F]3.109**. **[^{18}F]3.109** was synthesised in an overall AY of 5% *via* silver mediated halogen exchange followed by oxidative cyclisation. Upon isolation of the novel ^{18}F-trifluoromethylation reagent **[^{18}F]3.109**, a high orthogonality for the ^{18}F-trifluoromethylation of the cysteine residue was illustrated. The ^{18}F-trifluoromethylation with **[^{18}F]3.109** could be achieved in the presence of multiple carboxylic acid residues with the ^{18}F-trifluoromethylated products **[^{18}F]3.181**, **[^{18}F]3.182** and **[^{18}F]3.184** all accessed in good RCCs and RCYs. Finally, the [^{18}F]SCF_3 group was validated as a stable motif within naïve mouse models.

3.10 References

1 P. M. Matthews, E. A. Rabiner, J. Passchier, R. N. Gunn, *Br. J. Clin. Pharmacol.,* 2012, **73***,* 175.

2 S. Richter, F. Wuest, *Molecules* 2014, **19**, 20536.

3 C. L. Charron, J. L. Hickey, J. K. Nsiama, D. R. Cruickshank, W. L. Turnbull, G. L. Luyt, *Nat. Prod. Rep.* 2016, **33**, 761.

4 H. S. Krishnan, L. Ma, N. Vasdev, S. H. Liang, *Chem. Eur. J.,* 2017, **23**, 15553.

5 a) C. D. Spicer, B. G. Davis, *Nat. Commun.,* 2014, **5**, 1; b) O. Boutureira, G. Bernardes, *Chem. Rev.,* 2015, **115**, 2174.

6 T. J. Wright, B. J. Bower, J. M. Chalker, G. J. L. Bernardes, R. Wiewiora, W.-:. Ng, R. Raj, S. Faulkner, M. R. J. Vallée, A. Phanumartwiwath, O. D. Coleman, M.-L. Thézénas, M. Khan, S. R. G. Galen, L. Lercher, M. W. Schombs, S. Gerstberger, M. E. Palm-Espling, A. J. Baldwin, D. M. Kessler, T. D. W. Claridge, S. Mohammed, B. G. Davis, *Science*, 2016, **354**, 6312.

7 S. Kalkhof, A. Sinz, *Anal. Bioanal. Chem.,* 2008, **392**, 305.

8 D. R. Goddard, L. Micharlis, *J. Biol. Chem.,* 1935, **112**, 361.

9 J. M. Antos, J. M. MacFarland, A. T. Iavorone, M. B. Francis, *J. Am. Chem. Soc.,* 2009, **131**, 6301.

10 a) T. Weiland, E. Bokelmann, L. Bauer, H. U. Lang, L. H. Uber, *Liebigs Ann. Chem*., 1953, **583**, 129; b) B. A. Griffen. S. R. Adams, R. Y. Tsien, *Science,* 1998, **281**, 269; c) S. R. Adams, R. E. Campbell, L. A. Gross, B. R. Martin, G. K. Walkup, Y. Tao, J. Llopis, R. Y. Tsien, *J. Am. Chem. Soc.,* 2002, **124**, 6063.

11 a) N. Jentoft, D. G. Bearborn, *J. Biol. Chem.,* 1979, **254**, 4365; b) D. Chen, M. M. Disotuar, X. Xiong, Y. Wang, D. H.-C. Chou, *Chem. Sci.,* 2017, **8**, 2717.

12 a) A. Dirksen, P. E. Dawson, *Bioconjug. Chem.,* 2008, **19**, 2543; b) J. M. MacFarland, M. B. Francis, *J. Am. Chem. Soc.,* 2005, **127**, 13490.

13 F. Brotzel, H. Mayr, *Org. Biomol. Chem.,* 2007, **5**, 3814.

14 P. W. Miller, N. J. Long, R. Vilar, A. D. Gee, *Angew. Chem. Int. Ed.,* 2008, **47**, 8998.

15 S. Richter, F. Wuest, *Molecules,* 2014, **19**, 20536.

16 S. Preshlock, M. Tredwell, V. Gouverneur, *Chem. Rev.,* 2016, **116**, 719.

17 J. Becaud, L. Me, M. N. Karramkam, P. A. Schubiger, S. M. Ametamey, K. Graham, T. Stellfeld, L. Lehmann, S. Borkowski, D. Berndorff, *Bioconjugate Chem.,* 2009, **20**, 2254.

18 O. Jacobson, L. Zhu, Y. Ma, I. D. Weiss, X. Sun, G. Niu, D. O. Kiesemetter, X. Chen, *Bioconjugate Chem.,* 2011, **22**, 422.

19 U. Roehn, J. Becaud, L. Mu, A. Srinivasan, T. Stellfeld, A. Fitzner, K. Gragam, L. Dinkelborg, A. P. Schubiger, S. M. Ametamey, *J. Fluorine Chem.,* 2009, **130**, 902.

20 M. Winkler, J. Domarkas, L. F. Schweiger, D. O'Hagan, *Angew. Chem. Int. Ed.,* 2008, **47**, 10141.

21 H. Askenasy, M. Anbar, Y. Laor, Z. Lewitus, I. Kosary, S. Guttmann, Am. J. Roentgenol. *Radium Ther. Nucl. Med.*, 1962, **88**, 350.

22 W. Entzian, S. Aronow, A. Soloway, W. Sweet, *J. Nucl. Med.*, 1964, **5**, 542.

23 R. Ting, M. J. Adam, T. J. Ruth, D. M. Perrin, *J. Am. Chem. Soc.* 2005, **127**, 13094.

24 R. Ting, C. Harwig, U. auf dem Keller, S. McCormick, P. Austin, C. M. Overall, M. J. Adam, T. J. Ruth, D. M. Perrin, *J. Am. Chem. Soc.*, 2008, **130**, 12045.

25 U. auf dem Keller, C. L. Bellac, Y. Li, Y. Lou, P. F. Lange, R. Ting, C. Harwig, R. Kappelhoff, S. Dedhar, M. J. Adam, *Cancer Res.*, 2010, **70**, 7562.
26 Y. Li, Z. Liu, J. Lozada, M. Q. Wong, K.-S. Lin, D. Yapp, D. M. Perrin, *Nucl. Med. Biol.,* 2013, **40**, 959.
27 Z. Liu, Y. Li, J. Lozada, M. Q. Wong, J. Greene, K.-S. Lin, D. Yapp, D. M. Perrin, *Nucl. Med. Biol.,* 2013, **40**, 841.
28 Z. Liu, M. Pourghiasian, M. A. Radtke, J. Lau, J. Pan, G. M. Dias, D. Yapp, K. S. Lin, F. Bénard, D. M. Perrin, *Angew. Chem. Int. Ed.*, 2014, **53**, 11876.
29 D. M. Perrin, *Acc. Chem. Res.,* 2016, **49**, 1333.
30 R. Schirrmacher, G. Bradtmöller, E. Schirrmacher, O. Thews, J. Tillmanns, T. Siessmeier, H. G. Buchholz, P. Bartenstein, B. Wängler, C. M. Niemeyer, *Angew. Chem. Int. Ed.,* 2006, **45**, 6047.
31 L. Mu, A. Höhne, P. Schubiger, S. M. Ametamey, K. Graham, J. E. Cyr, L. Dinkelborg, T. Stellfeld, A. Srinivasan, U. Voigtmann, *Angew. Chem. Int. Ed.*, 2008, **47**, 4922.
32 J. Zhu, J. Chin, C. Wängler, B. Wängler, R. B. Lennox, R. Schirrmacher, *Bioconjugate Chem.,* 2014, **25**, 1143.
33 S. Niedermoser, J. Chin, C. Wängler, A. Kostikov, V. Bernard-Gauthier, N. Vogler, J.-P. Soucy, A. J. McEwan, R. Schirrmacher, B. Wängler, *J. Nucl. Med.*, 2015, **56**, 1100.
34 J.-P. Meyer, P. Adumeau, J. S. Lewis, B. M. Zeglis, *Bioconjugate Chem.,* 2016, **27**, 2791.
35 W. J. McBride, R. M. Sharkey, H. Karacay, C. A. D'Souza, E. A. Rossi, P. Laverman, C.-H. Chang, O. C. Boerman, D. M. Goldenberg, *J. Nucl. Med.*, 2009, **50**, 991.
36 W. J. McBride, C. A. D'Souza, R. M. Sharkey, H. Karacay, E. A. Rossi, C.-H. Chang, D. M. Goldenberg, *Bioconjugate Chem.*, 2010, **21**, 1331.
37 L. Lang, W. Li, N. Guo, Y. Ma, L. Zhu, D. O. Kiesewetter, B. Shen, G. Niu, X. Chen, *Bioconjugate Chem.*, 2011, **22**, 2415.
38 P. Laverman, C. A. D'Souza, A. Eek, W. J. McBride, R. M. Sharkey, W. J. Oyen, D. M. Goldenberg, O. C. Boerman, *Tumor Biol.*, 2012, **33**, 427.
39 F. Cleeren, J. Lecina, E. M. Billaud, M. Ahamed, A. Verbruggen, G. M. Bormans, *Bioconjugate Chem.*, 2016, **27**, 790.
40 F. Wuest, M. Berndt, R. Bergmann, J. van den Hoff, J. Pietzsch, *Bioconjugate Chem.*, 2008, **19**, 1202.
41 S. Maschauer, O. Prante, *BioMed Res. Int.*, 2014, **2014**, 16.
42 a) G. Vaidyanathan, M. R. Zalutsky, *Int. J. Rad. Appl. Instrum. B,* 1992, **19**, 275; b) G. Vaidyanathan, M. R. Zalutsky, *Nat. Protoc.,* 2006, **1**, 1655.
43 M. Kuchar, M. Pretze, T. Kniess, J. Steinbach, J. Pietzsch, R. Löser, *Amino Acids,* 2012, **43**, 1431.
44 a) G. Tang, W. Zeng, M. Yu, G. Kabalka, *J. Label. Compd. Radiopharm.,* 2008, **51**, 68; b) P. M-ding, F. Fuechtner, F. Wuest, *Appl. Radiat. Isot.,* 2005, **63**, 329; c) R. Bejot, A. M. Elizarov, E. Ball, J. Zhang, R. Miraghaie, H. C. Kolb, V. Gouverneur, *J. Label. Compd. Radiopharm.,* 2011, **54**, 117.
45 a) A. P. Kostikov, J. Chin, K. Orchowski, E. Schirrmacher, S. Neidermoser, K. Jurkschat, L. I.-Berends, C. Wängler, B. Wängler, R. Schirrmacher, *Nat. Protoc.,* 2012, **7**, 1956; b) J. -L. Zeng, J. Wang, J. -A. Ma, *Bioconjugate Chem.,* 2015, **26**, 1000.

46 D. E. Olberg, J. M. Arukwe, D. Grace, O. K. Hjelstuen, M. Solbakken, G. M. Kindberg, A. Cuthbertson, *J. Med. Chem.,* 2010, **53**, 1732.
47 Z. Li, L. Lang, Y. Ma, D. O. Kieswetter, *J. Label. Compd. Radiopharm.,* 2008, **51**, 23.
48 M. Glaser, M. Morrison, M. Solbakken, J. Arukwe, H. Karlsen, U. Wiggen, S. Champion, G. M. Kindberg, A. Cuthbertson, *Bioconjugate Chem.,* 2008, **19**, 951,
49 E. Schirrmacher, B. Wängler, M. Cypryk, G. Bradtmöller, M. Schäfer, M. Eisenhut, K. Jurkschat, R. Schirrmacher, *Bioconjugate Chem.,* 2007, **18**, 2085.
50 J. A. J. Inkster, K. Liu, S. A.-Mohand, P. Schaffer, B. Guérin, T. J. Ruth, T. Storr, *Chem. Eur. J.,* 2012, **18**, 11079.
51 S. Rojas, P. Nolis, J. D. Gispert, J. Spengler, F. Albericio, J. R. Herance, S. Abad, *RSC Adv.,* 2013, **3**, 8028.
52 E. Von Guggenberg, J. A. Sader, J. S. Wilson, S. Shahhosseini, I. Koslowsky, F. Wuest, J. R. Mercer, *Appl. Radiat. Isot.,* 2009, **67**, 1670.
53 B. De Bruin, B. Kuhnast, F. Hinnen, L. Yaouancq, M. Amessou, L. Johannes, A. Samson, R. Boisgard, B. Tavitian, F. Dollé, *Bioconjugate Chem.,* 2005, **16**, 406.
54 W. Cai, X. Zhang, Y. Wu, X. Chen, *J. Nucl. Med.,* 2006, **47**, 1172.
55 X. Yue, D. O. Kiesewetter, J. Guo, Z. Sun, X. Zhang, L. Zhu, G. Niu, Y. Ma, L. Lang, X. Chen, *Bioconjugate Chem.,* 2013, **24**, 1191.
56 X. Yue, X. Yan, C. Wu, G. Niu, Y. Ma, O. Jacobson, B. Shen, D. O. Kiesewetter, X. Chen, *Mol. Pharm.,* 2014, **11**, 3875.
57 O. Jacobson, X. Yan, Y. Ma, G. Niu, D. O. Kiesewetter, X. Chen, *Bioconjugate Chem.,* 2015, **26**, 2016.
58 R. Huisgen, *Angew. Chem*., 1963, **75**, 604.
59 J. Marik, J. L. Sutcliffe, *Tetrahedron Lett*., 2006, **47**, 6681.
60 M. Glaser, J. Goggi, G. Smith, M. Morrison, S. K. Luthra, E. Robins, E. O. Aboagye, *Bioorg. Med. Chem. Lett*., 2011, **21**, 6945.
61 M. Glaser, M. Solbakken, D. R. Turton, R. Pettitt, J. Barnett, J. Arukwe, H. Karlsen, A. Cuthbertson, S. K. Luthra, E. Årstad, *Amino Acids,* 2009, **37**, 717.
62 a) A. T. Blomquist, L. H. Liu, *J. Am. Chem. Soc.,* 1953, **75**, 2153; b) N. J. Agard, J. A. Prescher, C. R. Bertozzi, *J. Am. Chem. Soc.,* 2004, **126**, 15046; c) S. Arumugam, J. Chin, R. Schirrmacher, V. V. Popik, A. P. Kostikov, *Bioorg. Med. Chem. Lett.,* 2011, **21**, 6987.
63 L. S. Campbell-Verduyn, L. Mirfeizi, A. K. Schoonen, R. A. Dierkx, P. H. Elsinga, B. L. Feringa, *Angew. Chem. Int. Ed.,* 2011, **50**, 11117.
64 S. H. Hausner, R. D. Carpenter, N. Bauer, J. L. Sutcliffe, *Nucl. Med. Biol.,* 2013, **40**, 233.
65 N. J. Agard, J. M. Baskin, J. A. Prescher, A. Lo, C. R. Bertozzi, *ACS Cem. Biol.,* 2006, **1**, 644.
66 a) M. L. Blackman, M. Royzen, J. M. Fox., *J. Am. Chem. Soc.,* 2008, 130, 13518; b) R. D. Bach, *J. Am. Chem. Soc.,* 2009, **131**, 5233.
67 a) R. Selvaraj, S. Liu, M. Hassink, C.-W. Huang, L.-P. Yap, R. Park, J. M. Fox, Z. Li, P. S. Conti, *Bioorg. Med. Chem. Lett.,* 2011, **21**, 5011; b) S. Liu, M. Hassink, R. Selvarah, L.-P. Yap, R. Park, H. Wang, X. Chen, J. M. Fox, Z. Li, P. S. Conti, *Mol. Imaging,* 2013, **12**, 121.
68 T. L. Andersen, P. Nordeman, H. F. Christoffersen, H. Audrain, G. Antoni, T. Skrydstrup, *Angew. Chem. Int. Ed.,* 2017, **56**, 4549.

69 W. Zhao, H. G. Lee, S. L. Buchwald, J. M. Hooker, *J. Am. Chem. Soc.,* 2017, **139**, 7152.
70 P. W. Miller, N. J. Long, R. Vilar, A. D. Gee, *Angew. Chem. Int. Ed.,* 2008, **47**, 8998.
71 M. Imiolek, G. Karunanithy, W.-L. Ng, A. J. Baldwin, V. Gouverneur, B. G. Davis, *J. Am. Chem. Soc.,* 2018, **140**, 1568.
72 K. E. Arntson, W. C. K. Pomerantz, *J. Med. Chem.,* 2016, **59**, 5158.
73 W. E. Hull, B. D. Sykes, *J. Mol. Biol.* 1975, **98**, 121.
74 S. Barata-Vallejo, B. Lantaño, A. Postigo, *Chem. Eur. J.,* 2014, **20**, 16806.
75 S. Capone, I. Kieltsch, O. Flögel, G. Lelais, A. Togni, D. Seebach, *Helvetica Chimica Acta.,* 2008, **91**, 2035.
76 N. Ichiishi, J. P. Caldwell, M. Lin, W. Zhong, X. Zhu, E. Streckfuss, H.-Y. Kim, C. A. Parish, S. W. Krska, *Chem. Sci,* 2018, **9**, 4168.
77 V. Matoušek, E. Pietrasiak, R. Schwenk, A. Togni, *J. Org. Chem.,* 2013, **78**, 6763.
78 a) J.-C. Folest, J.-Y. Nédélec, J. Périchon, *Synth. Commun.,* 1988, **18**, 1491; b) H. P. Cao, Q. Y. Chen, *J. Fluor. Chem.,* 2007, **128**, 1187; c) B. R. Langlois, T. Billard, J. -C. Mulatier, C. Yezeguelian, *J. Fluor. Chem.,* 2007, **128**, 851.
79 M. Li, Y. Wang, X.-S. Xue, J.-P. Cheng, *Asian J. Org. Chem.,* 2017, **6**, 235.
80 T. Umemoto, B. Zhang, T. Zhu, X. Zhou, P. Zhang, S. Hu, Y. J. Li, *J. Org. Chem.,* 2017, **82**, 7708.
81 M. Li, X.-S. Xue, J. Guo, Y. Wang, J.-P. Cheng, *J. Org. Chem.,* 2016, **81**, 3119.
82 T. Umemoto, S. Ishihara, *Tetrahedron Lett*., 1990, **31**, 3579.
83 S. Mizuta, S. Verhoog, K. M. Engle, T. Khotavivattana, M. O'Duill, K. Wheelhouse, G. Rassias, M. Medebielle, V. Gouverneur, *J. Am. Chem. Soc.,* 2013, **135**, 2505.
84 S. Noritake, N. Shibata, Y. Nomura, Y. Huang, A. Marsnev, S. Nakamura, T. Torua, D. Cahard, *Org. Biomol. Chem.,* 2009, **7**, 3599.
85 X. Wang, L. Truesdale, J. Q. Yu, *J. Am. Chem. Soc*., 2010, **132**, 3648.
86 Y. Cheng, H. Jiang, Y. Zhang, S. Yu, *Org. Lett.,* 2013, **15**, 5520.
87 J. -J. Dai, C. Fang, B. Xiao, J. Li, J. Xu, Z. -J. Liu, X. Lu, L. Liu, Y. Fu, *J. Am. Chem. Soc.,* 2013, **135**, 8436.
88 T. Liu, Q. Shen, *Org. Lett.,* 2011, **13**, 2342.
89 S. B.-Vallejo, B. Lantaño, A. Postigo, *Chem. Eur. J.,* 2014, **20**, 16806.
90 Y. Mace, B. Raymondeau, C. Pradet, J.-C. Blazejewski, E. Magnier, *Eur. J. Org. Chem.,* 2009, **2009**, 1390.
91 T. Umemoto, S. J. Ishihara, *J. Am. Chem. Soc.,* 1993, **115**, 2156.
92 T. Khotavivattana, S. Verhoog, M. Tredwell, L. Pfeifer, S. Calderwood, K. Wheelhouse, T. L. Collier, V. Gouverneur, *Angew. Chem. Int. Ed.,* 2015, **54**, 9991.
93 M. D. Levin, T. Q. Chen, M. E. Neubig, C. M. Hong, C. A. Theulier, I. A. Kobylianskii, M. Janabi, J. P. O'Neill, F. D. Toste, *Science,* 2017, **356**, 1572.
94 S. M. Schwarzenboeck, I. Rauscher, C. Bluemel, W. P. Fendler, S. P. Rowe, M. G. Pomper, A. Asfhar-Oromieh, K. Herrmann, M. Eiber, *J. Nucl. Med.,* 2017, **58**, 1545.
95 H. -L. Huang, Y. -C. Huang, W. -Y. Lee, C. -N. Yeh, K. -J. Lin, C. -S. Yu, *PLoS One,* 2014, **9**, e104118.
96 U. Ackermann, L. Plougastel, C. Wichmann, Y. W. Goh, S. D. Yeoh, S. S. Poniger, H. J. Tochon-Danguy, A. M. Scott, *J. Label. Compd. Radiopharm.,* 2014, **57**, 115.

97 C. A. Foss, R. C. Mease, H. Fan, Y. Wang, H. T. Ravrt, R. F. Dannals, R. T. Olszewski, W. D. Heston, A. P. Kozikowski, M. G. Pomper, *Clin. Cancer Res.,* 2005, **11**, 4022.
98 R. Hatley, S. MacDonald, R. Slack, J. Le, S. Ludbrook, P. Lukey, *Angew. Chem. Int. Ed.,* 2018, **57**, 3298.
99 C. Gadais, N. S.-Rosa, E. Chelain, J. Pytkowicz, T. Brigaud, *Eur. J. Org. Chem.,* 2017, 246.
100 C. Gagais, N. Saraiva-Rosa, E. Chelain, J. Pytkowicz, T. Brigaud, *Eur. J. Org. Chem.,* 2017, **2017**, 246.

Chapter IV:

^{123}I-Iodination of Aryl Boronic Esters and Acids

4.1 Multimodal Imaging Techniques

As summarised in Chapter I, multimodality imaging such as positron emission tomography (PET) combined with computed tomography (CT) enables integrated anatomical and functional characterisation of the state of diseases.[1] In order to take advantage of these imaging techniques, significant efforts have been undertaken in the field of radiochemistry to streamline the preparation of ^{18}F-labelled PET radiotracers from a diverse range of precursors (Figure 4.1).[2-3]

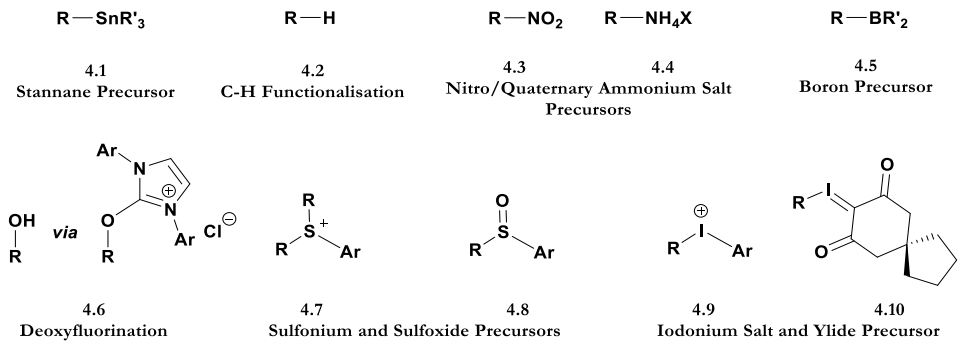

Figure 4.1. Common precursors and intermediates associated with non-metal radiochemistry

4.2 Single Photon Electron Computed Tomography (SPECT)

Whilst significant developments have been undertaken in the field of PET imaging, single photon electron computed tomography (SPECT) continues to be used widely within medical imaging. SPECT is comparable to PET in offering non-invasive imaging *via* use of tracer molecules containing radionuclides. Unlike PET however, which utilises positron emitting radionuclides, SPECT exploits those radionuclides that emit γ-radiation in electron capture and isomeric transition processes (Table 4.1).

Radionuclide	Half-Life (h)	Type of emission	Energy (keV)
^{123}I	13.2	Electron Capture	159
^{99m}Tc	6	Isomeric Transition	140
^{111}In	67.9	Electron Capture	537
^{67}Ga	78.3	Electron Capture	93

Table 4.1. Radionuclides utilised for SPECT

Typically, these radionuclides have longer half-lives than those used for PET and are of a lower energy. Whilst SPECT is a less sensitive technique than PET, the longer half-lives of the aforementioned radionuclides present several advantages. The first of these is the potential for greater distance between the production facility and imaging facility. Second, the longer half-life allows for greater flexibility in both the radiosynthesis and the imaging *in vivo* for longer biological processes.

4.3 Radioiodination of (Hetero)aromatics

Of those non-metal radioisotopes utilised within PET, SPECT and other imaging techniques such as radioisotope therapy (RIT), radioimmunoassay (RIA) and autoradiography, radioactive isotopes of iodine (^{123}I, ^{124}I, ^{125}I, ^{131}I) occupy a prominent place (Figure 4.2).[4]

Previous approaches for the formation of C-*I bonds have centered around three methods (Scheme 4.1). The first of these is a copper mediated halogen/isotopic exchange exemplified by Brownell for the radiolabeling of [^{123}I]IPEB **[^{123}I]4.12** (Scheme 4.1A), an imaging agent for the glutamine receptor.[5] Both alternatives involve an oxidative process *via* the initial formation of iodomonochloride from sodium iodide and a strong oxidant such as chloramine-T. This process has been utilised for both electrophilic aromatic substitution and

iododestannylation as exemplified by Gouverneur and Weiland for the radiolabeling of [^{123}I]DPA-713 **[^{123}I]4.14** and [^{123}I]MIBG **[^{123}I]4.16** respectively (Scheme 4.1B, 4.1C).[6,7]

Radionuclide	Production	Half-Life	Primary Decay Processes	Application
Iodine-123	^{124}Xe(p,pn)^{123}I	13.2 h	EC	SPECT
Iodine-124	^{124T}e(p,n)^{124}I	4.18 days	74,4% EC, 25.6% β^+	PET
Iodine-125	^{124}Xe(n,γ)^{125}I	54.9 days	EC	RIA, Binding
Iodine-131	$^{130'}$Te(n,γ)^{131}I	8.02 days	β^-	RIT, SPECT

Figure 4.2. Iodine-123, -125 and -131 main properties

Whilst these methods have allowed for the successful production for a small selection of tracers,[8] each has their own limitations. Halogen/isotopic exchange, has been shown to be highly substrate dependent whilst both S_EAr and destannylation processes rely upon electron rich aromatic systems to facilitate the radiolabelling step. Although the relatively long half-live of the radioactive isotopes of iodine does allow for multiple post-labelling transformations, this is not ideal. These reasons have fuelled the desire develop novel late stage radioiodination strategies.

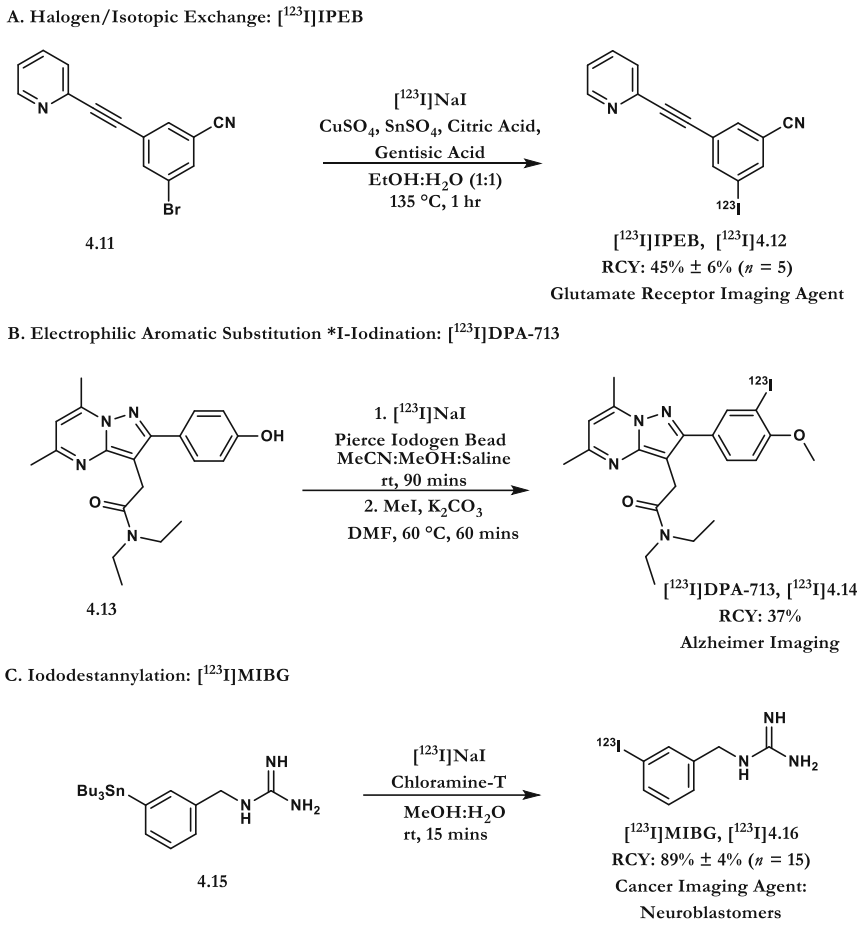

Scheme 4.1. Classical Methods for Radioiodination

4.4 Metal Mediated Radioiodination

In 2013, Sutherland and co-workers reported a nickel-mediated radioiodination of (hetero)aryl bromides using [^{125}I]NaI or [^{123}I]NaI (Scheme 4.2).[9] Whilst this reaction allowed for the use of the commercially available aryl-bromides, the harsh conditions and air sensitive $Ni(COD)_2$ complex makes this approach non-trivial for radiochemists.

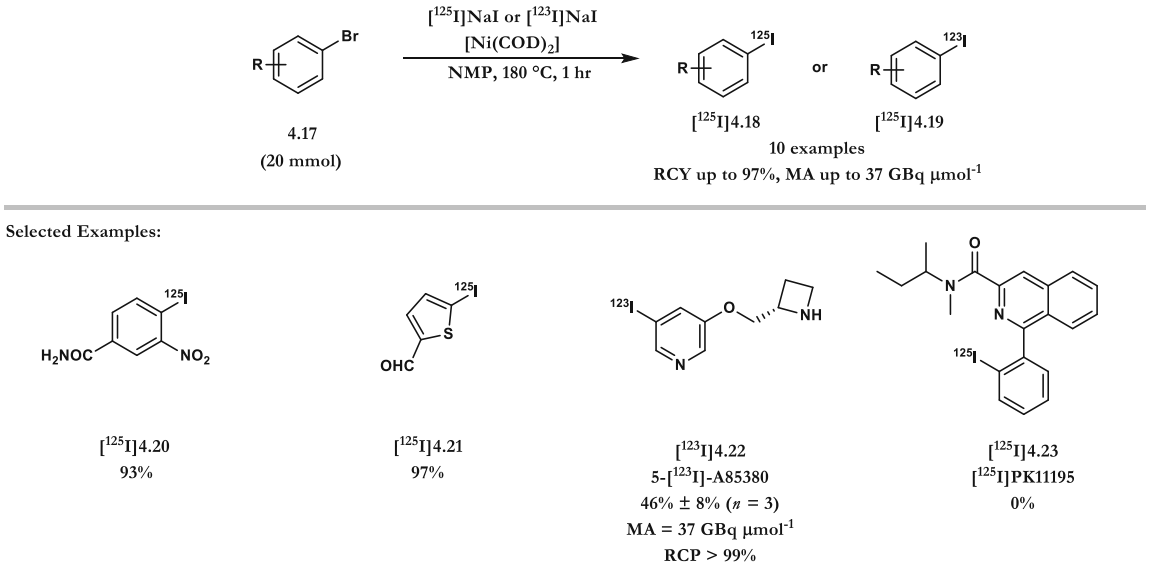

Scheme 4.2. Nickel Mediated Radioiodination of (Hetero)Aryl Bromides

In an effort to develop a methodology that proceeded under more mild conditions, Sutherland and co-workers reported an electrophilic C-H ^{125}I-iodination of (hetero)arenes. Using [^{125}I]NIS, generated *in-situ* by mixing NCS and [^{125}I]NaI, and the Lewis acid $AgNTf_2$, the authors successfully ^{125}I-iodinated electron rich aromatics (Scheme 4.3).[10] Whilst this method was reported using relatively mild conditions compared to those reported previously by Sutherland (Scheme 4.2), the lack of pre-functionalisation to aid in directing radioiodination could be a limitation when applied to complex targets bearing multiple, reactive sites.

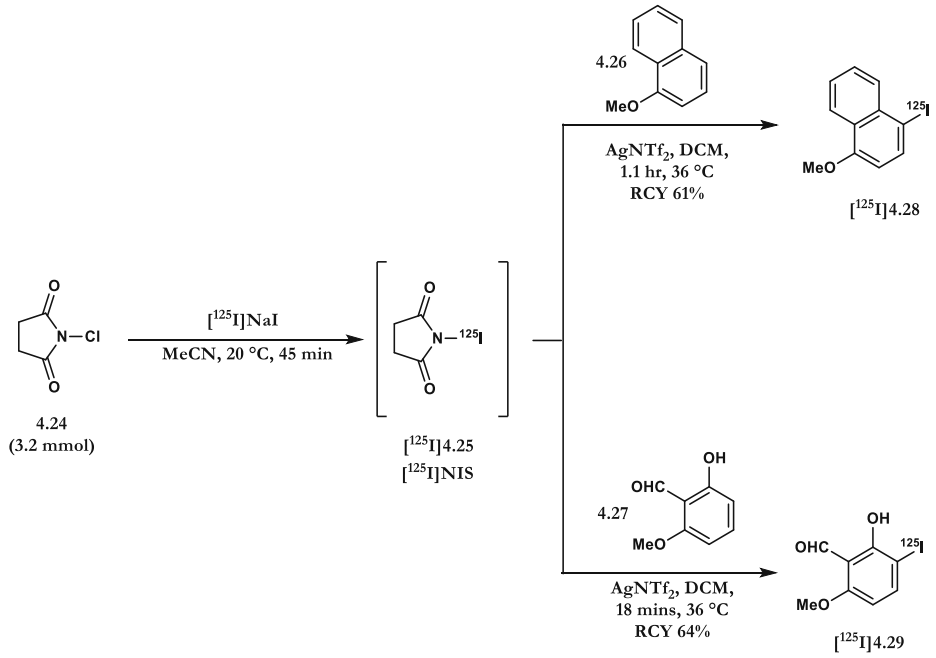

Scheme 4.3. Silver(I) catalysed iodination of arenes

4.5 Metal Free Radioiodination

Following the aforementioned works, Sutherland and co-workers, developed an efficient one-pot ^{125}I-iodination of anilines.[11] Under mild conditions, the *in-situ* formation of the corresponding diazonium salts was described. Following this formation, displacement with [^{125}I]NaI allowed access to a wide range of functionalised ^{125}I-labelled (hetero)aromatics in a regioselective manner. This was exemplified with the radioiodination of five clinically relevant radiotracers (Scheme 4.4). This transformation underlined the advantage that pre-functionalisation with bench stable precursors can have over C-H functionalisation processes.

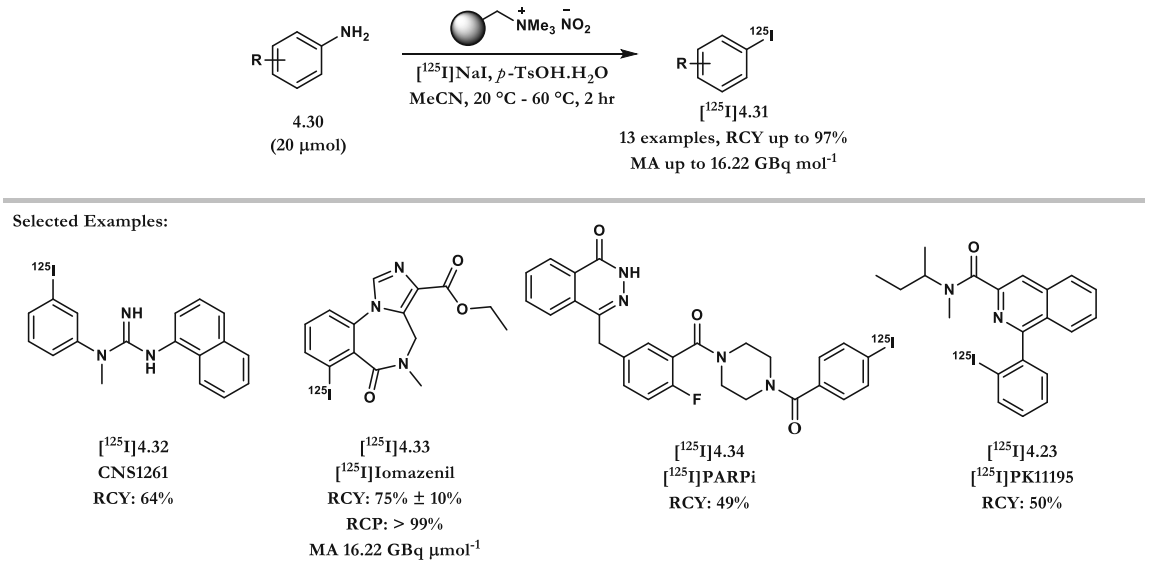

Scheme 4.4. A one-pot radioiodination of aryl amines via stable diazonium salts

4.6 Radioiodination of Boron Precursors

The use of boron precursors in radioiodination was first described by Knapp in the radiosynthesis of a ^{125}I-tagged barbituric acid analogue **[^{125}I]4.36** (Scheme 4.5).[12] In this work, starting from a vinylic boronic acid and [^{125}I]ICl generated *in-situ* from chloramine-T and [^{125}I]NaI, Knapp was able to perform radioiodination at room temperature with a moderate yield through an electrophilic substitution mechanism. Analogous conditions have since been applied to the radiolabeling of a variety of boron derivatives for C-*I bond formation (Scheme 4.6).[13-15]

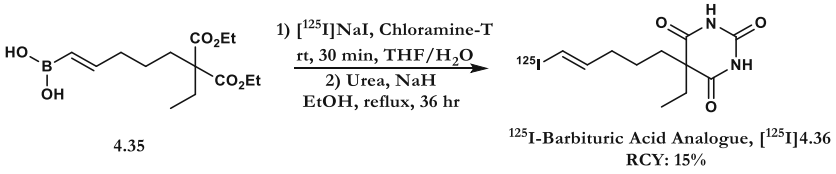

Scheme 4.5. Electrophilic *ipso*-iododeboronation for the synthesis of ^{125}I-tagged barbituric acid **[^{125}I]4.36**

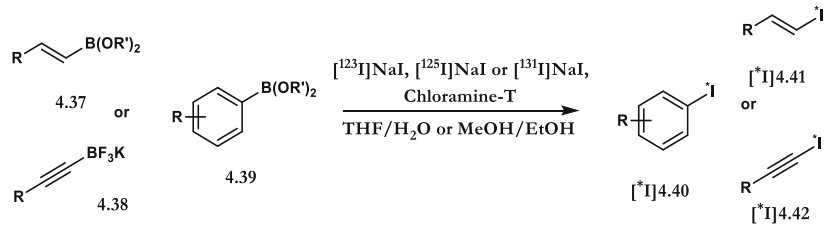

Scheme 4.6. Electrophilic *ipso*-iododeboronation of boron precursors

Whilst this method has been successfully applied to the radioiodination of more challenging targets (Scheme 4.7),[16,17,18] one of the main limitations is the need for electron rich alkenes and aromatics to facilitate efficient labelling. As highlighted in the work of Kabalka,[13] whilst electron rich aromatics underwent efficient iodination, substrates containing electron withdrawing substituents such as **[^{125}I]4.55** and **[^{125}I]4.56** either were unsuccessful or required elongated reaction times (Scheme 4.8).

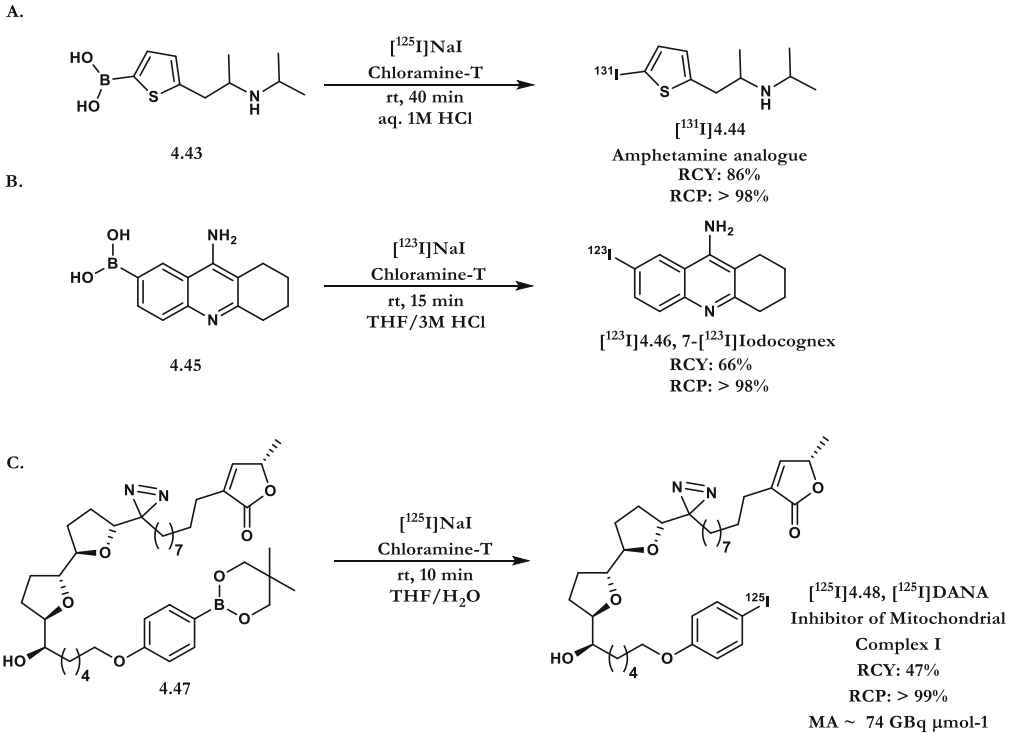

Scheme 4.7. Electrophilic *ipso*-iododeboronation for the synthesis of A) Amphetamine analogue **[^{131}I]4.44** B) [^{123}I]Iodocognex **[^{123}I]4.46** C) [^{125}I]DANA **[^{125}I]4.48**

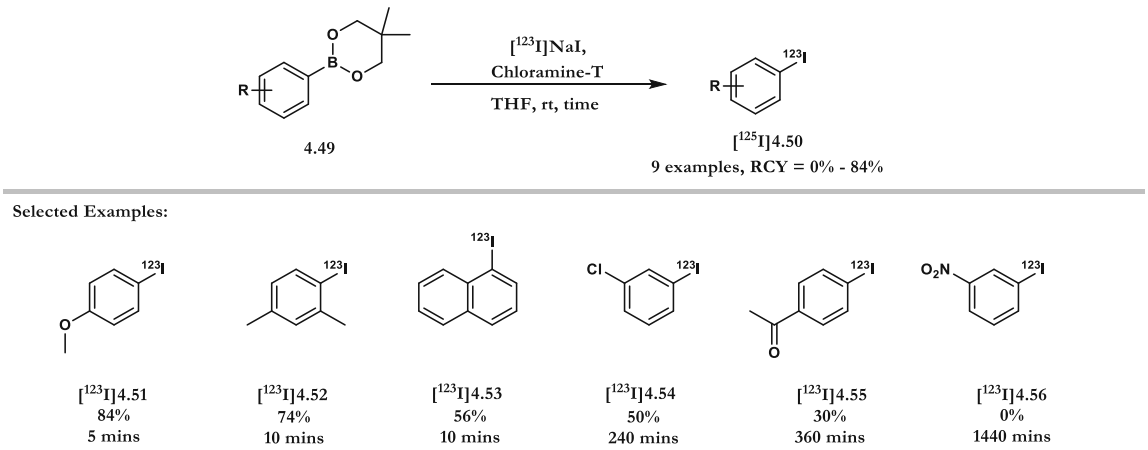

Scheme 4.8. Electrophilic Radioiodination of Aryl Boronic Esters

4.7 Results and Discussion

Given the previous work by our group on the copper mediated nucleophilic ^{18}F-fluorination of aryl pinacol boronic esters,[19] the prospect of using a common precursor for both radiofluorination and radioiodination prompted us to explore the copper-mediated reaction of aryl boron reagents with [^{123}I]NaI.[a]

4.7.1 Initial Investigations

In 2013, Hartwig and co-workers reported a one pot borylation-iodination of (hetero)arenes employing iridium(I) and copper(I)-catalysis (Scheme 4.9).[20] The authors established that CuI could be replaced by Cu_2O for reactions with iodide acting as the limiting reagent, a result boding well for possible iodination with radiolabelled NaI. This protocol served as a starting point for our investigation into the nucleophilic radioiodination of aryl boron reagents.

[a] The following work was undertaking in collaboration with G. McSweeney, T.Cailly, S. Preshlock, S. Verhoog and M. Tredwell. All specific contributions are highlighted in footnotes and Supporting Information

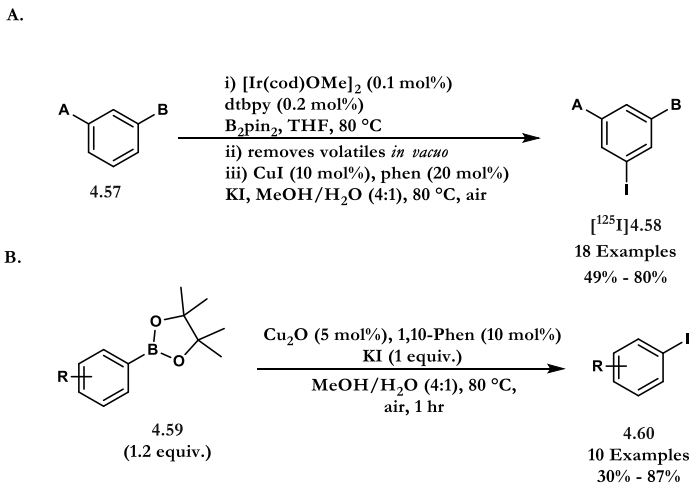

Scheme 4.9. A) Sterically controlled iodination of arenes via iridium-catalyzed C-H borylation B) Under limiting iodide conditions

Taking the naturally occurring isotope, iodine-127, a screen of copper sources, ligands and solvent was undertaken (Table 4.2). Since none of the copper(I) sources were found to improve upon Cu_2O, a range of copper(II) sources were investigated; $Cu(OCOCF_3)_2$ was found to be marginally superior (Table 4.2, Entry 11). Notably, $Cu(OTf)_2(py)_4$, used previously in the ^{18}F-fluoroination of aryl pinacol boronic esters, afforded none of desired product **4.51** (Table 4.2, Entry 9).

Finally, a range of ligands were screened. The use of a *bis*-phosphine ligand gave no desired product (Table 4.2, Entry 13). Furthermore, the nitrogen ligands 2,2'-bipyridine, bathophenanthroline, TMEDA and pyridine afforded little to no product formation.

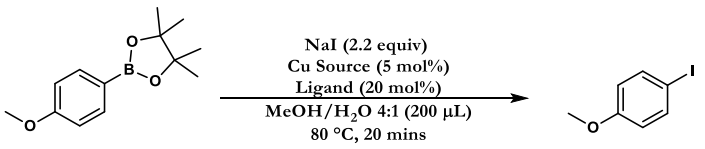

4.61
0.1 mmol

4.51

Entry	Copper Source	Ligand	NMR Yield/%[a]
1	Cu_2O	1,10-Phenanthroline	58
2	$Cu(OTf)(C_6H_6)$	1,10-Phenanthroline	4
3	$Cu(OTf)(C_6H_6)$	-	2
4	$Cu(OTf)(MeCN)_4$	1,10-Phenanthroline	24
5	$Cu(OTf)(MeCN)_4$	-	2
6	Cu(TC)	1,10-Phenanthroline	24
7	$Cu(OAc)_2$	-	8
8	$Cu(OAc)_2$	1,10-Phenanthroline	48
9	$Cu(OTf)_2(py)_4$	1,10-Phenanthroline	0
10	$Cu(OTf)_2$	1,10-Phenanthroline	5
11	**$Cu(OCOCF_3)_2$**	**1,10-Phenanthroline**	**60**
12	$Cu(OCOCF_3)_2$	1,2-Bis(diphenylphosphino)ethane	0
13	$Cu(OCOCF_3)_2$	2,2'-bipyridine	7
14	$Cu(OCOCF_3)_2$	Bathophenanthroline	0
15	$Cu(OCOCF_3)_2$	TMEDA	3
16	$Cu(OCOCF_3)_2$	Pyridine	2

[a]NMR yields measured using *tert*-butyl methyl ether as internal standard.

Table 4.2. Screening of copper sources and ligands

Following initial optimisation, a variety of electron rich, neutral and poor aryl boronic esters were screened. The conditions described by both Kabalka and Hartwig were examined in parallel in order to provide a comparison of each method before undertaking the radioiodination.[13,20] As predicted, when subjecting electron rich substrates to those Kabalka's conditions, excellent conversions were observed. However, when electron poor substrates were

employed, minimal to no conversion to the desired product was observed (Figure. 4.3).

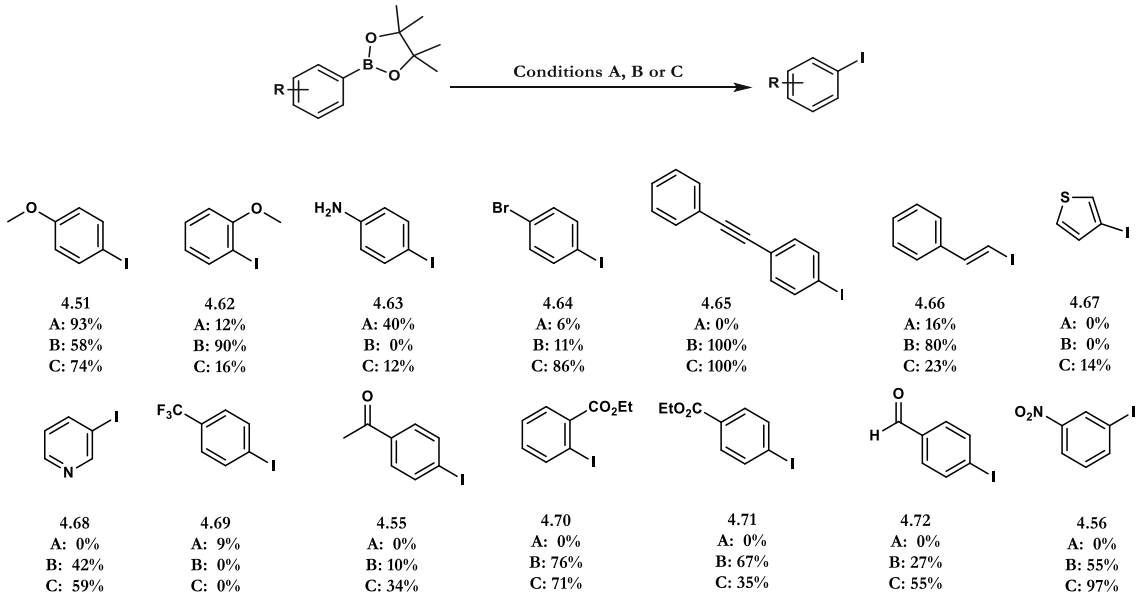

Conditions A: Substrate (0.05 mmol), NaI (2.2 equiv.), Chloramine-T (1.1 equiv.), 80 °C, 30 min, THF/1 M NaOH Conditions B: Substrate (0.05 mmol), NaI (2.2 equiv.), 10 mol% Cu_2O , 20 mol% 1,10-Phenanthroline, 80 °C, 30 min, MeOH/H_2O (4:1) Conditions C: Substrate (0.05 mmol), NaI (1.0 equiv.), 20 mol% 1,10-Phenanthroline, 10 mol% $Cu(OCOCF_3)_2$, 80 °C, 30 min, MeOH/H_2O (4:1) [d]Internal Standard: TBME (0.05 mmol)

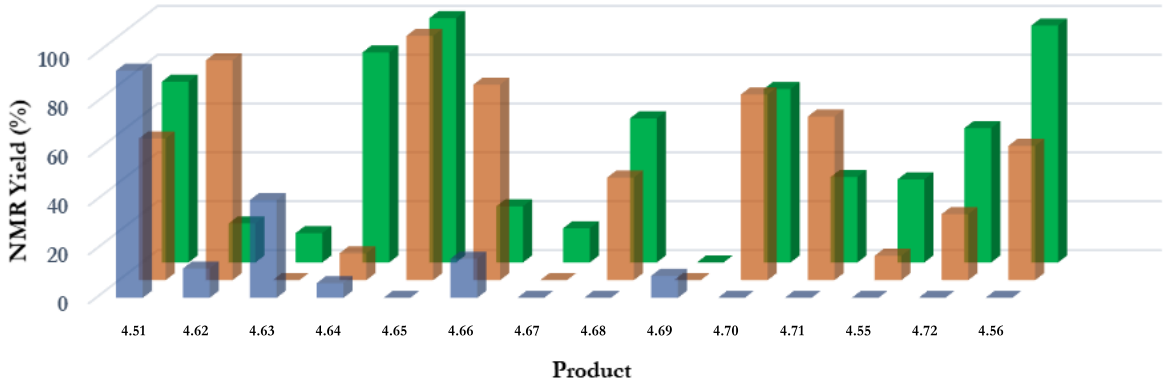

Series	Reaction Conditions
Kabalka[13]	NaI 2.2 equiv., Chloramine-T 1.1 equiv., THF/1M NaOH (200 µL, 1/1), 80 °C, 30 min
Hartwig[20]	NaI 2.2 equiv., Cu_2O 10 mol%, Phen 20 mol%, MeOH/H_2O (200 µL, 4/1), 80 °C, 30 min
This Work	NaI 1 equiv., $Cu(OCOCF_3)_2$ 10 mol%, 1,10-Phenanthroline 20 mol%, MeOH/H_2O (200 µL, 4/1), 80 °C, 30 min

Figure 4.3. A) Substrate scope of the ^{127}I-Iodination of aryl boronic esters B) Graphical representation of the ^{127}I-Iodination of aryl boronic esters

Whilst the use of $Cu(OCOCF_3)_2$ as a catalyst did lead to a general improvement when compared to those conditions reported by Hartwig, for a selection of substrates (**4.62**, **4.66**, **4.70**, **4.71**) Cu_2O proved to be a superior catalyst, and therefore both conditions were taken through for further investigations for the radiolabelling with iodine-123.

4.7.2 ^{123}I-Iodination: Preliminary Screenings

Studies with the model aryl boron precursors **4.61** demonstrated the viability of Cu-mediated nucleophilic ^{123}I-radioiodination, and its superiority to Kabalka's electrophilic radioiodination when applied to electron-deficient substrates (Table 4.3, Entry 2). Whilst our previous work with Cu_2O had led to similar NMR yields being observed, the radiochemical conversions (RCCs) with Cu_2O did not exceed 30% (Table 4.3, Entries 5-8). Nonetheless, by modifying the copper source, improved RCCs up to 79% were observed (Table 4.3, Entries 11).

Further optimisation, modifying the molar ratio of substrate versus copper complex and solvent revealed that the highest radiochemical conversions were obtained with 2 mol% of $Cu(OCOCF_3)_2$ and 2 mol% of 1,10-phenanthroline in $MeOH/H_2O$ (4:1) at 80 ^oC for 20 minutes (Table 4.3, entries 12). Pleasingly, aryl boronic acid **4.75**, trifluoroborate salt **4.76** and neopentyl glycol (nep) boronic ester **4.77** also underwent successful ^{123}I-iodination under these reaction conditions (Table 4.3, Entries 14-15).

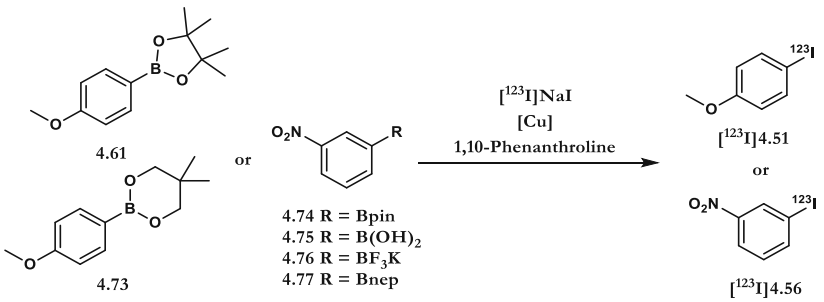

Entry[a]	Precursor	Copper Source	RCC[b] (*n* = 2)[c]
1	**4.61**	-[d]	93% ± 5%
2	**4.74**	-[d]	0% ± 0%
3	**4.73**	-[d]	84%[e]
4	**4.77**	-[d]	0%[f]
5	**4.61**	Cu_2O (140 mol%)[g]	15% ± 5%
6	**4.61**	Cu_2O (140 mol%)[g]	29% ± 5%
7	**4.61**	Cu_2O (140 mol%)[h]	5% ± 1%
8	**4.61**	Cu_2O (14 mol%)	29% ± 9%
9	**4.61**	$Cu(OCOCH_3)_2$ (10 mol%)	66% ± 15%
10	**4.61**	$Cu(OCOCF_3)_2$ (10 mol%)	79% ± 7%
11	**4.61**	$Cu(OCOCF_3)_2$ (5 mol%)	79% ± 15%
12	**4.61**	$Cu(OCOCF_3)_2$ (2 mol%)	87% ± 0%
13	**4.74**	$Cu(OCOCF_3)_2$ (2 mol%)	84% ± 6%
14	**4.75**	$Cu(OCOCF_3)_2$ (2 mol%)	73% ± 12%
15	**4.76**	$Cu(OCOCF_3)_2$ (2 mol%)	80% ± 2%

Table 4.3. Optimisation for the ^{123}I-Iodination of aryl boron reagents [a] Standard conditions: 1:1 [Cu]/1,10-phenanthroline in 200 μL of MeOH:H_2O (4:1) at 80 °C for 20 mins. [b] RCC = Radiochemical Conversion. [c] All reactions were repeated *n* times. [d] Conditions: Chloramine-T (1.8 equiv.), 200 μL of THF:H_2O (1:1) at rt for 20 mins. [e] RCY reported by G. W. Kabalka for **4.73** (See reference 17). [f] RCY reported by G. W. Kabalka for **4.77** (See reference 17). [g] 1,10-phenanthroline (6 equiv.). [h] No 1,10-phenanthroline. Pin = pinacol. Nep = Neopentyl glycol.

4.7.3 ^{123}I-Iodination: Substrate Scope

With the optimised conditions in hand (Table 4.6, Entry 12), an investigation was undertaken into the scope of the reaction with a selection of

pinacol derived (hetero)aryl boronic esters (Scheme 4.10). Excellent RCCs were obtained for a range of electron-rich and electron-deficient substrates. The reaction demonstrated a tolerance for both unprotected phenol and indole as exemplified with the ^{123}I-labelling of **[^{123}I]4.78** and **[^{123}I]4.79** respectively. Notably, the high regioselectivity of the product **[^{123}I]4.78**, illustrated that the product of S_EAr was incompatible with the reactions conditions. For the *ortho*-substituted aromatics **[^{123}I]4.70** and **[^{123}I]4.62**, a reduction in RCC was observed, potentially due to the steric hindrance of these substrates slowing down the transmetallation step.[21]

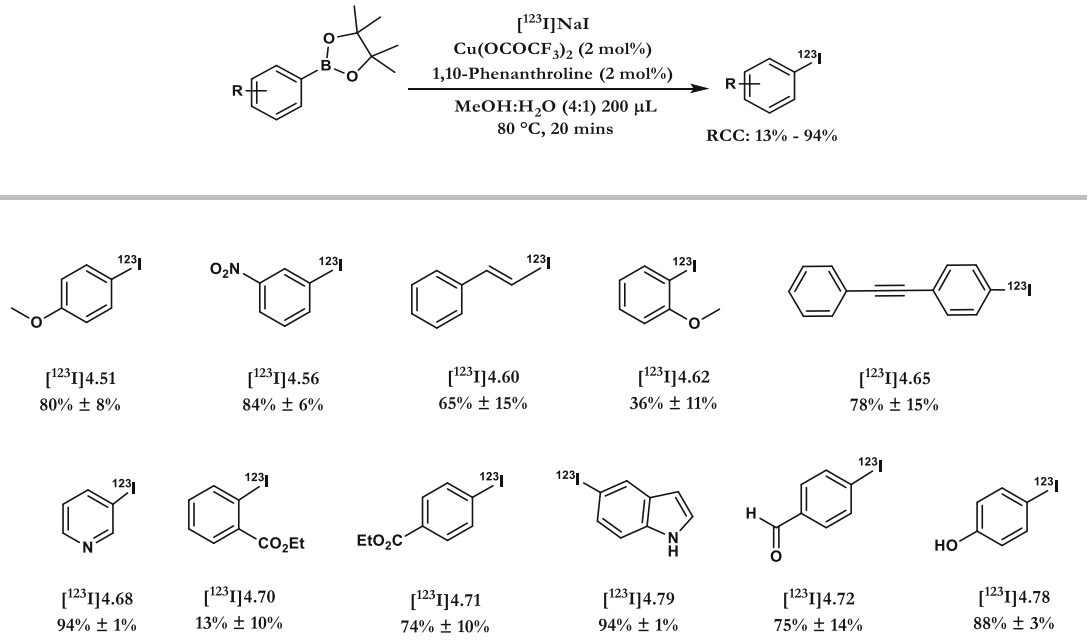

Scheme 4.10. Substrate scope for the copper mediated ^{123}I-iodination of (hetero)aryl boronic pinacol esters (n = 4 unless stated otherwise)

Next the reactivity of selected (hetero)aryl boronic acids was probed (Scheme 4.11). Again, high RCCs were observed for electron-rich **[^{123}I]4.78**, electron-poor **[^{123}I]4.56** and heterocycle **[^{123}I]4.79**.

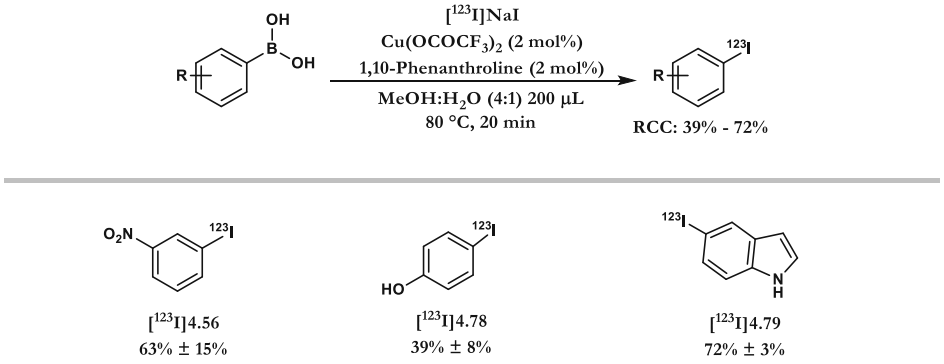

Scheme 4.11. Substrate scope for the Copper mediated ^{123}I-iodination of (hetero)aryl boronic acids (n = 4 unless stated otherwise)

4.7.4 ^{123}I-Iodination of Clinically Relevant SPECT Radiotracers:

Having established a modest scope, we sought to employ the protocol for the labelling of two clinically relevant SPECT tracers, [^{123}I]IMPY **[^{123}I]4.81** and [^{123}I]DPA-713 **[^{123}I]4.14**.

The first of these tracers, 6-[^{123}I]iodo-2-(4'-dimethylamino-)phenyl-imidazo[1,2-*a*]pyridine ([^{123}I]IMPY, **[^{123}I]4.81**), is a plaque imaging agent for the diagnosis of Alzheimer's disease that has previously been accessed via ^{123}I-iododestannylation in 20% - 60% RCY (Scheme 4.12A).[22,23] The corresponding boronic ester was prepared in 4 steps. A-Dibromination of 1-(4-(dimethylamino)phenyl)ethan-1-one **4.82** followed by mono-debromination with triethylamine and diethylphosphite afforded **4.84** in 70% yield over two steps. Condensation with 2-amino-5-iodopyridine furnished the heterocyclic core, after which, lithium-halogen exchange followed by quenching with

^{i}PrOBpin afforded the desired boronic pinacol ester **4.85**. Subjecting **4.85** to modified conditions described previously, [^{123}I]IMPY **[^{123}I]4.81** could be isolated in an RCY of 78% (4.12C).[b]

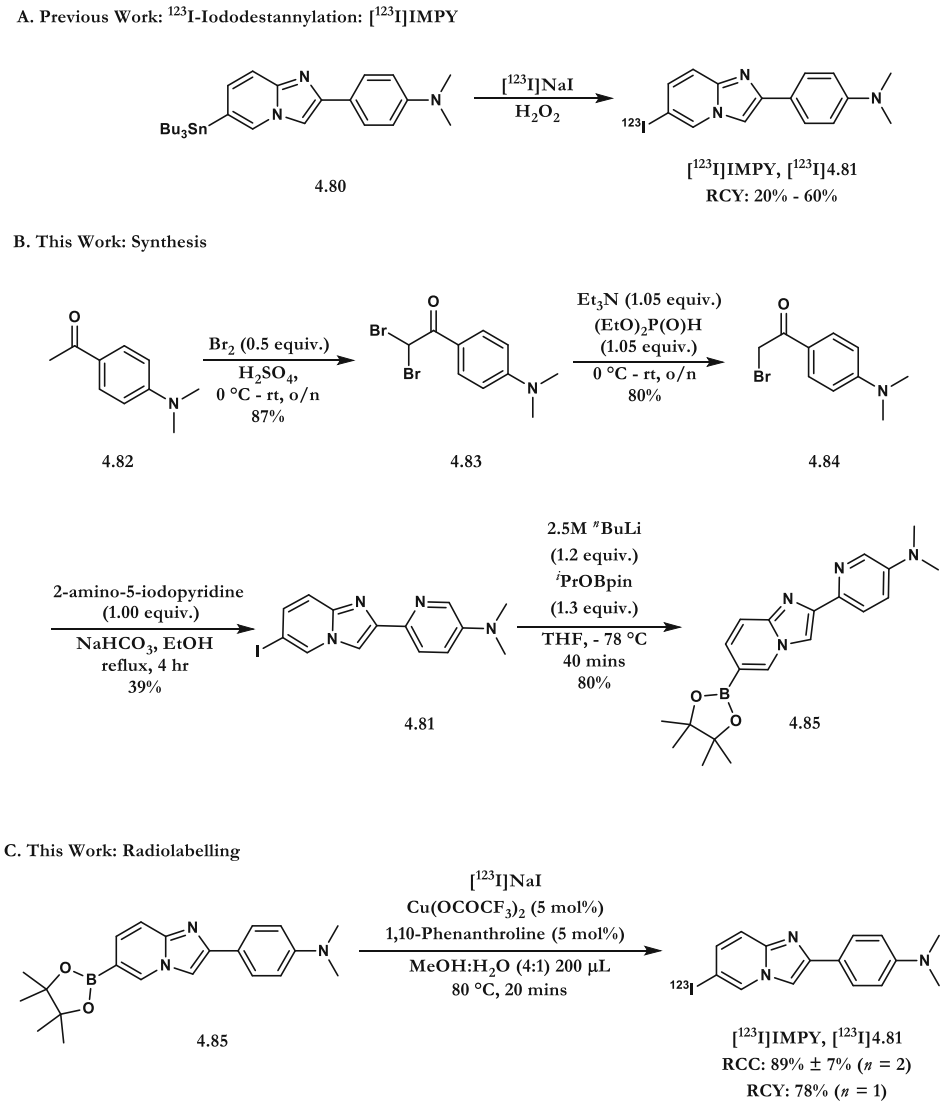

Scheme 4.12. A) Previous synthesis of [^{123}I]IMPY **[^{123}I]4.81** B) Copper mediated ^{123}I-iodination of aryl pinacol boronic ester **4.85**

The second tracer, *N*,*N*-diethyl-2-(2-(3-^{123}iodo-4-methoxyphenyl)-5,7-dimethylpyrazolo[1,5-*a*]pyrimidin-3-yl) acetamide [^{123}I]DPA-713 **[^{123}I]4.14**, previously labelled via an electrophilic iodination (Scheme 4.13A),[6] has been

[b] Synthesis of IMPY Boronic Ester Precursor and reference carried out by G. McSweeney

used as a translocator protein (TSPO) radioligand for the imaging of neurodegenerative diseases.[24]

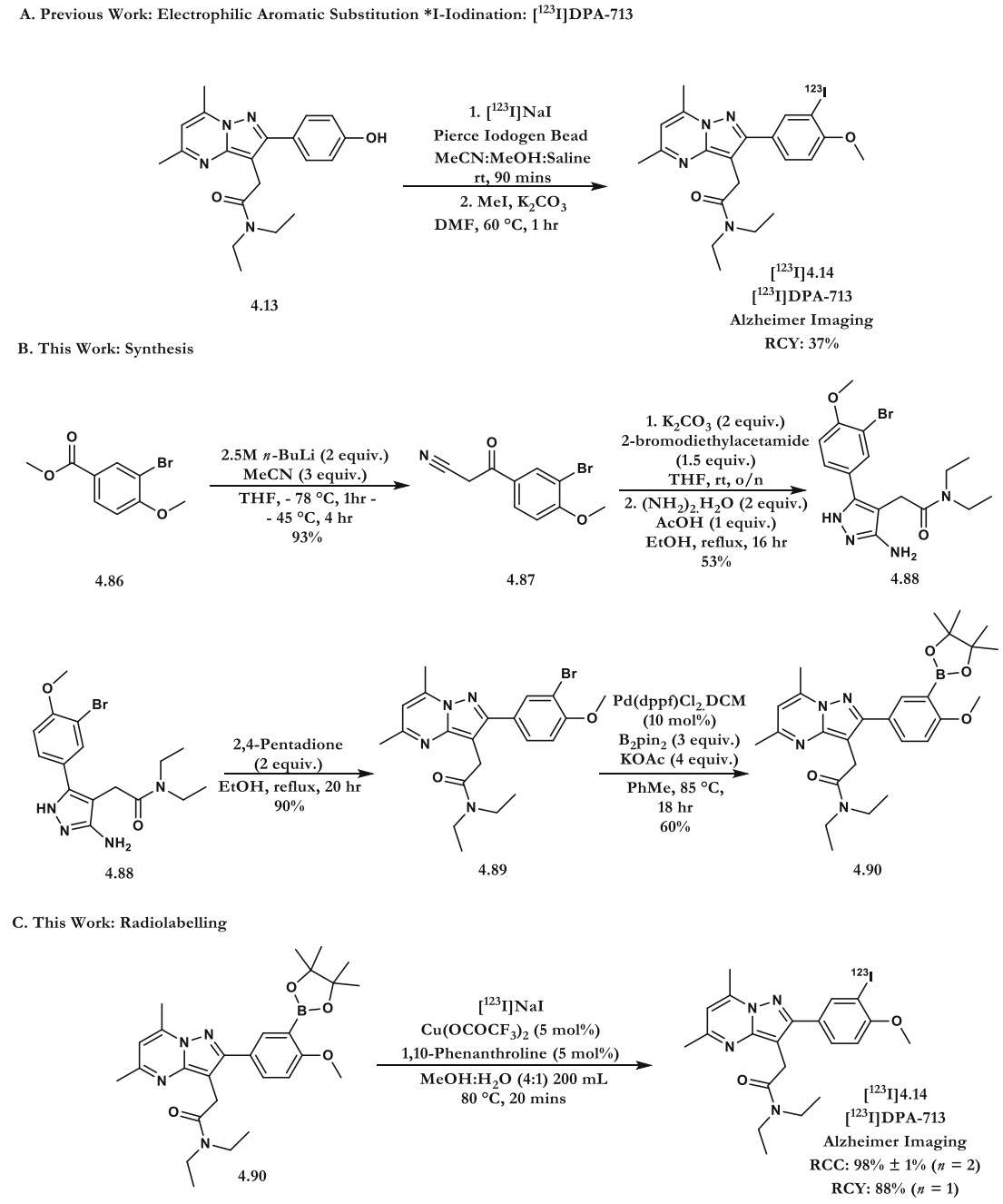

Scheme 4.13. A) Previous synthesis of [^{123}I]DPA-713 [^{123}I]**4.14** B) Synthesis of aryl pinacol boronic ester **4.90** C) Copper mediated ^{123}I-iodination of aryl pinacol boronic ester **4.90**

The synthesis of boronic ester precursor **4.90** began with deprotonation of MeCN with ^{n}BuLi, addition to methyl-3-bromo-4-methoxybenzoate to form

keto-nitrile **4.87**. Alkylation of **4.87** with 2-bromodiethylacetamide followed by treatment of hydrazine hydrate afforded aminopyridine **4.88**. Finally, condensation of **4.88** with 2,4-pentadione to form the pyrazolopyrimidine core, followed by Miyaura borylation allowed for the corresponding aryl pinacol boronic ester **4.90** to be isolated. When **4.90** was subjected to the modified copper mediated ^{123}I-iodination conditions, both high RCC (98% ±1%) and RCY (88%) were observed (4.13C).[c]

4.7.5 Divergent Radiohalogenation:

Having demonstrated the tolerance of the reaction towards two clinically relevant SPECT tracers, our final aim was to validate the aryl boronic ester as a precursor for divergent radiohalogenation with ^{18}F and ^{123}I (Scheme 4.14). Two tracers that had already been labelled with ^{18}F and ^{123}I from different precursors were investigated.[25-27] The first pair consists of 3-[^{18}F]fluoro-5-(pyridine-2-ylethynyl)benzonitrile [^{18}F]FPEB **[^{18}F]4.92** and 3-[^{123}I]iodo-5-(pyridine-2-ylethynyl)benzonitrile [^{123}I]IPEB **[^{123}I]4.12**, which are both radioligands for metabotropic glutamate receptors. Hamill and Brownell accessed [^{18}F]FPEB **[^{18}F]4.92** and [^{123}I]IPEB **[^{123}I]4.12** using two different precursors *via* S_NAr and halogen exchange, respectively (Scheme 4.14A, 4.14B).[5,27]

[c] Synthesis of DPA-713 boronic ester precursor **4.90** and reference carried out by G. McSweeney

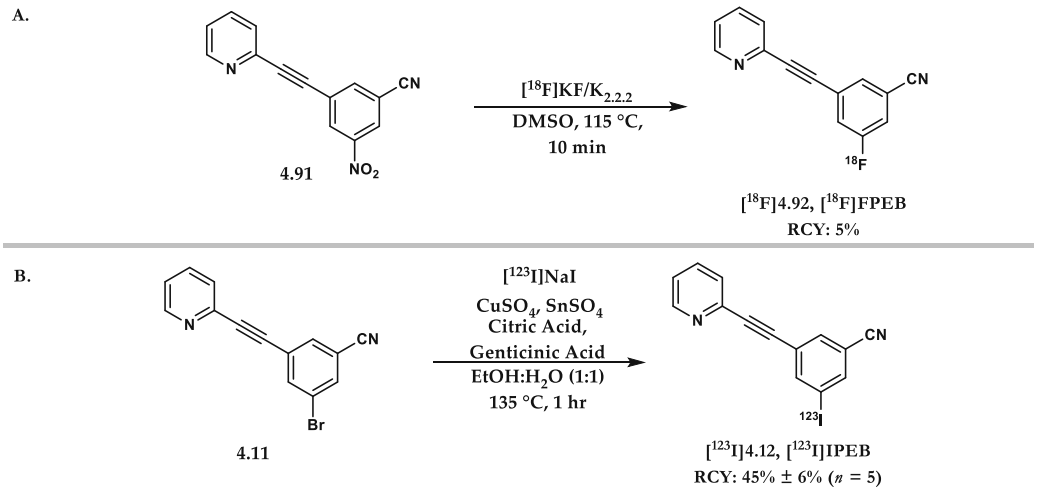

Scheme 4.14. Previous syntheses of [^{18}F]FPEB **[^{18}F]4.92** and [^{123}I]IPEB **[^{123}I]4.12**

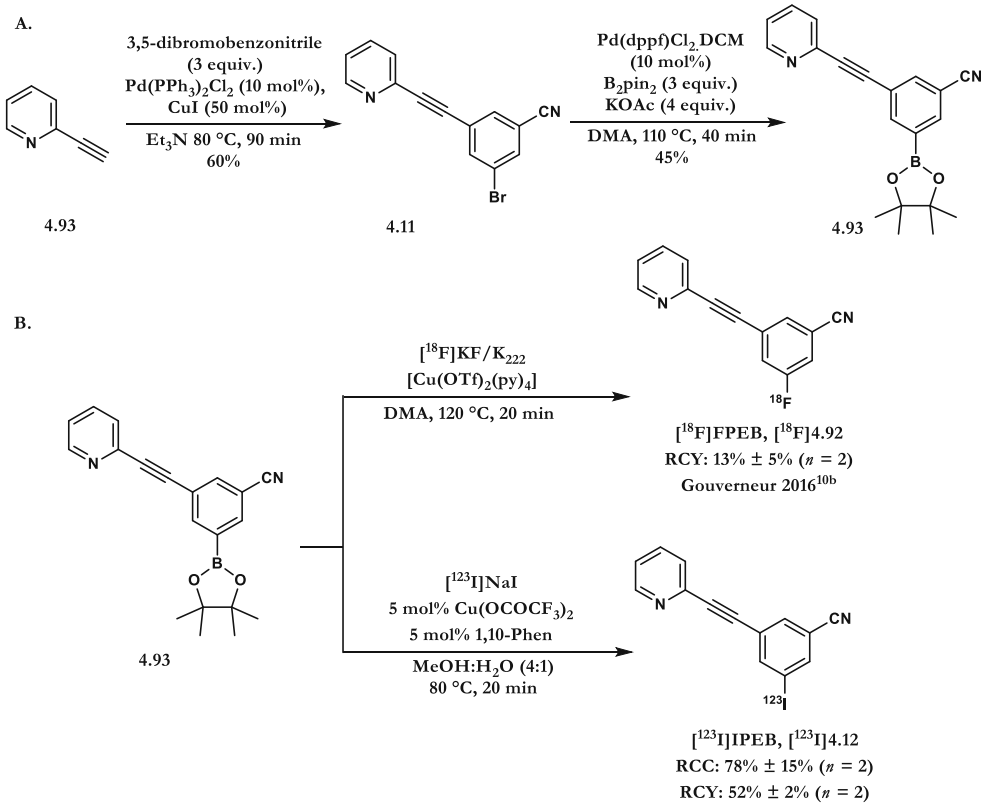

Scheme 4.15. A) Synthesis of aryl boron pinacol ester **4.93** B) Divergent synthesis from a common precursor for both [Cu] Mediated ^{123}I-iodination and ^{18}F-fluorination of aryl boronic ester **4.93**[d]

The corresponding boronic ester **4.93**, was prepared by coupling of 2-ethynylpyridine **4.93** with 3,5-dibromobenzonitrile under classical Sonogashira conditions to afford **4.11** in 60% yield. Miyaura borylation of **4.11**

[d] The borylation of compound **4.11** was carried out by Dr. S. Gruber. The ^{18}F-fluorodeboronation of **4.93** was carried out by Dr. S. Preshlock.

furnished boronic ester **4.93** in 45% yield. With the boronic ester precursor in hand, both [^{18}F]FPEB **[^{18}F]4.92** and [^{123}I]IPEB **[^{123}I]4.12** could be accessed in 13% ± 5% and 52% ± 2% RCY, respectively, under copper mediated nucleophilic radiohalogenation (Scheme 4.15).

A similar principle was applied to *meta*-[^{18}F]fluorobenzylguanidine [^{18}F]MFBG **[^{18}F]4.97** and *meta*-[^{123}I]iodobenzylguanidine [^{123}I]MIBG **[^{123}I]4.16**.[25,7] Lewis and co-workers have compared the efficacy of [^{18}F]MFBG **[^{18}F]4.97** and [^{123}I]MIBG **[^{123}I]4.16** in human norepinephrine transporter (hNET) gene-transduced C6 rat glioma cells and xenografts.[5d] For this pre-clinical study, the radiosynthesis of [^{18}F]MFBG **[^{18}F]4.97** was accomplished *via* nucleophilic aromatic substitution with [^{18}F]F$^-$ followed by two step post ^{18}F-fluorination, whilst an iododestannylation followed by deprotection was performed to access [^{123}I]MIBG **[^{123}I]4.16** (Scheme 4.16A, 4.16B).

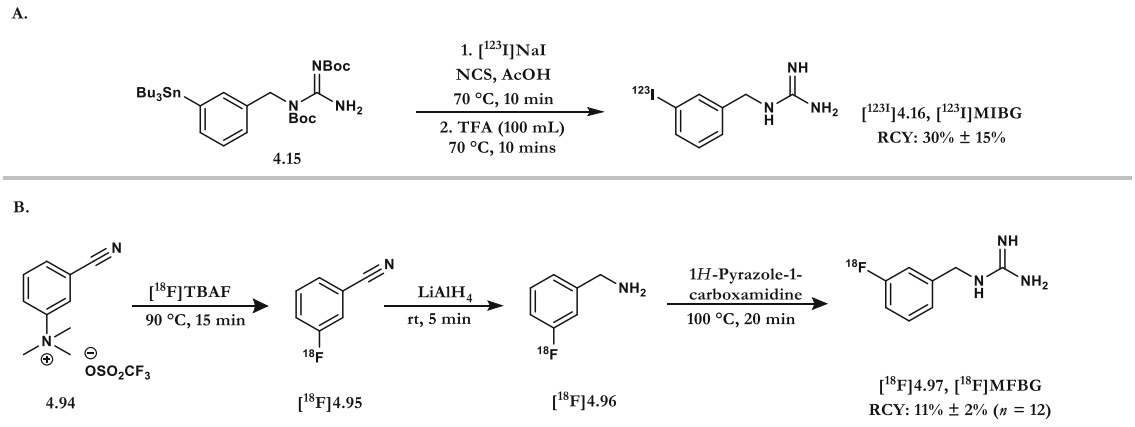

Scheme 4.16. Previous syntheses of [^{123}I]MIBG **[^{123}I]4.16** and [^{18}F]MFBG **[^{18}F]4.97**

We selected the protected aryl boronic ester **4.100** as a common precursor for both copper mediated ^{18}F-fluorination and ^{123}I-iodination.[14] Boronic ester **4.100** was prepared in three steps (Scheme 4.17A). Using analogous strategies

of radiohalogenation followed by deprotection, both [^{18}F]MFBG **[^{18}F]4.97** and [^{123}I]MIBG **[^{123}I]4.16** could be isolated in 25% ± 2% and in 37% RCY, respectively (Scheme 4.17). The molar activity of **[^{123}I]4.16** was calculated to be 19.8 GBq μmol^{-1} from a starting activity of 41.9 MBq (Graph 4.1). The molar activity of **[^{18}F]4.97** was calculated to be 15 – 23 GBq μmol^{-1} from starting activities of up to 6.3 GBq (Graph 4.2). These experiments validate the potential for aryl boronic pinacol esters to be used as common precursors for radiofluorination and radioiodination.

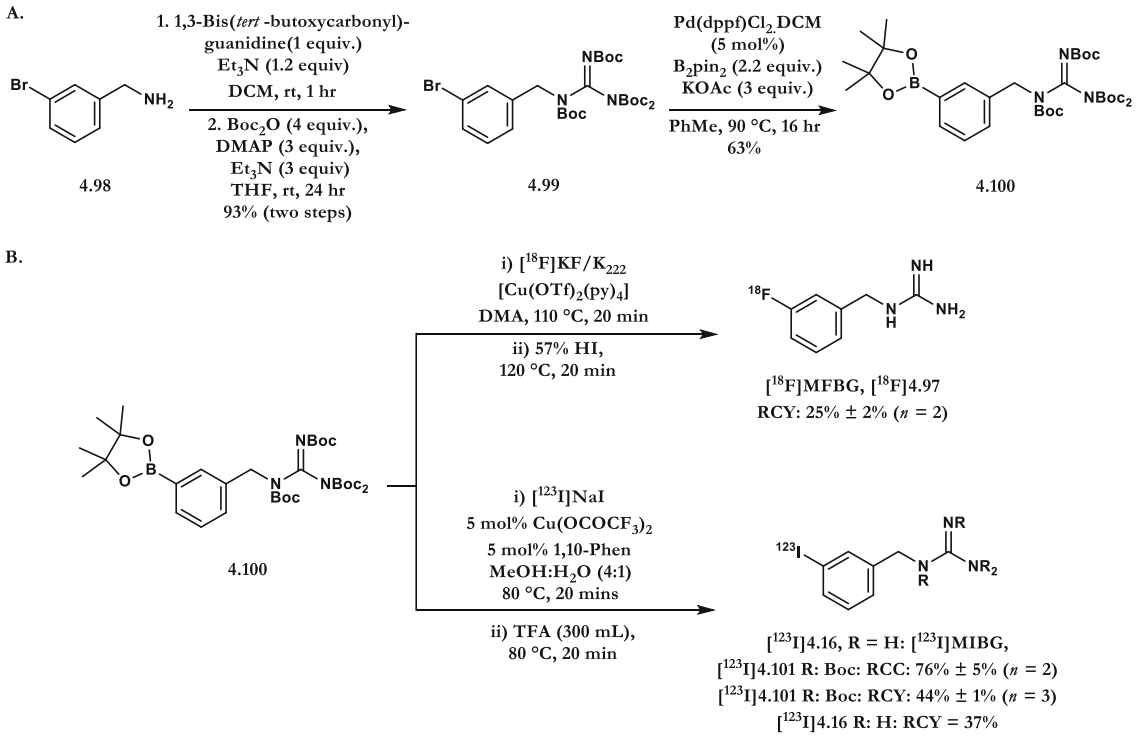

Scheme 4.17. A) Synthesis of aryl boronic ester precursor **4.100** B) Divergent synthesis from a common precursor for both [Cu] mediated ^{123}I-Iodination and ^{18}F-Fluorination of aryl boronic ester **4.100**[e]

[e] The ^{18}F-Fluorodeboronation of **4.100** was carried out in collaboration with Dr. S. Preshlock

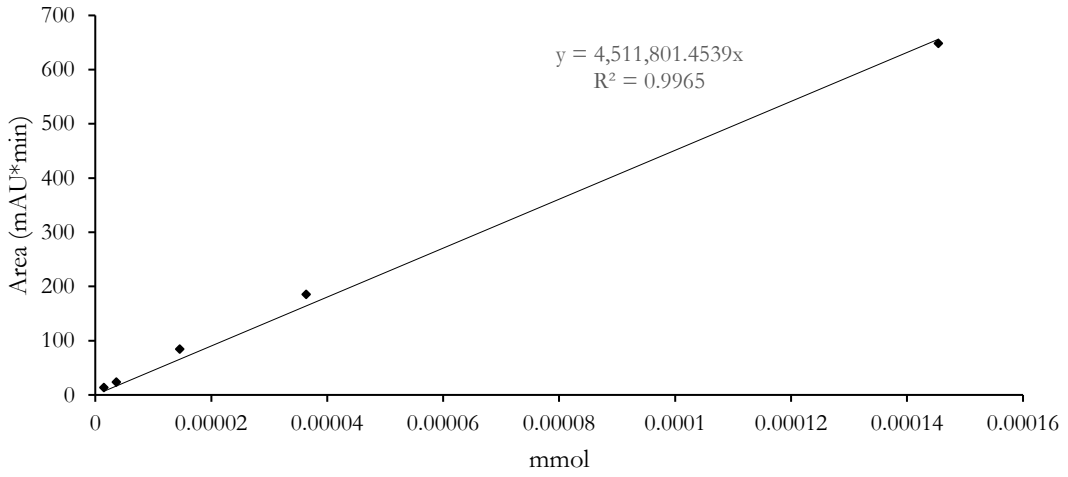

Injection Number	Activity (MBq)	Area (mAu*min)	Mmol injected	Specific Activity (GBq μmol^{-1})
1	0.6	0.1368	3.03205E-08	19.8

Graph 4.1 Calibration curve and molar activity calculation for [^{123}I]MIBG **[^{123}I]4.16**

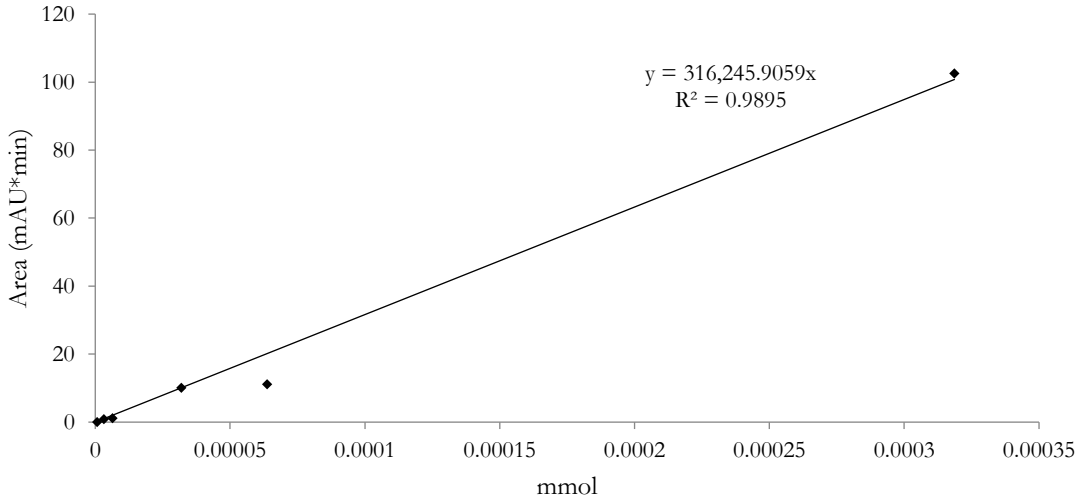

Injection Number	Activity (MBq)	Area (mAu*min)	Mmol injected	Specific Activity (GBq μmol^{-1})
1	4.8	0.0656	2.07434E-07	23.1
2	5.4	0.1148	3.63622E-07	14.9
3	3.0	0.0458	1.45069E-07	20.7
4	1.9	0.0262	8.29869E-08	22.9
5	3.2	0.0486	1.53938E-07	20.8

Graph 4.2 Calibration curve and molar activity calculation for [^{18}F]MFBG **[^{18}F]4.97**

4.8 Subsequent Development by Other Groups

An overview of the literature prior to the start of this project was given in the introduction to this chapter. However, during submission of this work and subsequently to this, several groups have reported innovative methodologies for radioiodination.

Most closely aligned to the work undertaken in this chapter was the copper mediated ^{131}I-iodination of aryl boronic acids reported by Zhang. In addition to demonstrating exceptionally high radiochemical yields, Zhang also, validated this transformation for translation *in vivo* with the imaging of c(RGDyk) peptide [^{125}I]4.106 labelled with [^{125}I]SIB (Scheme 4.18).[28]

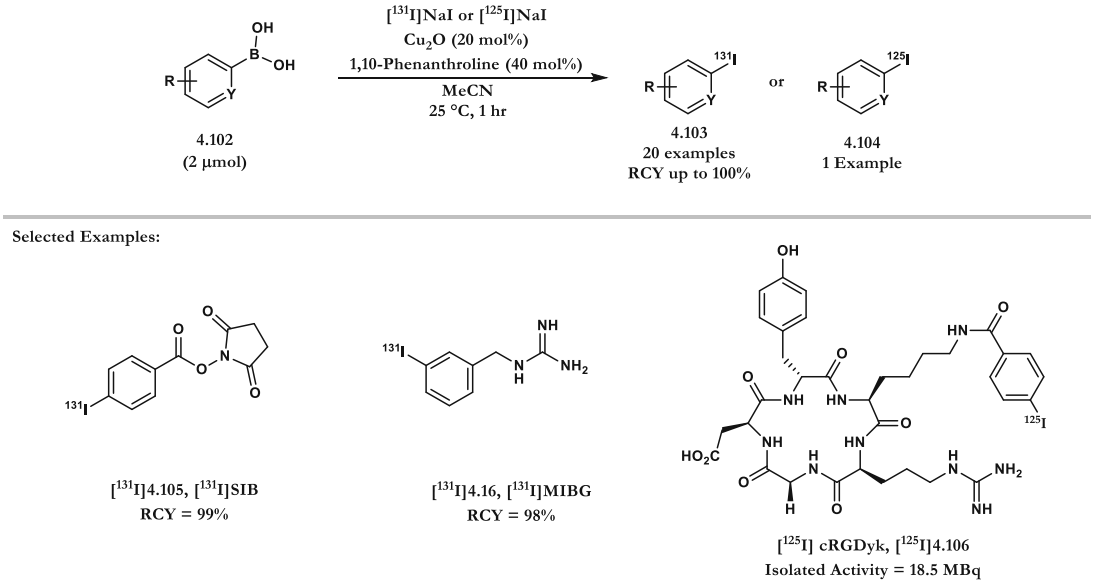

Scheme 4.18 Copper mediated radioiodination approach using aryl boronic acids

Following this work, in 2018, Mach and co-workers reported both ^{123}I-iodination and ^{211}As-astatination of aryl boronic esters and acids.[29] Under very mild conditions and fast reaction times, Mach and co-workers demonstrated the

versatility of this reaction with the labelling of two PARP inhibitors (Scheme 4.19). One highlight of this work was the use of $Cu(OTf)_2(py)_4$. This not only demonstrates the utility of boron precursors for divergent radiolabelling, but also the versatility of the catalyst which had been described by Gouverneur and co-workers for the nucleophilic ^{18}F-fluorination of aryl pinacol boronic esters.

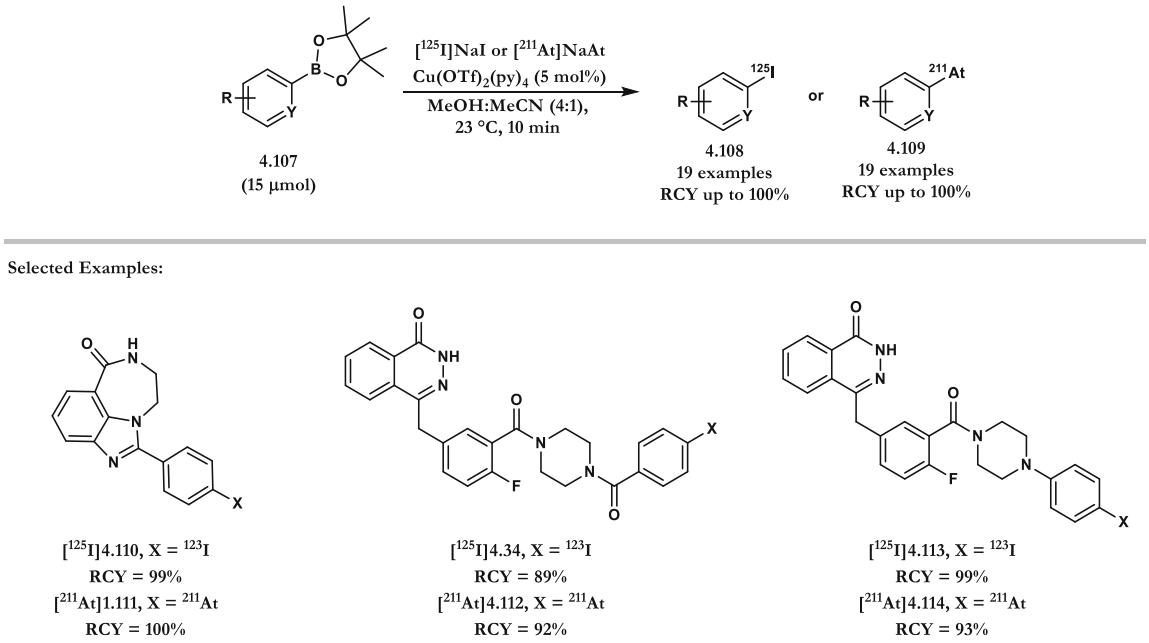

Scheme 4.19. Rapid Cu-catalyzed [^{211}At]astatination and [^{125}I]iodination of boronic esters at room temperature

Finally, in 2018, Sutherland and co-workers reported the gold(I) mediated *ipso*-iododeboronation of aryl boronic acids.[30] Using analogous conditions to the electrophilic C-H iodination described earlier (Scheme 4.3), an efficient and regioselective ^{125}I-iodination using PPh_3AuNTf_2 and *in situ* generated [^{125}I]NIS was described (Scheme 4.20). Sutherland and co-workers validated this method with the synthesis and purification of [^{125}I]MIBG **[^{125}I]4.16** in an isolated radiochemical yield of 28% and molar activity of > 2.73 GBq μmol^{-1} starting from 10.16 MBq [^{125}I]NaI.

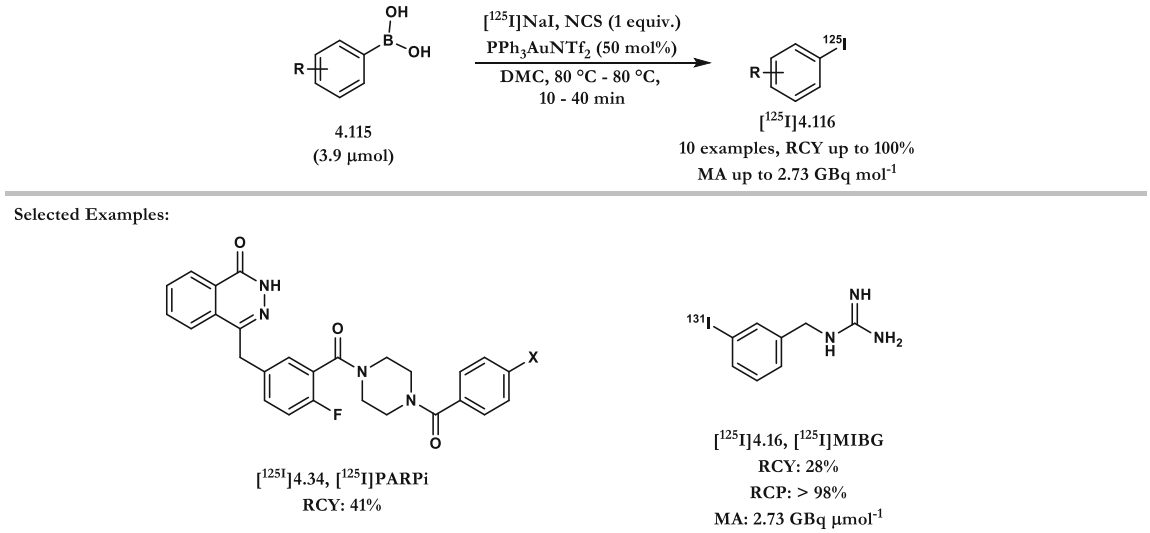

Scheme 4.20. Rapid ^{125}I-iodination under Gold(I) Catalysis

4.9 Conclusion

To conclude, this chapter reports the first copper mediated nucleophilic ^{123}I-radioiodination of aryl pinacol boronic esters and boronic acids. The reaction shows a high tolerance towards both electron-rich and electron-poor (hetero)aromatics. Following this, four clinically-relevant SPECT tracers [^{123}I]IMPY **[^{123}I]4.81**, [^{123}I]DPA-713 **[^{123}I]4.12**, [^{123}I]IPEB **[^{123}I]4.12** and [^{123}I]MIBG **[^{123}I]4.16** were synthesised, all in good RCC/RCYs. In addition, the concept of divergent radiohalogenation by reacting a common aryl boron reagent with either [^{18}F]fluoride or [^{123}I]iodide in the presence of a copper complex was validated. This was exemplified with the successful labelling of [^{18}F]FPEB /[^{123}I]IPEB and [^{18}F]MFBG/[^{123}I]MIBG.

4.10 References

1 P. M. Matthews, E. A. Rabiner, J. Passchier, R. N. Gunn, *Br. J. Clin. Pharmacol.,* 2012, **73***,* 175.

2 P. W. Miller, N. J. Long, R. Vilar and A. D. Gee, *Angew. Chem. Int. Ed.,* 2008, **47**, 8998.

3 S. Preshlock, M. Tredwell, V. Gouverneur, *Chem. Rev.,* 2016, **116**, 719.

4 R. H. Seevers, R. E. Counsell, *Chem. Rev.,* 1982, **82**, 575.

5 K.-E. Kil, A. Zhu, Z. Zhang, J.-K. Choi, S. Kura, C. Gong, A.-L. Brownell, *ACS. Med. Chem. Lett.,* **2014**, **5**, 652.

6 E. R. O'Brien, V. Kersemans, M. Tredwell, B. Checa, S. Serres, M. S. Soto, V. Gouverneur, D. Leppert, D. C. Anthony, N. R. Sibson, *J. Nucl. Med.*, 2014, **55**, 275.

7 D. M. Wieland, J. Wu, L. E. Brown, T. J. Mangner, D. P. Swanson, W. H. Beierwaltes., *J. Nucl. Med.,* 1980, **21**, 349.

8 S. Mushtaq, J. Jeon, A. Shaheen, B. S. Jang, S. H. Park, *J. Radioanal. Nucl. Chem.,* 2016, **309**, 859.

9 A. A. Cant, S. Champion, R. Bhalla, S. L. Pimlott, A. Sutherland, *Angew. Chem. Int. Ed.,* 2013, **52**, 7829.

10 D. T. Racys, S. A. I. Sharif, S. L. Pimlott, A. Sutherland*, J. Org. Chem*., 2016, **81**, 772.

11 N. L. Sloan, S. K. Luthra, G. McRobbie, S. L. Pimlott, A. Sutherland, *Chem. Commun.,* 2017, **53**, 11008.

12 P. C. Srivastava, a P. Callahan, E. B. Cunningham, and F. F. Knapp, *J. Med. Chem.,* 1983, **26**, 742.

13 G. W. Kabalka, M. R. Akula, and J. Zhang, *Nucl. Med. Biol.,* 2002, **29**, 841.

14 M. R. Akula, M.-L. Yao, and G. W. Kabalka, *J. Label. Compd. Radiopharm.,* 2011, **54**, 132.

15 G. W. Kabalka and A. R. Mereddy, *J. Label. Compd. Radiopharm.,* 2005, **48**, 359.

16 M. M. Goodman, G. W. Kabalka, R. C. Marks, F. F. Knapp, J. Lee, and Y. Liang, *J. Med. Chem.,* 1992, **35**, 280.

17 M. R. Akula, J. H. Zhang, and G. W. Kabalka, *J. Label. Compd. Radiopharm.,* 2001, **5**, 260.

18 S. Yamamoto, M. Abe, S. Nakanishi, M. Murai, and H. Miyoshi, *Tetrahedron Lett.,* 2011, **52**, 3090.

19 M. Tredwell, S. M. Preshlock, N. J. Taylor, S. Gruber, M. Huiban, J. Passchier, J. Mercier, C. Génicot, V. Gouverneur *Angew. Chem. Int. Ed.,* 2014, **53**, 7751.

20 B. M. Partridge, J. F. Hartwig, *Org. Lett.,* 2013, **15**, 140.

21 N. Ichiishi, A. F. Brooks, J. J. Topczewski, M. E. Rodnick, M. S. Sanford, *Org. Lett.,* 2014, **16**, 3224

22 A. B. Newberg, N. A. Wintering, K. Plössl, J. Hochold, M. G. Stabin, M. Watson, D. Skovronsky, C. M Clark, M. P. Kung, H. F. Kung, *J. Nucl. Med.,* 2006, **47**, 748.
23 Z. P. Zhuang, M. P. Kung, A. Wilson, C. W. Lee, K. Plössl, C. Hou, D. M. Holtzman, H. F. Kung*, J. Med. Chem*., 2003, **46**, 237.
24 H. Wang, M. Pullambhatia, T. R. Guilarte, R. C. Mease, M. G. Pomper, *Biochem. Biophys. Res. Commun.,* 2009, **389**, 80.
25 H. Zhang, R. Huang, N. V. K. Pillarsetty, D. L. J. Thorek, G. Vaidyanathan, I. Serganova, R. G. Blasberg, J. S. Lewis, *Eur. J. Nucl. Med. Mol. Imaging* 2014, **41***,* 322.
26 S. Preshlock, S. Calderwood, S. Verhoog, M. Tredwell, M. Huiban, A. Hienzsch, S. Gruber, T. C. Wilson, N. J. Taylor, T Cailly, M. Schedler, T. L. Collier, J. Passchier, R. Smits, J. Mollitor, A. Hoepping, M. Mueller, C. Génicot, J. Mercier, V. Gouverneur, *Chem. Commun.,* 2016, **52**, 8361.
27 T. G. Hamill, S. Krause, C. Ryan, C. Bonnefous, S. Govek, T J. Seiders, N. D. P. Cosford, J. Roppe, T. Kamenecka, S. Patel, R. E. Gibson, S. Sanabria, K. Riffel, W Eng, C. King, X. Yang, M. D. Green, S. S. O'Malley, R. Hargreaves, H. D. Burns, *Synapse* 2005, **56**, 205.
28 P. Zhang, R. Zhuang, Z. Guo, X. Su, X. Chen, X. Zhang, *Chem. Eur. J.* 2016, **47**, 16783.
29 S. W. Reilly, M. Makvandi, K. Xu, R. H. Mach, *Org. Lett.,* 2018, **20**, 1752.
30 S. Webster, K. M. O'Rourke, C. Fletcher, S. L. Pimlott, A. Sutherland, A.-L. Lee, *Chem. Eur. J.,* 2018, **24**, 937.

Thesis Summary

This thesis describes three different approaches for either the development of application of novel methodology for PET and SPECT imaging, all of which were carried out at the Siemens Organic Molecular Imaging Laboratory, University of Oxford.

The need for novel radiotracers for the imaging of cancer is one of great need within the community. Chapter II describes the application of the copper mediated ^{18}F-fluorodeboronation of aryl pinacol boronic esters for the radiosynthesis of [^{18}F]olaparib. [^{18}F]Olaparib could be accessed in good activity yields and molar activities. Following this, the successful imaging and quantification of PARP expression *in vivo* is carried out.

Chapter III discusses the radiosynthesis and application of the novel ^{18}F-trifluoromethylation reagent known as [^{18}F]Umemoto. Subsequently, the ^{18}F-trifluoromehtylation of unmodified peptides is reported. For the radiosynthesis of the reagent, the silver mediated nucleophilic ^{18}F-fluorination is employed. Although a modest activity yield is reported, this novel reagent has huge potential. Not only for the radiolabelling of biomolecules, but also the ^{18}F-trifluoromethylation of other motifs previously inaccessible.

Chapter IV describes a conventional research and development project for the copper mediated ^{123}I-iodination of aryl boronic esters and acids. Using $Cu(OCOCF_3)_2$ in combination with 1,10-phenanthroline, the ^{123}I-iodination of functionalised aromatics is reported. Subsequently, four radiotracers are successfully radiolabelled. This methodology provides a complementary approach to that of the copper mediated ^{18}F-fluorination of aryl pinacol boronic ester. This is exemplified with the

divergent labelling of common precursors for [^{123}I]MIBG and [^{18}F]MFBG as well as [^{123}I]IPEB and [^{18}F]FPEB.

The work described within this thesis has been published in the following peer reviewed articles:

Chapter II: ***T. C. Wilson***, M.-A. Xavier, J. Knight, S. Verhoog, J. Baguña Torres, M. Mosley, S. L. Hopkins, S. Wallington, D. Allen, V. Kersemans, R. Hueting, S. Smart, V. Gouverneur, B. Cornelissen., *J. Nuc. Med.,* **2018**, *Just Accepted*

Chapter III: S. Verhoog, C. W. Kee, Y. Wang, T. Khotavivattana, ***T. C. Wilson***, V. Kersemans, S. Smart, M. Tredwell, B. G. Davis, V. Gouverneur., *J. Am. Chem. Soc.* **2018**, *140*, 1572.

Chapter IV: ***T. C. Wilson***, G. McSweeney, S. Preshlock, S. Verhoog, M. Tredwell, T. Cailly, V. Gouverneur., *Chem. Commun*. **2016**, *52*, 13277.

Other works highlighted and discussed include:

1. S. Preshlock, S. Calderwood, S. Verhoog, M. Tredwell, M. Huiban, A. Hienzsch, S. Gruber, ***T. C. Wilson***, N. J. Taylor, T. Cailly, M. Schedler, T. L. Collier, J. Passchier, R. Smits, J. Mollitor, A. Hoepping, M. Mueller, C. Genicot, J. Mercier, V. Gouverneur, *Chemical Communications*, **2016**, *52*, 8361.
2. ***T. C. Wilson***, T. Cailly, V. Gouverneur. *Chem. Soc. Rev.,* **2018**, *47*, 6990.

Chapter V:

Experimental Data

5.1 General Experimental Information

All NMR spectra were recorded on Bruker DPX200, AV400 and AV500 spectrometers. Proton and carbon-13 NMR spectra are reported as chemical shifts (δ) in parts per million (ppm) relative to the solvent peak using the Bruker internal referencing procedure (edlock). Fluorine-19 NMR spectra are referenced relative to $CFCl_3$ in $CDCl_3$. Coupling constants (*J*) are reported in units of hertz (Hz). The following abbreviations are used to describe multiplicities - s (singlet), d (doublet), t (triplet), q (quartet), m (multiplet), br. (broad). High resolution mass spectra (HRMS, *m/z*) were recorded on a Bruker MicroTOF spectrometer using positiveelectrospray ionization (ESI^+), on a Micromass GCT spectrometer using filed ionization (FI^+) or chemical ionization (CI^+), or on a Waters GCT Classic GCMS using electron impact ionisation (EI). Infrared spectra were recorded either as the neat compound or in a solution using a Bruker Tensor 27 FT-IR spectrometer. Absorptions are reported in wavenumbers (cm^{-1}). Melting points of solids were measured on a Griffin apparatus and are uncorrected. Solvents were purchased from Sigma-Aldrich, Honeywell or Fisher. When dry solvents were required they were purified by expression through an activated alumina column built according to the procedures described by Pangborn and Grubbs. Chemicals were purchased from Acros, Alfa Aesar, Bachem, Fisher, Fluorochem, Sigma-Aldrich and used as received. Reactions were monitored by thin-layer chromatography (TLC) carried out on

Merck Kiesegel 60 F254 plates, silica gel column chromatography was performed over Merck silica gel C60 (40-60 μm). Unless stated otherwise, all experimental procedures and characterisation provided in this chapter are for compounds which I made.

5.2 General Radiochemical Information:

Working Procedures in SOMIL Whilst working in SOMIL, a minimum of two trained researchers were present to ensure that work was carried out in a safe manner. When carrying out small-scale aliquot reactions, two or three researchers worked together in order to make efficient use of the [^{18}F]fluoride. Reactions were carried out in duplicate (n = 2), from which a mean RCC was determined. For many reactions, two pairs were carried out, where possible on separate days, giving rise to n = 4 for these reactions.

Each reaction underwent several steps:

1. Weighing of solid reagents into vial.

2. Dispensing aliquot of [^{18}F]fluoride into vial.

3. Adding solvent (or solution of reagent in solvent) and putting reaction into heating block.

4. Removing reaction from heating block and quenching.

5. Preparing samples for radio-TLC and radio-HPLC analysis.

6. Injecting radio-HPLC sample.

7. Running radio-TLC plate and analysing using moving bed detector.

5.2.1 General information for radiofluorination procedures at the Chemistry Research Laboratory, University of Oxford

[^{18}F]Fluoride was produced by Alliance Medical (UK) via the ^{18}O(p,n)^{18}F reaction and delivered as [^{18}F]fluoride in ^{18}O-enriched-water. Radiosynthesis and azeotropic drying was performed on a NanoTek microfluidic device (Advion).

5.2.2 General information for radioiodination procedures at the Chemistry Research Laboratory, University of Oxford

General information for radiochemical procedures at the Chemistry Research Laboratory, University of Oxford. Sodium [^{123}I]Iodide was produced by GE Healthcare as none carrier added [^{123}I]Sodium Iodide in 0.05 M NaOH.

5.2.3 General information for the analysis of radioiodination and radiofluorination procedures at the Chemistry Research Laboratory, University of Oxford

HPLC analysis was performed with a Dionex Ultimate 3000 dual channel HPLC system equipped with shared autosampler, parallel UV-detectors and with Flowram analog output. Radio-TLC was performed on Merck Kiesegel 60 F254 plates. Analysis was performed using a LabLogic NaI/PMT-radiodetectors. All radiochemical conversions quoted are decay corrected and are calculated by radioTLC, taking into account the radiochemical purity observed by radio-HPLC.

5.3 Experimental Procedures and Characterisation for Compounds in Chapter II

4-(3-(4-(Cyclopropanecabonyl)piperazine-1-carbnonyl)-4-fluorobenzyl) phthalazin-1(*2H*)-one (Olaparib) (2.1)

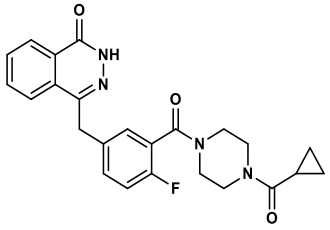

To a solution of 2-fluoro-5-((4-oxo3,4-dihydrophthalazin-1-yl)methyl)benzoic acid (500 mg, 1.68 mmol) in DMA (10 mL) was added DIPEA (560 μL, 3.36 mmol) and HBTU (640 mg, 1.70 mmol). The reaction mixture was stirred for 1 hour before addition of cyclopropylpiperazine-1-ylmethanone (241 μL, 1.70 mmol) was carried out. The reaction mixture was stirred at room temperature for 48 hours. The reaction mixture was then extracted with DCM (3 × 50 mL) and washed with water (3 × 200 mL). The organic layers were collected, dried with $MgSO_4$ and the excess solvent removed *in vacuo*. Purification *via* reverse phase HLPC was carried out affording 4-(3-(4-(cyclopropanecarbonyl)piperazine-1-carbonyl)-4-fluorobenzyl)phthalazin-1(*2H*)-one (olaparib) (465 mg, 1.07 mmol, 64**%**) as a white solid.

^{1}H NMR (400 MHz, $CDCl_3$) δ = 10.65 (s, 1H), 8.44 – 8.37 (m, 1H), 7.75 – 7.61 (m, 3H), 7.34 – 7.22 (m, 2H), 6.97 (t, *J* = 8.9 Hz, 1H), 4.22 (s, 2H), 3.90 – 3.09 (m, 8H), 1.79 – 1.52 (s, 1H), 0.99 – 0.88 (m, 2H), 0.81 – 0.63 (s, 2H); **{^{1}H}^{19}F NMR** (376 MHz, $CDCl_3$) δ = - 117.6; **M.P.** 69 - 71°C. Data is in accordance with known literature.[1]

2-Methylphthalazin-1(*2H*)-one (2.28)

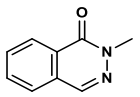

To a round bottom flask containing DMF (10 mL) under an atmosphere of argon was added, phthalazone (300 mg, 2.05 mmol). To solution was then cooled to 0 °C before sodium hydride (60% in dispersion oil, 61 mg, 2.53 mmol) was added portion wise before addition of iodomethane (119 μL, 1.92 mmol). The reaction was stirred overnight before the solvent was removed *in vacuo* and the crude material purified directly *via* flash column chromatography using *n*-pentane: EtOAc (10:1) affording 2-Methylphthalazin-1(*2H*)-one as a white solid (210 mg, 1.31 mmol, 64%).

^{1}H NMR (400 MHz, $CDCl_3$) δ = 8.42 – 8.38 (m, 1H), 8.12 (s, 1H), 7.81 – 7.70 (m, 2H), 7.69 – 7.65 (m, 1H), 3.83 (s, 3H); **^{13}C NMR** (100 MHz, $CDCl_3$) δ = 159.7, 137.6, 133.0, 131.6, 129.8, 127.8, 126.5, 126.0, 39.5. The data is in accordance with known literature.[2]

***tert*-Butyl 1-oxophthalazine-2(*1H*)-carboxylate (2.29)**

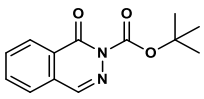

To a round bottom flask containing THF (10 mL) under an atmosphere of nitrogen was added, phthalazone (500 mg, 3.41 mmol), di-*tert*-butyl dicarbonate (1.11 g, 5.12 mmol) and DMAP (620 mg, 5.12 mmol). The reaction was stirred overnight at room temperature before the solvent was removed *in vacuo* and the crude material purified

directly *via* flash column chromatography using *n*-pentane: EtOAc (5:1) *tert*-Butyl 1-oxophthalazine-2(*1H*)-carboxylate as a white solid (765 mg, 3.11 mmol, 91%).

^{1}H NMR (400 MHz, $CDCl_3$) δ = 8.43 (dd, *J* = 7.9, 1.3 Hz, 1H), 7.83 (td, *J* = 7.5, 1.4 Hz, 1H), 7.77 (td, *J* = 7.6, 1.3 Hz, 1H), 7.68 (dd, *J* = 7.5, 1.3 Hz, 1H), 1.66 (s, 9H); **^{13}C NMR** (100 MHz, $CDCl_3$) δ = 158.3, 150.9, 138.9, 134.2, 132.3, 129.2, 128.7, 127.5, 126.4, 85.9, 27.8 (3C); **IR** (*ν,* cm^{-1}): 2980, 1720, 1641, 1470, 1325, 1130; **HRMS** (ESI) for $C_{13}H_{14}N_2O_3$ $[M+H]^+$ requires 247.1012 found 247.1015; **M.P.** 81 – 83 °C.

2-Allylphthalazin-1(*2H*)-one (2.30)

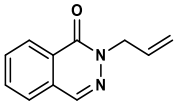

To a round bottom flask containing DMF (30 mL) under an atmosphere of nitrogen was added, phthalazone (500 mg, 3.42 mmol), anhydrous potassium carbonate (708 mg, 5.12 mmol) and allyl bromide (442 μL, 5.12 mmol). The reaction was stirred overnight at room temperature before the solvent was removed *in vacuo* and the crude material purified directly *via* flash column chromatography using *n*-pentane: EtOAc (3:1) affording 2-allylphthalazin-1(*2H*)-one as a brown oil (222 mg, 1.20 mmol, 35%)

^{1}H NMR (400 MHz, $CDCl_3$) δ = 8.42 (ddd, *J* = 7.5, 1.7, 0.7 Hz, 1H), 8.17 (d, *J* = 0.8 Hz, 1H), 7.83 – 7.72 (m, 2H), 7.71 – 7.67 (m, 1H), 6.04 (ddt, *J* = 17.2, 10.3, 5.9 Hz, 1H), 5.30 – 5.22 (m, 2H), 4.85 (dt, *J* = 5.9, 1.5 Hz, 2H); **^{13}C NMR** (100 MHz, $CDCl_3$) δ = 159.2, 138.1, 133.1, 132.5, 131.7, 129.7, 128.0, 126.8, 126.0, 118.0, 53.5. Data is in accordance with literature values.[3]

2-((2-Triethylsilyl)ethoxyl)methyl)phthalazin-1(*2H*)-one (2.31)

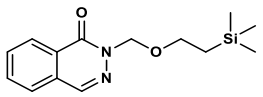

To a round bottom flask containing THF (10 mL) under an atmosphere of argon was added, phthalazone (480 mg, 3.28 mmol). To solution was then cooled to 0 °C before sodium hydride (60% in dispersion oil, 97 mg, 4.04 mmol) was added portion wise. The reaction was then stirred for 30 min at 0 °C before warming to room temperature after which 2-(trimethylsilyl)ethoxymethyl chloride (0.70 mL, 3.97 mmol) was added dropwise. The reaction mixture was left to stir overnight after which the solvent was removed *in vacuo*. The crude mixture was then extracted with DCM (3 x 10 mL) and washed with brine (3 x 10 mL). The organic layer was collected, dried with magnesium sulfate and the excess solvent removed *in vacuo*. The crude material was then purified by flash column chromatography (2:3 *n*-Pent:EtOAc) to afford 2-((2-triethylsilyl)ethoxyl)methyl) phthalazin-1(*2H*)-one as a colourless oil (435 mg, 1.57 mmol, 46%).

^{1}H NMR (400 MHz, $CDCl_3$) δ = 8.41 (d, *J* = 7.8 Hz, 1H), 8.15 (s, 1H), 7.76 (dt, *J* = 21.7, 7.6 Hz, 2H), 7.67 (d, *J* = 7.7 Hz, 1H), 5.55 (s, 2H), 3.74 – 3.68 (m, 2H), 0.99 – 0.92 (m, 2H), - 0.05 (s, 9H); **^{13}C NMR** (100 MHz, $CDCl_3$) δ = 161.4, 139.6, 134.9, 133.2, 131.2, 129.4, 128.4, 127.6, 80.4, 68.5, 19.5, 0.00 (3C); **IR** (*ν,* cm^{-1}): 1661, 1081, 833, 758; **HRMS** (ESI) for $C_{14}H_{20}N_2{}^{23}NaO_2{}^{28}Si$ $[M+Na]^+$ requires 299.1186 found 299.1185.

4-(3-(4-(Cyclopropanecarbonyl)piperazine-1-carbonyl)-4-(4,4,5,5-tetramethyl-1,3,2-dioxaborolan-2-yl)benzyl)-2-((2-trimethlsilyl)ethoxy)methyl)phthalazin-1(*2H*)-one (2.32)

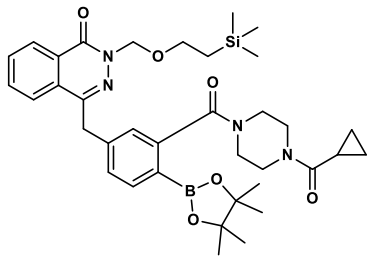

To a Schlenk tube under an atmosphere of argon was added, methyl-2-bromo-5-((4-oxo-((2-(trimethylsilyl)ethoxy)methyl)-3,4-dihydrophthalazin-1-yl)methyl)benzoate (1.48 g, 2.94 mmol), bis(pinacolato)diboron (1.49 g, 5.89 mmol), $Pd(dppf)Cl_2$ (72 mg, 0.09 mmol) and potassium acetate (0.87 g, 8.88 mmol). The reaction flask was then backfilled with argon and placed in an oil bath at 90 °C upon which degassed DMF (13 mL) was added and the reaction left to stir overnight. Upon completion, the reaction was cooled and passed through a plug of Celite before extracting with EtOAc (100 mL) and washing with lithium chloride solution (3 x 50 mL). The organic phases were collected, and the excess solvent was removed *in vacuo*. The crude material was then purified by flash column chromatography (10:3 *n*-Pent: EtOAc) to afford a mixture of methyl-5-((4-oxo-3-((2-(trimethylsilyl)ethoxy)methyl)-3,4-dihydro phthalazin-1-yl)methyl)-2-(4,4,5,5-tetramethyl-1,3,2-dioxaborolan-2-yl)benzoate and bis(pinacolato)diboron (2.00 g) with the following ^{1}H NMR spectra being observed. **^{1}H NMR** (400 MHz, $CDCl_3$) δ = 8.43 (d, *J* = 7.8 Hz, 1H), 7.85 (s, 1H), 7.76 – 7.57 (m, 2H), 7.53 (d, *J* = 8.0 Hz, 1H), 7.38 (s, 2H), 5.58 (s, 2H), 4.32 (s, 2H), 3.86 (s, 3H), 3.76 (t, *J* = 7.3 Hz, 1H), 1.37 (s, 12H), 0.99 (t, *J* = 7.6 Hz, 2H), - 0.03 (s, 9H). Peaks

reported only correspond to the product. The crude material was taken forward without further purification.

To a round bottom flask containing methyl-5-((4-oxo-3-((2-(trimethylsilyl)ethoxy) methyl)-3,4-dihydrophthalazin-1-yl)methyl)-2-(4,4,5,5-tetramethyl-1,3,2-dioxa borolan-2-yl)benzoate and bis(pinacolato) diboron (2.00 g) was added THF (100 mL) before cooling to 0 °C. Upon cooling, 2M lithium hydroxide (7 mL, 14 mmol) was added dropwise before allowing to reaction to stir for 30 min at 0 °C. 1M HCl was then added dropwise to the reaction mixture at 0 °C until reaching pH 4. The mixture was then extracted with EtOAc (3 x 80 mL) and washed with Brine (3 x 50 mL). The organic phases were combined and the excess solvent removed *in vacuo*. The crude material (1.4 g) was transferred to a round bottom flask upon which DCM (100 mL), HBTU (2.97 g, 7.84 mmol) and DIPEA (1.36 mL, 7.84 mmol) was added. After stirring at room temperature for 30 minutes, *N*-cyclopropylcarbonylpiperazine (1.11 mL, 7.85 mmol) was added and the reaction stirred overnight. After stirring for 16 hours, the excess solvent was removed *in vacuo* and the crude material isolated by flash column chromatography (Pure EtOAc) before purification by reverse phase HPLC was carried out to afford 4-(3-(4-(cyclopropanecarbonyl)piperazine-1-carbonyl)-4-(4,4,5,5-tetramethyl-1,3,2-dioxaborolan-2-yl)benzyl)-2-((2-trimethlsilyl)ethoxy) methyl)phthalazin-1(*2H*)-one (419 mg, 0.62 mmol, 22% - three steps) as a white solid in a mixture of rotamers. In each case the shift relating to the minor rotamer has been donated with an asterisk.*

^{1}H NMR (400 MHz, $CDCl_3$) δ = 8.46 (dd, *J* = 7.8, 1.6 Hz, 1H + 1H*), 7.79 – 7.55 (m, 4H + 4H*), 7.32 – 7.28 (m, 1H + 1H*), 7.14 (bs, 1H + 1H*), 5.59 (s, 2H + 2H*),

4.33 (s, 2H + 2H*), 3.87 – 3.04 (m, 10H + 10H*), 1.28 (s, 12H + 12H*), 1.04 – 0.97 (m, 4H + 4H*), 0.90 – 0.85 (m, 1H + 1H*), 0.83 – 0.71 (m, 2H + 2H*), 0.00 (s, 9H + 9H*); **^{13}C NMR** (100 MHz, $CDCl_3$) δ = 172.3 (1C + 1C*), 171.0 (1C + 1C*), 160.0 (1C + 1C*), 144.7 (1C + 1C*), 142.9 (1C + 1C*), 141.3 (1C + 1C*), 136.3 (1C + 1C*), 133.3 (1C + 1C*), 131.5 (1C + 1C*), 129.2 (1C + 1C*), 128.4 (1C + 1C*), 128.2 (1C + 1C*), 127.7 (1C + 1C*), 125.4 (1C + 1C*), 125.2 (1C + 1C*), 84.1 (2C + 2C*), 79.0 (1C + 1C*), 67.3 (1C + 1C*), 47.3 (1C*), 46.9 (1C), 45.2 (1C*), 44.8 (1C), 41.9 (1C*), 41.7 (2C), 41.4 (1C*), 39.1 (1C + 1C*), 24.9 (4C + 4C*), 18.1 (1C + 1C*), 11.1 (1C + 1C*), 7.66 (2C + 2C*), -1.36 (3C + 3C*) (the carbon bearing the boron substituent is not observed); **IR** (*ν,* cm^{-1}): 2981, 2889, 2360, 2341, 1641, 1382, 1354, 1146, 1087, 956; **HRMS** (ESI) for $C_{36}H_{49}N_4O_6{}^{10}B^{23}Na^{28}Si$ $[M+Na]^+$ requires 694.34429 found 694.34418; **M.P.** 78 – 80 °C.

4-(3-(4-(Cyclopropanecarbonyl)piperazine-1-carbonyl)-4-fluorobenzyl)-2-((2-trimethylsilyl) ethoxy)methyl)phthalazin-1(*2H*)-one (2.33) and (4-(cyclopropanecarbonyl)pipeazin-1-yl)(2-fluoro-5-((4-((2-(trimethylsilyl) ethoxy)methoxyl) phthalazine-1-yl)methyl)phenyl)methanone (2.38)

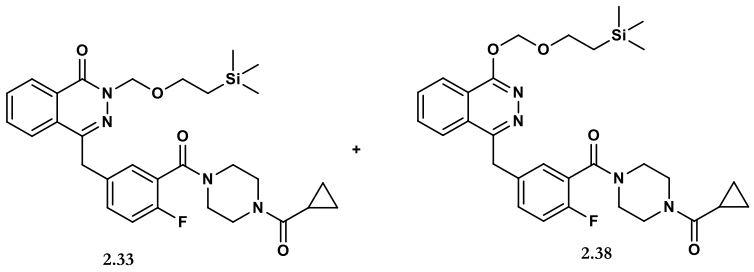

2.33 2.38

To a round bottom flask under an atmosphere of argon was added, 4-(3-(4-(cyclopropanecabonyl)piperazine-1-carbnonyl)-4-fluorobenzyl)phthalazin-1(*2H*)-one (olaparib) (500 mgs, 1.15 mmol), dry THF (30 mL). The mixture was cooled to 0 °C

and sodium hydride (60% in dispersion oil, 41 mg, 1.72 mmol) was added portion wise. The reaction was stirred at 0 °C for 30 minutes after which 2-(trimethylsilyl)ethoxymethyl chloride (0.24 mL, 1.37 mmol)was added dropwise. The reaction was warmed to room temperature and stirred overnight. After 16 hours the excess solvent was removed *in vacuo* and the crude material was purified directly *via* flash column chromatography (*n*-Pent: EtOAc 10:3 – Pure EtOAc) affording 4-(3-(4-(Cyclopropanecarbonyl)piperazine-1-carbonyl)-4-fluorobenzyl)-2-((2-trimethyl silyl)ethoxy)methyl)phthalazin-1(*2H*)-one and (4-(cyclopropanecarbonyl)pipeazin-1-yl)(2-fluoro-5-((4-((2-(trimethylsilyl)ethoxy)methoxyl)phthalazine-1-yl)methyl) phenyl)methanone as a white solid (389 mg, 60%) in a mixture of isomers (57:43) and rotamers. Where possible, the shift relating to the minor rotamer is denoted with an asterisk.

(2.33): ^{1}**H NMR** (400 MHz, $CDCl_3$) δ = 8.52 – 8.45 (m, 1H, 1H*), 7.73 (dt, *J* = 7.2, 3.4 Hz, 2H, 2H*), 7.66 (bs, 1H, 1H*), 7.40 – 7.28 (m, 2H + 2H*), 7.02 (td, *J* = 8.9, 3.2 Hz, 1H + 1H*), 5.59 (s, 2H + 2H*), 4.29 (s, 2H + 2H*), 3.92 – 3.14 (m, 10H + 10H*), 1.76 (bs, 1H, 1H*), 1.06 – 0.95 (m, 4H, 4H*) 0.85 – 0.70 (m, 2H + 2H*), 0.00 (s, 9H + 9H*); ^{13}**C NMR** (100 MHz, $CDCl_3$) δ = 172.3 (1C + 1C*), 165.2 (1C + 1C*), 159.8 (1C + 1C*), 157.0 (d, *J* = 247.5 Hz, 1C + 1C*), 144.6 (1C + 1C*), 134.5 (d, *J* = 3.4 Hz, 1C + 1C*), 133.5 (1C + 1C*), 131.6 (d, *J* = 6.5 Hz, 1C + 1C*), 129.2 (1C + 1C*), 129.1 (1C + 1C*), 128.4 (1C + 1C*), 127.8 (1C + 1C*), 127.8 (1C + 1C*), 125.0 (1C + 1C*), 123.7 (d, *J* = 18.2 Hz, 1C + 1C*), 116.2 (d, *J* = 22.0 Hz, 1C + 1C*), 79.0 (1C), 67.3 (1C + 1C*), 47.1 (1C*), 46.8 (1C), 45.7 (1C*), 45.2 (1C), 42.3 (2C), 42.1 (1C*), 41.7 (1C*), 37.9 (1C + 1C*), 18.1 (1C + 1C*), 11.0 (1C + 1C*), 7.73 (2C +

2C*), - 1.47 (3C + 3C*); **{^{1}H}^{19}F NMR** (376 MHz, $CDCl_3$) δ = -117.6 (s, 1F*), -117.7 (s, 1F);

(2.38): ^{1}H NMR (400 MHz, $CDCl_3$) δ = 8.52 – 8.45 (m, 1H, 1H*), 7.73 (dt, *J* = 7.2, 3.4 Hz, 2H, 2H*), 7.66 (bs, 1H, 1H*), 7.40 – 7.28 (m, 2H + 2H*), 7.02 (td, *J* = 8.9, 3.2 Hz, 1H + 1H*), 5.70 (s, 2H + 2H*), 4.30 (s, 2H +2H*), 3.92 – 3.14 (m, 10H + 10H*), 1.76 (bs, 1H, 1H*), 1.06 – 0.95 (m, 2H + 2H*) 0.95 – 0.85 (m, 2H + 2H*), 0.85 – 0.70 (m, 2H + 2H*), 0.00 (s, 9H + 9H*); **^{13}C NMR** (100 MHz, $CDCl_3$) δ = 172.3 (1C + 1C*), 165.2 (1C + 1C*), 159.9 (1C + 1C*), 156.9 (d, *J* = 247.5 Hz, 1C*), 144.6 (1C + 1C*), 134.6 (d, *J* = 3.4 Hz, 1C + 1C*), 133.4 (1C + 1C*), 131.5 (d, *J* = 8.1 Hz, 1C + 1C*), 129.1 (1C + 1C*), 129.0 (1C + 1C*), 128.4 (1C + 1C*), 127.8 (1C + 1C*), 127.8 (1C + 1C*), 125.0 (1C + 1C*), 123.7 (d, *J* = 18.2 Hz, 1C + 1C*), 116.2 (d, *J* = 22.0 Hz, 1C + 1C*), 94.2 (1C + 1C*), 67.3 (1C + 1C*), 47.1 (1C*), 46.8 (1C), 45.7 (1C*), 45.2 (1C), 42.3 (2C), 42.1 (1C*), 41.7 (1C*), 38.0 (1C + 1C*), 18.1 (1C + 1C*), 11.0 (1C + 1C*), 7.73 (2C + 2C*), - 1.37 (3C + 3C*); **{^{1}H}^{19}F NMR** (376 MHz, $CDCl_3$) δ = -117.6 (s, 1F*), -117.7 (s, 1F);

(2.33 + 2.38) IR (*ν,* cm^{-1}): 2980, 1635, 1433, 1224, 1009, 834, 690. **HRMS** (ESI) for $C_{30}H_{37}FN_4O_4{}^{23}Na^{28}Si$ $[M+Na]^+$ requires 587.2460 found 587.2462; **M.P.** 53 – 55 °C.

Dimethyl (3-oxo-1,3,-dihydroisobenzofuran-1-yl)phosphonate (2.35)

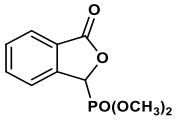

Dimethylphosphite (0.92 mL, 10.0 mmol) was added dropwise to a solution of sodium (0.58 g, 10.8 mmol) in MeOH (15 mL) at 0 °C. To the solution, 2-

carboxybenzaldehyde (1.00 g, 6.66 mmol) was added portion-wise while stirring. The mixture was gradually warmed to room temperature and stirred for 6 hours. methanesulfonic acid (0.77 mL, 11.9 mmol) was added dropwise and the mixture was stirred for another 30 minutes. The solution was concentrated in vacuo to produce a white solid, to which water was added (30 mL) and the crude product was extracted into DCM (3 × 30 mL). The organic layer was washed with water (2 × 30 mL), dried with $MgSO_4$ and filtered. The filtrate was concentrated in vacuo and washed with Et_2O (3 × 20 mL), affording dimethyl-(3-oxo-1,3-dihydrobenzofuran-1-yl)phosphonate (1.48 g, 92%) as a white solid.

^{1}H NMR (400 MHz, CD_3OD) δ = 7.96 (d, *J* = 7.5 Hz 1H), 7.81 (t, *J* = 7.5 Hz, 1H), 7.77 (d, *J* = 7.5 Hz, 1H), 7.65 (t, *J* = 7.5 Hz, 1H), 6.12 (d, *J* = 10.8, 1H), 3.90 (d, *J* = 10.8 Hz, 3H), 3.72 (d, *J* = 10.8 Hz, 3H); **M.P.** 90 – 92 °C; Data is in accordance with known literature.[1]

2-Fluoro-5-((3-oxoisobenzofuran-1(*3H*)-ylidene)methyl)benzonitrile (2.36)

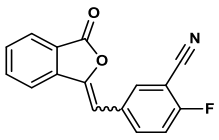

A solution of dimethyl-(3-oxo-1,3-dihydrobenzofuran-1-yl)phosphonate (1.00 g, 4.13 mmol) and 2-fluoro-5-formylbenzonitrile (0.62 g, 4.13 mmol) in THF (50 mL) was prepared at room temperature. The solution was then cooled to 0 °C followed by the addition of Et_3N (0.69 mL, 4.96 mmol). The reaction mixture was allowed to warm up to room temperature and was stirred for 48 h, followed by concentration in vacuo to produce a white solid. The solid was suspended in water, collected by vacuum filtration and washed with hexane (2 × 20 mL), Et_2O (2 × 20 mL), and MeOH (2 ×

20 mL) affording 2-Fluoro-5-((3-oxoisobenzofuran-1(*3H*)-ylidene)methyl)benzonitrile (0.99 g, 90%) as a white solid.

^{1}H NMR spectroscopy showed a 3:1 mixture of *E* and *Z* isomers. Where possible, the minor isomer is marked with an asterisk. **^{1}H NMR** (400 MHz, DMSO-d_6) δ = 8.22 – 8.10 (m, 2H + 2H*), 8.07 (d, *J* = 7.8 Hz, 1H), 7.98 (d, *J* = 7.7 Hz, 1H + 1H*), 7.94 – 7.89 (m, 1H + 1H*), 7.75 (t, *J* = 9.0 Hz, 1H + 1H*), 7.64 (t, *J* = 9.1 Hz, 1H + 1H*), 7.42 (d, *J* = 6.9 Hz, 1H*), 6.97 (s, 1H*) 6.95 (s, 1H); **M.P.** 163 – 165 °C. Data is in accordance with known literature.[4]

2-Fluoro-5-((4-oxo-3,4,-dihydrophthalazin-1-yl)methyl)benzoic acid (2.37)

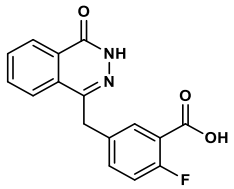

2-Fluoro-5-[(3'-oxo-2'-benzofuran-1'-ylidene)methyl]benzonitrile (0.50 g, 1.89 mmol) was suspended in water (3 mL) and 13 M NaOH was added (0.67 mL). The mixture was heated to 90 °C and stirred for 24 h, after which it was cooled to 70 °C, followed by the addition of hydrazine monohydrate (1.34 mL, 26.9 mmol) and a further 72 h of stirring. The mixture was then cooled to room temperature and acidified with 8 M HCl to an approximate pH of 4. The solid precipitate was collected by vacuum filtration and washed with water (3 × 25 mL) and Et_2O (4 × 25 mL) affording 2-Fluoro-5-((4-oxo3,4-dihydrophthalazin-1-yl)methyl)benzoic acid (0.54 g, 67%) as a red solid.

^{1}H NMR (400 MHz, DMSO-d_6) δ = 12.57 (s, 1H), 8.26 (dd, *J* = 7.8, 0.8 Hz, 1H), 7.98 (d, *J* = 7.9 Hz, 1H), 7.93 – 7.86 (m, 1H), 7.86 – 7.79 (m, 2H), 7.61 – 7.54 (m,

1H), 7.23 (dd, J 10.8, 8.5 Hz, 1H), 4.35 (s, 2H); **{^{1}H}^{19}F NMR** (376 MHz, DMSO-d_6) δ = -114.0; **M.P.** 217 – 219 °C. Data is in accordance with known literature.[1]

(4-(2-Iodobenzoyl)piperazin-1-yl)(cyclopropyl)methanone (2.39)

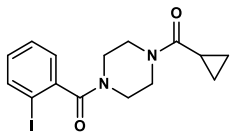

To a round bottom flask was added, 2-iodobenzoic acid (1.00 g, 4.03 mmol), DCM (40 mL), diisopropylethylamine (1.07 mL, 6.04 mmol) and HBTU (2.30 g, 6.04 mmol). The reaction mixture was then stirred for 30 minutes at room temperature before adding *N*-cyclopropylpiperazine-1-ylmethanone (1.26 mL, 6.04 mmol). The reaction was stirred overnight before the excess solvent with removed *in vacuo* and the crude material purified *via* flash column chromatography (EtOAc:MeOH 10:1) affording (4-(2-Iodobenzoyl)piperazin-1-yl)(cyclopropyl)methanone as a white solid (0.99 g, 2.57 mmol, 64%) in a mixture of rotamers. Where possible, the minor rotamer is marked with as asterisk.

^{1}H NMR (400 MHz, $CDCl_3$) δ = 7.83 (d, *J* = 7.9 Hz, 1H), 7.40 (t, *J* = 7.5 Hz, 1H), 7.19 (d, *J* = 7.5 Hz, 1H), 7.09 (t, *J* = 7.7 Hz, 1H), 4.04 – 3.55 (m, 6H), 3.37 – 3.08 (m, 2H), 1.76 (m, 1H), 0.98 (bs, 2H), 0.79 (bs, 2H); **^{13}C NMR** (100 MHz, $CDCl_3$) δ = 172.4 (1C +1C*), 169.6 (1C +1C*), 141.7 (1C +1C*), 139.3 (1C +1C*), 130.5 (1C +1C*), 128.6 (1C +1C*), 127.0 (1C +1C*), 92.4 (1C +1C*), 46.8 (1C*), 46.6 (1C), 45.6 (1C*), 45.1 (1C), 42.2 (1C*), 41.8 (1C + 1C*), 41.6 (1C), 11.0 (1C +1C*), 7.8 (2C +2C*); **IR** (*v,* cm^{-1}): 2980, 1633, 1439, 1221, 1009, 703; **HRMS** (ESI) for $C_{15}H_{18}{}^{127}IN_2O_2$ $[M+H]^+$ requires 385.0343 found 385.0355; **M.P.** 52 – 54 °C.

(4-(2-Bromobenzoyl)piperazin-1-yl)(cyclopropyl)methanone (2.40)

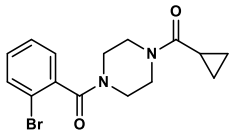

To a round bottom flask was added, 2-bromobenzoic acid (1.00 g, 4.97 mmol), DCM (40 mL), diisopropylethylamine (1.30 mL, 7.46 mmol) and HBTU (2.83 g, 7.46 mmol). The reaction mixture was then stirred for 30 minutes at room temperature before adding *N*-cyclopropylpiperazine-1-ylmethanone (1.52 mL, 7.46 mmol). The reaction was stirred overnight before the excess solvent with removed *in vacuo* and the crude material purified *via* flash column chromatography (EtOAc:MeOH 10:1) affording (4-(2-Bromobenzoyl)piperazin-1-yl)(cyclopropyl)methanone as a white solid in a mixture of rotamers (0.98 g, 2.93 mmol, 59%). The shifts relating to the minor rotamer has been donated with an asterisk.*

^{1}H NMR (400 MHz, $CDCl_3$) δ = 7.56 (d, *J* = 7.8 Hz, 1H), 7.35 (t, *J* = 7.4 Hz, 1H), 7.27 – 7.20 (m, 2H), 4.14 – 3.44 (m, 6H), 3.41 – 3.09 (m, 2H), 1.68 (d, *J* = 41.1 Hz, 1H), 0.96 (dt, *J* = 6.2, 3.2 Hz, 2H), 0.76 (bs, 2H); **^{13}C NMR** (100 MHz, $CDCl_3$) δ = 172.3 (1C +1C*), 167.9 (1C +1C*), 137.5 (1C +1C*), 132.9 (1C +1C*), 130.6 (1C +1C*), 127.9 (1C +1C*), 127.7 (1C +1C*), 119.1 (1C +1C*), 46.8 (1C*), 46.6 (1C), 45.6 (1C*), 45.1 (1C), 42.2 (1C*), 41.8 (1C + 1C*), 41.7 (1C), 11.0 (1C + 1C*), 7.71 (2C + 2C*); **IR** (*ν,* cm^{-1}): 1645, 1451, 1203, 996, 714; **HRMS** (ESI) for $C_{15}H_{18}{}^{79}BrN_2O_2$ $[M+H]^+$ requires 337.0481 found 337.0469; **M.P.** 63 – 65 °C.

2-(4,4,5,5-Tetramethyl-1,3,2-dioxaborolan-2-yl)benzoic acid

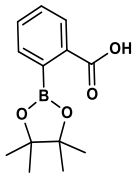

To a solution of anhydrous THF (20 mL) under an atmosphere of argon was added 2-boronobenzoic acid (1.00 g, 6.02 mmol), pinacol (0.71 g, 6.02 mmol) and magnesium sulfate (1.44 g, 12.04 mmol). The reaction was left to stir overnight at room temperature. Upon completion, the reaction was filtered and the excess solvent removed *in vacuo* affording 2-(4,4,5,5-tetramethyl-1,3,2-dioxaborolan-2-yl)benzoic acid as a white solid (1.49 g, 6.00 mmol, 99%).

^{1}H NMR (400 MHz, DMSO-d_6) δ = 7.83 (dd, J = 7.6, 0.9 Hz, 1H), 7.55 (td, J = 7.3, 1.3 Hz, 1H), 7.46 (td, J = 7.5, 1.4, 1H), 7.43 – 7.39 (m, 1H), 1.29 (s, 12H); **^{13}C NMR** (100 MHz, DMSO-d_6) δ = 169.6, 134.7, 132.2, 131.9, 129.2, 128.3, 83.4 (2C), 25.0 (4C) (the carbon bearing the boron substituent is not observed); **IR** (ν, cm^{-1}): 2972, 1679, 1344, 1304, 1141, 754; **HRMS** (ESI) for $C_{13}H_{16}{}^{10}BO_4$ [M-H]- requires 247.1212 found 247.1215; **M.P.** 118 – 120 °C.

(4-(Cyclopropanecarbonyl)piperazin-1-yl)(2-(4,4,5,5-tetramethyl-1,3,2-dioxaborolan-2-yl)phenyl)methanone (2.41)

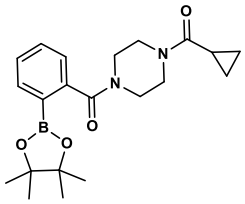

To a round bottom flask containing 2-(4,4,5,5-tetramethyl-1,3,2-dioxaborolan-2-yl)benzoic acid (1.00 g, 4.03 mmol) was added DCM (40 mL), diisopropylethylamine (1.05 mL, 6.04 mmol) and HBTU (2.29 g, 6.04 mmol). The reaction mixture was

stirred for 30 min before adding cyclopropylpiperazine-1-ylmethanone (0.86 mL, 6.04 mmol). The reaction was stirred overnight before the excess solvent with removed *in vacuo* and the crude material purified *via* flash column chromatography (EtOAc:MeOH 10:1) affording (4-(cyclopropanecarbonyl)piperazin-1-yl)(2-(4,4,5,5-tetramethyl-1,3,2-dioxaborolan-2-yl) phenyl)methanone as a white solid (1.08 g, 2.82 mmol, 70%) in a mixture of rotamers. The shifts relating to the minor rotamer has been donated with an asterisk.*

^{1}H NMR (400 MHz, $CDCl_3$) δ = 7.81 (d, *J* = 7.4 Hz, 1H + 1H*), 7.45 (td, *J* = 7.6, 1.5 Hz, 1H + 1H*), 7.35 (td, *J* = 7.5, 1.3 Hz, 1H + 1H*), 7.22 (d, *J* = 7.5 Hz, 1H + 1H*), 3.86 – 3.69 (m, 4H, 4H*), 3.67 – 3.50 (m, 2H, 2H*), 3.34 – 3.07 (m, 2H, 2H*), 1.81 – 1.52 (m, 1H + 1H*), 1.29 (s, 12H + 12H*), 1.04 – 0.95 (m, 2H + 2H*), 0.67 – 0.87 (m, 2H + 2H*); **^{13}C NMR** (100 MHz, $CDCl_3$) δ = 172.3 (1C + 1C*), 171.3 (1C + 1C*), 142.3 (1C + 1C*), 135.7 (1C + 1C*), 131.2 (1C + 1C*), 128.2 (1C + 1C*), 125.4 (1C + 1C*), 84.1 (2C + 2C*), 47.3 (1C*), 47.0, 45.2 (1C*), 44.9, 41.9 (2C), 41.6 (2C*) 24.9 (4C + 4C*), 11.0 (1C + 1C*), 7.65 (2C + 2C*) (the carbon bearing the boron substituent is not observed); **IR** (*ν,* cm^{-1}): 2970, 1634, 1467, 1213, 1014, 741; **HRMS** (ESI) for $C_{21}H_{30}{}^{10}BN_2O_4$ $[M+H]^+$ requires 384.2220 found 384.2218; **M.P.** 85 – 87 °C.

(4-benzoylpiperazin-1-yl)(cyclopropyl)methanone (2.42)

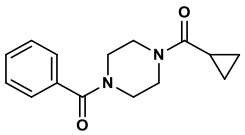

To a round bottom flask was added, benzoic acid (100 mg, 0.82 mmol), DCM (8 mL), diisopropylethylamine (0.21 mL, 1.23 mmol) and HBTU (466 mg, 1.23 mmol). The reaction mixture was then stirred for 30 minutes at room temperature before adding

cyclopropylpiperazine-1-ylmethanone (0.17 mL, 1.23 mmol). The reaction was stirred overnight before the excess solvent with removed *in vacuo* and the crude material purified *via* flash column chromatography (EtOAc:MeOH 10:1) affording (4-benzoylpiperazin-1-yl)(cyclopropyl)methanone as a colourless gum (162 g, 0.63 mmol 77%).

^{1}H NMR (400 MHz, $CDCl_3$) δ = 7.46 – 7.37 (m, 5H), 3.96 – 3.31 (m, 8H), 1.71 (bs, 1H), 1.06 – 0.91 (m, 2H), 0.86 – 0.68 (m, 2H); **^{13}C NMR** (100 MHz, $CDCl_3$) δ = 172.4, 170.7, 135.2, 130.1, 128.6 (2C), 127.1 (2C), 47.5, 45.3, 42.3 (2C), 11.0, 7.71 (2C); **IR** (*v,* cm^{-1}): 1624, 1438, 1230, 1020, 740; **HRMS** (ESI) for $C_{15}H_{19}N_2O_2$ $[M+H]^+$ requires 259.1376 found 259.1379.

(4-Benzylpiperazin-1-yl)(2-bromophenyl)methanone (2.43)

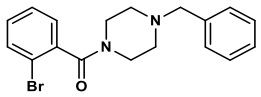

To a round bottom flask was added, 2-bromobenzoic acid (1.00 g, 4.97 mmol), DCM (40 mL), diisopropylethylamine (1.86 mL, 7.46 mmol) and HBTU (4.06 g, 7.46 mmol). The reaction mixture was then stirred for 30 minutes at room temperature before adding 1-benzylpiperaine (1.31 g, 7.46 mmol). The reaction was stirred overnight before the excess solvent with removed *in vacuo* and the crude material purified *via* flash column chromatography (Pure EtOAc) affording (4-Benzylpiperazin-1-yl)(2-bromophenyl)methanone as a white solid (1.43 g, 3.98 mmol, 80%).

^{1}H NMR (400 MHz, $CDCl_3$) δ = 7.47 (dd, *J* = 8.1, 1.2 Hz, 1H), 7.29 – 7.11 (m, 8H), 3.74 (t, *J* = 5.2 Hz, 2H), 3.44 (s, 2H), 3.15 (dddd, *J* = 39.4, 13.2, 6.9, 3.3 Hz, 2H), 2.57 – 2.38 (m, 3H), 2.57 – 2.38 (m, 4H); **^{13}C NMR** (100 MHz, $CDCl_3$) δ = 167.6, 138.1,

137.6, 132.8, 130.3, 129.1 (2C), 128.4 (2C), 127.7 (2C), 127.3, 119.2, 62.9, 53.1, 52.6, 46.8, 41.6; **IR** (*ν,* cm^{-1}): 3061, 2360, 2341, 1624, 1591, 1439, 1091, 836, 737; **HRMS** (ESI) for $C_{18}H_{20}{}^{79}BrN_2O$ $[M+H]^+$ requires 359.0689 found 359.0699; **M.P.** 58 – 60 °C.

(2-Bromophenyl)(piperidin-1-yl)methanone (2.46)

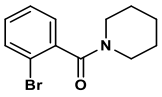

To a round bottom flask was added, 2-bromobenzoic acid (1.00 g, 4.97 mmol), DCM (40 mL), diisopropylethylamine (1.86 mL, 7.46 mmol) and HBTU (4.06 g, 7.46 mmol). The reaction mixture was then stirred for 30 minutes at room temperature before adding piperadine (0.74 mL, 7.46 mmol). The reaction was stirred overnight before the excess solvent with removed *in vacuo* and the crude material purified *via* flash column chromatography (10:7 *n*-Pentane: EtOAc) affording (2-bromophenyl)(piperidin-1-yl)methanone as a colourless oil (1.00 g, 3.78 mmol, 76%).

^{1}H NMR (400 MHz, $CDCl_3$) δ = 7.58 – 7.51 (m, 1H), 7.37 – 7.28 (m, 1H), 7.25 – 7.16 (m, 2H), 3.82 – 3.66 (m, 2H), 3.26 – 3.07 (m, 2H), 1.75 – 1.56 (m, 5H), 1.51 – 1.40 (m, 1H); **^{13}C NMR** (100 MHz, $CDCl_3$) δ = 167.5, 138.6, 132.8, 130.0, 127.6, 127.5, 119.2, 47.9, 42.5, 26.3, 25.5, 24.5. This data is found to be in accordance with the literature.[5]

Methyl-2-bromo-5-((4-oxo-((2-(trimethylsilyl)ethoxy)methyl)-3,4-dihydro phthalazin-1-yl)methyl) benzoate (2.53)

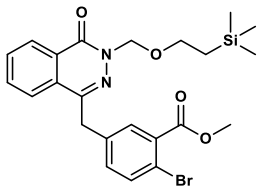

To a round bottom flask under an atmosphere of argon containing methyl-2-bromo-5-((4-oxo-((2-(trimethylsilyl)ethoxy)methyl)-3,4-dihydro phthalazin-1-yl)methyl) benzoate (11.0 g, 29.6 mmol) at 0 °C was added anhydrous THF (200 mL) and sodium hydride (60% in dispersion oil, 3.55 g, 88.8 mmol). The reaction was stirred at 0 °C for 30 min before warming to room temperature upon which 2-(trimethylsilyl)ethoxymethyl chloride (6.25 mL, 35.6 mmol) was added dropwise. The reaction was stirred overnight before the excess solvent was removed *in vacuo* and purified directly *via* flash column chromatography (*n*-Pent:EtOAc 10:3) affording methyl-2-bromo-5-((4-oxo-((2-(trimethylzilyl)ethoxy)methyl)-3,4-dihydro phthalazine-1-yl)methyl)benzoate as a white solid (10.7 g, 72%, 21.3 mmol).

^{1}H NMR (400 MHz, $CDCl_3$) δ = 8.52 – 8.45 (m, 1H), 7.77 – 7.68 (m, 3H), 7.66 – 7.58 (m, 1H), 7.21 (dd, *J* = 8.2, 2.3 Hz, 1H), 5.58 (s, 2H), 4.28 (s, 2H), 3.91 (s, 3H), 3.79 – 3.73 (m, 2H), 1.02 – 0.97 (m, 2H), 0.01 (s, 9H); **^{13}C NMR** (100 MHz, $CDCl_3$) δ = 167.8, 161.3, 145.7, 138.6, 136.0, 134.9, 133.9, 133.8, 133.0, 132.6, 130.5, 129.8, 129.2, 126.3, 121.3, 80.4, 68.6, 54.0, 39.5, 19.5, 0.00 (3C); **IR** (*ν,* cm^{-1}): 2952, 1721, 1652, 1431, 1294, 1223, 1074, 1027, 854, 832, 745; **HRMS** (ESI) for $C_{23}H_{27}{}^{79}BrN_2{}^{23}NaO_4{}^{28}Si$ $[M+Na]^+$ requires 525.0826 found 525.0827; **M.P.** 85 – 87 °C.

Methyl-2-bromo-5-((4-oxo-3,4-dihydrophthalazin-1-yl)methyl)benzoate (2.54)

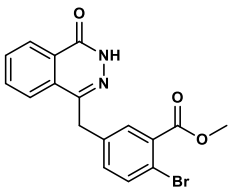

To a solution of 2-bromo-5-((4-oxo-3,4,-dihydrophthalazin-1-yl)methyl)benzoic acid (12.32 g, 34.4 mmol) in anhydrous DMF (100 mL) was added iodomethane (6.38 mL, 103.2 mmol) and anhydrous potassium carbonate (5.70 g, 41.3 mmol). The reaction was then heated to 50 °C and stirred overnight. Upon completion, the excess solvent was removed *in vacuo* and water (100 mL) was added to the crude material. The precipitate formed was filtered and washed with Et_2O (3 x 100 mL) before drying *in vacuo* affording methyl-2-bromo-5-((4-oxo-3,4-dihydrophthalazin-1-yl)methyl) benzoate as a dull brown solid (11.4 g, 30.6 mmol, 89%).

^{1}H NMR (400 MHz, DMSO-d_6) δ = 12.60 (s, 1H), 7.99 – 7.93 (m, 1H), 7.90 (ddd, *J* = 8.1, 7.1, 1.5 Hz, 1H), 7.83 (ddd, *J* = 8.4, 7.2, 1.3 Hz, 1H), 7.73 (d, *J* = 2.2 Hz, 1H), 7.67 (d, *J* = 8.2 Hz, 1H), 7.36 (dd, *J* = 8.2, 2.3 Hz, 1H), 4.35 (s, 2H), 3.83 (s, 3H); **^{13}C NMR** (100 MHz, DMSO-d_6) δ = 166.6, 159.8, 145.1, 138.6, 134.4, 134.1, 134.0, 132.8, 132.1, 131.6, 129.5, 128.3, 126.5, 125.9, 118.5, 53.1, 36.9; **IR** (*ν,* cm^{-1}): 2983, 1650, 1250, 1205, 1104, 772; **HRMS** (ESI) for $C_{17}H_{13}{}^{79}BrN_2{}^{23}NaO_3$ $[M+Na]_+$ requires 395.0002 found 395.0001; **M.P.** 211 – 213 °C.

2-Bromo-5-((4-oxo-3,4-dihydrophthalazin-1-yl)methyl)benzoic acid (2.55)

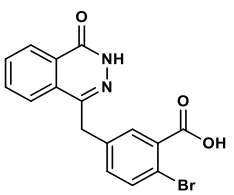

2-bromo-5-[(3'-oxo-2'- benzofuran-1'-ylidene)methyl]benzonitrile (12.0 g, 36.9 mmol) was suspended in water (75 mL) and 13 M NaOH was added (19 mL, 247 mmol). The mixture was heated to 90 °C and stirred for 24 h, after which it was warmed to reflux (140 °C), followed by the addition of hydrazine monohydrate (25.0 mL, 780 mmol) and a further 48 h of stirring. The mixture was then cooled to room temperature and acidified with 5M HCl to an approximate pH of 2. The solid precipitate was collected by vacuum filtration and washed with water (50 mL) and Et_2O (3 × 50 mL) affording 2-bromo-5-((4-oxo3,4-dihydrophthalazin-1-yl)methyl)benzoic acid (12.27 g, 88%) as a red solid.

^{1}H NMR (400 MHz, DMSO-d_6) δ = 12.61 (s, 1H), 8.25 (dd, *J* = 7.7, 1.4 Hz, 1H), 7.99 – 7.94 (m, 1H), 7.89 (ddd, *J* = 8.1, 7.1, 1.5 Hz, 1H), 7.83 (td, *J* = 7.5, 1.2 Hz, 1H), 7.71 (d, *J* = 2.3 Hz, 1H), 7.62 (d, *J* = 8.2 Hz, 1H), 7.36 (dd, *J* = 8.2, 2.3 Hz, 1H), 4.33 (s, 2H); **^{13}C NMR** (100 MHz, DMSO-d_6) δ = 167.7, 159.8, 145.2, 138.5, 134.3, 134.1, 133.4, 132.1, 131.4, 129.5, 128.3, 126.5, 125.9, 118.4, 100.0, 36.9; **IR** (*ν,* cm^{-1}): 2890, 1771, 1472, 1394, 970, 760, 689; **HRMS** (ESI) for $C_{16}H_{10}{}^{79}BrN_2O_3$ $[M-H]^-$ requires 356.9945 found 356.9948; **M.P.** > 250 °C.

2-Bromo-5-((3-oxoisobenzofuran-1(*3H*)-ylidene)methyl)benzonitrile (2.56)

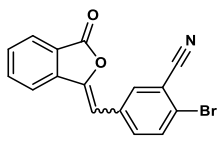

A solution of dimethyl-(3-oxo-1,3-dihydrobenzofuran-1-yl)phosphonate (5.00 g, 20.7 mmol) and 2-bromo-5-formylbenzonitrile (3.58 g, 17.2 mmol) in THF (100 mL) was prepared at room temperature. The solution was cooled to 0 °C followed by the addition of Et_3N (4.78 mL, 34.4 mmol). The reaction mixture was warmed to room

temperature and was stirred for 48 h, followed by concentration *in vacuo* to produce a white solid. The solid was suspended in water, collected by vacuum filtration and washed with hexane (2 × 20 mL) and Et_2O (3 × 20 mL) affording 2-Bromo-5-((3-oxoisobenzofuran-1(*3H*)-ylidene)methyl)benzonitrile (5.14 g, 15.8 mmol, 92%) as a white solid in an mixture of e:z stereoisomers (10:1) and a purity of 90%. NMR spectra showed a 10:1 mixture of E and Z isomers.

^{1}H NMR (400 MHz, DMSO-d_6) δ = 8.24 – 8.06 (m, 2H, 2H*), 8.01 – 7.90 (m, 3H, 3H*), 7.83 – 7.50 (m, 2H, 2H*), 7.00 (s, 1H*), 6.97 (s, 1H) (Where possible, shifts are assigned to each respective isomer); **^{13}C NMR** (100 MHz, DMSO-d_6) δ = 166.3, 146.6, 140.0, 135.9, 135.7, 135.4, 134.3, 134.1, 132.0, 131.6, 125.9, 123.9, 121.5, 117.5, 115.5, 103.9 (only those peaks corresponding to the major isomer are reported); **IR** (ν, cm^{-1}): 2977, 2225, 1776, 1643, 1495, 954, 745, 681; **HRMS** (ESI) for $C_{16}H_9{}^{79}BrNO_2$ $[M+H]^+$ requires 325.9746 found 325.9745; **M.P.** 118 – 120 °C.

2-Bromo-5-formylbenzonitrile (2.57)

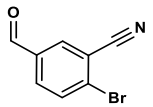

To a round bottom flask containing 2-amino-5-formylbenzonitrile (17.95 g, 126 mmol) at 0 °C was added 6M HCl (107 mL) and fuming H_2SO_4 (107 mL). After being allowed to cool, a solution of sodium nitrite (18.5 g, 268 mmol) in H_2O (40 mL) was added dropwise before allowing the reaction to stir for 30 minutes. The reaction mixture was then added dropwise to a solution of copper(II) bromide (40.1 g, 179 mmol) in 48% HBr (107 mL) at 0 °C. The reaction was then stirred at 0 °C for 60 min before being allowed to warm to room temperature and being stirred for another

hour. Upon completion, the reaction was poured into an ice/water mixture before the organic layer was extracted with DCM (3 x 150 mL). The organic layer was then dried with $MgSO_4$ and the excess solvent removed *in vacuo*. The crude material was purified by flash column chromatography (*n*-Pent:EtOAc 10:1) to afford 2-bromo-5-formylbenzonitrile as a pale yellow solid (16.8 g, 80.6 mmol, 64%).

^{1}H NMR (400 MHz, $CDCl_3$) δ = 10.00 (s, 1H), 8.14 (s, 1H), 7.95 (d, 8.4, 1H), 7.90 (d, *J* = 8.3 Hz, 1H); **^{13}C NMR** (100 MHz, $CDCl_3$) δ = 188.9, 135.4, 135.1, 134.3, 133.7, 131.9, 117.2, 116.1; **IR** (*ν,* cm^{-1}): 1702, 1562, 1174, 1008; **HRMS** (ESI) for $C_8H_5{}^{79}BrNO$ $[M+H]^+$ requires 209.9549 found 209.9551; **M.P.** 108 – 110 °C.

2-Amino-5-formylbenzonitrile (2.66)

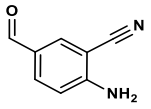

To a flame-dried round bottom flask was added 2-amino-5-bromo-benzonitrile (1.00 g, 5.08 mmol) and THF (30 mL). The solution was cooled to −78 °C before *n*-BuLi in hexanes (2.5 M, 4.49 mL, 11.2 mmol) was added dropwise. The reaction was left to stir at -78 °C for 2 h before quenching with DMF (0.92 mL, 12.7 mmol) and allowed to warm to room temperature. The solution was then extracted with $NaHCO_3$ (40 mL) and washed with DCM (3 x 30 mL). The organic layers were collected, dried with $MgSO_4$, and the excess solvent removed *in vacuo*. The crude material was then purified *via* flash column chromatography (*n*-Pent:EtOAc 4:1) affording 2-amino-5-formylbenzonitrile (0.53 g, 71%) as a pale yellow solid.

^{1}H NMR (400 MHz, $CDCl_3$) δ = 9.76 (s, 1H), 7.92 (d, *J* = 1.8 Hz, 1H), 7.87 (dd, *J* = 8.6, 1.8 Hz, 1H), 6.82 (d, *J* = 8.6 Hz, 1H), 5.00 (bs, 2H); **^{13}C NMR** (100 MHz, $CDCl_3$)

δ = 188.6, 153.7, 136.5, 134.3, 127.4, 116.2, 115.1, 95.9. The data is in accordance with known literature.[6]

2-(4-(Cyclopropanecarbonyl)piperazin-1-yl)(2-fluorophenyl)methanone (2.76)

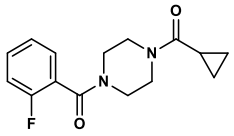

To a round bottom flask was added, 2-fluorobenzoic acid (1.00 g, 7.14 mmol), DCM (40 mL), diisopropylethylamine (1.86 mL, 10.7 mmol) and HBTU (4.06 g, 10.7 mmol). The reaction mixture was then stirred for 30 min at room temperature before adding cyclopropylpiperazine-1-ylmethanone (1.52 mL, 10.7 mmol). The reaction was stirred overnight before the excess solvent with removed *in vacuo* and the crude material purified *via* flash column chromatography (EtOAc:MeOH 10:1) affording (4-(cyclopropanecarbonyl)piperazin-1-yl)(2-(4,4,5,5-tetramethyl-1,3,2-dioxaborolan-2-yl)phenyl)methanone as a white solid (1.32 g, 4.78 mmol 67%) in a mixture of rotamers (2:1). In each case the shift relating to the minor rotamer has been donated with an asterisk.*

^{1}H NMR (400 MHz, $CDCl_3$) δ = 7.40 – 7.29 (m, 2H + 2H*), 7.16 (td, *J* = 7.5, 1.1 Hz, 1H + 1H*), 7.04 (ddd, *J* = 9.4, 8.3, 1.1 Hz, 1H + 1H*), 3.88 – 3.46 (m, 6H + 6H*), 3.38 – 3.20 (m, 2H + 2H*), 1.76 – 1.58 (m, 1H + 1H*), 0.98 – 0.88 (m, 2H + 2H*), 0.83 – 0.62 (m, 2H + 2H*); **^{13}C NMR** (100 MHz, $CDCl_3$) δ = 172.3 (1C + 1C*), 165.4 (1C + 1C*), 158.0 (d, *J* = 247.7 Hz, 1C + 1C*), 131.7 (d, *J* = 8.0 Hz, 1C + 1C*), 129.1 (1C + 1C*), 124.9 (d, *J* = 3.5 Hz, 1C + 1C*), 123.5 (d, *J* = 17.4, 1C + 1C*), 115.8 (d, *J* = 21.3, 1C + 1C*), 47.0 (1C*), 46.7 (1C), 45.6 (1C*), 45.1 (1C), 42.2 (2C), 41.9 (1C*), 41.7 (1C*), 11.0 (1C + 1C*), 7.64 (2C + 2C*); **{^{1}H}^{19}F NMR** (376

MHz, $CDCl_3$) δ = – 115.0 (s, 1F*), – 115.1 (s, 1F); **IR** (*ν,* cm^{-1}): 1630, 1460, 1219, 1004, 727; **HRMS** (ESI) for $C_{15}H_{18}{}^{19}FN_2O_2$ $[M+H]^+$ requires 277.1282 found 277.1285; **M.P.** 65 – 67 °C.

3-((4-oxo-3,4-dihydrophthalazin-1-yl)methyl)benzoic acid (2.83)

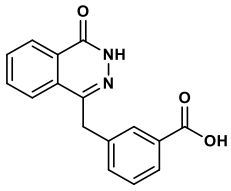

A solution of dimethyl-(3-oxo-1,3-dihydrobenzofuran-1-yl)phosphonate (7.25 g, 30.0 mmol) and 3-formylbenzonitrile (2.62 g, 20.0 mmol) in THF (250 mL) was prepared at room temperature. The solution was then cooled to 0 °C followed by the addition of Et_3N (6.10 mL, 30.0 mmol). The reaction mixture was warmed to room temperature and was stirred for 48 h, followed by concentration in vacuo to produce a white solid. The solid was suspended in water, collected by vacuum filtration and washed with hexane (2 × 20 mL) and Et_2O (3 × 20 mL) affording 3-((3-oxoisobenzofuran-1(3*H*)-ylidene)methyl)benzonitrile (4.40 g) as a crude white solid which was then taken through to the next step without further purification. 3-((3-oxoisobenzofuran-1(3*H*)-ylidene)methyl)benzonitrile (4.40 g, 17.8 mmol) was suspended in water (100 mL) and 13 M NaOH was added (26.4 mL, 238 mmol). The mixture was heated to 90 °C and stirred for 2 h, after which it was warmed to reflux (140 °C), followed by the addition of hydrazine monohydrate (7.48 mL, 240 mmol) and a further 16 h of stirring. The mixture was then cooled to room temperature and acidified with 5 M HCl to an approximate pH of 2. The solid precipitate was collected by vacuum filtration and washed with water (100 mL) and Et_2O (3 × 100 mL)

affording 3-((4-oxo-3,4-dihydrophthalazin-1-yl)methyl)benzoic acid (4.18 g, 15.0 mmol, 50%, two steps) as a white solid.

^{1}H NMR (400 MHz, DMSO-d_6) δ = 12.64 (s, 1H), 8.25 (dd, *J* = 7.9, 1.4 Hz, 1H), 7.96 (d, *J* = 7.9 Hz, 1H), 7.91 – 7.85 (m, 2H), 7.82 (dd, *J* = 7.6, 1.2 Hz, 1H), 7.80 – 7.75 (m, 1H), 7.58 (dt, *J* = 7.7, 1.5 Hz, 1H), 7.42 (t, *J* = 7.7 Hz, 1H), 4.38 (s, 2H); **^{13}C NMR** (100 MHz, DMSO-d_6) δ = 167.6, 159.8, 145.5, 139.1, 134.0, 133.7, 132.0, 131.4, 129.8, 129.5, 129.3, 128.3, 127.9, 126.5, 126.0; **IR** (*ν,* cm^{-1}): 3004, 1686, 1457, 1270, 1082, 937, 762, 666; **HRMS** (ESI) for $C_{16}H_{11}N_2O_3$ $[M-H]^-$ requires 279.0840 found 279.0647; **M.P.** > 250 °C.

4-(3-(4-(cyclopropanecabonyl)piperazine-1-carbnonyl)benzyl)phthalazin-1(*2H*)-one (2.84)

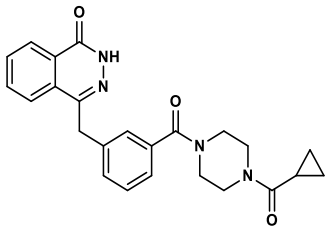

To a solution of 3-((4-oxo-3,4-dihydrophthalazin-1-yl)methyl)benzoic acid (1.00 g, 3.57 mmol) in DCM (100 mL) was added DIPEA (930 μL, 5.36 mmol) and HBTU (2.63 g, 5.36 mmol). The reaction mixture was stirred for 1 h before addition of cyclopropylpiperazine-1-ylmethanone (760 μL, 5.36 mmol) was carried out. The reaction mixture was then stirred at room temperature for 48 h, and the reaction mixture was extracted with DCM (3 × 50 mL) and washed with water (3 × 50 mL). The organic layers were collected, dried with $MgSO_4$ and the excess solvent removed *in vacuo*. Purification *via* reverse phase HLPC was then carried (Supplemental Figure

2) out affording 4-(3-(4-(cyclopropanecabonyl)piperazine-1-carbnonyl)benzyl) phthalazin-1(*2H*)-one (810 mg, 55**%**) as a white solid.

^{1}H NMR (400 MHz, $CDCl_3$) δ = 11.83 (bs, 1H), 8.46 – 8.39 (m, 1H), 7.73 – 7.67 (m, 3H), 7.37 – 7.30 (m, 3H), 7.27 – 7.20 (m, 1H), 4.33 (s, 2H), 3.89 – 3.18 (m, 8H), 1.78 – 1.60 (m, 1H), 1.00 – 0.90 (m, 2H), 0.82 – 0.64 (m, 2H); **^{13}C NMR** (100 MHz, $CDCl_3$) δ = 172.4, 170.4, 161.1, 145.7, 138.3, 135.5, 133.5, 131.5, 130.2, 129.6, 129.0, 128.2, 127.2, 127.0, 125.5, 125.1, 47.5, 45.3, 42.3 (2C), 38.5, 14.2, 11.0, 7.73; **IR** (*v,* cm^{-1}): 2925, 1632, 1430, 1353, 1101, 772; **HRMS** (ESI) for $C_{24}H_{25}N_4O_3$ $[M+H]^+$ requires 417.1856 found 417.2001; **M.P.** 82 – 84 °C.

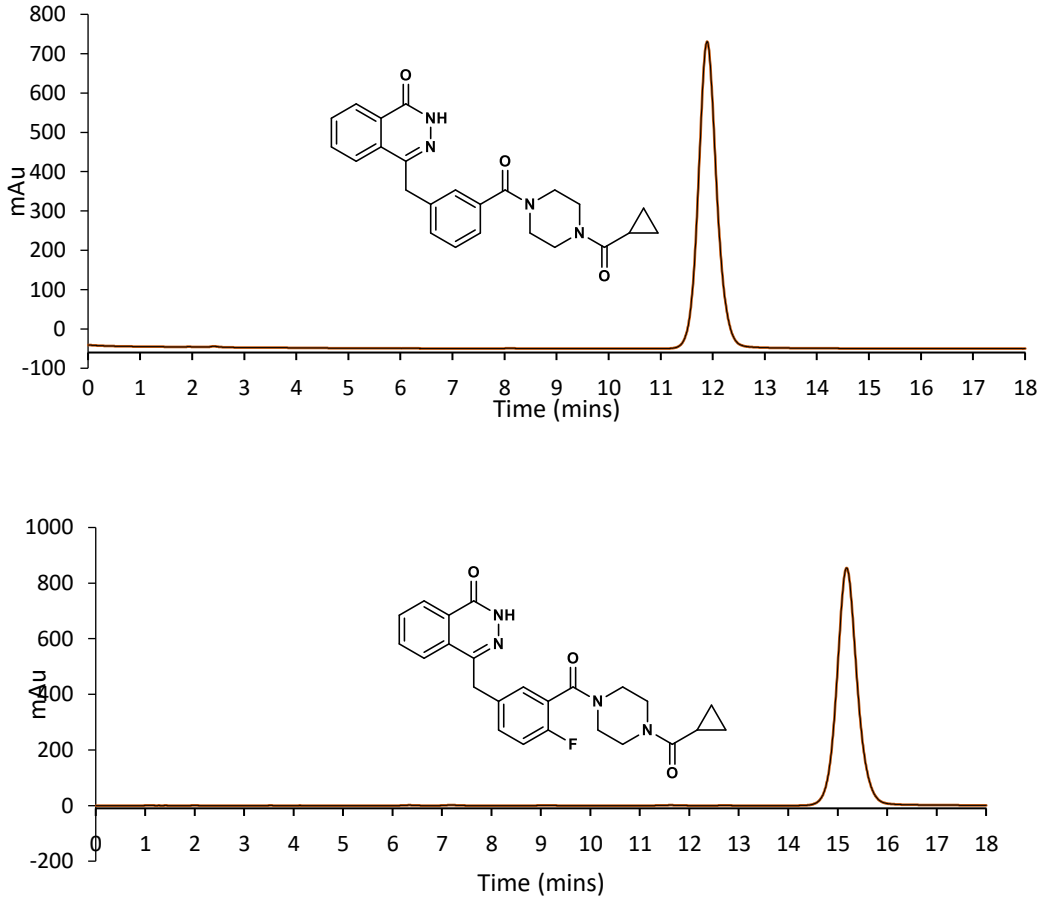

HPLC UV Trace of 4-(3-(4-(cyclopropanecabonyl)piperazine-1-carbnonyl)benzyl)phthalazin-1(2H)-one and olaparib. HPLC Eluent: Synergi 4 μm Hydro-RP 80A, 150 x 4.6 mm with 25% MeCN/75% H_2O (isocratic 1 mL/min) monitoring with UV (220 nm).

Synthesis of [$Cu(OTf)_2(impy)_4$] complex (2.68)

A solution of imidazo[1,2-*b*]pyridazine (impy) (758 mg, 6.36 mmol, 10 equiv.) in MeOH (1 mL) was added dropwise at 55 °C to a solution of $Cu(OTf)_2$ (230 mg, 0.636 mmol, 1.0 equiv.) in MeOH (1 mL). The blue precipitate which formed was washed with Et_2O (3 x 2 mL), then recrystallized from hot MeOH to afford [$Cu(OTf)_2(impy)_4$] (324 mg, 0.387 mmol, 61%).

Anal. Calcd. for $C_{26}H_{20}CuF_6N_{12}O_6S_2$: C, 37.26; H, 2.41; N, 20.05. Found: C, 37.07; H, 2.33; N, 19.91; **IR** (ATR, neat): (ν cm^{-1}) = 2981, 1620, 1541, 1503, 1374, 1352, 1306, 1281, 1241, 1221, 1149, 1071, 1027, 950, 918, 879, 801, 755, 733, 632.

5.4 Radiochemical Procedures and Characterisation for Chapter II:

Procedure for preparation of a solution of [^{18}F]KF/K_{222} in MeCN:

A solution of Kryptofix 222 (15 mg) and K_2CO_3 (3 mg) in 1 mL of MeCN/H2O, 4:1 was freshly prepared. [^{18}F]Fluoride (3.0-4.0 GBq) was separated from 18O-enriched-water using a Chromafix $PSHCO_3$ ^{18}F separation cartridge (45 mg) and subsequently released with 900 μL (in 6 x 150 μL portions) of the K_{222}/K_2CO_3 solution into a 5 mL V-vial containing a magnetic stir bar in the concentrator. The solution was dried with five cycles of azeotropic drying with MeCN (5 x 200 μL) under a flow of N_2 at 105 °C. The dried [^{18}F]KF/K_{222} residue was redissolved in anhydrous MeCN (500 - 1000 μL).

General procedure for small scale heterocycle screening experiments with 4-(4,4,5,5-tetramethyl- 1,3,2-dioxaborolan-2-yl)benzonitrile:

A solution of [^{18}F]KF/K_{222} in MeCN (20 - 30 MBq, 10-50 μL) was dispensed into a V-vial containing $Cu(OTf)_2(py)_4$ (0.0053 mmol), 4-(4,4,5,5-tetramethyl-1,3,2-

dioxaborolan-2-yl)benzonitrile (13.7 mg, 0.06 mmol) and a magnetic stirrer bar. Air (20 mL) was flushed through the reaction vial using a syringe and then a solution containing the heterocycle (0.06 mmol) in DMF (300 μL) was added via syringe. The sealed vial was heated at 110 °C for 20 min. The reaction was quenched by addition of water (200 μL). An aliquot was removed for analysis by radioTLC and HPLC for radiochemical conversion and product identity. Analysis was performed using a Waters Nova-Pak C18 column (4 μm, 3.9 x 150 mm) at a flow rate 1 mL/min. Radio-TLC was performed on Merck Kiesegel 60 F254 plates, using n-hexane/EtOAc (1:1) as eluent. Analysis was performed using a plastic scintillator/PMT detector.

General procedure for small scale ^{18}F-labeling of arenes:

A solution of [^{18}F]KF/K_{222} in MeCN (20 - 30 MBq, 10 - 50 μL) was dispensed into a V-vial containing Copper source (0.03 mmol), aryl pinacol boronate (0.02 mmol) and a magnetic stirrer bar. Air (20 mL) was flushed through the reaction vial using a syringe and then solvent (300 μL) was added via syringe. The sealed vial was heated at 110 °C for 20 min. The reaction was quenched by addition of water (200 μL). An aliquot was removed for analysis by radioTLC and HPLC for radiochemical conversion and product identity. Analysis was performed using the gradient given below with a Waters Nova-Pak C18 column (4 μm, 3.9 x 150 mm) at a flow rate 1 mL/min. Radio-TLC was performed on Merck Kiesegel 60 F254 plates, using as eluent DCM/MeOH (9:1). Analysis was performed using a plastic scintillator/PMT detector.

HPLC gradient for small scale heterocycle screening experiments and small scale ^{18}F-labeling of arenes:

Water/MeCN, 1 mL/min, Waters Nova-Pak C18 Column, 4 µm, 3.9 x 150 mm 0 - 1 min (5% MeCN) isocratic 1 - 10 min (5% MeCN to 95% MeCN) linear increase 10 - 14 min (95% MeCN) isocratic 14 - 15 min (95% MeCN to 5% MeCN) linear decrease 15 - 17 min (5% MeCN) isocratic.

Procedure for the Synthesis and Isolation of ^{18}F-Olaparib:

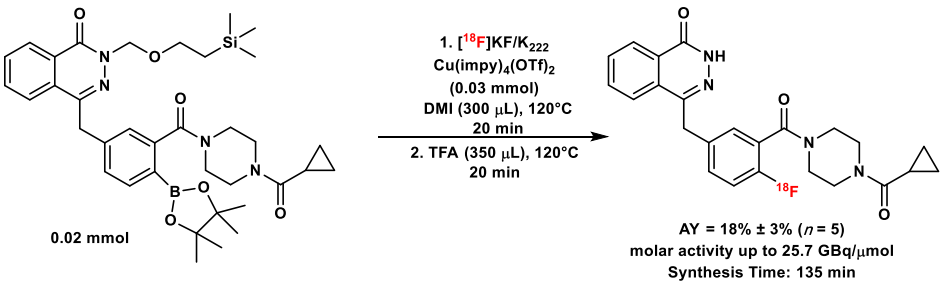

[^{18}F]Fluoride was separated from ^{18}O-enriched-water using an anion exchange cartridge (Sep-Pak Accell Plus QMA Carbonate Plus Light Cartridge, 46 mg Sorbent per Cartridge, 40 µm particle size, Waters) and released with 900 µL (in 6 x 150 µL portions) of a solution of $K_{222}/K_2C_2O_4/K_2CO_3$ (kryptofix 222 (6.3 mg), $K_2C_2O_4$ (1 mg) and K_2CO_3 (0.1 mg) in 1 mL of MeCN/H_2O, 4:1) into a 5 mL V-vial containing a magnetic stir bar in the concentrator. The solution was dried with five cycles of azeotropic drying with MeCN (5 x 200 µL) under a flow of N_2 at 105 °C. The 5 mL vial containing the dried [^{18}F]KF/K_{222} complex was purged with 30 mL of air using a syringe and then a solution of arylboronate precursor (13.4 mg, 0.02 mmol) and $Cu(OTf)_2(impy)_4$ (25 mg, 0.03 mmol) in anhydrous 1,3-dimethyl-2-imidazolidinone (DMI) (300 µL) was added. The mixture was heated at 120 °C for 20 min in a sealed vial with stirring. After 20 min, TFA (350 µL) was added and stirring was continued

at 120 °C for 20 min. The reaction was then cooled to room temperature before quenching with H_2O (6 mL) and eluting over an Oasis HLB Plus cartridge (preconditioned with 2 mL MeOH and 10 mL H_2O). The vial was then rinsed with CH_3CN:H_2O (1:9, 2.0 mL), and eluting over the Oasis HLB cartridge after which the product was eluted with CH_3CN (2.0 mL) into a 5 mL V-vial. The MeCN was evaporated under a flow of N_2 at 100 °C until approximately 50 μL remained. The reaction mixture was then diluted in with 28% MeCN/ 72% 25 mM NH_4HCO_2 in H_2O and loaded directly onto a 2 mL HPLC loop and injected on a semi-Prep HPLC column (Synergi 4μm Hydro-RP 250 x 10 mm) and eluted into a collection vial with 28% MeCN/ 72% 25 mM NH_4HCO_2 in H_2O monitoring with UV (254 nm) and radioactive traces. The ^{18}F-olaparib was collected in 10 mL of H_2O and eluted over an Oasis HLB Plus cartridge (preconditioned with 2 mL MeOH and 10 mL H_2O). The cartridge was washed with H_2O (1.0 mL), after which the product was eluted with EtOH (2.0 mL). The ethanol was evaporated under a flow of N_2 while heating at 100 °C. The dry residue was then re-dissolved in 10% DMSO/PBS (pH = 7.4).

The Molar Activity of [^{18}F]olaparib was assessed by radio-HPLC, using an analytical Synergi 4 μm Hydro-RP 80A column, 150 x 4.6 mm eluted with 25% MeCN/75% H2O (isocratic 1 mL/min), monitoring with UV (220 nm) and radioactive traces.

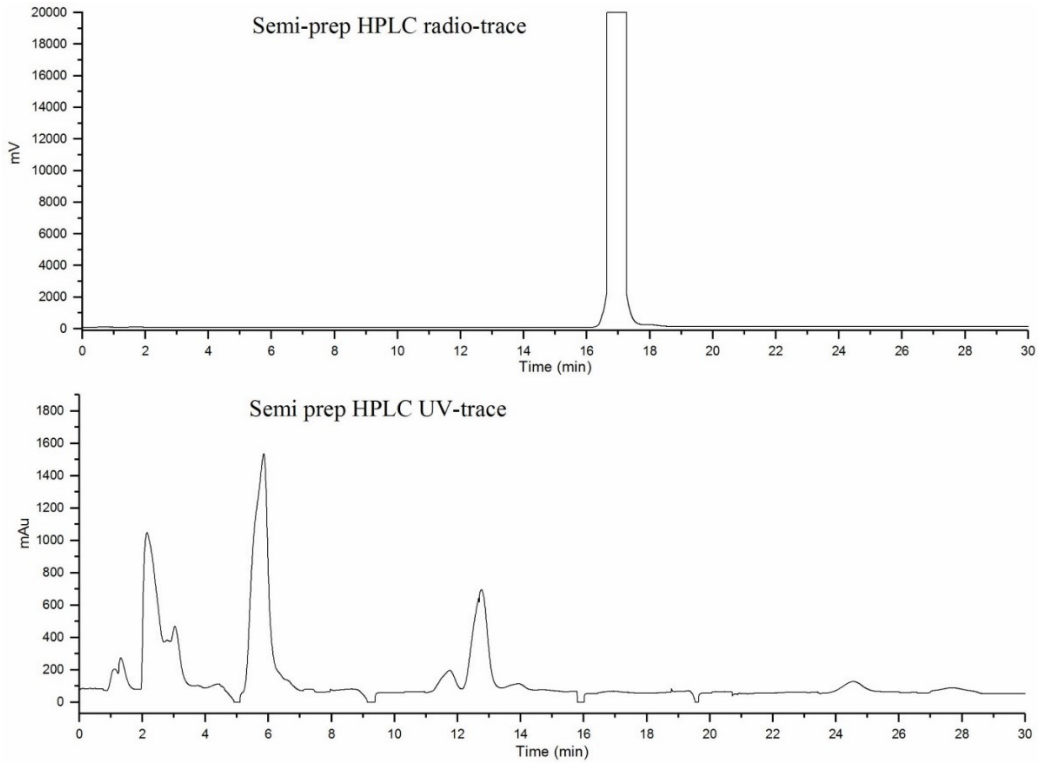

Semi-prep radioHPLC purification of ^{18}F-olaparib

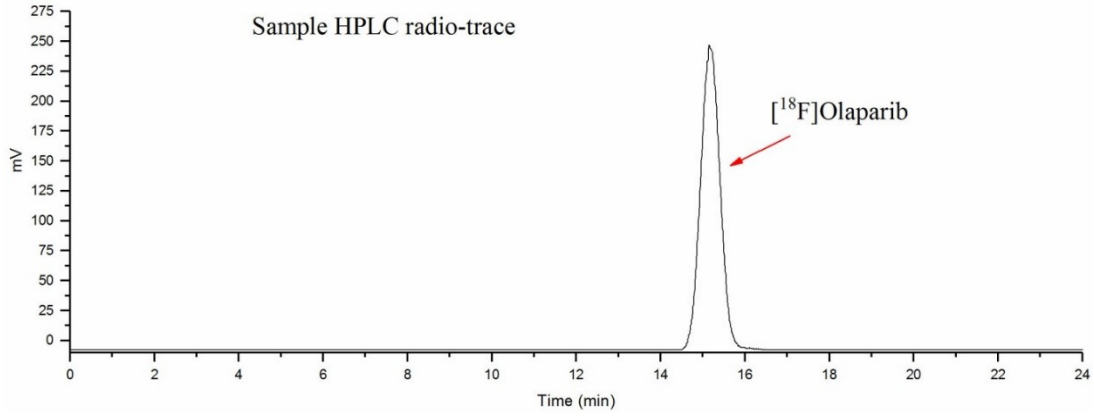

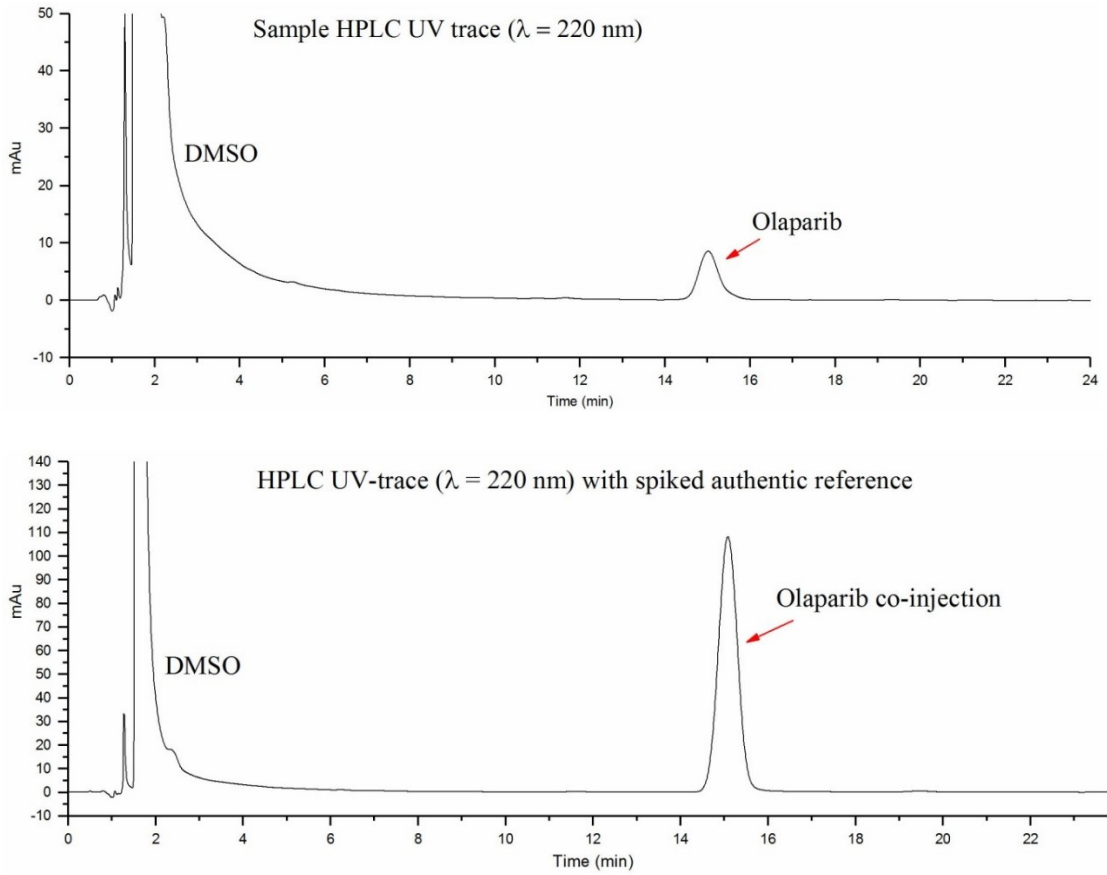

Purified ^{18}F-olaparib was injected onto an analytical column. Additionally, a sample spiked with an authentic reference sample of olaparib (0.7 μg) was analysed. Analytical HPLC conditions are listed in the previous section.

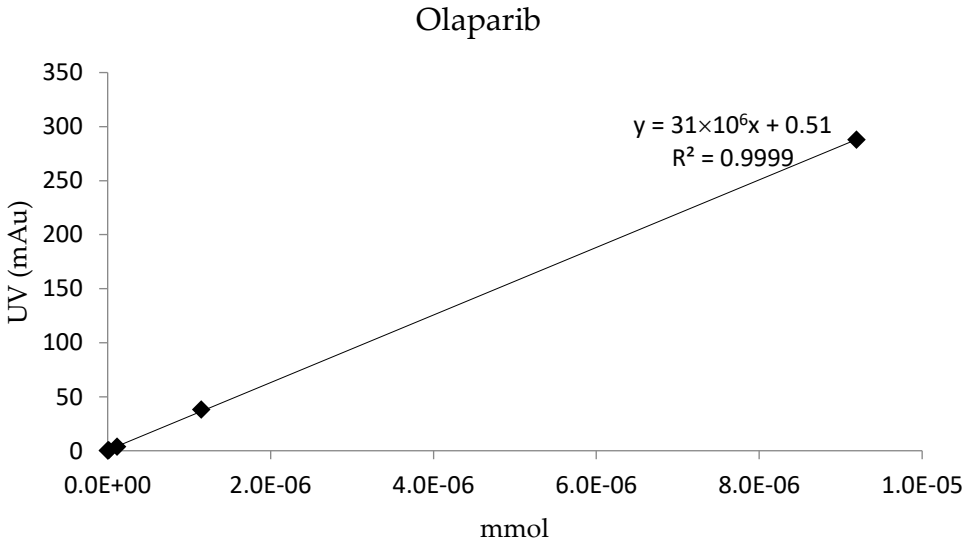

Injection Number	Activity (MBq)	Area (mAu)	Mmol injected (*10^{-7})	Molar Activity (GBq µmol^{-1})
1[a]	2.0	9.16	2.7	7.2
2[a]	1.4	4.82	1.3	10.4
3[a]	1.6	18.29	5.6	2.8
4[a]	0.7	2.73	0.71	9.8
5[a]	3.1	5.06	1.4	21.3
6[b]	1.1	3.67	1.0	10.9
7[b]	1.6	2.86	0.75	21.3
8[b]	1.7	2.58	0.66	25.7
9[b]	2.2	25.79	8.1	2.7
10[b]	2.6	5.79	1.7	15.4

Molar Activity Calculations for ^{18}F-olaparib Under oxalate drying conditions; [b]Under carbonate drying conditions.

5.5 Biological Procedures and Characterisation for Chapter II (carried out by M. A. Xavier and J. Knight):

5.5.1 Cells

PSN-1, MiaPaCa-2, and Capan-1 human pancreatic duct adenocarcinoma cells were originally purchased from ATCC. Cells were maintained in Dulbecco's Modified Eagle Medium (DMEM), supplemented with 10% foetal bovine serum (FBS), 2 mM L-glutamine, 100 units/mL penicillin, and 0.1 mg/mL streptomycin. Cells were grown in a 37 °C environment containing 5% CO_2 and were harvested and passaged as required using Trypsin-EDTA solution. Cells were authenticated by the provider and the cumulative length of culture was less than 6 months following retrieval from liquid nitrogen storage. Cells were regularly tested to confirm the absence of mycoplasma contamination. Capan-1 cells used in this study were subsequently found

by STR profiling not to match with the ATCC-held profile. However, low PARP enzyme expression was confirmed by Western blot and immunohistochemistry.

5.5.2 Western Blot

Western blot probing for PARP-1 was performed after cells were exposed to external beam radiation (0 or 10 Gy; 137Cs source, using a using an IBL-637 137Cs irradiator, Cisbio International; 1 Gy/min) with 2 or 24 hours recovery.

Total protein preparations were produced at 4 °C on approximately 1×10^7 cells using RIPA lysis buffer (50 mM Tris, pH 8, 1% NP40, 0.5% sodium deoxycholate, 0.1% sodium dodecyl sulphate, 150 mM sodium chloride, cOmplete™ protease inhibitor cocktail [Sigma-Aldrich]). The cell lysates were isolated by centrifugation after lysis through a 21G hypodermic syringe and 30 second sonication. Thirty microgram lysate samples were run on a 4-12% Bis-Tris MES gel (Novex), transferred to a PVDF membrane and exposed to a 1:500 dilution of anti-PARP-1 antibody (Proteintech 13371-ap-1, lot 00045356) or anti-PGP-1 (abcam 170904, 1:2000), followed by a 1:3000 dilution of the secondary goat anti-rabbit-HRP (Bio-Rad). The membrane was exposed to autoradiography film after development using an ECL western blot substrate solution (Pierce Thermo Scientific 32209). β-actin was used as the loading control.

5.5.3 Immunocytochemistry

Cells were plated onto 8-chamber slides (Falcon CultureSlides) at 7×10^4 cells per chamber in 0.75 mL culture media and incubated overnight in a 37 °C CO_2 incubator until approximately 80% confluent. The slides were briefly in phosphate-buffered

saline (PBS) pH 7.4, and the cells fixed in 4% formaldehyde/PBS for 10 min. The slides were washed in PBS for 3 x 5 minutes, and cells permeabilized in 0.5% Triton X100 (Sigma) for 10 min. The cells were washed as before and non-specific binding was blocked by incubation of the slides in 2% BSA/PBS for 1 hour. To each appropriate section approximately 100 μL primary antibody diluted 1:100 and 1:250 in 2% BSA/PBS, or just 2% BSA/PBS, was applied, and incubated in a humid chamber for 2 hours. The primary antibodies used was anti-PARP-1 rabbit polyclonal (ProteinTech 13371-ap-1). The slides were washed in PBS for 3 x 5 minutes, and the secondary goat-anti-rabbit IgG-594 antibody (Life Technologies Alexa Fluor, 1:500 dilution in 2% BSA/PBS), was applied and incubated for 1 hour. The slides were then washed in PBS for 3 x 5 minutes, excess fluid removed with a tissue, and a drop of Vectashield + DAPI (Vector Laboratories) was applied to each section. Finally, a coverslip was gently lowered onto each slide, and Covergrip (Biotium) used to seal the coverslips. Prepared slides were stored at 4 °C in the dark. The slides were analysed using a Leica SP8 confocal fluorescent microscope.

5.5.4 Cell uptake experiments

Cell uptake of [^{18}F]olaparib in PSN-1, MiaPaCa-2 and Capan-1 cells was determined as previously described (*8-10*). Aliquots of cells (1.5×105 cells/well) were seeded in 24-well plates in warm cell culture medium (500 μL) and the cells were allowed to adhere overnight. Cells were irradiated (10 Gy; dose rate 0.8 Gy/min) or sham-irradiated and then returned to an incubator (37 °C, 5% CO_2) for 2-48 h. The cell culture medium was then removed and cells were washed once with fresh cell culture medium (500 μL). In 500 μL of cell culture medium (not supplemented with FBS, L-

glutamine, or penicillin/streptomycin), [^{18}F]olaparib (50 kBq) was added to each well and the cells were then incubated at 37 °C. In the blocking groups, non-radioactive olaparib, talazoparib, or rucaparib were also added in increasing concentrations (10 pM - 10 μM. After 30 or 60 minutes, the cell culture medium was removed and combined with two washes (500 μL) of cell culture medium. The remaining monolayer of cells was then lysed with 0.1 M sodium hydroxide for 20 minutes at room temperature. The amount of radioactivity contained within the cell culture medium and the cell lysate fractions was measured using a gamma counter. Protein levels from parallel plates were quantified using a Pierce BCA protein assay kit (Thermo Scientific) according to the manufacturer's recommendations and bovine serum albumin was used as the protein standard. Cell uptake levels of 18F-olaparib were normalized to percent of the total added radioactivity per milligram protein. These experiments were performed in triplicate on at least three separate occasions. IC50 values were calculated using GraphPad Prism software (GraphPad Software, San Diego, CA, USA). Data are presented as mean ± SEM.

5.5.5 Radiation dose dependency

Aliquots of cells ($7.5\times10_4$ cells/well) were seeded in 24-well plates in warm cell culture medium (500 μL). After 4 h, cells were irradiated (0, 2, 4, 6, 8, or 10 Gy; dose rate 0.8 Gy/min) and then returned to an incubator (37 °C, 5% CO_2). After 24 or 48 h, the cell culture medium was then removed, and cells were washed once with fresh cell culture medium (500 μL). In 500 μL of cell culture medium (not supplemented with FBS, L-glutamine, or penicillin/streptomycin), [^{18}F]olaparib (50 kBq) was added to each well and the cells were then incubated at 37 °C. In the blocking groups, non-

radioactive olaparib was also added to each well to achieve a concentration of 10 μM. After 30 minutes, the cell culture medium was removed and combined with two washes (500 μL) of cell culture medium. The remaining monolayer of cells was then lysed with 0.1 M sodium hydroxide for 20 minutes at room temperature. The amount of radioactivity contained within the cell culture medium and the cell lysate fractions was measured using a gamma counter. Protein levels from parallel plates were quantified using a Pierce BCA protein assay kit (Thermo Scientific) according to the manufacturer's recommendations and bovine serum albumin was used as the protein standard. Radiotracer cell uptake levels were normalized to percent of the total added radioactivity per milligram protein.

5.5.6 In vivo tumour models

All animal procedures were performed in accordance with the UK Animals (Scientific Procedures) Act 1986 and with local ethical committee approval. Animals were housed in IVC cages in sex-matched groups up to 5 per cage, in an artificial day-night cycle facility, with ad libitum access to food and water.

5.5.7 PSN-1 and Capan-1

Cells were harvested using trypsin, washed twice using PBS, and reconstituted in DMEM. PSN-1 or Capan-1 xenograft tumours were established in the right hind flank of female NOD/SCID mice (Charles River, UK) by subcutaneous injection of 1×10^6 cells in PBS:matrigel (150 μL). Tumour volumes (V) were calculated after calliper measurement using the following equation: $V = (a^2 \times b)/2$, where a is the width of the tumour and b the length (small and large diameters, respectively). The

individual relative tumour volume (RTV) was defined as $Vt/V0$, where Vt is the volume at a given time and $V0$ at the start of treatment. Animals were entered in in vivo studies when their tumour was at least 200 mm^3.

5.5.8 CaNT

The murine adenocarcinoma NT (CaNT) was implanted subcutaneously onto the right thigh of 6 – 7 weeks old female CBA/Carl mice. 50 μL of a crude cell suspension, prepared by mechanical dissociation of an excised tumour from a donor animal, was injected. Tumours were selected for imaging when the geometric mean diameter reached 6-8 mm (volumes calculated as above), approximately 3 weeks after implantation.

5.5.9 Irradiation of tumours

Irradiation of subcutaneous tumour xenografts was performed using a Gulmay 320 kV system (2.0 Gy/min). A dose of 10 Gy was delivered to the tumour using 300 kV X-rays (Gulmay 320kV irradiator; 2 Gy/min). The radiation set-up allowed irradiation of the right hind quarter, including the tumour and right leg, only. Control mice were anesthetized and sham-irradiated for the same length of time. Irradiation was performed 2 hours prior to administration of [^{18}F]olaparib.

5.5.10 PET/CT Imaging: [^{18}F]olaparib PET imaging

Two hours prior to PET/CT imaging, animals were exposed to X-irradiation of the tumour (10 Gy or sham) (see schedule below). Radiation was delivered using a Gulmay 320 kV X-irradiator; 2.0 Gy/min. Anesthesia was maintained at 2.5 % isoflurane throughout the duration of the irradiation, and animals were allowed to

recover. To study the relationship of PARP-1 expression, [^{18}F]olaparib uptake and hypoxia, the same animals were administered EF_5 (0.6 μg in 200 μL 0.9% saline) intraperitoneally, one hour prior to PET/CT imaging. Some animals were administered an excess of cold, unlabelled olaparib (0.5 mg in 250 ml 10%DMSO (v/v) in PBS), intravenously, 30 minutes prior to administration of 18F-olaparib. Naïve CBA/Carl mice, not bearing tumours, were not irradiated, nor was EF_5 administered.

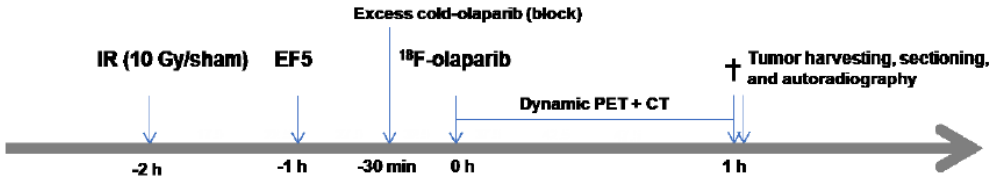

Dynamic PET/CT images were acquired using a VECTor4CT integrated PET/CT system. Mice were anesthetized by 4% isoflurane gas (0.5 L/min O_2) and placed on a custom-built imaging cradle in a prone position. Animals were intravenously injected with [^{18}F]olaparib or (3 – 5 MBq, 8 – 11 GBq μmol^{-1}, through a tail vein catheter, and dynamic imaging was performed over 45-60 min after radiolabeled compound administration. PET acquisition (150 s per frame, using list mode acquisition) using an ultra-high-resolution rat/mouse 1.8 mm collimator, followed by a cone-beam CT scan (55 kV, 0.19 mA) for anatomical reference and attenuation correction. Anesthesia was maintained at 2.5 % isoflurane throughout the duration of the image acquisition. PET images were reconstructed using U-SPECT-Rec3.22 software (MILabs, Utrecht, The Netherlands), applying a pixel-based algorithm with 8 subsets, 6 iterations and 0.8 mm voxel size for ^{18}F (energy window settings 477.9-584.1 keV).

5.5.11 Image analysis

Reconstructed images were viewed and analyzed using PMOD v.3.37 (PMOD Technologies, Zurich, Switzerland). The radioactivity in each volume of interest was calculated as percent injected dose per cubic cm (%ID/mL).

5.5.12 Ex vivo biodistribution

After PET/CT image acquisition, animals were euthanized by cervical dislocation and selected organs, tissues and blood were removed. The amount of radioactivity in each organ was measured using a 2480 WIZARD2 gamma counter (PerkinElmer). Counts per minute were converted into MBq using a calibration curve generated from known standards. Values were decay-corrected to the time of injection, and the percentage of the injected dose per gram (%ID/g) of each tissue was calculated.

5.5.13 Ex vivo analysis

5.5.14 Autoradiography

After imaging and automated gamma counting, selected tissues from mice were flash-frozen with dry ice. If required, samples were stored at −80 °C overnight. Frozen tissue was sectioned (8 μm) using an OTF5000 cryotome (Bright Instruments Ltd). Tissue sections were thaw-mounted onto Superfrost PLUS glass microscope slides (Menzel-Glaser, Thermo Scientific) and allowed to dry at room temperature. The slides were then exposed to a storage phosphor screen (PerkinElmer, Super Resolution, 12.5 x 25.2 cm) in a standard X-ray cassette for 15 h at 4 °C or −20 °C. The phosphor screen was then imaged using a Cyclone® Plus Storage Phosphor

System (PerkinElmer) and images were analysed with OptiQuant 5.0 (PerkinElmer) and ImageJ (NIH).

5.5.15 Immunohistochemistry

5.5.16 PARP-1 staining:

PSN-1 xenografts harvested from mice were flash frozen and 8 μm sections were prepared using a cryostat. Sections were stored at −80 °C until use. Slides were allowed to reach room temperature (10 minutes), then washed briefly in phosphate-buffered saline (PBS) pH 7.4. The slides were fixed in 4% formaldehyde/PBS for 10 min, then washed three times in PBS for 5 min. Sections were permeabilized in 0.5% Triton X100 (Sigma) for 10 min, washed, and non-specific binding was blocked by incubation of the slides in 2% BSA/PBS for 1 h. Slides were briefly allowed to dry and each section was isolated using a PAP pen (Sigma). To each appropriate section approximately 100 μL primary anti-PARP-1 polyclonal antibody (ProteinTech 13371-AP-1) diluted 1:250 in 2% BSA/PBS, or just 2% BSA/PBS, was applied, and incubated in a humid chamber overnight at 4 °C. The slides were washed three times in PBS for 5 min, and the secondary goat-anti-rabbit IgG-488 antibody (Life Technologies Alexa Fluor, 1:500 dilution in 2% BSA/PBS), was applied and incubated for 1 h. The slides were then washed in PBS, excess fluid removed, mounted using Vectashield containing DAPI (Vector Laboratories). Slides were stored at 4 °C in the dark. Images were acquired using a Leica SP8 confocal fluorescent microscope.

5.5.17 EF_5 staining:

Tumour hypoxia was confirmed by immunohistological staining for EF5 (2-(2-nitro-1H-imidazol-1-yl)-N-(2,2,3,3,3-pentafluoropropyl)-acetamide). For EF_5 studies, mice were administered with 10 mM EF5 in 0.9% saline i.v. 2 h prior to tumour excision (EF5 was obtained from Dr. Cameron Koch, University of Pennsylvania (*12*)). To determine the correlation between [^{18}F]olaparib uptake and hypoxia, tumour slices were analysed by both autoradiography and EF_5 IHC (*13*) (*11*) (*14*). Object-based overlap between both modalities was determined by first co-registering autoradiography and fluorescence microscopy images using a rigid transformation. Then, Manders' overlap coefficients (M1) were calculated using the JACoP plug-in for Image J (methods of Manders for spatial intensity correlation analysis with Costes method for automatic thresholding).

5.5.18 Statistical methods

All statistical analyses and nonlinear regression were performed using GraphPad Prism (GraphPad Software, San Diego, CA, USA). Data were tested for normality and analysed either by the unpaired, two-tailed Student's t-test where appropriate, or 1-way analysis of variance (ANOVA) for multiple comparisons, with Dunnet's post-tests to calculate significance of differences between groups. All data were obtained at least in triplicate and results reported as mean ± standard deviation, unless stated otherwise.

5.5.19 Biodistribution data

	%ID/g		
Blood	0.11	0.11	0.14
Heart	0.19	0.17	0.34
Lung	0.29	0.19	0.34
Liver	2.55	4.02	5.27
Spleen	2.09	1.91	3.68
Stomach	0.46	0.26	0.58
Large intestine	0.92	1.64	2.99
Small intestine	7.75	10.33	17.40
Pancreas	0.91	0.70	1.30
Kidney	0.59	0.60	1.01
Muscle	0.20	0.14	0.34
Skin	0.16	0.10	0.27
Fat	0.05	0.03	0.26

Ex vivo biodistribution [^{18}F]olaparib in naïve CBA/Carl mice.

	[^{18}F]olaparib						**[^{18}F]olaparib + IR (10 Gy)**			**[^{18}F]olaparib + block**			
Blood	0.41	0.73	0.57	0.24	0.21	0.19	0.63	0.83	1.17	2.12	2.29	2.51	1.06
Tumour	1.94	4.07	4.20	3.27	2.43	3.07	6.43	3.03	6.59	1.68	0.92	1.09	1.09
Heart	3.18	2.05	1.74	1.58	0.85	1.07	3.14	2.49	2.88	1.98	1.59	1.51	0.78
Lung	4.68	3.51	3.18	2.15	1.45	1.69	3.94	4.47	4.47	1.61	1.40	1.32	0.74
Liver	26.2	34.6	27.0	21.0	13.5	18.0	25.1	33.8	45.7	29.1	32.9	22.4	23.1
Spleen	17.5	13.7	11.3	14.0	7.36	8.01	45.0	20.5	14.3	1.62	1.46	1.24	0.69
Stomach	2.59	3.53	1.81	1.80	0.55	0.60	4.15	0.92	0.87	1.44	0.79	0.46	0.21
Large intestine	12.6	30.5	80.8	27.0	28.9	6.61	27.5	28.9	16.2	20.1	13.3	61.4	12.7
Small intestine	54.5	58.1	30.6	31.9	18.6	26.6	65.1	113	95.2	89.9	77.2	96.4	132
Pancreas	8.49	9.38	7.25	5.52	2.78	4.24	13.6	10.3	11.4	1.92	2.29	1.91	1.79
Kidney	10.5	7.95	6.02	7.04	3.41	3.66	10.0	9.25	10.6	13.1	5.09	3.98	2.44

Muscle	1.60	1.40	1.45	1.12	0.70	0.73	3.71	2.01	1.76	1.58	1.08	1.18	0.65
Bone	3.38	4.54	2.71	1.88	1.26	1.50	9.12	4.13	3.81	1.06	0.78	0.80	0.46
Skin	1.50	1.75	2.06	1.25	0.87	1.14	2.10	2.38	2.66	1.65	1.09	1.10	0.66
Fat	0.97	0.82	0.68	0.45	0.44	0.37	0.66	1.41	0.82	0.53	0.62	0.35	0.19

Ex vivo biodistribution [^{18}F]olaparib in PSN-1 xenograft bearing mice.

	[^{18}F]olaparib				**[^{18}F]olaparib + IR (10 Gy)**			**[^{18}F]olaparib + block**		
Blood	0.30	0.23	0.31	0.72	0.86	0.43	1.16	0.25	0.27	0.56
Tumour	2.48	3.21	2.94	1.73	1.85	1.70	2.48	1.27	1.04	0.69
Heart	1.75	0.87	1.81	2.24	0.92	0.48	0.80	0.53	1.62	1.83
Lung	2.60	1.49	2.66	3.97	0.83	0.60	0.85	0.90	2.04	1.86
Liver	11.78	5.79	10.32	22.63	9.16	5.93	6.67	3.62	6.88	9.79
Spleen	9.84	6.13	8.40	15.10	0.77	0.73	0.82	2.80	7.93	6.43
Stomach	1.55	0.63	1.14	3.42	0.38	0.36	0.64	0.30	0.49	0.94
Large intestine	4.99	4.50	4.14	8.14	5.21	3.30	5.86	2.91	4.06	5.00
Small Intestine	12.27	17.29	11.58	13.70	15.58	9.80	19.97	0.45	11.70	46.04
Pancreas	9.32	8.12	7.87	13.16	1.89	1.59	1.84	4.56	10.82	10.22
Kidney	4.32	2.05	4.91	5.22	4.66	1.03	3.67	1.26	3.32	4.16
Muscle	0.65	0.45	0.63	1.44	0.63	0.29	0.48	0.28	0.65	0.88
Bone	1.46	0.98	1.26	3.08	0.31	0.16	0.19	0.47	1.27	2.17
Skin	0.02	0.55	0.77	1.54	0.67	0.23	0.33	0.14	0.46	1.16
Fat	0.46	0.19	0.27	0.69	0.24	0.13	0.19	0.22	0.77	0.36
Brain	0.82	0.03	0.03	0.10	0.06	0.03	0.03	0.03	0.03	0.04
Caecum	5.11	4.35	3.31	24.11	7.58	4.46	5.92	9.13	4.00	5.07
Gallbladder	81.02	24.53	34.02	446.94	68.68	31.81	36.90	105.86	35.11	88.82

Ex vivo biodistribution [^{18}F]olaparib in Capan-1 xenograft bearing mice.

	[18F]olaparib		[18F]olaparib + IR (10 Gy)		[18F]olaparib + block
Blood	1.78	8.00	9.79	3.12	4.00
Tumour	1.48	2.83	1.43	1.92	0.98
Heart	7.34	0.00	8.74	7.03	2.51
Lung	12.5	9.73	10.9	9.61	2.29
Liver	84.6	110	93.2	100	74.3
Spleen	43.3	47.0	69.0	58.3	2.41
Stomach	6.17	12.8	9.40	4.20	4.09
Large intestine	24.0	47.8	60.1	47.0	61.2
Small intestine	200	279	455	190	603
Pancreas	15.1	20.8	29.5	23.6	3.41
Kidney	23.9	21.0	24.5	19.0	8.45
Muscle	5.84	4.63	5.45	5.31	2.65
Bone	11.7	10.2	15.7	11.5	5.18
Skin	3.82	4.65	5.02	5.12	1.16
Fat	7.19	1.12	2.52	2.34	1.57
Brain	0.29	0.23	0.20	0.25	0.22
Caecum	32.5	56.2	42.9	44.6	101
Gallbladder	953	126	155	57.3	194

Ex vivo biodistribution [18F]olaparib in CaNT allograft bearing CBA/Carl mice.

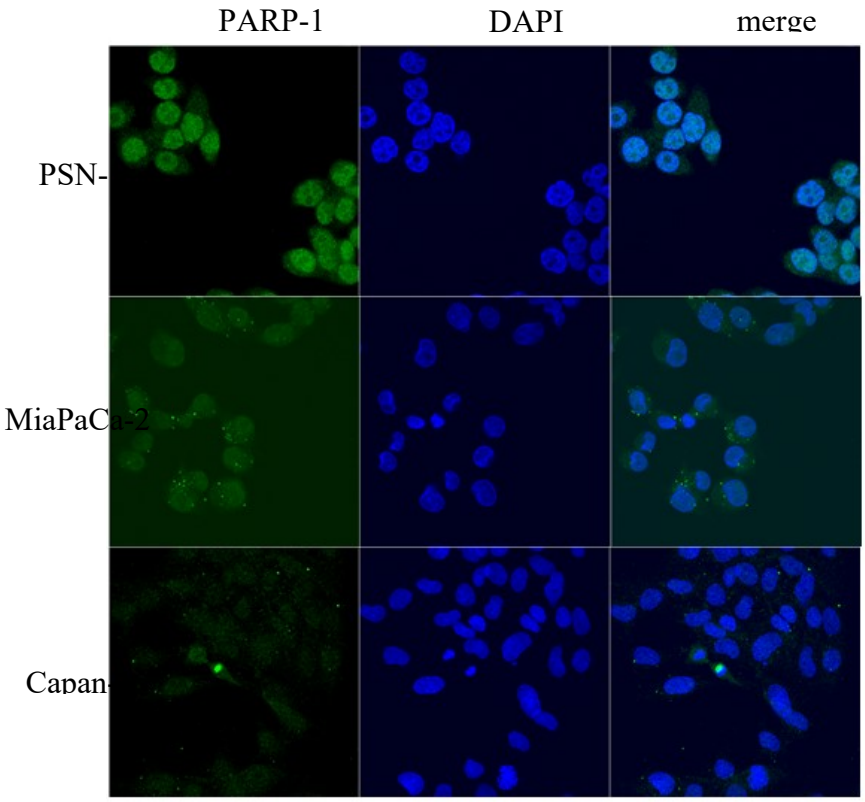

Immunocytochemistry of PARP-1 in a selection of PDAC cell lines.

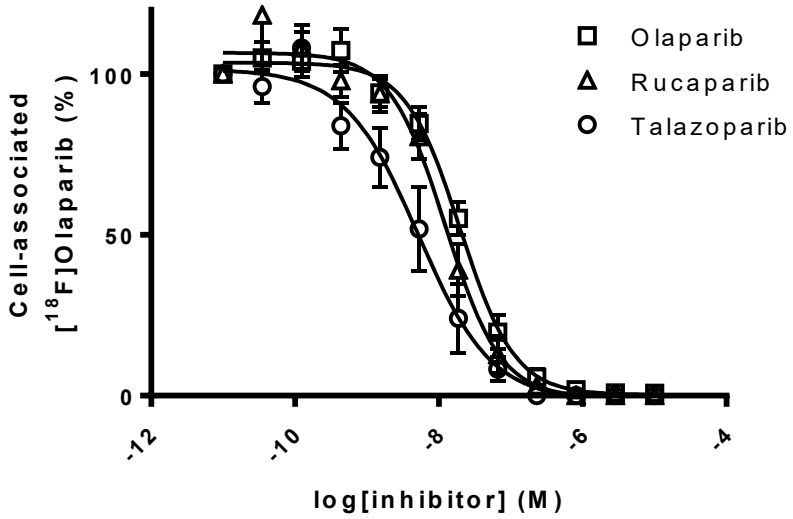

Displacement of [^{18}F]olaparib uptake in PSN-1 cells by a selection of several PARP inhibitors.

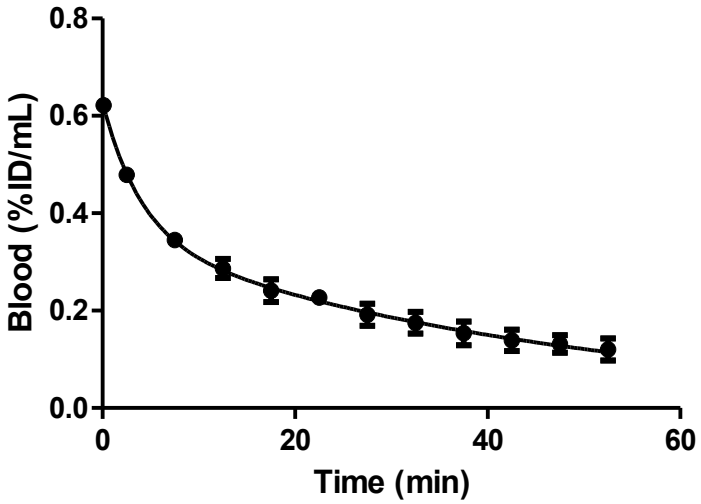

Concentration of [^{18}F]olaparib in blood of naïve CBA/Carl mice.

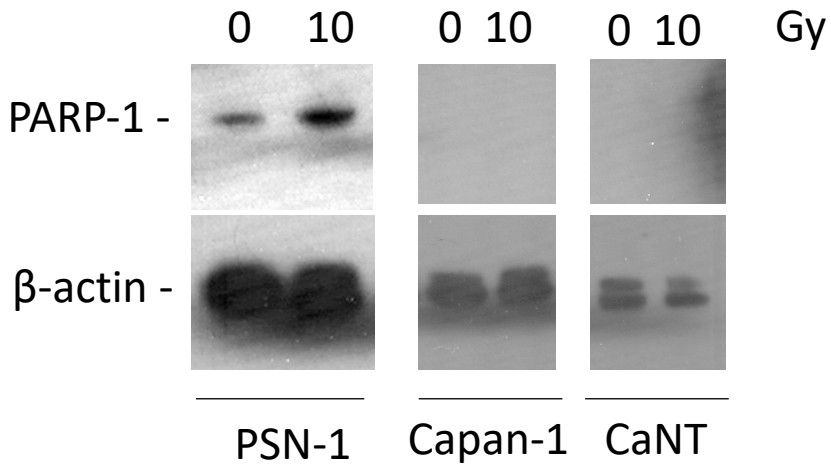

Western blot of xenograft tumour tissue from PSN-1, Capan-1, and CaNT tumours, after irradiation (10 Gy) or sham-irradiation (0 Gy). Xenografts from randomly selected animals were analysed.

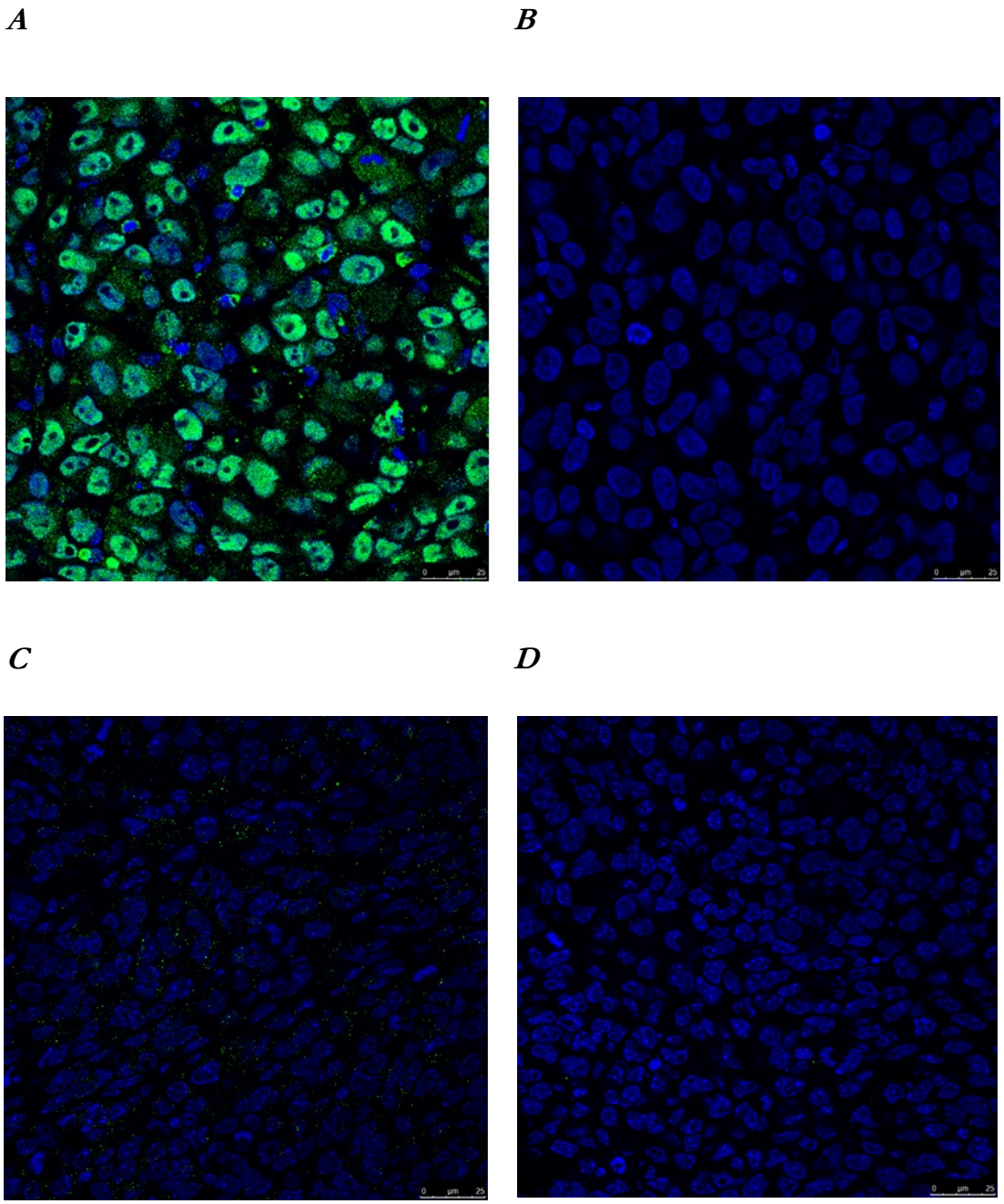

Immunohistochemistry staining for PARP-1 on xenograft tumour tissue from PSN-1 (A), CaNT tumours (C). Controls using only secondary antibody showed minimal non-specific staining (B, D).

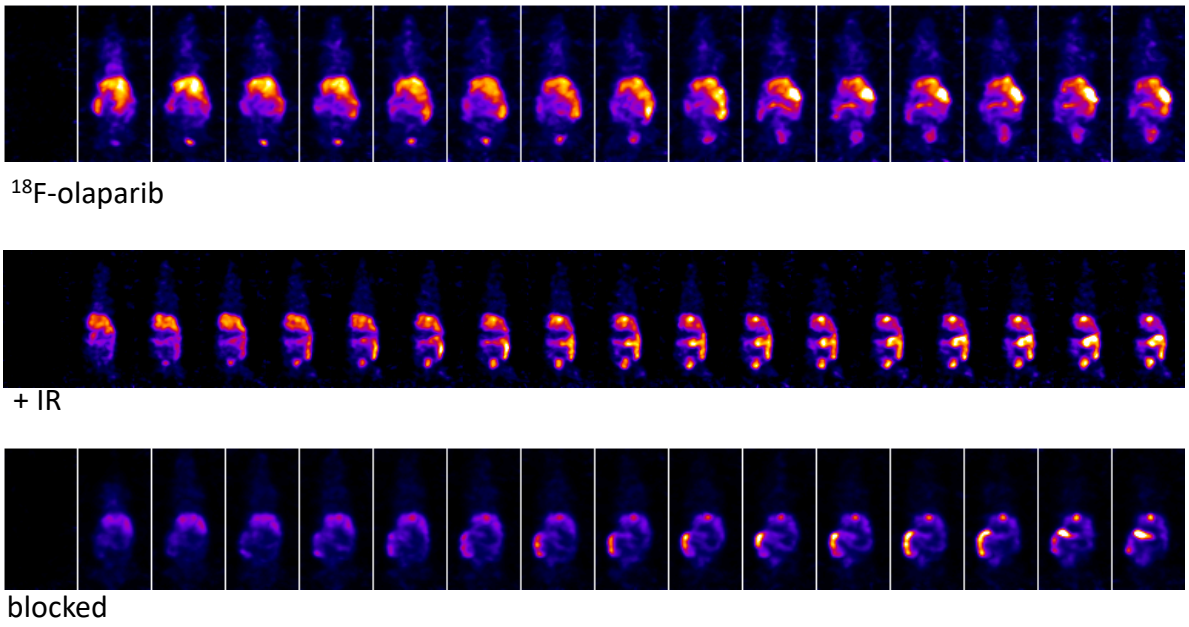

(A) Representative dynamic PET images after intravenous bolus injection of [18F]olaparib in PSN-1 tumour-bearing mice. Images are presented as coronal Maximum Intensity Projections

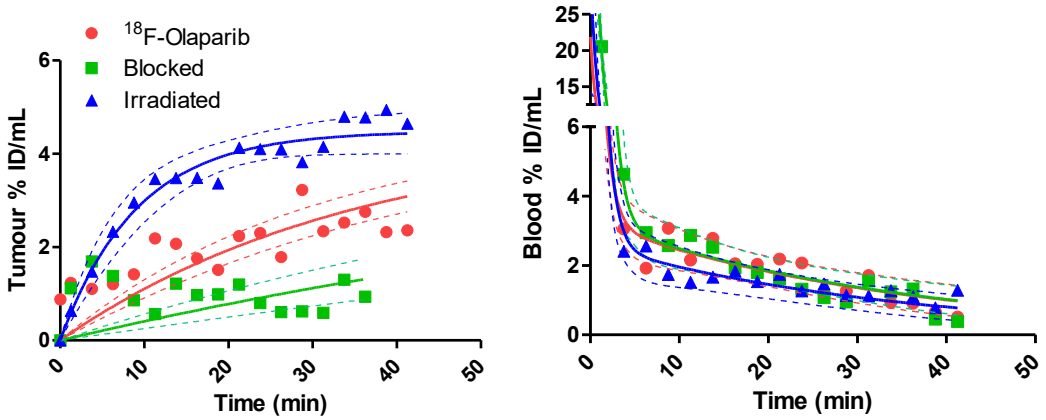

Image quantification of dynamic PET images after intravenous bolus injection of [18F]olaparib in PSN-1 tumour-bearing mice. Images

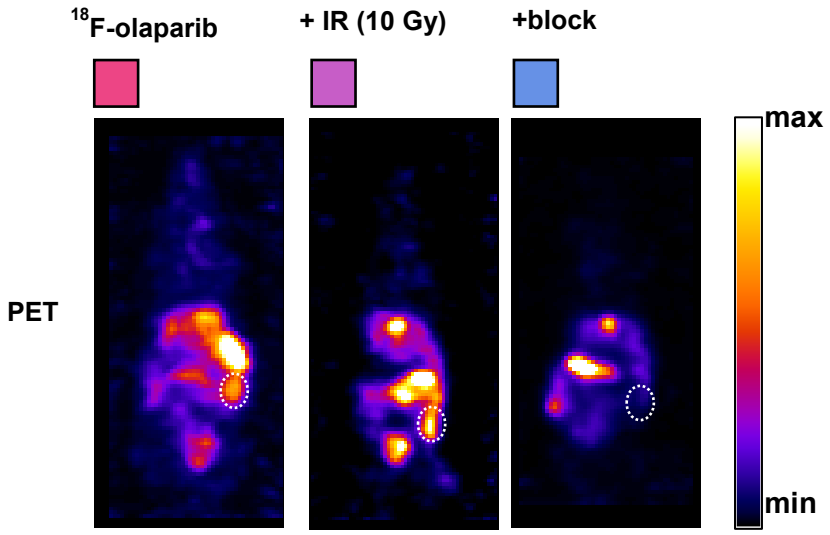

Maximum intensity projections of the same animals, using the same colour scale. Dashed circles indicate the position of the xenograft tumour.

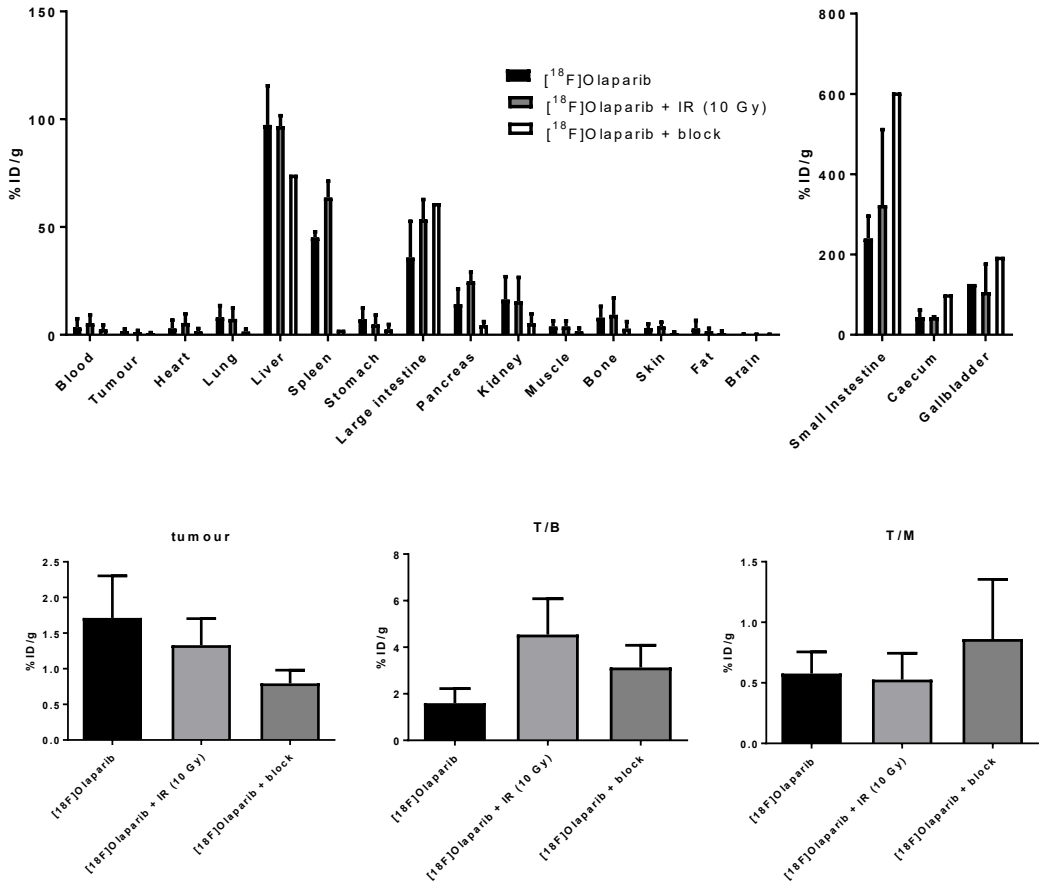

Ex vivo biodistribution of [18F]olaparib in CaNT tumour-bearing mice, 1 h after intravenous injection.

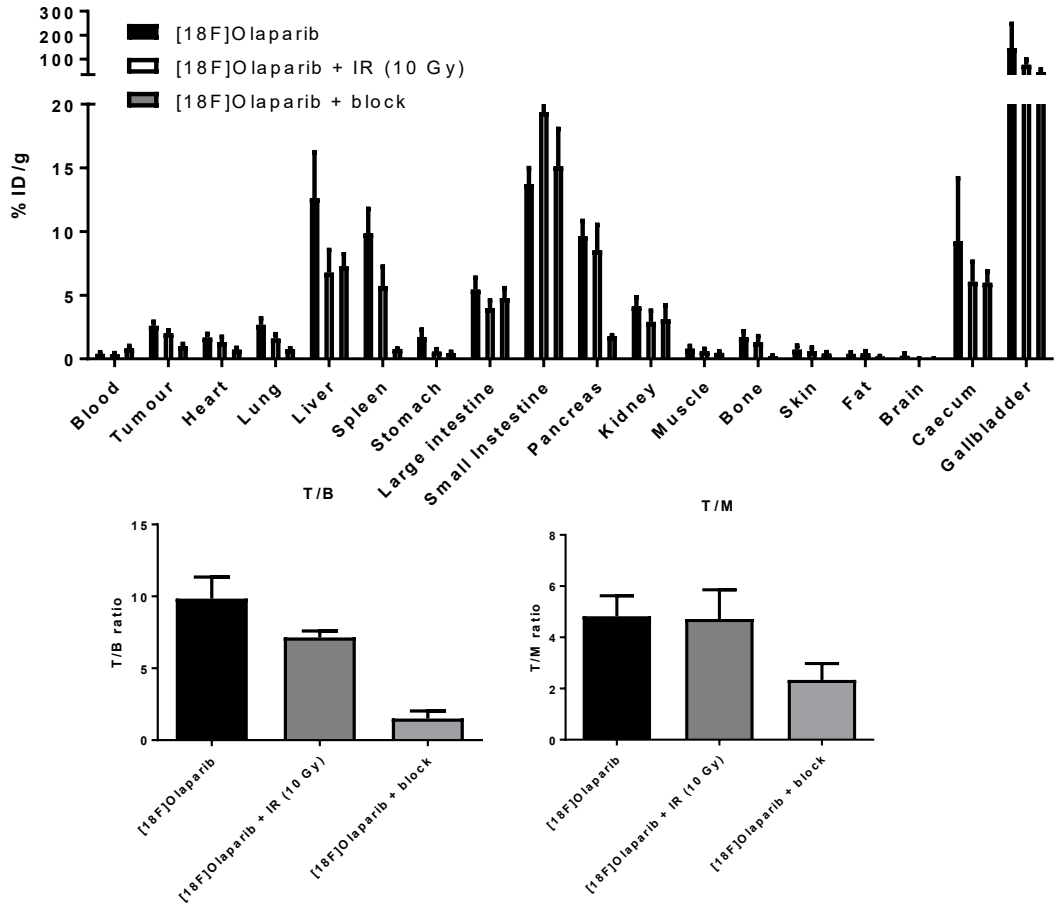

:

Ex vivo biodistribution of [^{18}F]olaparib in Capan-1 tumour-bearing mice, 1 h after intravenous injection.

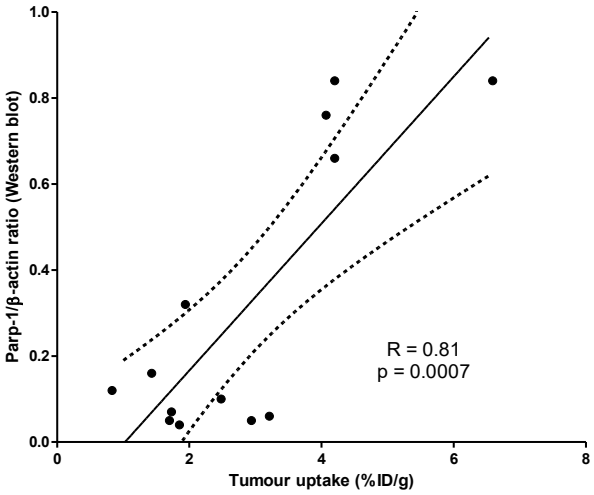

Correlation of tumour uptake determined by ex vivo biodistribution and PARP-1 expression measure via Western blot

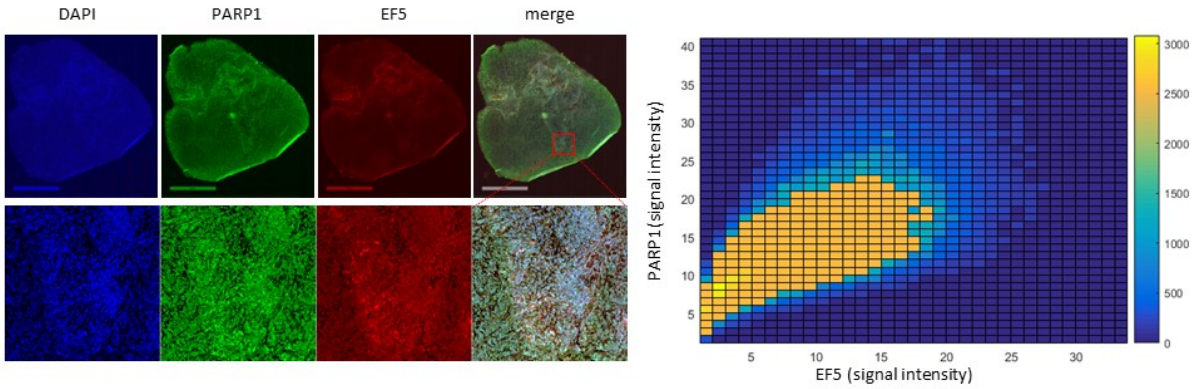

Representative section from a naive PSN-1 xenograft tumour, stained for PARP-1 and EF5, including a representative high-resolution detail, and a cytofluorogram comparing PARP-1 versus EF5 signal intensity in the high-resolution image.

5.6 Radiochemical Procedures and Characterisation for Compounds in Chapter III:

HPLC Eluents

Analysis was performed on a Phenomenex Synergi Hydro RP 4 μm 80A 150 x

4.6mm column unless otherwise noted.

Eluent A
Solvent A = H_2O + 0.1% HCO_2H, Solvent B = CH_3CN + 0.1% HCO_2H, flow rate = 1 mL/min
0 - 1 min = 25% B
1 - 10 min = 25% B to 95% B
10 - 14 min = 95% B
14 - 15 min = 95% B to 25% B
15 - 18 min = 25% B

Eluent B
Solvent A = H_2O + 0.1% HCO_2H, Solvent B = CH_3CN + 0.1% HCO_2H, flow rate = 1 mL/min
0 - 1 min = 5% B
1 - 10 min = 5% B to 95% B
10 - 14 min = 95% B
14 - 15 min = 95% B to 5% B
15 - 18 min = 5% B

Eluent C
Solvent A = H_2O + 0.1% HCO_2H, Solvent B = CH_3CN + 0.1% HCO_2H, flow rate = 1 mL/min
0 - 1 min = 5% B
1 - 20 min = 5% B to 95% B
20 - 24 min = 95% B
24 - 25 min = 95% B to 5% B
25 - 28 min = 5% B

Eluent D
Solvent A = H_2O + 0.1% HCO_2H, Solvent B = CH_3CN + 0.1% HCO_2H, flow rate = 0.8 mL/min
0 - 2 min = 5% B
2 - 20 min = 5% B to 50% B
20 - 22 min = 50% B
22 - 23 min = 50% B to 85% B
23 - 28 min = 85% B
28 - 29 min = 85% B to 5% B
29 - 33 min = 5% B

Eluent E
Solvent A = H_2O + 0.1% TFA, Solvent B = CH_3CN + 0.1% TFA, flow rate = 1 mL/min
0 - 2 min = 5% B
2 - 20 min = 5% B to 50% B
20 - 22 min = 50% B
22 - 23 min = 50% B to 85% B
23 - 28 min = 85% B
28 - 29 min = 85% B to 5% B
29 - 33 min = 5% B

Eluent F
Solvent A = H_2O + 0.1% HCO_2H, Solvent B = CH_3CN + 0.1% HCO_2H, flow rate = 0.8 mL/min
0 - 2 min = 5% B
2 - 32 min = 5% B to 65% B
32 - 34 min = 65% B
34 - 35 min = 65% B to 5% B
35 - 40 min = 5% B

Eluent G
Solvent A = H_2O + 0.1% TFA, Solvent B = CH_3CN + 0.1% TFA, flow rate = 1 mL/min
0 - 4 min = 0% B to 5% B
4 - 10 min = 5% B
10 - 20 min = 5% B to 80% B
20 - 23 min = 80% B
23 - 24 min = 80% B to 0% B
24 - 29 min = 0% B

Sep-Pak Cartridges Used for Purification

Waters Sep-Pak Al_2O_3 N light cartridge (part # WAT023561), Waters Sep-Pak SiO_2 light cartridge (part# WAT023537), Waters Sep-Pak SiO_2 plus cartridge (part # WAT020520), Waters Sep-Pak Dry Sodium Sulfate cartridge (part # WAT054265), Oasis MCX Plus cartridge (Waters, part # 186003516), Oasis HLB Plus cartridge (Waters, part # 186000132), Oasis HLB Light cartridge (Waters, part # 186005125), Oasis MAX Plus cartridge (Waters, part # 186003517).

All cartridges were preconditioned with MeOH (2 mL) followed by H_2O (10 mL) unless otherwise indicated.

5.6.1 General Procedure for the Generation of the [^{18}F]KF/diCy18-cr-6 Complex

[^{18}F]Fluoride (3.0-10.0 GBq) was separated from ^{18}O-enriched-water using an anion exchange cartridges (Waters Sep-Pak Accell Plus QMA Carbonate Plus Light Cartridge, 46 mg Sorbent per Cartridge (Part #186004540) which was activated with H_2O (1.0 mL) immediately prior to use) and released with 900 μL of a solution of diCy-18-cr-6/$K_2C_2O_4$/K_2CO_3 (dicyclohexano-18-crown-6 (14 mg, 38 μmol), potassium oxalate monohydrate (4 mg, 22 μmol) and potassium carbonate (0.2 mg, 0.72 μmol) in 1.0 mL CH_3CN/H_2O 4/1) into a 5 mL v-vial situated in the concentrator. The solution was dried with five cycles of azeotropic drying using acetonitrile (200 μL) under a flow of N_2 at 105 °C. This drying procedure resulted in recovery of 80-90% of the initial [^{18}F]F^- activity.

5.6.2 Isolation Procedure of 5-[^{18}F]-(Trifluoromethyl)benzothiophenium Trifluoromethanesulfonate ([^{18}F]3.109)

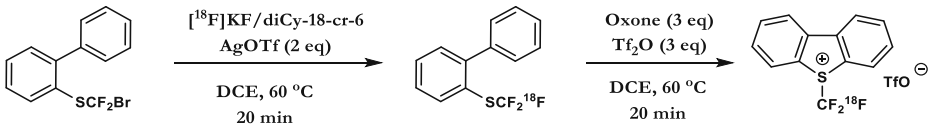

3.141 [^{18}F]3.142 [^{18}F]3.109

To a 5 mL v-vial (closed with a screw cap and septum) containing the dried [^{18}F]KF/diCy-18-cr-6 reagent was added a solution of AgOTf (21 mg, 80 μmol) (note 1) in dry MeOH/CH_3CN (3:2, 500 μL) and the solvent was removed by heating at 100 °C under a stream of nitrogen (4 min). Upon cooling of the v-vial, a solution of 2-{[bromo(difluoro)methyl]sulfanyl}biphenyl **3.141** (13 mg, 40 μmol) in DCE (300

μL) was added. The resulting brown suspension was allowed to stir at 60 °C for 20 minutes (note 2), after which the solvent was removed at 75 °C under a stream of nitrogen (2 minutes) with venting the outlet gasses through a Sep-Pak SiO_2-light cartridge as trap (note 3). The SiO_2-cartridge was then eluted with a solution of CH_3CN/H_2O/DMSO (DMSO (400 μL) in CH_3CN/H_2O 7:3 (800 μL)) back into the reaction vial (note 4), after which it was loaded through a syringe-filter (PTFE, Ø =13 mm, pore-size 0.22 μm, VWR part #514-0068) onto a SemiPrep HPLC column (Agilent 1200 Infinity Isocratic Pump system with a Phenomenex Synergi Hydro RP 4 μm 80A 250x10 mm column ; Eluent 75% CH_3CN/H_2O, flowrate = 4.0 ml/min) for purification. The reaction vial was rinsed with 70% CH_3CN/H_2O (400 μL), which was loaded onto the semi-prep HPLC in the same manner. The fraction of **[^{18}F]3.142** was collected at Rt = 17.0-18.5 min into a vial containing 20 mL of H_2O, and the resulting solution was eluted over a Sep-Pak C18 Plus cartridge. The cartridge was washed with 1 mL H_2O, blown dry with an N_2 flow and connected to a Sep Pak Dry Sodium Sulfate cartridge (cartridge not pre-conditioned). **[^{18}F]3.142** was eluted with DCE (1.4 mL) into a v-vial containing Oxone (37 mg, 120 μmol) (note 5, 6). A solution of Tf_2O (20 μL, 120 μmol) in DCE (150 μL) was added (note 7) and the resulting mixture was stirred at 60 °C for 20 minutes. Upon cooling of the v-vial $CHCl_3$ (1.0 mL) was added and the mixture was loaded onto a preconditioned Sep-Pak SiO_2-light cartridge. The cartridge was washed with $CHCl_3$ (1.5 mL) and dried with nitrogen, after which **[^{18}F]3.109** was eluted with CH_3CN (700 μL). An aliquot of the obtained solution of **[^{18}F]3.109** was analysed by radio-HPLC (Phenomenex Synergi Hydro RP 4 μm 80A 150x4.6mm, Eluent A) connected to an Advion CMS to determine radiochemical purity and product identity.

5.6.3 Additional notes for this procedure:

1) The yield of the ^{18}F halogen exchange reaction to provide **[^{18}F]3.109** can be influenced by the quality and storage conditions of the silver salt used. Although reproducible yields were obtained with new samples of AgOTf (Sigma Aldrich, >99.95% trace metal basis) weighed out on the bench, we found that older samples (>2 month storage on the bench) could lead to lower yields (Activity Yield <5%) or failure of the reaction to occur. To avoid these issues AgOTf was stored and weighed out in a nitrogen filled drybox.

2) Stirring is essential for the ^{18}F halogen exchange reaction to occur.

3) Activity losses of up to 20% occurred during solvent evaporation. It was found that part of this activity was **[^{18}F]3.109**, which was trapped on the SiO_2 cartridge and eluted back into the reaction vial. Routinely about 45% – 50% of the initial [^{18}F]F$^-$ activity remained in the reaction vial after this step.

4) DMSO was used to increase solubility and ensure efficient loading of the reaction mixture onto the semi-prep HPLC column.

5) The Activity Yield and Molar Activity of **[^{18}F]3.109** was recorded at this point.

6) It is essential that H_2O is removed in this step, or the cyclisation reaction to provide **[^{18}F]3.109** occurs in lower yields or fails.

7) Tf_2O was stored in a Schlenk flask under nitrogen atmosphere at room temperature.[18] The solution of Tf_2O in DCE (0.8M) was freshly prepared before addition and should be clear and colourless. If the solution is turbid this indicates the presence of TfOH (due to hydrolysis of Tf_2O during storage) which will result in lower yields for the cyclisation reaction.

5.6.4 Analysis of 5-[^{18}F]-(Trifluoromethyl)benzothiophenium Trifluoromethanesulfonate ([^{18}F]3.109)

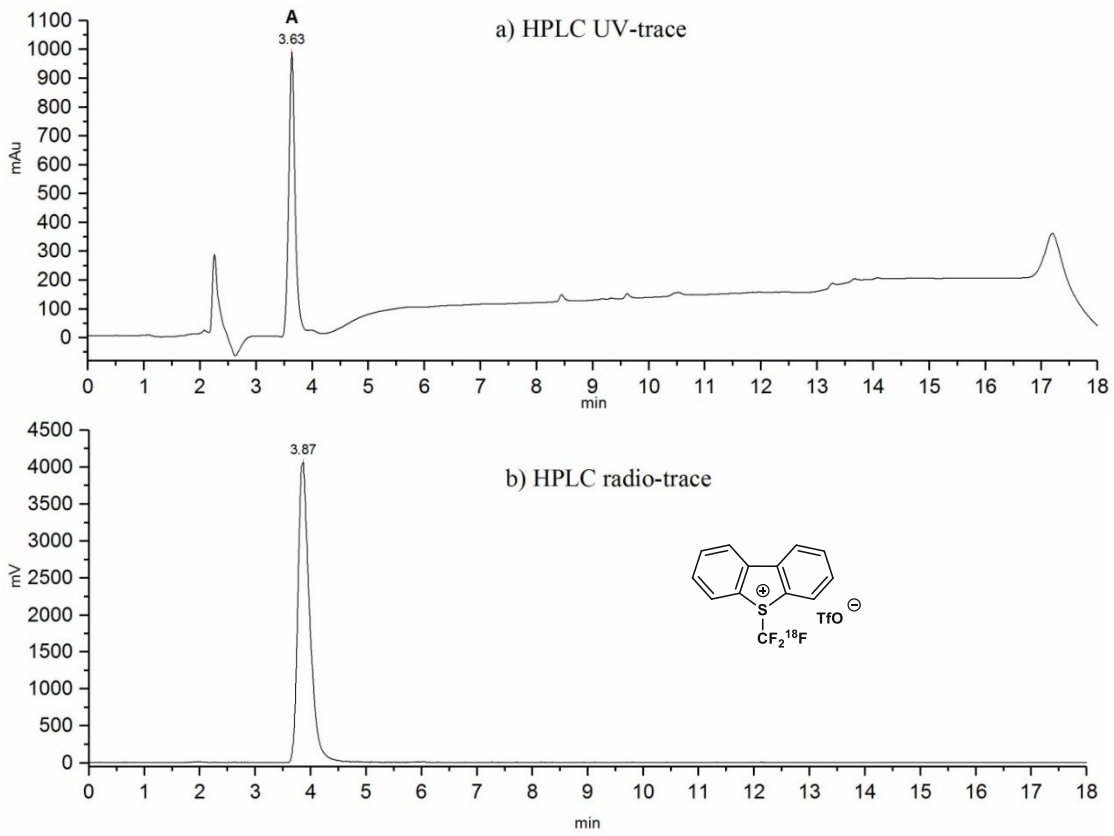

a) HPLC UV-trace (254 nm) and b) HPLC radio-trace of a sample of **[^{18}F]3.109** after isolation. Phenomenex Synergi Hydro RP 4 μm 80A 150x4.6mm column (Eluent A, flow rate = 0.7 ml/min).

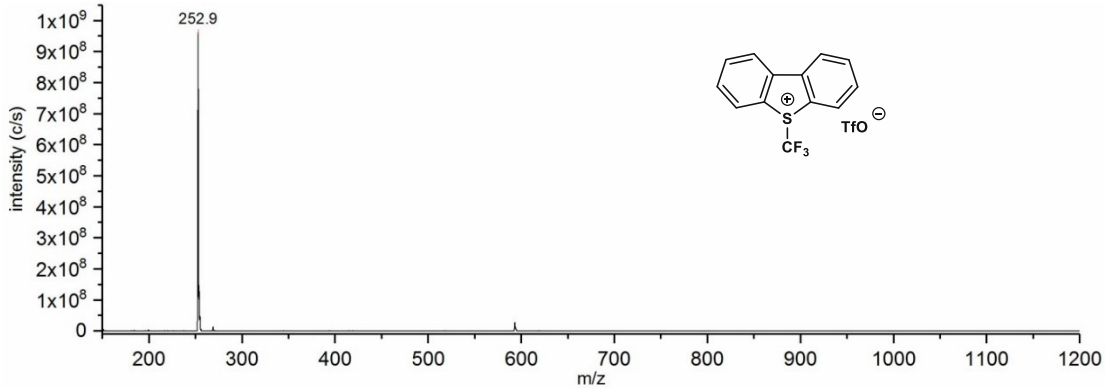

Peak A. *m/z* Calcd for $C_3H_8F_3S1$ $[M]^+$ 253.0, found 252.9.

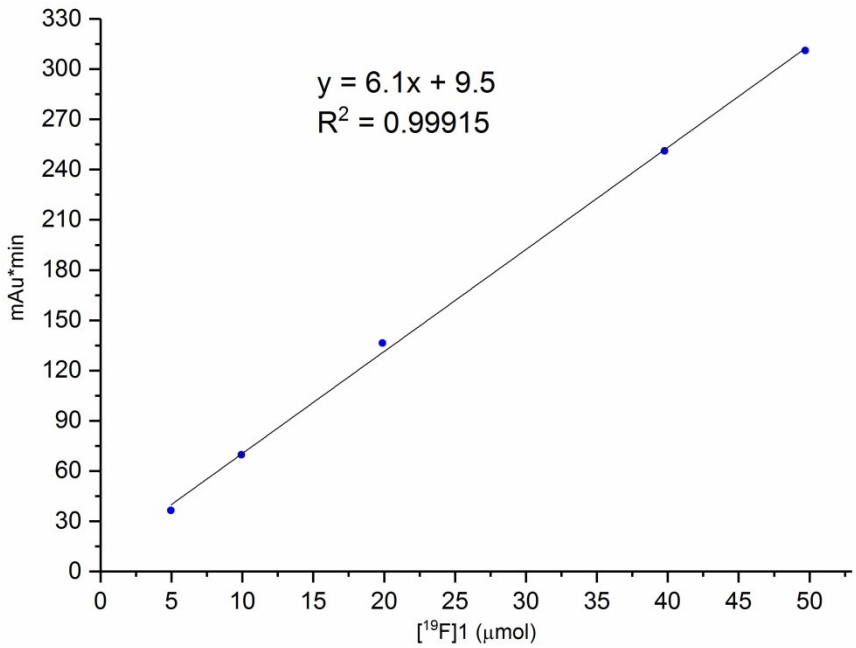

Calibration curve acquired with authentic standard (254 nm) for determination of molar activity of **[^{18}F]3.109**.

5.6.5 Radiochemical and Activity Yield Distribution

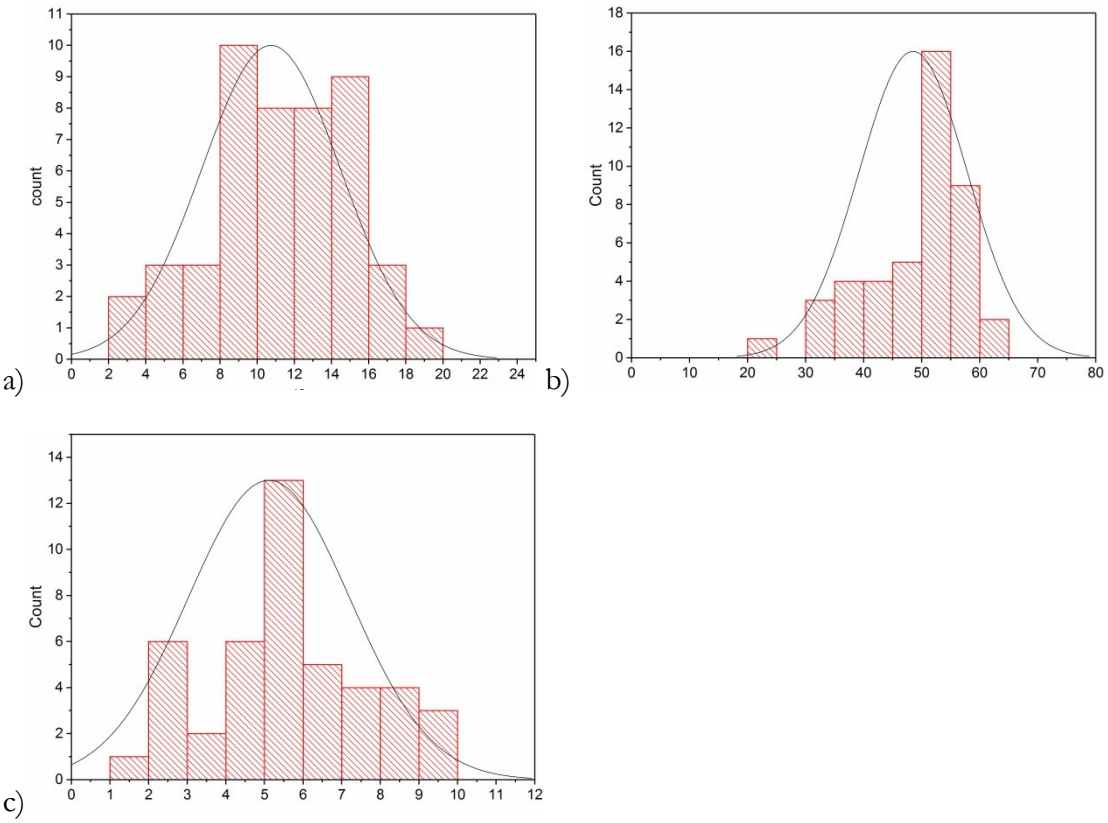

Yield distributions for a) The synthesis of **[^{18}F]3.142**, b) The cyclisation of **[^{18}F]3.142** to **[^{18}F]3.109** and c) The Activity Yield of **[^{18}F]3.109.**

5.6.6 General Procedure for the ^{18}F-Trifluoromethylation of Peptides using [^{18}F]3.109

An aliquot of a solution of ^{18}F-Umemoto's reagent **[^{18}F]3.109** in CH_3CN (20-300 μL, 20-100 MBq) was added to a v-vial and heated at 100 °C under a flow of nitrogen (2 minutes) to remove solvent. The vial was allowed to cool to room temperature, after which a solution of substrate (20 μmol) and additive (20 μmol) in solvent (100 μL) was added via syringe. The sealed vial was stirred at room temperature for 10-20 minutes.

5.6.7 Determination of radiochemical conversion:

The reaction mixture was diluted with CH_3CN/H_2O (1:2, 200 μL) and an aliquot was removed for analysis by radio-TLC and radio-HPLC to determine radiochemical conversion and product identity. Radio-HPLC was performed on a Phenomenex Synergi Hydro RP 4 μm 80A 150 x 4.6mm column. Radio-TLC was performed on Merck Kiesegel 60 F254 plates (eluent: CH_3CN/DCM 1/1). Analysis was performed using a plastic scintillator/PMT detector.

5.6.8 Isolation procedure using Oasis HLB cartridge:

The reaction was diluted with H_2O (7.0 mL) and loaded onto a preconditioned Oasis HLB Plus cartridge for purification. The cartridge was washed with CH_3CN/H2O (1:9, 1.0 mL), after which the product was eluted with a solution CH_3CN + 0.1% TFA (2.0 mL). An aliquot of the obtained solution was analysed by radio-HPLC to determine radiochemical purity and product identity.

5.6.9 Isolation procedure using Oasis MCX cartridge:

The reaction was diluted with 2% HCO_2H in H_2O (1.0 mL) and loaded onto a preconditioned Oasis MCX Plus cartridge for purification. The cartridge was washed

with 2% HCO_2H in H_2O (3.0 mL), followed by MeOH (2.0 mL). The product was eluted with a solution of 4N NH_3 in EtOH/H_2O (0.22 mL 35% NH_4OH, 0.78 mL EtOH). An aliquot of the obtained solution was analysed by radio-HPLC to determine radiochemical purity and product identity.

5.6.10 Isolation procedure using Oasis MAX cartridge:

The reaction was diluted with 5% NH_4OH solution (1.0 mL) and loaded onto a preconditioned Oasis MAX Plus cartridge for purification. The cartridge was washed with 5% NH_4OH solution (2.0 mL), followed by MeOH (2.0 mL). The product was eluted with a solution of 2% HCO_2H in MeOH (2.0 mL). An aliquot of the obtained solution was analysed by radio-HPLC to determine radiochemical purity and product identity.

Methyl 2-(benzoylamino)-3-[([^{18}F]trifluoromethyl)sulfanyl]propanoate ([^{18}F]3.146)

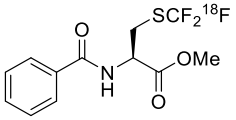

Prepared following the general procedure using methyl benzoyl-*L*-cysteinate (4.8 mg, 20 μmol), DMAP (2.4 mg, 20 μmol) and DMSO (100 μL). The reaction was stirred at room temperature for 20 min.

Reaction	Radio-TLC	Radio-HPLC	Radiochemical Conversion
1	79%	95%	75%
2	71%	97%	69%
3	72%	94%	68%
4	77%	97%	75%
Radiochemical Conversion + Standard Deviation			72% ± 4%

Radiochemical conversion of **[^{18}F]3.146** using DMAP in DMSO

Prepared following the general procedure using methyl benzoyl-*L*-cysteinate (4.8 mg, 20 μmol), DMAP (2.4 mg, 20 μmol) in DMSO/H_2O 4:1 (100 μL). The reaction was stirred at room temperature for 10 min.

Reaction	Radio-TLC	Radio-HPLC	Radiochemical Conversion
1	76%	90%	68%
2	68%	92%	63%
Radiochemical Conversion + Standard Deviation			66% ± 4%

Radiochemical conversion of **[^{18}F]3.146** using DMAP in DMSO/H_2O 4:1

Prepared following the general procedure using methyl benzoyl-*L*-cysteinate (4.8 mg, 20 μmol), 0.4M $KHCO_3$ in H_2O (50 μL, 20 μmol) and DMSO (50 μL). The reaction was stirred at room temperature for 10 min.

Reaction	Radio-TLC	Radio-HPLC	Radiochemical Conversion
1	77%	99%	76%
2	79%	96%	76%
3	68%	94%	64%
4	71%	97%	69%
Radiochemical Conversion + Standard Deviation			71% ± 6%

Radiochemical conversion of **[^{18}F]3.146** using $KHCO_3$ in DMSO/H_2O 1:1

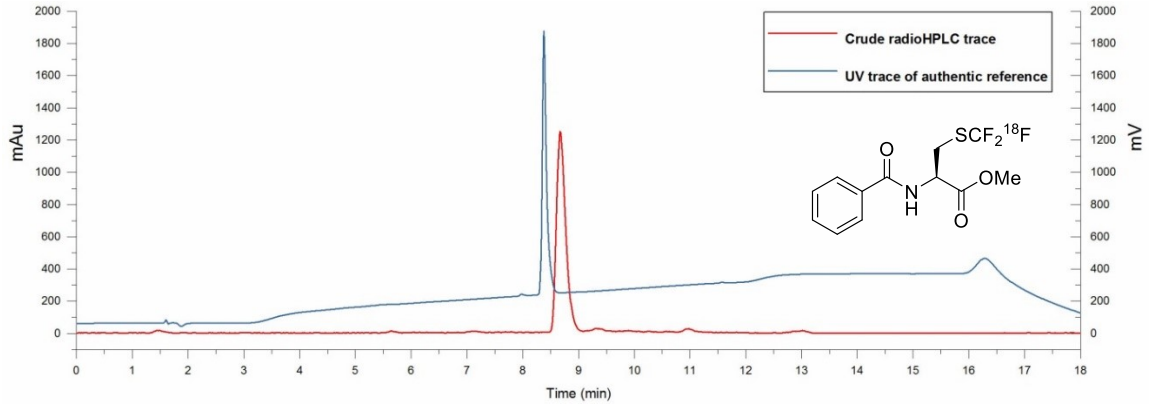

HPLC radio-trace of **[^{18}F]3.146** (red) overlaid with HPLC UV-trace (220 nm) of **[^{19}F]3.146** (blue).

Methyl (2*S*)-2-[(*tert*-butoxycarbonyl)amino]-4-[([^{18}F]trifluoromethyl)sulfanyl] butanoate ([^{18}F]3.147)

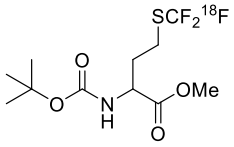

Prepared following the general procedure using methyl-2-[(*tert*-butoxycarbonyl)amino]-4-sulfanylbutanoate (5.3 mg, 20 μmol), DMAP (2.4 mg, 20 μmol) in DMSO (100 μL). The reaction was stirred at room temperature for 20 min.

Reaction	Radio-TLC	Radio-HPLC	Radiochemical Conversion
1	76%	88%	67%
2	85%	82%	70%
3	91%	89%	81%
4	93%	88%	82%
Radiochemical Conversion + Standard Deviation			75% ± 8%

Radiochemical Conversion of **[^{18}F]3.147**

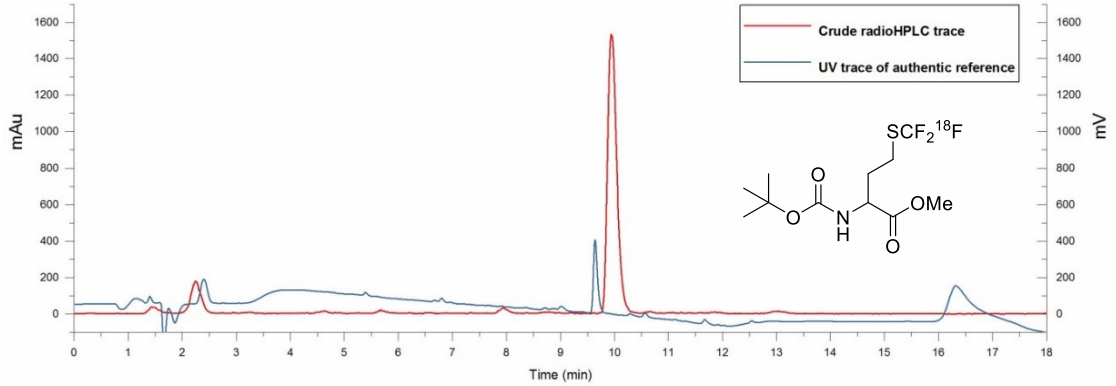

HPLC radio-trace of **[^{18}F]3.147** (red) overlaid with HPLC UV-trace (220 nm) of **[^{19}F]3.147** (blue).

(2*S*)-2-amino-4-[([^{18}F]trifluoromethyl)sulfanyl]butanoic acid ([^{18}F]3.148)

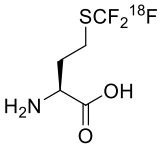

An aliquot of a solution of **[^{18}F]3.109** in CH_3CN (100-300 μL, 30-55 MBq) was added to a v-vial and heated at 100 °C under a nitrogen flow (2 minutes) to remove solvent. The vial was allowed to cool to room temperature, after which a solution of *L*-homocysteine (3.0 mg, 20 μmol) and $KHCO_3$ (4.0 mg, 40 μmol) in DMSO/H_2O (1:9,

100 μL) was added via syringe. The sealed vial was stirred at 40 °C for 20 minutes. The reaction was diluted with 2% HCO_2H solution (1.0 mL) and loaded onto a preconditioned Oasis MCX Plus cartridge for purification. The cartridge was washed with 2% HCOOH solution (3.0 mL), followed by MeOH (2.0 mL). The product **[^{18}F]3.148** was eluted with a solution of 4N NH_3 in EtOH/H_2O (0.22 mL 35% NH_4OH, 0.78 mL EtOH). An aliquot of the obtained solution was analysed by radio-HPLC (Eluent G) to determine radiochemical purity and product identity.

Reaction	Starting Activity (Mbq)	Isolated Activity after Sep-Pak (MBq)	radio-HPLC purity	Synthesis time (min)	RCY (n.d.c)
1	18.8	4.0	100%	39	21%
2	23.8	7.2	100%	40	30%
Radiochemical Conversion + Standard Deviation					26% ± 6%

Isolated Radiochemical Yield of **[^{18}F]3.148**

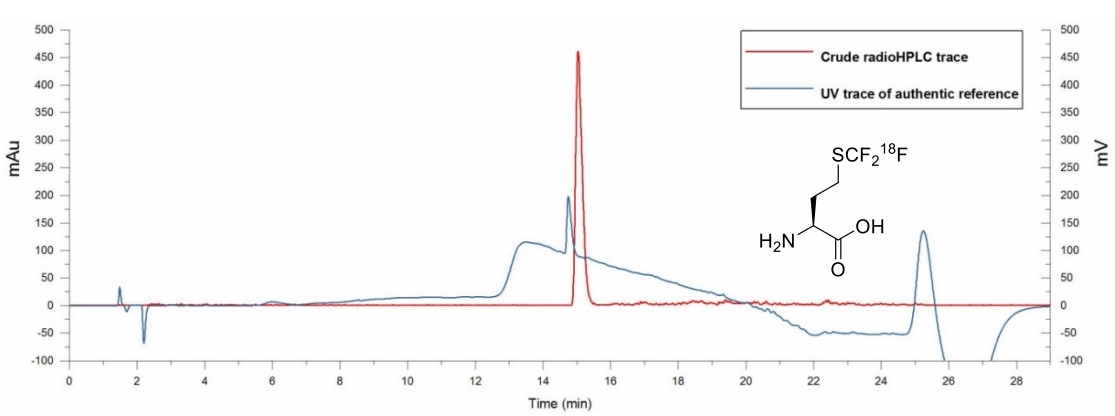

HPLC radio-trace of **[^{18}F]3.148** (red) overlaid with HPLC UV-trace (207 nm) of **[^{19}F]3.148** (blue).

Reaction of [^{18}F]3.109 with DMAP Without the Addition of Substrate

An aliquot of a solution of **[^{18}F]3.109** in CH_3CN (20-100 μL, 20-35 MBq) was added to a v-vial and heated at 100 °C under a nitrogen flow (2 minutes) to remove solvent. The vial cooled to room temperature, after which a solution of DMAP (2.4 mg, 20 μmol) in solvent (100 μL) was added via syringe. The sealed vial was stirred at room

temperature for 10 minutes. The reaction was diluted with CH_3CN/H_2O (1:2, 200 μL) and an aliquot was removed for analysis by radio-HPLC (Eluent A).

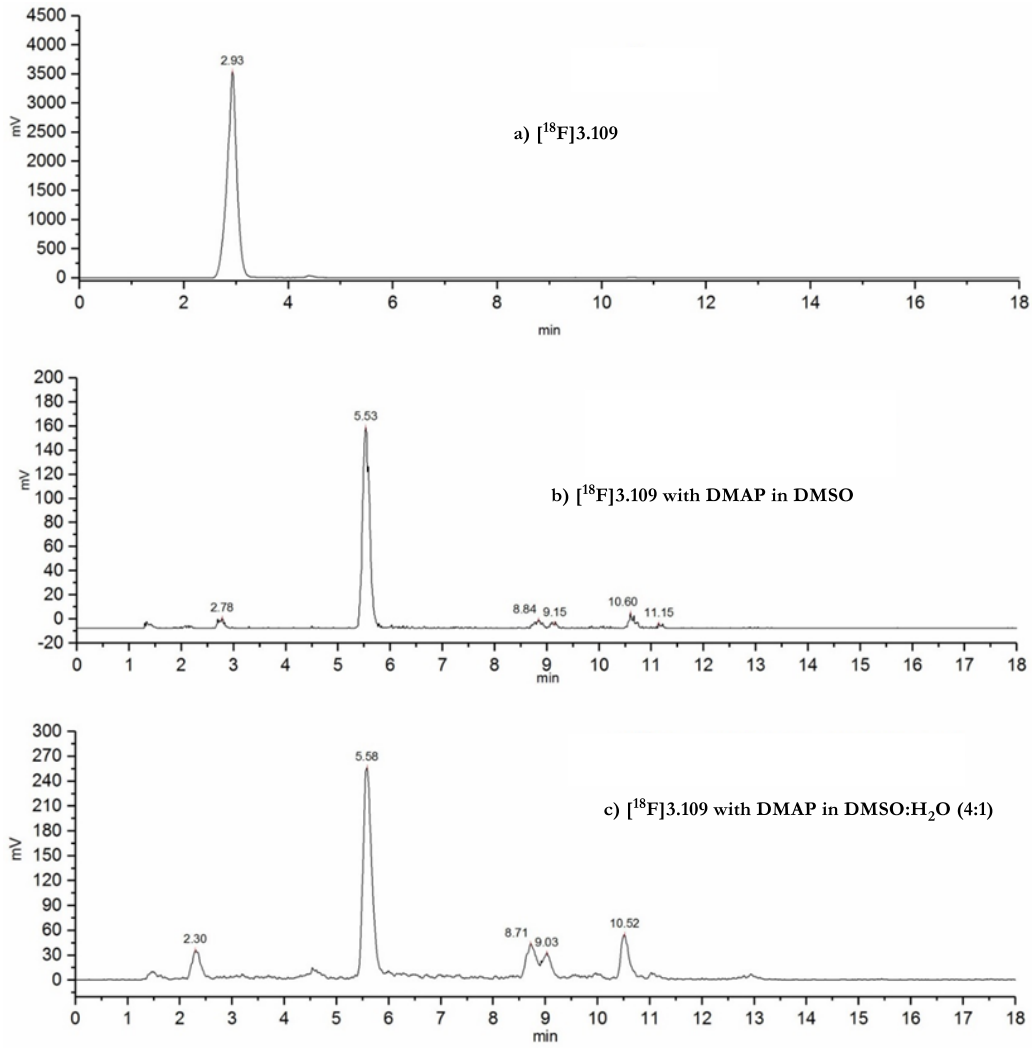

HPLC radio-trace of a) **[^{18}F]3.109**, b) Crude HPLC radio-trace after reaction of **[^{18}F]3.109** with DMAP (1 equiv.) in DMSO (100 μL) for 10 min at rt, c) Crude HPLC radio-trace after reaction of **[^{18}F]3.109** with DMAP (1 equiv.) in DMSO/H_2O 4:1 (100 μL) for 10 min at rt.

Full consumption of the ^{18}F-Umemoto reagent **[^{18}F]3.109** was observed on stirring with DMAP (20 μmol) for 10 min at room temperature in either DMSO or DMSO/H_2O 4:1 as solvent (100 μL). The main decomposition product in both reactions showed a radio peak at Rt = 5.5-5.6 min and could not be identified. No UV signal (220 nm) was found in the same region (not shown).

Methyl (2*R*)-2-({[(*tert*-butoxycarbonyl)amino]acetyl}amino)-3-[([^{18}F]trifluoromethyl) sulfanyl]propanoate ([^{18}F]3.151)

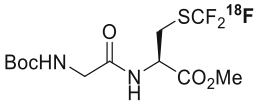

Prepared following the general procedure using methyl (*2R*)-2-({[(*tert*-butoxycarbonyl)amino]acetyl}amino)-3-sulfanylpropanoate (5.8 mg, 20 μmol), DMAP (2.4 mg, 20 μmol) in DMSO/H_2O 4:1 (100 μL). The reaction mixture was stirred at room temperature for 10 min. Radiochemical conversion was determined by radio-TLC and radio-HPLC (Eluent A).

Reaction	Radio-TLC	Radio-HPLC	Radiochemical Conversion
1	58%	93%	54%
2	54%	84%	45%
3	72%	84%	61%
4	74%	84%	62%
Radiochemical Conversion + Standard Deviation			55% ± 7%

Radiochemical Conversion of **[^{18}F]3.151**

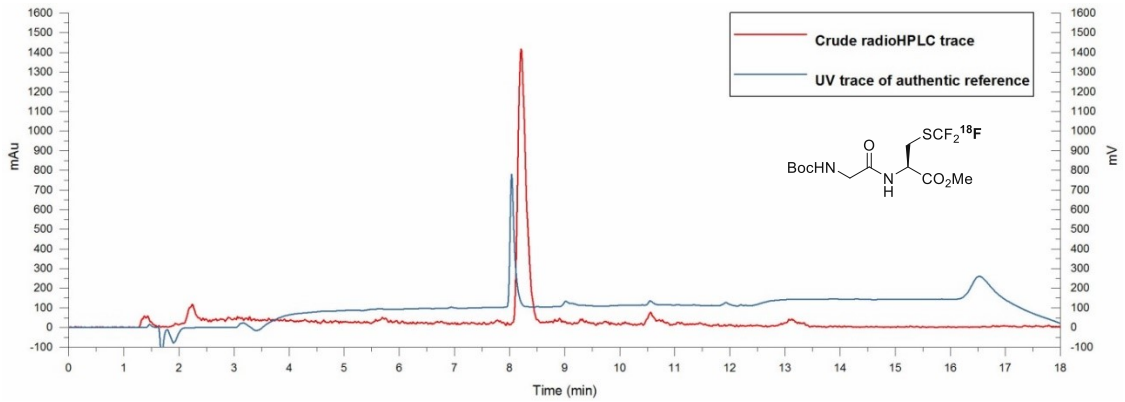

HPLC radio-trace of **[^{18}F]3.151** (red) overlaid with HPLC UV-trace (220 nm) of **[^{19}F]3.151** (blue).

Methyl-*N*-((*tert*-butoxycarbonyl)-*L*-alanyl)-*S*-([^{18}F]trifluoromethyl)-*L*-cysteinate ([^{18}F]3.152)

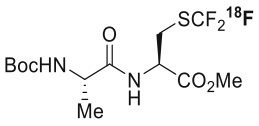

Prepared following the general procedure using methyl (*2R*)-2-({(2*S*)-2-[(*tert*-butoxycarbonyl)amino]propanoyl}amino)-3-sulfanylpropanoate (6.1 mg, 20 μmol),

DMAP (2.4 mg, 20 μmol) in DMSO/H_2O 4:1 (100 μL). The reaction mixture was stirred at room temperature for 10 min. Radiochemical conversion was determined by radio-TLC and radio-HPLC (Eluent A).

Reaction	Radio-TLC	Radio-HPLC	Radiochemical Conversion
1	55%	90%	50%
2	45%	82%	37%
3	77%	88%	68%
4	74%	92%	68%
Radiochemical Conversion + Standard Deviation			56% ± 15%

Radiochemical Conversion of **[^{18}F]3.152**

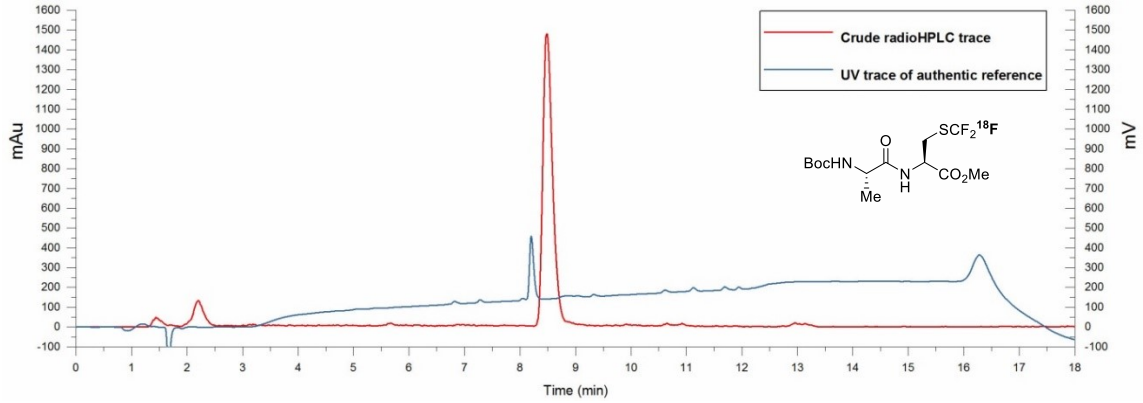

HPLC radio-trace of **[^{18}F]3.152** (red) overlaid with HPLC UV-trace (220 nm) of **[^{19}F]3.152** (blue).

Methyl-*N*-((*tert*-butoxycarbonyl)-*L*-alloisoleucyl)-S-([^{18}F]trifluoromethyl)-*L*-cysteinate, [^{18}F]3.153

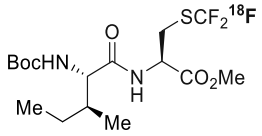

Prepared following the general procedure using methyl-(*tert*-butoxycarbonyl)-*L*-alloisoleucyl-*L*-cysteinate (7.0 mg, 20 μmol), DMAP (2.4 mg, 20 μmol) in DMSO (100 μL). The reaction mixture was stirred at room temperature for 10 min. Radiochemical conversion was determined by radio-TLC and radio-HPLC (Eluent A).

Reaction	Radio-TLC	Radio-HPLC	Radiochemical Conversion
1	81%	87%	71%
2	74%	81%	60%
3	77%	76%	59%
4	84%	76%	64%
Radiochemical Conversion + Standard Deviation			63% ± 5%

Radiochemical Conversion of **[^{18}F]3.153**

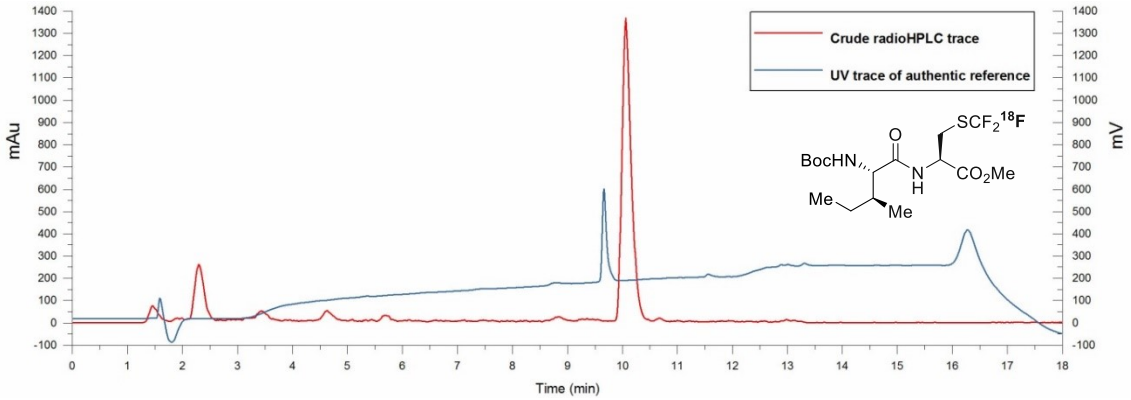

HPLC radio-trace of **[^{18}F]3.153** (red) overlaid with HPLC UV-trace (220 nm) of **[^{19}F]3.153** (blue).

Methyl N-((*tert*-butoxycarbonyl)-*L*-valyl)-S-([^{18}F]trifluoromethyl)-*L*-cysteinate, [^{18}F]3.154

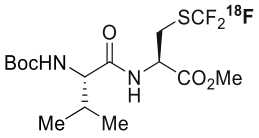

Prepared following the general procedure using methyl (*tert*-butoxycarbonyl)-*L*-valyl-*L*-cysteinate (7.0 mg, 20 μmol), DMAP (2.4 mg, 20 μmol) in DMSO/H_2O 4:1 (100 μL). The reaction mixture was stirred at room temperature for 10 min. Radiochemical conversion was determined by radio-TLC and radio-HPLC (Eluent A).

Reaction	Radio-TLC	Radio-HPLC	Radiochemical Conversion
1	76%	88%	67%
2	76%	87%	66%
3	75%	88%	66%
4	74%	88%	65%
Radiochemical Conversion + Standard Deviation			66% ± 1%

Radiochemical Conversion of **[^{18}F]3.154**

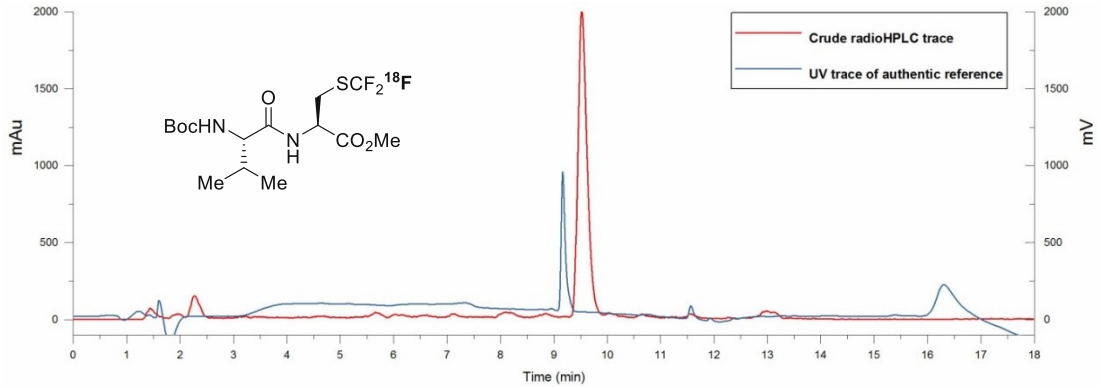

HPLC radio-trace of **[^{18}F]3.154** (red) overlaid with HPLC UV-trace (210 nm) of **[^{19}F]3.154** (blue).

(*S*)-4-((*tert*-Butoxycarbonyl)amino)-5-(((*R*)-1-methoxy-1-oxo-3-(([^{18}F]trifluoromethyl) thio)propan-2-yl)amino)-5-oxopentanoic acid ([^{18}F]3.155)

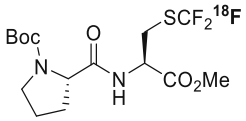

Prepared following the general procedure using *tert*-butyl (*S*)-2-(((*R*)-3-mercapto-1-methoxy-1-oxopropan-2-yl)carbamoyl)pyrrolidine-1-carboxylate (6.6 mg, 20 μmol), DMAP (2.4 mg, 20 μmol) in DMSO/H_2O 4:1 (100 μL). The reaction mixture was stirred at room temperature for 10 min. Radiochemical conversion was determined by radio-TLC and radio-HPLC (Eluent A).

Reaction	Radio-TLC	Radio-HPLC	Radiochemical Conversion
1	73%	86%	63%
2	76%	85%	65%
3	72%	84%	61%
4	76%	83%	63%
Radiochemical Conversion + Standard Deviation			63% ± 2%

Radiochemical Conversion of **[^{18}F]3.155**

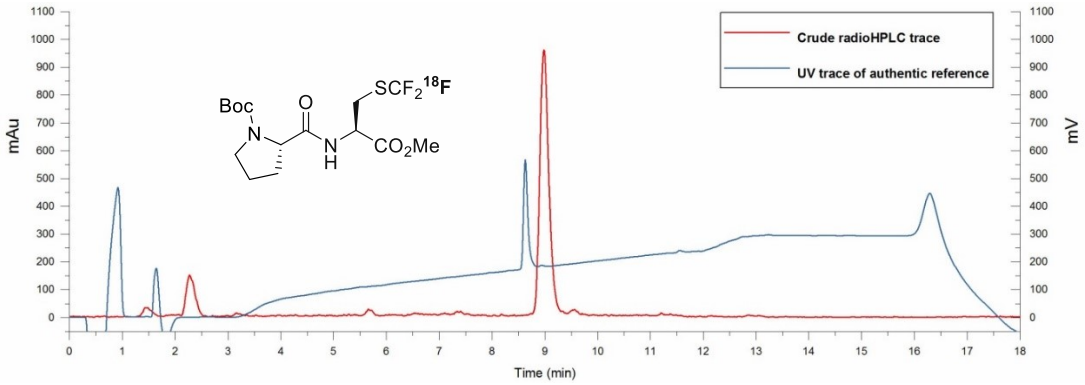

HPLC radio-trace of **[^{18}F]3.155** (red) overlaid with HPLC UV-trace (220 nm) of **[^{19}F]3.155** (blue).

Methyl N-((*tert*-butoxycarbonyl)-*L*-leucyl)-*S*-([^{18}F]trifluoromethyl)-*L*-cysteinate ([^{18}F]3.156)

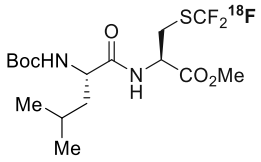

Prepared following the general procedure using methyl (*tert*-butoxycarbonyl)-*L*-leucyl-*L*-cysteinate (7.0 mg, 20 μmol), DMAP (2.4 mg, 20 μmol) in DMSO/H_2O 4:1 (100 μL). The reaction mixture was stirred at room temperature for 10 min. Radiochemical conversion was determined by radio-TLC and radio-HPLC (Eluent A).

Reaction	Radio-TLC	Radio-HPLC	Radiochemical Conversion
1	56%	85%	48%
2	76%	93%	71%
3	82%	95%	78%
Radiochemical Conversion + Standard Deviation			65% ± 16%

Radiochemical Conversion of **[^{18}F]3.156**

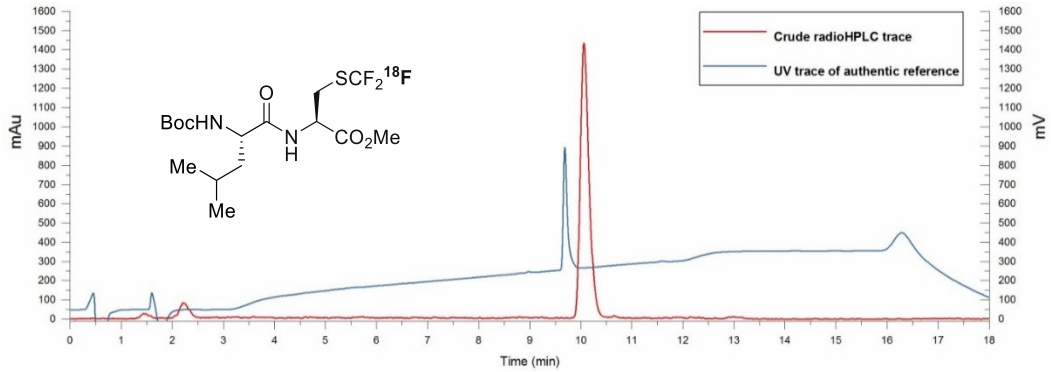

HPLC radio-trace of **[^{18}F]3.156** (red) overlaid with HPLC UV-trace (220 nm) of **[^{19}F]3.156** (blue).

Methyl N-((*tert*-butoxycarbonyl)-*L*-phenylalanyl)-*S*-([^{18}F]trifluoromethyl)-*L*-cysteinate ([^{18}F]3.157)

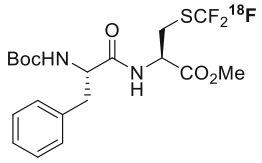

Prepared following the general procedure using methyl (*tert*-butoxycarbonyl)-*L*-phenylalanyl-*L*-cysteinate (7.6 mg, 20 μmol), DMAP (2.4 mg, 20 μmol) in DMSO/H_2O 4:1 (100 μL). The reaction mixture was stirred at room temperature for 10 min. Radiochemical conversion was determined by radio-TLC and radio-HPLC (Eluent A).

Reaction	Radio-TLC	Radio-HPLC	Radiochemical Conversion
1	77%	71%	55%
2	73%	75%	55%
3	71%	82%	58%
4	79%	87%	68%
Radiochemical Conversion + Standard Deviation			59% ± 7%

Radiochemical Conversion of **[^{18}F]3.157**

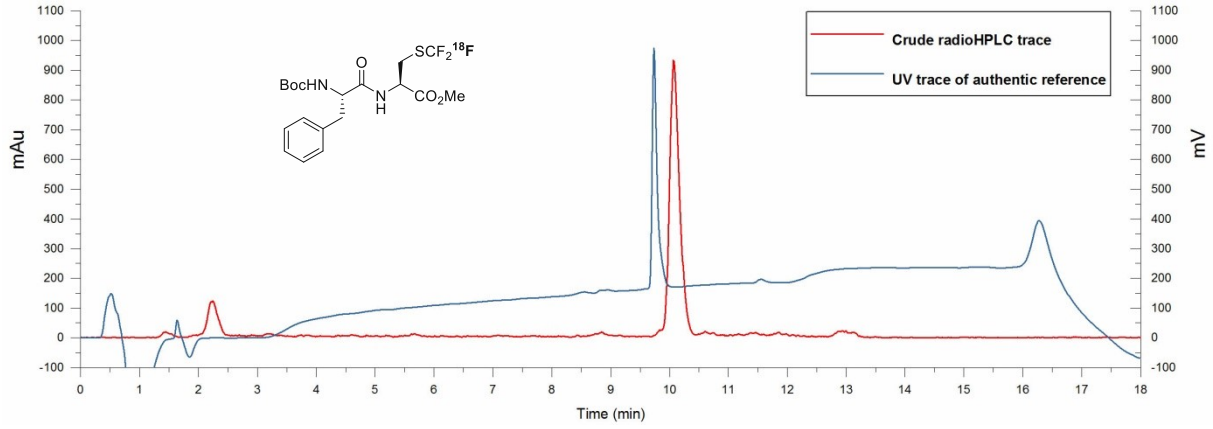

HPLC radio-trace of **[^{18}F]3.157** (red) overlaid with HPLC UV-trace (220 nm) of **[^{19}F]3.157** (blue).

Methyl N-((*tert*-butoxycarbonyl)-*L*-asparaginyl)-*S*-([^{18}F]trifluoromethyl)-*L*-cysteinate, [^{18}F]3.158

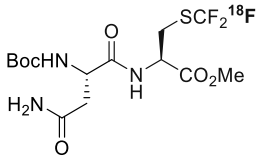

Prepared following the general procedure using methyl (*tert*-butoxycarbonyl)-*L*-asparaginyl-*L*-cysteinate (7.0 mg, 20 μmol), DMAP (2.4 mg, 20 μmol) in DMSO/H_2O 4:1 (100 μL). The reaction mixture was stirred at room temperature for 10 min. Radiochemical conversion was determined by radio-TLC and radio-HPLC (Eluent A).

Reaction	Radio-TLC	Radio-HPLC	Radiochemical Conversion
1	76%	88%	67%
2	64%	84%	54%
3	66%	93%	61%
4	72%	88%	63%
Radiochemical Conversion + Standard Deviation			61% ± 6%

Radiochemical Conversion of **[^{18}F]3.158**

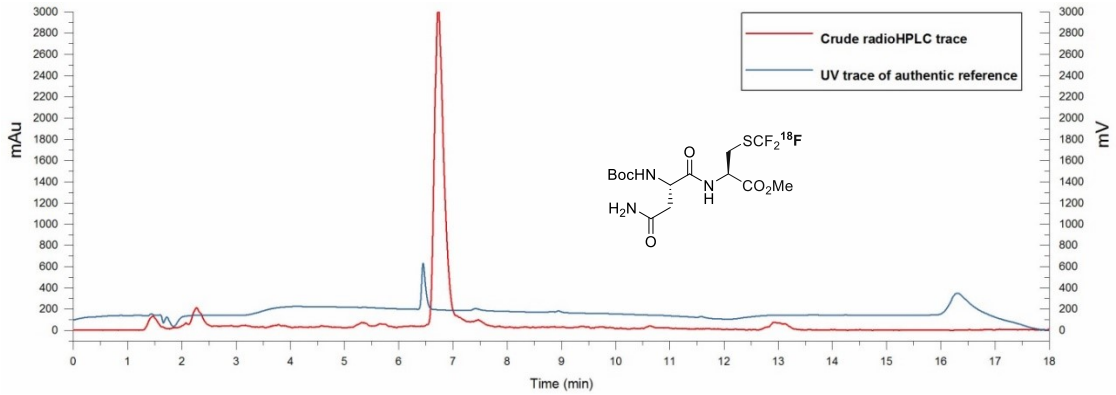

HPLC radio-trace of **[^{18}F]3.158** (red) overlaid with HPLC UV-trace (210 nm) of **[^{19}F]3.158** (blue).

Methyl N-((*tert*-butoxycarbonyl)-L-glutaminyl)-*S*-([^{18}F]trifluoromethyl)-*L*-cysteinate ([^{18}F]3.159)

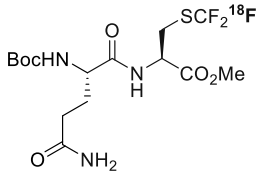

Prepared following the general procedure using methyl (*tert*-butoxycarbonyl)-*L*-glutaminyl-*L*-cysteinate (7.3 mg, 20 μmol), DMAP (2.4 mg, 20 μmol) in DMSO/H_2O 4:1 (100 μL). The reaction mixture was stirred at room temperature for 10 min. Radiochemical conversion was determined by radio-TLC and radio-HPLC (Eluent A).

Reaction	Radio-TLC	Radio-HPLC	Radiochemical Conversion
1	72%	84%	61%
2	73%	83%	61%
3	69%	85%	59%
4	75%	82%	62%
Radiochemical Conversion + Standard Deviation			60% ± 1%

Radiochemical Conversion of **[^{18}F]3.159**

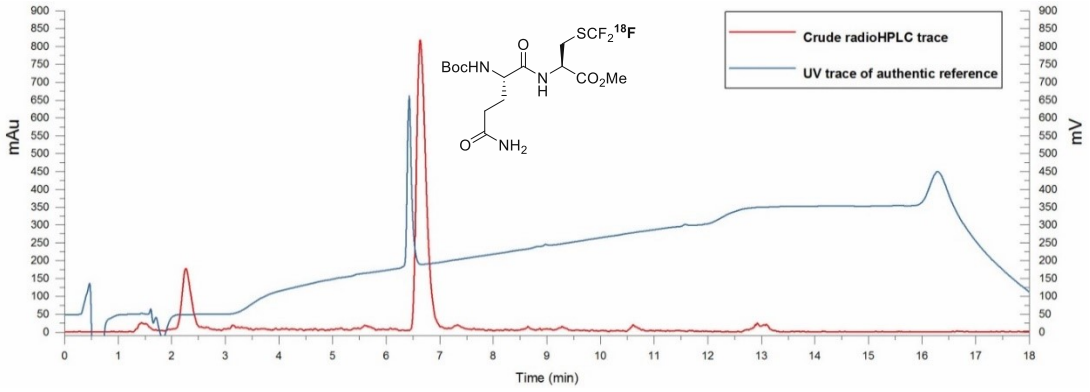

HPLC radio-trace of **[^{18}F]3.159** (red) overlaid with HPLC UV-trace (220 nm) of **[^{19}F]3.159** (blue).

Methyl N-((*tert*-butoxycarbonyl)-*L*-lysyl)-*S*-([^{18}F]trifluoromethyl)-*L*-cysteinate ([^{18}F]3.160)

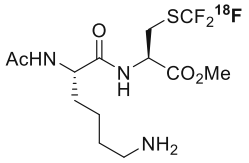

Prepared following the general procedure using methyl acetyl-*L*-lysyl-*L*-cysteinate TFA salt (7.6 mg, 20 μmol), DMAP (4.8 mg, 40 μmol) in DMSO 4:1 (100 μL). The reaction mixture was stirred at 40 °C for 20 minutes. **[^{18}F]3.160** was isolated by Oasis MCX cartridge purification. Radiochemical purity and product identity were determined by radio-HPLC (Eluent F).

Reaction	Starting Activity (Mbq)	Isolated Activity after Sep-Pak (MBq)	radio-HPLC purity	Synthesis time (min)	RCY (n.d.c)
1	24.8	12.0	16%	23	8%

Radiochemical Conversion of **[^{18}F]3.160**

Prepared following the general procedure using methyl acetyl-*L*-lysyl-*L*-cysteinate TFA salt (7.6 mg, 20 μmol), Et_4NHCO_3 (7.7 mg, 20 μmol) in DMSO 4:1 (100 μL). The reaction mixture was stirred at 40 °C for 20 minutes. **[^{18}F]3.160** was isolated by Oasis HLB cartridge purification. Radiochemical purity and product identity were determined by radio-HPLC (Eluent F).

Reaction	Starting Activity (Mbq)	Isolated Activity after Sep-Pak (MBq)	radio-HPLC purity	Synthesis time (min)	RCY (n.d.c)
1	20.0	7.2	91%	32	33%
2	39.2	7.9	95%	29	19%
3	43.7	11.5	94%	34	25%
Radiochemical Yield + Standard Deviation					26% ± 7%

Radiochemical Conversion of **[^{18}F]3.160**

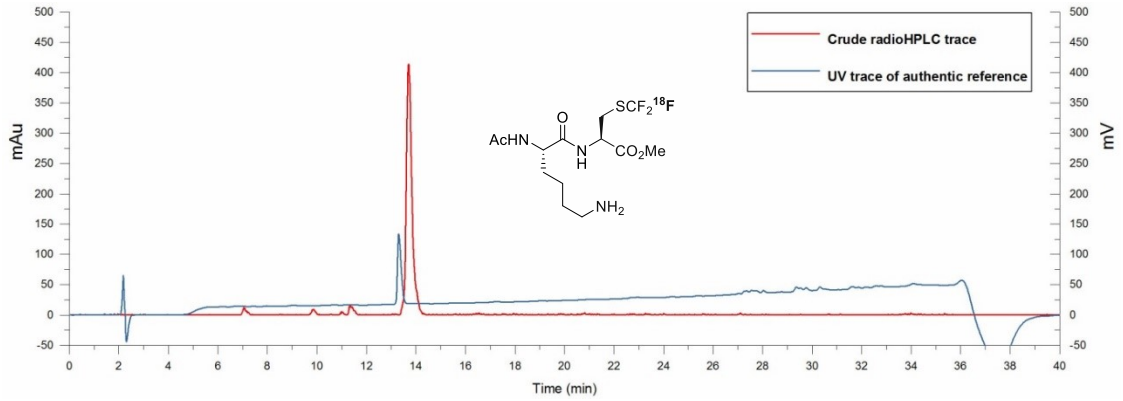

HPLC radio-trace of **[^{18}F]3.160** (red) overlaid with HPLC UV-trace (218 nm) of **[^{19}F]3.160** (blue).

(*S*)-4-((*tert*-Butoxycarbonyl)amino)-5-(((*R*)-1-methoxy-1-oxo-3-(([^{18}F]trifluoromethyl)thio)propan-2-yl)amino)-5-oxopentanoic acid ([^{18}F]3.161)

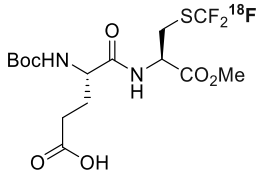

Prepared following the general procedure using (*S*)-4-((*tert*-butoxycarbonyl)amino)-5-(((*R*)-3-mercapto-1-methoxy-1-oxopropan-2-yl)amino)-5-oxopentanoic acid (7.3 mg, 20 μmol), DMAP (2.4 mg, 20 μmol) in DMSO/H_2O 4:1 (100 μL). The reaction mixture was stirred at room temperature for 10 min. Radiochemical conversion was determined by radio-TLC (eluent CH_3CN/DCM/AcOH 50:50:1) and radio-HPLC (Eluent A).

Reaction	Radio-TLC	Radio-HPLC	Radiochemical Conversion
1	74%	82%	61%
2	77%	88%	68%
3	72%	60%	43%
4	79%	82%	65%
Radiochemical Conversion + Standard Deviation			59% ± 11%

Radiochemical Conversion of **[^{18}F]3.161**

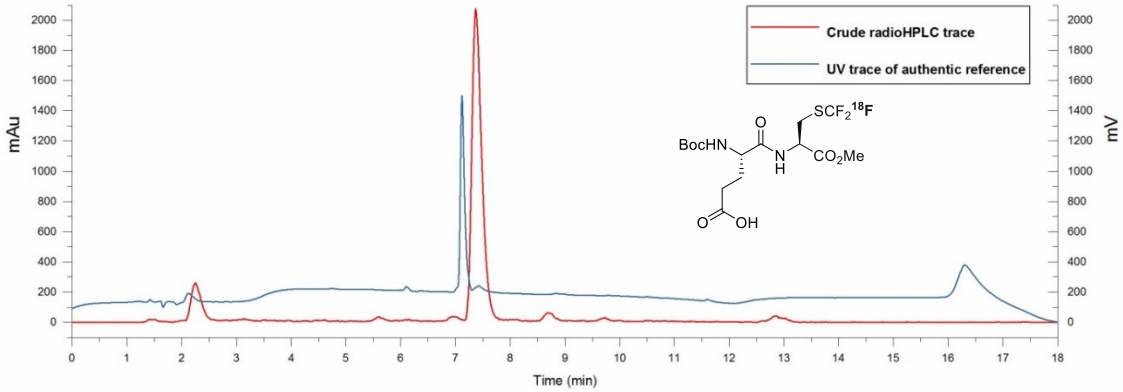

HPLC radio-trace of **[^{18}F]3.161** (red) overlaid with HPLC UV-trace (210 nm) of **[^{19}F]3.161** (blue).

Methyl N-((*tert*-butoxycarbonyl)-*L*-alloisoleucyl)-S-([^{18}F]trifluoromethyl)-*L*-cysteinate ([^{18}F]3.162)

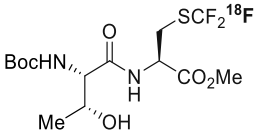

Prepared following the general procedure using methyl (*tert*-butoxycarbonyl)-*L*-allothreonyl-*L*-cysteinate (6.7 mg, 20 μmol), DMAP (2.4 mg, 20 μmol) in DMSO/H_2O 4:1 (100 μL). The reaction mixture was stirred at room temperature for 10 min. Radiochemical conversion was determined by radio-TLC and radio-HPLC (Eluent A).

Reaction	Radio-TLC	Radio-HPLC	Radiochemical Conversion
1	76%	83%	63%
2	81%	91%	74%
3	76%	84%	64%
4	78%	86%	67%
Radiochemical Conversion + Standard Deviation			67% ± 5%

Radiochemical Conversion of **[^{18}F]3.162**

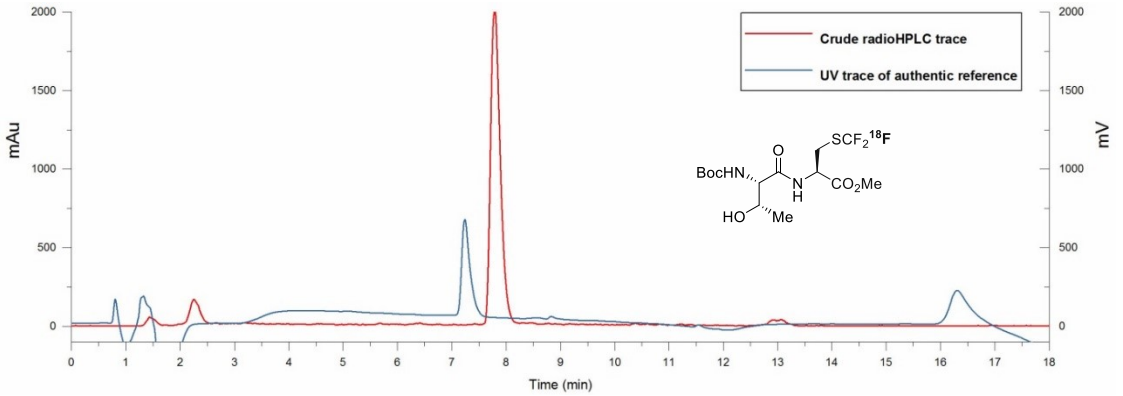

HPLC radio-trace of **[^{18}F]3.162** (red) overlaid with HPLC UV-trace (210 nm) of **[^{19}F]3.162** (blue).

Methyl N-((*tert*-butoxycarbonyl)-*L*-seryl)-S-([^{18}F]trifluoromethyl)-*L*-cysteinate ([^{18}F]3.163)

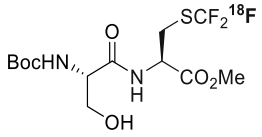

Prepared following the general procedure using methyl (*tert*-butoxycarbonyl)-*L*-seryl-*L*-cysteinate (6.4 mg, 20 μmol), DMAP (2.4 mg, 20 μmol) in DMSO 4:1 (100 μL). The reaction mixture was stirred at room temperature for 10 min. Radiochemical conversion was determined by radio-TLC and radio-HPLC (Eluent A).

Reaction	Radio-TLC	Radio-HPLC	Radiochemical Conversion
1	47%	81%	38%
2	48%	68%	33%
3	79%	79%	62%
4	70%	71%	50%
Radiochemical Conversion + Standard Deviation			46% ± 13%

Radiochemical Conversion of **[^{18}F]3.163**

Prepared following the general procedure using methyl (*tert*-butoxycarbonyl)-*L*-seryl-*L*-cysteinate (6.4 mg, 20 μmol), 0.4M $KHCO_3$ in H_2O (50 μL, 20 μmol) and DMSO (50 μL). The reaction mixture was stirred at room temperature for 10 min. Radiochemical conversion was determined by radio-TLC and radio-HPLC (Eluent A).

Reaction	Radio-TLC	Radio-HPLC	Radiochemical Conversion
1	72%	96%	69%
2	63%	98%	62%
3	76%	99%	75%
4	72%	97%	70%
Radiochemical Conversion + Standard Deviation			69% ± 6%

Radiochemical Conversion of **[^{18}F]3.163**

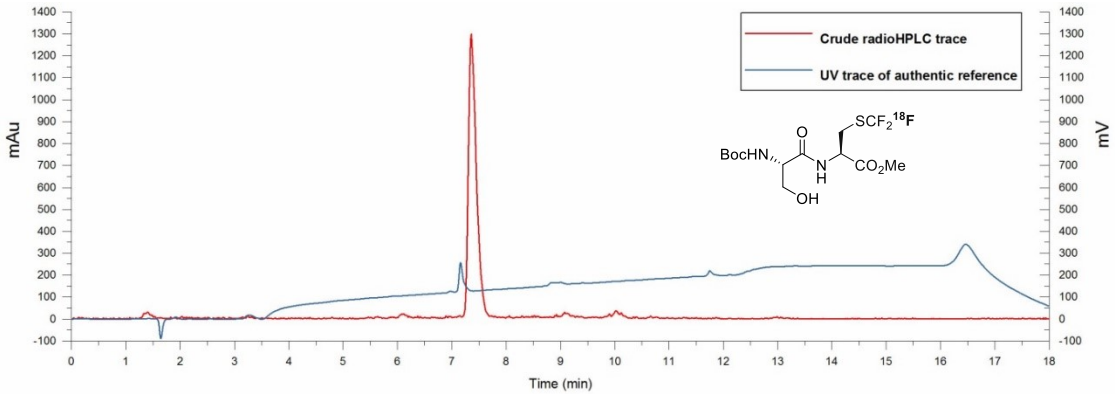

HPLC radio-trace of **[^{18}F]3.163** (red) overlaid with HPLC UV-trace (220 nm) of **[^{19}F]3.163** (blue).

Methyl N-((*tert*-butoxycarbonyl)-*L*-tyrosyl)-S-([^{18}F]trifluoromethyl)-*L*-cysteinate ([^{18}F]3.164)

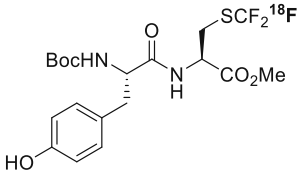

Prepared following the general procedure using methyl (*tert*-butoxycarbonyl)-*L*-tyrosyl-*L*-cysteinate (8.0 mg, 20 μmol), 0.4M $KHCO_3$ in H_2O (50 μL, 20 μmol) and DMSO (50 μL). The reaction mixture was stirred at room temperature for 10 min. Radiochemical conversion was determined by radio-TLC and radio-HPLC (Eluent A).

Reaction	Radio-TLC	Radio-HPLC	Radiochemical Conversion
1	75%	91%	68%
2	71%	94%	67%
3	51%	91%	46%
4	82%	88%	72%
Radiochemical Conversion + Standard Deviation			63% ± 12%

Radiochemical Conversion of **[^{18}F]3.164**

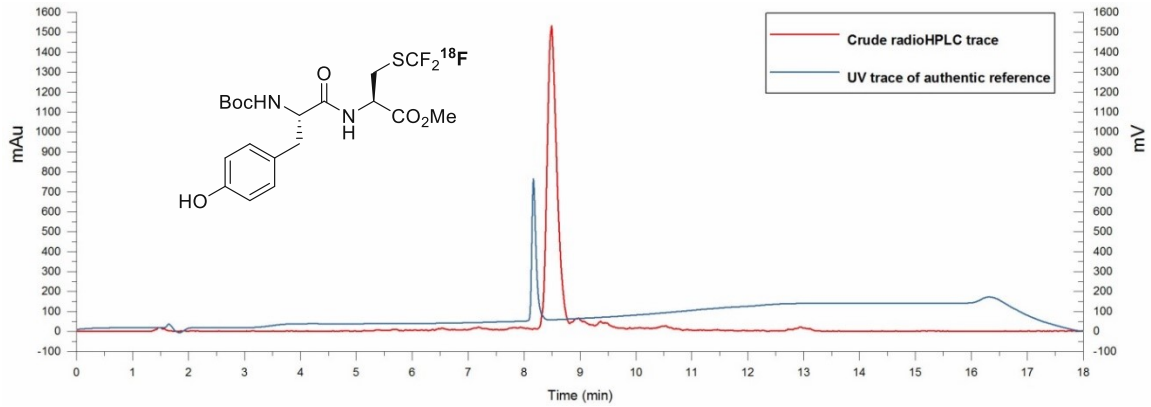

HPLC radio-trace of **[^{18}F]3.164** (red) overlaid with HPLC UV-trace (220 nm) of **[^{19}F]3.164** (blue).

Methyl N-((*tert*-butoxycarbonyl)-*L*-methionyl)-S-(trifluoromethyl)-*L*-cysteinate ([^{18}F]3.165)

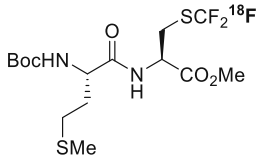

Prepared following the general procedure using methyl (*tert*-butoxycarbonyl)-*L*-methionyl-*L*-cysteinate (7.3 mg, 20 μmol), DMAP (2.4 mg, 20 μmol) in DMSO (100 μL). The reaction mixture was stirred at room temperature for 10 min. Radiochemical conversion was determined by radio-TLC and radio-HPLC (Eluent A).

Reaction	Radio-TLC	Radio-HPLC	Radiochemical Conversion
1	81%	82%	66%
2	75%	87%	65%
3	62%	77%	48%
4	77%	88%	65%
Radiochemical Conversion + Standard Deviation			62% ± 9%

Radiochemical Conversion of **[^{18}F]3.165**

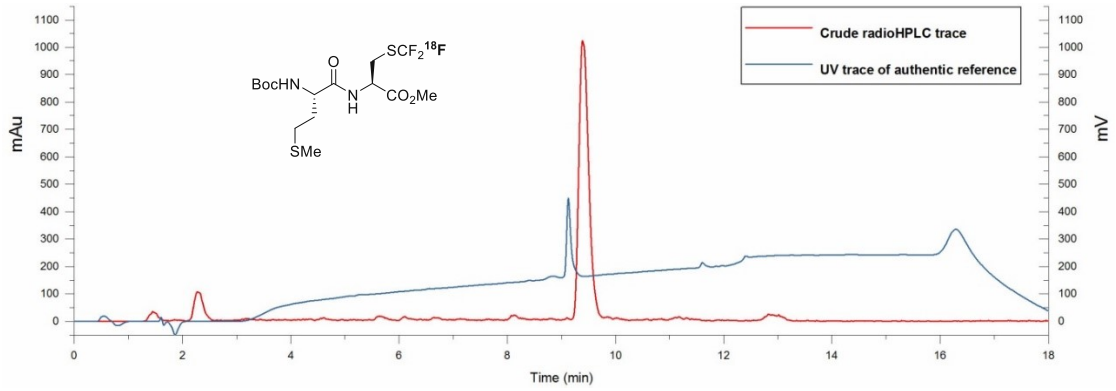

HPLC radio-trace of **[^{18}F]3.165** (red) overlaid with HPLC UV-trace (220 nm) of **[^{19}F]3.165** (blue).

^{18}F-Trifluoromethylation of methyl (tert-butoxycarbonyl)-*L*-histidyl-*L*-cysteinate ([^{18}F]3.166)

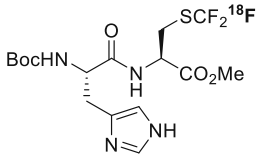

Prepared following the general procedure using methyl (tert-butoxycarbonyl)-*L*-histidyl-*L*-cysteinate (7.4 mg, 20 μmol), DMAP (2.4 mg, 20 μmol) in DMSO 4:1 (100 μL). The reaction mixture was stirred at room temperature for 10 min. Radiochemical conversion was determined by radio-TLC and radio-HPLC (Eluent D).

Reaction	Radio-TLC	Radio-HPLC	Radiochemical Conversion
1	40%	65%	26%
2	48%	61%	29%
Radiochemical Conversion + Standard Deviation			27% ± 2%

Radiochemical Conversion of **[^{18}F]3.166**

Prepared following the general procedure using methyl (*tert*-butoxycarbonyl)-*L*-histidyl-*L*-cysteinate (7.4 mg, 20 μmol), 0.4M $KHCO_3$ in H_2O (50 μL, 20 μmol) and DMSO (50 μL). The reaction mixture was stirred at room temperature for 10 min. Radiochemical conversion was determined by radio-TLC and radio-HPLC. An aliquot of the crude reaction mixture was analysed using HPLC and MS (ESI).

Reaction	Radio-TLC	Radio-HPLC	Radiochemical Conversion
1	56%	76%	43%
2	30%	75%	23%
3	84%	70%	59%
4	75%	51%	38%
Radiochemical Conversion + Standard Deviation			41% ± 15%

Radiochemical Conversion of **[^{18}F]3.166**

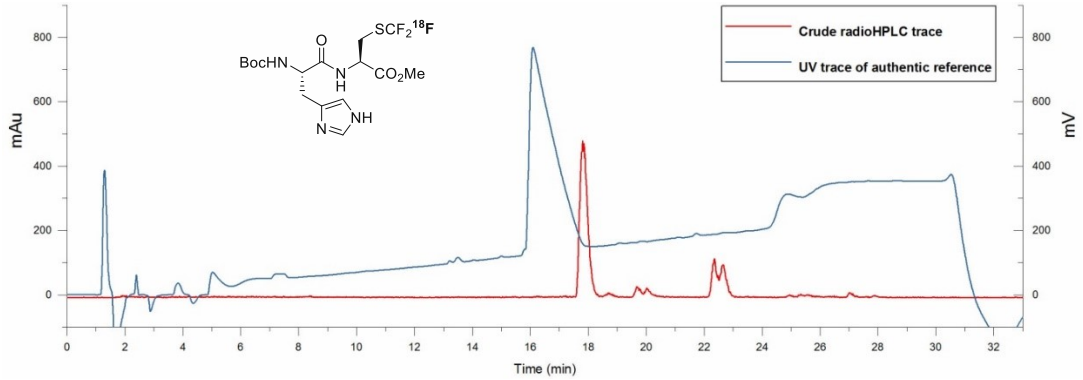

HPLC radio-trace of **[^{18}F]3.166** (red) overlaid with HPLC UV-trace (220 nm) of **[^{19}F]3.166** (blue).

^{18}F-Trifluoromethylation of methyl (tert-butoxycarbonyl)-*L*-tryptophyl-*L*-cysteinate ([^{18}F]3.167)

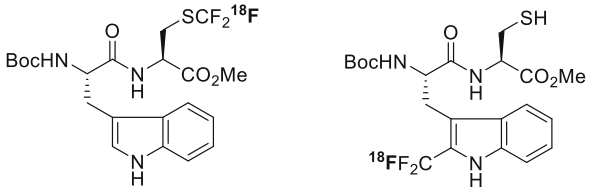

[^{18}F]3.167 [^{18}F]3.168

Prepared following the general procedure using methyl (tert-butoxycarbonyl)-*L*-tryptophyl-*L*-cysteinate (8.4 mg, 20 μmol), DMAP (2.4 mg, 20 μmol) in DMSO 4:1 (100 μL). The reaction mixture was stirred at room temperature for 10 min. Radiochemical conversion was determined by radio-TLC and radio-HPLC (Eluent C).

Reaction	Radio-TLC	Radio-HPLC		Radiochemical Conversion	
		[^{18}F]3.167	[^{18}F]3.168	[^{18}F]3.167	[^{18}F]3.168
1	76%	28%	26%	21%	19%

Radiochemical Conversion of **[^{18}F]3.167** and **[^{18}F]3.168**.

Prepared following the general procedure using methyl (*tert*-butoxycarbonyl)-*L*-tryptophyl-*L*-cysteinate (8.4 mg, 20 μmol), 0.4M $KHCO_3$ in H_2O (50 μL, 20 μmol) and DMSO (50 μL). The reaction mixture was stirred at room temperature for 10 min. Radiochemical conversion was determined by radio-TLC and radio-HPLC

(Eluent C). An aliquot of the crude reaction mixture was analysed using HPLC and MS (ESI).

Reaction Radio-TLC		Radio-HPLC		Radiochemical Conversion	
		[^{18}F]3.167	[^{18}F]3.168	[^{18}F]3.167	[^{18}F]3.168
1	93%	63%	19%	59%	18
2	93%	71%	11%	66%	10
3	91%	66%	14%	60%	13
4	94%	55%	21%	52%	20
Radiochemical Conversion + Standard Deviation				59 ± 6%	15 ± 4%

Radiochemical Conversion of **[^{18}F]3.167** and **[^{18}F]3.168**.

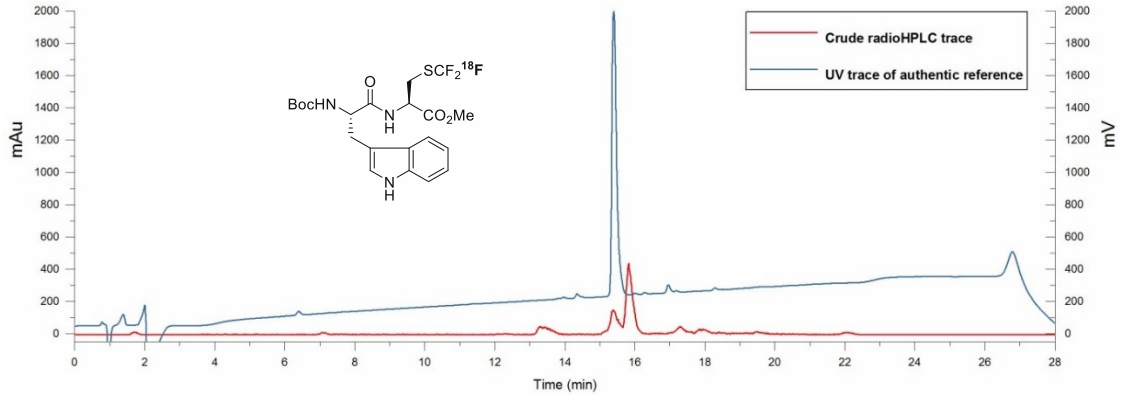

HPLC radio-trace of **[^{18}F]3.167** (red) overlaid with HPLC UV-trace (220 nm) of **[^{19}F]3.167** (blue).

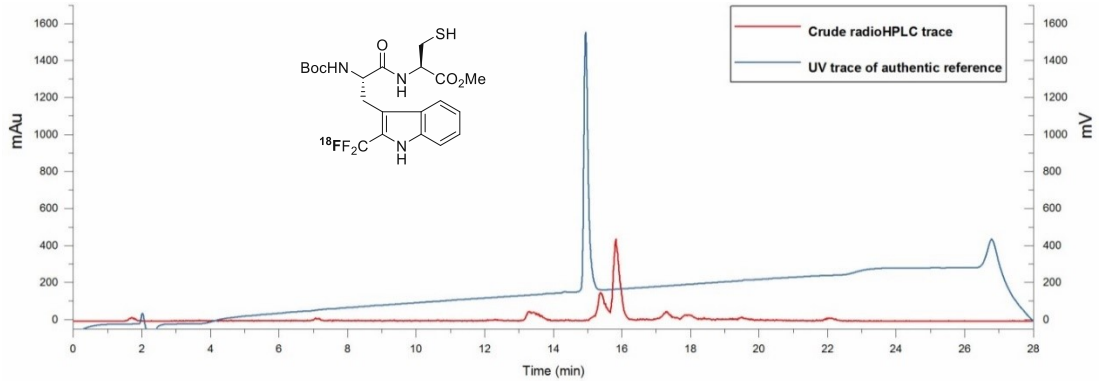

HPLC radio-trace of **[^{18}F]3.168** (red) overlaid with HPLC UV-trace (220 nm) of **[^{19}F]3.168** (blue).

(2*S*)-2-amino-4-{[(1*R*)-1-[(carboxymethyl)carbamoyl]-2-[([^{18}F]trifluoromethyl) sulfanylethyl]carbamoyl}butanoic acid ([^{18}F]3.181)

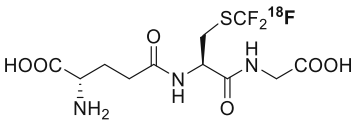

Prepared following the general procedure using *L*-glutathione (6.1 mg, 20 μmol), 0.95M $NaHCO_3$ (70 μL, 66 μmol) in DMSO (70 μL). The reaction mixture was stirred at 30 °C for

10 minutes. **[^{18}F]3.181** was isolated by Oasis MCX cartridge purification using 1.0M NaOH as elution solvent. Radiochemical purity and product identity were determined by radio-HPLC (eluent B).

Reaction	Starting Activity (Mbq)	Isolated Activity after Sep-Pak (MBq)	radio-HPLC purity	Synthesis time starting from [^{18}F]3.109 (min)	RCY (n.d.c)
1	53.7	13.0	98%	40	24%
2	35.7	10.4	>99%	26	29%
Radiochemical Yield + Standard Deviation					26% ± 4%

Isolated Radiochemical Yield of **[^{18}F]3.181**

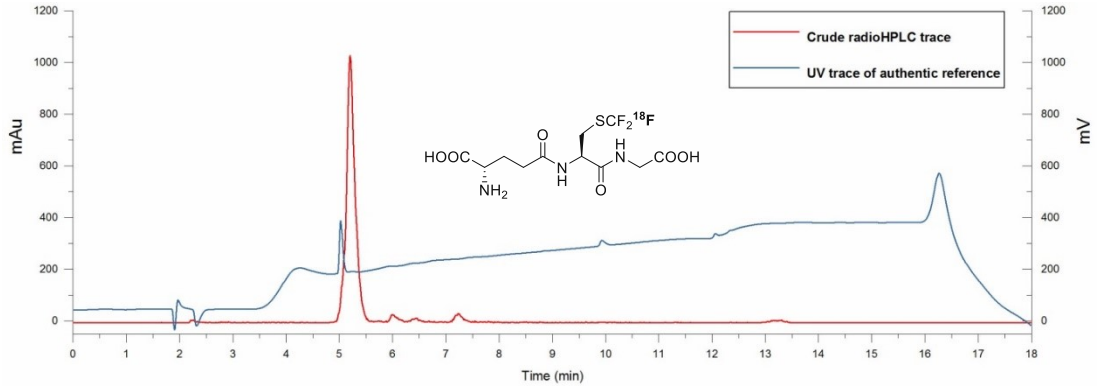

HPLC radio-trace of **[^{18}F]3.181** (red) overlaid with HPLC UV-trace (220 nm) of **[^{19}F]3.181** (blue).

(((*R*)-1-carboxy-2-((trifluoromethyl)thio)ethyl)carbamoyl)-*L*-glutamic acid ([^{18}F]3.182)

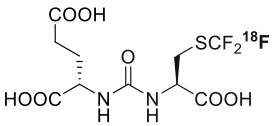

Prepared following the general procedure using (((*R*)-1-carboxy-2-mercaptoethyl)carbamoyl)-*L*-glutamic acid (5.9 mg, 20 μmol), 0.80M K_2CO_3 (50 μL, 40 μmol) in DMSO (50 μL). The reaction mixture was stirred at 40 °C for 20 minutes. **[^{18}F]3.182** was isolated by Oasis MAX cartridge purification. Radiochemical purity and product identity were determined by radio-HPLC (eluent B).

Reaction	Starting Activity (Mbq)	Isolated Activity after Oasis MAX (Mbq)	radio-HPLC purity	Synthesis time starting from [^{18}F]3.109 (min)	RCY (n.d.c)
1	36.7	3.8	81%	42	8%
2	38.8	4.7	90%	51	11%
Radiochemical Yield + Standard Deviation					10% ± 2%

Isolated Radiochemical Yield of **[^{18}F]3.182**

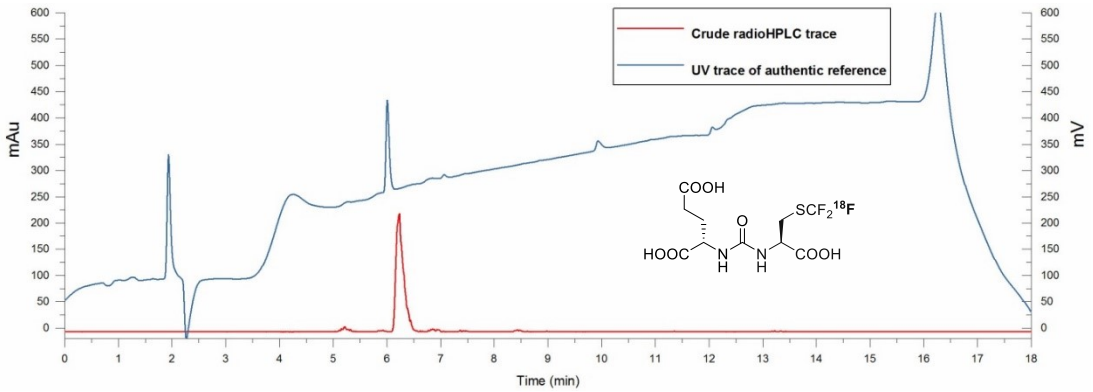

HPLC radio-trace of **[^{18}F]3.182** (red) overlaid with HPLC UV-trace (220 nm) of **[^{19}F]3.182** (blue).

Val-Val-Gly-Gly-Val-Met-Gly-Lys-Lys-Gly-Cys([^{18}F]CF_3) ([^{18}F]3.184)

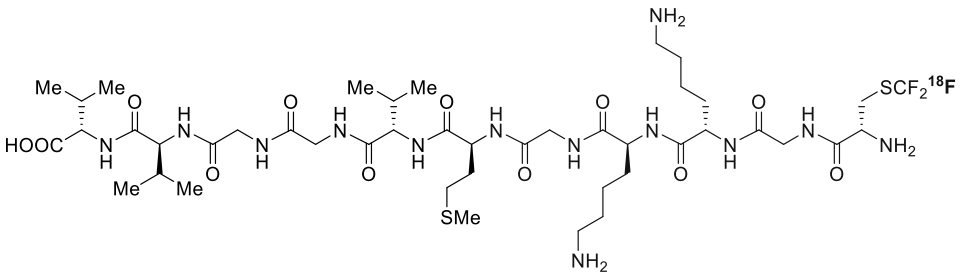

Prepared following the general procedure using H-Cys-Gly-Lys-Lys-Gly-Met-Val-Gly-Gly-Val-Val-OH trifluoroacetate salt (1.0 mg, 0.80 μmol), Et_4NHCO_3 (2.0 mg, 10 μmol) in DMSO 4:1 (40 μL). The reaction mixture was stirred at 40 °C for 20 minutes. **[^{18}F]3.184** was isolated by Oasis HLB cartridge purification. Radiochemical purity and product identity were determined by radio-HPLC (Eluent E).

Reaction	Starting Activity (Mbq)	Isolated Activity after Sep-Pak	radio-HPLC purity	[18F]1 remaining	Synthesis time (min)	RCY (n.d.c)
1	36.0	18.9	73%	25%	32	38%
2	26.7	17.0	35%	64%	29	22%
Radiochemical Yield + + Standard Deviation						30% ± 11%

Isolated Radiochemical Yield of **[18F]3.184**

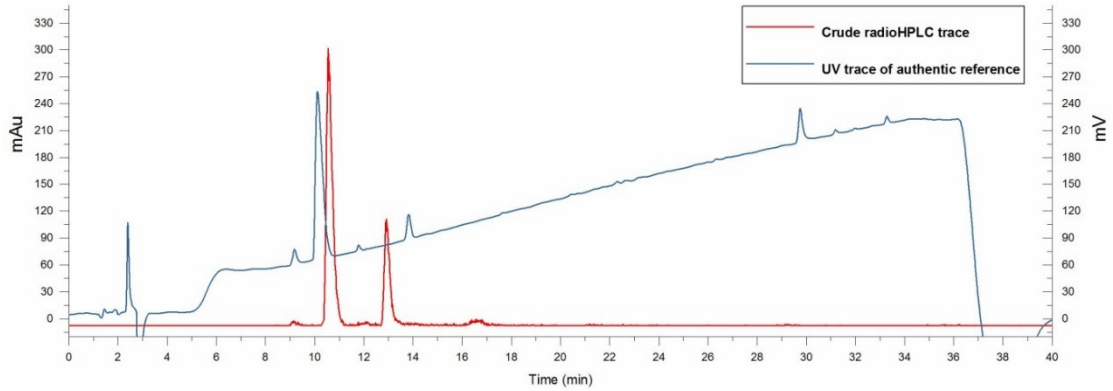

HPLC radio-trace of **[18F]3.184** (red) overlaid with HPLC UV-trace (220 nm) of **[19F]3.184** (blue).

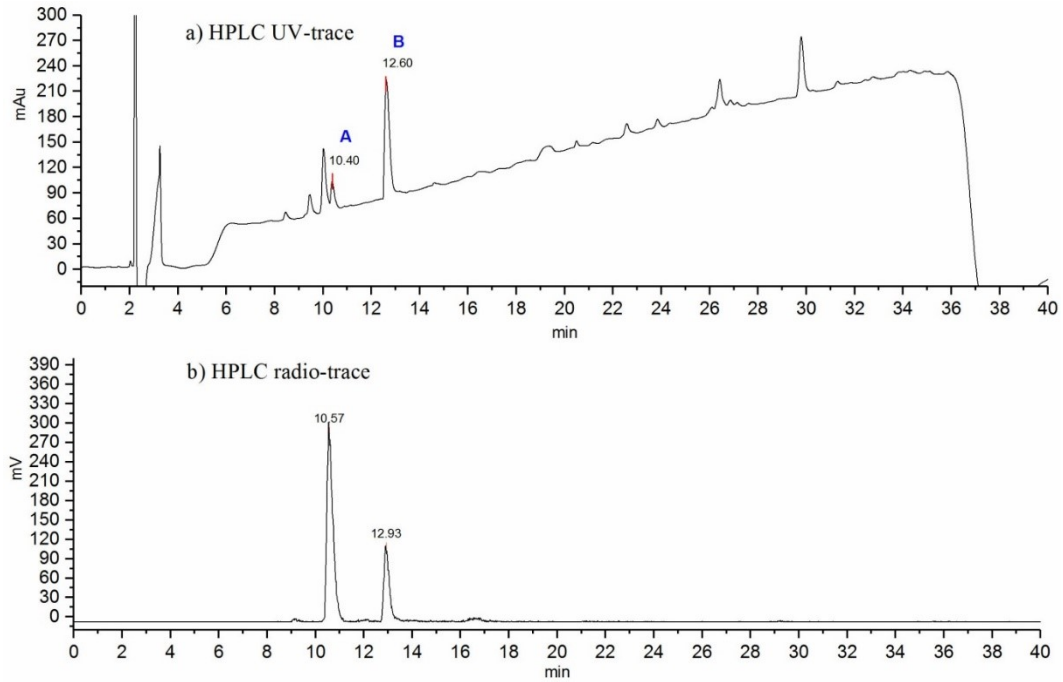

Crude HPLC UV-trace and HPLC radio-trace of the ^{18}F-trifluoromethylation of in H-Cys-Gly-Lys-Lys-Gly-Met-Val-Gly-Gly-Val-Val-OH trifluoroacetate salt in DMSO/H_2O 4:1 using Et_4NHCO_3 as base.

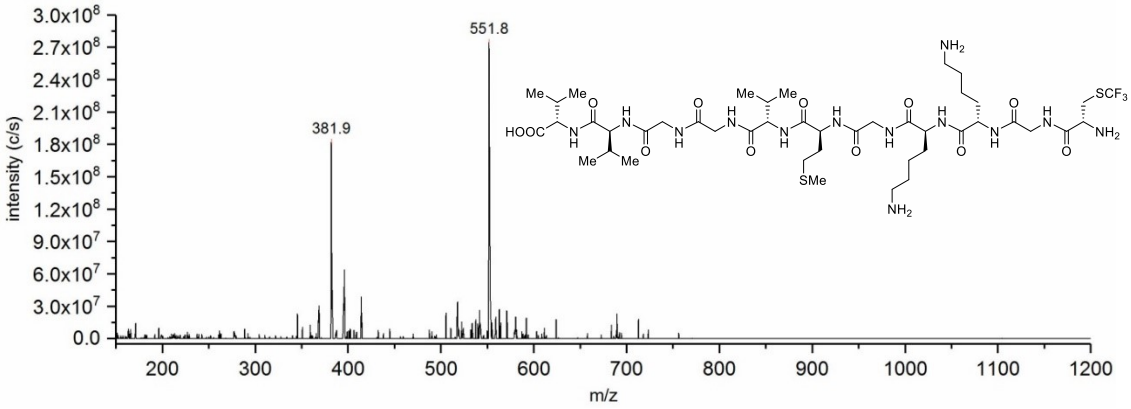

Peak A. *m/z* Calcd for $C_{44}H_{80}F_3N_{13}O_{12}S_2$ $[M+2H]^{2+}$ 551.8, found 551.8.

Cyclo(Arg-Gly-Asp-D-Phe-Cys($[^{18}F]CF_3$) ($[^{18}F]$3.186)

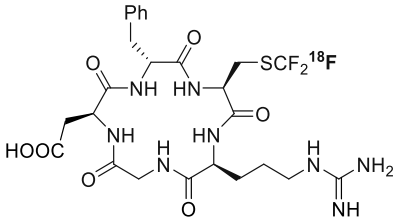

An aliquot of a solution of ^{18}F-Umemoto **[^{18}F]3.109** in CH_3CN (120 μL, 32-61 MBq) was added to a v-vial and heated at 100 °C under a nitrogen flow (2 minutes) to remove solvent. The vial was allowed to cool to room temperature, after which a solution of cyclo(Arg-Gly-Asp-D-Phe-Cys) acetate salt (2.0 mg, 3.1 μmol), Et_4NHCO_3 (2.0 mg, 10 μmol) in DMSO 4:1 (40 μL) was added via syringe. The sealed vial was stirred at for 20 minutes at 40 °C. The reaction mixture was diluted with MeOH/H_2O + 0.1% TFA (1:1, 120 μL) and loaded onto a semi-prep column (Phenomenex Luna C18(2) 150 x 100mm) for purification (Eluent E, flowrate 4.0 mL/min). **[^{18}F]3.186** was collected at Rt = 15.3-15.8 Min. Radiochemical purity and product identity were determined by radio-HPLC (Eluent E).

Reaction	Starting Activity (Mbq)	Isolated Activity after prep-HPLC (MBq)	Radio-HPLC purity	Molar Activity (GBq μmol^{-1})	RCY (n.d.c)
1	60.9	9.4	>99%	0.15	15%
2	30.2	7.2	>99%	0.16	22%
Radiochemical Yield + Standard Deviation					19% ± 5%

Isolated Radiochemical Yield of **[^{18}F]3.186**

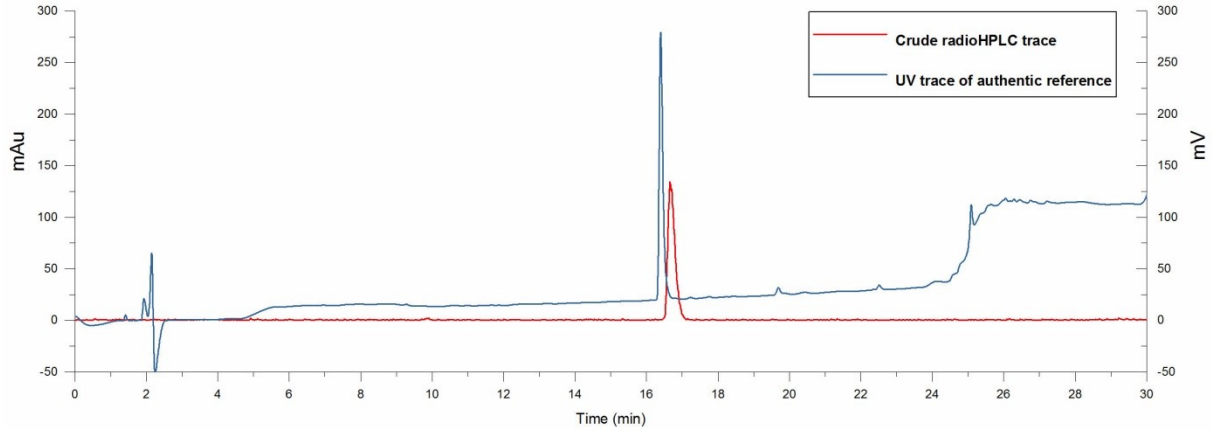

HPLC radio-trace of **[^{18}F]3.186** (red) overlaid with HPLC UV-trace (220 nm) of **[^{19}F]3.186** (blue).

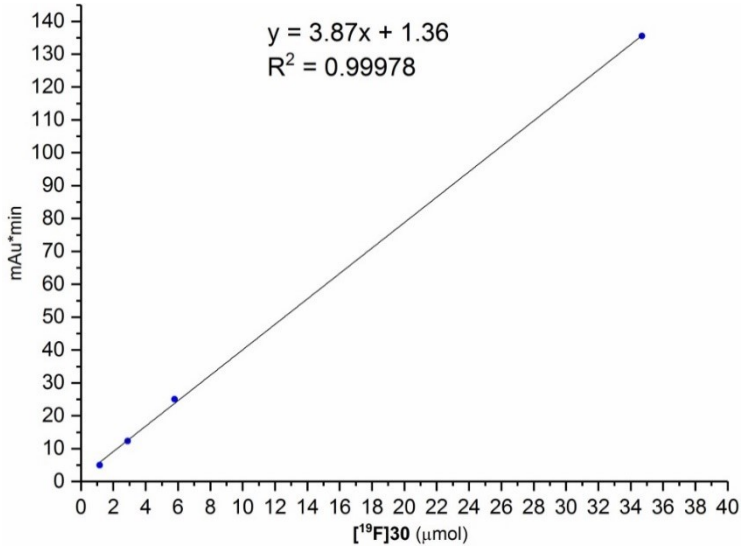

Calibration curve acquired with authentic standard (220 nm) for determination of molar activity of **[^{18}F]3.186**

5.7 Biological Procedures and Characterisation for Chapter III

The solution of cyclo(Arg-Gly-Asp-D-Phe-Cys([^{18}F]CF_3) **[^{18}F]3.186** obtained after prep-HPLC was diluted with H_2O (8 mL) and loaded onto an Oasis HLB plus cartridge, after which it was flushed with H_2O (2 mL) followed by air. **[^{18}F]3.186** was

eluted with EtOH (1.0 mL), and solvent was removed at 70 °C under a stream of nitrogen followed by reconstitution in 10 mM PBS buffer (pH 7.4).

Naïve CBA mice (n = 3) were anaesthetised using 2-4% isoflurane on room air/oxygen (80/20) and a tail vein cannula was placed for dosing of **[^{18}F]3.186** (1-3 MBq, 100 μL). Core body temperature of the mice was maintained at 37 ° C and respiration rate was monitored and kept at 40-60 BPM for the duration of the imaging protocol. Dynamic whole-body PET imaging using the VECTor^{4}CT fitted with the HE-UHR-RM collimator was performed (MIlabs, Utrecht, The Netherlands). Data were acquired in list mode and 12 frames of 5 minutes were recorded (10 bed positions per frame). The radiotracer was injected manually during the second frame.

The PET images were reconstructed with MILabs reconstruction software using pixel-based ordered-subset expectation maximization (POSEM) with 8 iterations and 16 subsets, on 0.8 mm isotropic 3D voxel grids. Triple-energy-window based scatter correction and CT-based non-uniform attenuation correction was applied. The CT scans were reconstructed using cone-beam filtered backprojection (Feldkamp algorithm) on a 0.2 mm voxel grid. The PET images were registered to the CT images and a quantification factor was applied to allow absolute quantitation of the PET data.

Reconstructed images were viewed and analysed using PMOD v.3.37 (PMOD Technologies, Zurich, Switzerland). The radioactivity in each volume of interest was calculated as % Injected dose per cubic cm (%ID/cm^3).

Immediately following imaging, mice were sacrificed with an overdose of anaesthesia and the organs and tissues were removed, washed, and weighted. The radioactivity of

the samples was counted by use of an auto γ-counting system (Hidex AMG, LabLogic, UK). The amount of radioactivity in the organs and tissues was calculated as % Injected dose per gram of tissue (%ID/g).

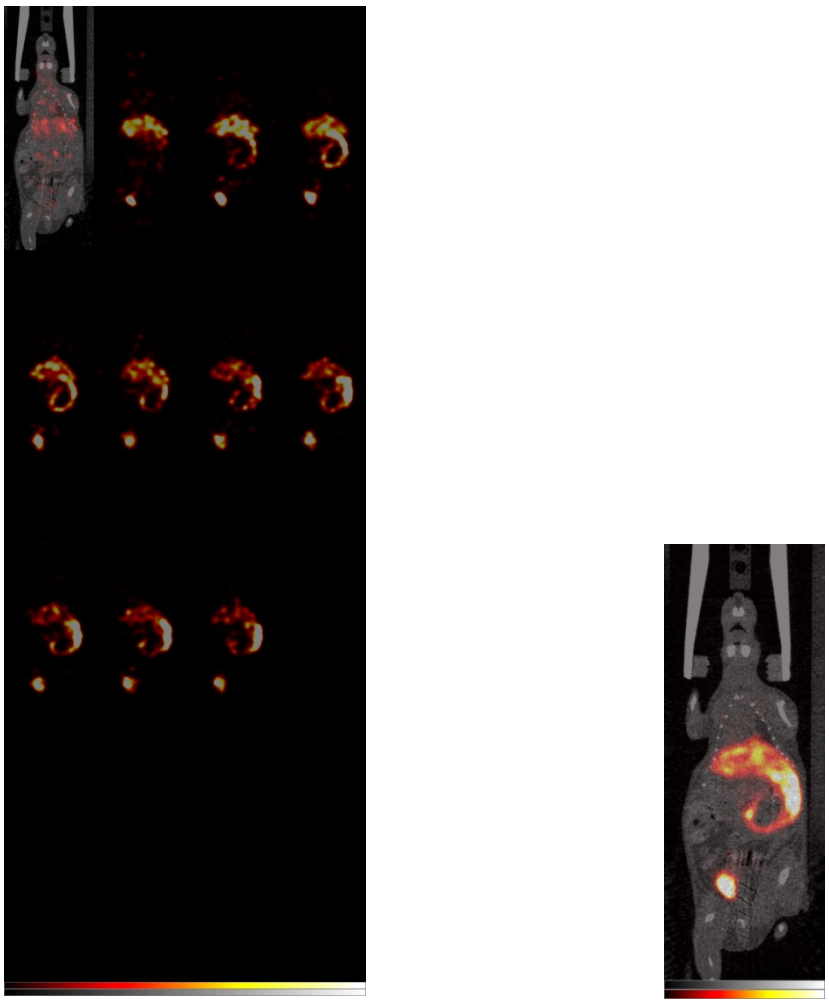

a) **b)**

a) Dynamic PET-CT images of cRGDfC([^{18}F]CF_3) **[^{18}F]3.186** over 60 min after intravenously injection into a naïve CBA mouse. b) Time averaged image.

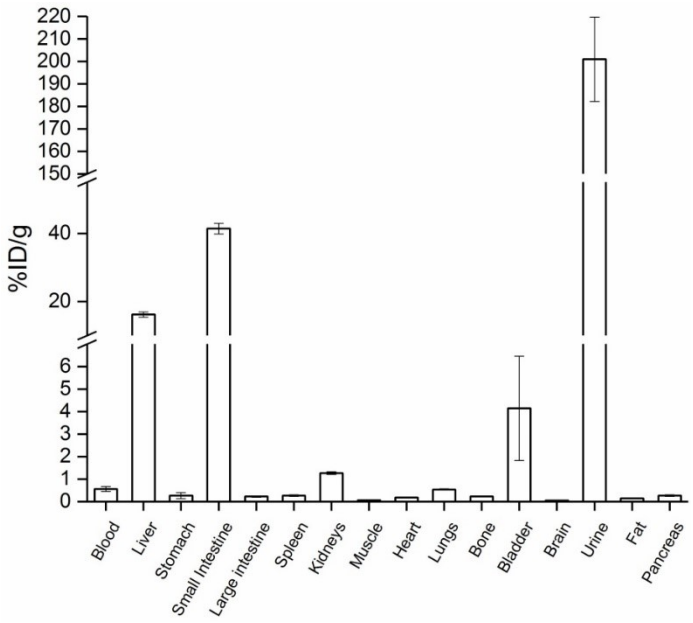

Biodistribution in selected organs of cRGDfC([^{18}F]CF_3) **[^{18}F]3.186** 1h post injection in naïve CBA mice (n = 3).

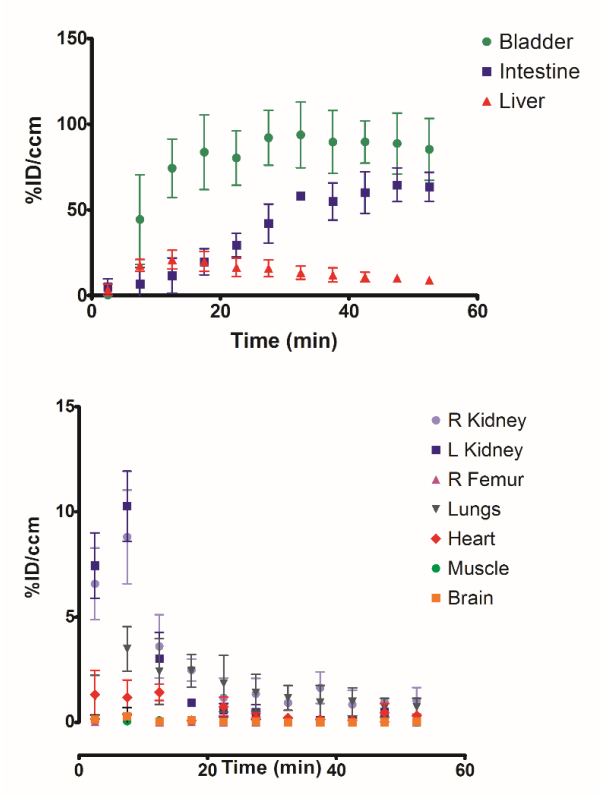

Time-activity curves of accumulation of cRGDfC([^{18}F]CF_3) **[^{18}F]3.186** in selected organs in naïve CBA mice (n = 3)

5.8 Experimental Procedures and Characterisation for Compounds in Chapter IV:

(*E*)-2-Iodoethenylbenzene (4.60)

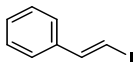

In a round bottom flask were introduced at room temperature 4,4,5,5-tetramethyl-2-[(*E*)-2-phenylethenyl]-1,3,2-dioxaborolane (104 mg, 0.45 mmol), NaI (149 mg, 0.99 mmol), Chloramine-T (140 mg, 0.49 mmol), THF (2 mL)and NaOH (1M solution in H_2O, 2 mL). The solution was allowed to stir at room temperature for 24 h, $Na_2S_2O_3$ saturated solution was added (20 mL) and extraction was performed with DCM (3 x 20 mL). The organic layers were dried with $MgSO_4$ and evaporated. Purification by silica gel chromatography using cyclohexane as eluent afforded (*E*)-2-iodoethenylbenzene as a colourless oil (64 mg, 62%).

^{1}H NMR (400 MHz, $CDCl_3$): δ = 7.44 (d, *J* = 14.9 Hz, 1H), 7.38 – 7.27 (m, 5H), 6.84 (d, *J* = 14.9 Hz, 1H); **^{13}C NMR** (100 MHz, $CDCl_3$): δ = 145.1, 137.8, 128.8, 128.5, 126.1, 76.8. Data consistent with literature values.[7]

1-Iodo-4-(2-phenylethynyl)benzene (4.65):

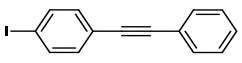

In a round bottom flask were introduced 4,4,5,5-tetramethyl-2-[4-(2-phenylethynyl)phenyl]-1,3,2-dioxaborolane (100 mg, 0.33 mmol), NaI (108 mg, 0.72 mmol), Cu_2O (2.3 mg, 1.65 μmol), 1,10-phenanthroline (11.8 mg, 0.066 mmol), MeOH (3.6 mL) and H_2O (0.8 mL). The mixture was heated for 1h at 80 °C and, after cooling down to room temperature, water (20 mL) was added and extraction was performed with DCM (3 x 20mL). The organic layers were dried with MgSO4

and evaporated. Purification by silica gel chromatography using cyclohexane as eluent afforded 1-iodo-4-(2-phenylethynyl)benzene as a white powder (68 mg, 68%).

^{1}H NMR (400 MHz, $CDCl_3$): δ = 7.71 – 7.67 (m, 2H), 7.55 – 7.50 (m, 2H), 7.38 – 7.33 (m, 3H), 7.26 (d, *J* = 8.4 Hz 2H); **^{13}C NMR** (100 MHz, $CDCl_3$): δ = 137.6, 133.2, 131.7, 128.7, 128.5, 123.1, 122.9, 94.2, 90.9, 88.6. Data consistent with literature values.[8]

Potassium-3-nitrophenyltrifluoroborate (4.76):

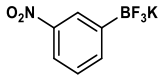

In a round bottom flask were introduced at room temperature 3-nitrophenyl boronic acid (400 mg, 2.40 mmol), potassium hydrogen difluoride (742 mg, 9.50 mmol) and a 1:1 mixture of H_2O:MeOH (15 mL). The solution was allowed to stir at room temperature for 2h before the solvent was removed *in vacuo*. To the crude mixture was added H_2O (20 mL) before extraction was performed with $CHCl_3$ (3 x 20 mL). The organic layers were then combined, dried with $MgSO_4$ and excess solvent removed *in vacuo* affording potassium-3-nitrophenyltrifluoroborate as a white solid (522 mg, 95%).

^{1}H NMR (400 MHz, $CDCl_3$): δ = 8.15 – 8.08 (m, 1H), 7.93 (ddd, *J* = 8.1, 2.6, 1.2 Hz, 1H), 7.74 (d, *J* = 7.2 Hz, 1H), 7.41 (t, *J* = 7.1 Hz, 1H); **^{19}F NMR** (376 MHz, $CDCl_3$): δ = - 140.0 – - 140.6 (bs, 3F). Data consistent with literature values.[9]

Synthesis of *N,N*-diethyl-2-(2-(3-iodo-4-methoxyphenyl)-5,7-dimethyl pyrazolo[1,5-*a*]pyrimidin-3-yl) acetamide: DPA-713[a]

General procedure A:

Under argon, to a 5 mL solution of THF at – 78 °C and *n*-butyllithium (12 mmol, 2.5 M in *n*-hexane), a solution of acetonitrile (18 mmol in 10 mL THF) was added drop-wise over a period of 20 minutes. The solution was left to stir at -78 °C for one hour before the chosen benzoate (6 mmol in 10 mL THF) was added over a period of 15 minutes. After one hour the reaction was warmed to – 45 °C and the stirring continued until complete consumption of starting material was observed *via* TLC. The reaction was quenched using 2M HCl (50 mL), diluted with EtOAc (50 mL) and the layers were separated. The organic layer was washed with brine (4 x 40 mL), dried with $MgSO_4$ and concentrated to afford the expected 3-oxo-3-phenylpropanenitrile derivatives.

General Procedure B:

Potassium carbonate (8 mmol) was added to a reaction vessel charged with, the chosen 3-oxo-3-phenylpropanenitrile derivative (4 mmol) in THF (30 mL). Subsequently, 2-bromodiethylacetamide (6 mmol) was added dropwise and the reaction was left to stir overnight. The reaction was quenched using 1 M HCl (50 mL), followed by dilution with ethyl acetate (60 mL) and the layers were separated. The mixture was washed with brine (3 x 50 mL), dried and concentrated *in vacuo*. The crude sample was flushed through a short plug of silica using EtOAc:cyclohexane (2:8 to

[a] The synthesis of the DPA-713 boronic ester precursor was carried out by G. McSweeney

4:6) as the eluent to give an oil. This oil was dissolved in ethanol (30 mL), treated with hydrazine monohydrate (8 mmol), glacial acetic acid (8 mmol) and was heated to reflux for 18 hours. The solvent was evaporated under reduced pressure and diluted with ethyl acetate before being washed with saturated sodium carbonate (3 x 50 mL). The organic layer was dried with $MgSO_4$ and concentrated i*n vacuo* prior to purification via flash column chromatography Methanol:DCM (3:97) as the eluent to afford the expected pyrazolo[1,5-*a*]pyrimidin-3-yl]acetamide derivatives.

General Procedure C:

2,4-Pentanedione (4 mmol) was added to a solution of the chosen pyrazolo[1,5-*a*]pyrimidin-3-yl]acetamide derivative (2 mmol in 10 mL of EtOH). The reaction mixture was heated at reflux for 20 h. Upon cooling to ambient temperature, the solvent was removed in *vacuo*. The crude material was purified by column chromatography using dichloromethane/methanol (9:1) as the eluent to give the expected DPA-713 analogues.

3-(3-Iodo-4-methoxyphenyl)-3-oxopropanenitrile

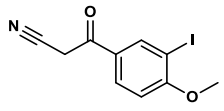

Synthesised following general procedure A, yielding 3-(3-iodo-4-methoxyphenyl)-3-oxopropanenitrile (1.80 g, 95% yield) as a white powder.

^{1}H NMR (400 MHz, $CDCl_3$): δ = 8.32 (d, *J* = 2.2 Hz, 1H), 7.92 (dd, *J* = 8.7, 2.2 Hz, 1H), 6.89 (d, *J* = 8.7 Hz, 1H), 4.02 (s, 2H), 3.98 (s, 3H); **^{13}C NMR** (100 MHz, $CDCl_3$): δ = 184.4, 163.0, 140.2, 130.9, 128.8, 113.7, 110.4, 86.5, 56.9, 29.1; **IR** (*ν,* cm^{-1}): 2941,

2269, 1707, 1583, 1256, 1203, 935, 818, 662; **HRMS** (ESI) for $C_{10}H_8O_2N^{127}I$ [M + Na]$^+$ requires m/z 323.9492, found 323.9490; **M.P.** 128 – 130 °C.

2-Bromo-*N,N*-diethylacetamide

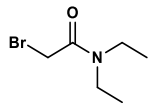

Freshly distilled diethylamine (2 mL, 19.8 mmol) was slowly added to a solution of bromoacetyl bromide (860 μL, 9.9 mmol) in 50 mL dichloromethane at – 78 °C. The mixture was allowed to warm to room temperature and left to stir for one hour. 25 mL of H_2O was added and the reaction mixture was extracted with dichloromethane (3 x 40 mL). The combined organic layers were dried with $MgSO_4$ and concentrated, yielding 2-bromo-*N,N*-diethylacetmide as a white solid (98%, 1.9 g, 9.8 mmol). The spectroscopic data matched that of the literature.[10]

^{1}H NMR (400 MHz; $CDCl_3$): δ = 3.86 (s, 2H), 3.41 (qd, *J* = 7.2, 2.6 Hz, 4H), 1.27 (t, *J* = 7.2 Hz, 3H), 1.16 (t, *J* = 7.2 Hz, 3H); **^{13}C NMR** ($CDCl_3$, 100 MHz): δ = 165.9, 42.9, 40.5, 26.4, 14.4, 12.5.

2-(3-Amino-5-(3-iodo-4-methoxyphenyl)-1*H*-pyrazol-4-yl)-*N,N*-diethylacetamide

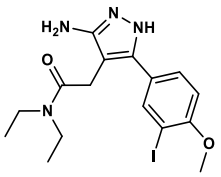

Synthesised following general procedure B, yielding 2-[5-amino-3-(3-iodo-4-methoxyphenyl)-*1H*-pyrazol-4-yl]-*N,N*-diethylacetamide (0.94 g, 55%) as a yellow

powder.

^{1}H NMR (400 MHz, $CDCl_3$): δ = 7.78 (d, *J* = 2.1 Hz, 1H), 7.34 (dd, *J* = 8.4, 2.1 Hz, 1H), 6.81 (d, *J* = 8.5 Hz, 1H), 5.97 (bs, 2H), 3.89 (s, 3H), 3.46 (s, 2H), 3.33 (q, *J* = 7.1 Hz, 2H), 3.12 (q, *J* = 7.1 Hz, 2H), 1.09 (t, *J* = 7.1 Hz, 3H), 0.98 (t, *J* = 7.1 Hz, 3H). (Signal due to pyrazole NH is not observed); **^{13}C NMR** (100 MHz, $CDCl_3$): δ = 170.3, 158.2, 153.8, 141.7, 138.6, 129.2, 125.2, 111.9, 97.7, 86.2, 56.5, 42.5, 40.7, 28.3, 14.3, 13.1; **IR** (*ν,* cm^{-1}): 3210, 2968, 1610, 1506, 1432, 1251, 1046, 814; **HRMS** (ESI) for $C_{16}H_{22}O_2N_4{}^{127}I$ $[M+H]^+$ requires *m/z* = 429.0782, found 429.0779; **M.P.** 87 – 89 °C.

***N*,*N*-Diethyl-2-(2-(3-iodo-4-methoxyphenyl)-5,7-dimethylpyrazolo[1,5-*a*]pyrimidin-3-yl)acetamide**

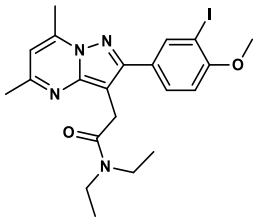

Synthesised following general procedure C, yielding *N*,*N*-diethyl-2-[2-(3-iodo-4-methoxyphenyl)-5,7-dimethylpyrazolo[1,5-*a*]pyrimidin-3-yl]acetamide (836 mg, 85% Yield) as a yellow powder. The data matched that of the literature.[11]

^{1}H NMR (400 MHz, $CDCl_3$): δ = 8.19 (d, *J* = 2.1 Hz, 1H), 7.87 (dd, *J* = 8.5, 2.1 Hz, 1H), 6.90 (d, *J* = 8.5 Hz, 1H), 6.52 (d, *J* = 0.6 Hz, 1H), 3.92 (s, 2H), 3.91 (s, 3H), 3.52 (q, *J* = 7.1 Hz, 2H), 3.42 (q, *J* = 7.1 Hz, 2H), 2.74 (d, *J* = 0.6 Hz, 3H), 2.55 (s, 3H), 1.24 (t, *J* = 7.1 Hz, 3H), 1.13 (t, *J* = 7.1 Hz, 3H); **^{13}C NMR** (101 MHz, $CDCl_3$): δ = 169.8, 158.2, 157.7, 153.5, 139.3, 130.1, 128.3, 110.7, 108.4, 101.0, 100.0, 86.1, 56.5,

42.4, 40.7, 28.1, 24.6, 17.0, 14.5, 13.2; **M.P.** 151 – 152 °C; The data is consistent with that of the literature.[6]

3-(3-Bromo-4-methoxyphenyl)-3-oxopropanenitrile (4.87)

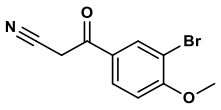

Synthesised following general procedure A, yielding 3-(3-bromo-4-methoxyphenyl)-3-oxopropanenitrile (1.42 g, 93%) as yellow powder.

^{1}H NMR (400 MHz, $CDCl_3$): δ = 8.11 (s, 1H), 7.88 (d, *J* = 8.7 Hz, 1H), 6.98 (d, *J* = 8.7 Hz, 1H), 4.05 (s, 2H), 3.99 (s, 3H); **^{13}C NMR** (101 MHz, $CDCl_3$): δ = 184.7, 160.9, 133.9, 129.9, 128.2, 113.8, 112.6, 111.5, 56.8, 29.2; **IR** (*ν,* cm^{-1}): 2980, 2915, 2255, 1687, 1589, 1285, 1202, 966, 828, 818, 774, 676; **HRMS** (ESI) for $C_{10}H_7O_2N^{79}Br$ $[M+H]^+$ requires *m/z* = 251.9665 found 251.9674; **M.P.** 110 – 112 °C.

2-(3-Amino-5-(3-bromo-4-methoxyphenyl)-1*H*-pyrazol-4-yl)-*N*,*N*-diethylacetamide (4.85)

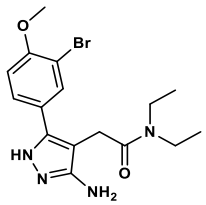

Synthesised following general procedure B, yielding 2-[5-amino-3-(3-bromo-4-methoxyphenyl)-*1H*-pyrazol-4-yl]-*N*,*N*-diethylacetamide (0.81 g, 53%) as a yellow powder.

^{1}H NMR (400 MHz, $CDCl_3$): δ = 7.53 (d, *J* = 2.1 Hz, 1H), 7.27 (dd, *J* = 8.5, 2.1 Hz, 1H), 6.83 (d, *J* = 8.5 Hz, 1H), 3.89 (s, 3H), 3.45 (s, 2H), 3.32 (q, *J* = 7.1 Hz, 2H), 3.10

(q, *J* = 7.1 Hz, 2H), 1.07 (t, *J* = 7.1 Hz, 3H), 0.96 (t, *J* = 7.1 Hz, 3H) (Signal due to pyrazole NH and NH_2 are not observed); **^{13}C NMR** (400 MHz, $CDCl_3$): δ = 170.4, 155.7, 153.3, 142.3, 132.5, 128.2, 125.1, 111.9, 111.7, 97.2, 56.3, 42.4, 40.7, 28.0, 14.4, 13.2; **IR** (*ν,* cm^{-1}): 3542, 2915, 1615, 1595, 1469, 1428, 1229, 1107, 971, 832, 747; **HRMS** (ESI) for $C_{16}H_{21}{}^{79}BrN_4O_2$ $[M+H]^+$ requires *m/z* 379.0775, found 379.0770; **M.P.** 84 – 86 °C.

2-(2-(3-Bromo-4-methoxyphenyl)-5,7-dimethylpyrazolo[1,5-*a*]pyrimidin-3-yl)-*N*,*N*-diethyl acetamide (4.89)

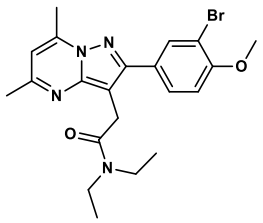

Synthesised following general procedure C, yielding *N*,*N*-diethyl-2-[2-(3-bromo-4-methoxyphenyl)-5,7-dimethylpyrazolo[1,5-*a*]pyrimidin-3-yl]acetamide (0.80 g, 90%) as a yellow powder.

^{1}H NMR (400 MHz, $CDCl_3$): δ = 7.99 (d, *J* = 2.1 Hz, 1H), 7.84 (dd, *J* = 8.5, 2.1 Hz, 1H), 6.97 (d, *J* = 8.5Hz, 1H), 6.51 (d, *J* = 0.9 Hz, 1H), 3.93 (s, 3H), 3.91 (s, 2H), 3.52 (q, *J* = 7.1 Hz, 2H), 3.41 (q, *J* = 7.1 Hz, 2H), 2.73 (d, *J* = 0.8 Hz, 4H), 2.53 (s, 3H), 1.23 (t, *J* = 7.1 Hz, 3H), 1.12 (t, *J* = 7.1 Hz, 3H); **^{13}C NMR** (101 MHz, $CDCl_3$): δ = 169.9, 157.8, 156.0, 153.6, 147.9, 144.9, 133.3, 129.1, 127.9, 111.9, 111.8, 108.5, 101.1, 56.4, 42.5, 40.8, 28.1, 24.8, 17.0, 14.5, 13.2; **IR** (*ν,* cm^{-1}): 2980, 1638, 1554, 1225, 1052, 945, 907, 845, 787, 763; **HRMS** (ESI) for $C_{21}H_{24}BrN_4O_2$ $[M+H]^+$ requires *m/z* 443.1088, found 443.1081; **M.P.** 145 – 146 °C.

***N,N*-Diethyl-2-(2-(4-methoxy-3-(4,4,5,5-tetramethyl-1,3,2-dioxaborolan-2-yl)phenyl)-5,7-dimethylpyrazolo[1,5-*a*]pyrimidin-3-yl)acetamide (4.90)**

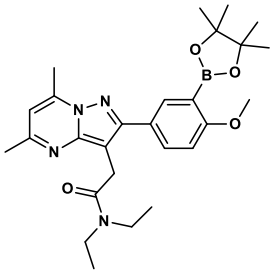

To a 10 mL round bottom under argon, flask charged with 2 mL of Toluene was added *N*,*N*-diethyl-2-[2-(3-bromo-4-methoxyphenyl)-5,7-dimethylpyrazolo[1,5-*a*]pyrimidin-3-yl]acetamide (177 mg, 0.4 mmol), $Pd(dppf)Cl_2.CH_2Cl_2$ (32 mg, 0.04 mmol), potassium acetate (157 mg, 1.6 mmol) and bis(pinacolato)diboron (305 mg, 1.2 mmol). The reaction was left to stir at 85 °C for 18 hours. The reaction was allowed to cool and the solvent removed in *vacuo* before addition of ethyl acetate (5 mL). The mixture was filtered through a short plug of celite, evaporated and subjected to column chromatography using acetone/DCM (1/9 to 2/8) as the eluent. Crystallization followed by filtration from petroleum ether and diethylether afforded *N*,*N*-diethyl-2-{2-[4-methoxy-3-(tetramethyl-1,3,2-dioxaborolan-2-yl)phenyl]-5,7-dimethylpyrazolo[1,5-*a*]pyrimidin-3-yl}acetamide as a white powder (118 mg, 60%).

^{1}H NMR (400 MHz, $CDCl_3$): δ = 8.03 (d, *J* = 2.3 Hz, 1H), 7.89 (dd, *J* = 8.6, 2.3 Hz, 1H), 6.94 (d, *J* = 8.6 Hz, 1H), 6.49 (d, *J* = 0.7 Hz,1H), 3.90 (s, 2H), 3.87 (s, 3H), 3.46 (q, *J* = 7.2 Hz, 2H), 3.39 (q, *J* = 7.1 Hz, 2H), 2.75 (d, *J* = 0.7 Hz, 3H), 2.52 (s, 3H), 1.36 (s, 12H), 1.18 (t, *J* = 7.2 Hz, 3H), 1.10 (t, *J* = 7.1 Hz, 3H); **^{13}C NMR** (400 MHz, $CDCl_3$): δ = 170.0, 164.4, 157.3, 155.1, 147.7, 144.7, 136.9, 133.2, 125.8, 110.5, 108.1, 100.9, 83.4, 56.0, 42.3, 40.7, 28.1, 24.9, 24.7, 17.0, 14.4, 13.1 (Signal due to carbon

bearing the boron is not observed); **IR** (ν, cm^{-1}): 2974, 1649, 1585, 1398, 1249, 1140, 1067, 1024, 859, 759. **HRMS** (ESI) for $C_{27}H_{38}{}^{11}BN_4O_4$ $[M+H]^+$ requires m/z 493.2978, found 493.2978; **M.P.** 120 - 122 °C.

(6-Iodo-2-(4'-dimethylamino)phenyl-imidazo[1,2-*a*]pyridine): IMPY[b]

2,2-Dibromo-1-(4-(dimethylamino)phenyl)ethan-1-one (4.83)

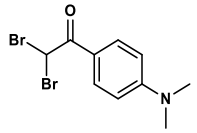

Prepared according to literature procedure.[6] Bromine (1.1 mL, 9.0 mmol) was added dropwise to a solution of 1-(5-(dimethylamino)phenyl-2-yl)ethanone (2.9 g, 18 mmol) in concentrated H_2SO_4 (95%, 18 mL) at 0 °C. The reaction mixture was stirred overnight at room temperature and subsequently poured into ice water and neutralized with 3% NaOH. The aqueous phase was extracted with EtOAc (3 x 70 mL). The organic layers were combined, washed with brine (3 x 70 mL), dried and concentrated in vacuo. Purification of the crude product by column chromatography using EtOAc/hexanes (1/9) afforded 2,2-dibromo-1-(5-(dimethylamino)pyridin-2-yl)ethanone as a yellow-green solid (5 g, 15.6 mmol, 87%).

^{1}H NMR (400 MHz, $CDCl_3$): δ = 7.96 – 7.92 (m, 2H), 6.67 (s, 1H), 6.65 – 6.61 (m, 2H), 3.07 (s, 6H); **^{13}C NMR** (101 MHz, $CDCl_3$): δ = 184.3, 154.3, 132.4, 117.7, 110.9, 77.5, 77.2, 76.8, 40.7, 40.2. Data consistent with literature values.[12]

[b] The synthesis of the IMPY boronic ester precursor was carried out by G. McSweeney

2-Bromo-1-(4-(dimethylamino)phenyl)ethan-1-one (4.84)

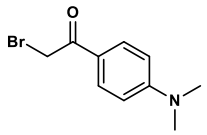

Prepared according to literature procedure.[7] To a solution of 2,2-dibromo-1-(5-(dimethylamino)pyridin- 2-yl)ethanone (3.0 g, 9.3 mmol) in 50 mL of anhydrous THF was added triethylamine (1.4 mL, 10 mmol) and diethyl phosphite (1.3 mL, 10 mmol) at 0 °C. The reaction was stirred overnight at room temperature. The mixture was diluted with ethyl acetate and the aqueous phase further extracted with ethyl acetate (3 x 70 mL). The combined organic layers were washed with brine (3 x 50 mL), dried and concentrated in vacuo. Purification of the crude product via column chromatography using EtOAc/hexanes (1:9) afforded 2-bromo-1-(4-(dimethylamino)phenyl)ethan-1-one as a green solid (1.8 g, 7.5 mmol, 80%).

^{1}H NMR (400 MHz, $CDCl_3$): δ = 8.07 (d, *J* = 1.5 Hz, 1H), 7.98 (d, *J* = 4.4 Hz, 1H), 6.97 (dd, = 4.4, 1.5 Hz, 1H), 4.80 (s, 2H), 3.10 (s, 6H); **^{13}C NMR** (101 MHz, $CDCl_3$): δ = 189.6, 154.2, 132.0 (2C), 121.6, 110.9 (2C), 40.3 (2C), 31.3. Data matched that of the literature.[12]

4-(6-Iodoimidazo[1,2-*a*]pyridin-2-yl)-*N*,*N*-dimethylaniline (4.81)

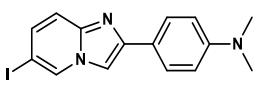

Prepared according to literature procedure.[7] A mixture of 2-bromo-1-(4-(dimethylamino)phenyl)ethan-1-one (484 mg, 2 mmol) and 2-amino-5-iodopyridine (440 mg, 2 mmol) in EtOH (25 mL) was stirred at reflux for 2 hours. The mixture

was allowed to cool and $NaHCO_3$ (250 mg) was then added. Subsequently the mixture was stirred at reflux for 4 hours before being cooled and the precipitate was filtered and washed with cold EtOH giving 4-(6-iodoimidazo[1,2-*a*]pyridin-2-yl)-*N*,*N*-dimethylaniline as a green solid (280 mg, 0.7 mmol, 39% yield).

^{1}H NMR (400 MHz, $CDCl_3$): δ = 7.90 (s, 1H), 7.39 – 7.37 (m, 2H), 6.96 (d, *J* = 9.3 Hz, 1H), 6.85 (dd, *J* = 9.3, 1.4 Hz, 1H), 6.36 – 6.34 (m, 2H), 2.58 (s, 6H).**^{13}C NMR** (101 MHz, $CDCl_3$): δ = 150.5, 147.0, 144.1, 131.8, 130.0, 127.0 (C), 121.2, 118.0, 112.4 (2C), 106.2, 74.4, 40.4; **IR** (*ν,* cm^{-1}): 2981, 2360, 1615, 1512, 1383, 1196, 950, 820, 671; **HRMS** (ESI) for $C_{15}H_{14}IN_3$ $[M+H]^+$ requires *m/z* 364.0305, found 364.0312; **M.P.** 230 – 232 °C; Data consistent with literature values.[13]

N,*N*-Dimethyl-4-(6-(4,4,5,5-tetramethyl-1,3,2-dioxaborolan-2-yl)imidazo[1,2-*a*]pyridin-2-yl)aniline (4.85)

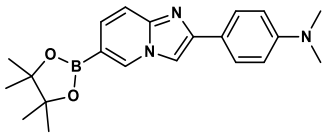

To a solution of 4-(6-iodoimidazo[1,2-*a*]pyridin-2-yl)-*N*,*N*-dimethylaniline (73 mg, 0.2 mmol) in THF (2 mL) at - 78 °C was added 2.5 M nBuLi (96 μL, 0.24 mmol). After 10 minutes 2-Isopropoxy-4,4,5,5-tetramethyl-1,3,2-dioxaborolane (53 μL, 0.26 mmol) was added dropwise. The reaction was left to stir for 30 minutes before addition of NH_4Cl (10 mL). The aqueous layer was extracted with dichloromethane (3 x 20 mL), washed with brine (3 x 20 mL), dried and concentrated in vacuo. The reaction was subjected to column chromatography using MeOH:DCM (2:8) as the eluent affording *N*,*N*-dimethyl-4-(6-(4,4,5,5-tetramethyl-1,3,2-dioxaborolan-2-

yl)imidazo[1,2-*a*]pyridin-2-yl)aniline as an off white solid (58 mg, 1.6mmol, 80% yield).

^{1}H NMR (400 MHz, $CDCl_3$): δ = 8.51 (s, 1H), 7.85 (d, *J* = 8.7 Hz, 2H), 7.70 (s, 1H), 7.57 (d, *J* = 9.0 Hz, 1H), 7.43 (d, *J* = 9.0 Hz, 1H), 6.79 (d, *J* = 8.7 Hz, 2H), 3.00 (s, 6H), 1.37 (s, 12H); **^{13}C NMR** (100 MHz, $CDCl_3$): δ = 149.4, 145.7, 145.2, 131.5, 127.6, 126.0 (2C), 120.6, 115.0, 111.4 (2C), 105.2, 83.2 (2C), 39.5, 23.9 (4C) (Signal due to carbon bearing the boron is not observed); **IR** (*ν,* cm^{-1}): 2980, 2360, 1614, 1538, 1493, 1383, 1271, 965, 948, 820; **HRMS** (ESI) for $C_{21}H_{26}BN_3O_2$ $[M+H]^+$ requires *m/z* 364.2191, found 364.2183; **M.P.** 219 – 222 °C.

***Meta*-fluorobenzyl guanidine*Meta*-iodobenzyl guanidine: MFBG/MIBG**

***tert*-Butyl-{(*Z*)-[(*tert*-butoxycarbonyl)amino][(3-bromobenzyl)amino] methylidene} carbamate**

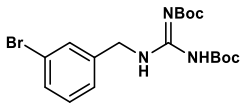

To a stirred solution of 3-bromobenzylamine (0.67 mL, 5.4 mmol) in DCM (10 mL) was added triethylamine (0.89 mL, 6.5 mmol). After 5 minutes stirring, *N,N*'- bis(*tert*-butoxycarboyl)-*N*''-triflylguanidine (2.06 g, 5.4 mmol) was added before leaving the reaction mixture to stir for 30 min. Upon completion, the excess solvent was removed *in vacuo* before adding water (50 mL) and extracting the organic layer with DCM (3 × 30 mL). The organic layers were combined, washed with water (2 × 50 mL) and brine (50 mL), dried with MgSO4, filtered and the solvent removed *in vacuo* affording *tert*-Butyl-{(*Z*)-[(*tert*-butoxycarbonyl)amino][(3-fluorobenzyl)amino]methylidene} carbamate as a white solid (1.75 g, 99%).

^{1}H NMR (400 MHz, $CDCl_3$): δ = 11.54 (s, 1H), 8.60 (bs, 1H), 7.47-7.19 (m, 4H), 4.60 (d, *J* = 6 Hz, 2H), 1.51 (s, 9H), 1.48 (s, 9H); **^{13}C NMR** (125.8 MHz, $CDCl_3$): δ = 163.6, 156.2, 153.2, 139.8, 130.9, 130.7, 130.3, 126.4, 122.7, 83.4, 79.5, 44.2, 28.3, 28.1; **IR**: (ν, cm^{-1}) 2979, 1723, 1643, 1620; **HRMS** (ESI): $C_{18}H_{27}{}^{79}BrN_3O_4$ $[M+H]^+$ requires 428.11795 found 428.11743; **M.P.** 111 - 113 °C

***tert*-Butyl-*N*-[(1*Z*)-{bis[(*tert*-butoxy)carbonyl]amino}({[(*tert*-butoxy) carbonyl] ({[3-(bromo)phenyl]methyl})amino})methylidene]carbamate (4.99)**

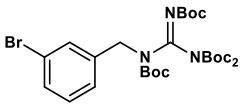

To a round bottom flask was added, *tert*-Butyl-{(*Z*)-[(*tert*-butoxycarbonyl)amino][(3-bromobenzyl)amino]methylidene} carbamate (0.11g, 0.26 mmol), di-*tert*-butyl dicarbonate (0.17 g, 0.77 mmol), dimethylaminopyridine (0.63 mg, 0.52 mmol), triethylamine (0.11 mL, 0.77 mmol) and THF (5 mL). The reaction was then left to stir at room temperature for 16 hours. The solvent was then removed *in vacuo* and the product purified via flash column chromatography (9:1 cyclohexane: EtOAc) gave *tert*-Butyl *N*-[(1*Z*)- {bis[(*tert*-butoxy)carbonyl]amino}({[(*tert*-butoxy)carbonyl]({[3-(bromo) phenyl]methyl}) amino})methylidene] carbamate as a colourless oil (0.15 g, 93%).

^{1}H NMR (400 MHz, $CDCl_3$) δ 7.52 (t, *J* = 1.8 Hz, 1H), 7.36 (ddd, *J* = 7.9, 1.9, 1.0 Hz, 1H), 7.34 - 7.30 (m, 1H), 7.14 (t, 1H, *J* = 7.9), 4.97 (s, 2H), 1.47 (s, 9H), 1.45 (s, 18H), 1.39 (s, 9H); **^{13}C NMR** (100 MHz, $CDCl_3$) δ 157.3, 152.2, 151.1, 147.3, 144.4, 139.8, 136.7, 130.3, 129.9, 126.5, 122.3, 84.1, 83.8, 82.1, 81.0, 49.6, 28.0 (3C), 27.9

(6C), 27.8 (3C); **IR**: (ν, cm^{-1}) 2980, 1808, 1727, 1658, 1380, 1125, 875; **HRMS** (ESI) for $C_{28}H_{42}{}^{79}BrN_3O_8$ $[M+H]^+$ requires 627.2155 found 627.2159.

***tert*-Butyl *N*-[(1*Z*)-{bis[(*tert*-butoxy)carbonyl]amino}({[(*tert*butoxy)carbonyl]({[3-(tetramethyl-1,3,2-dioxaborolan-2-yl)phenyl]methyl})amino}) methylidene] carbamate (4.100):**

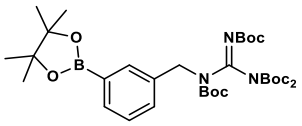

To a dried schlenk tube under an atmosphere of argon was added *tert*-Butyl-*N*-[(1*Z*)-{bis[(*tert*-butoxy)carbonyl]amino}({[(*tert*-butoxy)carbonyl]({[3-(bromo)phenyl] methyl})amino})methylidene]carbamate (0.15g, 0.24 mmol), bis(pinacolato)diboron (133 mg, 5.3 mmol), potassium acetate (67 mg, 0.012 mmol), dichloro[1,1'-bis(diphenylphosphino)ferrocene]-palladium(II) dichloromethane adduct (10 mg, 0.14 mmol) and DMF (3 mL) for 16 h. Upon completion, the reaction was extracted in DCM (10 mL) and washed with Brine (3 × 30 mL). The organic layer was combined, dried with $MgSO_4$, filtered and the solvent removed *in vacuo* affording a crude mixture of *tert*-Butyl *N*-[(1*Z*)-{bis[(*tert*-butoxy)carbonyl]amino}({[(*tert*-butoxy)carbonyl] ({[3-(tetramethyl-1,3,2-dioxaborolan-2-yl)phenyl]methyl})amino}) methylidene] carbamate and bis(pinacolato)diboron (0.15 g). The crude product was then purified by reverse phase prep-HPLC, affording *tert*-Butyl *N*-[(1*Z*)-{bis[(*tert*-butoxy)carbonyl]amino}({[(*tert*butoxy)carbonyl]({[3-(tetramethyl-1,3,2-dioxaborolan -2-yl)phenyl]methyl})amino}) methylidene] carbamate as a colourless oil (0.10 g, 63%, 0.08 mmol).

^{1}H NMR (400 MHz, $CDCl_3$): δ = 7.78 (s, 1H), 7.69-7.66 (m, 1H), 7.53-.48 (m, 1H), 7.29 (d, J = 7.5, 1H), 5.03 (s, 2H), 1.48 (s, 9H), 1.45 (s, 18H), 1.38 (s, 9H), 1.32 (s, 12H); **^{13}C NMR** (100 MHz, $CDCl_3$): δ = 157.5, 151.3, 147.4, 144.5, 136.7, 134.3, 133.5, 130.6, 127.7, 83.7, 83.7, 83.6, 81.9, 50.0, 28.0, 27.9, 27.8, 24.9 (note: CAr-B was not observed); **IR** (ν, cm^{-1}): 2979, 1806, 1727, 1653, 1127, 1102, 852; **HRMS** (ESI) for $C_{34}H_{55}{}^{10}BN_3O_{10}$ $[M+H]^+$ requires 675.4011 found 675.3996.

***tert*-Butyl{(*Z*)-[(3-iodobenzyl)amino][(*tert*-butoxycarbonyl)amino] methylidene}carbamate**.

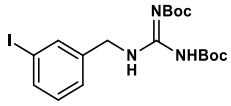

To a stirred solution of 3-iodobenzylamine (0.50 g, 1.05 mmol) in DCM (10 mL) was added triethylamine (0.43 mL, 3.15 mmol). After 5 minutes stirring, *N,N*'-bis(*tert*-butoxycarboyl)-*N*''-triflylguanidine (0.411 g, 1.05 mmol) was added before leaving the reaction mixture to stir for 30 mins. Upon completion, the excess solvent was removed *in vacuo* before adding water (10 mL) and extracting the organic layer with DCM (3 × 10 mL). The organic layers were combined, washed with water (2 × 10 mL) and brine (10 mL), dried with $MgSO_4$, filtered and the solvent removed *in vacuo* affording the *tert*-Butyl{(*Z*)-[(3-iodobenzyl)amino][(*tert*-butoxycarbonyl)amino] methylidene} carbamate as a white solid (0.40 g 81%).

^{1}H NMR (400 MHz, $CDCl_3$) δ = 11.53 (s, 1H), 8.59 (bs, 1H), 7.66 (s, 1H), 7.61 (dd, *J* = 7.8, 1.6 Hz, 1H), 7.27 (d, *J* = 7.8, 1H), 7.07 (t, *J* = 7.8 Hz, 1H), 4.57 (d, *J* = 5.4 Hz, 2H), 1.51 (s, 9H), 1.48 (s, 9H); **^{13}C NMR** (101 MHz, $CDCl_3$) δ = 163.6, 156.3, 153.3, 139.9, 137.0, 136.8, 130.6, 127.2, 94.7, 83.5, 79.7, 44.2, 28.4, 28.2; **IR** (*ν,* cm^{-1}):

2980, 1720, 1639, 1617, 1457, 1327, 1157, 1133; **HRMS** (ESI) for $C_{18}H_{27}N_3O_4{}^{127}I$ $[M+H]^+$ requires 476.1040 found 476.1039; **M.P.** 95 – 97 °C.

***tert*-Butyl-*N*-[(1*Z*)-{bis[(*tert*-butoxy)carbonyl]amino}({[(tert-butoxy) carbonyl][(3-iodophenyl) methyl]amino})methylidene]carbamate**.

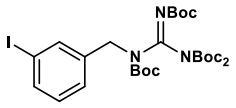

To a round bottom flask was added, *tert*-butyl{(*Z*)-[(3-iodobenzyl)amino][(*tert*-butoxycarbonyl)amino]methylidene}carbamate (0.61 g, 1.28 mmol), di-*tert*-butyl dicarbonate (0.89 g, 5.12 mmol), dimethyl amino pyridine (0.47 g, 3.84 mmol), triethylamine (0.71 mL, 5.12 mmol) and THF (10 mL). The reaction was then left to stir at room temperature 17 hours. Upon completion, the solvent was removed *in vacuo* and the product purified via flash column chromatography (8:2 cyclohexane: EtOAc) affording *tert*-butyl-*N*-[(1*Z*)-{bis[(*tert*-butoxy)carbonyl]amino}({[(*tert*-butoxy)carbonyl][(3-iodophenyl)methyl]amino}) methylidene] carbamate as a colourless oil (0.59 g, 68%).

^{1}H NMR (400 MHz, $CDCl_3$): δ = 7.74 (t, *J* = 1.5 Hz, 1H), 7.61 – 7.53 (m, 1H), 7.39 (d, *J* = 7.8, 1H), 7.02 (t, *J* = 7.8 Hz, 1H), 4.96 (s, 2H), 1.49 (s, 9H), 1.46 (s, 18H), 1.41 (s, 9H); **^{13}C NMR** (101 MHz, $CDCl_3$): δ = 157.4, 151.2, 147.4, 144.3, 140.0, 136.9, 136.4, 130.1, 127.4, 94.1, 84.2, 83.9, 82.2, 49.5, 28.1, 28.0, 28.0; **IR** (*ν,* cm^{-1}): 2980, 1808, 1727, 1652, 1368, 1279, 1252, 1127, 1102; **HRMS** (ESI) for $C_{28}H_{42}N_3O_8{}^{127}I^{23}Na$ $[M+Na]^+$ requires 698.1909 found 698.1906; **M.P.** 61 – 63 °C.

***tert*-Butyl{(*Z*)-[(3-fluorobenzyl)amino][(*tert*-butoxycarbonyl)amino] methylidene} carbamate**

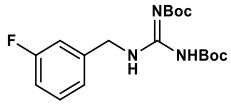

To a stirred solution of 3-fluorobenzylamine (0.23 mL, 2.00 mmol) in DCM (2 mL) was added triethyamine (0.28 mL, 2.00 mmol). After 5 minutes stirring, *N,N′*-Di-Boc-1*H*-pyrazole-1-carboxamidine (0.75 g, 2.4 mmol) was added before leaving the reaction mixture to stir for 30 mins. Upon completion, the excess solvent was removed *in vacuo* before re-dissolving in Et_2O (10 mL) The organic layer was washed with water (2 × 10 mL) and brine (10 mL) before extraction. The organic layer was dried with $MgSO_4$ and the solvent removed *in vacuo*. Purification *via* column chromatography (4:1 Hex: EtOAc) afforded the *tert*-Butyl{(*Z*)-[(3-fluorobenzyl)amino][(*tert*-butoxycarbonyl)amino] methylidene} carbamate as a white solid (0.66 g, 1.79 mmol, 91 %)

^{1}H NMR (400 MHz, $CDCl_3$): δ = 11.48 (s, 1H), 8.55 (bs, 1H), 7.26-7.19 (m, 1H), 7.02 – 6.87 (m, 3H), 4.56 (d, J = 6 Hz, 2H), 1.44 (s, 9H), 1.42 (s, 9H); **^{13}C NMR** (125.8 MHz, $CDCl_3$): δ = 164.2, 163.6, 161.8, 154.7 (d, J = 300 Hz), 139.9 (d, J = 7 Hz), 130.2 (d, J = 8 Hz), 123.3 (d, J = 3 Hz), 114.7 (d, J = 17 Hz), 114.5 (d, J = 17 Hz), 83.3, 79.5, 44.3 (d, J = 2 Hz), 28.3 (3C), 28.1 (3C); {^{1}H}^{19}F NMR (376 MHz, $CDCl_3$): δ = − 112.7; **IR** (ν, cm^{-1}) 2980, 1720, 1639, 1616; **HRMS (ESI)** for $C_{18}H_{27}FN_3O_4$ $[M+H]^+$ requires 368.19801 found 368.19764; **M.P.** 119 - 120 °C.

***tert*-Butyl-N-[(1Z)-{*bis*[(tert-butoxy)carbonyl]amino}({[(*tert*-butoxy)carbonyl][(3-fluorophenyl)methyl]amino})methylidene]carbamate**

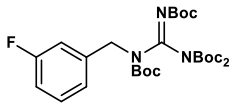

To a round bottom flask was added, *tert*-butyl{(*Z*)-[(3-fluorobenzyl)amino][(*tert*-butoxycarbonyl)amino]methylidene}carbamate (0.20 g, 0.54 mmol), di-*tert*-butyl dicarbonate (0.36 g, 1.63 mmol), dimethylaminopyridine (0.13 g, 1.09 mmol), triethylamine (0.21 mL, 1.63 mmol) and THF (5 mL). The reaction was then left to stir at room temperature overnight. Upon completion, the solvent was removed *in vacuo* and the product purified via flash column chromatography (8:2 cyclohexane: EtOAc) afford *tert*-Butyl-N-[(1Z)-{*bis*[(tert-butoxy)carbonyl]amino}({[(*tert*-butoxy)carbonyl][(3-fluoro phenyl)methyl]amino})methylidene]carbamate as a white powder (0.27 g, 0.47 mmol, 86%).

^{1}H NMR (400 MHz, $CDCl_3$): δ = 7.24 (td, 1H, J = 7.9, 5.9 Hz), 7.14 (d, 1H, J = 7.7 Hz), 7.12 – 7.07(m, 1H), 6.96 – 6.88 (m, 1H), 5.01 (s, 2H), 1.48 (s, 9H), 1.47 (s, 18H), 1.38 (s, 9H); **^{13}C NMR** (100 MHz, $CDCl_3$): δ = 163.0 (d, J = 245 Hz), 157.4, 151.2, 147.4 (2C), 144.6, 140.2 (d, J = 7.2 Hz), 129.8 (d, J = 8.2 Hz), 123.3 (d, J = 2.9 Hz), 114.5 (d, J = 21.8 Hz), 114.1 (d, J = 21.2 Hz), 84.1, 84.0 (2C), 82.2, 49.8 (d, J = 1.2 Hz), 28.1 (3C), 28.0 (6C), 28.0 (3C); **^{19}F NMR** (376 MHz, $CDCl_3$): δ = − 113.63 (td, J = 9.3, 5.9 Hz); **IR**: (ν, cm^{-1}) 2980, 1806, 1725, 1652, 1368, 1123, 1099, 850; **HRMS (ESI)** for $C_{28}H_{43}FN_3O_8$ $[M+H]^+$ requires 568.30287 found 568.30129; **M.P.** 81 – 83 °C.

1-[(3-Fluorophenyl)methyl]guanidine hydrochloride (4.97)

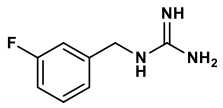

To a round bottom flask under an atmosphere of argon was added, tert-butyl{(Z)-[(3- fluorobenzyl)amino][(tert-butoxycarbonyl)amino] methylidene}carbamate (0.20 g, 0.54 mmol), methanol (10 mL) and conc. hydrochloric acid (0.17 mL, 2.16 mmol). The reaction was heated to 65 °C and left to reflux for 16 h. Upon completion, the solvent was removed in vacuo affording 1-[(3-fluorophenyl)methyl]guanidine hydrochloride as an off white solid (0.06 g, 98 %).

^{1}H NMR (400 MHz, DMSO-d_6): δ = 8.35 (t, J = 6.3 Hz, 1H), 7.61 – 7.28 (m, 3H), 7.25 – 6.99 (m, 3H), 4.42 (d, J = 6.4 Hz, 2H); **^{13}C NMR** (100 MHz, DMSO-d_6): δ = 162.7 (d, J = 244 Hz), 157.3, 140.9 (d, J = 7 Hz), 131.0 (d, J = 8 Hz), 123.7 (d, J = 3 Hz), 114.7 (d, J = 21 Hz), 114.4 (d, J = 22 Hz), 43.7; 19F NMR (376 MHz, DMSO-d_6): δ = -113.0 -113.1 (m, 1F); **IR** (ν, cm^{-1}): 3159, 2938, 2361, 2342, 1653, 668; **HRMS (ESI)** for $C_8H_{11}N_3F$ [M-HCl+H]+ requires 168.0934 found 168.0931; **M.P**.: 69-71 °C.

3-Iodo-5-(pyridine-2-ylethynyl)benzonitrile: IPEB

3-Bromo-5-(pyridine-2-ylethynyl)benzonitrile (4.11)

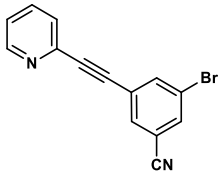

A mixture slurry of 2-ethynylpyridine (0.5 mL, 5.0 mmol), 3,5-dibromobenzonitrile (3.9 g, 15.0 mmol), trans-dichlorobis(triphenyl-phosphine)palladium (350 mg, 0.5

mmol), CuI (475 mg, 2.5 mmol) and PPh_3 (262 mg, 1.0 mmol) in Et_3N (14.0 mL, 99.9 mmol) was heated in a Schlenk tube at 80 °C for 1.5 h. After cooling to rt the resulting reaction mixture was diluted with sat. NH_4Cl (100 mL) and extracted with Et_2O (3 x 80 mL). The combined organic layers were dried over Na_2SO_4, filtered and concentrated in vacuum. The residue was dissolved in hexane/EtOAc (4/1) and filtered through a small silica-gel column (washed several times) and concentrated in vacuum. The crude product was purified by crystallization from hot hexane/EtOAc (placed in the freezer) to afford the product as a white solid (852 mg, 60%).

^{1}H NMR (400 MHz, $CDCl_3$): δ = 8.65 (ddd, J = 4.9, 1.8, 1.0 Hz, 1H), 7.95 (dd, J = 1.9, 1.5 Hz, 1H), 7.80 – 7.76 (m, 2H), 7.73 (td, J = 7.7, 1.8 Hz, 1H), 7.54 (dt, J = 7.8, 1.1 Hz, 1H), 7.31 (ddd, J = 7.7, 4.9, 1.2 Hz, 1H); **^{13}C NMR** (101 MHz, $CDCl_3$): δ = 150.4, 142.2, 138.9, 136.4, 134.7, 133.8, 127.6, 125.7, 123.8, 122.9, 116.6, 114.5, 92.0, 84.9. Data consistent with literature values. Data consistent with literature values.[14]

3-Iodo-5-(pyridine-2-ylethynyl)benzonitrile (4.12)

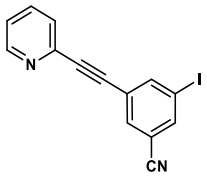

To a dried schlenk tube under an atmosphere of argon was added, 3-Bromo-5-(pyridine-2-ylethynyl)benzonitrile (200 mg, 0.71 mmol), copper iodide (6 mg, 0.032 mmol), *N*,*N*'-dimethylethylenediamine (10 μL, 0.071 mmol) and sodium iodide (212 mg, 1.41 mmol). The reaction flask was then heated to 90 °C before dioxane (14 mL) was added. The reaction was then left to stir at 90 °C overnight. After stirring for 16 hr, the reaction was cooled and filtered through celite. To the crude mixture was

added H_2O (30 mL) before extraction was performed with DCM (3 x 30 mL). The organic layers were then combined, dried with $MgSO_4$ and excess solvent removed *in vacuo*. The crude product was initially purified *via* flash column chromatography (10 : 3 Petane: EtOAc) affording a mixture of 3-bromo-5-(pyridine-2-ylethynyl)benzonitrile and 3-Iodo-5-(pyridine-2-ylethynyl)benzonitrile after which reverse phase HPLC purification was carried out affording 3-iodo-5-(pyridine-2-ylethynyl)benzonitrile as a white solid (55 mg, 23%, 0.17 mmol)

^{1}H NMR (400 MHz, $CDCl_3$): δ = 8.66 (d, *J* = 5.0 Hz, 1H), 8.17 (s, 1H), 7.97 (s, 1H), 7.82 (s, 1H), 7.74 (td, *J* = 7.5. 1.0 Hz, 1H), 7.55 (d, *J* = 8.0 Hz, 1H), 7.32 (dd, *J* = 7.5, 5.5 Hz, 1H); **^{13}C NMR** (101 MHz, $CDCl_3$): δ = 150.7, 145.0, 142.5, 140.6, 136.8, 134.6, 127.8, 125.8, 124.0, 116.7, 114.8, 93.9, 92.2, 85.2. Data consistent with literature values.[15]

3-(Pyridin-2-ylethynyl)-5-(4,4,5,5-tetramethyl-1,3,2-dioxaborolan-2-yl)benzonitrile (4.93):[c]

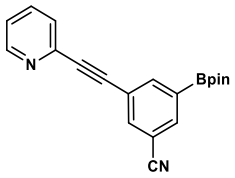

Nitrogen was bubbled through a mixture of 3-bromo-5-(pyridin-2-ylethynyl)benzonitrile (640.0 mg, 2.26 mmol), bis(pinacolato)diboron (631 mg, 2.49 mmol), potassium acetate (887.0 mg, 9.04 mmol), dichloro[1,1'-bis(diphenylphosphino)ferrocene]-palladium(II) dichloromethane adduct (110.8 mg, 0.14 mmol) and N,N-dimethylacetamide (7 mL) for 1 h. Then the reaction was heated

[c] The following step was carried out by S. Gruber

at 110° C for 40 min, cooled to room temperature and diluted with H_2O (100 mL), and extracted with EtOAc (4 x 35 mL). The combined organic extracts were washed with brine (35 mL), dried ($MgSO_4$), filtered, and concentrated in vacuum to give a residue that was dissolve in Et_2O/hexane (5/1) and filtered through a small silica-gel column. The filtrate was concentrated in vacuum and the residue was purified by crystallization from hot acetonitrile (placed in the freezer) to afford the product as a white solid (332 mg, 45%).

^{1}H NMR (400 MHz, CD_2Cl_2): δ = 8.65 – 8.56 (m, 1H), 8.21 (s, 1H), 8.04 (t, *J* = 1.3 Hz, 1H), 7.92 (t, *J* = 1.6 Hz, 1H), 7.72 (td, *J* = 7.8 Hz, 1.8, 1H), 7.55 (dd, *J* = 7.8, 1.5 Hz, 1H), 7.29 (ddd, *J* = 7.5, 4.9, 1.2 Hz, 1H), 1.35 (s, 12H); **^{13}C NMR** (101 MHz, CD_2Cl_2): δ = 150.6, 143.1, 142.3, 138.4, 137.4, 136.6, 127.8, 123.7, 123.7, 118.3, 113.0, 91.0, 86.4, 85.2, 25.0 (note: the aromatic carbon bound to the BPin was not observed). Data consistent with literature values.[14]

3-Fluoro-5-(pyridin-2-ylethynyl)benzonitrile (4.92)[d]

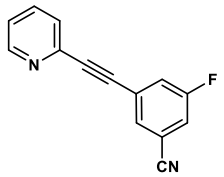

A mixture slurry of 2-ethynylpyridine (0.5 mL, 5.0 mmol), 3-dibromo-5-fluorobenzonitrile (3.0 g, 15.0 mmol), trans-dichlorobis(triphenyl-phosphine)palladium (350 mg, 0.5 mmol), CuI (475 mg, 2.5 mmol, and PPh_3 (262 mg, 1.0 mmol) in Et_3N (14.0 mL, 99.9 mmol) was heated in a Schlenk tube at 80 °C for 1.5 h. After cooling to room temperature, the resulting reaction mixture was diluted

[d] The following step was carried out by S. Gruber

with sat. NH_4Cl (100 mL) and extracted with Et_2O (3 x 80 mL). The combined organic layers were dried over Na_2SO_4, filtered and concentrated in vacuum. The residue was dissolved in hexane/EtOAc (4:1) and filtered through a small silica-gel column (washed several times) and concentrated in vacuum. The crude product was purified by crystallization from hot hexane/EtOAc (placed in the freezer) to afford the product as a white solid (684 mg, 62%). **^{1}H NMR** (500 MHz, $CDCl_3$): δ = 8.66 – 8.54 (m, 1H), 7.70 (td, J = 7.7 Hz, 1.8, 1H), 7.64 (t, J = 1.4 Hz, 1H), 7.52 (dt, J = 7.8 Hz, 1.1, 1H), 7.49 (ddd, J = 8.7, 2.5, 1.3 Hz, 1H), 7.33 (ddd, J = 7.9, 2.5, 1.3 Hz, 1H), 7.29 (ddd, J = 7.7, 4.8, 1.2 Hz, 1H); **^{13}C NMR** (101 MHz, $CDCl_3$): δ = 161.9 (d, J = 252 Hz), 150.4, 142.2, 136.4, 131.5 (d, J = 4 Hz), 127.6 , 126.1 (d, J = 10 Hz), 123.8 , 123.5 (d, J = 23 Hz), 119.5 (d, J = 25 Hz), 116.8 (d, J = 3 Hz), 114.4 (d, J = 10 Hz), 91.7, 85.1 (d, J = 3 Hz); ^{19}F NMR (376 MHz, $CDCl_3$): δ = –108.9. Data consistent with literature values.[14]

5.9 Radioiodination Procedures and Characterisation for Compounds in Chapter IV:

5.9.1 General procedure for the ^{123}I-Iodination of Aryl Bpin or $B(OH)_2$ substrates:

To a V-vial containing a magnetic stirrer bar, arylBpin (15 μmol) or arylB$(OH)_2$ (15 μmol) and [^{123}I]NaI (ca. 20 MBq, 5 μL MeOH approx.) was added $Cu(OCOCF_3)_2$ (0.30 μmol), 1,10-phenanthroline (0.30 μmol) in MeOH:H_2O (4:1, 200 μL) from a stock solution. The reaction vial was then heated to 80 °C for 20 minutes. The reaction was quenched by addition of 10 mol% sodium thiosulfate (200 μL) and MeCN (100 μL). An aliquot was removed for analysis by radio-TLC and HPLC to calculate the radiochemical conversion (RCC) and purity respectively.

5.9.2 Procedure for the ^{123}I-Iodination of ArylBpin Tracers: [^{123}I]DPA-713, [^{123}I]IMPY, Boc Protected [^{123}I]MIBG and [^{123}I]IPEB:

The optimised method started with the preparation of a V-vial containing a magnetic stirrer bar and [^{123}I]NaI (ca. 4 MBq, 5 μL MeOH approx.) to which arylBpin (5 μmol), $Cu(OCOCF_3)_2$ (0.25 μmol), 1,10-phenanthroline (0.25 μmol) in MeOH:H_2O (4:1, 200 μL). The reaction vial was then heated to 80 °C for 20 minutes. The reaction was quenched by addition of 10 mol% sodium thiosulfate (400 μL) and MeCN (100 μL). An aliquot was removed for analysis by thin-layer chromatography (radio-TLC) and high performance liquid chromatography (radio-HPLC) to calculate the radiochemical conversion and purity respectively.

5.9.3 Procedure for the ^{123}I-Iodination and determination of RCY of ArylBpin Tracers: [^{123}I]DPA-713, [^{123}I]IMPY, and [^{123}I]IPEB:

The optimised method started with the preparation of a V-vial containing a magnetic stirrer bar, arylBpin (5 μmol) and [^{123}I]NaI (ca. 4 – 36 MBq, 5 - 15 μL MeOH approx.) to which $Cu(OCOCF_3)_2$ (0.25 μmol), 1,10-phenanthroline (0.25 μmol) in MeOH:H_2O (4:1, 200 μL). The reaction vial was then heated to 80 °C for 20 minutes. The reaction was diluted in H_2O (6 mL) and loaded onto a C-18 SepPak Plus cartridge. This was then flushed with H_2O (2 mL) and air (2 mL) followed by elution of the ^{123}I-iodinated product with MeCN (2 mL). The radiochemical yield was then calculated as a percentage of activity (MBq) found in the MeCN elute compared to the starting activity (MBq). An aliquot was removed for analysis by HPLC to calculate the radiochemical yield and purity respectively.

5.9.4 Procedure for the ^{123}I-iodination, deprotection and determination of RCY of [^{123}I]MIBG ([^{123}I]4.16):

The optimised method started with the preparation of a V-vial containing a magnetic stirrer bar, arylBpin (5 μmol) and [^{123}I]NaI (ca. 3 – 7 MBq, 5 μL MeOH approx.) to which $Cu(OCOCF_3)_2$ (0.25 μmol), 1,10-phenanthroline (0.25 μmol) in 4:1 MeOH:H_2O (200 μL). The reaction vial was then heated to 80 °C for 20 minutes. The reaction was diluted in H_2O containing 10% MeOH (6 mL) and loaded onto a C-18 SepPak Plus cartridge and flushed with H_2O:MeOH (9:1, 6 mL). [^{123}I[MIBG was then eluted with DCM (2 x 1 mL) followed by air (2 x 1 mL). At this point the radiochemical yield was calculated as a percentage of activity (MBq) found in the DCM collected compared to the starting activity (MBq). Following this, the DCM was removed at 50 °C under a stream of N_2. Once dry, either; 300 μL of 57% HI was added and the reaction stirred for 10 minutes at 125 °C, or 300 μL of TFA was added and the reaction stirred for 10 minutes at 80 °C. After 10 minutes, an aliquot was removed for analysis by high performance liquid chromatography (radioHPLC) to calculate the conversion of the deprotection step and the purity respectively.

HPLC gradient A: water/acetonitrile, 1 mL/min, Waters Nova-Pak C18 Column, 4 μm, 3.9 x 150 mm

0-1 min (5% MeCN) isocratic
1-10 min (5% MeCN to 95% MeCN) linear increase
10-14 min (95% MeCN) isocratic
14-15 min (95% MeCN to 5% MeCN) linear decrease
15-17 min (5% MeCN) isocratic

HPLC gradient B: water/acetonitrile containing 0.1 mg/mL TFA, 1 mL/min, Waters Nova-Pak C18 Column, 4 μm, 3.9 x 150 mm

0-2 min (5% MeCN containing 0.1 mg/mL TFA) isocratic

1-10 min (5% MeCN containing 0.1 mg/mL TFA to 95% MeCN containing 0.1 mg/mL TFA) linear increase
10-14 min (95% MeCN containing 0.1 mg/mL TFA) isocratic
14-15 min (95% MeCN containing 0.1 mg/mL TFA to 5% MeCN containing 0.1 mg/mL TFA) linear decrease
15-17 min (5% MeCN containing 0.1 mg/mL TFA) isocratic

Compound	**Starting Activity (MBq)**	**MeCN Flush Activity (MBq)**	**H_2O Flush Activity (MBq)**	**QMA Activity (MBq)**	**RCP (%)**	**RCY (%)***
[^{123}I]DPA-713	36.5	32.0	0.7	1.0	> 99%	88%
[^{123}I]IMPY	15.2	11.8	1.5	1.7	> 99%	78%
[^{123}I]IPEB	15.9	8.4	2.8	0.0	> 99%	53%
[^{123}I]IPEB	4.9	2.2	2.7	0.0	> 99%	45%

Calculation of Radiochemical Yields for [^{123}I]DPA-713, [^{123}I]IMPY, and [^{123}I]IPEB

Starting Activity (MBq)	**MeOH Flush Activity (MBq)**	**H_2O Flush Activity (MBq)**	**RCP (%)**	**RCY* (%) (Protected Species)**	**Deprotection Condition**	**Conversion (%)**	**RCC (%) ([^{123}I]MIBG Salt)**
15.8	7.1	3.5	> 99	45	-	-	-
8.1	3.6	1.1	-	44	57% HI (300 µL), 125 °C, 10 mins	79	35
41.9	18.1	11.1	-	43	TFA (300 µL), 80 °C, 10 mins	86	37

*Radiochemical yield calculated as a percentage of activity in the MeOH or DCM flush (MBq) compared to the starting activity. Loss in activity due to transfer losses.

Calculation of Radiochemical Yields for Boc Protected [^{123}I]MIBG and [^{123}I]MIBG

5.9.5 Radio-HPLC Tracers

Radio-HPLC traces with authentic UV references (blue line) overlaid Crude Radio-HPLC (black line) traces of the crude mixture following the general procedure, with authentic UV references overlaid are shown below. The solid blue line indicates the UV trace for cold reference material and the solid black line is the crude radio-HPLC trace. All samples were run using HPLC gradient A unless otherwise specified.

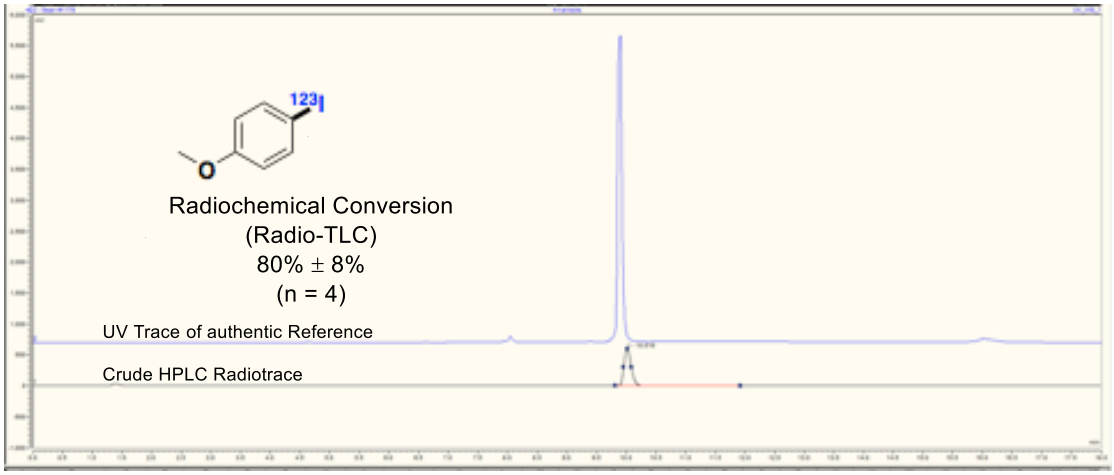

HPLC radio-trace of **[^{123}I]4.51** (black) overlaid with HPLC UV-trace (220 nm) of **[^{127}I]4.51** (blue).

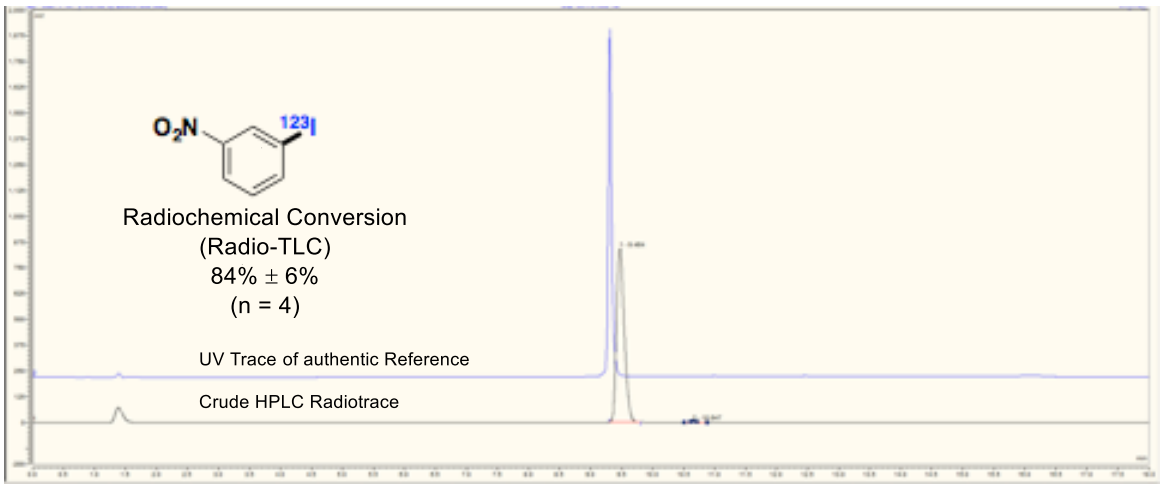

HPLC radio-trace of **[^{123}I]4.56** (black) overlaid with HPLC UV-trace (220 nm) of **[^{127}I]4.56** (blue).

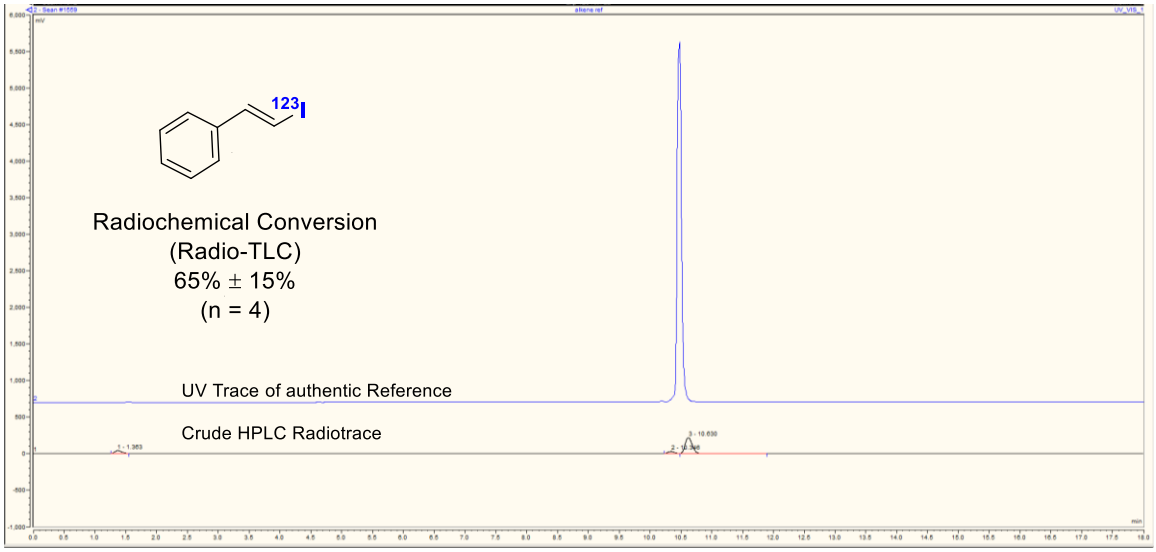

HPLC radio-trace of **[^{123}I]4.60** (black) overlaid with HPLC UV-trace (220 nm) of **[^{127}I]4.60** (blue).

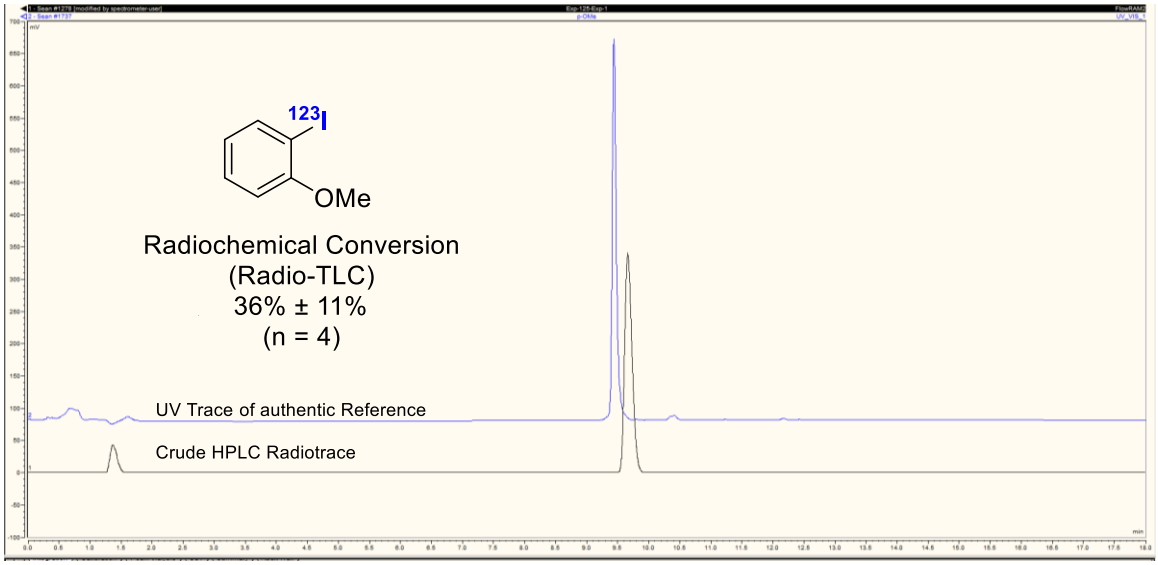

HPLC radio-trace of **[^{123}I]4.62** (black) overlaid with HPLC UV-trace (220 nm) of **[^{127}I]4.62** (blue).

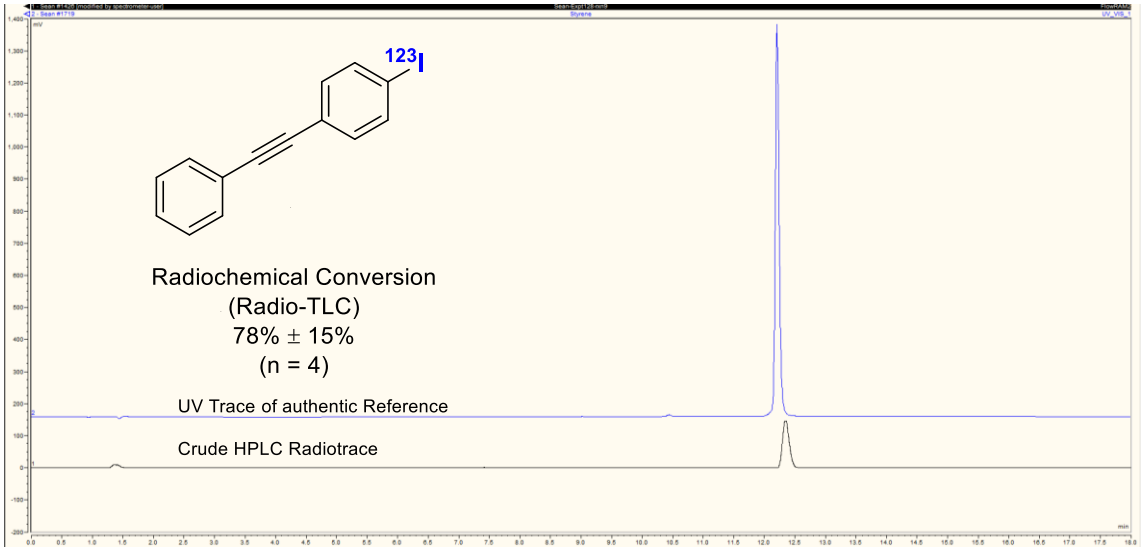

HPLC radio-trace of **[^{123}I]4.65** (black) overlaid with HPLC UV-trace (220 nm) of **[^{127}I]4.65** (blue).

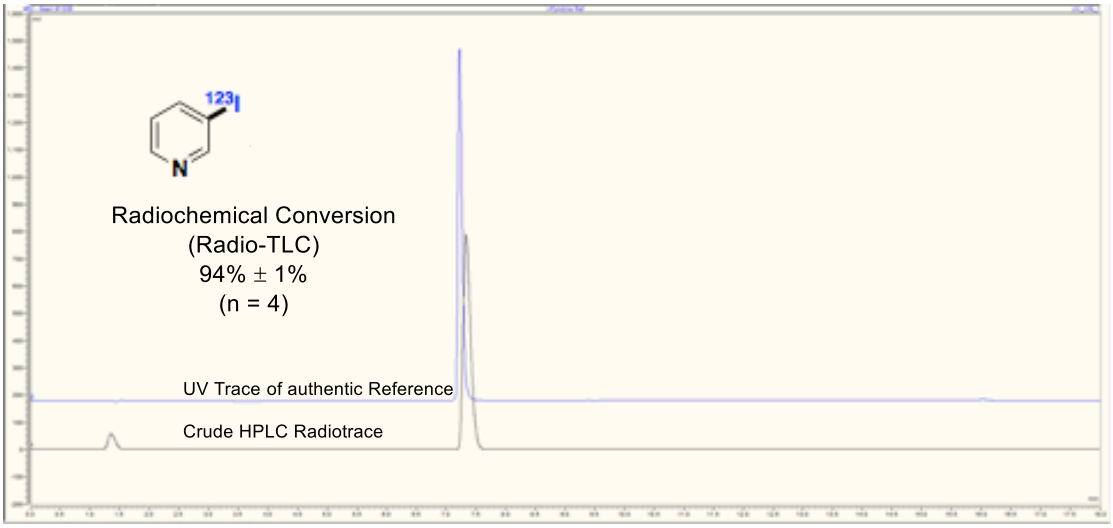

HPLC radio-trace of **[^{123}I]4.68** (black) overlaid with HPLC UV-trace (220 nm) of **[^{127}I]4.68** (blue).

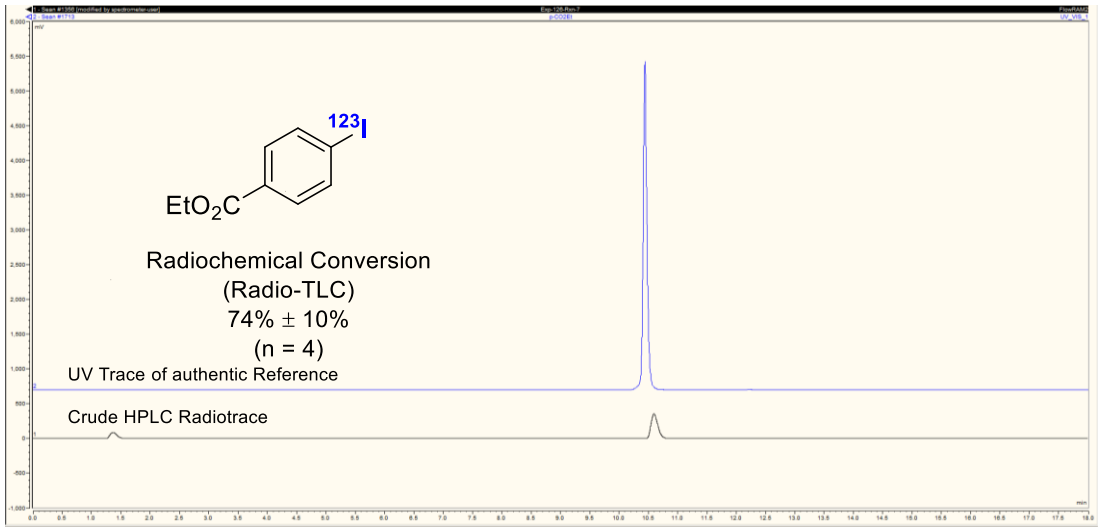

HPLC radio-trace of **[^{123}I]4.71** (black) overlaid with HPLC UV-trace (220 nm) of **[^{127}I]4.71** (blue).

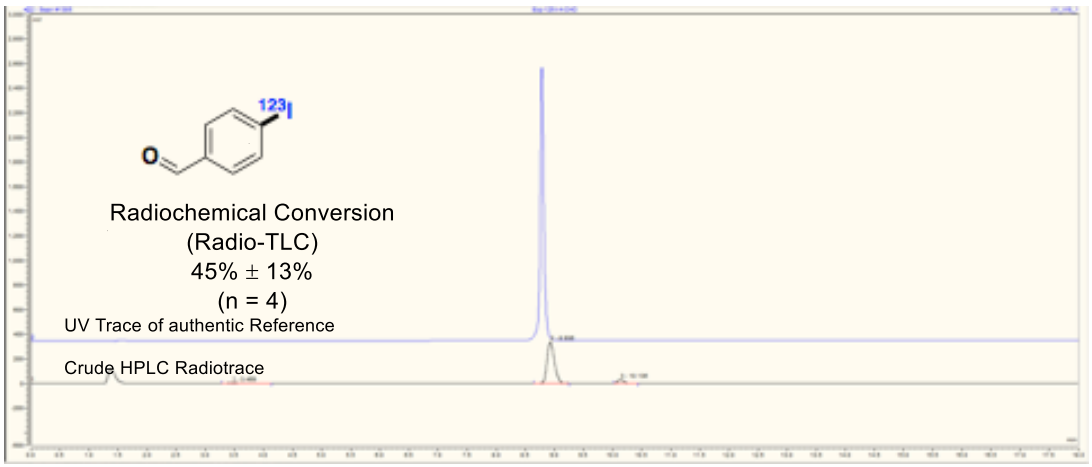

HPLC radio-trace of **[^{123}I]4.72** (black) overlaid with HPLC UV-trace (220 nm) of **[^{127}I]4.72** (blue).

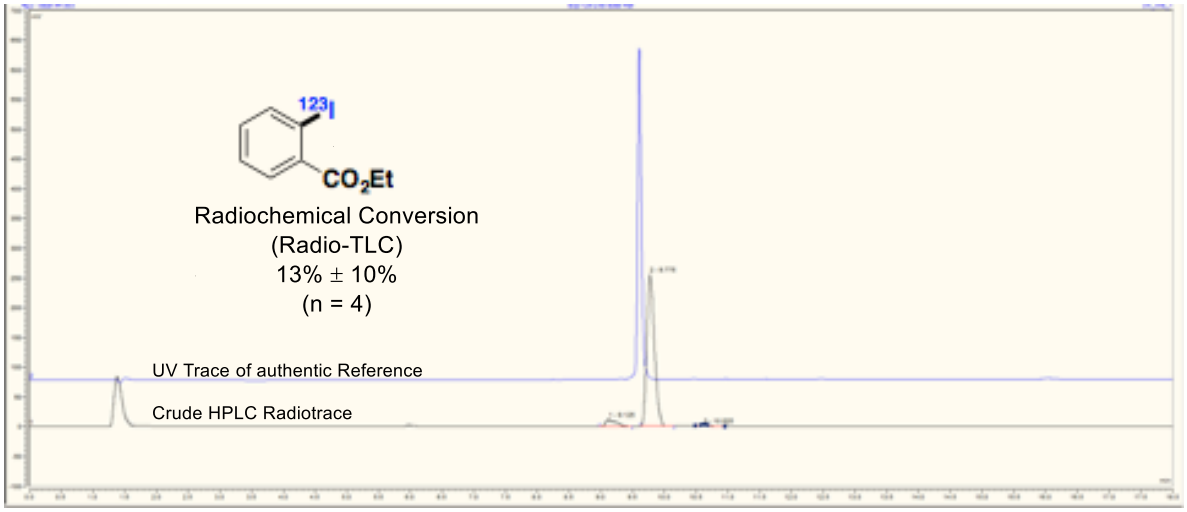

HPLC radio-trace of **[^{123}I]4.76** (black) overlaid with HPLC UV-trace (220 nm) of **[^{127}I]4.76** (blue).

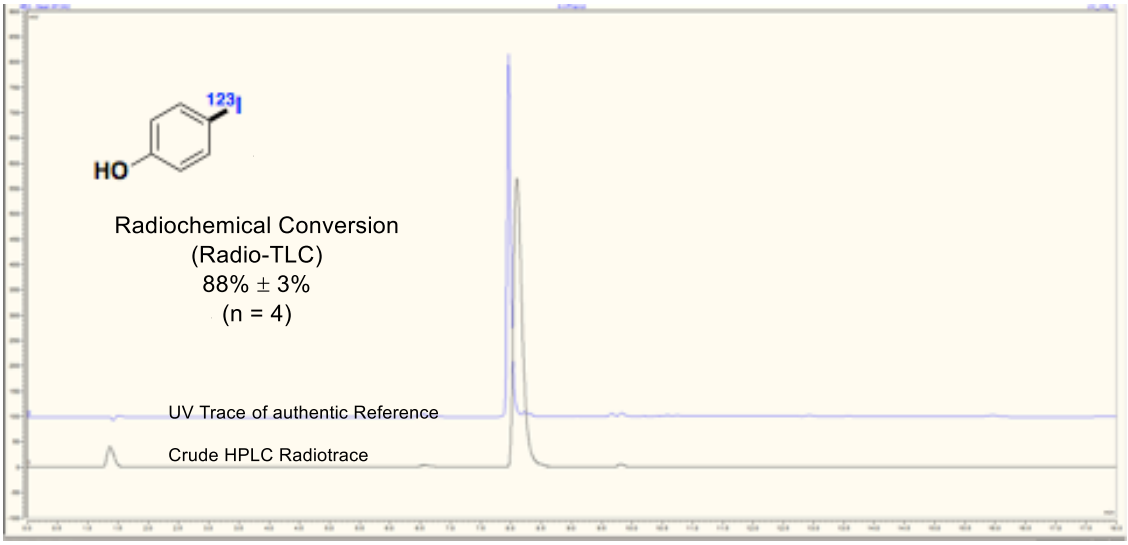

HPLC radio-trace of **[^{123}I]4.78** (black) overlaid with HPLC UV-trace (220 nm) of **[^{127}I]4.78** (blue).

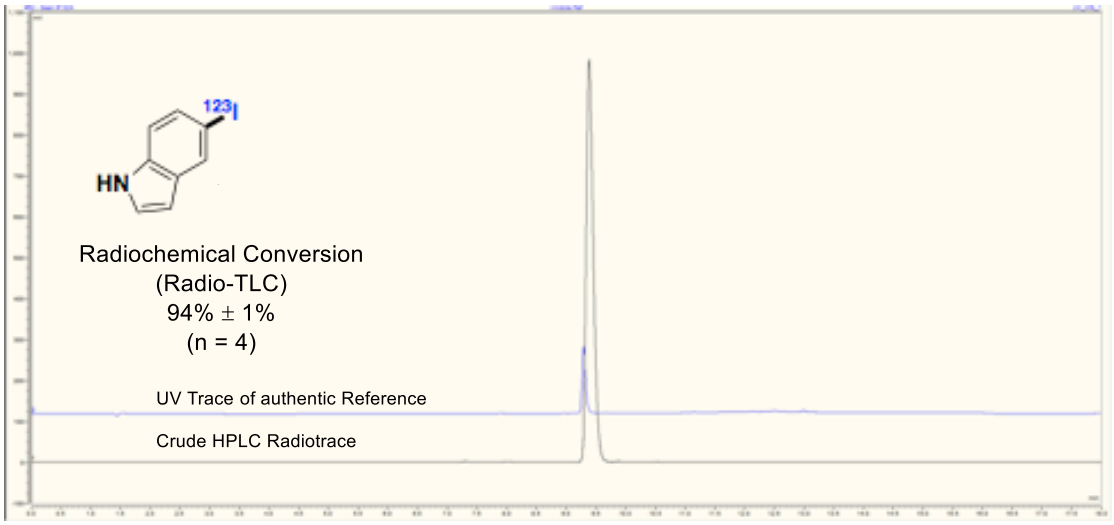

HPLC radio-trace of **[^{123}I]4.79** (black) overlaid with HPLC UV-trace (220 nm) of **[^{127}I]4.79** (blue).

5.9.6 HPLC Traces Derived from Boronic Acid Starting Materials (all traces recorded using HPLC gradient B)

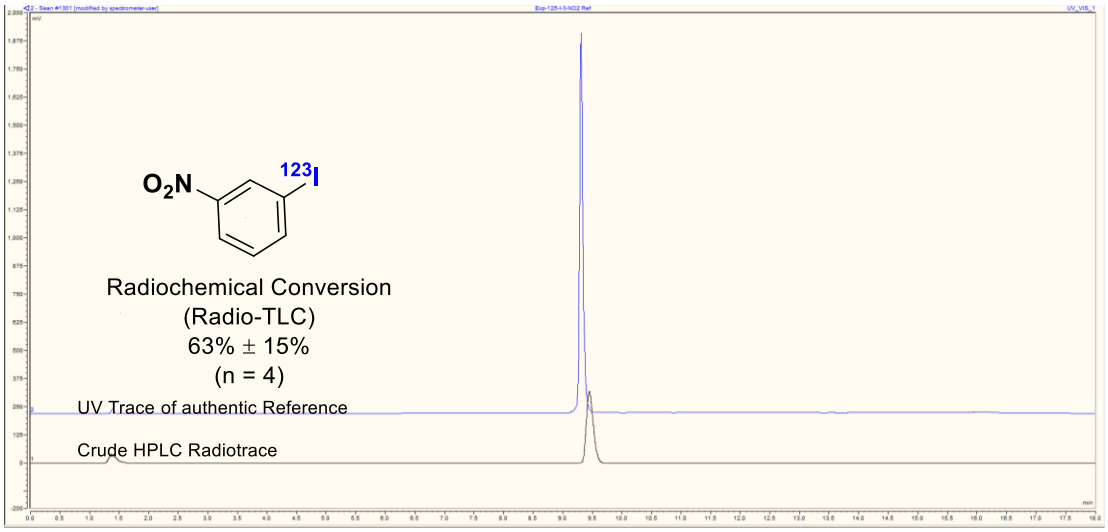

HPLC radio-trace of **[^{123}I]4.56** (black) overlaid with HPLC UV-trace (220 nm) of **[^{127}I]4.56** (blue).

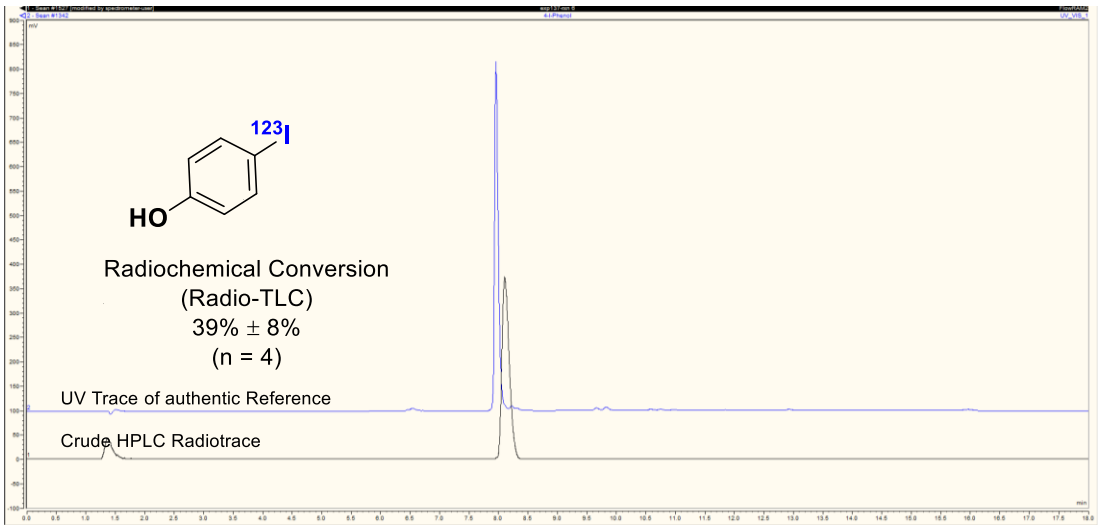

HPLC radio-trace of **[^{123}I]4.78** (black) overlaid with HPLC UV-trace (220 nm) of **[^{127}I]4.78** (blue).

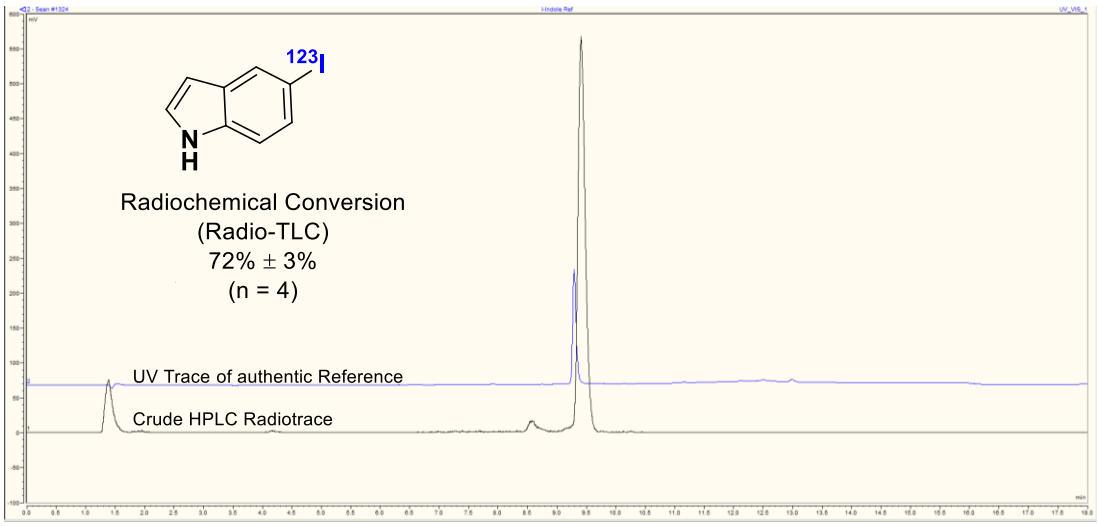

HPLC radio-trace of **[^{123}I]4.79** (black) overlaid with HPLC UV-trace (220 nm) of **[^{127}I]4.79** (blue).

5.9.7 HPLC Traces of SPECT Traces (all traces taken using HPLC gradient A unless otherwise specified)

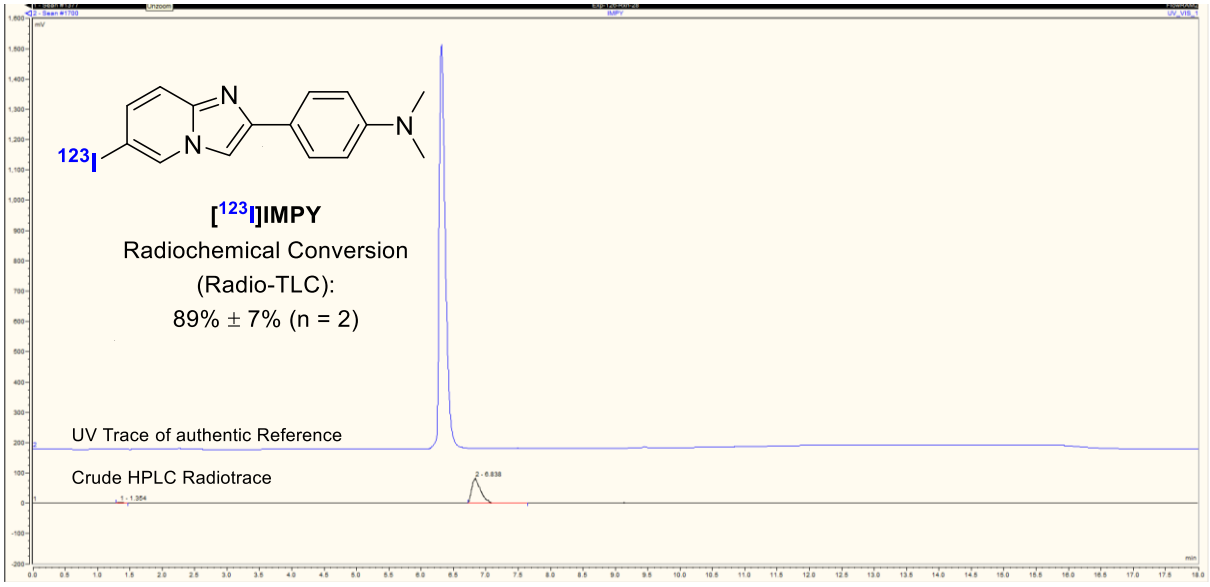

HPLC radio-trace of **[^{123}I]4.81** (black) overlaid with HPLC UV-trace (220 nm) of **[^{127}I]4.81** (blue). Trace recorded using HPLC gradient B

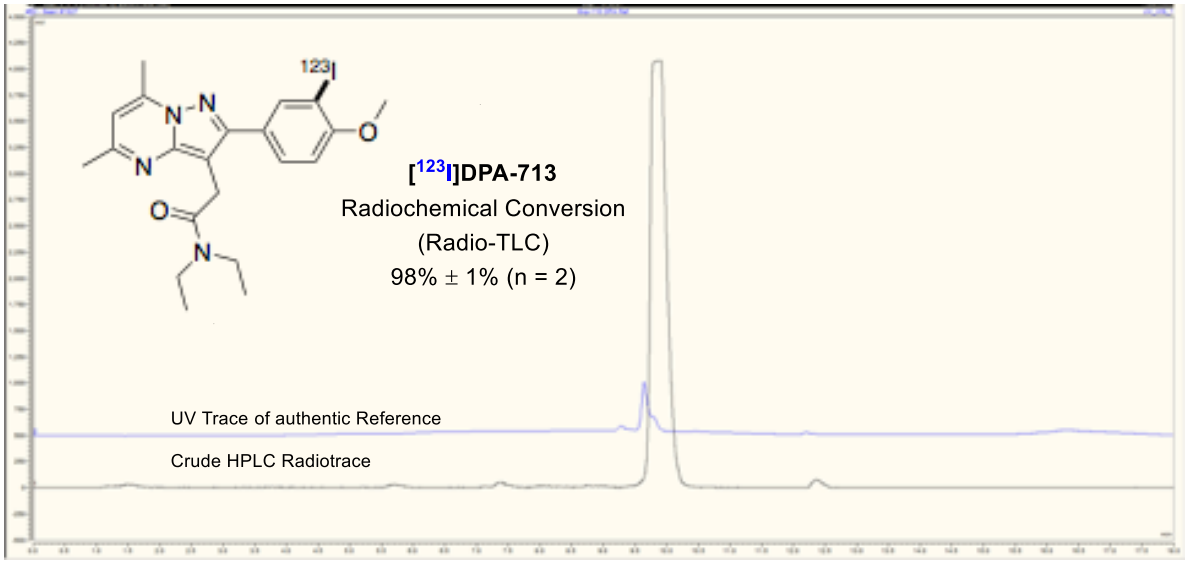

HPLC radio-trace of **[^{123}I]4.14** (black) overlaid with HPLC UV-trace (220 nm) of **[^{127}I]4.14** (blue).

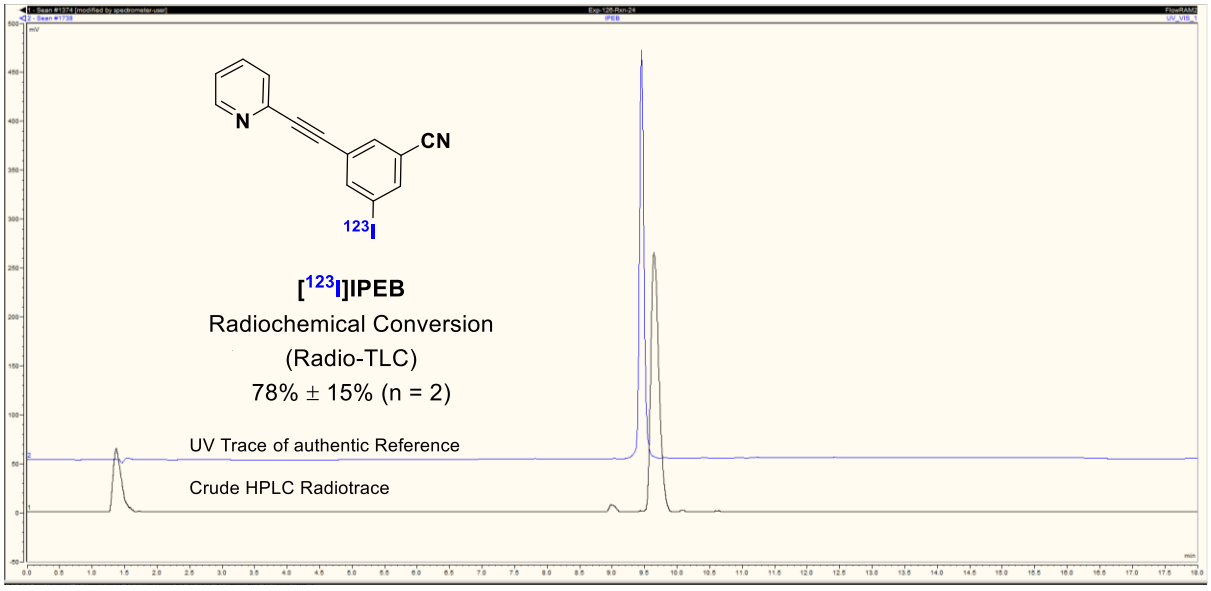

HPLC radio-trace of **[^{123}I]4.12** (black) overlaid with HPLC UV-trace (220 nm) of **[^{127}I]4.12** (blue).

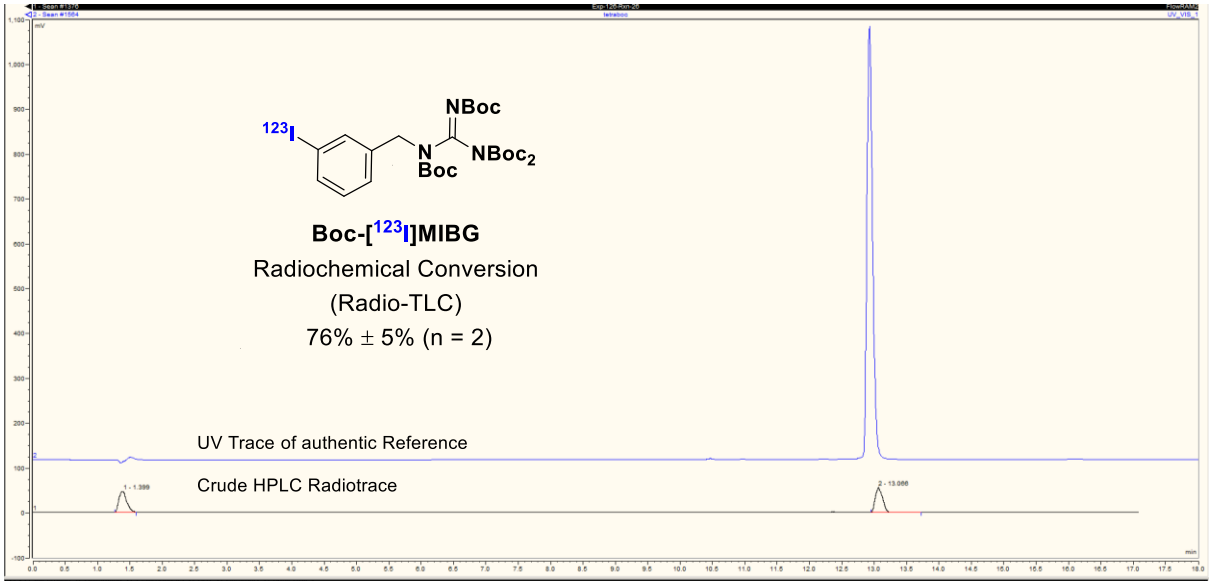

HPLC radio-trace of **[^{123}I]4.101** (black) overlaid with HPLC UV-trace (220 nm) of **[^{127}I]4.101** (blue).

Radio-trace for [^{123}I]MIBG ([^{123}I]4.16).

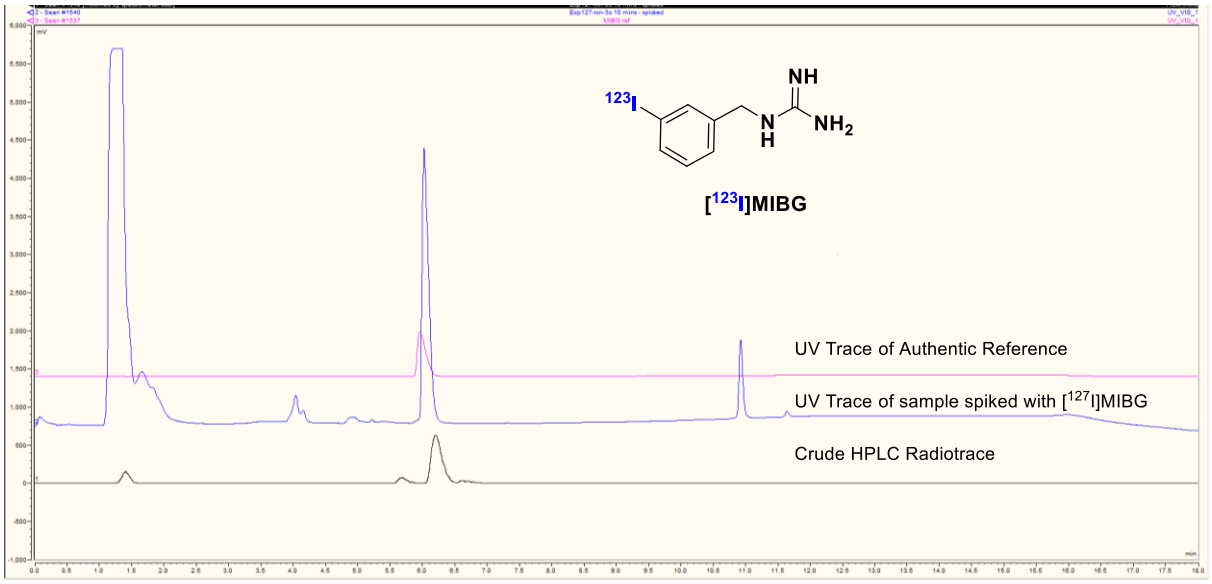

HPLC radio-trace of **[^{123}I]4.16** (black) overlaid with HPLC UV-trace (220 nm) of **[^{127}I]4.16** (blue). The product injected onto an analytical column overlaid with a UV-spectra spiked with an authentic reference sample. Trace carried out using HPLC gradient B

5.10 Radiofluorination Procedures and Characterisation for Compounds in Chapter IV:

Isolation procedure for [^{18}F]MFBG [^{18}F]4.97:

[^{18}F]Fluoride (3.0-10.0 GBq) was separated from ^{18}O-enriched-water using anion exchange cartridge (see section 2.3) and subsequently released with 900 μL (in 6 x 150 μL portions) of a solution of $K_{222}/K_2C_2O_4/K_2CO_3$ (kryptofix 222 (6.3 mg), $K_2C_2O_4$ (1 mg) and K_2CO_3 (0.1 mg) in 1 mL of MeCN/H_2O, 4:1) into a 5 mL V-vial containing a magnetic stir bar in the concentrator. The solution was dried with five cycles of azeotropic drying with MeCN (5 x 200 μL) under a flow of N_2 at 105 °C. The 5 mL vial containing the dried [^{18}F]KF/K_{222} complex was purged with 30 mL of air using a syringe and then a solution of arylboronate precursor (13 mg, 0.02 mmol) and $Cu(OTf)_2(py)_4$ (14 mg, 0.02 mmol) in anhydrous DMF (400 μL) was added. The mixture was heated at 120 °C for 20 min in a sealed vial with stirring. $HI_{(aq)}$ (57%, 300 μL) was added via syringe and the reaction was stirred at 120 °C for 10 min. The reaction mixture was then allowed to cool to room temperature and partially neutralized with NaOH(aq) (6.75 M, 300 μL) and further diluted with 25 mM NH_4HCOO(aq) (800 μL) and filtered before loading onto a 2 mL HPLC loop and injected on a semi-Prep HPLC column (Synergi 4μm Hydro-RP 250x10mm) and eluted with 10% MeCN/90% 25 mM NH_4HCOO (isocratic 4 mL/min) monitoring with UV (254 nm) and radioactive traces. (Note: Precipitate formed after HI deprotection and led to poor transfer efficiency and loss of activity deposited on the syringe filter prior to loading HPLC.) MA of [^{18}F]MFBG in collected fraction was assessed using an analytical Synergi 4μm Hydro-RP 80A, 150 x 4.6 mm with 10%

MeCN/90% NH_4HCOO(aq) (isocratic 1 mL/min)monitoring with UV (254 nm) and radioactive traces.

Radio-trace for [^{18}F]MFBG ([^{18}F]4.97):

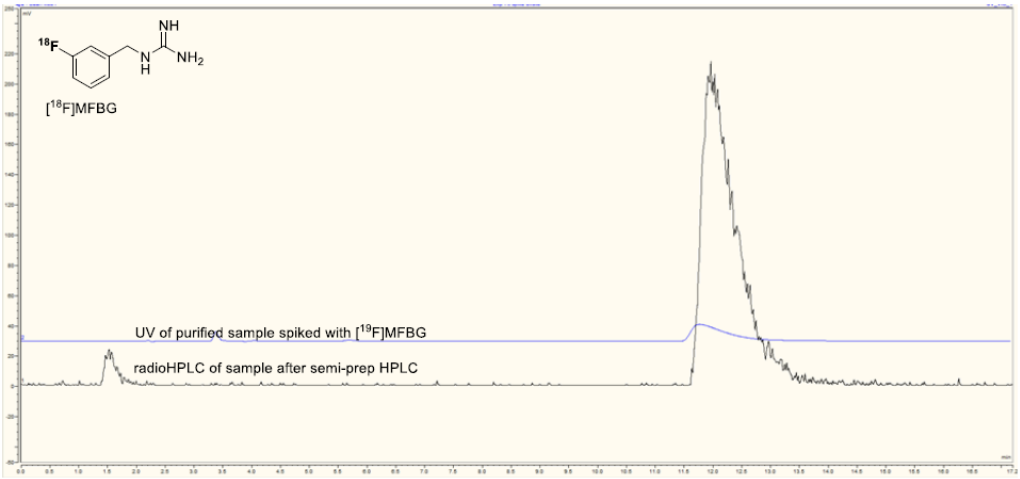

HPLC radio-trace of **[^{123}I]4.97** (black) overlaid with HPLC UV-trace (220 nm) of **[^{127}I]4.97** (blue).

Isolation procedure for [^{18}F]FPEB [^{18}F]4.92:

[^{18}F]Fluoride (3.0-10.0 GBq) was separated from ^{18}O-enriched-water using anion exchange cartridge (see section 2.3) and subsequently released with 900 µL (in 6 x 150 µL portions) of a solution of $K_{222}/K_2C_2O_4/K_2CO_3$ (kryptofix 222 (6.3 mg), $K_2C_2O_4$ (1 mg) and K_2CO_3 (0.1 mg) in 1 mL of MeCN/H2O, 4:1) into a 5 mL V-vial containing a magnetic stir bar in the concentrator. The solution was dried with five cycles of azeotropic drying with MeCN (5 x 200 µL) under a flow of N2 at 105 °C. The 5 mL vial containing the dried [^{18}F]KF/K_{222} complex was purged with 30 mL of air using a syringe and then a solution of arylboronate precursor (10 mg, 0.03 mmol) and $Cu(OTf)_2(py)_4$ (27 mg, 0.04 mmol) in anhydrous DMA (400 µL) was added. The mixture was heated at 120 °C for 20 min in a sealed vial with stirring, after which, the reaction mixture was diluted with 1 mL of 40% MeCN/ 60% 25 mM NH_4HCOO(aq) and loaded directly onto a 2 mL HPLC loop and injected on a semi-Prep HPLC

column (Synergi 4µm HydroRP 250x10mm) and eluted with 50% MeCN/50% 25 mM NH_4HCOO (isocratic 4 mL/min) monitoring with UV (254 nm) and radioactive traces. MA of [^{18}F]FPEB in collected fraction was assessed using an analytical Synergi 4µm Hydro-RP 80A, 150 x 4.6 mm with 40% MeCN/60% H_2O (isocratic 1 mL/min)monitoring with UV (254 nm) and radioactive traces.

Radio-trace for [^{18}F]FPEB ([^{18}F]4.92):

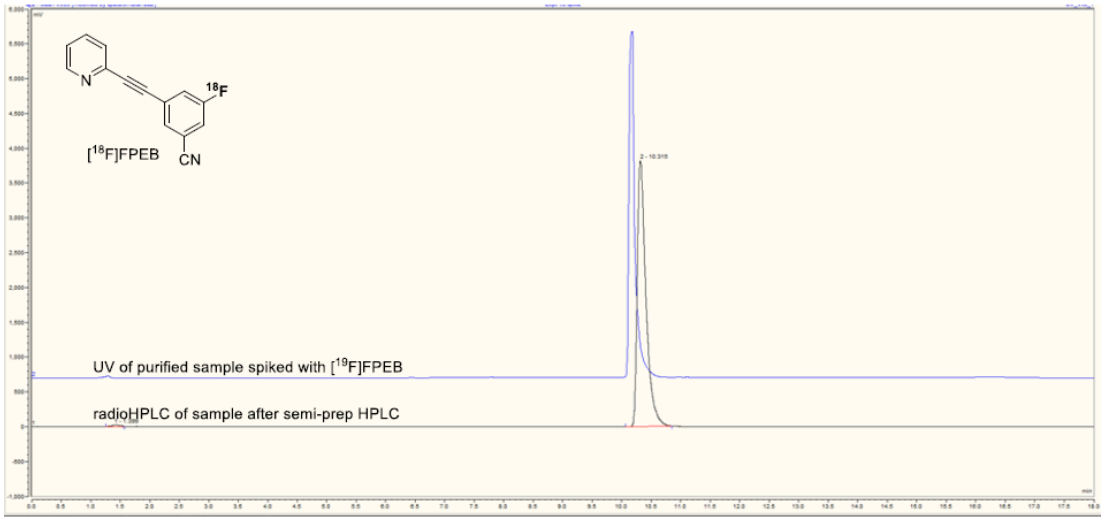

HPLC radio-trace of **[^{123}I]4.92** (black) overlaid with HPLC UV-trace (220 nm) of **[^{127}I]4.92** (blue).

5.11 References

[1] K. A. Menear, C. Adcock, R. Boulter, X.-L. Cockcroft, L. Copsey, A. Cranston, K. J. Dillon, J. Drzewiecki, S. Garman, S. Gomez, H. Javaid, F. Kerrigan, C. Knights, A. Lau, V. M. Loh Jr., I. T. W. Matthews, S. Moore, M. J. O'Connor, G. C. M. Smith, N. M. B. Martin, *J. Med. Chem.,* 2008, **51**, 6581.

[2] V. M. Outerbridge, S. M. Landge, H. Tamaki, B. Török, Microwave-Promoted Solid-Acid Catalyzed One-Pot Synthesis of Phthalazinones. *Synthesis.* 2009, **11**, 1801.

[3] A. O. H. Nezhawy, S. T. Gaballah, M. A. A. Radwan, *Tetrahedron Letters.* 2009, **50**, 6646.

[4] PCT Int. Appl., WO2008047082, 2008

[5] F.-C. Qiu, W.-C. Yang, Y.-Z. Chang, B.-T. Guan, *Asian J. Org. Chem.,* 2017, **6**, 1361.

[6] P. Ravat, Y. Borozdina, Y. Ito, V. Enkelmann, M. Baumgarten, *Cryst. Growth Des.,* 2014, **14**, 5840.

[7] X. Zhang, P. Li, Y. Ji,; L. Zhang,; L. Wang, *Synthesis,* 2011, 2975.

[8] C. Morrill, R. H. Grubbs, *J. Org. Chem.* 2003, **68**, 6031.

[9] P. G. Wilson, J. M. Mercy, J. M. Redmond, A. W. McCarter, *J. Org. Chem.,* 2012, **77**, 6384.

[10] S. L. Riches, C. Saha, N. F. Filgueira, E. Grange, E. M. McGarrigle, V. K. Aggarwal, *J. Am. Chem. Soc.,* 2010, **132**, 7626.

[11] H. Wang, M. Pullambhatla, T. R. Guilarte, R. C. Mease, M. G. Pomper, *Biochem. Biophys. Res. Commun.,* 2009, **389**, 80.

[12] Z. Diwu; C. Beachdel; Dieter. H. Klaubert, *Tetrahedron Letters*, 1998 , 39, 4987 – 4990

[13] J.-S. Choi, J. J. Braymer, S. K. Park, S. Mustafa, J. Chae, M. H. Lim, *Metallomics* 2011, **3**, 284.

[14] S. Preshlock, S. Calderwood, S. Verhoog, M. Tredwell, M. Huiban, A. Hienzsch, S. Gruber, T. C. Wilson, N. J. Taylor, T Cailly, M. Schedler, T. L. Collier, J. Passchier, R. Smits, J. Mollitor, A. Hoepping, M. Mueller, C. Genicot, J. Mercier, V. Gouverneur, *Chem. Commun.,* 2016, **52**, 8361.

[15] K.-E. Kil, A. Zhu, Z. Zhang, J.-K. Choi, S. Kura, C. Gong, A.-L. Brownell, *ACS. Med. Chem. Lett.,* 2014, **5**, 652.